EMERGING INFECTIOUS DISEASES®

CDC
Centers for Disease Control and Prevention

Viral Infections

May 2022

Lorser Feitelson (1898–1978), *Magical Forms*, 1947. Oil on canvas, 36 in x 30 in / 91.4 cm x 76.2 cm. The Feitelson / Lundeberg Art Foundation Collection, courtesy Louis Stern Fine Arts © The Feitelson / Lundeberg Art Foundation, Portland, Oregon, USA.

EMERGING INFECTIOUS DISEASES®

Emerging Infectious Diseases is published monthly by the Centers for Disease Control and Prevention, 1600 Clifton Rd NE, Mailstop H16-2, Atlanta, GA 30329-4027, USA. Telephone 404-639-1960; email, eideditor@cdc.gov

EMERGING INFECTIOUS DISEASES®

Viral Infections **May 2022**

On the Cover

Lorser Feitelson (1898–1978), *Magical Forms*, 1947. Oil on canvas, 36 in x 30 in / 91.4 cm x 76.2 cm. The Feitelson/ Lundeberg Art Foundation Collection, courtesy Louis Stern Fine Arts © The Feitelson / Lundeberg Art Foundation, Portland, Oregon, USA.

About the Cover p. 1085

Synopses

Medscape EDUCATION ACTIVITY

Research

Medscape EDUCATION ACTIVITY

Dispatches

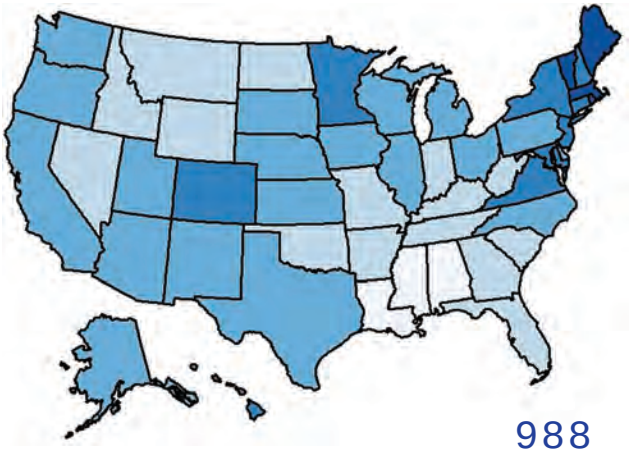

988

EMERGING INFECTIOUS DISEASES®

May 2022

Research Letters

1003

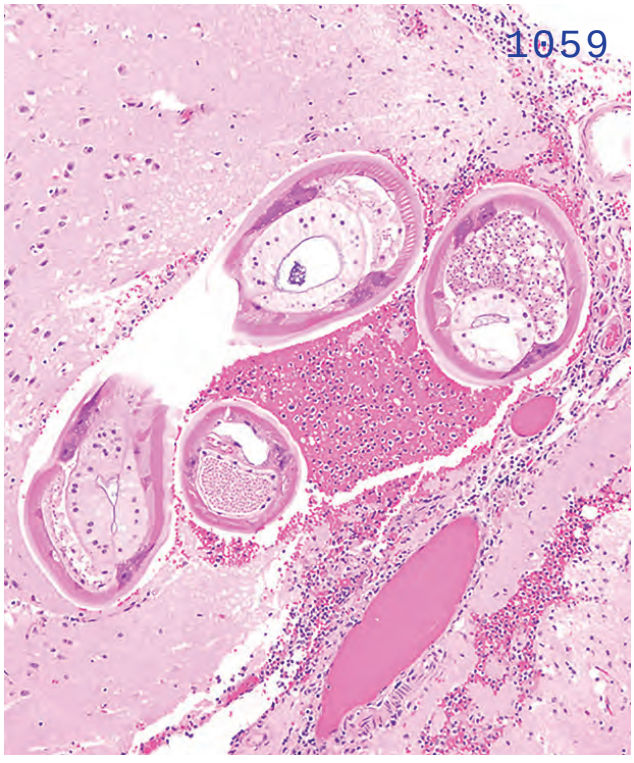

EMERGING INFECTIOUS DISEASES®

May 2022

Comment Letters

About the Cover

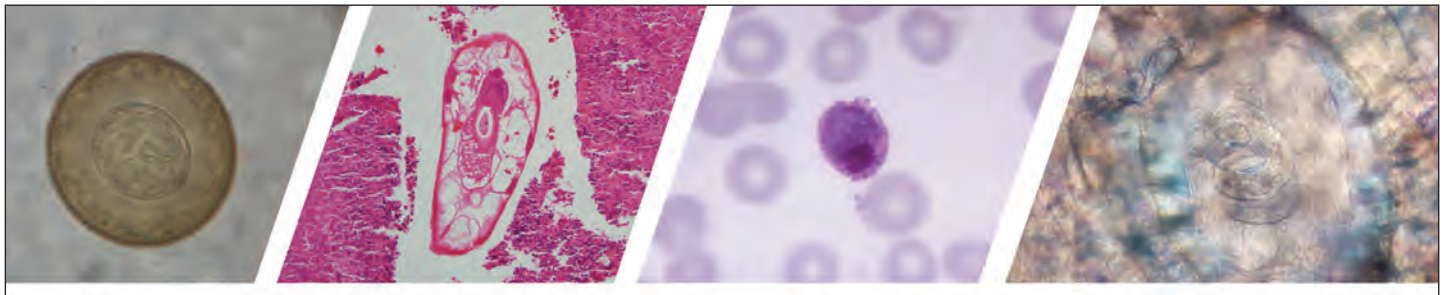

DPDx

Diagnostic Assistance and Training in Laboratory Identification of Parasites

A free service of CDC available to laboratorians, pathologists, and other health professionals in the United States and abroad

- Diagnosis from photographs of worms, histological sections, fecal, blood, and other specimen types
- Expert diagnostic review
- Formal diagnostic laboratory report
- Submission of samples via secure file share

Visit the DPDx website for information on laboratory diagnosis, geographic distribution, clinical features, parasite life cycles, and training via Monthly Case Studies of parasitic diseases.

www.cdc.gov/dpdx
dpdx@cdc.gov

U.S. Department of Health and Human Services
Centers for Disease Control and Prevention

CS272346-DE

Invasive Group A *Streptococcus* Outbreaks Associated with Home Healthcare, England, 2018–2019

Laura E. Nabarro, Colin S. Brown, Sooria Balasegaram, Valérie Decraene, James Elston, Smita Kapadia, Pauline Harrington, Peter Hoffman, Rachel Mearkle, Bharat Patel, Derren Ready, Esther Robinson, Theresa Lamagni

Medscape EDUCATION ACTIVITY

In support of improving patient care, this activity has been planned and implemented by Medscape, LLC and Emerging Infectious Diseases. Medscape, LLC is jointly accredited by the Accreditation Council for Continuing Medical Education (ACCME), the Accreditation Council for Pharmacy Education (ACPE), and the American Nurses Credentialing Center (ANCC), to provide continuing education for the healthcare team.

Medscape, LLC designates this Journal-based CME activity for a maximum of 1.00 ***AMA PRA Category 1 Credit(s)™***. Physicians should claim only the credit commensurate with the extent of their participation in the activity.

Successful completion of this CME activity, which includes participation in the evaluation component, enables the participant to earn up to 1.0 MOC points in the American Board of Internal Medicine's (ABIM) Maintenance of Certification (MOC) program. Participants will earn MOC points equivalent to the amount of CME credits claimed for the activity. It is the CME activity provider's responsibility to submit participant completion information to ACCME for the purpose of granting ABIM MOC credit.

All other clinicians completing this activity will be issued a certificate of participation. To participate in this journal CME activity: (1) review the learning objectives and author disclosures; (2) study the education content; (3) take the post-test with a 75% minimum passing score and complete the evaluation at http://www.medscape.org/journal/eid; and (4) view/print certificate. For CME questions, see page 1089.

Release date: April 18, 2022; Expiration date: April 18, 2023

Learning Objectives

Upon completion of this activity, participants will be able to:

- Analyze characteristics of invasive group A *Streptococcus*
- Evaluate demographics and outcomes of the current study of invasive group A *Streptococcus* outbreaks
- Assess the source of invasive group A *Streptococcus* outbreaks based on investigations
- Distinguish infection control measures employed during invasive group A *Streptococcus* outbreaks

CME Editor

Amy J. Guinn, BA, MA, Technical Writer/Editor, Emerging Infectious Diseases. *Disclosure: Amy J. Guinn, BA, MA, has disclosed no relevant financial relationships.*

CME Author

Charles P. Vega, MD, Health Sciences Clinical Professor of Family Medicine, University of California, Irvine School of Medicine, Irvine, California. *Disclosure: Charles P. Vega, MD, has disclosed the following relevant financial relationships: served as an advisor or consultant for GlaxoSmithKline; Johnson & Johnson.*

Authors

Laura E. Nabarro, FRCPath; Colin S. Brown, MD, FRCPath; Sooria Balasegaram, MBChB; Valérie Decraene, PhD; James Elston, FFPH; Smita Kapadia, MBBS; Pauline Harrington, MSc; Peter Hoffman, BSc; Rachel Mearkle, MBBS; Bharat Patel, MD, FRCPath; Derren Ready, PhD; Esther Robinson, MD, FRCPath; and ***Theresa Lamagni, PhD.***

Author affiliation: Public Health England, London, UK

DOI: https://doi.org/10.3201/eid2805.211497

Healthcare-associated invasive group A *Streptococcus* (iGAS) outbreaks are common worldwide, but only England has reported outbreaks associated with home healthcare (HHC). We describe 10 outbreaks during 2018–2019 in England. A total of 96 iGAS cases (range 2–39 per outbreak) and 28 deaths (case-fatality rate 29%) occurred. Outbreak duration ranged from 3–517 days; median time between sequential cases was 20.5 days (range 1–225 days). Outbreak identification was difficult, but *emm* typing and whole-genome sequencing improved detection. Network analyses indicated multiple potential transmission routes. Screening of 366 HHC workers from 9 outbreaks identified group A *Streptococcus* carriage in just 1 worker. Outbreak control required multiple interventions, including improved infection control, equipment decontamination, and antimicrobial prophylaxis for staff. Transmission routes and effective interventions are not yet clear, and iGAS outbreaks likely are underrecognized. To improve patient safety and reduce deaths, public health agencies should be aware of HHC-associated iGAS.

Streptococcus pyogenes (group A *Streptococcus*; GAS) is a common community-acquired pathogen, predominantly affecting skin, soft tissues, and the respiratory tract. Invasive GAS (iGAS) infection, characterized by entry of the bacterium into sterile body fluids, including blood, has a mortality rate of 8%–16% (*1*–*4*). Person-to-person iGAS transmission is thought to occur through direct skin contact or via respiratory droplets from symptomatic infections and asymptomatic carriers. Throat, nose, skin, and anogenital carriage have been linked to healthcare-associated outbreaks (*5*–*8*), which have been recorded in hospital, long-term care, and outpatient facilities worldwide (*9*–*11*). Environmental and fomite transmission are less well characterized.

In England, most community nursing care is performed by practitioners traveling between patients to deliver healthcare in the patients' homes, termed home healthcare (HHC). HHC is administered by a variety of healthcare workers, including district nurses, community nurses, healthcare assistants, general practitioners, podiatrists, hospital outreach teams, and palliative care staff. A substantial part of HHC is wound care, but HHC workers (HHCWs) also administer medication, assist with rehabilitation, and perform catheter and end of life care. During a single working week, an HHCW could perform many of these duties for different patients.

The home environment is not designed for healthcare and has unique infection control challenges. HHCWs and their equipment could become contaminated directly from the patient or the patient's home, and the patient risks infection from practitioners or their equipment (*12*,*13*).

In England, iGAS cases are notifiable to local health protection teams (HPTs) under the Health Protection (Notification) Regulations 2010 (*14*) as a means of beginning immediate public health actions as needed, including contact tracing, according to national guidelines (*15*). Guidance also requests that all sterile site GAS isolates be sent for typing to the Respiratory and Vaccine Preventable Bacteria Reference Unit (RVPBRU) of Public Health England (PHE). All isolates, including GAS isolates from possible healthcare-associated infections, should be referred for typing or stored locally for future outbreak investigations. RVPBRU returns results to the referring hospital and local HPT within 6 days. RVPBRU also provides whole-genome sequencing (WGS) to support outbreak investigations.

In 2013, PHE identified the first HHC-associated iGAS outbreak in England (*16*). PHE has regularly recorded outbreaks since then, and HPTs managed outbreaks with advice from national leads for streptococcal surveillance and reference microbiology units. We describe HHC-associated iGAS outbreaks reported during January 2018–August 2019, including identification, investigation, and management, to inform public health response in England and elsewhere.

Methods

Case Definition and Data Sources

In this study, we included HHC-associated iGAS outbreaks identified in England during January 1, 2018–August 31, 2019. We identified outbreaks cross-referenced from PHE's case and outbreak logging software, HPZone, and the RVPBRU streptococcal outbreak dataset. In addition, we contacted the healthcare-associated infection leads of each PHE center to identify any outbreaks not reported in the 2 datasets. We chose this short timeframe to ensure we could examine each outbreak in detail and maximize accurate data collection.

We included outbreaks with ≥2 cases of iGAS infection of the same *emm* type and linked to the same defined HHC service. We excluded outbreaks in which other exposures offered a more plausible transmission route, such as within residential care or another healthcare setting.

The inclusion criteria for individual cases within an outbreak varied between outbreaks and were set by the investigating outbreak control team (OCT). The broadest inclusion criterion for cases was defined as iGAS of the same *emm* type linked to the same defined HHC service. In outbreaks for which WGS was deployed, the inclusion criteria were honed to include

only cases linked by sequencing, defined as ≤5 SNPs between strains. Noninvasive GAS infections and colonization were not systematically investigated or recorded in all outbreaks.

To investigate temporal trends in outbreaks, we also searched HPZone for outbreaks during January 1, 2013–December 31, 2017. We did not search other sources for outbreaks during this period and did not collect further data because the outbreaks were too distant in time for data to be accurate. We provide operational definitions used in this study (Table 1).

Data Collection and Analysis

We conducted a 1-hour qualitative semistructured telephone interview with the chair of each OCT or other nominated staff member. We asked participants standardized open-ended questions grouped into themes surrounding outbreak identification, microbiology, investigation, and infection control. We encouraged participants to elaborate on answers by asking probing follow-up questions and incorporated themes that emerged in early interviews into subsequent interviews. We explored barriers to investigation and management in a similar way and encouraged participants to identify learning points and recommendations for future outbreaks. We collected data by using a standardized interview protocol and captured audio recordings of interviews to enable further review by the interviewer. We used thematic analysis to analyze qualitative data.

When available, we collected quantitative data regarding the number of HHCWs and patients screened and treated. We collected standardized pseudonymized data on case-patients, including age, iGAS onset date, hospitalization, and outcome. When sequencing was performed, we identified cases linked by sequence data (these data are not reported here). We recorded and analyzed data in Excel (Microsoft, https://www.microsoft.com) and Stata version 15 (StataCorp LLC, https://www.stata.com) and managed data in line with PHE's information governance policy.

Ethics Approval

This study was performed by PHE as part of its legal obligation to collect and process information about communicable disease surveillance and control under section 251 of the National Health Service Act 2006 (https://www.legislation.gov.uk/ukpga/2006/41/contents). No further ethics approval was required.

Results

Outbreak Characteristics

During 2013–2017, a total of 7 HHC-associated iGAS outbreaks were identified in England; during January 1, 2018–August 23, 2019, a total of 10 HHC-associated iGAS outbreaks were identified (Figure 1). In these 10 outbreaks, 96 iGAS cases and 28 attributable deaths (case-fatality rate 29%) were reported. Outbreaks ranged from 2 to 39 (median 7) iGAS cases; case-level data and results of HHCW screening for 1 outbreak (outbreak number 10) were unavailable (Tables 2, 3).

The median age of case-patients was 83 (range 42–100) years; 68% of cases were among female patients and 32% among male patients. Among 96 cases, 92 (96%) patients received nursing care administered by HHC services. Of the 4 cases that did not receive direct HHC care, 2 were household contacts of patients receiving HHC and neither had an identified GAS infection at the time. An epidemiologic link to HHC was not established for the other 2 cases, but those 2 were linked to other outbreaks by WGS.

Among 5 outbreaks with recorded wound swab sample results, GAS was cultured from 104 case-patients (range 1–95 cases per outbreak). The number of bacterial swab samples taken in these outbreaks was not documented by investigating teams, and available

Table 1. Definitions used in a study of invasive group A *Streptococcus* infection associated with home healthcare, England, 2018–2019

Term	Definition
Invasive group A *Streptococcus* (iGAS) infection	Isolation of GAS from a normally sterile site, either by PCR or culture. For this study, iGAS also includes GAS infections in which GAS was isolated from a normally nonsterile site in combination with a severe clinical presentation, such as streptococcal toxic shock syndrome or necrotizing fasciitis
Group A *Streptococcus* (GAS) infection	Isolation of GAS from a nonsterile site in combination with clinical symptoms attributable to bacterial infection including fever (temperature ≥38°C), sore throat, wound infection, or cellulitis
Group A *Streptococcus* carriage	Isolation of GAS from a nonsterile site but no symptoms attributable to infection with this microorganism
Home healthcare (HHC)	Community health services, including district nursing teams, general practitioners, podiatry (chiropody), community midwifery, hospital outreach, and palliative care, which provide medical or nursing care within a patient's home
Residential care	Live-in accommodation that provides 24-hour care and support to its residents

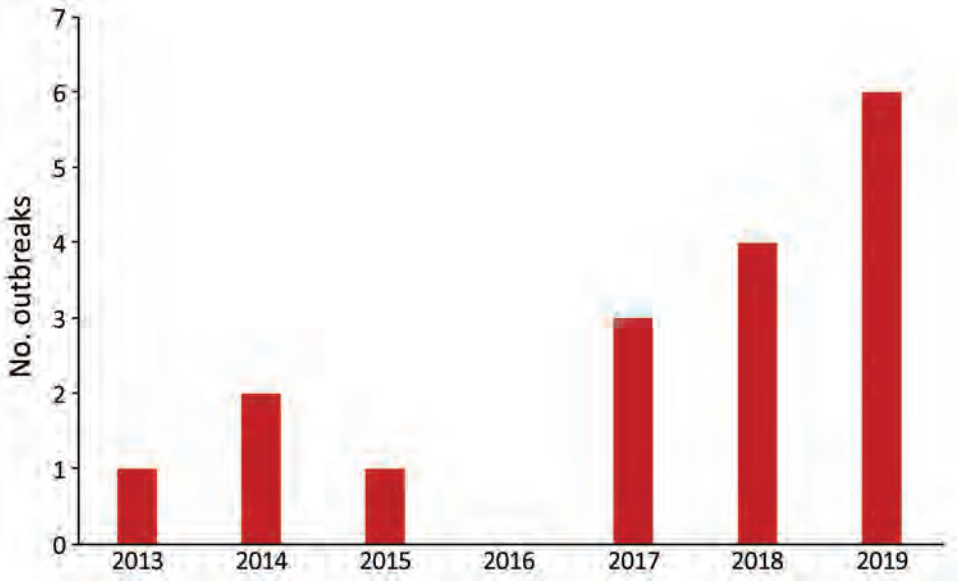

Figure 1. Annual number of home healthcare–associated invasive group A *Streptococcus* (iGAS) infection outbreaks reported to Public Health England, January 1, 2013–August 31, 2019. A total of 17 outbreaks occurred during this timeframe, but outbreaks sharply increased during 2018–2019.

data did not enable distinction between GAS carriage and noninvasive infection (Table 2).

Outbreak Identification

Nine outbreaks were identified through statutory notifications of individual iGAS cases to local HPTs; 1 outbreak (outbreak 4) was identified through WGS at the RVPBRU Streptococcal Reference Laboratory. The median time between first identified case and the date the outbreak was declared was 40 days (range 3–517 days), but these data were not available for outbreak 10. Some cases were identified retrospectively when investigation teams reviewed previously notified iGAS cases of the same *emm* type to reinvestigate a link to HHC (Figure 2).

Six outbreaks were caused by *S. pyogenes* type *emm*1 or *emm*89, the 2 most common iGAS-causing *emm* types circulating in England during this period. Among the remaining 4 outbreaks, 2 were caused by *emm*94, 1 by *emm*87, and 1 by *emm*44. WGS was performed for 6 outbreaks involving *emm*1 (n = 2), *emm*89 (n = 3), and *emm*94 (n = 1) to establish whether cases of common *emm* types with epidemiologic links constituted an outbreak. Outbreak 10 (*emm*44) was sequenced because of the substantial number of cases and long duration (Table 2).

In the 6 outbreaks of common *emm* types (*emm*1, *emm*89, *emm*94), WGS confirmed that epidemiologically linked cases formed a genomic cluster in each outbreak. In 3 of these outbreaks, WGS identified ≥1 case of the same *emm* type with epidemiologic links to the outbreak that did not cluster with the other cases, enabling exclusion of the case from the outbreak. In 2 outbreaks, WGS confirmed that 2 sequential cases diagnosed >5 months apart but cared for by the same HHC team formed a genomic cluster and were likely part of the same outbreak. None of the sequenced outbreaks had close genomic relationships with each other, indicating each was a distinct outbreak.

Table 2. Summary of home healthcare–associated invasive group A *Streptococcus* infection outbreaks, England, 2018–2019*

Outbreak no.	No. iGAS cases	No. GAS cases†	No. deaths	No. days from first to last case	No. cases without identified HHC input	*emm* type	WGS
1	14	2	2	136	1	87	N
2	7	1	2	148	0	94	N
3	6	0	3	222	0	94	Y
4	7	0	2	388	0	89	Y
5	5	5	2	179	2	89	N
6	3	0	0	75	0	1	Y
7	4	0	0	219	0	1	Y
8	2	0	1	3	0	89	Y
9	9	1	1	507	0	89	Y
10	39	95	15	487	1	44	Y
Total	96	104	28	NA	4	NA	NA

*GAS, group A *Streptococcus*; HHC, home healthcare; iGAS, invasive group A *Streptococcus*; NA, not applicable; WGS, whole-genome sequencing.
†Noninvasive GAS was not systematically investigated or recorded in all outbreaks. Available data did not enable distinction between carriage and noninvasive infection.

One outbreak (outbreak 4) was not initially recognized by the local HPT but was identified by the reference laboratory from a set of local WGS controls used to investigate another HHC-associated iGAS outbreak (outbreak 9) (Table 2). The discovery of outbreak 4 revealed a separate *emm*89 iGAS in patients cared for by a single HHC team. Outbreak 4 involved 7 cases and 2 deaths over a period of 388 days, and the last case was notified 74 days before the outbreak was identified; no further cases were identified in the 60 days after the outbreak was identified. Although case-patients were cared for by a single HHC team, the epidemiologic link between cases was not identified earlier because the outbreak involved *emm*89, a common type; long intervals passed between sequential cases; and the HPT did not routinely ask about HHC exposures.

Table 3. Characteristics of home healthcare–associated invasive group A *Streptococcus* infection outbreaks, England, 2018–2019*

Characteristics	No. (%)	IQR (range)
All outbreaks, n = 10		
Total cases	96 (100)	NA
Total deaths	28 (29)	NA
Median cases	7	4–9 (2–39)
Median outbreak duration, d	199	139–347 (3–507)
Outbreaks with case data, n = 9		
Case-patient characteristics, n = 57		
Median age, y	83	77–90 (42–100)
Sex		
F	39 (68)	NA
M	18 (32)	NA
Median days between cases	21	6–46 (1–225)
Type of residence, n = 48		
Residential care	17 (35)	NA
Own home	31 (65)	NA
HHCW exposure, n = 96		
Patient receiving care	92 (96)	NA
Household contact of recipient	2 (4)	NA
None identified†	2 (4)	NA

*HHCW, home healthcare worker; NA, not applicable.
†Cases linked to outbreaks through whole-genome sequencing but without any identified connection to home healthcare services.

Outbreak Duration

Duration of outbreaks varied greatly. The median time between specimen collection from the first and last identified case in each outbreak was 199 days (range 3–507 days). Long intervals often passed between cases (median 20.5 days, range 1–225 days) (Figures 2, 3).

In outbreaks 2, 4, 8, and 9, the last recognized case occurred before the outbreak was formally declared, and these outbreaks might have self-terminated after HHC teams instigated improved infection control and before the HPT became involved (Figure 2). Specifically, outbreaks 4 and 9 occurred in a region with a large concurrent HHC-associated iGAS outbreak in which HHC services had recently reviewed their infection control procedures. In the other 6 outbreaks, a median of 130 days (range 31–181 days) passed between outbreak declaration and the last identified case.

Once outbreaks were identified, time to link outbreaks to HHC was often delayed. Among 48

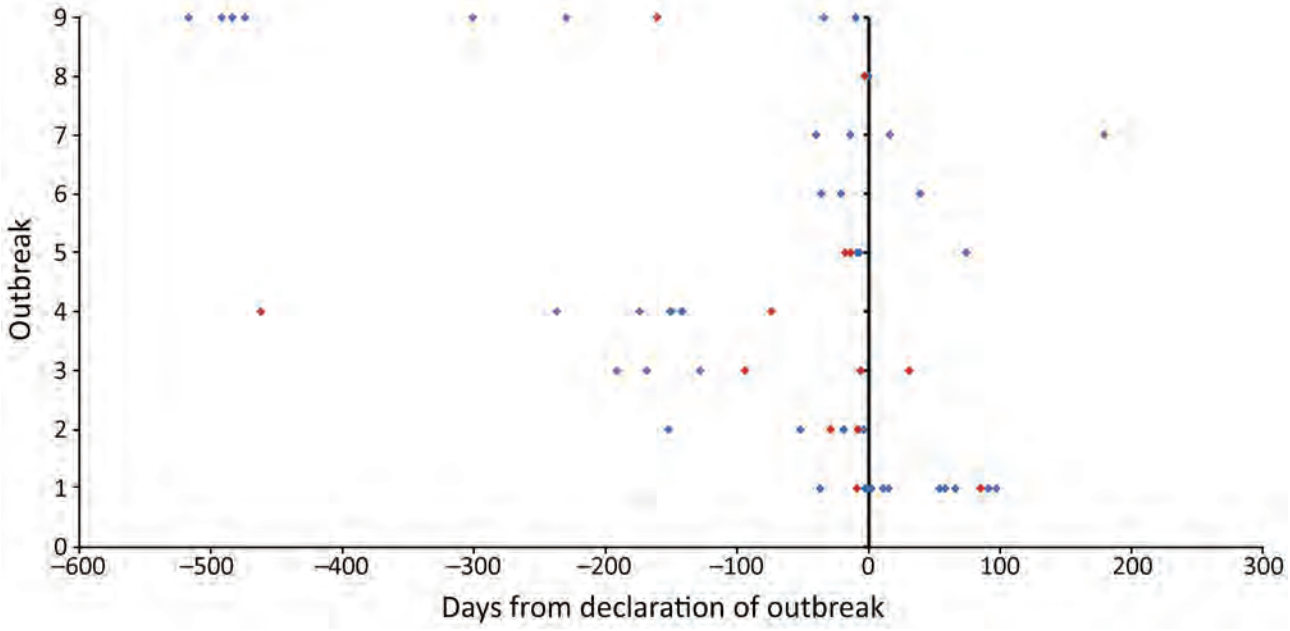

Figure 2. Timeline of cases in 9 home healthcare–associated invasive group A *Streptococcus* (iGAS) infection outbreaks, England, January 1, 2018–August 31, 2019. Vertical black line indicates date that outbreak was declared. Diamonds indicate day of initial detection of iGAS cases: blue diamonds represent patients that survived, red diamonds patients that died. Data from outbreak 10 (39 cases, 15 deaths) were not available.

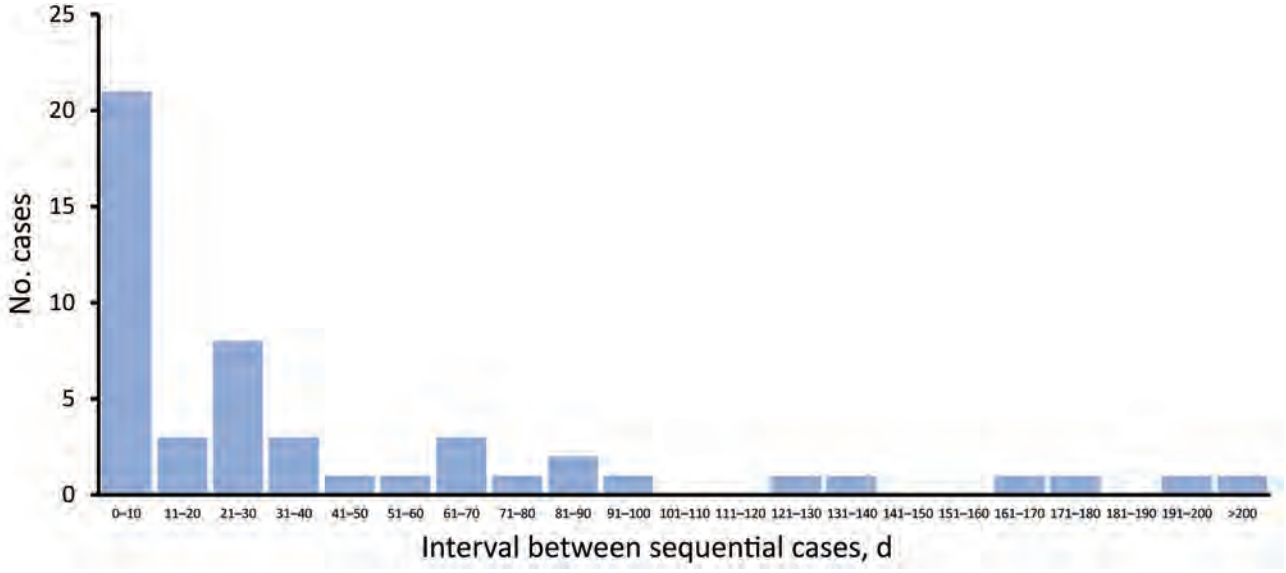

Figure 3. Intervals between sequential invasive group A *Streptococcus* cases in 9 home healthcare–associated outbreaks, England, January 1, 2018–August 31, 2019. Data from outbreak 10 were not available.

case-patients for whom place of residence was documented, 17 (35%) lived in residential care but also received HHC services. Transmission within the residential care facility initially was investigated before further cases were identified outside this environment and HHC links were explored.

Outbreak Investigation

Investigating teams performed network analyses during outbreak investigations through records provided by HHC teams. These investigations did not identify a single HHCW in contact with all case-patients during the 7 days before symptom onset. HHCWs visited up to 20 patients per day, and multiple HHCWs might visit a patient each week, making investigation complex. In 5 outbreaks, ≥1 HHCW described symptoms suggestive of GAS before or during the associated iGAS outbreak. In addition, 8/10 OCTs reported difficulty obtaining information from HHC teams because of poor record keeping and time pressures on already overstretched services.

After network analyses, HHCWs were screened with throat swab samples for bacterial culture in all 10 outbreaks. The aim of screening was to identify HHCWs who might have acted as a common source and posed an ongoing risk to patients. In the 9 outbreaks for which data were available, a total of 411 HHCWs were identified for screening and 366 were screened by throat swab. A median of 22 (range 3–160) HHCWs were screened per outbreak. A single (0.36%) throat swab sample cultured GAS but unfortunately was not typed. In 7 outbreaks, any reported wounds or skin breaks among HHCWs were screened for GAS by swab and culture, but all were negative. In 3 outbreaks, a few HHCWs with negative throat swab samples but strong epidemiologic links to cases were screened with swab samples from piercing sites, perineum, and vagina; none were positive. The logistics of screening HHCWs in the community were complex, predominantly because of inadequate occupational health provision (6/8 outbreaks) and delays of up to 6 weeks between the decision to screen and commencement of screening. In addition, HHCW screening involved associated sensitivities, including concern about the use of screening to attribute blame and potential personal shame if swab samples were positive.

In 3 outbreaks, patient wounds were systematically screened for GAS carriage. In the 2 outbreaks with data available, 107 patients were screened but no GAS-positive samples identified. Although full data are not available for the third outbreak, GAS carriage and infection was detected in a small proportion of patients. In 7 outbreaks, patient wound screening was not systematically performed, but in 4 of these outbreaks HHCWs were encouraged to send swab samples from any wound with suspected infection. Although the number of swab samples sent for this indication is unknown, 6 swab samples from 2 outbreaks tested GAS-positive, but these were not *emm* typed, so they cannot be directly linked to other outbreaks.

In 2 outbreaks, environmental screening was performed. Bacterial swab samples were taken for culture from communal and storage areas at the HHCW

base and from items that were difficult to clean, including portable electronic devices (e.g., tablets or smart phones), equipment, bags, blood pressure cuffs, and Doppler machines. Although the total number of swab samples taken was not recorded, a single swab sample taken from the handle of an equipment bag cultured GAS-positive, and subsequent WGS confirmed it to be the outbreak strain.

Source and Transmission Mode

The sources and modes of transmission were not definitively established in any outbreak. The common hypothesis among investigating teams was that GAS was transmitted between colonized or infected patients and HHCWs and that numerous possible transmission events caused each outbreak. The role of fomites was unclear, but teams recognized the challenges associated with adequately decontaminating HHCW equipment in the home environment.

Infection Control Methods

Infection control procedures were reviewed in each outbreak. Recommendations included infection control training for HHCWs and enhanced cleaning of HHCW bases and equipment storage areas in their cars. In 5 outbreaks, investigators noted that HHCWs carried equipment that was difficult to clean, such as fabric bags, portable electronic devices, and Doppler machines. This finding led to replacing fabric bags with impermeable, surface-wipeable bags (n = 3) or plastic, wipeable crates (n = 1), along with developing standard operating procedures for cleaning equipment that was difficult to decontaminate (n = 2). After outbreak 10 was identified, HHCWs were given disposable long aprons to wear during wound care procedures.

In 7 outbreaks, HHCWs were treated with antimicrobial drugs, which were intended to decolonize staff with potential occult carriage and interrupt transmission. In 6 outbreaks, HHCWs who had direct contact with a case-patient were initially treated with a 10-day course of penicillin V (median 2 [range 1–3] HHCWs per outbreak). When further cases occurred in 5 outbreaks, mass penicillin V prophylaxis for HHCWs was advised by the OCT and administered. In 4 outbreaks for which data were available, 139 HHCWs received prophylaxis (median 26 [range 22–65] per outbreak). In 3 of these outbreaks, no iGAS cases were notified after mass prophylaxis. HHCWs voiced opposition to antimicrobial drug prophylaxis in 3 outbreaks because of perceived lack of need after negative screening and concerns about antimicrobial resistance. In outbreak 1, the HPT directly engaged with HHCWs through presentations and discussions to achieve reasonable coverage and compliance with antimicrobial prophylaxis. Overall, HHCW compliance to antimicrobial prophylaxis is unknown.

Patients whose wounds cultured GAS-positive were treated with antimicrobial drug therapy. Mass antimicrobial prophylaxis was not administered to patients in any outbreak.

Discussion

GAS outbreaks in hospitals, residential care facilities, and outpatient facilities are well documented, and guidelines exist for their investigation and management (*9*,*15*,*17*,*18*). However, despite a rising trend in HHC provision in Europe and the United States, the only published reports of HHC-associated iGAS outbreaks have come from England (*16*).

HHC-associated infections are common. Data from the United States suggest that 3.2% of HHC patients become infected and require hospitalization or emergency care treatment and that wound infections are among the most common (*13*). The home environment poses infection control challenges that differ from acute healthcare settings, including limited ability to decontaminate hands, equipment, and the environment, and a lower quality of environmental cleaning. In addition, family members who sometimes help nursing staff do not have adequate training in infection control. A recent study from Belgium highlighted the need for better data on HHC-associated infections and for developing infection control guidelines specific to this setting (*19*).

In England, the first HHC-associated iGAS outbreak was identified in 2013, and outbreak detection has been rapidly rising since then (*17*). Although all iGAS cases were notifiable in England during 2013–2021, characterization of isolates by the national reference laboratory is typically the trigger point for investigating clusters and no changes in isolate referral requirements were made during this period. However, local HPTs might have increasingly sought information on HHC after receiving advice from national teams, increased awareness, or both.

HHC services are under growing pressure because of a 46% reduction in qualified district nurses since 2010 and rising demand from an aging population with increasingly complex care needs. Nonspecialist nurses and healthcare assistants frequently are employed to deliver HHC. Among district nurses responding to a Queen's Nursing Institute survey, 48% reported deferring visits or delaying patient care daily,

75% had unfilled vacancies on their teams, and 90% worked unpaid overtime hours (*20*). A King's Fund report cited staff concerns over the quality and safety of care and reported wound care was particularly likely to be deprioritized during busy periods (*21*).

We noted substantial delays in outbreak identification; 1 outbreak in our study (outbreak 4) was only identified when sporadic case isolates were used as sequencing controls to investigate another outbreak. Although detection delays were polyfactorial, a major contributing factor was that most outbreaks were caused by the 2 most common *emm* types in England, *emm*1 and *emm*89, making it difficult to distinguish outbreaks from sporadic cases. Compounding this problem were long intervals, up to 7 months, between sequential cases and no standardized method for HPTs to record and review *emm* types. Although HPTs were mandated by national guidelines to inquire about previous hospitalization and residential care, they did not routinely ask about HCC.

The value of WGS in investigating iGAS outbreaks is becoming increasingly recognized. In this study, the increased discrimination of WGS over *emm* typing confirmed that epidemiologically linked cases of common *emm* types formed genomic clusters. WGS also identified epidemiologically linked cases that did not form genomic clusters with outbreak cases, enabling exclusion of cases from investigation. WGS identification of genomic case clusters focused outbreak investigations and management, particularly where complex HHC-associated cases had multiple common exposures, such as residential care, wound management teams, and podiatry. Routine and timely WGS of all iGAS isolates could result in early and accurate identification of outbreaks.

WGS findings highlight the complexities of GAS transmission within the community, including cryptic carriage and infection or fomite transmission as the most credible connection between genomic case clusters in patients with distant epidemiologic links. In this study, HHCW screening by throat swab with bacterial culture in 9 outbreaks identified only 1 GAS carrier. Possible reasons for this low detection rate include delays in instigating screening because of lack of occupational health support and resistance from HHCW, which might mean that GAS infection or carriage resolved before screening. In addition, some HHCWs swabbed themselves or their colleagues, which might have introduced bias resulting from concerns about attributing blame. Finally, most HHCWs were screened by throat swab alone, and multiple published outbreaks have shown that HHCW GAS carriage from other sites can be responsible for transmission. Negative throat swab samples should not be used to exclude infection in a HHCW with an epidemiologic link to cases (*16*,*18*).

GAS can persist on inanimate surfaces for up to 4 months and can contaminate fomites (*22*,*23*), but the role of fomites in GAS transmission is difficult to establish. Previous published outbreaks were attributed to a diverse range of sources, including showerheads and bed curtains, but these objects were not definitively established as the only GAS source (*17*,*24*). Because fomite surface contamination can be transient and superficial contamination can be readily lost via subsequent contacts, failure to find GAS on any specific item does not exonerate the item from the transmission pathway. In this study, a single swab sample from a fabric bag handle tested positive for GAS, but insufficient data were available on number of swabs taken, and insufficient environmental swab samples were taken in other outbreaks, to establish whether fomites were a common transmission pathway. However, this positive sample highlights that equipment and hand contact surfaces can become contaminated. All HHCW equipment should be easy to decontaminate between patients' homes, and single-use equipment should be available where possible.

The first limitation of this study is that data were collected retrospectively and might have been subject to recall bias. No recommended guidelines on investigation of HHCW outbreaks were available when this study was performed, and OCTs did not have standardized data collection methods, resulting in missing data in some outbreaks. HHCW teams were not interviewed as part of this study and their insight on outbreak management would have been useful.

In conclusion, HHC-associated iGAS outbreaks are now common and increasingly recognized in England and have high mortality rates. Further work is needed to elaborate GAS transmission dynamics within the HHC environment and guidelines are required to guide HPTs in the investigation and management of these outbreaks. Outbreak control is complex and can require multiple interventions, including improved infection control, equipment decontamination, and prophylactic antimicrobial drug therapy for staff. Nonetheless, public health agencies should be aware of HHC-associated iGAS. Although outbreaks can be difficult to identify among sporadic iGAS cases, prompt *emm* typing and WGS offer a means for timely recognition of case clusters.

About the Author

Dr. Nabarro is a consultant in infectious disease and medical microbiology who previously worked for Public Health England. Her research interests include parasitic infections and control of communicable disease.

References

1. O'Grady KA, Kelpie L, Andrews RM, Curtis N, Nolan TM, Selvaraj G, et al. The epidemiology of invasive group A streptococcal disease in Victoria, Australia. Med J Aust. 2007;186:565–9. https://doi.org/10.5694/j.1326-5377.2007.tb01054.x
2. O'Loughlin RE, Roberson A, Cieslak PR, Lynfield R, Gershman K, Craig A, et al.; Active Bacterial Core Surveillance Team. The epidemiology of invasive group A streptococcal infection and potential vaccine implications: United States, 2000–2004. Clin Infect Dis. 2007;45:853–62. https://doi.org/10.1086/521264
3. Nelson GE, Pondo T, Toews KA, Farley MM, Lindegren ML, Lynfield R, et al. Epidemiology of invasive group A streptococcal infections in the United States, 2005–2012. Clin Infect Dis. 2016;63:478–86. https://doi.org/10.1093/cid/ciw248
4. Lamagni TL, Neal S, Keshishian C, Powell D, Potz N, Pebody R, et al. Predictors of death after severe *Streptococcus pyogenes* infection. Emerg Infect Dis. 2009;15:1304–7. https://doi.org/10.3201/eid1508.090264
5. Rutishauser J, Funke G, Lütticken R, Ruef C. Streptococcal toxic shock syndrome in two patients infected by a colonized surgeon. Infection. 1999;27:259–60. https://doi.org/10.1007/s150100050024
6. Paul SM, Genese C, Spitalny K. Postoperative group A β-hemolytic *Streptococcus* outbreak with the pathogen traced to a member of a healthcare worker's household. Infect Control Hosp Epidemiol. 1990;11:643–6. https://doi.org/10.2307/30146867
7. Berkelman RL, Martin D, Graham DR, Mowry J, Freisem R, Weber JA, et al. Streptococcal wound infections caused by a vaginal carrier. JAMA. 1982;247:2680–2. https://doi.org/10.1001/jama.1982.03320440028027
8. Ejlertsen T, Prag J, Holmskov A, Pettersson E. A 7-month outbreak of relapsing postpartum group A streptococcal infections linked to a nurse with atopic dermatitis. Scand J Infect Dis. 2001;33:734–7. https://doi.org/10.1080/00365540131707451 8
9. Saavedra-Campos M, Simone B, Balasegaram S, Wright A, Usdin M, Lamagni T. Estimating the risk of invasive group A *Streptococcus* infection in care home residents in England, 2009–2010. Epidemiol Infect. 2017;145:2759–65. https://doi.org/10.1017/S0950268817001674
10. Ibrahim LA, Sellick JA Jr, Watson EL, McCabe LM, Schoenhals KA, Martinello RA, et al. An outbreak of severe group A *Streptococcus* infections associated with podiatric application of a biologic dermal substitute. Infect Control Hosp Epidemiol. 2016;37:306–12. https://doi.org/10.1017/ice.2015.306
11. Beaudoin AL, Torso L, Richards K, Said M, Van Beneden C, Longenberger A, et al. Invasive group A *Streptococcus* infections associated with liposuction surgery at outpatient facilities not subject to state or federal regulation. JAMA Intern Med. 2014;174:1136–42. https://doi.org/10.1001/jamainternmed.2014.1875
12. Unsworth J, Collins J. Performing an aseptic technique in a community setting: fact or fiction? Prim Health Care Res Dev. 2011;12:42–51. https://doi.org/10.1017/S1463423610000198
13. Shang J, Wang J, Adams V, Ma C. Risk factors for infection in home health care: analysis of national Outcome and Assessment Information Set data. Res Nurs Health. 2020;43:373–86. https://doi.org/10.1002/nur.22053
14. The Health Protection (Notification) Regulations 2010 (SI 2010/659) [cited 2022 Mar 4]. https://www.legislation.gov.uk/uksi/2010/659/contents/made
15. Steer JA, Lamagni T, Healy B, Morgan M, Dryden M, Rao B, et al. Guidelines for prevention and control of group A streptococcal infection in acute healthcare and maternity settings in the UK. J Infect. 2012;64:1–18. https://doi.org/10.1016/j.jinf.2011.11.001
16. Olufon O, Iyanger N, Cleary V, Lamagni T. An outbreak of invasive group A streptococcal infection among elderly patients receiving care from a district nursing team, October 2013–May 2014. J Infect Prev. 2015;16:174–7. https://doi.org/10.1177/1757177415572646
17. Mahida N, Beal A, Trigg D, Vaughan N, Boswell T. Outbreak of invasive group A streptococcus infection: contaminated patient curtains and cross-infection on an ear, nose and throat ward. J Hosp Infect. 2014;87:141–4. https://doi.org/10.1016/j.jhin.2014.04.007
18. Health Protection Agency, Group A Streptococcus Working Group. Interim UK guidelines for management of close community contacts of invasive group A streptococcal disease. Commun Dis Public Health. 2004;7:354–61.
19. Hoxha A, Duysburgh E, Mortgat L. Healthcare-associated infections in home healthcare: an extensive assessment, 2019. Euro Surveill. 2021;26. https://doi.org/10.2807/1560-7917.ES.2021.26.5.1900646
20. Swift A, Punshon G. District nursing today. The view of district nurse team leaders in the UK. London: The Queen's Nursing Institute; 2019.
21. Maybin J, Charles A, Honeyman M. Understanding quality in district nursing services: learning from patients, carers and staff. London: The Kings Fund; 2016.
22. Wißmann JE, Kirchhoff L, Brüggemann Y, Todt D, Steinmann J, Steinmann E. Persistence of pathogens on inanimate surfaces: a narrative review. Microorganisms. 2021;9:343. https://doi.org/10.3390/microorganisms9020343
23. Marks LR, Reddinger RM, Hakansson AP. Biofilm formation enhances fomite survival of *Streptococcus pneumoniae* and *Streptococcus pyogenes*. Infect Immun. 2014;82:1141–6. https://doi.org/10.1128/IAI.01310-13
24. Claesson BE, Claesson UL. An outbreak of endometritis in a maternity unit caused by spread of group A streptococci from a showerhead. J Hosp Infect. 1985;6:304–11. https://doi.org/10.1016/S0195-6701(85)80135-3

Address for correspondence: Theresa Lamagni, Public Health England, 61 Colindale Ave, London NW9 5EQ, UK; email: Theresa.lamagni@phe.gov.uk

Genomic Epidemiology of Global Carbapenemase-Producing *Escherichia coli*, 2015–2017

Gisele Peirano, Liang Chen, Diego Nobrega, Thomas J. Finn, Barry N. Kreiswirth, Rebekah DeVinney, Johann D.D. Pitout

Medscape EDUCATION ACTIVITY

In support of improving patient care, this activity has been planned and implemented by Medscape, LLC and Emerging Infectious Diseases. Medscape, LLC is jointly accredited by the Accreditation Council for Continuing Medical Education (ACCME), the Accreditation Council for Pharmacy Education (ACPE), and the American Nurses Credentialing Center (ANCC), to provide continuing education for the healthcare team.

Medscape, LLC designates this Journal-based CME activity for a maximum of 1.00 ***AMA PRA Category 1 Credit(s)™***. Physicians should claim only the credit commensurate with the extent of their participation in the activity.

Successful completion of this CME activity, which includes participation in the evaluation component, enables the participant to earn up to 1.0 MOC points in the American Board of Internal Medicine's (ABIM) Maintenance of Certification (MOC) program. Participants will earn MOC points equivalent to the amount of CME credits claimed for the activity. It is the CME activity provider's responsibility to submit participant completion information to ACCME for the purpose of granting ABIM MOC credit.

All other clinicians completing this activity will be issued a certificate of participation. To participate in this journal CME activity: (1) review the learning objectives and author disclosures; (2) study the education content; (3) take the post-test with a 75% minimum passing score and complete the evaluation at http://www.medscape.org/journal/eid; and (4) view/print certificate. For CME questions, see page 1090.

Release date: April 13, 2022; Expiration date: April 13, 2023

Learning Objectives

Upon completion of this activity, participants will be able to:

- Assess the global distribution of different carbapenemase genes, based on a genome sequencing study of 229 carbapenemase-producing *Escherichia coli* (2015–17) from 36 countries
- Evaluate antimicrobial resistance determinants and plasmid replicon types, virulence-associated factors, and carbapenemase gene flanking regions and plasmid analysis, based on a genome sequencing study of 229 carbapenemase-producing *Escherichia coli* (2015–17) from 36 countries
- Determine the public health implications of the global distribution of different carbapenemase genes and associated factors, based on a genome sequencing study of 229 carbapenemase-producing *Escherichia coli* (2015–17) from 36 countries

CME Editor

Jude Rutledge, BA, Technical Writer/Editor, Emerging Infectious Diseases. *Disclosure: Jude Rutledge has disclosed no relevant financial relationships.*

CME Author

Laurie Barclay, MD, freelance writer and reviewer, Medscape, LLC. *Disclosure: Laurie Barclay, MD, has disclosed the following relevant financial relationships: stocks, stock options, or bonds from AbbVie (former).*

Authors

Gisele Peirano, PhD; Liang Chen, PhD; Diego Nobrega, PhD; Thomas J. Finn, PhD; Barry N. Kreiswirth, PhD; Rebekah DeVinney, PhD; and ***Johann D.D. Pitout, MD.***

Author affiliations: University of Calgary, Calgary, Alberta, Canada (G. Peirano, T.J. Finn, R. DeVinney, J.D.D. Pitout); Alberta Precision Laboratories, Calgary (G. Peirano, J.D.D. Pitout); Hackensack Meridian School of Medicine, Nutley, New Jersey, USA (L. Chen, B.N. Kreiswirth); University of Guelph, Guelph, Ontario, Canada (D. Nobrega); University of Pretoria, Pretoria, South Africa (J.D.D. Pitout)

DOI: https://doi.org/10.3201/eid2805.212535

We describe the global molecular epidemiology of 229 carbapenemase-producing *Escherichia coli* in 36 countries during 2015–2017. Common carbapenemases were oxacillinase (OXA) 181 (23%), New Delhi metallo-β-lactamase (NDM) 5 (20%), OXA-48 (17%), *Klebsiella pneumoniae* carbapenemase 2 (15%), and NDM-1 (10%). We identified 5 dominant sequence types (STs); 4 were global (ST410, ST131, ST167, and ST405), and 1 (ST1284) was limited to Turkey. OXA-181 was frequent in Jordan (because of the ST410-B4/*H*24RxC subclade) and Turkey (because of ST1284). We found nearly identical IncX3-$bla_{OXA-181}$ plasmids among 11 STs from 12 countries. NDM-5 was frequent in Egypt, Thailand (linked with ST410-B4/*H*24RxC and ST167-B subclades), and Vietnam (because of ST448). OXA-48 was common in Turkey (linked with ST11260). Global *K. pneumoniae* carbapenemases were linked with ST131 C1/*H*30 subclade and NDM-1 with various STs. The global carbapenemase *E. coli* population is dominated by diverse STs with different characteristics and varied geographic distributions, requiring ongoing genomic surveillance.

Carbapenems are effective options available for treating serious infections caused by multidrug-resistant (MDR) Enterobacterales bacteria (*1*). The emergence of carbapenem resistance is a major public health concern, and the World Health Organization has identified carbapenem-resistant Enterobacterales as critical-priority bacteria (*2*).

Carbapenemases are important causes of carbapenem resistance (*3*). Carbapenemase genes can be transferred between Enterobacterales species. The most common carbapenemases among Enterobacterales are *Klebsiella pneumoniae* carbapenemases (KPCs), imipenemases (IMPs), Verona integron–encoded metallo-β-lactamases (VIMs), New Delhi metallo-β-lactamases (NDMs), and oxacillinase (OXA) 48–like enzymes. *Escherichia coli* is the second most common carbapenemase-producing Enterobacterales species (*4*,*5*).

Because *E. coli* is mainly responsible for human community-associated infections (*6*), it evades conventional hospital-based infection-prevention measures (*7*). *E. coli* is an important One Health (i.e., human, animal, environmental health) reservoir for antimicrobial resistance (AMR) genes (*8*). Tracking global mobile genetic elements and *E. coli* clones associated with carbapenemase genes is a public health priority (*9*) and aids in designing management and prevention strategies.

Comprehensive epidemiology data about carbapenemase-producing *E. coli* is limited to institutional, regional, or countrywide surveys (*10*). We used short-read whole-genome sequencing (WGS) to describe the molecular characteristics and international distribution of carbapenemase-producing *E. coli*. We describe the geographic distribution of different carbapenemase genes (including their associations with dominant sequence types [STs], clades and underlying mobile genetic elements), other β-lactamases, AMR genes, and virulence factors.

Materials and Methods

Bacterial Isolates

We obtained ethics approval for this study through the University of Calgary Conjoint Health Research Ethics Board (approval no. REB17-1010). We included 229 clinical, nonrepeat *E. coli* isolates collected from 2 global surveillance programs (SMART and INFORM) during 2015–2017 (Appendix, https://wwwnc.cdc.gov/EID/article/28/5/21-2535-App1.pdf). Isolates had undergone identification and susceptibility testing using Clinical Laboratory and Standards Institute guidelines (*4*,*5*,*11*). Carbapenem nonsusceptible isolates underwent molecular screening for bla_{KPC}, bla_{VIM}, bla_{NDM}, $bla_{OXA-48-like}$, bla_{IMP}, and bla_{GES}, as described previously (*4*,*5*). Overall, we collected 87,182 Enterobacterales for the period 2015–2017 from 62 countries: 27,444 were identified as *E. coli* and 275 (1%) tested nonsusceptible to ≥1 of the carbapenems. Most (229 [83%]) were positive for either bla_{KPC}, $bla_{OXA-48-like}$, bla_{NDM}, bla_{VIM}, or bla_{IMP} and were included in this study. The remaining 46 were negative for bla_{KPC}, bla_{VIM}, bla_{NDM}, $bla_{OXA-48-like}$, bla_{IMP}, and bla_{GES}.

We defined major STs as representing >10% and minor STs as representing 5%–10% of the total *E. coli* carbapenemase population (*12*). Dominant STs were both major and minor STs.

Genomic Analysis

We subjected the carbapenemase-producing *E. coli* (n = 229) to short-read WGS by using NovoSeq (Illumina, https://www.illumina.com) with 151 × 2 paired-end reads (*13*,*14*). We obtained draft genomes by using SPAdes 3.15 (*15*). We used BLAST (http://blast.ncbi.nlm.nih.gov/Blast.cgi) to determine AMR genes, plasmid replicons, and virulence genes against the following databases or typing schemes: National Center for Biotechnology Information Bacterial Antimicrobial Resistance Reference Gene Database (https://www.ncbi.nlm.nih.gov/bioproject/PRJNA313047), ResFinder (*16*), PlasmidFinder (*17*), multilocus sequence typing (*18*), and virulence finder (*19*). We conducted multilocus sequence typing by using *mlst* 2.19 (https://github.com/tseemann/mlst). We identified ST410 and ST131 clades and subclades as described previously (*20*,*21*).

For phylogenetic analyses, we mapped trimmed raw reads from each genome to a reference genome sequence (EC958 [GenBank accession no. HG941718] for ST131, JS316 [GenBank accession no. CP058618] for ST410, WCHEC005237 [GenBank accession no. CP026580] for ST167, and AR_0015 [GenBank accession no. CP024862] for ST405) by using snippy (https://github.com/tseemann/snippy). We filtered single-nucleotide polymorphisms (SNPs) among prophages, repeated sequences, or insertion sequences as previously described (*22*), and we generated a maximum-likelihood phylogenetic tree inferred from the resulting SNP alignment by using RAxML 8.2.12 by using a general time-reversible model of nucleotide substitution and 4 discrete γ categories of rate heterogeneity (*23*). We identified phylogenetic clades by using hierarchical Bayesian analysis of the population structure in R by using RhierBAPS with 10 initial clusters at 2 clustering levels (*24*). We defined clades by using the first level of clustering and subclades at the second level of clustering (*25*). We annotated the phylogenetic trees in iTOL (*26*). We deposited all sequencing data in the National Center for Biotechnology Information database (BioProject PRJNA780590).

Statistical Analyses

We conducted all analyses in R 3.6.1 (*27*). Initially, we attempted to fit generalized linear mixed models with country-level random effects to summarize comparisons between dominant STs with respect to antimicrobial and virulence genes. Most models failed to converge, possibly because of the low number of isolates

Table. Global molecular epidemiology of 229 carbapenemase-producing *Escherichia coli* isolates, 36 countries, 2015–2017*

Carbapenemases (no. isolates)	Geographic location (no. isolates)	Sequence types (no. isolates)
KPCs (50)		
KPC-2 (35)	Argentina (4), Brazil (5), Colombia (8), Greece (1), Guatemala (4), Israel (2), Puerto Rico (2), United States (4), Venezuela (1), Vietnam (4)	ST10 (3), ST46 (2), ST69 (2), ST95 (3), ST131 (7), ST349 (1), ST405 (3), ST410 (3), ST538 (1), ST540 (1), ST607 (1), ST617 (1), ST648 (1), ST1193 (1), ST1196 (1), ST2172 (1), ST2279 (1), ST3580 (1)
KPC-3 (14)	Colombia (1), Israel (1), Italy (8), United States (4)	ST12 (1), ST73 (1), ST131 (7), ST141 (1), ST191 (1), ST617 (1), ST973 (1), ST1148 (1)
KPC-18 (1)	United States (1)	ST131 (1)
NDMs (66)		
NDM-1 (19)	Egypt (3), Guatemala (2), Kuwait (1), Morocco (4), Philippines (1), Romania (1), Russia (3), Serbia (1), Thailand (2), Vietnam (1)	ST38 (1), ST44 (1), ST69 (1), ST95 (1), ST131 (4), ST167 (3), ST345 (1), ST361 (1), ST617 (2), ST1193 (1), ST1434 (1), ST1470 (1), ST4553 (1),
NDM-4 (1)	Vietnam (1)	ST405 (1)
NDM-5 (40)	Canada (1), Egypt (16), Italy (2), Jordan (4), Lebanon (1), Thailand (8), United Kingdom (2), Vietnam (6)	ST131 (1), ST156 (1), ST167 (11), ST361 (4), ST405 (3), ST410 (12), ST448 (2), ST648 (4), ST2003 (2)
NDM-6 (1)	Guatemala (1)	ST38 (1)
NDM-7 (5)	Philippines (4), Vietnam (1)	ST156 (2), ST410 (1), ST448 (1), ST5229 (1)
OXA-48–like (96)		
OXA-48 (40)	Austria (1), Belgium (2), Egypt (3), Georgia (3), Israel (1), Lebanon (2), Mexico (1), Morocco (2), Saudi Arabia (1), Spain (2), Thailand (1), Tunisia (1), Turkey (15), United Kingdom (1), Vietnam (4)	ST10 (2), ST12 (1), ST34 (1), ST38 (8), ST58 (1), ST131 (2), ST224 (1), ST349 (1), ST354 (6), ST361 (1), ST405 (4), ST410 (2), ST624 (1), ST648 (1), ST1431 (1), ST11260 (6)
OXA-181 (48)	Egypt (6), Germany (1), Jordan (15), Kuwait (1), Lebanon (1), Malaysia (1), South Africa (2), Taiwan (1), Thailand (2), Turkey (18)	ST46 (1), ST131 (1), ST167 (2), ST205 (1), ST354 (1), ST410 (21), ST648 (1), ST1284 (18), ST1487 (1), ST6802 (1)
OXA-232 (5)	Malaysia (1), Mexico (3), Thailand (1)	ST127 (1), ST131 (1), ST361 (3)
OXA-244 (3)	Egypt (3)	ST58 (1), ST648 (1), ST1722 (1)
VIMs (4)		
VIM-1 (2)	Greece (1), Spain (1)	ST88 (1), ST404 (1)
VIM-23 (2)	Mexico (2)	ST410 (2)
IMPs (2)		
IMP-59 (2)	Australia (2)	ST357 (2)
Two carbapenemases (11)		
NDM-1 + VIM-1 (1)	Egypt (1)	ST131 (1)
NDM-1 + OXA-181 (2)	Egypt (2)	ST46 (2)
NDM-5 + OXA-48 (1)	Egypt (1)	ST167 (1)
NDM-5 + OXA-181 (5)	Egypt (3), South Korea (1), Vietnam (1)	ST410 (4), ST448 (1)
NDM-5 + OXA-232 (2)	United Kingdom (2)	ST2083 (2)

*KPC, *Klebsiella pneumoniae* carbapenemase; NDM, New Delhi metallo-β-lactamase; OXA, oxacillinase; ST, sequence type; VIM, Verona integron–encoded metallo-β-lactamase.

for some STs and the large number of countries involved. Thereafter, we attempted to use exact logistic regression models for clustered data, as previously described (*28*). Similarly, most models failed to converge, particularly for comparisons involving ST1284 where all isolates were obtained from a single country. We then used Fisher exact tests to perform pairwise comparisons of antimicrobial and virulence genes among dominant STs. We used Mann-Whitney tests for comparison of virulence scores between dominant STs. We adjusted p values for multiple comparisons within each outcome by using the false discovery rate (*29*). We defined statistical significance as $p \geq 0.05$.

Results

Global Distribution of Carbapenemases

Overall, 218 isolates were positive for a single carbapenemase and 11 isolates were positive for 2 carbapenemases (Table). The OXA-48–like (n = 106) were the most common carbapenemases, followed by NDMs (n = 77), KPCs (n = 50), VIMs (n = 5), and IMPs (n = 2). The OXA-48–like carbapenemases consisted of OXA-48 (n = 41), OXA-181 (n = 55), OXA-244 (n = 3), and OXA-232 (n = 7). *E. coli* with OXA-48, OXA-181, and OXA-232 had a global distribution. OXA-244 was limited to Egypt (Table). The NDMs consisted of NDM-1 (n = 22), NDM-4 (n = 1), NDM-5 (n = 48), NDM-6 (n = 1), and NDM-7 (n = 5). *E. coli* with NDM-1 and NDM-5 had a global distribution. NDM-4 was limited to Vietnam and NDM-6 to Guatemala; NDM-7 was found in the Philippines and Vietnam (Table). The KPCs consisted of KPC-2 (n = 35), KPC-3 (n = 14), and KPC-18 (n = 1). *E. coli* with KPC-2 and KPC-3 had a global distribution, and KPC-18 was obtained from the United States (Table). *E. coli* with VIMs (VIM-1 and VIM-23) were found in Greece, Spain, Mexico, and Egypt; *E. coli* with IMP-59 were obtained from Australia (Table).

Global Distribution of Dominant *E. coli* Sequence Types and Clades

We identified 2 major STs (ST410 [20%] and ST131 [12%]) and 3 minor STs (ST1284 [8%], ST167 [7%], and ST405 [5%]) among this collection. The next most common STs did not fulfill the definition of a dominant ST: ST38 (n = 10 [4%]), ST354 (n = 7 [3%]), ST361 (n = 9 [4%]), ST648 (n = 8 [4%]), and ST11260 (n = 6 [3%]).

ST410 was the most common ST (n = 45/229 [20%]) and was positive for KPC-2 (7%), NDM-5 (27%), NDM-7 (2%), OXA-48 (4%), OXA-181 (47%), and VIM-23 [4%]) (Appendix Table 1). ST410 belonged to 2 subclades: B3/*H24*Rx (n = 10) and B4/*H24*RxC (n = 35) (*21*).

ST131 was the second most common ST (n = 26/229 [12%]) and was positive for KPC-2 (n = 8), KPC-3 (n = 7), KPC-18 (n = 1), NDM-1 (n = 5), NDM-5 (n = 1), OXA-48 (n = 2), OXA-181 (n = 1), and OXA-232 (n = 1). One NDM-1 isolate was also positive for VIM-1. ST131 belonged to clade A/*H41* (n = 2) and subclades C1_nonM27 (n = 10), C1_M27 (n = 4), and C2 (n = 10). We also note the global distribution of different minor STs (ST1284, ST167, ST405) and their clades (Appendix).

AMR Determinants and Plasmid Replicon Types

We determined quinolone resistance–determining regions mutations, β-lactamases (noncarbapenemases), aminoglycoside modifying enzymes, and plasmid replicon types among the different *E. coli* STs (Appendix Table 1). TEM-1, CTX-M-15, *aac(6')-Ib-cr*, and *sul1* were common among isolates.

Virulence Associated Factors

We assessed the presence of 37 putative virulence factors among the different dominant STs (Appendix Table 2). The following factors were present among most of isolates: *fimH* (100%), *fyuA* (55%), *traT* (64%), and *iss* (52%). Some virulence factors were associated with certain STs: *papA* (81%), *iha* (77%), *sat* (81%), *fyuA* (100%) *usp* (100%), *ompT* (100%), and *malX* (100%) with ST131, and *astA* (100%) and *iutA* (100%) with ST1284. ST131 had the highest overall number of virulence genes (n = 11), and ST410 had the lowest number of virulence genes (n = 2) (Appendix Table 2).

Carbapenemase Gene Flanking Regions and Plasmid Analysis

Because of the limitations of short-read sequencing (*30*), analyses of the immediate carbapenemase gene flanking regions and plasmids harboring carbapenemase genes were insufficient, especially for $bla_{\text{OXA-48}}$ and bla_{VIMs}. We obtained results for 20/22 of $bla_{\text{NDM-1}}$, 2/2 of $bla_{\text{NDM-4}}$, 46/48 of $bla_{\text{NDM-5}}$, 1/1 of $bla_{\text{NDM-6}}$, 4/5 of $bla_{\text{NDM-7}}$, 34/35 of $bla_{\text{KPC-2}}$, 14/14 of $bla_{\text{KPC-3}}$, 1/1 of $bla_{\text{KPC-18}}$, 1/41 $bla_{\text{OXA-48}}$, 55/55 of $bla_{\text{OXA-181}}$, 3/3 of $bla_{\text{OXA-244}}$, and 7/7 of $bla_{\text{OXA-232}}$.

Among $bla_{\text{KPC-2}}$, 15 were situated in Tn*4401* elements (Tn*4401a* [n = 4] in ST131 and ST46, Tn*4401b* [n = 9] in 7 STs, and Tn*4401e* [n = 2] in ST131 and ST1193). Nineteen were associated with non-Tn*4401* mobile elements (NTM_{KPC}) (*31*), including 4 ST131 and 3 ST405 strains. The $bla_{\text{KPC-3}}$ genes were associated with Tn*4401a* (n = 9), Tn*4401b* (n = 3), and Tn*4401d* (n = 2). The $bla_{\text{KPC-18}}$ was located on a novel Tn*4401* variant (186 bp deletion). The bla_{NDM}s were located on truncated Tn*125*

elements, and the bla_{NDM} upstream regions showed substantial diversities with various IS element insertions (e.g., IS*630*, IS*Aba125*, IS*1*, and IS*903* with bla_{NDM-1}; IS*Ecp1* and IS*1* with bla_{NDM-5}; and IS*5* with bla_{NDM-7}).

All $bla_{OXA-232}$ genes were located on the same 6.1 kb colKp3 plasmids (pOXA-232) (*32*). Sequence similarities (95%–100%) of bla_{KPC-3} isolates with previously sequenced plasmids in GenBank showed that most (n = 9) were harbored within IncFIBQil plasmids (*33*); 2 KPC-3 genes were within pKPC-CAV1193 (*34*), 1 bla_{KPC-3} was within the IncFIA plasmid pBK30683 (*35*), and 1 bla_{KPC-3} was in the IncI2 plasmid pBK15692 (*36*). The $bla_{OXA-181}$ (n = 55) were situated within Tn*2013* harbored on the identical IncX3 plasmids with 99%–100% similarities to plasmid p72_X3_OXA181 (*37*). p72_X3_ OXA181 contained the IncX3 and truncated ColKp3 replicons (*13*).

Discussion

A World Health Organization report showed the lack of adequate surveillance programs in many parts of the world, especially from lower- and middle-income countries (LMICs) (*38*). That report identified bacteria, including carbapenem-resistant *E. coli*, where global surveillance data are urgently required. LMICs bear a considerable share of the disease burden attributable to MDR *E. coli* but lack adequate genomic surveillance systems (*39*). Our study aimed to describe the global molecular epidemiology of 229 carbapenemase-producing *E. coli* obtained from 36 countries (including 20 LMICs) during 2015–2017. Isolates with multiple AMR genes dominated the population. The most common carbapenemase group was the OXA-48-like carbapenemases (44%), followed by NDMs (32%), KPCs (21%), VIMs (2%), and IMPs (1%). OXA-48-like carbapenemases were numerous in Egypt, Jordan, and Turkey; NDMs were numerous in Egypt, Thailand, and Vietnam, and KPCs were numerous in Colombia, Italy, and the United States.

We identified 5 dominant STs and their respective clades and subclades; 4 were global: ST410 subclades B3/*H24*Rx and B4/*H24*RxC; ST131 clade A/*H*41, subclades C1_nonM27/*H*30, C1_M27/*H*30, and C2/*H*30; ST167 subclades B1, B2, and B3; and ST405 clades A and B (Appendix Figure). ST1284 (1 clade) was limited to Turkey, and the ST167-A clade was limited to Guatemala. Dominant STs and their respective clades and subclades were associated with different underlying mobile genetic elements: ST410 was linked with NDM-5 and OXA-181; ST131 was linked with KPCs, ST1284 was linked with OXA-181, ST167 was linked with NDM-5, and ST405 was linked with various carbapenemases.

A recent survey of global carbapenemase-producing *E. coli* for the period 2002–2017 included 343 carbapenem-resistant isolates obtained mainly from the United States (*40*). KPC (16%), NDM (16%), and OXA-48–like (13%) carbapenemases were common. The study screened for different *E. coli* phylogroups and certain STs (ST131, ST648, and ST405). Phylogroup B2 isolates were common, and phylogroup A was dominant in Asia. Global ST131 with bla_{KPC}s was the most common ST, followed by ST648 with $bla_{OXA-48-like}$ and ST405 with bla_{NDM}s.

The most frequent individual carbapenemases in our survey were OXA-181 (23%), NDM-5 (20%), OXA-48 (17%), KPC-2 (15%), and NDM-1 (10%). This result was different from carbapenemase-producing *K. pneumoniae* and *Enterobacter cloacae* complex with carbapenemases obtained from the same surveillance programs (*14*,*41*). The *K. pneumoniae* population was dominated by ST258 with KPC-2 from Greece and KPC-3 from the United States (*41*). The *E. cloacae* complex isolates (various STs) were dominated by VIM-1 from Greece and Italy (*14*). *K. pneumoniae* (*42*) and *E. cloacae* complex (*43*) are mainly hospital pathogens, whereas *E. coli* was mainly a community pathogen (*6*), which could partly be responsible for the different carbapenemase types among these species.

Molecular-based surveillance studies have shown that OXA-48–like enzymes are common among global carbapenemase-producing Enterobacterales (*4*,*5*). OXA-48 is currently the most common OXA-48–like derivative and OXA-181 the second most common derivative (*44*). OXA-48 is endemic in North Africa, Middle East, and Turkey (*44*). *E. coli* with bla_{OXA-48} is linked to various STs (*44*). In our study, OXA-48 was identified among 18 STs from 15 countries. *E. coli* with bla_{OXA-48} was common in Turkey, where it was linked with ST11260.

OXA-181 is linked with certain *E. coli* STs, especially ST410 (*44*). *E. coli* ST410 belongs to phylogroup A and is divided into 2 clades (A/*H*53 and B/*H*24). Clade B is divided into subclades B1/*H*24, B2/*H*24R, B3/*H*24Rx, and B4/*H*24RxC (*21*). The B2/*H*24R subclade is associated with fluroquinolone resistance, B3/*H*24Rx with $bla_{CTX-M-15}$, and B4/*H*24RxC with $bla_{OXA-181}$ (*21*). In our survey, OXA-181 was identified among 11 different STs obtained from 12 countries. All the OXA-181 genes were situated within Tn*2013* harbored on near identical IncX3 plasmids (≈100% similarly to p72_X3_OXA181). *K. pneumoniae* ST307 with p72_X3_OXA181 was previously responsible for large outbreaks in South Africa (*13*,*37*). *E. coli* with $bla_{OXA-181}$ was frequent in Jordan, Egypt (linked with ST410- B4/*H24*RxC subclade), and Turkey (linked with ST1284). The ST410-B4/*H24*RxC subclade with

bla$_{OXA-181}$ was also found in Thailand and South Korea. The ST410-B3/*H24*Rx subclade with *bla*$_{OXA-181}$ was present in South Africa and Kuwait.

Molecular-based surveillance studies have shown that NDMs are often the most common carbapenemase in certain regions (e.g., the Indian subcontinent) (*4*,*5*). NDM-1 is the most frequent NDM enzyme and associated with various STs within diverse plasmid platforms (*45*). In our survey, NDM-1 was identified among 14 different STs obtained from 10 countries. *E. coli* with *bla*$_{NDM-1}$ was not linked with a specific ST and was evenly distributed among the different countries.

E. coli with NDM-5 is numerous among *E. coli* with NDMs from India, China, and sub-Saharan Africa (*45*). NDM-5, in our survey, was found among 9 different STs from 9 countries. It was common in Egypt (linked with ST410 [B4/*H24*RxC] and ST167 [B1 and B3]), Thailand (linked with ST410 [B4/*H24*RxC] and ST167 [B2]), and Vietnam (linked with ST448). ST167 belongs to phylogroup A and is an emerging carbapenemase clone associated with *bla*$_{NDM-5}$ (*46*). We divided ST167 into 2 clades (A and B) and 3 subclades (B1, B2, and B3). Subclade B3 was the most dominant clade and associated with *bla*$_{NDM-5}$ obtained from Egypt and Italy. Other subclades were less common and linked with *bla*$_{NDM-5}$, *bla*$_{NDM-1}$, and *bla*$_{OXA-181}$ obtained in Guatemala (clade A), Egypt (subclades B1 and B2), and Thailand (subclade B2).

E. coli with *bla*$_{KPC}$ is associated with ST131 (*47*) on diverse plasmid platforms (*48*). *E. coli* ST131 is global MDR high-risk clone associated with fluoroquinolone resistance and *bla*$_{CTX-M}$s (*49*). ST131 belongs to clades A/*H*41, B/*H*22, and C/*H*30 (*50*). C/*H*30 is divided into subclades C0, C1_nonM27, C1_M27, and C2. In our survey, KPC genes were found among 26 different STs from 11 countries. *E. coli* with *bla*$_{KPC}$ was common in Colombia linked with various STs. ST131 was responsible for 32% of KPC isolates and obtained from Italy, Israel, Guatemala, Puerto Rico, and the United States (including Puerto Rico). ST131 with *bla*$_{KPC}$ was dominated by the C1_nonM27 subclade. This dominance is different from that observed by Johnson et al. study (*40*), where the C2 subclade was common. The ST131-C1_M27 subclade in our survey was positive for *bla*$_{NDM-1}$ and *bla*$_{OXA-232}$.

Among this study's strengths is that it included a large global collection of recent isolates representing multiple LMICs. We characterized all isolates using short-read WGS and provided novel information regarding the geographic distribution and MDR determinants of dominant STs and their respective clades and subclades (e.g., global ST410 was linked with *bla*$_{OXA-181}$, ST131 with *bla*$_{KPCs}$, ST167 with *bla*$_{NDM-5}$, and ST405 with various carbapenemases).

We showed that the underlying molecular epidemiology within the same carbapenemase groups were very different (e.g., NDM-1 was linked with various STs, including ST131-C2/*H*30, whereas NDM-5 was linked with ST167-B and ST410B4/*H*24Rx). The geographic distribution of isolates with NDM-1 and NDM-5 was different (e.g., NDM-1 showed global distribution whereas those with NDM-5 were numerous in Egypt, Thailand, and Vietnam). Similar differences were described for isolates with OXA-48 (various STs) and OXA-181 (linked with ST410B4/*H*24Rx). Future genomic surveys should use methodologies that characterize individual carbapenemases.

We also showed that global *bla*$_{OXA-181}$ was harbored on near identical IncX3 plasmids (irrespective of the ST or geographic location). This finding suggests that highly similar IncX3 plasmids were mainly responsible for the global distribution of OXA-181 genes, the most common carbapenemase in this collection. The control of such IncX3 plasmids should be a public health priority.

Limitations of this study include the fact that flanking regions and plasmids harboring carbapenemases were not fully reconstructed because of the limitations of short-read sequencing (*30*). The characterization of plasmids is vital to fully comprehend the molecular epidemiology of global carbapenemase-producing *E. coli*, and a follow-up study using long-read sequencing is under way. Several countries included only few isolates (Table) and therefore may not be fully representative of what carbapenemase-producing *E. coli* dominates in that region.

In summary, the global carbapenemase-producing *E. coli* population is dominated by diverse STs with different characteristics and varied geographic distributions. This characterization was especially apparent within certain carbapenemases groups (i.e., NDM-1 vs. NDM-5 or OXA-48 vs. OXA-181). Ongoing genomic surveillance to characterize individual carbapenemases will assist in designing management and prevention strategies to help curtail the spread of AMR bacteria.

Acknowledgments

We thank Merck and AstraZeneca for providing the SMART and INFORM isolates.

This work was supported by a research grant from the Joint Programming Initiative on Antimicrobial Resistance–Canadian Institute Health Research program (grant no. 10016015) and the US National Institutes of Health (grant no. 10028552).

About the Author

Dr. Peirano is a research associate at Alberta Precision Laboratories and the University of Calgary. Her research interests include the molecular epidemiology of antimicrobial-resistant organisms.

References

1. Tompkins K, van Duin D. Treatment for carbapenem-resistant Enterobacterales infections: recent advances and future directions. Eur J Clin Microbiol Infect Dis. 2021; 40:2053–68. https://doi.org/10.1007/s10096-021-04296-1
2. Tacconelli E, Carrara E, Savoldi A, Harbarth S, Mendelson M, Monnet DL, et al.; WHO Pathogens Priority List Working Group. Discovery, research, and development of new antibiotics: the WHO priority list of antibiotic-resistant bacteria and tuberculosis. Lancet Infect Dis. 2018;18:318–27. https://doi.org/10.1016/S1473-3099(17)30753-3
3. Pitout JD, Nordmann P, Poirel L. Carbapenemase-producing *Klebsiella pneumoniae*, a key pathogen set for global nosocomial dominance. Antimicrob Agents Chemother. 2015;59:5873–84. https://doi.org/10.1128/AAC.01019-15
4. Karlowsky JA, Lob SH, Kazmierczak KM, Young K, Motyl MR, Sahm DF. In vitro activity of imipenem/relebactam against *Enterobacteriaceae* and *Pseudomonas aeruginosa* isolated from intraabdominal and urinary tract infection samples: SMART Surveillance United States 2015–2017. J Glob Antimicrob Resist. 2020;21:223–8. https://doi.org/10.1016/j.jgar.2019.10.028
5. Kazmierczak KM, Karlowsky JA, de Jonge BLM, Stone GG, Sahm DF. Epidemiology of carbapenem resistance determinants identified in meropenem-nonsusceptible *Enterobacterales* collected as part of a global surveillance program, 2012 to 2017. Antimicrob Agents Chemother. 2021;65:e0200020. https://doi.org/10.1128/AAC.02000-20
6. Pitout JD. Extraintestinal pathogenic *Escherichia coli*: an update on antimicrobial resistance, laboratory diagnosis and treatment. Expert Rev Anti Infect Ther. 2012;10:1165–76. https://doi.org/10.1586/eri.12.110
7. Pitout JDD. Population dynamics of *Escherichia coli* causing bloodstream infections over extended time periods. MSphere. 2021;6:e0095621. https://doi.org/10.1128/msphere.00956-21
8. Léger A, Lambraki I, Graells T, Cousins M, Henriksson PJG, Harbarth S, et al. Characterizing social-ecological context and success factors of antimicrobial resistance interventions across the One Health spectrum: analysis of 42 interventions targeting *E. coli*. BMC Infect Dis. 2021;21:873. https://doi.org/10.1186/s12879-021-06483-z
9. Nordmann P, Poirel L. The difficult-to-control spread of carbapenemase producers among *Enterobacteriaceae* worldwide. Clin Microbiol Infect. 2014;20:821–30. https://doi.org/10.1111/1469-0691.12719
10. Manges AR, Geum HM, Guo A, Edens TJ, Fibke CD, Pitout JDD. Global extraintestinal pathogenic *Escherichia coli* (ExPEC) lineages. Clin Microbiol Rev. 2019;32:e00135-18. https://doi.org/10.1128/CMR.00135-18
11. Clinical and Laboratory Standards Institute. Performance standards for antimicrobial susceptibility testing. Twenty-fifth information supplement (M100–S25). Wayne (PA): The Institute; 2015.
12. Holland MS, Nobrega D, Peirano G, Naugler C, Church DL, Pitout JDD. Molecular epidemiology of *Escherichia coli* causing bloodstream infections in a centralized Canadian region: a population-based surveillance study. Clin Microbiol Infect. 2020;26:1554.e1–e8.
13. Lowe M, Kock MM, Coetzee J, Hoosien E, Peirano G, Strydom KA, et al. *Klebsiella pneumoniae* ST307 with $bla_{OXA-181}$, South Africa, 2014–2016. Emerg Infect Dis. 2019;25:739–47. https://doi.org/10.3201/eid2504.181482
14. Peirano G, Matsumura Y, Adams MD, Bradford P, Motyl M, Chen L, et al. Genomic epidemiology of global carbapenemase-producing *Enterobacter* spp., 2008–2014. Emerg Infect Dis. 2018;24:1010–9. https://doi.org/10.3201/eid2406.171648
15. Nurk S, Bankevich A, Antipov D, Gurevich AA, Korobeynikov A, Lapidus A, et al. Assembling single-cell genomes and mini-metagenomes from chimeric MDA products. J Comput Biol. 2013;20:714–37. https://doi.org/10.1089/cmb.2013.0084
16. Zankari E, Hasman H, Cosentino S, Vestergaard M, Rasmussen S, Lund O, et al. Identification of acquired antimicrobial resistance genes. J Antimicrob Chemother. 2012;67:2640–4. https://doi.org/10.1093/jac/dks261
17. Carattoli A, Zankari E, García-Fernández A, Voldby Larsen M, Lund O, Villa L, et al. In silico detection and typing of plasmids using PlasmidFinder and plasmid multilocus sequence typing. Antimicrob Agents Chemother. 2014;58:3895–903. https://doi.org/10.1128/AAC.02412-14
18. Zhou Z, Alikhan NF, Mohamed K, Fan Y, Achtman M; Agama Study Group. The EnteroBase user's guide, with case studies on *Salmonella* transmissions, *Yersinia pestis* phylogeny, and *Escherichia* core genomic diversity. Genome Res. 2020;30:138–52. https://doi.org/10.1101/gr.251678.119
19. Joensen KG, Scheutz F, Lund O, Hasman H, Kaas RS, Nielsen EM, et al. Real-time whole-genome sequencing for routine typing, surveillance, and outbreak detection of verotoxigenic *Escherichia coli*. J Clin Microbiol. 2014;52:1501–10. https://doi.org/10.1128/JCM.03617-13
20. Matsumura Y, Pitout JDD, Peirano G, DeVinney R, Noguchi T, Yamamoto M, et al. Rapid identification of different *Escherichia coli* sequence type 131 clades. Antimicrob Agents Chemother. 2017;61:e00179-17. https://doi.org/10.1128/AAC.00179-17
21. Roer L, Overballe-Petersen S, Hansen F, Schønning K, Wang M, Røder BL, et al. *Escherichia coli* sequence type 410 is causing new international high-risk clones. MSphere. 2018;3:e00337-18. https://doi.org/10.1128/mSphere.00337-18
22. Wang M, Earley M, Chen L, Hanson BM, Yu Y, Liu Z, et al. Clinical outcomes and bacterial characteristics of carbapenem-resistant *Klebsiella pneumoniae* complex among patients from different global regions (CRACKLE-2): a prospective, multicentre, cohort study. Lancet Infect Dis. 2021 Nov 9 [Epub ahead of print]. https://doi.org/10.1016/S1473-3099(21)00399-6
23. Stamatakis A. RAxML version 8: a tool for phylogenetic analysis and post-analysis of large phylogenies. Bioinformatics. 2014;30:1312–3. https://doi.org/10.1093/bioinformatics/btu033
24. Tonkin-Hill G, Lees JA, Bentley SD, Frost SDW, Corander J. RhierBAPS: An R implementation of the population clustering algorithm hierBAPS. Wellcome Open Res. 2018; 3:93. https://doi.org/10.12688/wellcomeopenres.14694.1
25. Cheng L, Connor TR, Sirén J, Aanensen DM, Corander J. Hierarchical and spatially explicit clustering of DNA sequences with BAPS software. Mol Biol Evol. 2013;30:1224–8. https://doi.org/10.1093/molbev/mst028
26. Letunic I, Bork P. Interactive tree of life (iTOL) v3: an online tool for the display and annotation of phylogenetic and other

trees. Nucleic Acids Res. 2016;44(W1):W242-5. https://doi.org/10.1093/nar/gkw290
27. R Core Team. R: a language and environment for statistical computing. Vienna: R Foundation for Statistical Computing; 2017.
28. Troxler S, Lalonde T, Wilson JR. Exact logistic models for nested binary data. Stat Med. 2011;30:866–76. https://doi.org/10.1002/sim.4157
29. Benjamini Y, Hochberg Y. Controlling the false discovery rate: a practical and powerful approach to multiple testing. J R Stat Soc B. 1995;57:289–300. https://doi.org/10.1111/j.2517-6161.1995.tb02031.x
30. Arredondo-Alonso S, Willems RJ, van Schaik W, Schürch AC. On the (im)possibility of reconstructing plasmids from whole-genome short-read sequencing data. Microb Genom. 2017;3:e000128. https://doi.org/10.1099/mgen.0.000128
31. Chen L, Mathema B, Chavda KD, DeLeo FR, Bonomo RA, Kreiswirth BN. Carbapenemase-producing *Klebsiella pneumoniae*: molecular and genetic decoding. Trends Microbiol. 2014;22:686–96. https://doi.org/10.1016/j.tim.2014.09.003
32. Potron A, Rondinaud E, Poirel L, Belmonte O, Boyer S, Camiade S, et al. Genetic and biochemical characterisation of OXA-232, a carbapenem-hydrolysing class D β-lactamase from *Enterobacteriaceae*. Int J Antimicrob Agents. 2013;41:325–9. https://doi.org/10.1016/j.ijantimicag.2012.11.007
33. García-Fernández A, Villa L, Carta C, Venditti C, Giordano A, Venditti M, et al. *Klebsiella pneumoniae* ST258 producing KPC-3 identified in italy carries novel plasmids and OmpK36/OmpK35 porin variants. Antimicrob Agents Chemother. 2012;56:2143–5. https://doi.org/10.1128/AAC.05308-11
34. Sheppard AE, Stoesser N, Sebra R, Kasarskis A, Deikus G, Anson L, et al. Complete genome sequence of KPC-producing *Klebsiella pneumoniae* strain CAV1193. Genome Announc. 2016;4:e01649-15. https://doi.org/10.1128/genomeA.01649-15
35. Chen L, Chavda KD, Melano RG, Hong T, Rojtman AD, Jacobs MR, et al. Molecular survey of the dissemination of two bla_{KPC}-harboring IncFIA plasmids in New Jersey and New York hospitals. Antimicrob Agents Chemother. 2014;58:2289–94. https://doi.org/10.1128/AAC.02749-13
36. Chen L, Chavda KD, Al Laham N, Melano RG, Jacobs MR, Bonomo RA, et al. Complete nucleotide sequence of a bla_{KPC}-harboring IncI2 plasmid and its dissemination in New Jersey and New York hospitals. Antimicrob Agents Chemother. 2013;57:5019–25. https://doi.org/10.1128/AAC.01397-13
37. Strydom KA, Chen L, Kock MM, Stoltz AC, Peirano G, Nobrega DB, et al. *Klebsiella pneumoniae* ST307 with OXA-181: threat of a high-risk clone and promiscuous plasmid in a resource-constrained healthcare setting. J Antimicrob Chemother. 2020;75:896–902. https://doi.org/10.1093/jac/dkz550
38. World Health Organization. Antimicrobial resistance: global report on surveillance 2014. Geneva: World Health Organization; 2014. p. 257.
39. Acharya KP, Subramanya SH, Pitout JDD. Inclusion of next-generation leaders and cost-effective precision diagnostic techniques are vital in combatting antimicrobial resistance in low- and middle-income countries. JAC Antimicrob Resist. 2020 Jun 23 [Epub ahead of print]. https://doi.org/10.1093/jacamr/dlaa032
40. Johnston BD, Thuras P, Porter SB, Anacker M, VonBank B, Vagnone PS, et al. Global molecular epidemiology of carbapenem-resistant *Escherichia coli* (2002–2017). Eur J Clin Microbiol Infect Dis. 2021 Jul 19 [Epub ahead of print]. https://doi.org/10.1007/s10096-021-04310-6
41. Peirano G, Bradford PA, Kazmierczak KM, Chen L, Kreiswirth BN, Pitout JD. Importance of clonal complex 258 and $IncF_{K2\text{-}like}$ plasmids among a global collection of *Klebsiella pneumoniae* with bla_{KPC}. Antimicrob Agents Chemother. 2017;61:e02610-16. https://doi.org/10.1128/AAC.02610-16
42. Peirano G, Chen L, Kreiswirth BN, Pitout JDD. Emerging antimicrobial-resistant high-risk *Klebsiella pneumoniae* clones ST307 and ST147. Antimicrob Agents Chemother. 2020;64:e01148-20. https://doi.org/10.1128/AAC.01148-20
43. Stokes W, Peirano G, Matsumara Y, Nobrega D, Pitout JDD. Population-based surveillance of *Enterobacter cloacae* complex causing blood stream infections in a centralized Canadian region. Eur J Clin Microbiol Infect Dis. 2021 Jul 14 [Epub ahed of print]. https://doi.org/10.1007/s10096-021-04309-z
44. Pitout JDD, Peirano G, Kock MM, Strydom KA, Matsumura Y. The global ascendency of OXA-48-type carbapenemases. Clin Microbiol Rev. 2019;33:e00102-19. https://doi.org/10.1128/CMR.00102-19
45. Wu W, Feng Y, Tang G, Qiao F, McNally A, Zong Z. NDM metallo-β-lactamases and their bacterial producers in health care settings. Clin Microbiol Rev. 2019;32:e00115-18. https://doi.org/10.1128/CMR.00115-18
46. Cummins EA, Snaith AE, McNally A, Hall RJ. The role of potentiating mutations in the evolution of pandemic *Escherichia coli* clones. Eur J Clin Microbiol Infect Dis. 2021 Nov 17 [Epub of print]. https://doi.org/10.1007/s10096-021-04359-3
47. Peirano G, Bradford PA, Kazmierczak KM, Badal RE, Hackel M, Hoban DJ, et al. Global incidence of carbapenemase-producing *Escherichia coli* ST131. Emerg Infect Dis. 2014;20:1928–31. https://doi.org/10.3201/eid2011.141388
48. Stoesser N, Sheppard AE, Peirano G, Anson LW, Pankhurst L, Sebra R, et al. Genomic epidemiology of global *Klebsiella pneumoniae* carbapenemase (KPC)-producing *Escherichia coli*. Sci Rep. 2017;7:5917. https://doi.org/10.1038/s41598-017-06256-2
49. Mathers AJ, Peirano G, Pitout JD. The role of epidemic resistance plasmids and international high-risk clones in the spread of multidrug-resistant *Enterobacteriaceae*. Clin Microbiol Rev. 2015;28:565–91. https://doi.org/10.1128/CMR.00116-14
50. Pitout JDD, Finn TJ. The evolutionary puzzle of *Escherichia coli* ST131. Infect Genet Evol. 2020;81:104265. https://doi.org/10.1016/j.meegid.2020.104265

Address for correspondence: Johann D.D. Pitout, University of Calgary, #9, 3535 Research Rd NW, Calgary, AB T2L 2K8, Canada; email: jpitout@ucalgary.ca

Risk for Asymptomatic Household Transmission of *Clostridioides difficile* Infection Associated with Recently Hospitalized Family Members

Aaron C. Miller, Alan T. Arakkal, Daniel K. Sewell, Alberto M. Segre, Sriram V. Pemmaraju, Philip M. Polgreen; CDC MInD-Healthcare Group

We evaluated whether hospitalized patients without diagnosed *Clostridioides difficile* infection (CDI) increased the risk for CDI among their family members after discharge. We used 2001–2017 US insurance claims data to compare monthly CDI incidence between persons in households with and without a family member hospitalized in the previous 60 days. CDI incidence among insurance enrollees exposed to a recently hospitalized family member was 73% greater than enrollees not exposed, and incidence increased with length of hospitalization among family members. We identified a dose-response relationship between total days of within-household hospitalization and CDI incidence rate ratio. Compared with persons whose family members were hospitalized <1 day, the incidence rate ratio increased from 1.30 (95% CI 1.19–1.41) for 1–3 days of hospitalization to 2.45 (95% CI 1.66–3.60) for >30 days of hospitalization. Asymptomatic *C. difficile* carriers discharged from hospitals could be a major source of community-associated CDI cases.

Clostridioides difficile infection (CDI) is one of the most commonly occurring types of healthcare-associated infection and is predominately associated with hospitals (*1*,*2*). Thus, CDI-related investigations and interventions primarily have focused on hospital settings. More recently, reports of community-associated CDI cases, in which patients without a history of recent hospitalization are infected, have become more common (*3*,*4*). Although healthcare-associated CDI remains a considerable problem, more emphasis on community-associated CDI cases also is needed.

Risk factors for community-associated CDI are similar to risk factors for hospital-associated cases. For example, antimicrobial drug and proton-pump inhibitor (PPI) use increase the risk for community-associated CDI (*4*,*5*). For some community-associated CDI cases, exposure to healthcare settings beyond hospitalization, including clinics and emergency departments (*6*,*7*), are associated with an increased risk for CDI. However, for some CDI cases, no clear exposure to healthcare facilities can be identified. To find a source of *C. difficile* in community settings, other potential exposures have been proposed. Food is one such potential exposure, and *C. difficile* has been recovered from several different edible substances, including meat and vegetables (*8*,*9*). Pets have also been implicated (*10*). In addition, the possibility of household transmission of CDI between family members has been proposed, and having a symptomatic family member is a risk factor for CDI (*10*,*11*).

In addition to symptomatic CDI cases, patients with asymptomatic *C. difficile* colonization might contribute to transmission (*12*,*13*). In whole-genome sequencing studies, identifying epidemiologic links between symptomatic CDI among hospitalized patients has often been difficult (*14*,*15*), suggesting a potential role for asymptomatic *C. difficile* colonization. Asymptomatic colonized patients might contribute less to environmental contamination than symptomatic cases, but in sufficient numbers they could still play a role in *C. difficile* transmission in healthcare settings (*16*). Furthermore, if asymptomatically colonized patients contribute to *C. difficile* transmission within the hospital, then they could contribute to transmission in the community after they are discharged and especially could play a role in transmission among other household members. Finally, because hospitalized patients can remain asymptomatically colonized with

Authors affiliation: University of Iowa, Iowa City, Iowa, USA

DOI: https://doi.org/10.3201/eid2805.212023

C. difficile after discharge (*17*–*20*), this patient population could represent a large reservoir of CDI outside healthcare settings.

We investigated whether recently hospitalized patients increased the risk for CDI among household members in the period after discharge. Specifically, we were interested in the risk posed to household members by patients who are discharged without a CDI diagnosis and who are not diagnosed with CDI after discharge. If the risk for asymptomatic *C. difficile* colonization increases with length of stay, we hypothesized that the risk for CDI among household members should increase as a function of their recently hospitalized family members' lengths of stay.

Methods

Data Source

We constructed our study population from the US Commercial Claims and Medicare Supplemental datasets of IBM MarketScan Research Databases (https://www.ibm.com) from 2001–2017. These databases contain employer-sponsored commercial insurance claims and Medicare supplemental claims for >195 million enrollees during the 17-year study period. This dataset represents one of the largest longitudinal administrative databases in the United States. The databases provided insurance claims for inpatient, outpatient, and emergency department encounters, along with outpatient medications, demographic characteristics, employment, and enrollment characteristics. We were able to link claims from multiple family members in the same enrollment plan by using a family identifier along with a variable indicating each enrollee's relationship to the primary enrollee, which indicated spouse, child, or dependent.

Study Population

We restricted our study population to enrolled households in which ≥2 family members could be identified on the same insurance plan. Our analysis was based on monthly CDI incidence, so we restricted our study population to those enrollees that were continuously enrolled for an entire month. We used code 008.45 from International Classification of Diseases, 9th Revision (ICD-9), and codes A04.7, A04.71, and A04.72 from the International Classification of Diseases, 10th Revision, Clinical Modification (ICD-10-CM), to identify CDI cases in outpatient and inpatient settings. To eliminate recurrent infections or subsequent care for the same infection, we focused on CDI cases in which the patient had no prior CDI diagnosis ≤60 days prior to the index month.

To isolate the potential effect of asymptomatic household transmission attributable to a prior hospitalization, we applied 2 additional restrictions to remove potential symptomatic exposures that might confound our results. First, we restricted our analysis to only enrollees that did not have a family member with CDI diagnosed in the period ≤60 days prior to the index month. Second, we restricted our analysis to those enrollees who were not hospitalized themselves ≤60 days prior to the index month.

Analysis

We compared the monthly incidence of CDI between persons in households where another family member had been recently hospitalized and discharged, ≤60 days prior to the index month, to those without recently hospitalized family members. We used a regression model to stratify enrollees into monthly enrollment strata based on the year and month, along with other demographic and patient characteristics, such as age, sex, prior antimicrobial drug use, PPI use, presence of an infant ≤2 years of age in the household, and exposure to a recently hospitalized family member. We then estimated the CDI incidence within each monthly enrollment strata, as a function of these various characteristics (Appendix, https://wwwnc.cdc.gov/EID/article/28/5/21-2023-App1.pdf).

We separated enrollees into categories for ages 0–17, 18–40, 41–65, and >65 years. We also categorized antimicrobial drugs into separate risk strata for high-CDI-risk antibiotics (clindamycin, fluoroquinolones, cephalosporins, carbapenems, ampicillin/sulbactam, pipercillin/tazobactam, and later-generation cephalosporins) or low-CDI-risk antibiotics (penicillin, macrolides, sulfonamides, trimethoprim, tetracyclines, and first-generation cephalosporins). We identified patients taking 1 of the following PPIs within 30 days before the CDI index date: omeprazole, esomeprazole, lansoprazole, rabeprazole, pantoprazole, dexlansoprazole, and omeprazole with sodium bicarbonate. We included an indicator for the presence of an infant ≤2 years old in the household because higher colonization rates have been found in infants (*17*,*21*).

Quantifying Exposure to Recently Hospitalized Family Members

We evaluated the effect of exposure to a recently hospitalized family member in 2 ways. First, we defined a single dichotomous stratification based on whether any other family member spent time in the hospital ≤60 days prior to the index month. We then analyzed the incidence rate ratio (IRR) of CDI

associated with exposure to a recently hospitalized family member. Second, we investigated whether a dose-response relationship existed between risk for CDI and the total amount of time that recently hospitalized family members spent in the hospital ≤60 days prior to the index month by computing the total days of within-family hospitalization. Specifically, we summed the lengths of stay across recently hospitalized family members' inpatient stays that overlapped the previous 60-day exposure window. For example, a case-patient with 2 family members discharged in the prior 60 days, 1 with a length of stay of 2 days and the other 3 days, would have 5 total days of within-family hospitalization (Appendix Figure 1). Finally, we sorted total days of within-family hospitalization into categories of 0, 1–3, 4–10, 11–20, 21–30, and >30 days by using 0 days (i.e., no hospitalization or a hospitalization of <1 day) of prior exposure as the reference.

Statistical Approach

We started by computing monthly CDI incidence for each of the patient characteristics used to define the various strata we described. We then estimated IRRs for the various patient strata while accounting for potential confounding effects by using a log-linear regression model, along with a quasi-Poisson distribution to account for overdispersion. Specifically, we estimated the mean CDI incidence in each monthly enrollment strata as a function of the binary criteria that define a stratum (Appendix). Of note, this approach and study population previously have been used to estimate the risk for secondary CDI infections among family members in household settings (*11*).

Sensitivity Analyses

We conducted 2 sensitivity analyses. First, we evaluated whether underlying susceptibility at a household level might confound our results. For example, households with family members more susceptible to CDI also could be more likely to have longer or more frequent hospitalizations (Appendix Figure 2). To evaluate this effect, we analyzed 2 models in which we reversed the temporal order and evaluated whether CDI risk is associated with future hospitalizations in a family (Appendix).

Second, we explored the time window used to define prior exposures. Specifically, we considered a 90-day exposure window before index CDI events to compute total days of within household exposure and prior exposure to antimicrobial drugs.

Results

We identified a total of 142,125,247 enrollees with ≥2 family members enrolled in the same insurance plan for an entire month (Table 1), which resulted in just over 5.1 billion enrollment months that we could observe over the study period. Most (53.2%) households contained ≥4 persons in the same insurance plan. We identified a total of 224,818 CDI cases across 194,424 enrollees; 55.9% of cases occurred among female enrollees and 74.6% among enrollees >40 years of age. Of all CDI cases, 6,575 cases represented a possible *C. difficile* transmission that occurred within 60 days after hospitalization of a family member. After we removed enrollees who were exposed to a family member with diagnosed CDI or who were hospitalized themselves, 164,650 CDI cases remained, of which 3,871 represented a potential asymptomatic *C. difficile* transmission from a recently hospitalized family member.

Table 1. Baseline enrollment characteristics of families with multiple infected members using a 60-day exposure window in study of asymptomatic *Clostridioides difficile* transmission among household members, United States*

Characteristics	All enrollees. no. (%)	No. (%) episodes of index CDI diagnosis†	No. (%) cases of possible transmission after family member hospitalization
No. CDI cases	NA	224,818	6,575
No. enrollees	142,125,247 (100)	194,424 (100)	6,453 (100)
Age group at enrollment or CDI diagnosis, y			
0–17	47,733,847 (33.6)	19,719 (8.8)	547 (8.3)
18–40	46,634,859 (32.8)	37,259 (16.6)	1,156 (17.6)
41–65	44,039,682 (31.0)	103,430 (46.0)	1,822 (27.7)
>65	3,716,859 (2.6)	64,410 (28.6)	3,050 (46.4)
Sex			
M	70,485,475 (49.6)	99,133 (44.1)	2,798 (42.6)
F	71,639,772 (50.4)	125,685 (55.9)	3,777 (57.4)
Family size			
2	36,598,138 (25.8)	134,644 (59.9)	4,166 (63.4)
3	29,857,746 (21.0)	36,236 (16.1)	905 (13.8)
4	40,705,784 (28.6)	34,559 (15.4)	839 (12.8)
5	21,536,725 (15.2)	13,517 (6.0)	409 (6.2)
>5	13,426,854 (9.4)	5,862 (2.6)	256 (3.9)

*CDI, *Clostridioides difficile* infection; NA, not applicable.
†Events occurring ≥60 days before another episode.

We calculated CDI incidence rates of cases per 100,000 enrollment months and unadjusted IRRs by the various demographic and exposure groups (Table 2). Consistent with established CDI risk factors, we found CDI incidence was greater among female persons; persons >40 years of age, especially persons >65 years of age; persons with exposure to low-CDI-risk and high-CDI-risk antibiotics; and persons taking PPIs. Overall, the CDI incidence was ≈73% greater (IRR 1.73) among persons exposed to a recently hospitalized family member (incidence of 5.56 cases/100,000 enrollment months) than among persons who were not exposed to recently a hospitalized family member (incidence of 3.22 cases/100,000 enrollment months). At a bivariate level across nearly all enrollment characteristics, the CDI incidence rate was greater among enrollees in households with recently hospitalized family members (Table 3). CDI incidence increased monotonically across the various levels of within-household hospitalization from 3.22 cases/100,000 enrollment months for 0 days of within-household hospitalization to 8.73 cases/100,000 enrollment months for >30 total days of within-household hospitalization.

For stratified regression analyses, we divided enrollees into 357,348 enrollment-month strata based on different combinations of demographics, enrollment characteristics, and risk factors (Table 4). For each within-household hospitalization exposure group, we computed IRRs relative to the baseline group in which family members spent <1 day in the hospital during the previous 60 days. Compared with enrollees whose family members spent <1 day in the hospital, the IRR of CDI continuously increased across the exposure bins from 1.30 (95% CI 1.19–1.41) for persons with 1–3 days of within-family hospitalization up to 2.45 (95% CI 1.66–3.60) for those with >30 days of within-family hospitalization.

Known CDI risk factors also were associated with greater incidence. Antimicrobial drug exposure was associated with an increased CDI incidence rate; for low-CDI-risk antibiotics the IRR was 2.69 (95% CI 2.59–2.79), and for high-CDI-risk antibiotics IRR was 8.83 (95% CI 8.63–9.03). PPI usage was also associated with statistically significant CDI incidence, an IRR of 2.23 (95% CI 2.15–2.30). CDI incidence increased with age; relative to ages 0–17 years the IRR continuously increased from 1.71 (95% CI 1.65–1.78) for ages 18–40 years to 9.32 (95% CI 8.92–9.73) for ages >65 years. Female persons had a higher incidence compared with male persons (IRR 1.30, 95% CI 1.28–1.33). Households with an infant also had a higher CDI incidence than those without (IRR 1.51, 95% CI 1.44–1.58).

We performed a sensitivity analysis to determine whether our results were confounded by household-level susceptibility (Appendix Table 1). When we reversed the temporal order of hospital exposure, we found little evidence that our primary results can be

Table 2. Bivariate comparisons of unadjusted incidence rates and incidence rate ratios for infection incidence across various patient strata using a 60-day exposure window in study of asymptomatic *Clostridioides difficile* transmission among household members, United States*

	Exposed to previously hospitalized family member ≤60 days			Not exposed to previously hospitalized family member ≤60 days			
Variable	CDI cases	Total enrollee months	CDI incidence†	CDI cases	Total enrollee months	CDI incidence†	Unadjusted IRR
Overall	3,871	69,675,026	5.56	160,779	4,998,101,178	3.22	1.73
Age group, y							
0–17	317	24,432,280	1.30	15,615	1,445,786,086	1.08	1.20
18–40	567	19,978,891	2.84	29,718	1,427,785,479	2.08	1.37
41–65	1,193	19,281,059	6.19	74,803	1,868,106,655	4.00	1.55
>65	1,794	5,982,798	29.99	40,643	256,422,958	15.85	1.89
Sex							
M	1,698	37,945,564	4.47	67,378	2,488,714,427	2.71	1.65
F	2,173	31,729,463	6.85	93,401	2,509,386,752	3.72	1.84
Outpatient antimicrobial drug use within 60 days							
None	2,419	63,230,032	3.83	100,792	4,575,861,567	2.20	1.74
Low-risk drugs	292	2,979,748	9.80	11,944	201,200,918	5.94	1.65
High-risk drugs	1,160	3,465,248	33.48	48,043	221,038,693	21.74	1.54
PPI use within 30 days							
N	3,477	68,273,806	5.09	146,185	4,913,346,960	2.98	1.71
Y	394	1,401,221	28.12	14,594	84,754,218	17.22	1.63
Infant age <2 y in family							
N	3,489	48,618,765	7.18	151,291	4,597,497,625	3.29	2.18
Y	382	21,056,262	1.81	9,488	400,603,553	2.37	0.76

*IRRs compare CDI incidence among persons exposed to a family member previously hospitalized for ≥1 d relative incidence for to those not exposed to a previously hospitalized family member. The overall incidence rate ratio among those exposed to a previously hospitalized family member relative to those unexposed was 1.73 and was >1 across all strata. CDI, *Clostridioides difficile* infection; IRR, incidence rate ratio; PPI, proton-pump inhibitor.
†Cases per 100,000 enrollee months.

Table 3. Number of cases and enrollee-months in each exposure bin for total days of household-hospitalization using a 60-day exposure window in study of asymptomatic *Clostridioides difficile* transmission among household members, United States*

No. days family members spent hospitalized	60-day exposure window		
	No. CDI cases	Total enrollment months	Incidence†
0	160,267	4,980,648,694	3.22
1–3	2,336	52,798,719	4.42
4–10	1,519	27,457,461	5.53
11–20	315	4,338,929	7.26
21–30	107	1,317,610	8.12
>30	106	1,214,792	8.73

*CDI, *Clostridioides difficile* infection.
†Cases per 100,000 enrollment months.

explained by confounding due to CDI susceptibility among family members. The point estimates for our primary dose-response curve remained relatively unchanged and were considerably larger than the effect estimates associated with future hospital visits among family members.

As a second sensitivity analysis, we considered a 90-day exposure window for capturing recently hospitalized family members (Appendix Tables 2–4). In general, the results of the analysis using a 90-day exposure window were consistent with the 60-day window, and we noted a similar dose-response relationship between the total days of within-household hospitalization among recently hospitalized family members and risk for CDI. However, the magnitude of some of the point estimates was slightly attenuated using the 90-day window compared with the 60-day window. For example, the IRR for the 1–3 day within-family hospitalization category was 1.24 for the 90-day window, compared with 1.30 for the 60-day window. However, the CIs for both sets of analyses overlapped the point estimates of the other.

Table 4. Results of regression analysis of incidence rate ratio for *Clostridioides difficile* infection using quasi-Poisson model and 60-day exposure window in study of asymptomatic *C. difficile* transmission among household members, United States*

Variable	IRR (95% CI)
No. days member was hospitalized within 60 d	
0	Referent
1–3	1.30 (1.19–1.41)
4–10	1.46 (1.32–1.62)
11–20	1.79 (1.43–2.23)
21–30	2.17 (1.48–3.18)
>30	2.45 (1.66–3.60)
Age group, y	
0–17	Referent
18–40	1.71 (1.65–1.78)
41–65	2.97 (2.86–3.08)
>65	9.32 (8.92–9.73)
Sex	
M	Referent
F	1.30 (1.28–1.33)
Outpatient antimicrobial drug use within 60 d	
None	Referent
Low-risk drugs	2.69 (2.59–2.79)
High-risk drugs	8.83 (8.63–9.03)
PPI use within 30 d	2.23 (2.15–2.30)
Infant <2 y in family	1.51 (1.44–1.58)

*Models were adjusted for year, month, and family size. Regression models included an offset for number of enrollment months. Because family hospitalization exposure group was followed for 60 days to identify secondary *Clostridioides difficile* infection, the length of their enrollment period is 60 days. For the unexposed group, the length of enrollment was the length of a given month. IRR, incident rate ratio; PPI, proton-pump inhibitor.

Discussion

In this study, we found that persons exposed to recently hospitalized family members were at substantially increased risk for CDI within 60 days after the family member's hospital discharge. Furthermore, CDI risk among family members increased as total days of within-household hospitalization increased. Because CDI was not diagnosed in recently hospitalized and discharged family members during or after their hospitalization, and because persons in our analysis were not hospitalized themselves, the increased risk could be attributable to asymptomatic *C. difficile* colonization at the time of hospital discharge in the hospitalized family member.

We also conducted several sensitivity analyses. First, to evaluate whether household confounding because of greater hospitalization in more susceptible family members could explain our findings, we reversed the temporal ordering of hospital exposure and found that incorporating future hospitalizations did not attenuate our primary effect estimates. This finding reinforces our primary hypothesis that the increased risk we observed is attributable to transmission from family members who become asymptomatically colonized during a prior hospital stay. Second, we used a 90-day exposure window and found consistent results but the dose-response effect appeared slightly attenuated. This finding could suggest that household exposures occurring >60 days in the past might convey minimal risk.

Our results have several implications. First, we provide further support for the role of asymptomatic *C. difficile* carriers in bacterial transmission. Second, we identify a previously underappreciated potential CDI reservoir outside healthcare settings that

could support the spread of community-associated *C. difficile*. Finally, our results suggest that, if patients who are asymptomatically colonized during a hospital stay contribute to transmission in the community, not all CDI cases attributable to hospital exposure can be directly identified based on hospital discharge records.

In hospital settings, patients asymptomatically colonized with *C. difficile* are increasingly viewed as a major contributor to CDI spread (*12*,*13*). Indeed, asymptomatic *C. difficile* transmission has been posited as an explanation for the missing epidemiologic links in whole-genome sequencing studies (*14*). Asymptomatic *C. difficile* colonization among hospitalized patients is not uncommon (*12*,*17*–*20*). For example, a meta-analysis found that ≈10% of hospitalized patients in North America become colonized (*20*). In addition, the likelihood of colonization increases with longer hospital stays (*17*), as well as the use of chemotherapy (*22*), PPIs or H2 blockers (*22*), and steroids (*23*). Furthermore, colonization likely persists for some time after discharge. For example, prior hospitalization, even 6 months in the past, has been found to be a risk factor for colonization at hospital admission (*18*). Because asymptomatically colonized patients can contaminate the environment and *C. difficile* spores are resistant to many cleaning solutions, household environments could feasibly lead to both symptomatic and asymptomatic CDI in family members.

Despite the increase in community-acquired CDI, relatively little research has focused on the household setting. Instead, most efforts to find the exposure sources for community-associated CDI have focused on healthcare settings outside hospitals, such as outpatient clinics and emergency departments (*6*,*7*), and nonhealthcare sources such as food (*8*), household pets (*10*), and even exposure to the agricultural industry (*24*). A few relatively small studies (*10*,*25*) and 1 large study (*11*) did identify potential secondary *C. difficile* transmission from symptomatic cases among household members. Thus far, however, few studies, except studies focusing on newborns, have questioned the role of asymptomatic carriers in household settings. Because infants frequently are colonized with *C. difficile* in their first several months of life, our findings and those from other studies that exposure to infants is potential risk factor for community-associated *C. difficile* (*17*,*21*) are not surprising.

Household transmission has been documented for other gastrointestinal infections, including rotavirus, norovirus, and *Giardia* (*26*–*30*). In addition, household transmission has been documented for another major healthcare-associated infection, methicillin-resistant *Staphylococcus aureus* (*31*,*32*). For at least some of these pathogens, asymptomatic or minimally symptomatic cases contribute to disease transmission. Of note, transmission of methicillin-resistant *S. aureus*, like *C. difficile,* was first thought to be almost exclusively confined to hospital settings; awareness of spread in community settings emerged later. Close household contact can also contribute to the spread of other fecal–oral pathogens, such as rotavirus and norovirus (*27*), via environmental contamination, providing further support for the plausibility of household spread of *C. difficile*.

In addition to providing support for the contribution of asymptomatic *C. difficile* colonization to household transmission, our results also might have implications for future *C. difficile* surveillance and intervention-based investigations. Prior investigations have shown that cases of symptomatic hospital-associated CDI often do not appear until after a patient is discharged (*33*) and that some of those cases might generate additional symptomatic cases among family members (*11*). However, our results raise the policy question of whether secondary symptomatic cases among household members should be considered when measuring the broader costs of healthcare-associated infections, especially those that have a reasonable epidemiologic link (e.g., using genotyping) with discharged patients who are asymptomatically colonized. Our results clearly suggest that hospital-based interventions to control both symptomatic and asymptomatic *C. difficile* transmission can help reduce spread in the community. Measures based on standard surveillance efforts might also underestimate the full effectiveness of hospital-based infection and antimicrobial stewardship interventions because those measures might not capture potential, positive downstream effects in the community.

One limitation of our study is that we cannot directly identify the exact point of exposure where *C. difficile* transmission might have occurred. Exposure could have occurred in a household setting after a family member was discharged from the hospital; alternatively, a family member might have become colonized while visiting another family member in the hospital. However, several reasons exist to suspect that family members visiting the hospital are unlikely to fully explain our observed effect. First, healthcare workers often have lower colonization rates than discharged patients (*17*). Second, visitors and visiting hours often are limited or restricted and only represent a small portion of a patient's total length of stay. Third, we did not count persons as exposed in our

analysis when their corresponding CDI index date occurred before their family members were discharged from the hospital; we only consider exposure to a recently hospitalized family member after discharge occurred. Thus, if visiting the hospital were the primary mechanism driving our results, our analytical method would be greatly biased toward the null.

Another limitation of our study is that we depended on insurance claims data and diagnostic codes to identify CDI events. We did not have access to laboratory test results to confirm CDI diagnoses, nor did we have access to genetic data to confirm whether subsequent CDI cases in family members were genetically related. We also could not observe or confirm that household contact actually occurred in the assumed household setting; family members could be residing in different locations even if they were enrolled in the same insurance plan. Finally, our data might not capture all family members residing in a single location. We only had access to information for family members that are actively enrolled in the same insurance plan, and family members in the same household are often enrolled in different plans. Despite these limitations, our results demonstrate the importance of considering asymptomatic carriers in spread of CDI in household settings.

In conclusion, because patients are frequently colonized with *C. difficile* during hospitalization and at discharge, and because ≈25 million persons each year have overnight hospital stays in the United States alone (*34*), patients recently discharged from hospitals could be spreading *C. difficile* outside hospital settings. Asymptomatic *C. difficile* carriers discharged from hospitals could be a major source of community-associated CDI cases and should be considered during surveillance and intervention-based investigations.

About the Author

Dr. Miller is a research assistant professor in the Department of Internal Medicine at the University of Iowa Roy J. and Lucille A. Carver College of Medicine. His primary research interests include the modeling and epidemiologic study of infectious diseases, in particular healthcare-associated infections, and application of data-science techniques to study patient safety and diagnostic errors for infectious diseases.

References

1. Lessa FC, Mu Y, Bamberg WM, Beldavs ZG, Dumyati GK, Dunn JR, et al. Burden of *Clostridium difficile* infection in the United States. N Engl J Med. 2015;372:2369–70. https://doi.org/10.1056/NEJMoa1408913
2. Lim SC, Knight DR, Riley TV. *Clostridium difficile* and One Health. Clin Microbiol Infect. 2020;26:857–63. https://doi.org/10.1016/j.cmi.2019.10.023
3. Ofori E, Ramai D, Dhawan M, Mustafa F, Gasperino J, Reddy M. Community-acquired *Clostridium difficile*: epidemiology, ribotype, risk factors, hospital and intensive care unit outcomes, and current and emerging therapies. J Hosp Infect. 2018;99:436–42. https://doi.org/10.1016/j.jhin.2018.01.015
4. Deshpande A, Pasupuleti V, Thota P, Pant C, Rolston DD, Sferra TJ, et al. Community-associated *Clostridium difficile* infection and antibiotics: a meta-analysis. J Antimicrob Chemother. 2013;68:1951–61. https://doi.org/10.1093/jac/dkt129
5. Dial S, Delaney JA, Barkun AN, Suissa S. Use of gastric acid-suppressive agents and the risk of community-acquired *Clostridium difficile*–associated disease. JAMA. 2005;294:2989–95. https://doi.org/10.1001/jama.294.23.2989
6. Simecka JW, Fulda KG, Pulse M, Lee JH, Vitucci J, Nguyen P, et al. Primary care clinics can be a source of exposure to virulent *Clostridium* (now *Clostridioides*) *difficile*: an environmental screening study of hospitals and clinics in Dallas-Fort Worth region. PLoS One. 2019;14:e0220646. https://doi.org/10.1371/journal.pone.0220646
7. Guh AY, Adkins SH, Li Q, Bulens SN, Farley MM, Smith Z, et al. Risk factors for community-associated *Clostridium difficile* infection in adults: a case-control study. Open Forum Infect Dis. 2017;4:ofx171. https://doi.org/10.1093/ofid/ofx171
8. Rupnik M, Songer JG. *Clostridium difficile*: its potential as a source of foodborne disease. Adv Food Nutr Res. 2010;60:53–66. https://doi.org/10.1016/S1043-4526(10)60003-4
9. Lim SC, Androga GO, Knight DR, Moono P, Foster NF, Riley TV. Antimicrobial susceptibility of *Clostridium difficile* isolated from food and environmental sources in Western Australia. Int J Antimicrob Agents. 2018;52:411–5. https://doi.org/10.1016/j.ijantimicag.2018.05.013
10. Loo VG, Brassard P, Miller MA. Household transmission of *Clostridium difficile* to family members and domestic pets. Infect Control Hosp Epidemiol. 2016;37:1342–8. https://doi.org/10.1017/ice.2016.178
11. Miller AC, Segre AM, Pemmaraju SV, Sewell DK, Polgreen PM. Association of household exposure to primary *Clostridioides difficile* infection with secondary infection in family members. JAMA Netw Open. 2020;3:e208925. https://doi.org/10.1001/jamanetworkopen.2020.8925
12. Galdys AL, Curry SR, Harrison LH. Asymptomatic *Clostridium difficile* colonization as a reservoir for *Clostridium difficile* infection. Expert Rev Anti Infect Ther. 2014;12:967–80. https://doi.org/10.1586/14787210.2014.920252
13. Sheth PM, Douchant K, Uyanwune Y, Larocque M, Anantharajah A, Borgundvaag E, et al. Evidence of transmission of *Clostridium difficile* in asymptomatic patients following admission screening in a tertiary care hospital. PLoS One. 2019;14:e0207138. https://doi.org/10.1371/journal.pone.0207138
14. Eyre DW, Cule ML, Wilson DJ, Griffiths D, Vaughan A, O'Connor L, et al. Diverse sources of *C. difficile* infection identified on whole-genome sequencing. N Engl J Med. 2013;369:1195–205. https://doi.org/10.1056/NEJMoa1216064
15. Kociolek LK, Gerding DN, Espinosa RO, Patel SJ, Shulman ST, Ozer EA. *Clostridium difficile* whole genome sequencing reveals limited transmission among symptomatic children: a single-center analysis. Clin Infect Dis. 2018;67:229–34. https://doi.org/10.1093/cid/ciy060

16. García-Fernández S, Frentrup M, Steglich M, Gonzaga A, Cobo M, López-Fresneña N, et al. Whole-genome sequencing reveals nosocomial *Clostridioides difficile* transmission and a previously unsuspected epidemic scenario. Sci Rep. 2019;9:6959. https://doi.org/10.1038/s41598-019-43464-4
17. Crobach MJT, Vernon JJ, Loo VG, Kong LY, Péchiné S, Wilcox MH, et al. Understanding *Clostridium difficile* colonization. Clin Microbiol Rev. 2018;31:e00021-17. https://doi.org/10.1128/CMR.00021-17
18. Anjewierden S, Han Z, Brown AM, Donskey CJ, Deshpande A. Risk factors for *Clostridioides difficile* colonization among hospitalized adults: a meta-analysis and systematic review. Infect Control Hosp Epidemiol. 2021;42:565–72. https://doi.org/10.1017/ice.2020.1236
19. McFarland LV, Mulligan ME, Kwok RY, Stamm WE. Nosocomial acquisition of *Clostridium difficile* infection. N Engl J Med. 1989;320:204–10. https://doi.org/10.1056/NEJM198901263200402
20. Zacharioudakis IM, Zervou FN, Pliakos EE, Ziakas PD, Mylonakis E. Colonization with toxinogenic *C. difficile* upon hospital admission, and risk of infection: a systematic review and meta-analysis. Am J Gastroenterol. 2015;110:381–90, quiz 391. https://doi.org/10.1038/ajg.2015.22
21. Wilcox MH, Mooney L, Bendall R, Settle CD, Fawley WN. A case-control study of community-associated *Clostridium difficile* infection. J Antimicrob Chemother. 2008;62:388–96. https://doi.org/10.1093/jac/dkn163
22. Loo VG, Bourgault AM, Poirier L, Lamothe F, Michaud S, Turgeon N, et al. Host and pathogen factors for *Clostridium difficile* infection and colonization. N Engl J Med. 2011;365:1693–703. https://doi.org/10.1056/NEJMoa1012413
23. Leekha S, Aronhalt KC, Sloan LM, Patel R, Orenstein R. Asymptomatic *Clostridium difficile* colonization in a tertiary care hospital: admission prevalence and risk factors. Am J Infect Control. 2013;41:390–3. https://doi.org/10.1016/j.ajic.2012.09.023
24. Squire MM, Riley TV. *Clostridium difficile* infection in humans and piglets: a 'One Health' opportunity. Curr Top Microbiol Immunol. 2013;365:299–314. https://doi.org/10.1007/978-3-662-45792-4_237
25. Pépin J, Gonzales M, Valiquette L. Risk of secondary cases of *Clostridium difficile* infection among household contacts of index cases. J Infect. 2012;64:387–90. https://doi.org/10.1016/j.jinf.2011.12.011
26. Wikswo ME, Parashar UD, Lopman B, Selvarangan R, Harrison CJ, Azimi PH, et al. Evidence for household transmission of rotavirus in the United States, 2011–2016. J Pediatric Infect Dis Soc. 2020;9:181–7. https://doi.org/10.1093/jpids/piz004
27. Quee FA, de Hoog MLA, Schuurman R, Bruijning-Verhagen P. Community burden and transmission of acute gastroenteritis caused by norovirus and rotavirus in the Netherlands (RotaFam): a prospective household-based cohort study. Lancet Infect Dis. 2020;20:598–606. https://doi.org/10.1016/S1473-3099(20)30058-X
28. Marsh ZA, Grytdal SP, Beggs JC, Leshem E, Gastañaduy PA, Rha B, et al. The unwelcome houseguest: secondary household transmission of norovirus. Epidemiol Infect. 2018;146:159–67. https://doi.org/10.1017/S0950268817002783
29. Phattanawiboon B, Nonthabenjawan N, Boonyos P, Jetsukontorn C, Towayunanta W, Chuntrakool K, et al. Norovirus transmission mediated by asymptomatic family members in households. PLoS One. 2020;15:e0236502. https://doi.org/10.1371/journal.pone.0236502
30. Waldram A, Vivancos R, Hartley C, Lamden K. Prevalence of *Giardia* infection in households of *Giardia* cases and risk factors for household transmission. BMC Infect Dis. 2017;17:486. https://doi.org/10.1186/s12879-017-2586-3
31. Lakhundi S, Zhang K. Methicillin-resistant *Staphylococcus aureus*: molecular characterization, evolution, and epidemiology. Clin Microbiol Rev. 2018;31:e00020-18. https://doi.org/10.1128/CMR.00020-18
32. David MZ, Daum RS. Community-associated methicillin-resistant *Staphylococcus aureus*: epidemiology and clinical consequences of an emerging epidemic. Clin Microbiol Rev. 2010;23:616–87. https://doi.org/10.1128/CMR.00081-09
33. Kuntz JL, Polgreen PM. The importance of considering different healthcare settings when estimating the burden of *Clostridium difficile*. Clin Infect Dis. 2015;60:831–6. https://doi.org/10.1093/cid/ciu955
34. Centers for Disease Control and Prevention. Hospital utilization (in non-federal short-stay hospitals) [cited 2021 May 7]. https://www.cdc.gov/nchs/fastats/hospital.htm

Address for correspondence: Aaron C. Miller, Department of Internal Medicine, Roy J. and Lucille A. Carver College of Medicine, University of Iowa, 200 Hawkins Dr, Iowa City, IA 52242, USA; email: aaron-miller@uiowa.edu

Estimating Relative Abundance of 2 SARS-CoV-2 Variants through Wastewater Surveillance at 2 Large Metropolitan Sites, United States

Alexander T. Yu,[1] Bridgette Hughes,[1] Marlene K. Wolfe, Tomas Leon, Dorothea Duong, Angela Rabe, Lauren C. Kennedy, Sindhu Ravuri, Bradley J. White, Krista R. Wigginton, Alexandria B. Boehm, Duc J. Vugia

Monitoring severe acute respiratory syndrome coronavirus 2 (SARS-CoV-2) variants of concern (VOCs) is critical for public health management of coronavirus disease. Sequencing is resource-intensive and incompletely representative, and not all isolates can be sequenced. Because wastewater SARS-CoV-2 RNA concentrations correlate with coronavirus disease incidence in sewersheds, tracking VOCs through wastewater is appealing. We developed digital reverse transcription PCRs to monitor abundance of select mutations in Alpha and Delta VOCs in wastewater settled solids, applied these to July 2020–August 2021 samples from 2 large US metropolitan sewersheds, and compared results to estimates of VOC abundance from case isolate sequencing. Wastewater measurements tracked closely with case isolate estimates (Alpha, rp 0.82–0.88; Delta, rp 0.97). Mutations were detected in wastewater even at levels <5% of total SARS-CoV-2 RNA and in samples available 1–3 weeks before case isolate results. Wastewater variant monitoring should be strategically deployed to complement case isolate sequencing.

By November 2021, the coronavirus disease (COVID-19) pandemic, caused by severe acute respiratory syndrome coronavirus 2 (SARS-CoV-2), had claimed >5 million lives worldwide, including >700,000 in the United States (*1*–*3*). Since its emergence in late 2019, SARS-CoV-2 has mutated, resulting in some variants categorized by the World Health Organization as variants of concern (VOCs). VOCs have evidence of potential increased infectiousness, immune evasion, and clinical severity, and they have spread globally. Some VOCs, such as Alpha and Delta, have become the predominant strain at different times and regions (*4*,*5*). COVID-19 diagnostics, therapeutics, or vaccines may have decreased effectiveness against VOCs (*6*,*7*). As of November 2021, VOCs in the United States included the Alpha (B.1.1.7), Beta (B.1.351), Gamma (P.1), and Delta (B.1.617.2) variants (*3*).

Monitoring for VOCs is critical for management of the ongoing COVID-19 pandemic, enabling public health officials to track their public health impact, implement control measures, and allocate resources effectively. Detection of SARS-CoV-2 variants occurs primarily through genomic sequencing of isolates collected for PCR-based diagnosis of persons with active COVID-19 infection. Sequencing is resource- and time-intensive and has limits on capacity because of equipment, reagents, and trained personnel (*8*). As such, complete and timely sequencing of case isolates is not feasible or practical, particularly when case numbers have been high. During January 2020–September 2021, <3% of COVID-19 cases in the United States had isolates that were sequenced and available on public repositories (*3*). Nonrandom selection of isolates for sequencing and nonuniform result reporting could make results susceptible to bias and not truly representative of circulating variants (*4*,*8*,*9*). Also,

Author affiliations: California Department of Public Health, Richmond, California, USA (A.T. Yu, T. Leon, A. Rabe, S. Ravuri, D.J. Vugia); California Department of Public Health, Sacramento, California, USA (A.T. Yu, T. Leon, A. Rabe, S. Ravuri, D.J. Vugia); Verily Life Sciences, South San Francisco, California, USA (B. Hughes, D. Duong, B.J. White); Stanford University, Stanford, California, USA (M.K. Wolfe, L.C. Kennedy, A.B. Boehm); Emory University, Atlanta, Georgia, USA (M.K. Wolfe); University of Michigan, Ann Arbor, Michigan, USA (K.R. Wigginton)

DOI: https://doi.org/10.3201/eid2805.212488

[1]These first authors contributed equally to this article.

substantial delays can occur between isolate collection, sequencing and availability of results to public health (*9*). Given its timeliness, representativeness, and comparatively low costs, wastewater surveillance for VOCs can be a useful supplement to case-based sequencing surveillance (*10*–*12*).

Since early in the pandemic, wastewater samples have been collected and analyzed to quantify the amount of SARS-CoV-2 RNA in sewage. Estimates of viral RNA abundance in sewage correlate closely with reported COVID-19 case counts for the catchment area (sewershed) (*13*,*14*) and provide a comprehensive snapshot of real-time community transmission independent of individual care-seeking or testing behavior. Therefore, there is a strong interest in determining if wastewater can also provide useful information on circulating VOCs (*15*). Both sequencing and PCR assays targeting specific mutations have been proposed as methods to detect mutations and deletions in SARS-CoV-2 RNA in wastewater.

Variant monitoring using environmental samples presents technical challenges. Variants are characterized by the presence of multiple mutations on the same RNA genome, and some share ≥1 mutations (*16*). Unlike isolates from an individual case, which consist of a single genome, wastewater samples likely contain material from multiple SARS-CoV-2 variants shed from different persons, each variant at low concentrations and in various states of genomic integrity because of degradation (*17*). Therefore, because wastewater contains a complex mixture of SARS-CoV-2 RNA fragments, the presence of ≥1 variant mutation sequences does not alone prove that the variant is present in wastewater.

We developed targeted digital reverse transcription PCR mutation assays to retrospectively and prospectively monitor wastewater settled solids for the presence and abundance of mutations present in the Alpha (B.1.1.7) and Delta (B.1.617.2) VOCs. We chose wastewater solids because they contain orders of magnitude higher concentrations of viral RNA than wastewater influent (*18*,*19*); previous work has documented a strong coupling between SARS-CoV-2 RNA concentrations in wastewater solids and incidence in the associated population contributing to the wastewater (*19*). We prospectively monitored wastewater solids of a large metropolitan sewershed in California (San Jose), USA, during July 2020–August 2021 for a deletion present in the Alpha variant. We then retrospectively measured the abundance of this deletion in a second large metropolitan area (Sacramento, CA, USA) where samples had been routinely collected. We also measured concentrations of mutations suggestive of Delta in both sewersheds. We then compared these totals against estimates of Alpha and Delta abundance in each of these sewersheds by using COVID-19 case isolate sequencing data available to the California Department of Public Health (CDPH).

Methods

Mutation Assay Development for Alpha and Delta Variants

We developed assays in silico to target mutations present in Alpha (HV69-70) and Delta (Del156–157/R158G). We screened primers and probe sequences (Appendix Table, https://wwwnc.cdc.gov/EID/article/28/5/21-2488-App1.pdf) for specificity using BLAST (http://blast.ncbi.nlm.nih.gov/Blast.cgi), and then tested them in vitro against a wide range of viral genomes, including wild-type SARS-CoV-2 and SARS-CoV-2 VOCs, including Alpha and Delta. We further tested the sensitivity and specificity of the assays by diluting variant gRNA containing the mutations in no (0 copies), low (100 copies), and high (10,000 copies) background of wild-type gRNA (Appendix).

Wastewater Sample Collection

This study used samples from 2 publicly owned treatment works (POTWs) that serve ≈1.5 million residents of Santa Clara County, California, USA (San Jose), and Sacramento County, California, USA (Sacramento). Details of collection processes have been described (*14*).

We collected samples from the POTWs to span the period before and including the presumed emergence of Alpha and Delta variants in the communities. Before presumed emergence, sampling was 1–4 times per month; during the periods of suspected emergence, sampling was 3–7 times per week. At San Jose, 133 (HV69–70) and 48 (del156–157/R158G) samples and at Sacramento, 64 (HV69–70) and 48 (del156–157/R158G) samples were included for analyses of each mutation.

We extracted RNA from the settled solids and processed within 24 hours of sample collection to measure concentrations of the nucleoprotein (N) gene using digital droplet reverse transcription PCR (Appendix) (*20*). The N gene codes for the SARS-CoV-2 nucleocapsid; the specific region of the genome targeted by the assay is conserved on SARS-CoV-2 genomes. We included internal recovery controls. Thereafter, we stored RNA samples at –80°C for 0–300 days before analyzing them a second time for the N

gene and the Delta mutation (Del156–157/R158G) or the Alpha mutation (HV69-70), using digital droplet reverse transcription PCR. By comparing the N gene concentration in the samples before and after storage, we confirmed negligible RNA degradation. All wastewater data are publicly available (https://doi.org/10.25740/zf117dn1545).

Incident COVID-19 Cases and Case Isolate Sequences

Each POTW provided sewershed boundary shapefiles. We determined the number of PCR-confirmed COVID-19 cases reported to CDPH as a function of episode date (earliest of either specimen collection or symptom onset date) residing within each sewershed using methods reported previously (*20*) (Appendix).

COVID-19 case isolate whole-genome sequence data available to CDPH included data from the CDC and laboratory partners. We assigned sequence data to a sewershed on the basis of residential home postal code for the sample. We assigned the PANGO lineage based on the software version available at the time data was extracted; most recent results used pangoLEARN and pango-designation version 1.2.66 (*21*).

We calculated VOC abundance estimates by dividing the number of sequences identified as Alpha or Delta (using the World Health Organization definition and including all PANGO sublineages Q.*, for Alpha, and AY.*, for Delta) by the total number of isolates sequenced from persons residing in the sewersheds over 14-day periods. To estimate time between isolate sample collection and sequence result and to measure the effect of that time delay on VOC estimates, we compared 14-day VOC abundance estimates over time against a final estimate generated on August 24, 2021. We chose a 14-day VOC window (versus a 7- or 28-day window) to balance timeliness of results and number of available case isolates sequenced within the window, given that fewer case isolates increase the uncertainty of estimates.

We performed Pearson correlations between the wastewater mutation and case isolate variant datasets, comparing the mean ratio of mutations in wastewater (HV69-70 and Del156-157/R158G to the N gene) to the proportion of case isolates sequenced and characterized as Alpha or Delta, each averaged over the previous 14 days. We used 0 as a replacement for samples where the measurement was below the limit of detection (nondetect); we repeated the analysis by using half the detection limit (500 copies/g), and the results were the same. We set statistical significance at $p<0.05$ and performed analyses in R studio version 1.4.1106 (https://www.rstudio.com).

Results

Variant Mutation Assay Specificity and Sensitivity

In silico analysis indicated no cross-reactivity between the assays and deposited sequences in GenBank. When challenged against wild-type gRNA, the respiratory virus panel, and actual or synthetic variant gRNA, no cross-reactivity occurred. Positive controls and no-template controls run on the sample plate performed according to expectations. Variant mutation concentrations were measured in no, low, and high background of wild-type gRNA, which does not contain the mutations. Results of mutation assays in the presence of high and low background wild-type gRNA are similar to their results in the absence of background wild-type gRNA (Appendix Figure 1), indicating that the assays are sensitive and specific.

Variant Mutation Concentrations in Wastewater Solids

Results for positive and negative controls were as expected, and recovery controls indicated consistent RNA recovery from samples and lack of substantial inhibition (Appendix). We measured HV69-70 concentrations up to 1 time/day at San Jose and up to 3 times/week at Sacramento; concentrations ranged from not detected to >10,000 copies/g (Figure 1, 2). N and HV69-70 concentrations at San Jose before 15 Feb 2021 are not presented graphically; samples collected during July and September 2020 did not have measurable HV69-70. HV69-70 was measured for the first time in San Jose solids on November 25, 2020, at concentrations of ≈103 copy/g. We did not detect HV69-70 in Sacramento wastewater solids before late February 2021; results for samples collected in October 2020 (not shown in plot) and late January 2021 were nondetect for HV69-70. At both locations, the concentration of HV69-70 relative to the N gene (HV69-70/N ratio) increased over time beginning in early March 2021, peaked in early June 2021 at San Jose and May 2021 at Sacramento when HV69-70/N was ≈1, and then fell until HV69-70 became undetectable at San Jose and present at very low relative concentrations at Sacramento (0.01) in late July 2021 (Figure 1, 2).

Del156–157/R158G concentrations were measured as frequently as three times per week at both San Jose and Sacramento and ranged from not detected to 100,000 copies/g (Figure 1, 2). We observed Del156-157/R158G nondetects in samples collected before early April 2021 at both sites, and then both sites experienced a small peak in Del156–157/R158G concentration in early to mid-May 2021 (Del156–157/

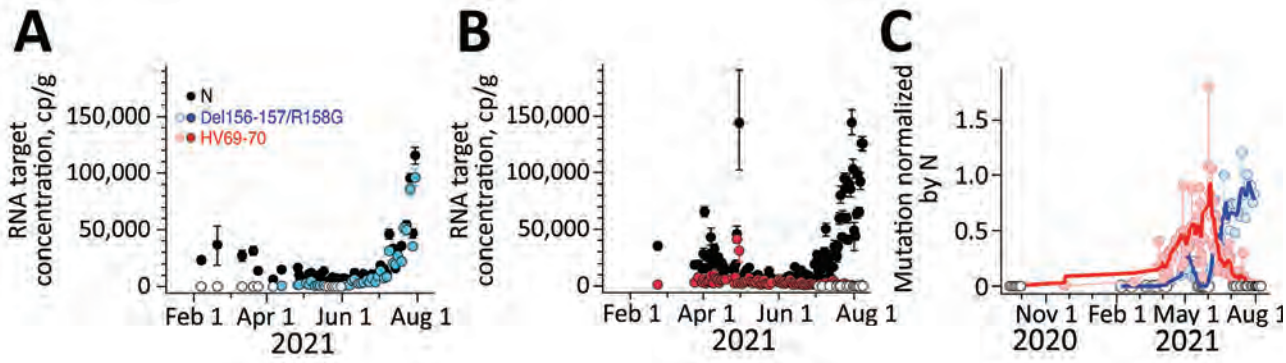

Figure 1. Measurements of severe acute respiratory syndrome coronavirus 2 variants of concern in wastewater solids, San Jose, California, USA. Concentrations of N gene and mutations found in Delta (Del156-157/R158G; panel A), and Alpha (HV69-70; panel B) variants in wastewater solids and their ratio (panel C). Error bars in panels A and B represent SDs derived from the 10 replicates run for each sample; open white circles are nondetects (below the limit of detection) and shown as 0. Errors include technical and replication errors. If error bars are not visible, then errors are smaller than the symbol. Panel C shows smoothed lines for visual reference for mutation ratios. For Del156-157/R158G/N ratio, the smoothed line is a 3-point running average, and for the HV69-70/N ratio, the smoothed line is a 7-point running average; each approximates a weekly average. The timescale for the HV69-70 data (B) is truncated for visualization; additional data on dates before February 15, 2021, are described in the article and shown (C), with the exception of data from July 14, 2020, which was nondetect. N, nucleoprotein.

R158G relative to N ≈0.2–0.3 at the 2 sites), followed by a decline to undetectable levels over ≈2 weeks, followed by a sharp increase until the end of the data series. During this time, N gene concentrations in wastewater increased contemporaneously. The concentration of Del156–157/R158G relative to N (Del156–157/R158G/N ratio) (Figure 1, 2) increased to ≈0.8 at the sites by the end of the data series.

Trends in Variants in Sequenced Case Isolates from Sewersheds

We analyzed trends in Alpha and Delta variants confirmed from case isolates collected from residents (case isolates) of the San Jose and Sacramento sewersheds from early February through late July 2021 (Figure 3). Alpha proportions increased in both sewersheds from early March, peaking in May–June and decreasing in early July. Delta was first identified in isolates in early April and by the end of July accounted for almost all sequenced isolates. In San Jose, a small peak in Delta occurred in May, before a large sustained increase in June; a similar peak is also evident, to a lesser extent, in the Sacramento Delta data. During this period, the 7-day average laboratory-confirmed incident COVID-19 cases ranged from 1 to 30/100,000 population (Appendix Figure 2) in each sewershed. Incident COVID-19 cases in each sewershed is positively and significantly correlated with N gene measurements in the settled solids (Pearson R [r_p] 0.8, df 46–131, $p<10^{-10}$ for both San Jose and Sacramento N gene datasets, regardless of whether they were generated when measuring the Delta or Alpha mutation).

Relationship between Proportion of Alpha and Delta Variants in Case Isolates and Wastewater Mutation Data

We compared ratios of HV69-70 and Del156-157/R158G mutations to the N gene (VOC abundance estimates based on wastewater) against the proportion of all case isolates sequenced and identified as Alpha and Delta variant (VOC abundance estimates based on case isolate sequencing) from each sewershed (Figure 3). Trends of wastewater VOC abundance estimates follow closely and temporally the trends of case isolate sequencing VOC abundance estimates during this period at both sewersheds, including features such as an early peak in Delta in May. Alpha and Delta mutation gene ratios from wastewater were strongly correlated with the corresponding ratios of each VOC from case isolates sequenced: r_p 0.82 ($p<10^{-5}$, df 19 in San Jose) and 0.88 ($p<10^{-7}$, df 21 in Sacramento) for Alpha; r_p 0.97 ($p<10^{-15}$, df 23 for both San Jose and Sacramento) for Delta. When compared to the opposing variant, the mutation gene ratios were not correlated ($p>0.05$ for all).

Completeness of and Delays in Receiving SARS-CoV-2 Isolate Sequence Data

During February 1–August 1, 2021, the total number of case isolates sequenced over a 14-day period in our 2 sewersheds varied (2–520 median for 8% of all sequenced case isolates from San Jose and 6% from Sacramento). Earliest isolate sequencing results were available to CDPH ≈5 days after sample collection date. Approximately 75% of all sequenced isolate results in our dataset were available within 2–3 weeks. As more isolate sequencing data were received, estimated

proportions of VOCs changed over time. Around 3 weeks were required for 95% of VOC estimates (14-day window) to be within 10% of the final estimate.

Discussion

Our results show that the HV69-70 and Del156-157/R158G mutation assays as used for wastewater settled solids were sensitive and specific. By using these PCR mutation assays, we found strong correlation between wastewater estimates and case isolate sequencing–derived estimates of circulating Alpha and Delta in 2 large metropolitan communities in California, USA. Mutations were detected in wastewater samples collected 1–3 weeks earlier than when Alpha and Delta variant estimates generated by case-isolate sequencing were available and reliable. Targeted mutation assays applied to SARS-CoV-2 RNA extracted from wastewater solids can be a rapid, efficient, and reliable way to monitor VOCs introduced to and circulating in a community. Monitoring for VOCs using wastewater may provide earlier complementary surveillance data than from case isolate sequencing data, if mutation assays are or can be developed for new and existing VOCs and put into use in a timely manner.

Use of PCRs targeting characteristic mutations thought to be particular to a SARS-CoV-2 variant may concurrently detect other SARS-CoV-2 strains that carry the same mutations. Targeting a single mutation in wastewater, as was done in our study for Alpha, carries an increased potential risk for mischaracterization. For example, on September 8, 2021, according to GISAID (https://www.gisaid.org), a global repository of case isolate sequence data, 1,043,561 (97%) of the 1,077,360 Alpha (B.1.1.7 and Q sublineages) sequences contained the HV69-70 mutation. However, HV69-70 was also present in other variants, such as B.1.258.19, where it was present in all 141 B.1.258.19 sequences in GISAID, and B.1.617.2, where it was present in 647 (0.2%) of 402,038 sequences. Targeting multiple mutations, as was done in our study with Delta, can increase specificity. Of the 937,570 sequences in GISAID classified as Delta (B.1.617.2 and AY sublineages), 842,354 (90%) have the Del156–157/R158G mutations (referred to as E156G/del157–158 in GISAID). Although this combination of mutations can be present in other variants, it is rarer; the non-Delta variant with the highest percentage of sequences with these mutations is B.1.617.3, for which there were 266 isolates in the global GISAID database and only 77 (29%) possessing these mutations. The non-Delta variant with these mutations for which there are the largest number of isolates in GISAID is B.1.1.7, for which 6 (0.0006%) of the >1,053,637 million sequences have these mutations.

Our findings show that use of mutation assays (HV69-70 for Alpha, Del156-157/R158G for Delta) to estimate circulating variants in wastewater correlated well with estimates from case isolate sequencing data. Wastewater estimates for Alpha, based on a single deletion assay, were robust over time in 2 large municipalities over 8 months (r_p 0.82, $p<10^{-5}$ in San Jose; r_p 0.88, $p<10^{-7}$ in Sacramento), including periods of high (tail of 2020 winter, 2021 summer) and low (2021 spring) community SARS-CoV-2 transmission. Similarly, estimates for Delta, based on multiple mutations, correlated highly with estimates from sequenced case isolates (r_p 0.97, $p<10^{-15}$ for both San Jose

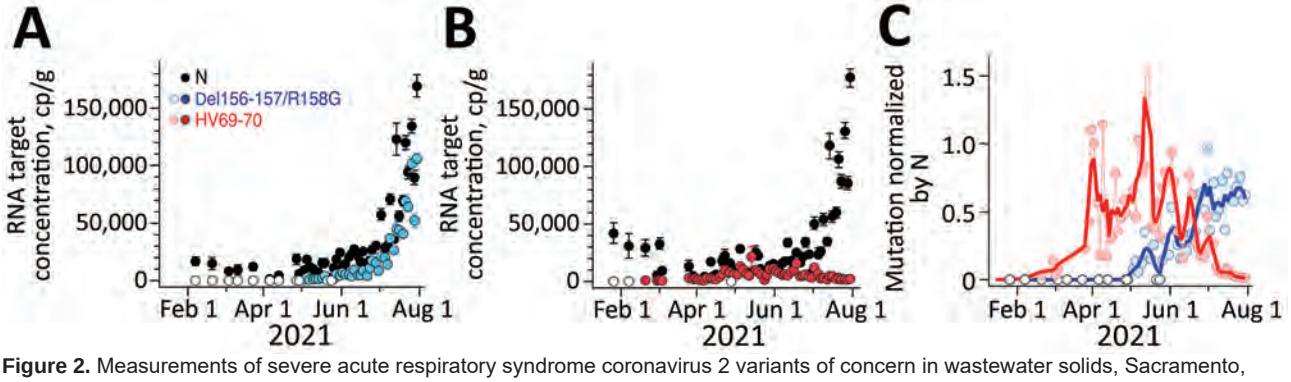

Figure 2. Measurements of severe acute respiratory syndrome coronavirus 2 variants of concern in wastewater solids, Sacramento, California, USA. Concentrations of N gene and mutations found in Delta (Del156-157/R158G; panel A), and Alpha (HV69-70; panel B) severe acute respiratory syndrome coronavirus 2 in wastewater solids and their ratio (panel C). Error bars in panels A and B represent SDs derived from the 10 replicates run for each sample; open white circles are nondetects ((below the limit of detection) and shown as 0. Errors include technical and replication errors. If error bars are not visible, then errors are smaller than the symbol. For Del156-157/R158G/N ratio, the smoothed line is a 3-point running average, and for the HV69-70/N ratio, the smoothed line is a 7-point running average; each approximates a weekly average. The timescale for the HV69-70 data (B) is truncated for visualization; additional data on dates before January 15, 2021, are described in the article and were nondetects. One data point is located beyond the upper bound of the y-axis (C): the value for HV69-70/N on May 14, 2021, was 2.4. N, nucleoprotein.

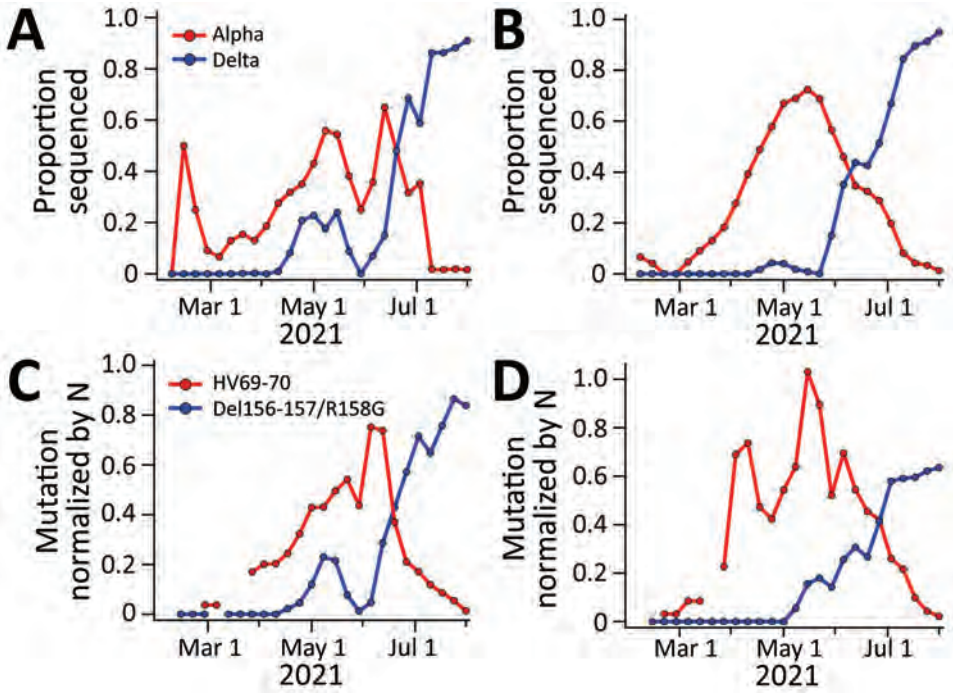

Figure 3. Comparison of severe acute respiratory syndrome coronavirus 2 variants of concern in wastewater solids with coronavirus disease case isolates, San Jose and Sacramento, California, USA, February 1–July 31, 2021. A, B) Proportion of circulating severe acute respiratory syndrome coronavirus 2 attributable to the Alpha and Delta variants, estimated from isolate sequencing data from cases collected and sequenced over the previous 14-day period in San Jose (A) and Sacramento (B) sewersheds. C, D) Concentrations of mutations found in Alpha (HV69-70) and Delta (Del156-157/R158G) variant viruses, normalized by N gene concentrations in wastewater, averaged over the previous 14 days in San Jose (C) and Sacramento (D). No data are shown for dates for which no measurements were made within the previous 14 days. N, nucleoprotein.

and Sacramento). Concurrent monitoring of VOCs in both wastewater and case isolates can confirm whether targeted mutation assays used are correlated with the VOCs being monitored and mitigate risks for misinterpreting wastewater results. Discrepant or divergent estimates between the 2 datasets should be noticeable within weeks and would suggest another variant with the same mutations circulating at abundance, prompting investigation if unexpected.

Emergence of the Omicron VOC in November 2021 (3) provides an excellent example of the importance of interpreting wastewater mutation assay data in the context of case isolate sequencing data. Omicron also includes the HV69-70 mutation. At the time this study was conducted, the HV69-70 mutation, as noted previously, was rarely circulating in non-Alpha variants, suggesting that positive detections likely represented Alpha. However, Alpha disappeared from California circulation by end of summer 2021 and by December 2021, public health concern was for Omicron. With zero Alpha case isolates detected in either sewershed during September 1–December 1, the HV69-70 mutation assay was deployed on wastewater to screen for presence of Omicron, a more likely VOC to emerge in California than Alpha, while a more specific assay was developed (22).

For validated assays deployed in established wastewater sites, wastewater surveillance for VOCs could be an important adjunctive estimate of variant circulation. Because cost and limited genomic testing capacity make sequencing all COVID-19 isolates impractical, especially during times of high case incidence, health departments and decision-makers extrapolate information from relatively small numbers or proportions of sequenced isolates, which may be biased and unrepresentative. For our case dataset, 14-day VOC estimates were derived from as few as 2–20 total case isolates and <1% of total cases sequenced.

Wastewater variant monitoring can overcome biases and delays seen with case isolate sequencing. Because everyone living in a sewershed contributes waste to the system, wastewater monitoring is independent of testing and care accessibility biases and results are more representative of cases in that sewershed. In addition, wastewater mutation assay results are available in a shorter time than VOC estimates from sequencing of case isolates. In our monitored sewersheds, the total average turnaround time from wastewater collection to testing results was <8 hours. In contrast, for our 2 sewersheds, it took 2–3 weeks after sample collection date for 75% of case isolate sequence results to be received and 3 weeks for most 14-day VOC estimates to be within 10% of their final estimate. These delays do not include the additional delay between case symptom onset and test taking that could further accentuate time advantages of wastewater variant monitoring.

Several limitations exist for using wastewater (solids or liquids) for SARS-CoV-2 variant monitoring.

Laboratory limits of detection for SARS-CoV-2 RNA in wastewater and for targeted mutations may result in no detection, especially at times with lower community COVID-19 case counts and consequent lower overall concentrations of SARS-COV-2 RNA in wastewater. However, even in mid-May 2021, when case counts in these 2 sewersheds were as low as 1–2 cases/100,000 population, both SARS-CoV-2 RNA levels and variant abundance could still be measured and accurately estimated. Estimates of circulating Alpha and Delta mutations were also able to be consistently detected even at levels <5% of total SARS-CoV-2 RNA. Limits of detection, both for SARS-CoV-2 and for different mutations associated with variants, are likely to vary depending on laboratory methods used and which mutation is targeted; delineating these limits for each laboratory, sewershed, and assay is important for interpreting what a nondetect result implies about variant circulation.

Because newly identified variants to be monitored require new mutation assays to be designed, the time needed to design, test, and begin using assays is a crucial consideration (Appendix Figure 3). Although the time to design an assay in silico (<1 day) and test its sensitivity and specificity in vitro (3–5 days) is short, the time to receive reagents, including synthesized oligos and positive control RNA, from vendors can take 4–6 weeks because of supply chain issues and increased demand during the pandemic. In addition, before an assay can be designed, variant sequences and mutations must be accurately characterized, which can delay the assay design process. Efforts to develop assays before variants become VOCs and proactively order reagents can help ensure assays are available when needed for public health response.

Monitoring for VOCs will continue to be an important public health function and a need that will become more salient if SARS-CoV-2 testing of cases and sequencing resources or utilization decrease over time. Difficulty in surveillance based on case isolate sequencing, including difficulties attributable to nonrepresentative sampling and delayed results, mean that complementary variant surveillance methods are needed. Detection and monitoring of variants in wastewater has been proposed as an adjunct methodology, and our experiences monitoring for 2 VOCs in 2 large California municipalities support the use of targeted PCR mutation assays as a useful method to estimate abundance of circulating VOCs and inform public health. In conjunction with continued COVID-19 case isolate sequencing, wastewater variant monitoring can be strategically deployed as an adjunct public health surveillance tool.

Acknowledgments

We thanks the many people who contributed to wastewater sample collection, including Srividhya Ramamoorthy, Michael Cook, Ursula Bigler, James Noss, Lisa C. Thompson, Payak Sarkar, Noel un Enoki, and Amy Wong. We also thank the many groups involved in the sequencing of case isolates, including California, Santa Clara, and Sacramento County Public Health departments and the many public, private, and academic laboratories who have dedicated substantial resources towards the understanding of SARS-CoV-2 variants. In addition, we thank the California Department of Public Health COVID-19 Epidemiology and Data teams for their help with COVID-19 data.

Parts of this study were performed at Stanford University, which sits on the ancestral and unceded lands of the Muwekma Ohlone people. We pay our respects to them and their Elders, past and present, and are grateful for the opportunity to live and work here.

This work is supported in part by a gift from the CDC Foundation. This study was supported in part by the Epidemiology and Laboratory Capacity for Infectious Diseases Cooperative Agreement (no. 6NU50CK000539-03-02) from CDC. B.W., D.D., and B.H. are employees of Verily Life Sciences.

About the Author

Dr. Yu is a public health medical officer at the California Department of Public Health, where he works on enteric and waterborne diseases surveillance, as well as on the COVID-19 pandemic response. His research interests include enhanced and environmental surveillance methods for infectious diseases and climate change–related infectious diseases.

References

1. State of California. Tracking COVID-19 in California [cited 2021 Sep 28]. https://covid19.ca.gov/state-dashboard
2. World Health Organization. COVID-19 dashboard [cited 2021 Sep 28]. https://covid19.who.int
3. Centers for Disease Control and Prevention. COVID data tracker [cited 2021 Sep 28]. https://covid.cdc.gov/covid-data-tracker
4. Campbell F, Archer B, Laurenson-Schafer H, Jinnai Y, Konings F, Batra N, et al. Increased transmissibility and global spread of SARS-CoV-2 variants of concern as at June 2021. Euro Surveill. 2021;26:2100509. https://doi.org/10.2807/1560-7917.ES.2021.26.24.2100509
5. Twohig KA, Nyberg T, Zaidi A, Thelwall S, Sinnathamby MA, Aliabadi S, et al.; COVID-19 Genomics UK (COG-UK) consortium. Hospital admission and emergency care attendance risk for SARS-CoV-2 delta (B.1.617.2) compared with alpha (B.1.1.7) variants of concern: a cohort study. Lancet Infect Dis. 2022;22:35–42. https://doi.org/10.1016/S1473-3099(21)00475-8

6. Sanders RW, de Jong MD. Pandemic moves and countermoves: vaccines and viral variants. Lancet. 2021;397:1326–7. https://doi.org/10.1016/S0140-6736(21)00730-3
7. World Health Organization Regional Office for Africa. Weekly bulletin on outbreak and other emergencies: week 39: 21–27 September 2020. 2020 Sep 28 [cited 2021 Sep 28]. https://apps.who.int/iris/handle/10665/335723
8. Walensky RP, Walke HT, Fauci AS. SARS-CoV-2 variants of concern in the United States—challenges and opportunities. JAMA. 2021;325:1037–8. https://doi.org/10.1001/jama.2021.2294
9. World Health Organization Regional Office for Europe. Methods for the detection and identification of SARS-CoV-2 variants, March 2021 [cited 2021 Sep 28]. https://apps.who.int/iris/handle/10665/340067
10. Crits-Christoph A, Kantor RS, Olm MR, Whitney ON, Al-Shayeb B, Lou YC, et al. Genome sequencing of sewage detects regionally prevalent SARS-CoV-2 variants. MBio. 2021;12:e02703–20. https://doi.org/10.1128/mBio.02703-20
11. Izquierdo-Lara R, Elsinga G, Heijnen L, Munnink BBO, Schapendonk CME, Nieuwenhuijse D, et al. Monitoring SARS-CoV-2 circulation and diversity through community wastewater sequencing, the Netherlands and Belgium. Emerg Infect Dis. 2021;27:1405–15. https://doi.org/10.3201/eid2705.204410
12. Bar-Or I, Weil M, Indenbaum V, Bucris E, Bar-Ilan D, Elul M, et al. Detection of SARS-CoV-2 variants by genomic analysis of wastewater samples in Israel. Sci Total Environ. 2021;789:148002. https://doi.org/10.1016/j.scitotenv.2021.148002
13. Kirby AE, Walters MS, Jennings WC, Fugitt R, LaCross N, Mattioli M, et al. Using Wastewater surveillance data to support the COVID-19 response—United States, 2020–2021. MMWR Morb Mortal Wkly Rep. 2021;70:1242–4. https://doi.org/10.15585/mmwr.mm7036a2
14. Wolfe MK, Archana A, Catoe D, Coffman MM, Dorevich S, Graham KE, et al. Scaling of SARS-CoV-2 RNA in settled solids from multiple wastewater treatment plants to compare incidence rates of laboratory-confirmed COVID-19 in their sewersheds. Environ Sci Technol Lett. 2021;8:393–404. https://doi.org/10.1021/acs.estlett.1c00184
15. Peccia J, Zulli A, Brackney DE, Grubaugh ND, Kaplan EH, Casanovas-Massana A, et al. Measurement of SARS-CoV-2 RNA in wastewater tracks community infection dynamics. Nat Biotechnol. 2020;38:1164–7. https://doi.org/10.1038/s41587-020-0684-z
16. Chakraborty C, Bhattacharya M, Sharma AR. Present variants of concern and variants of interest of severe acute respiratory syndrome coronavirus 2: their significant mutations in S-glycoprotein, infectivity, re-infectivity, immune escape and vaccines activity. Rev Med Virol. 2021 Jun 27 [Epub ahead of print]. https://doi.org/10.1002/rmv.2270
17. Wurtzer S, Waldman P, Ferrier-Rembert A, Frenois-Veyrat G, Mouchel JM, Boni M, et al.; OBEPINE consortium. Several forms of SARS-CoV-2 RNA can be detected in wastewaters: Implication for wastewater-based epidemiology and risk assessment. Water Res. 2021;198:117183. https://doi.org/10.1016/j.watres.2021.117183
18. Li B, Di DYW, Saingam P, Jeon MK, Yan T. Fine-scale temporal dynamics of SARS-CoV-2 RNA abundance in wastewater during A COVID-19 lockdown. Water Res. 2021;197:117093. https://doi.org/10.1016/j.watres.2021.117093
19. Graham KE, Loeb SK, Wolfe MK, Catoe D, Sinnott-Armstrong N, Kim S, et al. SARS-CoV-2 RNA in wastewater settled solids is associated with COVID-19 cases in a large urban sewershed. Environ Sci Technol. 2021;55:488–98. https://doi.org/10.1021/acs.est.0c06191
20. Wolfe MK, Topol A, Knudson A, Simpson A, White B, Vugia DJ, et al. High-frequency, high-throughput quantification of SARS-CoV-2 RNA in wastewater settled solids at eight publicly owned treatment works in northern California shows strong association with COVID-19 incidence. mSystems. 2021;6:e0082921. https://doi.org/10.1128/mSystems.00829-21
21. Rambaut A, Holmes EC, O'Toole Á, Hill V, McCrone JT, Ruis C, et al. A dynamic nomenclature proposal for SARS-CoV-2 lineages to assist genomic epidemiology. Nat Microbiol. 2020;5:1403–7. https://doi.org/10.1038/s41564-020-0770-5
22 KQED News. Scientists find traces of Omicron in sewage from Sacramento and Merced [cited 2021 Dec 8]. https://www.kqed.org/news/11898161/scientists-find-traces-of-omicron-in-sewage-from-sacramento-and-merced

Address for correspondence: Alexander T. Yu, California Department of Public Health, 850 Marina Bay Pkwy, Building P, Richmond, CA 94804, USA; email: alexander.yu@cdph.ca.gov

Effectiveness of BNT162b2 Vaccine Booster against SARS-CoV-2 Infection and Breakthrough Complications, Israel

Aharona Glatman-Freedman, Michal Bromberg, Yael Hershkovitz, Hanna Sefty, Zalman Kaufman, Rita Dichtiar, Lital Keinan-Boker

We estimated vaccine effectiveness (VE) of the BNT162b2 (Pfizer-BioNTech, https://www.pfizer.com) booster dose against SARS-CoV-2 infection and reduction of complications (hospitalization, severe disease, and death) among breakthrough cases in persons in Israel ≥16 years of age for ≤20 weeks. VE estimates reached 96.8% (95% CI 96.0%–97.5%) for persons 16–59 years of age and 93.1% (95% CI 91.8%–94.2%) for persons ≥60 years of age on week 3. VE estimates remained at these levels for 8 weeks in the 16–59 age group and 11 weeks in those ≥60. A slow decline followed, becoming more pronounced in the last 2–3 weeks of evaluation. Estimates in the last week of evaluation were 77.6% (95% CI 68.4%–84.2%) and 61.3% (52.5%–68.4%) for persons 16–59 years and ≥60 years , respectively. The more pronounced VE decline coincided with rapid increase in Omicron variant activity. Rate reduction of breakthrough complications remained moderate to high throughout the evaluation.

The mass severe acute respiratory syndrome coronavirus 2 (SARS-CoV-2) BNT162b2 (Pfizer-BioNTech, https://www.pfizer.com) vaccination campaign in Israel was associated with a decline in the number of SARS-CoV-2 infections, hospitalizations, and deaths, reaching a nadir by mid-May 2021 (*1*). However, beginning the third week of June 2021, a new rise in the number of SARS-CoV-2 cases was observed, including cases among fully vaccinated persons (*1*,*2*). Waning humoral immune response after the second vaccine dose was then found to be associated with increased incidence of SARS-CoV-2–related infections, hospitalizations, and deaths caused primarily by the B.1.617.2 (Delta) variant (*3*). In response to the increasing illness and deaths, the Israel Ministry of Health (MOH) recommended a third (booster) BNT162b2 vaccine dose for persons for whom at least 5 months had passed after receiving the second vaccine dose (*4*). The elderly and other high-risk groups were prioritized at first (*4*), and other age groups were added rapidly thereafter (*5*). We estimated the booster dose vaccine effectiveness (VE) against SARS-CoV-2 infection and the rate reduction of complications in breakthrough coronavirus disease (COVID-19) cases after the BNT162b2 booster dose in persons ≥16 years of age, by age group, for up to 20 weeks after receipt of the booster dose.

Author affiliations: Tel Aviv University School of Public Health, Tel Aviv, Israel (A. Glatman-Freedman, M. Bromberg); Israel Center for Disease Control, Ministry of Health, Ramat Gan, Israel (A. Glatman-Freedman, M. Bromberg, Y. Hershkovitz, H. Sefty, Z. Kaufman, R. Dichtiar, L. Keinan-Boker); Haifa University School of Public Health, Haifa, Israel (L. Keinan-Boker)

DOI: https://doi.org/10.3201/eid2805.220141

Methods

Study Design

We conducted a retrospective longitudinal cohort study using 2 MOH national repositories: the COVID-19 vaccine repository and the SARS-CoV-2 test repository. The national COVID-19 vaccine repository includes vaccine type, vaccine lot number, and date of dose administration for each person vaccinated in Israel. The national SARS-CoV-2 PCR test database includes the results of each test performed, the date of testing, and the date results were obtained for each person. It also includes the date of hospitalization, severity of illness, and date of death of persons with COVID-19, if applicable. Personal identifiers such as unique personal identity number, age, and sex of each person registered in the repositories (because of PCR testing or vaccination) are included in both databases. We retrieved individual deidentified data from both databases and matched

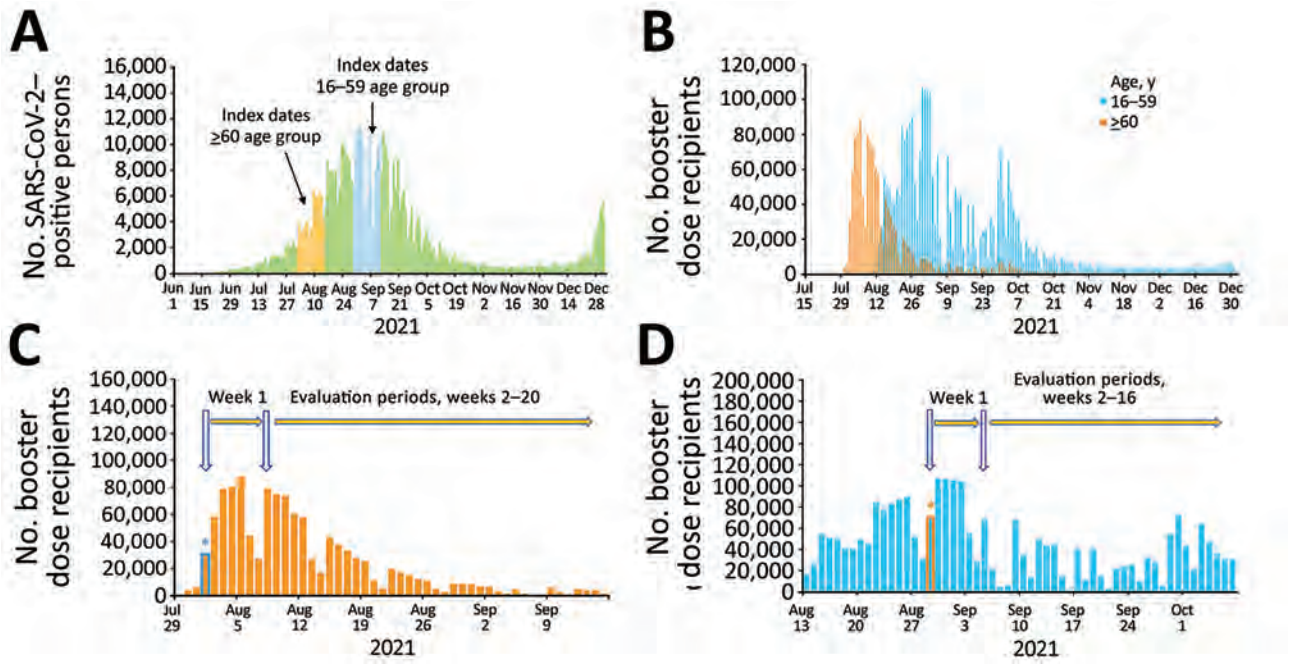

Figure 1. Estimations of effectiveness of BNT162b2 vaccine booster (Pfizer, https://www.pfizer.com) against SARS-CoV-2 infection and breakthrough complications, Israel. A) Epidemic curve of new PCR-confirmed SARS-CoV-2–positive persons, June 1, 2021–January 1, 2022. Index dates are highlighted in orange (for persons ≥60 years of age) and light blue (for persons 16–59 years of age). B) Daily booster dose recipients by age group. C) Graphic illustration of the booster dose vaccine effectiveness evaluation method for a single cohort of persons ≥60 years of age that received the booster dose on August 1, 2021. Orange bars represent the number of persons who received the booster dose each day; light blue asterisk represents the date persons ≥60 years of age included in cohort 1 received the booster dose. D) Graphic illustration of the booster dose vaccine effectiveness evaluation method for a single cohort of persons 16–59 years of age who received the booster dose on August 29, 2021. Light blue bars represent the number of persons who received the booster dose each day; orange asterisk represents the date persons 16–59 years of age included in cohort 1 received the booster dose.

persons by using twice-encrypted unique personal identity numbers.

During the first stage of our study, we determined VE for booster dose vaccine recipients against SARS-CoV-2 infection by using unvaccinated persons as controls. During the second stage, we determined the rate reduction for hospitalizations, severe or critical disease, and deaths among persons who tested positive for SARS-CoV-2 after the booster dose (i.e., breakthrough cases).

We defined as index dates the dates on which third-dose vaccine recipients in our study received the booster dose (Figure 1, panel A). Booster dose recipients and unvaccinated controls included in each index date represented a single cohort. We performed analyses for persons 16–59 years of age across 14 consecutive cohorts with the index dates August 29, 2021–September 11, 2021. These dates were selected because, by that period, persons 16–59 years of age had already been approved by the MOH to receive the booster dose (Appendix Figure 1). Analyses for persons ≥60 years of age were performed across 14 consecutive cohorts with index dates occurring during August 1, 2021–August 14, 2021. These dates were chosen for this age group because this group was the first to receive the booster dose (Figure 1, panel B) and because most persons ≥60 years of age received the third dose before August 29, 2021 (Appendix Figure 1). We followed each cohort through January 1, 2022.

Estimation of VE

We excluded residents of Israel who tested positive for SARS-CoV-2 by PCR before the evaluation periods from the analyses (Appendix Table 1, Figures 2, 3). We estimated VE for the 16–59-year and ≥60-year age groups, as well as for age groups 16–29 years, 30–39 years, 40–49 years, and 50–59 years (Appendix Figures 2, 3). We first estimated VE for each cohort starting week 2 after the index date. We then estimated VE for all 14 cohorts combined. Because of the different index dates for these age groups, we followed persons 16–59 years of age for 16 weeks and persons ≥60 years of age for 20 weeks (Figure 1, panels C, D; Appendix Table 2).

Hospitalizations, Severe Disease, and Death among SARS-CoV-2–Positive Booster Dose Recipients

We determined rates of SARS-CoV-2–related hospitalizations, severe or critical disease, and deaths for booster-dose recipients and for unvaccinated persons who tested positive for SARS-CoV-2 by PCR during the evaluation period described previously (breakthrough cases). The time allotted for the occurrence of hospitalization and severe or critical disease after the first positive PCR test was 14 days (*6*). We did not set a time limit for death after the first positive PCR test. We determined disease severity in accordance with US National Institutes of Health guidelines (*7*).

Statistics

We determined VE and 95% CI using the formula (1 – incidence rate ratio [IRR]) × 100. The IRR represents the ratio of PCR-confirmed SARS-CoV-2 infection rate in the group of booster-dose recipients to the corresponding rate in the unvaccinated control group. For persons who tested positive for SARS-CoV-2 by PCR several times during the evaluation period, we included only the first positive test result in the analysis.

We excluded persons who had a positive SARS-CoV-2 PCR test before the evaluation periods from the analysis, regardless of their vaccination status. Unvaccinated persons included in the study who were vaccinated during the cohort evaluation period were censored (removed from the study) on their vaccination dates.

We computed the number of unvaccinated controls by age and sex for each cohort by subtracting the number of residents of Israel, by age and sex, who were vaccinated with any number of BNT162b2 vaccine doses before or on the cohort vaccination date (index date) from the number of residents who did not have a recorded positive SARS-CoV-2 PCR test by that date. We calculated the number of person-days each person contributed as unvaccinated during each evaluation period. The number of residents (total, by age and by sex) was based on the 2021 Central Bureau of Statistics statistical abstract (*8*). We took into account unvaccinated participants who were included in >1 cohort when calculating VEs and CIs.

VE was first calculated for each age group daily cohort by week starting the second week after the booster dose. VE was estimated separately for each week that passed since the index date. For the combined VE estimate (for all 14 cohorts together), we took several steps. First, we summed the number of booster-vaccinated and unvaccinated SARS-CoV-2–positive cases for the evaluation period. Second, we counted the days at risk for each age-group cohort on the basis of the number of person-days for each booster-vaccinated and unvaccinated person from the start of the study until the person became SARS-CoV-2–positive or until the end of follow-up, whichever date was earlier. Third, we summed the days at risk for each age group cohort during the evaluation period to provide the total number of person-days at risk in the booster-vaccinated or unvaccinated status for all age group cohorts. Finally, we calculated IRR for the age group cohorts combined.

We evaluated the reduction in SARS-CoV-2–related hospitalizations, illness severity during hospitalizations, and death in persons who received 3 BNT162b2 vaccine doses compared with unvaccinated persons using the formula (1 – IRR) × 100. We performed adjustment of IRR and 95% CI for age group (16–29, 30–39, 40–49, and 50–59 years for persons 16–59 years of age; 60–79 and ≥80 years for persons ≥60 years of age), sex and epidemiologic week, provided the data sizes were sufficiently large, by using Poisson regression. Statistical analysis was performed using SAS Enterprise Guide 7.1 software (SAS Institute, https://www.sas.com). The study was approved by the superior ethical committee of the Israel MOH (protocol no. CoR-MOH-081–2021) with exemption from informed consent.

Results

Booster Dose Vaccination Campaign

By October 31, 2021, persons ≥60 years of age reached a vaccination rate of ≈80% (Appendix Figure 1). Vaccination rates by that date were 70.2% for the 50–59-year age group, 62.4% for the 40–49-year age group, 53.1% for the 30–39-year age group, and 44.7% for the 16–29-year age group (Appendix Figure 1).

Booster Dose VE in Persons 16–59 Years of Age

Adjusted VE point estimates reached 92.8% (95% CI 91.3%–94.0%) in week 2 of the evaluation period and 96.8% (95% CI 96.0%–97.5%) by week 3 (Figure 2, panel A; Appendix Table 3). The adjusted VE remained above 95% until week 10 and thereafter started to slowly decline, reaching VE of 89.6% (95% CI 85.4%–92.7%) in week 14. In weeks 15 and 16, VE point estimates declined by 12%, reaching a point estimate of 77.6% (95% CI 68.4%–84.2%) (Figure 2, panel A; Appendix Table 3). The evaluation dates of weeks 15 and 16 occurred during December 2021 (Appendix

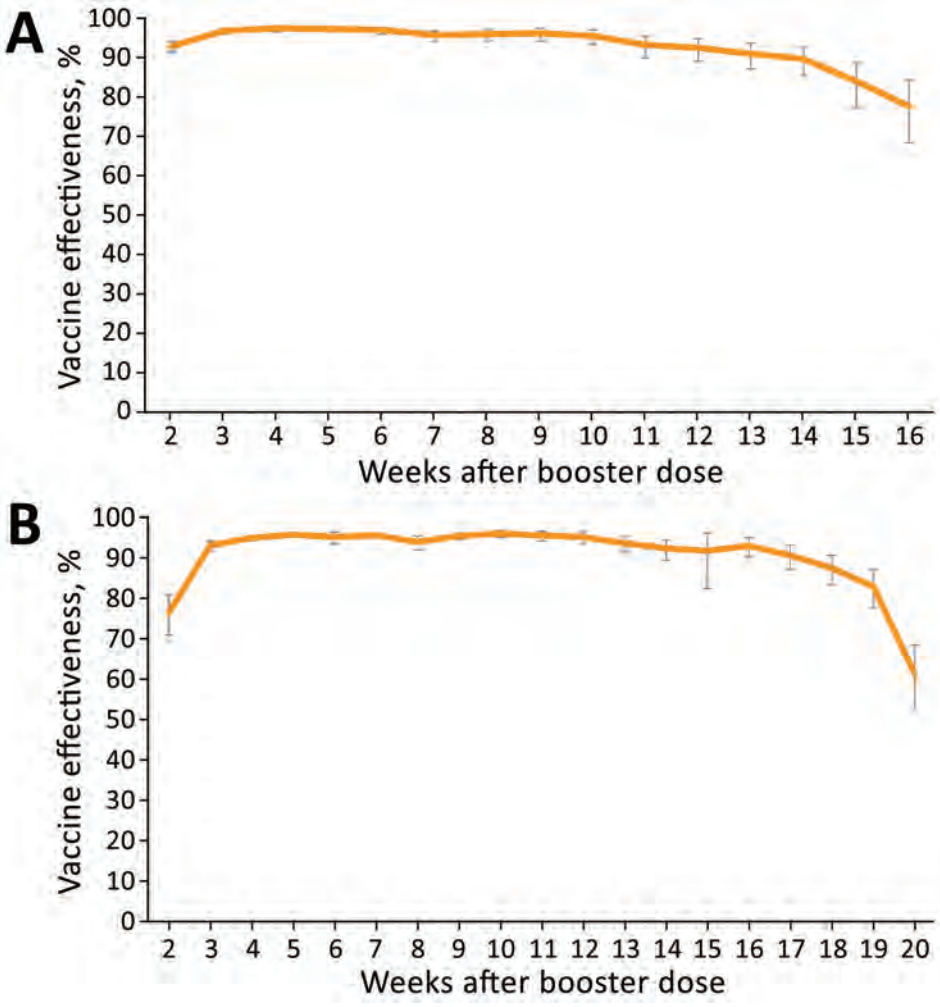

Figure 2. Adjusted vaccine effectiveness against severe acute respiratory syndrome coronavirus 2 infection in persons 16–59 years of age, by week, September 6, 2021–January 1, 2022 (A), and ≥60 years of age, by week, August 9, 2021–January 1, 2022 (B), Israel. Adjustments were performed for sex, age, and epidemiologic week. Error bars represent 95% CIs.

Table 2), when the percentage of the B.1.1.529 (Omicron) variant among reported sequenced samples in Israel rapidly increased (Figure 3) (*9*). VE estimation by age groups demonstrated similar patterns (Appendix Figure 4).

Booster Dose VE in Persons ≥60 Years of Age

Adjusted VE point estimates reached 76.4% (95% CI 70.9%–80.9%) on week 2 of the evaluation period and 93.1% (95% CI 91.8%–94.2%) by week 3 (Figure 2, panel B; Appendix Table 3). The adjusted VE remained above

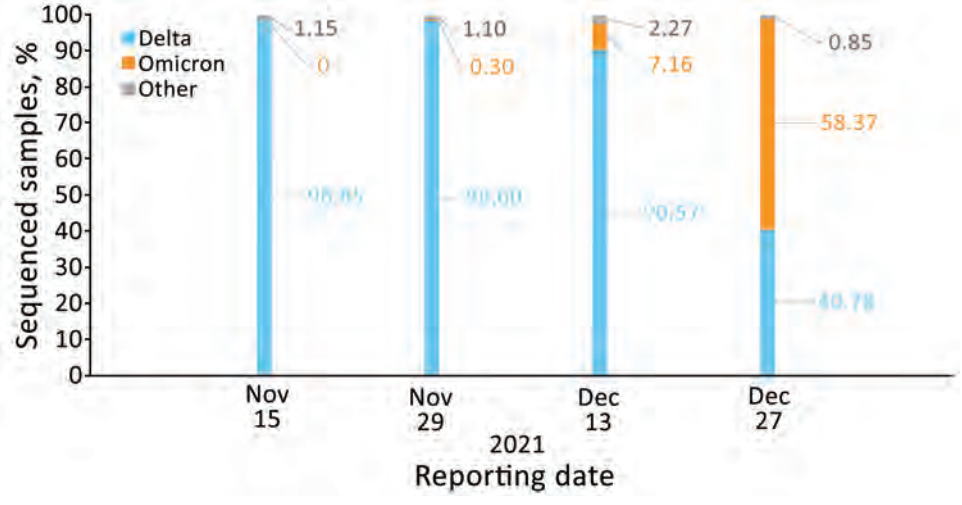

Figure 3. Percentage of sequenced severe acute respiratory syndrome coronavirus 2 samples by variant and reporting date, Israel, November 15, November 29, December 13, and December 27, 2021. Based on (*9*). Numbers within the figure represent percentages of sequenced samples.

93% until week 13, and thereafter started to slowly decline, reaching VE of 90.6% (95% CI 87.2%–93.1%) at week 17. In weeks 18 and 19, VE point estimates declined by 7% and in week 20, VE declined by 21.6%, reaching a point estimate of 61.3% (95% CI 52.5%–68.4%) (Figure 2, panel B; Appendix Table 3). The evaluation dates of weeks 19 and 20 occurred during December 2021 (Appendix Table 2), when the percentage of the B.1.1.529 (Omicron) variant among reported sequenced samples in Israel rapidly increased (Figure 3) (*9*).

Hospitalizations among SARS-CoV-2–Positive Booster Dose Vaccine Recipients

We analyzed rate reductions of hospitalizations among persons who became SARS-CoV-2-positive by week and for all evaluation weeks combined (Table 1). The hospitalization rate reduction by week for persons 16–59 years of age was between 62.8% (95% CI −0.6% to 86.2%) and 100.0%. The combined rate reduction for weeks 2–16 was 89.2% (95% CI 79.1%–94.4%) (Table 1).

The hospitalization rate reduction by week for persons ≥60 years of age was between 54.9% (95% CI −35.9 to 85.1%) and 95.0% (95% CI 72.1%–99.1%). The combined rate reduction for weeks 2–20 was 75.1% (95% CI 71.3%–78.5%) (Table 1).

Severe Disease among SARS-CoV-2–Positive Booster Dose Vaccine Recipients

The severe or critical disease rate reduction for persons 16–59 years of age was 92.0% (95% CI 70.0%–97.9%) on week 2 (Table 2). No cases of severe or critical disease were recorded among booster-dose recipients for weeks 3–16. The combined rate reduction for weeks 2–16 was 97.3% (95% CI 89.7%–99.3%) (Table 2).

Table 1. Rate reduction of hospitalizations among SARS-CoV-2–positive persons who received the BNT162b2 COVID-19 vaccine booster dose, Israel*

Age group, y	Time of first positive SARS-CoV-2 PCR test after index date, wk	Unvaccinated SARS-CoV-2–positive persons		Vaccinated SARS-CoV-2–positive persons		Adjusted 1 – IRR, % (95% CI)†
		Hospitalized	Total	Hospitalized	Total	
16–59	2	889	22,545	4	1,343	92.2 (77.9–97.3)
	3	770	18,232	3	455	83.9 (46.7–95.1)
	4	590	12,962	2	293	84.6 (47.1–95.5)
	5	414	8,555	1	210	90.1 (44.5–98.2)
	6	259	5,531	1	138	84.3 (15.1–97.1)
	7	175	3,573	0	131	100.0
	8	120	2,626	1	83	74.0 (−52.5 to 95.6)
	9	92	2,013	0	54	100.0
	10	72	1,714	0	57	100.0
	11	69	1,401	0	66	100.0
	12	68	1,385	0	90	100.0
	13	72	1,442	0	118	100.0
	14	62	1,569	1	154	84.4 (5.9–97.4)
	15	64	2,145	4	351	62.8 (−0.6 to 86.2)
	16	71	4,088	1	884	94.0 (47.9–99.3)
	2–16 combined	1,662	41,135	18	4,427	89.2 (79.1–94.4)
>60	2	644	1,985	98	1,314	77.5 (71.5–82.3)
	3	666	2,200	39	464	73.0 (64.4–79.5)
	4	647	2,160	36	375	68.2 (52.7–78.6)
	5	619	2,164	25	319	73.2 (48.2–86.2)
	6	593	2,033	20	296	77.3 (62.5–86.3)
	7	501	1,724	29	271	64.5 (50.2–74.7)
	8	375	1,276	23	221	65.3 (40.2–79.9)
	9	254	869	6	147	86.7 (72.6–93.6)
	10	163	577	10	86	64.1 (27.1–82.3)
	11	108	376	9	63	54.9 (−35.9 to 85.1)
	12	80	258	4	44	71.0 (21.5–89.3)
	13	56	208	3	52	80.2 (54.4–91.4)
	14	56	183	3	49	81.9 (45.8–94.0)
	15	58	170	6	47	67.5 (32.6–84.4)
	16	53	162	5	44	65.7 (23.4–84.6)
	17	46	151	1	56	94.4 (57.3–99.2)
	18	42	147	1	69	95.0 (72.1–99.1)
	19	38	184	5	125	82.6 (57.7–92.8)
	20	46	305	13	432	81.4 (67.0–89.5)
	2–20 combined	1,976	6,673	336	4,474	75.1 (71.3–78.5)

*COVID-19, coronavirus disease; IRR, incidence rate ratio; SARS-CoV-2, severe acute respiratory syndrome coronavirus 2.
†Adjusted for sex and epidemiologic week.

Table 2. Rate reduction of severe or critical disease among SARS-CoV-2–positive persons who received the BNT162b2 COVID-19 vaccine booster dose, Israel*

Age group, y	Time of first positive SARS-CoV-2 PCR test after index date, wk	Unvaccinated SARS-CoV-2–positive persons		Vaccinated SARS-CoV-2–positive persons		Adjusted 1 – IRR, % (95% CI)†
		Severe or critical disease	Total	Severe or critical disease	Total	
16–59	2	422	22,545	2	1,343	92.0 (70.0–97.9)
	3	358	18,232	0	455	100.0
	4	262	12,962	0	293	100.0
	5	170	8,555	0	210	100.0
	6	113	5,531	0	138	100.0
	7	63	3,573	0	131	100.0
	8	40	2,626	0	83	100.0
	9	32	2,013	0	54	100.0
	10	27	1,714	0	57	100.0
	11	29	1,401	0	66	100.0
	12	24	1,385	0	90	100.0
	13	25	1,442	0	118	100.0
	14	21	1,569	0	154	100.0
	15	30	2,145	0	351	100.0
	16	30	4,088	0	884	100.0
	2–16 combined	727	41,135	2	4,427	97.3 (89.7–99.3)
≥60	2	450	1,985	56	1,314	81.9 (75.4–86.7)
	3	470	2,200	27	464	73.5 (61.0–82.0)
	4	464	2,160	18	375	77.8 (63.1–86.8)
	5	469	2,164	15	319	78.9 (66.8–86.6)
	6	447	2,033	9	296	86.6 (74.2–93.0)
	7	390	1,724	12	271	81.4 (63.1–90.6)
	8	299	1,276	13	221	75.6 (54.1–87.0)
	9	207	869	2	147	94.6 (85.3–98.0)
	10	128	577	9	86	58.6 (11.1–80.7)
	11	78	376	2	63	86.2 (39.1–96.9)
	12	52	258	3	44	69.0 (−15.3 to 91.7
	13	40	208	1	52	91.0 (63.8–97.8)
	14	42	183	2	49	84.0 (44.8–95.3)
	15	45	170	3	47	78.5 (49.3–90.8)
	16	37	162	3	44	70.3 (30.0–87.4)
	17	32	151	1	56	91.7 (43.4–98.8)
	18	28	147	0	69	100.0
	19	33	184	4	125	83.6 (47.0–94.9)
	20	42	305	7	432	89.0 (75.8–95.0)
	2–20 combined	1,465	6,673	187	4,474	81.6 (78.3–84.3)

*COVID-19, coronavirus disease; IRR, incidence rate ratio; SARS-CoV-2, severe acute respiratory syndrome coronavirus 2.
†Adjusted for sex and epidemiologic week.

The rate reduction of severe or critical disease by week for persons ≥60 years of age was between 58.6% (95% CI 11.1%–80.7%) and 100%. The combined rate reduction for weeks 2–20 was 81.6% (95% CI 78.3%–84.3%) (Table 2).

Deaths among SARS-CoV-2-Positive Booster Dose Vaccine Recipients

No deaths were recorded among booster-dose recipients 16–59 years of age during the evaluation weeks, compared with 1–45 deaths per week in the unvaccinated group, a rate reduction of 100% (Table 3). The death rate reduction by week for persons ≥60 years of age was between 49.1% (95% CI −44.3% to 82.1%) and 100%. The combined rate reduction for weeks 2–20 was 77.1% (95% CI 71.2%–81.8%) (Table 3). Analysis of death rate reduction by using only deaths that were highlighted by hospitals as deaths caused by COVID-19 and limiting the time from positive PCR test to death by up to 28 days yielded similar results (Appendix Tables 4, 5).

Discussion

Our results demonstrate that, after the BNT16b2 booster dose, VE against SARS-CoV-2 infection reached levels that were observed shortly after the second vaccine dose (*6*). VE point estimates of >90% were observed in week 2 in persons 16–59 years of age and in week 3 in persons ≥60 years of age. Similar delay in achieving high VE among elderly persons was also shown after the second BNT162b2 vaccine dose (*6*). Highest-level VE was maintained for up to 11 weeks, as shown in persons ≥60 years of age included in our study. The decline in VE that occurred afterward was initially mild, still maintaining VE point estimates ≥90% for up to week 17 of the evaluation period in persons ≥60 years

of age. The decline in VE became steeper during the last 2 weeks of the evaluation period.

The B.1.617.2 (Delta) variant was the most prevalent variant in Israel through November 2021. However, the last 2 evaluation weeks, which occurred in December 2021 (Appendix Table 2), coincided with the beginning of a new wave of illness and the sharp rise in the B.1.1.529 (Omicron) variant in Israel. Waning immunity was shown several months after the second BNT162b2 vaccine dose (*2*,*3*,*10*) and was temporarily associated with the rise of the B.1.617.2 (Delta) variant in Israel. However, a fresh 2-dose BNT162b2 vaccination regimen was found to be highly effective against the B.1.617.2 (Delta) variant (*1*).

Early evaluations suggest that VE of 2 doses of the BNT162b2 against B.1.1.529 (Omicron) variant–related infection, symptomatic disease, and hospitalizations was reduced compared with VE against the B.1.617.2 (Delta) variant (*11*,*12*; C.H. Hansen et al., unpub. data, https://www.medrxiv.org/content/10.1101/2021.12.20.21267966v3; N. Andrews et al., unpub. data, https://www.medrxiv.org/content/10.1101/2021.12.14.21267615v1). VE of the BNT162b2 booster dose against infection and symptomatic disease caused by the B.1.1.529 (Omicron) variant was also lower than for the B.1.617.2 (Delta) variant (*11*; C.H. Hansen et al., unpub. data; N. Andrews et al., unpub. data). The difference in VE against the B.1.1.529 (Omicron) and B.1.617.2 (Delta) variants increased as time passed from booster dose administration (*11*). Therefore, the steeper decrease in the 3-dose VE in the last 2 weeks of our study period could be caused, at least in part, by the rapid spread of the B.1.1.529 (Omicron) variant in Israel.

Several studies have evaluated the shorter-term effect of the BNT162b2 booster dose on SARS-CoV-2 infection and complications (*13*–*17*; N. Andrews et al., unpub. data, https://www.medrxiv.org/content/

Table 3. Rate reduction of deaths among SARS-CoV-2–positive persons who received the BNT162b2 COVID-19 vaccine booster dose, Israel*

Age group, y	Time of first positive SARS-CoV-2 PCR test after index date, wk	Unvaccinated SARS-CoV-2–positive persons		Vaccinated SARS-CoV-2–positive persons		Adjusted 1 – IRR, % (95% CI)†
		Deaths	Total	Deaths	Total	
16–59	2	45	22,545	0	1,343	100
	3	36	18,232	0	455	100
	4	27	12,962	0	293	100
	5	17	8,555	0	210	100
	6	11	5,531	0	138	100
	7	6	3,573	0	131	100
	8	5	2,626	0	83	100
	9	4	2,013	0	54	100
	10	3	1,714	0	57	100
	11	3	1,401	0	66	100
	12	3	1,385	0	90	100
	13	2	1,442	0	118	100
	14	1	1,569	0	154	100
	15	1	2,145	0	351	100
	16	1	4,088	0	884	100
	2–16 combined	72	41,135	0	4,427	100
≥60	2	243	1,985	31	1,314	81.9 (70.4–88.9)
	3	246	2,200	13	464	76.0 (55.3–87.2)
	4	226	2,160	13	375	68.1 (49.6–79.8)
	5	229	2,164	11	319	68.7 (42.7–82.9)
	6	201	2,033	7	296	76.5 (55.9–87.4)
	7	166	1,724	8	271	70.5 (29.4–87.7)
	8	122	1,276	8	221	63.1 (29.4–80.7)
	9	89	869	2	147	87.6 (53.7–96.7)
	10	59	577	5	86	49.1 (−44.3 to 82.1)
	11	30	376	0	63	100.0
	12	19	258	1	44	67.7 (−189.8 to 96.4)
	13	19	208	1	52	78.7 (−89.9 to 97.6)
	14	22	183	1	49	85.0 (8.5–97.5)
	15	21	170	1	47	85.3 (−21.3 to 98.2)
	16	17	162	0	44	100.0
	17	11	151	1	56	74.6 (−225.9 to 98.0)
	18	10	147	0	69	100.0
	19	7	184	2	125	56.5 (−144.3 to 92.3)
	20	8	305	3	432	70.7 (−2.7 to 91.7)
	2–20 combined	686	6,673	108	4,474	77.1 (71.2–81.8)

*COVID-19, coronavirus disease; IRR, incidence rate ratio; SARS-CoV-2, severe acute respiratory syndrome coronavirus 2.
†Adjusted for sex and epidemiologic week.

10.1101/2021.11.15.21266341v1) and found that a high degree of protection was achieved. Some of these studies used booster-eligible 2-dose vaccine recipients as controls (*13*–*15*,*17*), but our study evaluated VE by using unvaccinated persons as controls. Booster dose VE analysis using unvaccinated persons as controls is paramount, because the baseline VE against SARS-CoV-2 for booster dose recipient is >0%, and time to eligibility for a booster dose might vary among countries. Furthermore, our analysis shows the magnitude of protection offered by the booster dose in a manner that enables easy comparison with other VE studies.

Analyzing the reduction in complications among SARS-CoV-2 vaccine recipients is crucial for public health policy. Our results demonstrated substantial protection from complications among booster-dose vaccine recipients throughout the evaluation period and, further, suggest that this protection may be higher than the protection found shortly after the receipt of the second dose (*6*). Although a study from a health maintenance organization in Israel demonstrated VE estimates of 93% against hospitalizations, 92% against severe disease, and 81% against death (*15*), such analysis cannot distinguish between complications averted because of reductions in SARS-CoV-2 infections and reduction of complications among breakthrough cases. Further analysis is necessary to determine whether rate reductions of complications in booster-dose recipients are affected by the spread of the B.1.1.529 (Omicron) variant and whether those rate reductions are waning over time.

Our study's first limitation is that the size of the unvaccinated control study group was calculated on the basis of Israel Central Bureau of Statistics data. Nevertheless, these data included population size by sex and age, which enables statistical adjustment. Furthermore, data concerning hospitalizations, disease severity, and deaths were available in the SARS-CoV-2 PCR test repository for unvaccinated SARS-CoV-2–positive persons. The lack of information regarding the presence of comorbidities constitutes another limitation. However, the use of multiple cohorts, the size of the population included in our study, the consistent VE estimates among various age groups, and the successful use of similar methodology in previous SARS-CoV-2 VE studies (*1*,*6*) support the validity of our results.

In this evaluation, we did not estimate VE against symptomatic disease. When the number of PCR-positive persons increases, the ability to conduct epidemiologic investigation and determine whether symptoms were present greatly diminishes. A further limitation was the low number of weekly complications in SARS-CoV-2–positive persons, particularly in weeks of lower SARS-CoV-2 circulation (Tables 1–3). However, this limitation was less evident among persons ≥60 years of age, for whom the number of weekly complications is higher than for persons 16–59 years of age.

SARS-CoV-2 PCR testing and vaccination practices could vary among persons. Such differences can stem from behavior, occupation (such as being a healthcare worker), or health factors (such as having symptoms or risk factors or residing in a nursing home) and can potentially affect VE estimates against infection. Because SARS-CoV-2 PCR testing has been commonly performed among hospitalized patients, determination of reductions in hospitalizations, severe or critical disease, and death rate were probably not affected by factors that might affect testing practices of nonhospitalized patients.

No distinction was available in the MOH SARS-CoV-2 data repository between persons who were hospitalized because of COVID-19 and those who were hospitalized because of other reasons and were SARS-CoV-2–positive. However, the severity status that is registered in the repository is given to COVID-19 patients on the basis of National Institutes of Health guidelines (*7*).

In conclusion, our results showing high VE of the BNT162b2 booster dose against SARS-CoV-2 cases and the maintenance of positive effects among breakthrough cases demonstrate the duration of the booster-dose effect during a period in which the Delta variant was predominant. However, the reduced VE in an Omicron-variant setting indicates that additional tools are required to combat new variants of concern.

A.G.-F. and L.K.-B. conceived the study. A.G.-F. designed the study, wrote the protocol, led data analysis, and wrote the first draft of the manuscript. Y.H. and R.D. retrieved the data and performed data analysis. H.S. and Z.K. drafted the figures and tables with input from A.G.-F. A.G.-F., M.B., L.K.-B., H.S., and Z.K. interpreted the data and edited the final manuscript. Y.H. and R.D. verified the underlying data. All authors revised the manuscript critically for important intellectual content and approved the final manuscript.

About the Author

Dr. Glatman-Freedman is the department director of infectious diseases at the Israel Center for Disease Control and is affiliated academically with the School of Public Health at Tel Aviv University. Her primary research interests are the epidemiology of respiratory viruses, syndromic surveillance, and vaccine effectiveness.

References

1. Glatman-Freedman A, Hershkovitz Y, Kaufman Z, Dichtiar R, Keinan-Boker L, Bromberg M. Effectiveness of BNT162b2 vaccine in adolescents during outbreak of SARS-CoV-2 Delta variant infection, Israel, 2021. Emerg Infect Dis. 2021;27:2919–22. https://doi.org/10.3201/eid2711.211886
2. Goldberg Y, Mandel M, Bar-On YM, Bodenheimer O, Freedman L, Haas EJ, et al. Waning immunity after the BNT162b2 vaccine in Israel. N Engl J Med. 2021;385:e85. https://doi.org/10.1056/NEJMoa2114228
3. Levin EG, Lustig Y, Cohen C, Fluss R, Indenbaum V, Amit S, et al. Waning immune humoral response to BNT162b2 COVID-19 vaccine over 6 months. N Engl J Med. 2021;385:e84. https://doi.org/10.1056/NEJMoa2114583
4. Israel Ministry of Health. The vaccination advisory committee presented data and recommended the administration of a third dose to older adults. 2021 Jul 30 [cited 2021 Nov 21]. https://www.gov.il/en/departments/news/29072021-04
5. Israel Ministry of Health. Discussions on administering the third vaccine to additional populations. 2021 Aug 20 [cited 2021 Nov 21]. https://www.gov.il/en/departments/news/19082021-04
6. Glatman-Freedman A, Bromberg M, Dichtiar R, Hershkovitz Y, Keinan-Boker L. The BNT162b2 vaccine effectiveness against new COVID-19 cases and complications of breakthrough cases: a nation-wide retrospective longitudinal multiple cohort analysis using individualised data. EBioMedicine. 2021;72:103574. https://doi.org/10.1016/j.ebiom.2021.103574
7. National Institutes of Health. Coronavirus disease 2019 (COVID-19) treatment guidelines: clinical spectrum of SARS-CoV-2 infection [cited 2021 Feb 25]. https://www.covid19treatmentguidelines.nih.gov
8. Central Bureau of Statistics. Statistical abstract of Israel 2021—no. 72 [cited 2021 Nov 22]. https://www.cbs.gov.il/en/publications/Pages/2021/Population-Statistical-Abstract-of-Israel-2021-No.72.aspx
9. Our World in Data. SARS-CoV-2 variants in in analyzed sequences, Israel. 2022 [cited 2022 March 6]. https://ourworldindata.org/grapher/covid-variants-area?country=~ISR
10. Bayart JL, Douxfils J, Gillot C, David C, Mullier F, Elsen M, et al. Waning of IgG, total and neutralizing antibodies 6 months post-vaccination with BNT162b2 in healthcare workers. Vaccines (Basel). 2021;9:1092. https://doi.org/10.3390/vaccines9101092
11. UK Health Security Agency. SARS-CoV-2 variants of concern and variants under investigation in England. Technical briefing 33. 2021 [cited 2022 Jan 9]. https://assets.publishing.service.gov.uk/government/uploads/system/uploads/attachment_data/file/1043807/technical-briefing-33.pdf
12. Collie S, Champion J, Moultrie H, Bekker LG, Gray G. Effectiveness of BNT162b2 vaccine against Omicron variant in South Africa. N Engl J Med. 2022;386:494–6. https://doi.org/10.1056/NEJMc2119270
13. Bar-On YM, Goldberg Y, Mandel M, Bodenheimer O, Freedman L, Kalkstein N, et al. Protection of BNT162b2 vaccine booster against COVID-19 in Israel. N Engl J Med. 2021;385:1393–400. https://doi.org/10.1056/NEJMoa2114255
14. Bar-On YM, Goldberg Y, Mandel M, Bodenheimer O, Freedman L, Alroy-Preis S, et al. Protection against COVID-19 by BNT162b2 booster across age groups. N Engl J Med. 2021;385:2421–30. https://doi.org/10.1056/NEJMoa2115926
15. Barda N, Dagan N, Cohen C, Hernán MA, Lipsitch M, Kohane IS, et al. Effectiveness of a third dose of the BNT162b2 mRNA COVID-19 vaccine for preventing severe outcomes in Israel: an observational study. Lancet. 2021;398:2093–100. https://doi.org/10.1016/S0140-6736(21)02249-2
16. Tartof SY, Slezak JM, Puzniak L, Hong V, Frankland TB, Ackerson BK, et al. Effectiveness of a third dose of BNT162b2 mRNA COVID-19 vaccine in a large US health system: a retrospective cohort study. Lancet Reg Health Am. 2022 Feb 14 [Epub ahead of print]. https://doi.org/10.1016/j.lana.2022.100198
17. Andrews N, Stowe J, Kirsebom F, Toffa S, Sachdeva R, Gower C, et al. Effectiveness of COVID-19 booster vaccines against covid-19 related symptoms, hospitalisation and death in England. Nat Med. 2022 Jan 14 [Epub ahead of print]. https://doi.org/10.1038/s41591-022-01699-1

Address for correspondence: Aharona Glatman-Freedman, The Israel Center for Disease Control, Israel Ministry of Health, Gertner Institute Building, Tel Hashomer, Ramat Gan 5265601, Israel; email: aharona.freedman@moh.gov.il

Effects of Tick-Control Interventions on Tick Abundance, Human Encounters with Ticks, and Incidence of Tickborne Diseases in Residential Neighborhoods, New York, USA

Felicia Keesing,[1] Stacy Mowry, William Bremer, Shannon Duerr, Andrew S. Evans Jr., Ilya R. Fischhoff, Alison F. Hinckley, Sarah A. Hook, Fiona Keating, Jennifer Pendleton, Ashley Pfister, Marissa Teator, Richard S. Ostfeld[1]

Tickborne diseases (TBDs) such as Lyme disease result in ≈500,000 diagnoses annually in the United States. Various methods can reduce the abundance of ticks at small spatial scales, but whether these methods lower incidence of TBDs is poorly understood. We conducted a randomized, replicated, fully crossed, placebo-controlled, masked experiment to test whether 2 environmentally safe interventions, the Tick Control System (TCS) and Met52 fungal spray, used separately or together, affected risk for and incidence of TBDs in humans and pets in 24 residential neighborhoods. All participating properties in a neighborhood received the same treatment. TCS was associated with fewer questing ticks and fewer ticks feeding on rodents. The interventions did not result in a significant difference in incidence of human TBDs but did significantly reduce incidence in pets. Our study is consistent with previous evidence suggesting that reducing tick abundance in residential areas might not reduce incidence of TBDs in humans.

Lyme disease is an emerging zoonosis caused by the spirochete bacterium *Borrelia burgdorferi*, which is transmitted between vertebrate hosts, including humans, by ticks in the *Ixodes ricinus* complex. Annual cases of Lyme disease in the United States, as reported to the Centers for Disease Control and Prevention (*1*), have grown from a few hundred in the early 1980s to >30,000 in recent years. A recent study estimated that actual clinician diagnoses of Lyme disease in the past decade exceed 450,000 per year (*2*,*3*). Increasing incidence over the past few decades reflects both upward trends in case numbers within Lyme disease–endemic locations and a dramatic geographic spread from both northeastern and Midwestern foci (*4*–*6*). Beyond the effects of Lyme disease on human health, economic costs of patient care are estimated at ≈$1 billion/year in the United States (*7*).

Preventing exposure to *B. burgdorferi* and other tickborne pathogens can be aided by personal practices such as applying repellents, checking for ticks, and avoiding tick habitats. However, the efficacy of these methods is unclear, and considerable differences in effects have been reported (*8*,*9*). Although specific methods of property and wildlife management (e.g., deer hunting) are advocated by some agencies (*10*), knowledge of the effectiveness of these recommendations in reducing human encounters with ticks and incidence of tickborne diseases (TBDs) is limited (*11*–*13*).

Author affiliations: Bard College, Annandale, New York, USA (F. Keesing); Cary Institute of Ecosystem Studies, Millbrook, New York, USA (S. Mowry, W. Bremer, S. Duerr, I.R. Fischhoff, F. Keating, J. Pendleton, A. Pfister, M. Teator, R.S. Ostfeld); Dutchess County Department of Behavioral and Community Health, Poughkeepsie, New York, USA (A.S. Evans Jr.); Centers for Disease Control and Prevention, Fort Collins, Colorado, USA (A.F. Hinckley, S.A. Hook)

DOI: https://doi.org/10.3201/eid2805.211146

[1]These authors contributed equally to this article and were co-principal investigators.

Controlling the size of tick populations is generally considered a promising way of reducing human exposure to TBDs. Researchers pursuing these methods have identified chemical and biological agents, including synthetic pyrethroids, organophosphates, and entomopathogenic fungi, that are lethal to ticks (*14*–*19*). Field trials generally show that application of chemical or biologic acaricides can reduce the number of ticks by 50%–90% (*20*–*22*). Combining acaricides with other interventions (e.g., wildlife and landscape management) has also been assessed. However, studies evaluating whether these integrated approaches reduce human exposure to ticks are limited by design constraints, such as the lack of masking of researchers to treatment assignments, lack of appropriate placebo controls, small scale of deployment, unbalanced designs, and low statistical power. Studies also do not generally include data on human health outcomes, particularly incidence of TBDs (*23*,*24*).

A recent study (*23*) rectified many of these deficiencies by applying an acaricide (bifenthrin) to 2,727 residential properties in 3 states; using a masked, placebo-controlled design; and including tick abundance, human encounters with ticks, and cases of TBDs as response variables. Despite showing >60% reduction in tick populations on properties treated with the acaricide versus the placebo control (water), the study (*23*) showed no reduction in either tick encounters or cases of TBDs. One potential reason for this lack of effect is that the treatments did not reduce tick abundance below some putative threshold needed for reduced disease risk. A second possibility is that humans might frequently encounter ticks in locations other than their yards. In both cases, tick control might be more effective at reducing tick exposures when applied throughout a residential neighborhood.

This study, the Tick Project (*25*), was designed to determine whether tick control, when implemented more broadly in residential neighborhoods and by using multiple approaches to tick management, could reduce TBD risk and incidence. We designed a randomized, replicated, fully crossed, placebo-controlled, masked experiment to evaluate whether 2 environmentally safe methods to manage ticks, used separately or together, reduced tick abundance, human and pet encounters with ticks, and human and pet cases of TBDs.

Methods

We tested the effects of 2 methods of tick control, used separately or together, on tick abundance, tick encounters with humans and pets, and cases of TBDs over 4 years (2017–2020) in 24 neighborhoods in Dutchess County, New York, USA. The first intervention, the Tick Control System (TCS) (Select TCS, Tick Box Technology Corporation, http://www.tickboxtcs.com), consists of baited boxes that attract the small mammal hosts most likely to infect ticks with pathogens. When inside the box, these mammals are brushed with a dose of the acaricide fipronil. The second intervention, Met52 (Novozymes Biologicals, https://biosolutions.novozymes.com), is a fungal spray developed to kill questing ticks. Both interventions have been demonstrated to have extremely low toxicity to humans, pets, and wildlife as applied (*21*); high specificity for ticks (*26*); evidence of efficacy in tick-control as revealed in small-scale studies (*15*,*20*–*22*,*27*); and commercial availability at the time of the study.

The design was fully crossed so that 4 treatments were used: placebo TCS boxes and placebo Met52, placebo TCS boxes and active Met52, active TCS boxes and placebo Met52, and active TCS boxes and active Met52. All participating properties within a neighborhood received the same treatment. We included 6 replicate neighborhoods in each of 4 treatment categories to achieve 80% power to detect an effect size of 60%. Given the intensity of treatments and length of the study, increasing the sample size to achieve greater power was infeasible. Selected neighborhoods had high incidence of Lyme disease and moderate to high density of 1- and 2-family residences. During April 2016–June 2017, residents were recruited by mail, telephone, and in-person visits. Neighborhood treatments were randomly assigned, and study participants and scientific personnel that collected or managed data on response variables were masked to treatment assignments (Appendix).

Beginning in spring 2017, we deployed the 4 treatment combinations on participating properties (Appendix Table 1, https://wwwnc.cdc.gov/EID/article/28/5/21-1146-App1.pdf). We deployed TCS boxes or placebo boxes that contained no acaricide at densities consistent with product labeling during spring and summer, corresponding to the activity peaks for nymphal and larval blacklegged ticks (*28*). We placed boxes ≥10 meters apart in all habitat types that we sampled for ticks and placed them in protected locations, such as along building foundations and under vegetation, that are frequently used by small mammals.

If effective, TCS bait boxes would kill larval (hatchling stage) ticks feeding on small-mammal hosts in summer and fall, leading to fewer nymphs

(second immature stage) the following spring. Met52 would kill questing nymphal ticks in spring. Our tick sampling focused on the abundance of questing nymphal ticks in spring and ticks on small mammals in summer.

Met52, which contains spores of the F52 strain of the entomopathogenic fungus *Metarhizium brunneum*, was prepared according to product label instructions and applied by using truck-mounted high-pressure sprayers. Identical trucks and sprayers were filled with water for the placebo controls. Spraying was conducted twice each year preceding and during the peak of activity of questing nymphal ticks (*28*). For properties that included extensive forested areas, spraying extended 12 meters into the forest.

During the peak activity period for questing nymphal ticks and at least 1 week after spraying, we used 1-m × 1-m white corduroy cloth to flag-sample ticks at 20 randomly chosen participating properties within each neighborhood, sampling 3 habitat types on each property: lawn, forest, and shrub or garden, whenever present. To assess tick burdens on small mammals, we conducted mark-recapture sampling by using Sherman live traps at 10 participating properties in each neighborhood during August and September 2017–2019, corresponding to the activity peak of the larval stage (*28*). We did not conduct sampling in 2020 because of the coronavirus disease pandemic.

In an introductory survey, we asked the primary contact for each household where and how frequently each member of the household spent time outdoors and what approaches to personal tick prevention they used. From spring through late fall each year (Appendix Table 2), we distributed biweekly surveys to each participating household, asking whether any full-time resident, including pets that spent time outdoors, had encountered a tick or had a TBD diagnosed in the previous 2 weeks. We asked participants who reported TBD in humans to consider signing a medical consent form to enable confirmation of the case by their healthcare provider.

We generally evaluated effects of treatments by analyzing data aggregated at the neighborhood level to determine the effects of each treatment alone and in combination (Appendix). For tick encounters and cases of TBDs for humans and pets, we accounted for numbers of participants within neighborhoods. The Institutional Review Board and the Institutional Animal Care and Use Committee of the Cary Institute of Ecosystem Studies (Millbrook, NY, USA) approved protocols involving informed consent by human participants and the live-trapping and handling of small mammals.

Results

Characteristics of Neighborhoods and Participants

The average neighborhood was 27.5 (range 12.9–39.2) hectares and contained 118 (range 77–162) properties; average parcel size was (range 0.02–1.8) 0.19 hectares. A mean of 43% (range 18%–63%) of the neighborhood consisted of forested habitat, whereas lawns, shrubs, and gardens together accounted for ≈30% (range 14%–48%).

During the recruitment phase, ≈25% of households in each neighborhood did not respond to repeated attempts at contact, ≈25% declined to participate, and ≈10% were either ineligible (e.g., because they used pesticides) or failed to fully enroll (Appendix Figure 1). By the end of the recruitment phase, an average of 34% (range 24%–44%) of the properties in a given neighborhood were enrolled in the project. Neither the proportion of properties enrolled (Appendix Table 3, Figure 1) nor the habitat composition of the neighborhoods (Appendix Tables 4, 5) varied significantly by treatment group.

When the study began, a mean of 101 (range 62–136) persons and 35 (range 14–58) outdoor pets were enrolled in each neighborhood, for a total of 2,384 human participants and 849 pets. Enrollment numbers did not vary significantly by treatment group (Table 1). On average, participants had a median age of 49 years, and 40% of households had an annual

Table 1. Characteristics of participants for the 24 residential neighborhoods together and for the 6 neighborhoods in each of the 4 treatment groups of tick-control interventions, New York, USA*

Characteristic	Overall	Neither active	Active Met52	Active bait boxes	Both active
No. neighborhoods	24	6	6	6	6
Mean no. human participants per neighborhood	97 (± 19)	110 (± 13)	94 (± 26)	94 (± 13)	90 (± 18)
Mean no. outdoor pets per neighborhood	30 (± 8)	26 (± 9)	33 (± 9)	29 (± 5)	31 (± 10)
Average median age of human participants, y	49 (± 5)	48 (± 4)	51 (± 3)	48 (± 6)	49 (± 6)
Per capita no. preventive behaviors	1.27 (± 0.27)	1.20 (± 0.35)	1.37 (± 0.27)	1.27 (± 0.24)	1.27 (± 0.24)
Self-reported cases of diagnosed TBDs per capita before study onset, 2011–2016	0.07 (± 0.03)	0.05 (± 0.02)	0.07 (± 0.03)	0.07 (± 0.02)	0.07 (± 0.05)

*Data on age, previous cases of TBDs, and preventive behaviors were self-reported on the introductory survey administered during 2016–2017. Data on the number of participants and pets who spent time outside were averaged over the length of the study. Values in parentheses represent the standard error of the mean. TBDs, tickborne diseases.

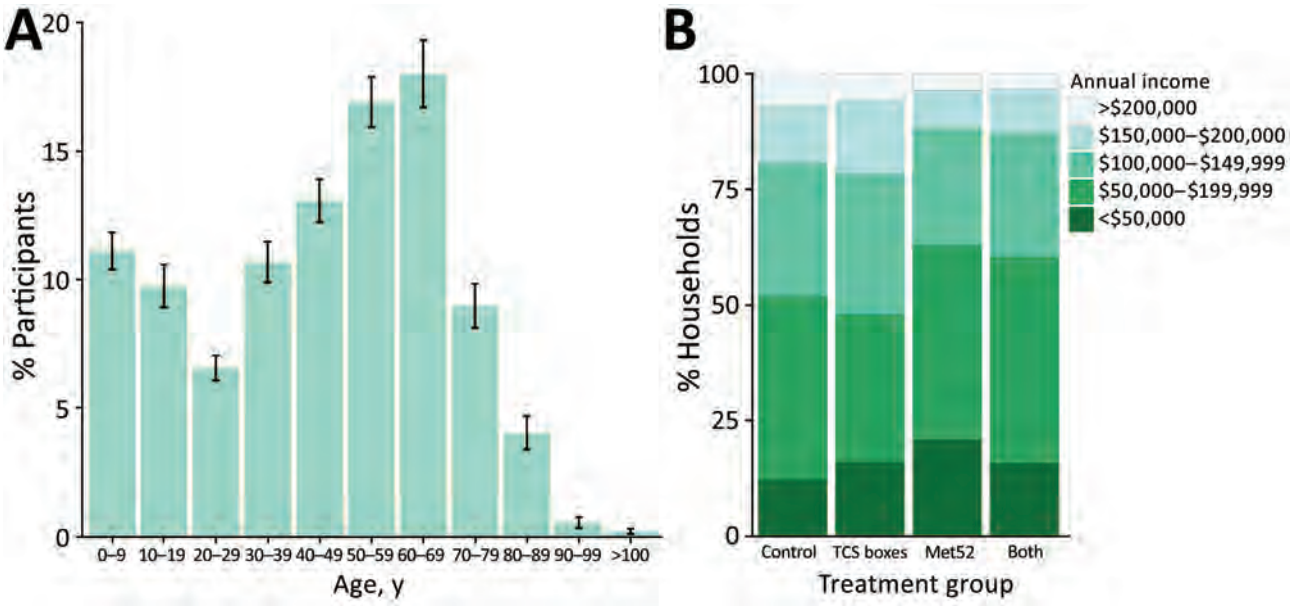

Figure 1. Characteristics of participants in study of tick-control interventions in residential neighborhoods, New York, USA. A) Mean percentage of participants in each age category at the time of enrollment, averaged for 24 neighborhoods. Error bars represent SEM. B) Mean percentage of households in each category of annual household income, averaged for the 6 neighborhoods in each treatment group. TCS, Tick Control System.

household income of $50,000–100,000 (Figure 1). Participants reported that when they spent time outside, most of their time was spent on their own properties or away from their neighborhoods (Appendix Figure 4). Participants reported regularly practicing just over 1 preventive behavior (e.g., tick checks) to protect themselves from ticks and TBDs (mean 1.2 ± 0.3 SEM; Table 1).

Tick Abundance

Questing Nymphal Ticks

Per sampling interval, more of the 4,040 questing nymphal ticks collected in the study were found in forested areas of properties than on lawns or in shrubs or gardens (Figure 2, panel A). At the neighborhood level of analysis, the presence of active TCS boxes was associated with a 53% reduction in the number of questing nymphal ticks in forest habitats compared with placebo controls, a statistically significant difference (Figure 2, panel A; Appendix Table 6). Despite an apparent reduction in tick abundance (compared with placebo controls) associated with Met52 treatment in forest habitats (Figure 2, panel A), this effect was not statistically significant, nor was there a significant effect of the 2 treatments used together (a significant interaction) (Appendix Table 6). Shrub and garden habitats showed a similar pattern; 40% fewer questing nymphal ticks were detected on properties with active TCS boxes than those with placebo controls (Figure 2, panel A; Appendix Table 7). This effect was statistically significant, but no significant effect of either active Met52 or the 2 treatments together was seen (Figure 2, panel A; Appendix Table 7). In lawn habitats at the neighborhood level of analysis, no statistically significant effect of either of the treatments used alone or together was seen (Figure 2, panel A; Appendix Table 8).

At the property level, ticks were detected in forested habitats on 75% of properties that received no active treatments but on only 45% of properties treated with active TCS boxes (Figure 2, panel B). A similar and statistically significant pattern was observed for the other 2 habitat types (Figure 2, panel B; Appendix Tables 9–11). There was no significant effect of active Met52 on the probability of detecting ticks in any of the 3 habitats, nor was there an effect of the treatments used together.

Larval and Nymphal Tick Burdens on Small Mammals

Averaged across all years and all treatments, white-footed mice had mean (± SEM) tick burdens of 3.7 ± 0.4 ticks/animal and chipmunks had 0.7 ± 0.1 ticks/animal (Figure 3). The presence of active TCS boxes was associated with a reduction in the mean number of ticks per white-footed mouse by about half (Figure 3, panel A; Appendix Table 12). There was no significant effect of either active Met52 or the treatments together on the average tick burden on mice (Appendix

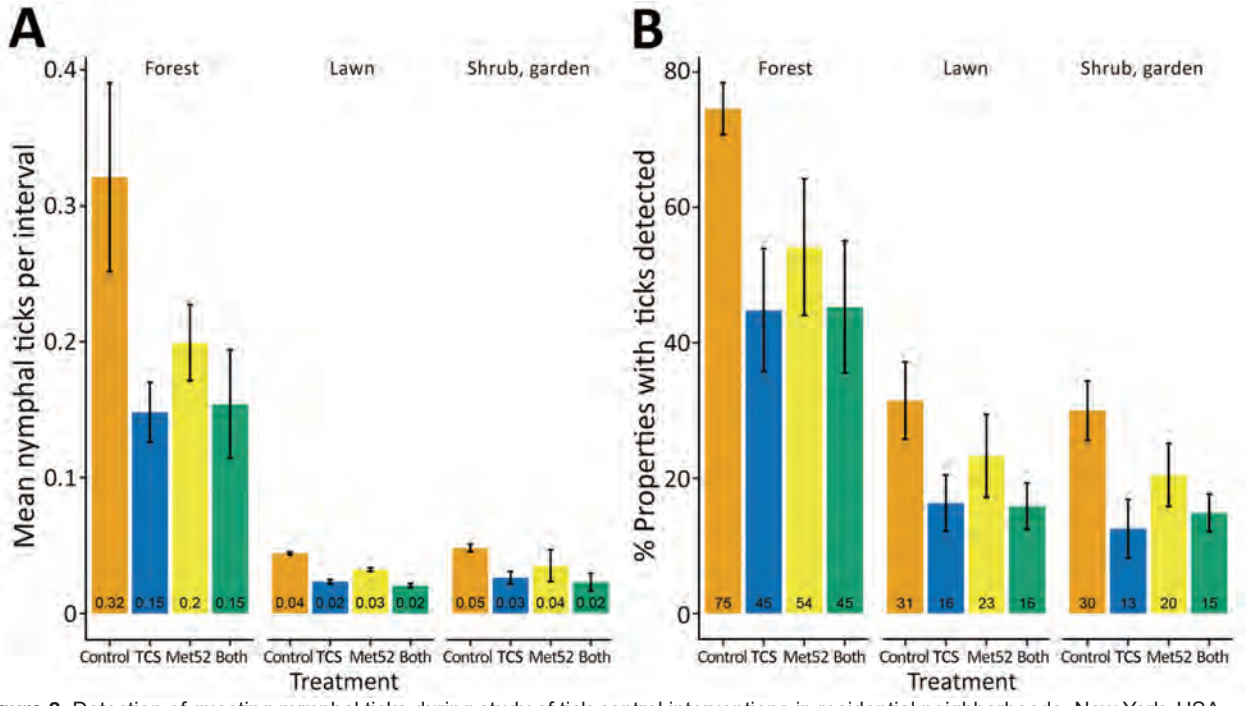

Figure 2. Detection of questing nymphal ticks during study of tick-control interventions in residential neighborhoods, New York, USA. A) Mean number of questing nymphal ticks per flagging interval (Appendix, https://wwwnc.cdc.gov/EID/article/28/5/21-1146-App1.pdf). B) Mean percentage of properties with questing nymphal ticks detected for each treatment group and in each habitat type (forest, lawn, shrub or garden). Totals are averaged over 3 years for each neighborhood. Data include ticks from the nymphal sampling period in May–July. Error bars represent SEM. TCS, Tick Control System.

Table 12). Neither treatment had a significant effect on the probability of tick presence on chipmunks or on nonzero tick burdens on chipmunks (Figure 3; Appendix Table 13).

Case and Encounter Data for Humans

We received 1,664 reports of encounters between ticks and human participants. The cumulative number of reported human encounters with ticks was ≈20% lower in neighborhoods treated with both active TCS boxes and active Met52, but this difference was not statistically significant (Figure 4, panel A), nor was there a significant effect of either of the active treatments alone (Appendix Table 14).

We received a total of 130 reports of TBD diagnoses in humans during 2017–2020. The active treatments, either alone or in combination, demonstrated no effect on the number of self-reported human cases of TBDs (Table 2; Figure 4, panel C; Appendix Table 15). We received permission to pursue confirmation for 84 (65%) of these cases and received 52 responses from healthcare providers. Of these, 35 (67%) confirmed

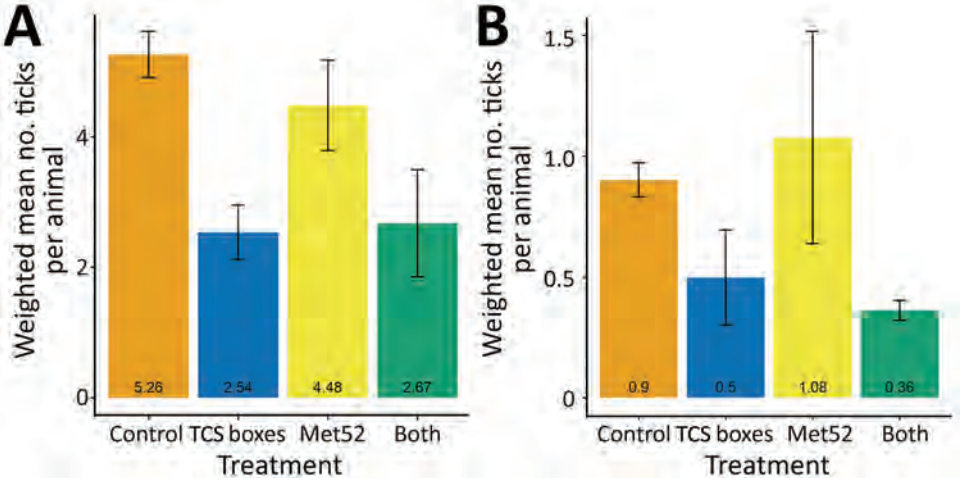

Figure 3. Weighted mean number of ticks on white-footed mice (A) and chipmunks (B) as a function of tick-control treatment, New York, USA, 2017–2019. Means represent the average of the 6 neighborhoods in each treatment group, whereas error bars represent SEs. Note that the scale of the y-axes differs. TCS, Tick Control System.

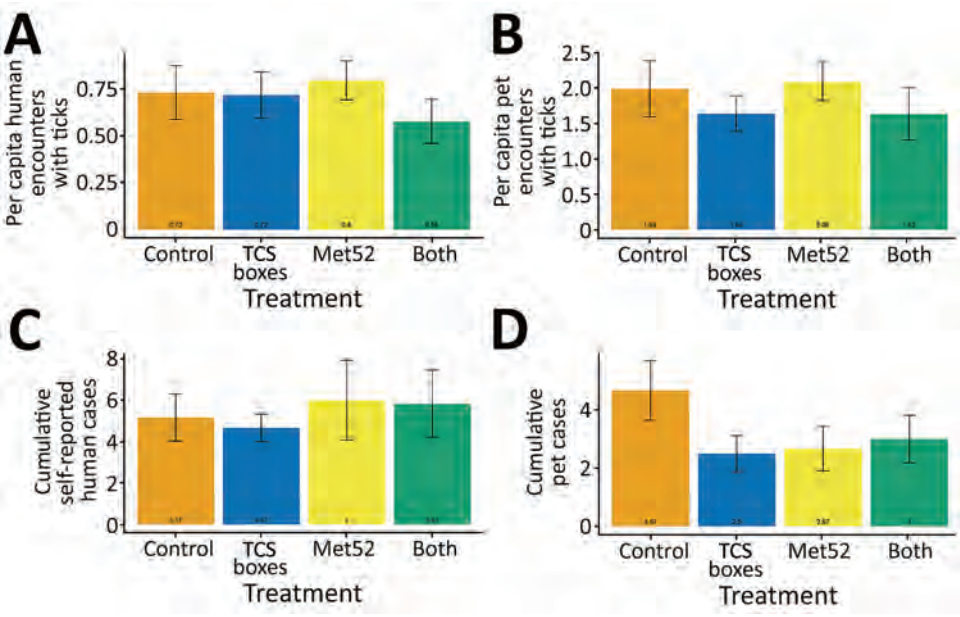

Figure 4. Mean per capita human and pet encounters with ticks and cumulative numbers of cases per neighborhood of tick-borne diseases for humans and pets in study of tick-control interventions, New York, USA. A) Human encounters; B) pet encounters; C) self-reported human cases; D) pet cases. Data represent the mean of the cumulative value (± SEM) over the 4 years of treatments (2017–2020), averaged across neighborhoods in a treatment group. Note that the scale of the y-axes differs. TCS, Tick Control System.

diagnoses of a TBD. There was no significant effect of the active treatments, either alone or in combination, on the number of human cases of TBDs confirmed by healthcare providers (Table 2; Appendix Table 16).

Case and Encounter Data for Pets

We received 1,307 reports of tick encounters for outdoor pets during 2017–2020. The cumulative number of reported pet encounters with ticks was ≈20% lower in neighborhoods with active TCS boxes, but this difference was not statistically significant, nor was there a significant effect of active Met52 treatments (Figure 4, panel B; Appendix Table 17). We received 77 reports of TBD diagnoses in pets during 2017–2020, as reported by owners. The incidence of owner-reported cases of TBDs in pets was lower by about half in neighborhoods with active TCS boxes or active Met52, and these differences were statistically significant (Table 2; Figure 4, panel D; Appendix Table 18).

Effectiveness of Masking Procedures

Of 874 households participating in December 2020, a total of 507 primary contacts (58%) completed the final survey; 438 (86%) of those contacts said they did not know their neighborhood's treatment assignment. Of the 65 who thought they knew their neighborhood's treatment assignment, their guesses were incorrect (54%) more frequently than they were correct (46%) (Appendix).

Discussion

We conducted a large-scale, randomized, masked, placebo-controlled study of the effects of 2 methods of tick control in residential neighborhoods. The central goal was to evaluate whether community-level control of ticks could reduce the threat of TBDs to public health. We documented significant reductions in tick abundance within certain treatment groups, most consistently within forest and garden habitats. These effects were not associated with significant reductions in human exposure to ticks or TBDs. However, TBD incidence in outdoor pets was significantly lower in neighborhoods that received the interventions.

Deploying active TCS boxes in neighborhoods was associated with fewer questing nymphal ticks by >50% and fewer ticks on rodents by ≈50% compared with placebo controls. Active Met52 spray showed no effect on the abundance of either questing or attached ticks compared with placebo controls. Not surprisingly, using those 2 methods of tick control together did not show multiplicative effects, as indicated by the lack of statistically significant interactions between the interventions.

The protocols for TCS and Met52 used in this study complied with product labels. The low efficacy of Met52 may have arisen from degradation and low residual effects of the acaricide after applications (*29*). Other studies using TCS boxes or Met52 are not directly comparable to ours because they used multiple tick-control methods with unbalanced designs or lacked placebo controls (*20*,*21*,*30*), which are necessary to account for the presence of the food and shelter TCS boxes provide and to ensure that personnel collecting data are unaware of treatment assignments. Also, previous studies have

tended to restrict TCS box placement or Met52 application to habitat edges, whereas we treated more broadly across habitat types. For example, a recent study placed TCS boxes in a single line along forest–lawn ecotones and found no effect (*31*). Keeping these important differences in mind, the reductions we observed in questing ticks and ticks on rodents in the neighborhoods with active TCS boxes and active Met52 were similar in magnitude to some previous studies using these tick-control methods (*22*) but differed from others (*15*,*20*,*31*,*32*).

Human encounters with ticks have been demonstrated to be a proxy for cases of TBD (*33*). We received 20% fewer cumulative reports of encounters between human participants and ticks, and between outdoor pets and ticks, in neighborhoods treated with both active TCS boxes and active Met52 than for placebo controls. However, this difference was not statistically significant, which might have been caused by stochastic variation among neighborhoods associated with relatively low numbers of cases.

The weak effects of tick reduction on tick encounters and reported cases of TBDs in humans could have arisen from one or more of the following reasons. First, despite persistent, energetic efforts throughout the first year of the study to recruit as many households as possible within neighborhoods, we enrolled 24%–44% of the households in each neighborhood (Appendix Figure 1). Although dozens of individual properties were treated per neighborhood, these treated areas might have been too sparse to provide added benefits over the treatment of individual properties. If more households in each neighborhood had participated, we might have observed greater reductions in tick numbers and an associated reduction in incidence of TBDs. However, increasing participation substantially in future interventions targeted at neighborhoods might not be feasible (Appendix Figure 1). General enthusiasm among residents was high, and the retention and response rates suggest high motivation among those who did participate.

Second, a total of 130 cases of TBDs were reported for all 24 neighborhoods cumulatively over the 4 years of treatments in this study, for a mean of only 5.5 cases per neighborhood. Such a low number of cases might have curtailed our ability to detect effects of the interventions. However, despite only 77 reported cases of TBDs in outdoor pets, or 3.7 cases per neighborhood on average, we detected a significant reduction in neighborhoods with active interventions compared with placebo controls. The absence of effects of treatment on incidence of self-reported and physician-confirmed cases of TBD in humans cannot be attributed solely to a limited number of cases.

A third possibility, related to the second, is that residents of our focal county frequently take actions to prevent exposure to tick bites and tickborne pathogens, which might have limited the effects observed from the interventions. Our study population within Dutchess County, New York, began experiencing high exposure to Lyme disease and other TBDs in the early 1990s, and many residents

Table 2. Cumulative diagnosed cases of tickborne diseases, averaged across the 6 residential neighborhoods in each treatment group of tick-control interventions, New York, USA*

Cases and treatment groups	Per capita cases (SE)	Cases/neighborhood (SE)	p value
Cases of diagnosed tickborne diseases in humans reported by participants, n = 130			
Control	0.05 (0.01)	5.17 (2.11)	
Active TCS boxes	0.05 (0.01)	4.67 (1.91)	NS
Active Met52	0.06 (0.02)	6.00 (2.45)	NS
Active TCS boxes and active Met52	0.06 (0.01)	5.83 (2.38)	NS
Cases of diagnosed tickborne diseases in humans confirmed by healthcare providers, n = 35†			
Control	0.009 (0.00)	1.00 (0.41)	
Active TCS boxes	0.012 (0.00)	1.17 (0.48)	NS
Active Met52	0.019 (0.01)	2.17 (0.88)	NS
Active TCS boxes and active Met52	0.016 (0.01)	1.50 (0.61)	NS
Cases of diagnosed tick-borne diseases in outdoor pets reported by participants, n = 77			
Control	0.17 (0.03)	4.67 (1.91)	
Active TCS boxes	0.08 (0.02)	2.50 (1.02)	‡
Active Met52	0.08 (0.03)	2.67 (1.09)	‡
Active TCS boxes and active Met52	0.11 (0.04)	3.00 (1.22)	NS

*For detailed statistical results, see Appendix Tables 16, 18, and 19 (https://wwwnc.cdc.gov/EID/article/28/5/21-1146-App1.pdf). Data represent the mean of the cumulative value (±SEM) over the 4 years of treatments, averaged across neighborhoods in a treatment group. NS, not significant.
†Cases in humans confirmed by healthcare providers were less common than cases reported by participants because some participants did not grant permission to the investigators to pursue confirmation from healthcare providers, some healthcare providers did not respond to repeated requests for information, and some diagnoses from healthcare providers did not confirm patient reports.
‡Statistically significant differences.

habitually engage in efforts to reduce risk, including use of repellents, protective clothing, tick checks, and yard management (*8*,*9*,*34*). In addition, awareness of relative risk might lead residents to spend more time in lawn and garden areas of their yards than in forested areas, where ticks were more abundant and the effects of treatments were stronger. These preventive behaviors could weaken the link between our tick-control interventions and disease incidence in the human population. If so, we would expect stronger effects of tick control in areas where residents demonstrate lower adherence to methods of personal protection. To examine this possibility, future studies could compare effectiveness of tick control interventions in areas of high and low adoption of personal protection measures.

The significant effect of active interventions observed for TBDs in outdoor pets but not in humans could have been caused by different patterns of space use (e.g., if outdoor pets spend more time in forested habitats within yards or use more of the neighborhood outside the individual property of residence). Use of repellents and other individual-based preventive measures might be less variable for pets than for humans, potentially increasing the ability to detect effects on pets. More information on how humans and pets use space, both within and outside residential areas, could help improve future tick-control interventions.

The observed effect of the active interventions on TBDs in outdoor pets should be interpreted cautiously. We observed no corresponding effect on tick encounters among pets, and we did not seek confirmation of pet diagnoses with veterinarians. Further, the incidence of TBDs in pets was the only outcome for which active Met52 treatments showed a significant effect.

In summary, although active TCS bait boxes were associated with reduced abundance of questing ticks, ticks attached to rodents, and TBD diagnoses in outdoor pets compared with placebo treatments, these interventions were not associated with significant reductions in human encounters with ticks or incidence of TBDs in humans. Thus, our study is consistent with that of Hinckley et al. (*23*) in suggesting that reducing the size of tick populations in residential areas might not result in strong effects on incidence of TBDs in human populations. More research is needed to address where in the environment, and under what conditions, humans most frequently encounter infected ticks, and in which geographic locations tick reductions will have the greatest impact on human health. One important conclusion for public health is that studies investigating tick reductions should also measure actual outcomes for people, such as disease incidence or tick encounters.

Acknowledgments

We are grateful for the support we received from the Steven & Alexandra Cohen Foundation; the Centers for Disease Control and Prevention; New York State; the Dutchess County Water and Wastewater Authority; the Ian Mactaggart Trust; the John Drulle, MD Memorial Lyme Fund, Inc.; the Pershing Square Foundation; The Walbridge Fund; Nina Brown deClercq; Susan and Jim Goodfellow; Elyse Harney; Eric Roberts; Pamela and Scott Ulm; and other private donors. We thank our partners: the Cary Institute of Ecosystem Studies, Bard College, the Centers for Disease Control and Prevention, the New York State Department of Health, and the Dutchess County Department of Community and Behavioral Health. The Cary Institute of Ecosystem Studies provided extensive logistical support. We benefited enormously from the expertise and dedication of the team at Arkus, Inc., especially Amy Bucciffero. Salesforce.org, Pardot, SMSMagic, FormAssembly, and DocUSign provided software and support at reduced fees. Our colleagues at Pestech Pest Solutions provided the professional applications of our treatments, under the committed leadership of Rob Robinson and Noah Startup. We are indebted to the staff of the Tick Project: Rose Adelizzi, Shefali Azad, Daniella Azulai, Kate Badour, Connor Baush, Mohammad Harris Bayan, Anna Butler, Reilly Carlson, Samantha Cassata, Adrian D'Souza, Dylan Dahan, Deanna DePietro, Joshua DiPaola, Lizzy Elliott, Michelle Ferrell, Amanda Gabryszak, Abigail Johnson, Amanda Jones, Alyssa Kamrowski, Ashley Kolton, Troy Koser, Beckett Lansbury, Rachel Livengood, Morgan Long, Sara McBride, Mica McCarty-Glen, Waynette McCracken, Sarah McGregor, Timothy McSweeny, Vince Meyer, Alison Molnar, Victoria Palfini, Nadine Pershyn, Nick Petterelli, Nicole Pierro, Luke Porter, Sophia Raithel, Madeline Rivard, Jared Russ, Samantha Sambado, Makayla Says, Megan Schierer, Brandi Strand, Katie Sweeney, Charlene Gray Tarsa, Abraham Turner, Nick Urbin, Agatha Winiarski, and Alex Wolf. The project benefited from the professional support of Josh Ginsberg, Holly Talbot, Lori Quillen, David Fischer, Amanda Johnson, Heather Malcom, Fred Merritt, Catherine Forbes, Ben Beard, Lars Eisen, Paul Mead, Jill Auerbach, Sue Serino, Didi Barrett, Robert S. Wills, and Sarah Dunphy-Lelii. This research was made possible by the generousparticipation of thousands of residents of Dutchess County, New York, and we extend our great appreciation to all of them. Two anonymous reviewers and an editor provided useful comments and suggestions that improved the manuscript.

This work was supported by a grant from the Steven & Alexandra Cohen Foundation, with additional financial and in-kind support from the Centers for Disease Control, New York State, the Dutchess County Water and Wastewater Authority, the Ian Mactaggart Trust, the John Drulle, MD Memorial Lyme Fund, Inc., the Pershing Square Foundation, The Walbridge Fund, Nina Brown deClercq, Susan and Jim Goodfellow, Elyse Harney, Eric Roberts, Pamela and Scott Ulm, and other private donors.

R.S.O. and F.K. designed the study. A.F.H., S.A.H., and A.S.E. provided input on study protocols. W.B., S.D., J.P., and M.T. collected data. F. Keating, A.P., and S.M. coordinated treatments and data. F.K. and S.M. analyzed the data. F.K. and R.S.O. wrote the first draft of the manuscript and all authors edited it.

About the Author

Dr. Keesing is David & Rosalie Rose Distinguished Professor of the Sciences, Mathematics, and Computing at Bard College. Her research focuses on the ecology of infectious diseases, particularly tickborne diseases in the northeastern United States.

References

1. Centers for Disease Control and Prevention. Lyme disease in Morbidity and Mortality Weekly Reports (MMWR). 2021 [cited 2021 Mar 16]. https://www.cdc.gov/lyme/stats/mmwr.html
2. Schwartz AM, Kugeler KJ, Nelson CA, Marx GE, Hinckley AF. Use of commercial claims data for evaluating trends in Lyme disease diagnoses, United States, 2010–2018. Emerg Infect Dis. 2021;27:499–507. https://doi.org/10.3201/eid2702.202728
3. Kugeler KJ, Schwartz AM, Delorey MJ, Mead PS, Hinckley AF. Estimating the frequency of Lyme disease diagnoses, United States, 2010–2018. Emerg Infect Dis. 2021;27:616–9. https://doi.org/10.3201/eid2702.202731
4. Burtis JC, Sullivan P, Levi T, Oggenfuss K, Fahey TJ, Ostfeld RS. The impact of temperature and precipitation on blacklegged tick activity and Lyme disease incidence in endemic and emerging regions. Parasit Vectors. 2016;9:606. https://doi.org/10.1186/s13071-016-1894-6
5. Eisen RJ, Eisen L, Beard CB. County-scale distribution of Ixodes scapularis and *Ixodes pacificus* (Acari: Ixodidae) in the continental United States. J Med Entomol. 2016;53:349–86. https://doi.org/10.1093/jme/tjv237
6. Schwartz AM, Hinckley AF, Mead PS, Hook SA, Kugeler KJ. Surveillance for Lyme Disease—United States, 2008–2015. MMWR Surveill Summ. 2017;66:1–12.
7. Adrion ER, Aucott J, Lemke KW, Weiner JP. Health care costs, utilization and patterns of care following Lyme disease. PLoS One. 2015;10:e0116767. https://doi.org/10.1371/journal.pone.0116767
8. Fischhoff IR, Keesing F, Ostfeld RS. Risk factors for bites and diseases associated with black-legged ticks: A meta-analysis. Am J Epidemiol. 2019;188:1742–50. https://doi.org/10.1093/aje/kwz130
9. Fischhoff IR, Bowden SE, Keesing F, Ostfeld RS. Systematic review and meta-analysis of tick-borne disease risk factors in residential yards, neighborhood, and beyond [Erratum in: BMC Infect Dis. 2019;19:1035]. BMC Infect Dis. 2019;19:1–11.
10. Stafford KC III. Tick management handbook. Connect Agric Exp Station Bull. 2007;1010(1010):9–18 [cited 2022 Apr 4]. https://portal.ct.gov/-/media/CAES/DOCUMENTS/Publications/Bulletins/b1010pdf.pdf
11. Kugeler KJ, Jordan RA, Schulze TL, Griffith KS, Mead PS. Will culling white-tailed deer prevent Lyme disease? Zoonoses Public Health. 2016;63:337–45. https://doi.org/10.1111/zph.12245
12. Fischhoff IR, Keesing F, Pendleton J, DePietro D, Teator M, Duerr STK, et al. Assessing effectiveness of recommended residential yard management measures against ticks. J Med Entomol. 2019;56:1420–7. https://doi.org/10.1093/jme/tjz077
13. Ostfeld RS. Lyme disease: the ecology of a complex system. New York: Oxford University Press; 2010.
14. Ostfeld RS, Price A, Hornbostel VL, Benjamin MA, Keesing F. Controlling ticks and tick-borne zoonoses with biological and chemical agents. Bioscience. 2006;56:383–94. https://doi.org/10.1641/0006-3568(2006)056[0383:CTATZW]2.0.CO;2
15. Schulze TL, Jordan RA, Schulze CJ, Healy SP. Suppression of *Ixodes scapularis* (Acari: Ixodidae) following annual habitat-targeted acaricide applications against fall populations of adults. J Am Mosq Control Assoc. 2008;24:566–70. https://doi.org/10.2987/08-5761.1
16. Bron GM, Lee X, Paskewitz SM. Do-it-yourself tick control: Granular gamma-cyhalothrin reduces *Ixodes scapularis* (Acari: Ixodidae) nymphs in residential backyards. J Med Entomol. 2021;58:749–55. https://doi.org/10.1093/jme/tjaa212
17. Dolan MC, Maupin GO, Schneider BS, Denatale C, Hamon N, Cole C, et al. Control of immature *Ixodes scapularis* (Acari: Ixodidae) on rodent reservoirs of *Borrelia burgdorferi* in a residential community of southeastern Connecticut. J Med Entomol. 2004;41:1043–54. https://doi.org/10.1603/0022-2585-41.6.1043
18. Kirkland BH, Westwood GS, Keyhani NO, Kirkland BH, Westwood GS. Pathogenicity of entomopathogenic fungi *Beauveria bassiana* and *Metarhizium anisopliae* to Ixodidae tick species *Dermacentor variabilis, Rhipicephalus sanguineus*, and *Ixodes scapularis*. J Med Entomol. 2004;41:705–11. https://doi.org/10.1603/0022-2585-41.4.705
19. Zhioua E, Browning M, Johnson PW, Ginsberg HS, LeBrun RA. Pathogenicity of the entomopathogenic fungus Metarhizium anisopliae (Deuteromycetes) to Ixodes scapularis (Acari: Ixodidae). J Parasitol. 1997;83:815–8. https://doi.org/10.2307/3284273
20. Williams SC, Little EAH, Stafford KC III, Molaei G, Linske MA. Integrated control of juvenile Ixodes scapularis parasitizing *Peromyscus leucopus* in residential settings in Connecticut, United States. Ticks Tick Borne Dis. 2018;9:1310–6. https://doi.org/10.1016/j.ttbdis.2018.05.014
21. Williams SC, Stafford KC III, Molaei G, Linske MA. Integrated control of nymphal *Ixodes scapularis*: effectiveness of white-tailed deer reduction, the entomopathogenic fungus *Metarhizium anisopliae*, and fipronil-based rodent bait boxes. Vector Borne Zoonotic Dis. 2018;18:55–64. https://doi.org/10.1089/vbz.2017.2146
22. Little EAH, Williams SC, Stafford KC III, Linske MA, Molaei G. Evaluating the effectiveness of an integrated tick management approach on multiple pathogen infection in Ixodes scapularis questing nymphs and larvae

parasitizing white-footed mice. Exp Appl Acarol. 2020;80:127–36. https://doi.org/10.1007/s10493-019-00452-7
23. Hinckley AF, Meek JI, Ray JAE, Niesobecki SA, Connally NP, Feldman KA, et al. Effectiveness of residential acaricides to prevent Lyme and other tick-borne diseases in humans. J Infect Dis. 2016;214:182–8. https://doi.org/10.1093/infdis/jiv775
24. Wilson AL, Boelaert M, Kleinschmidt I, Pinder M, Scott TW, Tusting LS, et al. Evidence-based vector control? Improving the quality of vector control trials. Trends Parasitol. 2015;31:380–90. https://doi.org/10.1016/j.pt.2015.04.015
25. Keesing F, Ostfeld RS. The Tick Project : testing environmental methods of preventing tick-borne diseases [Erratum in: Trends Parasitol. 2018;34:541]. Trends Parasitol. 2018;34:447–50. https://doi.org/10.1016/j.pt.2018.02.008
26. Fischhoff IR, Keesing F, Ostfeld RS. The tick biocontrol agent *Metarhizium brunneum* (= *M. anisopliae*) (strain F52) does not reduce non-target arthropods. PLoS One. 2017;12:e0187675. https://doi.org/10.1371/journal.pone.0187675
27. Schulze TL, Jordan RA, Williams M, Dolan MC. Evaluation of the SELECT tick control system (TCS), a host-targeted bait box, to reduce exposure to *Ixodes scapularis* (Acari: Ixodidae) in a Lyme disease endemic area of New Jersey. J Med Entomol. 2017;54:1019–24. https://doi.org/10.1093/jme/tjx044
28. Levi T, Keesing F, Oggenfuss K, Ostfeld RS. Accelerated phenology of blacklegged ticks under climate warming. Philos Trans R Soc Lond B Biol Sci. 2015;370:370. https://doi.org/10.1098/rstb.2013.0556
29. Dyer MC, Requintina MD, Berger KA, Puggioni G, Mather TN. Evaluating the effects of minimal risk natural products for control of the tick, Ixodes scapularis (Acari: Ixodidae). J Med Entomol. 2021;58:390–7.
30. Schulze TL, Jordan RA, Schulze CJ, Healy SP, Jahn MB, Piesman J. Integrated use of 4-Poster passive topical treatment devices for deer, targeted acaricide applications, and Maxforce TMS bait boxes to rapidly suppress populations of *Ixodes scapularis* (Acari: Ixodidae) in a residential landscape. J Med Entomol. 2007;44:830–9. https://doi.org/10.1093/jmedent/44.5.830
31. Hinckley AF, Niesobecki SA, Connally NP, Hook SA, Biggerstaff BJ, Horiuchi K, et al. Prevention of Lyme and other tickborne diseases using a rodent-targeted approach: a randomized controlled trial in Connecticut. Zoonoses Public Health. 2021;68:578–87.
32. Jordan RA, Schulze TL. Ability of two commercially available host-targeted technologies to reduce abundance of *Ixodes scapularis* (Acari: Ixodidae) in a residential landscape. J Med Entomol. 2019;56:1095–101. https://doi.org/10.1093/jme/tjz046
33. Hook SA, Nawrocki CC, Meek JI, Feldman KA, White JL, Connally NP, et al. Human-tick encounters as a measure of tickborne disease risk in Lyme disease endemic areas. Zoonoses Public Health. 2021;68:384–92. https://doi.org/10.1111/zph.12810
34. McKenna D, Faustini Y, Nowakowski J, Wormser GP. Factors influencing the utilization of Lyme disease-prevention behaviors in a high-risk population. J Am Acad Nurse Pract. 2004;16:24–30. https://doi.org/10.1111/j.1745-7599.2004.tb00368.x

Address for correspondence: Felicia Keesing, Program in Biology, Bard College, PO Box 5000, Annandale, NY 12504, USA; email: keesing@bard.edu

Pertactin-Deficient *Bordetella pertussis* with Unusual Mechanism of Pertactin Disruption, Spain, 1986–2018

Alba Mir-Cros,[1] Albert Moreno-Mingorance,[1] M. Teresa Martín-Gómez, Raquel Abad, Iván Bloise, Magda Campins, Alejandro González-Praetorius, M. Nieves Gutiérrez, Héctor Martín-González, Carmen Muñoz-Almagro, M. Ángeles Orellana, Manuela de Pablos, Josep Roca-Grande, Carlos Rodrigo, M. Elena Rodríguez, Sonia Uriona, M. José Vidal, Tomàs Pumarola, M. Nieves Larrosa, Juan José González-López

Bordetella pertussis not expressing pertactin has increased in countries using acellular pertussis vaccines (ACV). The deficiency is mostly caused by pertactin gene disruption by IS*481*. To assess the effect of the transition from whole-cell vaccine to ACV on the emergence of *B. pertussis* not expressing pertactin in Spain, we studied 342 isolates collected during 1986–2018. We identified 93 pertactin-deficient isolates. All were detected after introduction of ACV and represented 38% of isolates collected during the ACV period; 58.1% belonged to a genetic cluster of isolates carrying the unusual *prn*::del(–292, 1340) mutation. Pertactin inactivation by IS*481* insertion was identified in 23.7% of pertactin-deficient isolates, arising independently multiple times and in different phylogenetic branches. Our findings support the emergence and dissemination of a cluster of *B. pertussis* with an infrequent mechanism of pertactin disruption in Spain, probably resulting from introduction of ACV.

Bordetella pertussis is the main causative agent of pertussis, an acute upper respiratory tract infection of humans. The most effective strategy for preventing and controlling this disease is vaccination. In Spain during 1998–2005, pertussis vaccination with whole-cell vaccine (WCV) was progressively replaced by vaccination with acellular pertussis vaccine (ACV), which contains a combination of several antigens. Although vaccines and vaccination programs might differ among countries, the 3-component ACV containing pertussis toxin (PT), filamentous hemagglutinin (FHA), and pertactin is largely used for pertussis vaccination in many countries, including Spain. Specifically, the pertactin component has been included in most vaccines used throughout the history of pertussis vaccination in Spain (Table 1).

Despite extensive vaccination campaigns and high vaccination rates, pertussis has resurged in the past 20 years, and outbreaks have occurred worldwide. One of the main causes postulated for the change in pertussis epidemiology is evolution of circulating bacteria to vaccine/immunity-evasive phenotypes (*1*–*4*). In 2007, after the introduction of ACV,

Author affiliations: Hospital Universitari Vall d'Hebron Campus, Barcelona, Spain (A. Mir-Cros, A. Moreno-Mingorance, M.T. Martín-Gómez, M. Campins, H. Martín-González, J. Roca-Grande, S. Uriona, T. Pumarola, M.N. Larrosa, J.J. González-López); Universitat Autònoma de Barcelona, Barcelona (A. Mir-Cros, A. Moreno-Mingorance, T. Pumarola, M.N. Larrosa, J.J. González-López); Instituto de Salud Carlos III, Madrid, Spain (R. Abad); Hospital Universitario La Paz, Madrid (I. Bloise, M. de Pablos); Hospital Universitario de Guadalajara, Guadalajara, Spain (A. González-Praetorius, M.E. Rodríguez); Complejo Asistencial Universitario de Salamanca, Salamanca, Spain (M.N. Gutiérrez); Institut de Recerca Sant Joan de Déu, Esplugues de Llobregat, Spain (C. Muñoz-Almagro); Universitat Internacional de Catalunya, Barcelona (C. Muñoz-Almagro); CIBER de Epidemiología y Salud Pública, Barcelona (C. Muñoz-Almagro); Hospital Universitario 12 de Octubre, Madrid (M.Á. Orellana); Hospital Universitari Germans Trias i Pujol, Badalona, Spain (C. Rodrigo); Agència de Salut Pública de Catalunya, Barcelona (M.J. Vidal); CIBER de Enfermedades Infecciosas, Barcelona (T. Pumarola, M.N. Larrosa, J.J. González-López)

DOI: https://doi.org/10.3201/eid2805.211958

[1]These authors contributed equally to this article.

Table 1. Changes in the pertussis vaccination program in Spain, 1986–2018*

	Primary doses			Booster doses		
Year	Vaccine type	Schedule, mo	Pertussis components	Vaccine type	Schedule	Pertussis components
1975	WCV	3, 5, 7	Inactivated whole cell	NA	No booster	NA
1996	WCV	2–3, 4–5, 6–7	Inactivated whole cell	WCV	15–18 mo	Inactivated whole cell
1998/1999	WCV	2–3, 4–5, 6–7	Inactivated whole cell	ACV	18 mo	PT, FHA, PRN
2001	WCV	2, 4, 6	Inactivated whole cell	ACV	18 mo, 4–6 y	PT, FHA, PRN
2004†	NA	NA	NA	acv	Health workers caring for newborns	PT, FHA, PRN or PT, FHA, PRN, FIM2, FIM3‡
2005/2006	ACV	2, 4, 6	PT, FHA, PRN	ACV	18 mo, 4–6 y	PT, FHA, PRN
2012	ACV	2, 4, 6	PT, FHA, PRN	ACV/acv	18 mo (ACV), 4–6 y (acv)	PT, FHA, PRN or PT, FHA, PRN, FIM2, FIM3‡
2013	ACV	2, 4, 6	PT, FHA, PRN	ACV/acv	18 mo (ACV), 6 y (acv)	PT, FHA, PRN or PT, FHA, PRN, FIM2, FIM3‡
2014/2015§	NA	NA	NA	acv	From 27–28 through 32–36 wk of pregnancy	PT, FHA, PRN or PT, FHA, PRN, FIM2, FIM3‡
2017	ACV	2, 4, 11	PT, FHA, PRN or PT, FHA¶	ACV/acv#	6 y	PT, FHA, PRN or PT, FHA, PRN, FIM2, FIM3‡

*acv, diphtheria–tetanus–acellular pertussis vaccine with reduced antigenic load of diphtheria, tetanus and pertussis; ACV, diphtheria–tetanus–acellular pertussis vaccine; FHA, filamentous haemagglutinin; FIM2, type 2 fimbriae; FIM3, type 3 fimbriae; NA, not applicable; PRN, pertactin; PT, pertussis toxin; WCV, diphtheria–tetanus–whole-cell pertussis vaccine.
†Introduction of healthcare worker vaccination.
‡The 5-component ACV, which also contains FIM2 and FIM3, is used in some booster doses.
§Introduction of maternal pertussis vaccination.
¶At the end of 2013, use of an ACV not including the PRN component in primary vaccination was approved in Spain.
#ACV vaccine is administered to children vaccinated with the 2+1 schedule when they reach 6 y of age. Children vaccinated with the 3+1 schedule receive the acv vaccine.

pertactin-deficient isolates were detected in France and subsequently in other countries that had adopted ACV (*5*–*9*). Pertactin-deficient strains have demonstrated a greater ability than pertactin-producing strains to colonize ACV-vaccinated animals. Thus, the expansion of pertactin-deficient strains in human populations vaccinated with pertactin-containing vaccines indicates that such strains apparently have a selective advantage in these populations (*10*). The mechanisms associated with loss of pertactin expression are multiple and diverse, including, among others, insertion of the IS*481* and IS*1002* elements in several positions of the pertactin gene, deletions of small parts of or the entire pertactin gene, inversions, and presence of point mutations leading to stop codons (*6*,*11*). Globally, the main factor for pertactin deficiency is still the IS*481* insertion, but other mechanisms are increasing, such as the large inversion in the promotor area and the point mutations in the structural gene (i.e., in positions 223 and 1273 in *prn2*) (*12*–*14*).

To determine the presence of pertactin-deficient *B. pertussis* strains in Spain, we elucidated the genetic mechanisms involved in pertactin loss and bacterial population dynamics, and we analyzed whether replacing WCV with ACV affects emergence of pertactin-deficient *B. pertussis* strains. The study was approved by the Ethics Committee of the Hospital Universitari Vall d'Hebron (reference no. PR(AG)694/2020).

Methods

Bacterial Isolates and Study Period

We studied 342 nonduplicate *B. pertussis* clinical isolates collected at 5 hospitals at different locations in Spain during 1986–2018 (Appendix 1, https://wwwnc.cdc.gov/EID/article/28/5/21-1958-App1.pdf). All isolates were obtained from cultures of nasopharyngeal samples collected from patients with pertussis; we excluded isolates collected during studies of contacts. The study period was divided into 3 parts, based on the vaccine type used for routine vaccination in Spain: period 1 (1986–1997; 46/342 isolates) was defined by the exclusive use of WCV; period 2 (1998–2005; 51/342 isolates) was the period of transition to ACV; and period 3 (2006–2018, 245/342 isolates) was when ACV had completely replaced WCV. Isolates were collected from patients with different vaccination status: vaccinated, nonvaccinated, and partially vaccinated (incomplete primary vaccination [1–2 doses] and complete primary vaccination [3–4 doses]).

Vaccine Antigen Expression

We evaluated production of pertactin, PT, FHA, and fimbrial proteins FIM2 and FIM3. We used an indirect whole-cell ELISA with specific antibodies (97/558 for pertactin, 99/512 for PT S1 subunit, 99/572 for FHA, 06/124 for FIM2, and 06/128 for FIM3; National Institute for Biological Standards and Control, https://www.nibsc.org), as previously described (Appendix 1) (*15*–*17*).

Whole-Genome Sequencing and Data Analysis

We sequenced all pertactin-deficient isolates detected by ELISA and a proportional random selection of pertactin-producing isolates by using the MiSeq platform (Illumina, https://www.illumina.com) according to a 2 × 300 paired-end protocol. We obtained Bayesian phylogenetic reconstruction with BEAST version 1.10.4 (https://beast.community) by using the general time reversible substitution model, strict clock, and coalescent constant population (Appendix 1). We deposited the genome sequence reads of all 184 *B. pertussis* strains in the National Center for Biotechnology Inform ation database (BioProject no. PRJNA667582) (Appendix 2 Table 1, https://wwwnc.cdc.gov/EID/article/28/5/21-1958-App2.xlsx).

Results

Temporal Distribution of Pertactin-Deficient *B. pertussis*

All pertactin-deficient isolates (93/342) were collected during period 3, representing 38% of the isolates obtained during the period of exclusive ACV administration (Figures 1, 2). The first pertactin-deficient *B. pertussis* isolate was collected in 2007, when prevalence of pertactin-negative *B. pertussis* reached 29.4% of the total isolates collected. Since then, the number of pertactin-deficient isolates progressively increased; prevalence was highest in 2015, the last epidemic year of the disease in Spain, when 71.4% of *B. pertussis* isolates obtained did not express this antigen. Thereafter, prevalence of pertactin-deficient isolates decreased; 33.3% of the isolates collected during 2018 were deficient in production of this antigen. We observed no statistical differences in vaccination status between patients with pertactin-deficient and pertactin-producing *B. pertussis* infections (χ^2 test, p>0.05; Appendix 2 Table 1).

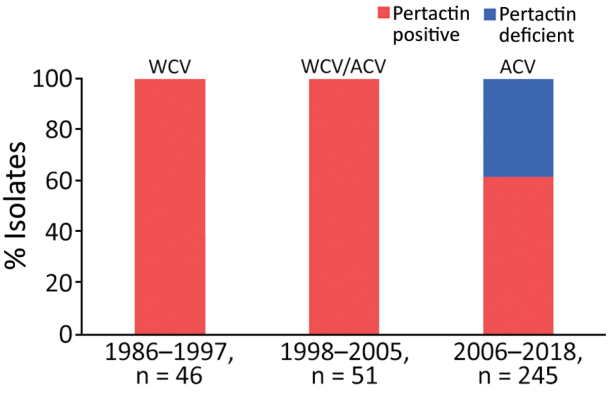

Figure 1. Temporal distribution of pertactin-deficient *Bordetella pertussis* isolates in Spain, 1986–2018. ACV, acellular vaccine WCV, whole-cell vaccine.

Molecular Mechanisms of Pertactin Deficiency

We identified 7 mechanisms involved with pertactin deficiency (Table 2; Appendix 2 Table 1). Among these mechanisms, we found partial deletion of the promoter zone and part of the pertactin-encoding gene located between positions –292 and 1340 (*prn*::del(–292, 1340)) in 54 (58.1%) of the 93 pertactin-deficient isolates. This mutation had been observed in 1 isolate collected in 2009 and was the most detected mechanism of pertactin deficiency since 2011, except for 2012 (Table 2; Figure 2). The second most common mechanism of pertactin deficiency was the IS*481* insertion at position 1613–1614 in reverse orientation (*prn*::IS*481*-1613rev). This mutation was identified in 12 (12.9%) of the pertactin-deficient isolates; it was identified in 2010 and remained as a

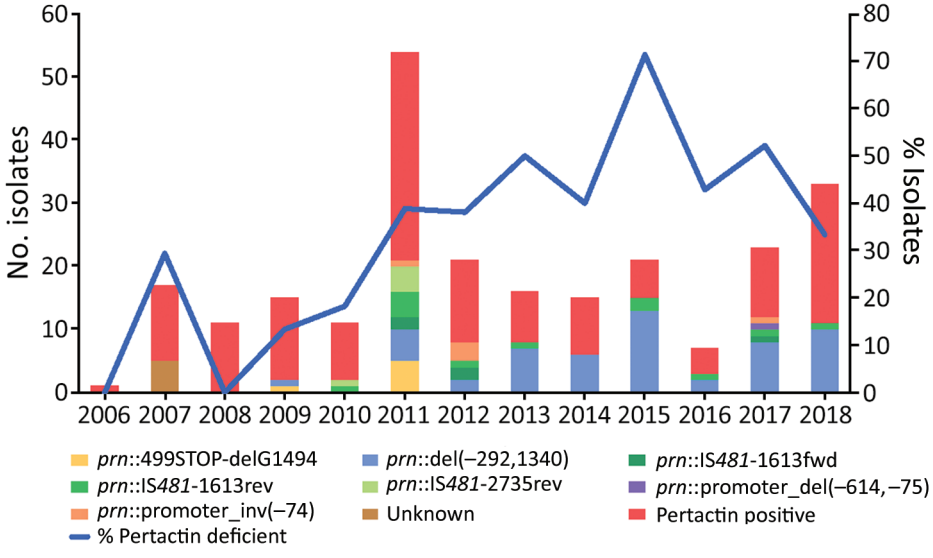

Figure 2. Temporal distribution of pertactin-deficient isolates and temporal trend of molecular mechanisms of pertactin deficiency in pertactin-deficient *Bordetella pertussis* isolates in Spain, 2006–2018 (study period 3). del, deletion; fwd, forward; inv, inversion; IS, insertion sequence; *prn*, pertactin gene; rev, reverse.

Table 2. Genomic mechanisms leading to origin deficiency of pertactin among *Bordetalla pertussis* isolates in Spain, 2006–2018*

Mechanism type	Mechanism name	Mechanism description	Genomic location†	Isolates, no. (%)	Reference
Deletion	*prn*::499STOP-delG1494	G deletion	1494	6 (6.5)	This study
	prn::del(–292, 1340)	Within promoter and first part of *prn* gene	–292 to 1340	54 (58.1)	(*18*)
	prn::promoter_del(–614, –75)	Within promoter	–614 to –75	1 (1.1)	This study
Insertion	*prn*::IS*481*-1613fwd	IS*481* within *prn*, forward direction	1613–1614	5 (5.4)	(*6*)
	prn::IS*481*-1613rev	IS*481* within *prn*, reverse direction	1613–1614	12 (12.9)	(*6*)
	prn::IS*481*-2735rev	IS*481* within *prn*, reverse direction	2735–2736	5 (5.4)	(*6*,*19*)
Inversion	*prn*::promoter_inv(-74)	22 kb large inversion within promoter	–20892 to –75	5 (5.4)	(*6*)

*del, deletion; fwd, forward insertion; inv, inversion; IS, insertion element; *prn*, pertactin gene; rev, reverse insertion.
†Numbers indicate the position of each mechanism relative to the *prn2* start codon.

mechanism of pertactin deficiency over the following years, except for 2014, when it was not found in any of the isolates collected (Table 2; Figure 2). Occasionally, we identified other minor causes of pertactin deficiency (Table 2; Figure 2; Appendix 2 Table 1). It was not possible to identify the genetic mechanism underlying the pertactin deficiency in 5 (5.4%) of the pertactin-deficient isolates collected during 2007 because no mutation was identified in the pertactin promoter or the structural gene (Figure 2; Appendix 2 Table 1).

Phylogenetic Analysis

To gain insight into the pertactin-deficient *B. pertussis* population dynamics in Spain, we reconstructed Bayesian phylogeny with a selection of 184 isolates: the 93 pertactin-deficient isolates and 91 pertactin-producing isolates randomly collected over the entire period. Whole-genome sequence variation analysis identified 1,255 single-nucleotide polymorphisms (SNPs). Bayesian evolution analysis conducted with BEAST estimated the mean evolutionary rate of *B. pertussis* as 2.7×10^{-7} substitutions/site/year (95% highest posterior density [HPD] $2.4–3 \times 10^{-7}$ substitutions/site/year), corresponding to 1.1 substitutions/genome/year. Bayesian model comparison confirmed that the general time reversible substitution model, strict clock, and coalescent constant population were the best fitting for the alignment. According to the type 3 fimbriae allele and the genetic identity of the isolates, we defined 3 clades within the phylogenetic tree (Figure 3, panel A; Appendix 2 Table 1). We found a strong association between the period and the clades of the circulating isolates (Figure 3, panel B). All isolates belonging to clades I, II, and III were producers of PT and FHA, regardless of pertactin loss (Appendix 2 Table 1).

Clade I, which was the most predominant clade during the exclusive WCV period, included 13 isolates obtained during 1986–1999 and 1 isolate collected in 2014. Overall, 84.6% contained the *ptxA1/ptxP1/fim2-1/fim3-1* allelic combination; for pertactin, 38.5% encoded *prn2*, 38.5% *prn3*, and 23.1% *prn1*. With regard to fimbrial serotypes, 46.2% were FIM3, 38.5% FIM2, and 15.4% FIM2/3. No pertactin-deficient isolates were observed among the isolates belonging to this clade (Figure 3; Appendix 2 Table 1).

Clade II, which predominated during the period of transition from WCV to ACV, included 64 isolates collected during 1998–2018, of which 93.8% contained the *ptxA1/ptxP3/prn2/fim2-1/fim3-2* allelic combination (Figure 3; Appendix 2 Table 1). With regard to fimbrial serotypes, 96.9% expressed FIM3 and 3.1% expressed both types of fimbriae simultaneously (FIM2/3). BEAST analysis estimated the time to the most recent common ancestor of the clade II isolates to be 1989 (95% HPD 1987–1992). With regard to pertactin production, 24 (37.5%) of the isolates from this clade were pertactin deficient. Of these, 13 (54.2%) contained a mutation associated with any of the IS*481* insertions described at position 1613–1614, distributed in different branches within the clade. Among these isolates, we identified a cluster of 6 isolates possessing the *prn*::IS*481*-1613rev mutation. The isolates were obtained in Barcelona during 2011–2017 (range 1–11 SNPs). In addition, 6 (25%) of the pertactin-deficient isolates within clade II shared the *prn*::499STOP-delG1494 mutation; all were genetically closely related, as they clustered together (range 0–4 SNPs). Samples containing these isolates were collected in Barcelona, and all but 1 was obtained during March–September 2011. No epidemiologic link was identified among the patients from whom these isolates were obtained. One pertactin-deficient isolate found in clade II showed the *prn*::promoter_del(–614, –75) mutation. All pertactin-deficient isolates from this clade, including *prn*::IS*481*-1613, *prn*::499STOP-delG1494 and

prn::promoter_del(–614, –75) mutations, presented the FIM3 serotype (Figure 3; Appendix 2 Table 1).

Clade III, which was the most predominant during the exclusive ACV period, consisted of 107 isolates collected during 2005–2018, of which 89.7% possessed the *ptxA1/ptxP3/prn2/fim2-1/fim3-1* allelic combination (Figure 3; Appendix 2 Table 1). With regard to fimbrial serotype, 72% of isolates of this clade expressed FIM2 and 28% FIM3, observed as FIM2 isolates replaced the previously predominant fimbrial serotype FIM3 from 2013 and coinciding with the incremental detection of pertactin-deficient isolates (Figure 4; Appendix 2 Table 1). BEAST analysis identified the time to the most recent common ancestor of clade III isolates as 1995 (95% HPD 1992–1998). Regarding pertactin production, 69 (64.5%) of the isolates of this clade were pertactin deficient. Of these, 54 (78.3%) possessed the *prn*::del(–292, 1340) mutation, forming a large cluster of isolates (range 0–19 SNPs of difference among them) obtained during 2009–2018 in Barcelona, Madrid, and Salamanca, Spain (estimated divergence occurring in 2007 [95% HPD 2005–2008]). Two other minor clusters of pertactin-deficient isolates with the same mechanism of pertactin deficiency were identified in clade III. The first cluster included 5 (7.2%) of the pertactin-deficient isolates within the clade (range 0–5 SNPs); all shared the *prn*::IS*481*-2735rev mutation and were collected during 2010–2011 in Barcelona, Madrid, and Salamanca. The second cluster also included 5 (7.2%) of the pertactin-deficient isolates within the clade (range 3–20 SNPs), possessed the *prn*::promoter_inv(–74) mutation, and was obtained during 2011–2017 in Barcelona, Madrid, and Salamanca. Of this clade, 4 (5.8%) pertactin-deficient isolates possessed a mutation associated with any of the described insertions of IS*481* at position

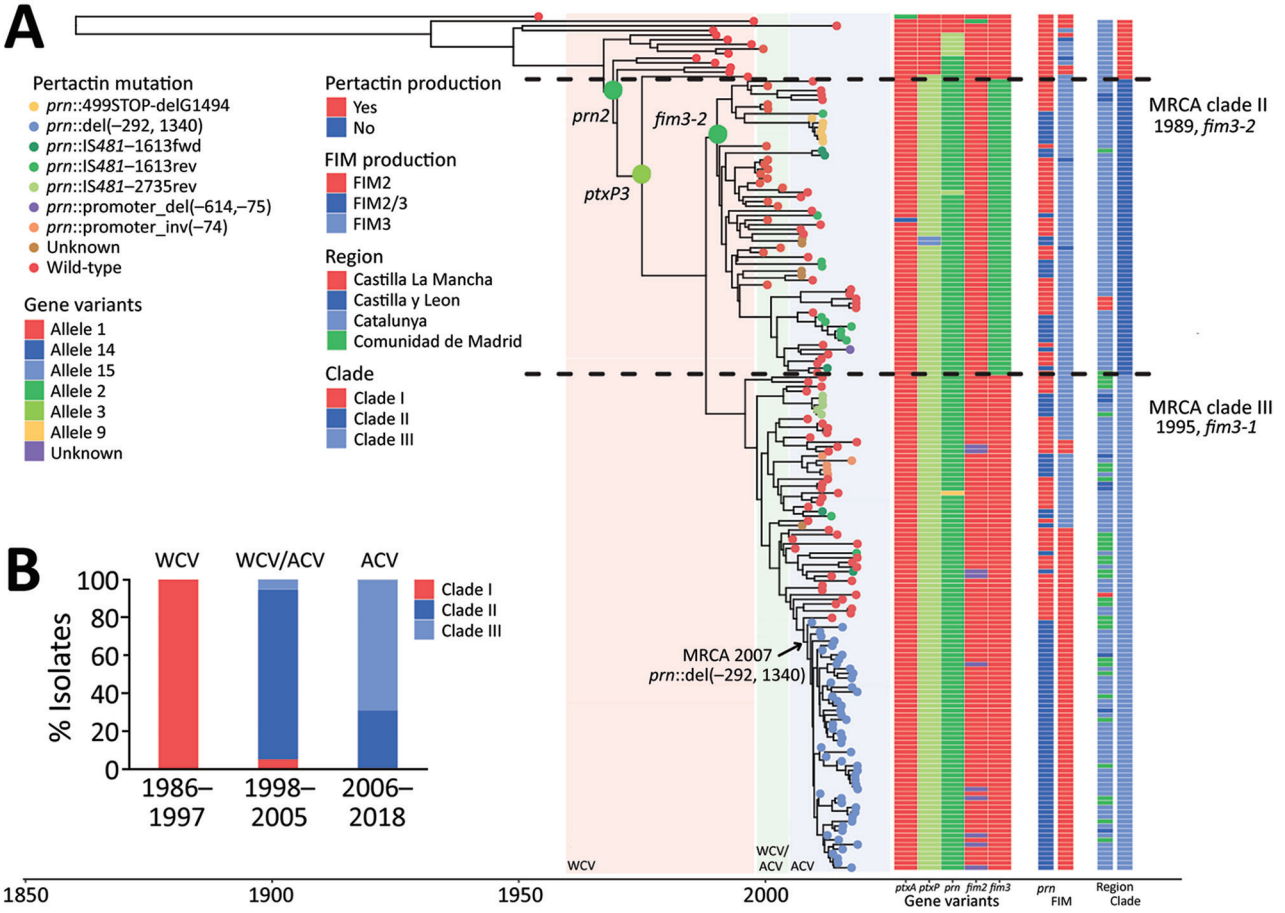

Figure 3. Time-scaled phylogeny of *Bordetella pertussis* isolates collected in Spain, 1986–2018. A) Bayesian phylogenetic reconstruction of 184 *B. pertussis* isolates and the reference Tohama I (GenBank accession no. NZ_CP031787). Shaded regions indicate periods of WCV, WCV/ACV, and ACV use. Colored dots at the end of the tree branches indicate pertactin production for each isolate. Alleles of *ptxA*, *ptxP*, *prn*, *fim2*, and *fim3* are indicated for each isolate, on the right. Data associated with expression (serotyping) of FIM2/FIM3 are also indicated for each isolate; B) Temporal distribution of the isolates' clades of *B. pertussis* based on the vaccine type(s) used for routine vaccination. ACV, acellular vaccine; del, deletion; FIM, fimbrial serotype; fwd, forward; inv, inversion; IS, insertion sequence; MRCA, most recent common ancestor; *prn*, pertactin gene; rev, reverse; WCV, whole-cell vaccine.

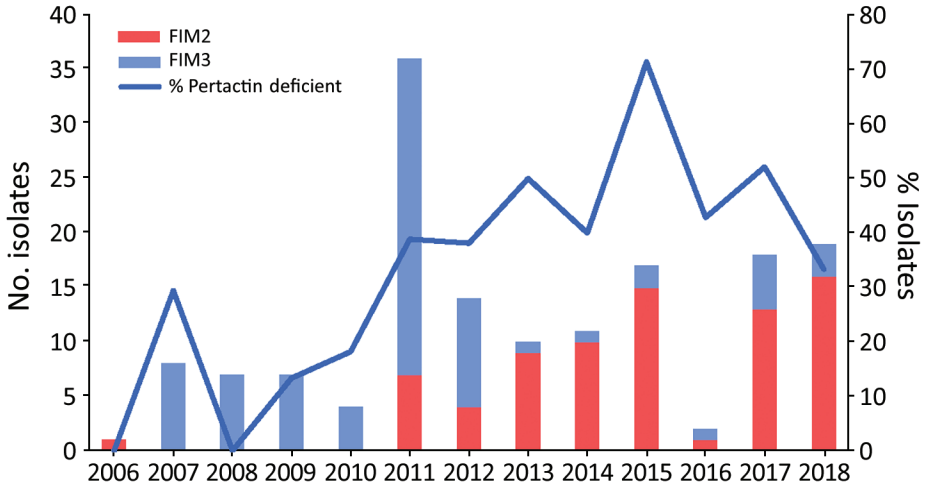

Figure 4. Temporal distribution of fimbrial serotypes and frequency of pertactin-deficient *Bordetella pertussis* isolates collected in Spain, 2006–2018 (study period 3). FIM, fimbrial serotype.

1613–1614; all were distributed randomly at different branches along the clade. Combining the deficiency of pertactin and the fimbrial serotype, *prn*::del(–292, 1340) isolates were associated with FIM2 expression, whereas *prn*::IS*481*-2735rev and *prn*::promoter_inv (–74) isolates were related to the FIM3 serotype. Last, 50% of pertactin-deficient isolates of clade III with the *prn*::IS*481*-1613 mutation expressed FIM2 and 50% possessed the FIM3 serotype (Figure 3; Appendix 2 Table 1).

We performed an SNP analysis to identify the genetic relationship among pertactin-deficient isolates showing clonal expansion in this study (i.e., *prn*::promoter_inv(–74), *prn*::del(–292, 1340), and *prn*::IS*481*-2735rev) and isolates that possessed the same pertactin gene mutation but were identified in other countries (i.e., Australia, France, and the United States) (Appendix 2 Table 2). The analysis revealed that isolates with the same pertactin gene–disruption mechanism nested together independently of the country in which they were obtained (Appendix 1 Figure).

Discussion

Pertactin-deficient isolates have been reported in several countries with a history of widespread vaccination with ACV containing pertactin. Nonetheless, there are no data for the pertactin-deficient *B. pertussis* strains in Spain. We detected pertactin-deficient isolates in Spain emerging concurrently with the introduction of ACV. We found pertactin-deficient isolate prevalence to be 38% during 2006–2018, the period of exclusive ACV use in this country.

In Spain, booster vaccination with ACV was introduced in the late 1990s and primary vaccination with ACV was begun in 2005. In 2007, shortly after implementation of ACV as the only vaccine administered against pertussis, the first pertactin-deficient isolate of this study was identified. After that, prevalence of pertactin-deficient *B. pertussis* progressively increased, reaching the highest prevalence (71.4%) in 2015. These results suggest that ACV use has probably driven an antigenic shift of *B. pertussis* toward loss of pertactin expression. This finding is in line with previously reported findings from several other countries, supporting the hypothesis that emergence of pertactin-deficient isolates depends on time since introduction of ACV containing pertactin (*6*,*13*). In a multicenter study conducted in Europe, in which ACV was introduced in several countries at the end of the 1990s, the proportion of pertactin-deficient isolates identified during 2007–2009 was 6.4% and during 2012–2015, the proportion increased to 24.9% (*13*). In Japan, ACV was first introduced in 1981 and 41% of pertactin-deficient isolates were detected during 2005–2007 (*20*). Similarly, in the United States, where ACV was introduced in 1991, 85% of *B. pertussis* isolates collected during 2011–2013 were pertactin deficient; and in Australia, the proportion of pertactin-deficient isolates reached 78% in 2012, after introduction of ACV in 1997 (*8*,*14*,*21*). However, a recent study conducted in Japan revealed a surprising decrease (to <10%) in prevalence of pertactin-deficient *B. pertussis* during 2014–2016. Furthermore, a genotypic replacement from the *ptxA2/ptxP1/prn1* to the *ptxA1/ptxP3/prn2* profile coinciding with the decline in pertactin-deficient *B. pertussis* was observed (*7*,*20*,*22*,*23*). The most likely explanation was the effect of the 2012 introduction of ACV not including the pertactin component (*20*). In our study, a decrease in pertactin-deficient

isolates within the *B. pertussis* population has been observed since 2016. No changes have been detected in vaccination coverage in Spain (>95% of coverage in primary vaccination since 1999) (*24*). However, introduction of a vaccine without the pertactin component used for primary vaccination was approved in Spain in 2013 and has been administered in 5 of 19 regions (not in Catalunya or the Comunidad de Madrid). Given that its use in Spain remains limited, establishing a possible causal relationship between its introduction and the loss of selective pressure towards pertactin-deficient isolates is difficult. Another factor that might have contributed to the increase of pertactin-producing isolates could be the progressive increase of the population with no immunity against pertactin as a consequence of natural immunization after infection by pertactin-deficient isolates over recent years. Nonetheless, in countries in which monocomponent vaccines (including PT only) or WCV were used, pertactin-deficient isolates were also observed. Examples include Denmark and Poland, where 14.8% of isolates collected during 2012–2015 and 15.4% of isolates collected during 2010–2016 were pertactin deficient (*13*,*25*). Intercountry circulation of pertactin-deficient strains among neighboring countries in which the ACV vaccine is used could explain dissemination of these isolates in these countries. To the contrary, few or no pertactin-deficient isolates were detected in countries such as Iran or Argentina, where WCV is used for primary vaccination, because there may be less selection pressure and less advantage for pertactin-deficient strains to emerge in a WCV-immunized population (*26*,*27*). Overall, these observations would support the hypothesis that pertactin-deficient isolates are selected in response to host immunity against pertactin after vaccination with ACV that contains this antigen (*20*).

Emergence of pertactin-deficient *B. pertussis* isolates in Spain has not resulted from an event of clonal emergence and dissemination because no single common ancestor has been found for all these isolates. We found that diverse mechanisms of pertactin gene disruption originated in different lineages distributed throughout the phylogeny of *B. pertussis*. This same phenomenon has been described in the United States, Japan, Australia, and several countries in Europe (*6*,*14*,*22*,*28*). The most commonly observed mechanism of disruption in our study (58.1%) was the unusual *prn*::del(–292, 1340), which implies a deletion of ≈1.6 kb. The second most commonly observed mechanism of pertactin deficiency (23.7%) was the IS*481* insertion at different locations along the pertactin gene (at positions 1613–1614 and 2735–2736, in either forward or reverse orientation). To the contrary, this mechanism has been the most frequently detected mechanism for pertactin deficiency in studies performed in other countries, such as Australia, Europe, and the United States, where 88.6%, 48.5% and 47.4% of the *B. pertussis* collected showed IS*481* as the main mechanism involved in pertactin gene disruption (*13*,*14*,*28*). Surprisingly, although *prn*::del(–292, 1340) has been identified sporadically in isolates from other countries, as far as we know, it has not been detected as a major mechanism of pertactin deficiency as observed in this collection of *B. pertussis* isolates in Spain. Specifically, this deletion has recently been detected in the United States in 1 isolate obtained in 2016 (*18*). It has also been detected in 5.9% of the pertactin-deficient isolates in Slovenia in a study conducted during 2006–2017, in 2.9% in Australia in a study conducted during 2013–2017, and in 5.6% of the recent pertactin-deficient isolates detected in France (*12*,*28*,*29*). All these isolates had the *ptxA1/ptxP3/fim3.1* genotype as observed in the isolates identified in our study (no data available for isolates from France) (*14*,*28*,*29*). As previously stated, vaccination coverage has not changed over the past 2 decades and no other demographic or epidemiologic factors that might have been involved in the successful dissemination of *prn*::del(–291, 1340) isolates in Spain have been identified. In addition, these isolates clustered together in the *B. pertussis* phylogeny and arose within the period of ACV use in Spain, suggesting that ACV implementation might have contributed to emergence of isolates containing this mutation and their dissemination in the environment. That the high prevalence observed is not the result of an event of outbreak-related dissemination is suggested by the genetic distance they possess; the fact that they have been found in different regions of Spain in different years; and the finding that isolates from Australia, France, and the United States possess this mutation also grouped in a monophyletic cluster with the isolates from our study (range 0–19 SNPs). Therefore, expansion of these isolates in Spain but not in other countries could be interpreted as successful intracountry dissemination of this lineage of isolates. Continued monitoring of their prevalence and evolution, especially among neighboring countries, is needed.

Our findings revealed that the fimbrial serotype of the *B. pertussis* circulating strains has shifted over the years, although most of the ACV

used does not contain FIM antigens because FIM2 isolates replaced the previously predominant fimbrial serotype FIM3 from 2013, coinciding with increased detection of pertactin-deficient isolates. Although information regarding the type of ACV vaccine administered is not available, fimbrial serotype replacement in *B. pertussis* is common and has been previously associated with immunity induced by vaccine or natural infection (*30*,*31*). When comparing the fimbrial serotype with pertactin deficiency, we observed that pertactin-deficient isolates collected at the beginning of the ACV period (2007–2012) were mostly associated with FIM3. Likewise, pertactin-deficient isolates collected in the last years of the ACV period (2013–2018) were mainly associated with FIM2, concurring with the shift in fimbrial serotype observed in the circulating *B. pertussis* population. Similarly, in other studies conducted in Europe, 84.9% of pertactin-deficient isolates obtained during 1998–2015 were FIM3, whereas all pertactin-deficient isolates collected in Slovenia during 2014–2017 were FIM2, denoting fimbrial serotype replacement as a consequence of immunity induced by the previous circulation of FIM3 isolates (*13*,*29*). In our study, the fimbrial serotype shift toward FIM2 mostly likely resulted from emergence of isolates with the *prn*::del(–292, 1340) mutation, suggesting a possible link between the 2 characteristics, which could provide an adaptive advantage of the isolates to escape population immunity, whether generated by vaccination or by natural infection by FIM3-producing *B. pertussis*.

One study limitation might be underdetection of low-prevalence *prn* mutations as a consequence of the number of isolates included per year, the overrepresentation of isolates from the ACV period, and the higher number of isolates collected from the Catalunya region. However, we provide a representative view of the mutations that have conditioned the emergence of pertactin-deficient *B. pertussis* in Spain because we did not include isolates from contacts of case-patients and the most prevalent pertactin-deficiency mechanisms found were detected in different regions of Spain in different years.

Our results show how introduction of ACV concurred with emergence of pertactin-deficient *B. pertusiss* in Spain. Several mechanisms are responsible for this phenomenon; the most identified mutation is *prn*::del(–292, 1340), found in a specific cluster of *B. pertussis*, which emerged after the implementation of vaccination with ACV. This finding is contrary to what has been observed in other countries, in which an IS*481*-mediated pertactin gene disruption has been the main mechanism identified. Other factors may have contributed to the dissemination of pertactin-deficient isolates in Spain, reinforcing the value of long-term surveillance of *B. pertussis* populations and their antigenic characteristics to assess the role that different pathogen adaptation mechanisms may have in the emergence of pertussis.

Acknowledgments

We are grateful to Nicole Guiso and Sophie Guillot for kindly providing the reference pertactin-deficient *B. pertussis* isolate from France used in this study and to Sylvain Brisse and Valérie Bouchez for sharing the reads of pertactin-deficient reference *B. pertussis* isolates from France used in phylogenetic analysis. We thank Adelaida Ferrer for her contribution to the creation of the *B. pertussis* isolates collection in the Hospital Universitari Vall d'Hebron.

This work was supported by the Ministerio de Economía y Competitividad, Instituto de Salud Carlos III, and cofinanced by the European Regional Development Fund "A Way to Achieve Europe" (Spanish Network for Research in Infectious Diseases, grant no. FIS PI18/00703) and by the Centro de Investigación Biomédica en Red (CIBER de Enfermedades Infecciosas), the Red Española de Investigación en Patología Infecciosa (grant no. CB21/13/00054). A.M.C. is supported by the Agència de Gestió d'Ajuts Universitaris i de Recerca de la Generalitat de Catalunya at Vall d'Hebron Institut de Recerca (Ajuts per a la Contractació de Personal Investigador FI, grant no. 2020FI_B2_00145) and by the Spanish Network for Research in Infectious Diseases (grant no. RD16/0016/0003). A.M.M. is supported by a grant from the Fondo de Investigación Sanitaria at Vall d'Hebron Institut de Recerca (Contratos Predoctorales de Formación en Investigación, grant no. FI19/00315).

About the Authors

Ms. Mir-Cros and Mr. Moreno-Mingorance are PhD students working at the Clinical Microbiology Research Group of the Hospital Universitari Vall d'Hebron Research Institute, Barcelona, Spain. Ms. Mir-Cros's research interests are the epidemiology and molecular characterization of *B. pertussis* and other related species, and Mr. Moreno-Mingorance's research interests are the use of bioinformatics in the study of bacterial populations and the characterization of antibiotic-resistant bacteria.

References

1. van Gent M, Heuvelman CJ, van der Heide HG, Hallander HO, Advani A, Guiso N, et al. Analysis of *Bordetella pertussis* clinical isolates circulating in European countries during

the period 1998-2012. Eur J Clin Microbiol Infect Dis. 2015;34:821–30. https://doi.org/10.1007/s10096-014-2297-2
2. Octavia S, Sintchenko V, Gilbert GL, Lawrence A, Keil AD, Hogg G, et al. Newly emerging clones of *Bordetella pertussis* carrying prn2 and ptxP3 alleles implicated in Australian pertussis epidemic in 2008-2010. J Infect Dis. 2012;205:1220–4. https://doi.org/10.1093/infdis/jis178
3. Mir-Cros A, Moreno-Mingorance A, Martín-Gómez MT, Codina G, Cornejo-Sánchez T, Rajadell M, et al. Population dynamics and antigenic drift of *Bordetella pertussis* following whole cell vaccine replacement, Barcelona, Spain, 1986-2015. Emerg Microbes Infect. 2019;8:1711–20. https://doi.org/10.1080/22221751.2019.1694395
4. Barkoff A-M, Mertsola J, Pierard D, Dalby T, Hoegh SV, Guillot S, et al. Surveillance of circulating *Bordetella pertussis* strains in Europe during 1998-2015. J Clin Microbiol. 2018;56:e01998–17. https://doi.org/10.1128/JCM.01998-17
5. Bouchez V, Brun D, Cantinelli T, Dore G, Njamkepo E, Guiso N. First report and detailed characterization of *B. pertussis* isolates not expressing pertussis toxin or pertactin. Vaccine. 2009;27:6034–41. https://doi.org/10.1016/j.vaccine.2009.07.074
6. Zeddeman A, van Gent M, Heuvelman CJ, van der Heide HG, Bart MJ, Advani A, et al. Investigations into the emergence of pertactin-deficient *Bordetella pertussis* isolates in six European countries, 1996 to 2012. Euro Surveill. 2014;19:20881. https://doi.org/10.2807/1560-7917.ES2014.19.33.20881
7. Otsuka N, Han H-J, Toyoizumi-Ajisaka H, Nakamura Y, Arakawa Y, Shibayama K, et al. Prevalence and genetic characterization of pertactin-deficient *Bordetella pertussis* in Japan. PLoS One. 2012;7:e31985. https://doi.org/10.1371/journal.pone.0031985
8. Lam C, Octavia S, Ricafort L, Sintchenko V, Gilbert GL, Wood N, et al. Rapid increase in pertactin-deficient *Bordetella pertussis* isolates, Australia. Emerg Infect Dis. 2014;20:626–33. https://doi.org/10.3201/eid2004.131478
9. Pawloski LC, Queenan AM, Cassiday PK, Lynch AS, Harrison MJ, Shang W, et al. Prevalence and molecular characterization of pertactin-deficient *Bordetella pertussis* in the United States. Clin Vaccine Immunol. 2014;21:119–25. https://doi.org/10.1128/CVI.00717-13
10. Safarchi A, Octavia S, Luu LDW, Tay CY, Sintchenko V, Wood N, et al. Pertactin negative *Bordetella pertussis* demonstrates higher fitness under vaccine selection pressure in a mixed infection model. Vaccine. 2015;33:6277–81. https://doi.org/10.1016/j.vaccine.2015.09.064
11. Barkoff A-M, He Q. Molecular epidemiology of *Bordetella pertussis*. Adv Exp Med Biol. 2019;1183:19–33. https://doi.org/10.1007/5584_2019_402
12. Bouchez V, Guillot S, Landier A, Armatys N, Matczak S, Toubiana J, et al.; French Pertussis Microbiology Study Group. Evolution of *Bordetella pertussis* over a 23-year period in France, 1996 to 2018. Euro Surveill. 2021;26:2001213. https://doi.org/10.2807/1560-7917.ES.2021.26.37.2001213
13. Barkoff A-M, Mertsola J, Pierard D, Dalby T, Hoegh SV, Guillot S, et al. Pertactin-deficient *Bordetella pertussis* isolates: evidence of increased circulation in Europe, 1998 to 2015. Euro Surveill. 2019;24:1700832. https://doi.org/10.2807/1560-7917.ES.2019.24.7.1700832
14. Weigand MR, Williams MM, Peng Y, Kania D, Pawloski LC, Tondella ML; CDC Pertussis Working Group. Genomic survey of *Bordetella pertussis* diversity, United States, 2000–2013. Emerg Infect Dis. 2019;25:780–3. https://doi.org/10.3201/eid2504.180812
15. Barkoff A-M, Guiso N, Guillot S, Xing D, Markey K, Berbers G, et al. A rapid ELISA-based method for screening *Bordetella pertussis* strain production of antigens included in current acellular pertussis vaccines. J Immunol Methods. 2014;408:142–8. https://doi.org/10.1016/j.jim.2014.06.001
16. Tsang RSW, Sill ML, Advani A, Xing D, Newland P, Hallander H. Use of monoclonal antibodies to serotype *Bordetella pertussis* isolates: comparison of results obtained by indirect whole-cell enzyme-linked immunosorbent assay and bacterial microagglutination methods. J Clin Microbiol. 2005;43:2449–51. https://doi.org/10.1128/JCM.43.5.2449-2451.2005
17. Heikkinen E, Xing DK, Ölander R-M, Hytönen J, Viljanen MK, Mertsola J, et al. *Bordetella pertussis* isolates in Finland: serotype and fimbrial expression. BMC Microbiol. 2008;8:162. https://doi.org/10.1186/1471-2180-8-162
18. Weigand MR, Peng Y, Cassiday PK, Loparev VN, Johnson T, Juieng P, et al. Complete genome sequences of *Bordetella pertussis* isolates with novel pertactin-deficient deletions. Genome Announc. 2017;5:e00973–17. https://doi.org/10.1128/genomeA.00973-17
19. Weigand MR, Peng Y, Loparev V, Batra D, Bowden KE, Burroughs M, et al. The history of *Bordetella pertussis* genome evolution includes structural rearrangement. J Bacteriol. 2017;199:e00806–16. https://doi.org/10.1128/JB.00806-16
20. Hiramatsu Y, Miyaji Y, Otsuka N, Arakawa Y, Shibayama K, Kamachi K. Significant decrease in pertactin-deficient *Bordetella pertussis* isolates, Japan. Emerg Infect Dis. 2017;23:699–701. https://doi.org/10.3201/eid2304.161575
21. Martin SW, Pawloski L, Williams M, Weening K, DeBolt C, Qin X, et al. Pertactin-negative *Bordetella pertussis* strains: evidence for a possible selective advantage. Clin Infect Dis. 2015;60:223–7. https://doi.org/10.1093/cid/ciu788
22. Zomer A, Otsuka N, Hiramatsu Y, Kamachi K, Nishimura N, Ozaki T, et al. *Bordetella pertussis* population dynamics and phylogeny in Japan after adoption of acellular pertussis vaccines. Microb Genom. 2018;4:e000180. https://doi.org/10.1099/mgen.0.000180
23. Miyaji Y, Otsuka N, Toyoizumi-Ajisaka H, Shibayama K, Kamachi K. Genetic analysis of *Bordetella pertussis* isolates from the 2008-2010 pertussis epidemic in Japan. PLoS One. 2013;8:e77165. https://doi.org/10.1371/journal.pone.0077165
24. Centro Nacional de Epidemiología, Instituto de Salud Carlos III. Situación de la Tosferina en España, 1998-2016 [cited 2022 Jan 30]. https://www.isciii.es/QueHacemos/Servicios/VigilanciaSaludPublicaRENAVE/EnfermedadesTransmisibles/Documents/archivos%20A-Z/TOSFERINA/Situación%20de%20la%20Tosferina%20en%20España,%201998-2016.pdf
25. Polak M, Zasada AA, Mosiej E, Krysztopa-Grzybowska K, Witkowski L, Rzeczkowska M, et al. Pertactin-deficient *Bordetella pertussis* isolates in Poland–a country with whole-cell pertussis primary vaccination. Microbes Infect. 2019;21:170–5. https://doi.org/10.1016/j.micinf.2018.12.001
26. Safarchi A, Octavia S, Nikbin VS, Lotfi MN, Zahraei SM, Tay CY, et al. Genomic epidemiology of Iranian *Bordetella pertussis*: 50 years after the implementation of whole cell vaccine. Emerg Microbes Infect. 2019;8:1416–27. https://doi.org/10.1080/22221751.2019.1665479
27. Carriquiriborde F, Regidor V, Aispuro PM, Magali G, Bartel E, Bottero D, et al. Rare detection of *Bordetella pertussis* pertactin-deficient strains in Argentina. Emerg Infect Dis. 2019;25:2048–54. https://doi.org/10.3201/eid2511.190329
28. Xu Z, Octavia S, Luu LDW, Payne M, Timms V, Tay CY, et al. Pertactin-negative and filamentous hemagglutinin-negative *Bordetella pertussis*, Australia, 2013–2017. Emerg

Infect Dis. 2019;25:1196–9. https://doi.org/10.3201/eid2506.180240
29. Kastrin T, Barkoff A-M, Paragi M, Vitek MG, Mertsola J, He Q. High prevalence of currently circulating *Bordetella pertussis* isolates not producing vaccine antigen pertactin in Slovenia. Clin Microbiol Infect. 2019;25:258–60. https://doi.org/10.1016/j.cmi.2018.10.005
30. Elomaa A, Advani A, Donnelly D, Antila M, Mertsola J, Hallander H, et al. Strain variation among *Bordetella pertussis* isolates in Finland, where the whole-cell pertussis vaccine has been used for 50 years. J Clin Microbiol. 2005;43:3681–7. https://doi.org/10.1128/JCM.43.8.3681-3687.2005
31. Gorringe AR, Vaughan TE. *Bordetella pertussis* fimbriae (Fim): relevance for vaccines. Expert Rev Vaccines. 2014;13:1205–14. https://doi.org/10.1586/14760584.2014.930667

Address for correspondence: Juan José González-López, Department of Clinical Microbiology, Hospital Universitari Vall d'Hebron, Pg Vall d'Hebron 119-129, 08035 Barcelona, Spain; email: jjgonzal@vhebron.net

Determining Existing Human Population Immunity as Part of Assessing Influenza Pandemic Risk

Jonathan Tin Lai Cheung, Tim K. Tsang, Hui-ling Yen, Ranawaka A.P.M. Perera, Chris Ka Pun Mok, Yong Ping Lin, Benjamin J. Cowling, Malik Peiris

Zoonotic influenza infections continue to threaten human health. Ongoing surveillance and risk assessment of animal viruses are needed for pandemic preparedness, and population immunity is an important component of risk assessment. We determined age-stratified hemagglutinin inhibition seroprevalence against 5 swine influenza viruses circulating in Hong Kong and Guangzhou in China. Using hemagglutinin inhibition seroprevalence and titers, we modeled the effect of population immunity on the basic reproduction number (R_0) if each virus were to become transmissible among humans. Among 353 individual serum samples, we reported low seroprevalence for triple-reassortant H1N2 and Eurasian avian-like H1N1 influenza viruses, which would reduce R_0 by only 18%–20%. The smallest R_0 needed to cause a pandemic was 1.22–1.24, meaning existing population immunity would be insufficient to block the spread of these H1N1 or H1N2 variants. For human-origin H3N2, existing population immunity could suppress R_0 by 47%, thus reducing pandemic risk.

An influenza pandemic can occur when an influenza A virus with gene segments derived in part or whole from animal viruses becomes able to efficiently and sustainably transmit among humans (*1*,*2*). Lack of prior immunity among the human population to the hemagglutinin (HA) of a novel virus enables pandemic spread of that virus. New influenza vaccines require >7 months to develop, but pandemics spread faster than that; a new vaccine would not be available in time to prevent a first pandemic wave, as was seen during the 2009 influenza (H1N1) pandemic (*1*,*3*). Because of this delay, surveillance and risk assessment are used to anticipate pandemic threats (*4*,*5*), enabling preemptive vaccine development to be initiated. Prepandemic actions might include developing vaccine seed strains, experimental vaccine seed lots, or even phase 1 clinical trials of prepandemic vaccine candidates, depending on risk assessment data. The World Health Organization (WHO) and Centers for Disease Control and Prevention (CDC) developed the Tool for Influenza Pandemic Risk Assessment and Influenza Risk Assessment Tool in response to the need for standardized and transparent tools to assess the pandemic potential of influenza viruses (*5*,*6*). Based on the properties of the virus, attributes in the human population, and virus ecology in animal hosts (*6*), such assessments attempt to determine emergence risk, the potential of an animal virus to become able to efficiently transmit among humans, and effect risk, the effect and severity if that virus were to spread among humans. Population immunity is an important feature of assessing risk.

Pandemic spread depends on the ability of a virus to transmit among humans, which is measured as the basic reproduction number (R_0), the average number of secondary cases generated by 1 infected person in a completely susceptible population. If R_0 is ≥1, the outbreak will tend to spread or persist, but if R_0 is <1, the outbreak will likely not spread or persist. At the start of some pandemics, such as the H1N1 pandemic in 2009, immunity levels may differ among some age groups, and the effective reproduction number, R_t, better reflects transmissibility. This value depends on virus characteristics (biological transmissibility), population density and social mixing, and existing human population immunity, which can reduce transmission efficiency. Existing cross-reactive population immunity is a key factor that can inhibit the spread of the virus among humans and also one key risk element for assessing emergence risk.

Author affiliations: University of Hong Kong, Hong Kong (J.T.L. Cheung, T.K. Tsang, H. Yen, R.A.P.M. Perera, C.K.P. Mok, B.J. Cowling, M. Peiris); Chinese University of Hong Kong, Hong Kong (C.K.P. Mok); First Affiliated Hospital of Guangzhou Medical University, Guangdong, China (Y.P. Lin)

DOI: https://doi.org/10.3201/eid2805.211965

Hemagglutination inhibition (HAI) antibody is a well-established immune correlate of protection against influenza. Data from experimentally infected humans show a correlation between increasing HAI titer to an influenza A virus and decreasing probability of infection; ≈50% of persons protected at an HAI titer of 40 became infected (*7*,*8*). However, there is a gradient of protection above and below this threshold HAI titer of 40. Estimates of population immunity in risk assessment algorithms would benefit from greater precision and scientific rationale (*6*). Current algorithms do not use the range or age-stratified distribution of HAI titers in the population, which might affect measures of overall population immunity. In a previous study (*9*), we assessed the effect on the R_t of age-stratified distribution of HAI titers to H2N2 influenza viruses. In this study, we refined and extended this approach, including the use of data on antibody titers, and applied it to assess human population immunity to swine influenza viruses (SIVs).

Eurasian avian (EA)–like H1 SIVs have circulated in China since 2001 (*10*) and have been the dominant strain in southern China since 2005 (*11*). Triple-reassortant internal gene (TRIG) H1 SIVs from North America have been detected in swine in China since 2002 and Vietnam since 2011 (*12*). Swine carry pandemic H1N1 virus gene segments acquired by reassortment (*11*,*13*–*15*).

China and Vietnam are the largest swine producers in Asia and together account for 40.2% of global production (https://www.statista.com/statistics/273232/net-pork-production-worldwide-by-country). Swine are often raised in close proximity to avian species and humans, with low biosecurity, enhancing risks of pandemic emergence (*1*,*4*). In this study, we assessed age-stratified levels of HAI antibodies to swine influenza A viruses recently circulating in China in human serum samples collected in Hong Kong and Guangzhou, then used these data to quantify population immunity to infection. In addition, as a case study, we modeled pre-2009 population immunity to the 2009 H1N1 virus (H1N1pdm09) as an example of an actual swine virus that emerged in pandemic form (*16*).

Methods

Cross-Sectional Age-Stratified Serum Panels

We used serum samples collected December 6, 2013–March 29, 2014 from children and adults in Hong Kong as part of a community-based cohort study (*17*). We recruited study participants on the household level, identifying households using random digit dialing. The study protocol was approved by the institutional review board of the University of Hong Kong.

We selected an age-stratified subset of 173 serum samples from this larger study for the present investigation. We selected an additional age-stratified panel of 180 anonymized serum samples from residual serum samples from patients with nonrespiratory and noninfectious illnesses admitted to the First Affiliated Hospital of Guangzhou Medical University, February 9–March 31, 2015. The study was approved by the ethics committee of the First Affiliated Hospital of Guangzhou Medical University (reference no. 2015-8).

Virus Antigens

As antigens for HAI tests, we selected 5 H1 and H3 subtype swine influenza viruses representing predominant lineages of viruses circulating in China: EA H1 swine virus A/swine/Hong Kong/NS4003/2016 (H1N1)(NS4003); TRIG H1-lineage virus A/swine/Hong Kong/NS301/2013 (H1N2) (NS301); H1N1pdm09-like swine H1N1 virus A/swine/Hong Kong/1436/2016 (H1N1) (TS1436); and a Binh Duong-like H3N2 swine virus A/swine/Hong Kong/4348/2016 (H3N2) (TS4348), which originated from the human H3N2 seasonal viruses in 2004–2006 (Appendix Figure 1, https://wwwnc.cdc.gov/EID/article/28/5/21-1965-App1.pdf) (*13*,*18*). The fifth lineage was a recombinant virus we generated, EA-lineage A/swine/Guangdong/104/2013 (H1N1) (GD104), reported elsewhere to have low cross-reactivity with human serum samples (*19*). We synthesized the HA gene of wild-type GD104 virus (GenBank accession no. KJ725040), cloning it into the pHW2000 vector (*20*,*21*) and a recombinant virus $A/PR/8/34^{PB2,PB1,PA,NP,NA,M,NS}$ × $A/swine/Guangdong/104/2013^{HA}$ (Rg-PR8 × $GD104^{HA}$) containing the HA gene derived from A/swine/Guangdong/104/2013 (H1N1) (GD104) and the 7 other genes from A/PR/8/34 (H1N1), rescued by virus reverse genetics (Appendix) (*21*). We also recorded the origins of the 8 gene segments of each virus (Appendix Figure 2). We propagated the SIVs in MDCK cells as described elsewhere (*14*).

HAI Assay

We pretreated serum samples with receptor-destroying enzyme (Denka Seiken, https://www.denka.co.jp), followed by heat inactivation at 56°C for 30 min, then serially diluted treated serum samples 2-fold (1:10–1:1,280) into microtiter plates. We

performed HAI with 0.5% turkey red blood cells using an equal volume of virus with 8 HA units/50 µL in duplicate (*22*). We determined HAI titer by the highest dilution of serum that prevented complete hemagglutination.

For calculating geometric mean titers (GMTs), we assigned a value of 5 to serum samples with a titer <10 and a value of 1,280 to those with a titer ≥1,280. We used antibody titers of 10 and 40 as cutoff values and used the Fisher exact test to compare the differences in seroprevalence between groups. We considered differences with a p value <0.05 statistically significant. We conducted all statistical analyses using R version 3.6.1 (https://cran.r-project.org/bin/windows/base/old/3.6.1).

Reproduction Number Modeling

We partitioned the seroprevalence data into 8 age groups by decade (e.g., 0–10 y, 11–20 y) and 9 HAI titer levels: <10, 10, 20, 40, 80, 160, 320, 640, and ≥1,280. We obtained population age distribution from the most recent census data from Hong Kong (2016; https://www.censtatd.gov.hk/en/scode459.html) and Guangzhou (2015; http://tjj.gz.gov.cn/pchb/2015n1rkcydc/content/post_2787426.html). We used data from a human challenge study to determine the protection against infection associated with each HAI antibody titer (*7*,*23*), then estimated the proportion of population in each HAI titer group for each age group using Bayesian inference with Dirichlet conjugates for multinomial likelihood assuming noninformative priors (Appendix). We calculated the proportion of the population that was immune by weighting the age-stratified sample immunity profile to the corresponding population age structure. We then constructed the next-generation transmission matrix using the social contact matrix for Hong Kong (*24*) and used the social contact matrix for the UK population for comparison (*25*). We defined R_0 as the largest eigenvalue of the transmission matrix (*26*,*27*), then constructed another transmission matrix in which we subtracted the population protected by HAI antibodies from the total, thus including only the susceptible population from each age group, meaning R_t was the largest eigenvalue of this matrix. Given that population immunity profile, we calculated the corresponding relative reduction in transmissibility, then computed the smallest R_0 needed to cause a pandemic for each test virus. We generated 95% credible intervals (CrI) for the estimated parameters using 10,000 repeated samples randomly drawn from the joint posterior distribution for each age group (Appendix).

Historical Pandemic Strain Simulation

To test our methodology on data from an actual recent pandemic, we used the same methods to assess population immunity to H1N1pdm09 in human serum samples collected before its spread in Hong Kong. Prior to the emergence of the 2009 pandemic, only those >50 years of age had cross-reactive HAI antibodies to H1N1pdm09 at a seroprevalence of >10% (*16*,*28*). We retrieved A/California/4/2009 HAI data from 2 serologic surveys performed in the population of Hong Kong in November–December 2008 and July–August 2009, before the onset of the first wave of the 2009 pandemic in Hong Kong (*29*,*30*). We imputed those HAI data into our reproduction number model to assess all-age population serologic immunity and susceptibility in a prepandemic setting against a virus of proven pandemic potential. We also retrieved HAI data on the H2N2 pandemic strain A/Singapore/1/57(H2N2) from a serologic survey conducted in Hong Kong in 2011 (*9*). Only those persons born before 1968 would be expected to carry detectable antibodies for the H2N2 viruses. We used methods from this study to assess the effect of current age-specific human population immunity against a H2-subtype influenza virus if it were to reemerge as a pandemic strain.

Results

Age-Stratified Seroprevalence

Among serum samples with HAI titers ≥40 from the Hong Kong and Guangzhou (Figure 1), stratified by 10-year age intervals, we found no significant differences across all age groups in the seroprevalence to A/Sw/HK/NS4003/2016 (H1N1), A/Sw/GD/104/2013 (H1N1), A/Sw/HK/NS301/2013 (H1N2), or A/Sw/HK/1436/2016 (H1N1). We found a significant difference in the seroprevalence of A/Sw/HK/4348/2016 (H3N2) virus HAI only in the age group 41–50 years; seroprevalence was significantly higher in serum samples from Guangzhou than Hong Kong ($p = 0.003$). Considering the overall similarity of the patterns of seroprevalence in Hong Kong and Guangzhou, we combined data from the 2 cities for further analysis to assess population-level immunity.

Data on the overall HAI seroprevalence at titers of ≥10 and ≥40 and GMTs of antibodies to 5 tested viruses overall (Table 1) and age-stratified data (Table 2) showed an overall low seroprevalence to 2 H1N1 EA viruses and the H1N2 TRIG virus. In contrast, 41.4% of samples had antibody titers ≥40 to H1N1pdm09-like virus (Table 1); we found greater seroprevalence levels in children and younger adults ≤30

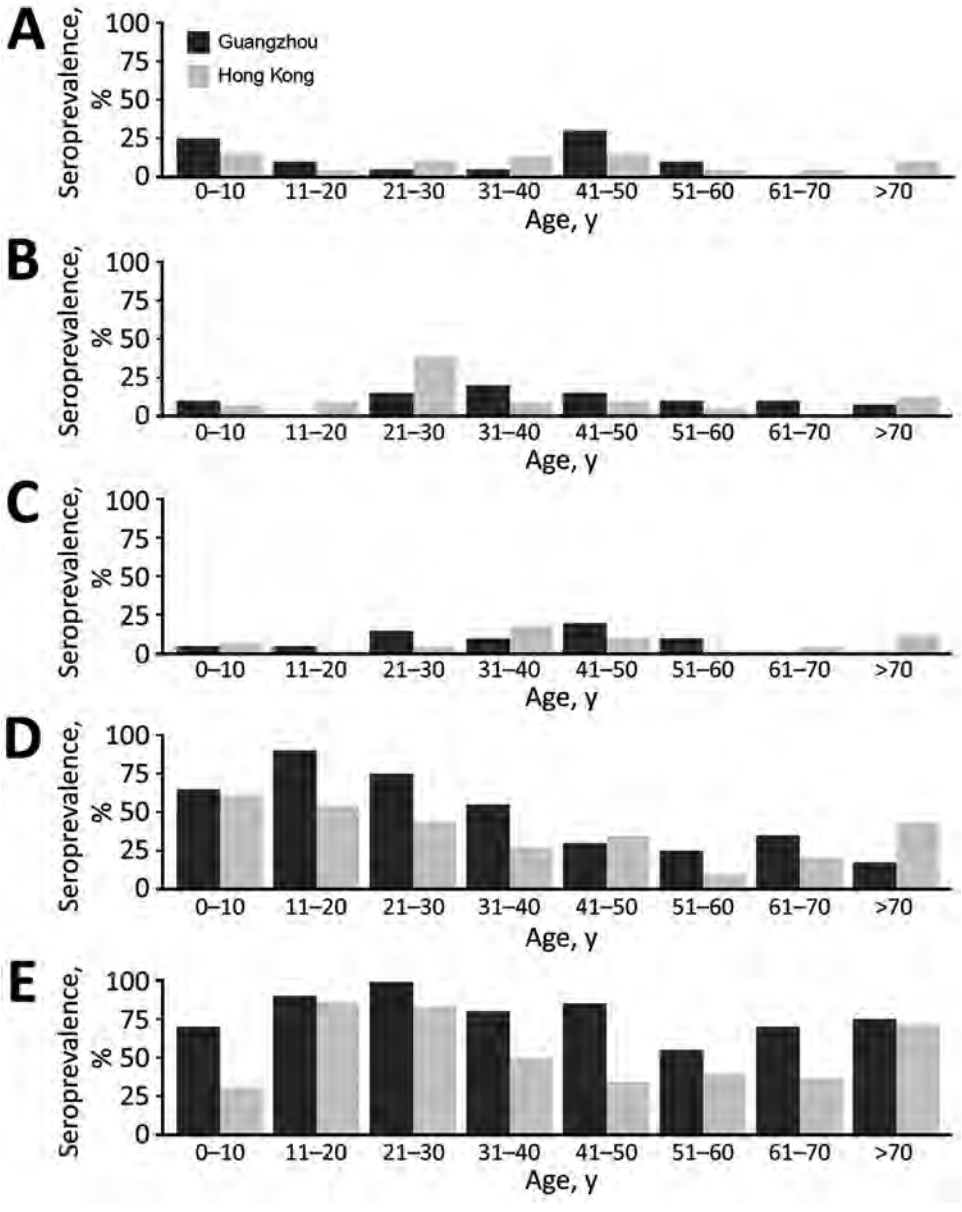

Figure 1. Seroprevalence of hemagglutination inhibition antibodies to different swine influenza viruses, by age group and location, A) A/swine/Hong Kong/NS4003/2016 (EA); B) A/swine/Guangdong/104/2013 (EA); C) A/swine/Hong Kong/NS301/2013 (TR); D) A/swine/Hong Kong/1436/2016 (pdm09); E) A/swine/Hong Kong/4348/2016 (BD-like H3). BD, Binh Duong; EA, Eurasian avian-like; pdm09, 2009 pandemic strain; TR, triple-reassortant. in study to determine existing human population immunity as part of assessing influenza pandemic risk.

years of age (Table 2). Overall, >67% of persons from Hong Kong and Guangzhou had titers ≥40 to the Binh Duong-like H3N2 virus A/Sw/HK/4348/2016, the predominant H3N2 virus lineage circulating in China and Vietnam, which has an HA derived from seasonal influenza viruses that circulated in humans in 2004. Persons in age groups 11–20 and 21–30 years had higher seroprevalence and GMT (Table 2).

Assessment of Population Immunity

From our estimates of overall population immunity against different H1 and H3 swine influenza viruses and its potential effect on R_0 and R_t (Figure 2), we determined that after weighting the protection conferred by each HAI titer level and by age distribution using the population age structure, only ≈19%–20% of the population was immune to A/swine/HK/NS4003/2016, A/swine/GD/104/2013, and A/swine/HK/NS301/2013 viruses (Appendix Table 2). We used a social contact matrix for Hong Kong to parametrize our estimates (Figure 2). We estimated that the population immunity in Guangzhou and Hong Kong would reduce R_0 of A/swine/HK/NS4003/2016, rg-A/swine/GD/104/2013, or A/swine/HK/NS301/2013 by only ≈18%–20%. Because the smallest R_0 needed to cause a pandemic is in the 1.22−1.24 range, if viruses with any of these HAs were to emerge in a form efficiently transmissible

Table 1. Seroprevalence and geometric mean titer for swine influenza viruses of H1 and H3 subtype in serum specimens from 353 persons in Hong Kong and Guangzhou, China*

Virus	Virus abbreviation	Virus lineage	No. (%) persons		GMT
			Seroprevalence ≥40	Seroprevalence ≥10	
A/swine/HK/NS4003/2016 (H1N1)	NS4003	EA	34 (9.6)	105 (29.7)	7.67
A/swine/GD/104/2013 (H1N1)	GD104	EA	39 (11.0)	89 (25.2)	7.84
A/swine/HK/NS301/2013 (H1N2)	NS301	TRIG	27 (7.6)	115 (32.6)	7.76
A/swine/HK/1436/2016 (H1N1)	TS1436	Pandemic (pdm09)	146 (41.4)	222 (62.9)	20.96
A/swine/HK/4348/2016 (H3N2)	TS4348	Seasonal (BD-like H3)	239 (67.7)	308 (87.3)	48.77

*Serum samples were collected during 2013–2014 in Hong Kong and during 2015 in Guangzhou. BD, Binh Duong; EA, Eurasian avian-like; GMT, geometric mean titer; TRIG, triple-reassortant internal gene.

in humans, the cross-reactive human population immunity would impede its spread only modestly (Figure 2).

In contrast, if A/swine/HK/4348/2016 (H3N2) were to acquire efficient biological transmissibility among humans, ≈49% of the population would be immune, which would suppress the inherent transmissibility of the virus by 47%; a pandemic would be prevented if the R_0 of the emergent virus was <1.9 (95% CrI 1.81–1.99) (Figure 2). The H1N1pdm09-like A/swine/HK/1436/2016 (H1N1) virus would spread globally if R_0 was ≥1.49 (95% CrI 1.43–1.56). In fact, antigenically drifted A/Michigan/45/2015-like viruses formed a subclade 6B.1A and continued to spread as seasonal H1N1 influenza during 2017–2020 (*31*). The estimates of reproduction numbers for seasonal influenza viruses are ≈1.28 (interquartile range 1.19–1.37) (*32*).

We have also presented the analysis of the data for the populations of Hong Kong and Guangzhou considered separately (Appendix Table 1); the results were very similar, and statistically significant differences were seen only with A/swine/HK/4348/2016 (H3N2). Guangzhou, compared with Hong Kong, showed significantly higher population immunity to A/swine/HK/4348/2016, providing a greater reduction in R_0.

For a sensitivity analysis, we investigated how critical the social contact matrix data were to the final outcome, by using the UK social contact matrix instead of the matrix for Hong Kong as a comparison model (*25*) (Appendix Table 2). The modeled estimates with the 2 contact matrixes gave similar results; we observed statistically significant differences only for A/swine/HK/1436/2016 (H1N1). Using the UK social contact matrix led to a significantly greater reduction in R_t, attributable to higher-contact frequencies in child and young adult populations in the United Kingdom.

The H1N1pdm09 virus caused a pandemic in 2009 even though there were some cross-reactive HAI antibodies in older adults. Using serum samples collected before the spread of H1N1pdm09 in Hong Kong, we showed that only ≈12% (95% CrI 10%–14%) of the general population was immune to the pandemic virus (A/California/4/2009) before the first pandemic wave (Tables 3, 4). R_0 would only have been reduced by ≈12% (95% CrI 10%–14%) and

Table 2. Age-stratified seroprevalence and GMT to swine influenza viruses of different lineages among 353 persons in Hong Kong and Guangzhou, China*

Patient age, y	NS4003 EA, H1N1		GD104 EA, H1N1		NS301 TRIG, H1N2		TS1436 H1N1pdm09		TS4348 BD-like H3N2	
	Sero† (%)	GMT (95% CI)	Sero† (%)	GMT (95% CI)	Sero† (%)	GMT (95% CI)	Sero† (%)	GMT (95% CI)	Sero† (%)	GMT (95% CI)
≤10	7/33 (21.2)	11 (7–16)	3/33 (9.1)	7 (5–9)	2/33 (6.1)	8 (6–10)	21/33 (63.6)	63 (34–119)	18/33 (54.5)	28 (15–51)
11–20	3/42 (7.1)	8 (6–9)	2/42 (4.8)	7 (5–9)	1/42 (2.4)	7 (6–8)	30/42 (71.4)	54 (36–81)	37/42 (88.1)	115 (81–162)
21–30	3/38 (7.8)	8 (6–10)	10/38 (26.3)	13 (8–19)	4/38 (10.5)	8 (6–10)	23/38 (60.5)	34 (22–52)	35/38 (92.1)	154 (106–225)
31–40	4/42 (9.5)	7 (6–9)	6/42 (14.3)	9 (7–12)	6/42 (14.3)	10 (8–14)	17/42 (40.5)	20 (13–29)	27/42 (64.3)	40 (27–59)
41–50	9/40 (22.5)	11 (8–15)	5/40 (12.5)	7 (5–10)	6/40 (15)	9 (7–13)	13/40 (32.5)	14 (10–21)	24/40 (60)	33 (23–48)
51–60	3/40 (7.5)	7 (5–10)	3/40 (7.5)	7 (5–9)	2/40 (5)	8 (6–11)	7/40 (17.5)	10 (7–15)	19/40 (47.5)	28 (18–42)
61–70	1/39 (2.5)	6 (5–7)	2/39 (5.1)	6 (5–8)	1/39 (2.6)	7 (6–8)	11/39 (28.2)	12 (8–17)	21/39 (53.8)	27 (19–38)
>70	4/79 (5.1)	7 (6–7)	8/79 (10.1)	8 (7–10)	5/79 (6.3)	7 (6–8)	24/79 (30.4)	15 (12–20)	58/79 (73.4)	54 (42–68)

*Serum samples were collected during 2013–2014 in Hong Kong and during 2015 in Guangzhou. BD, Binh Duong; EA, Eurasian–avian-like; GMT, geometric mean titer; sero, seroprevalence; TRIG, triple-reassortant internal gene.
†Proportion of persons with hemagglutination inhibition antibody titers ≥1:40.

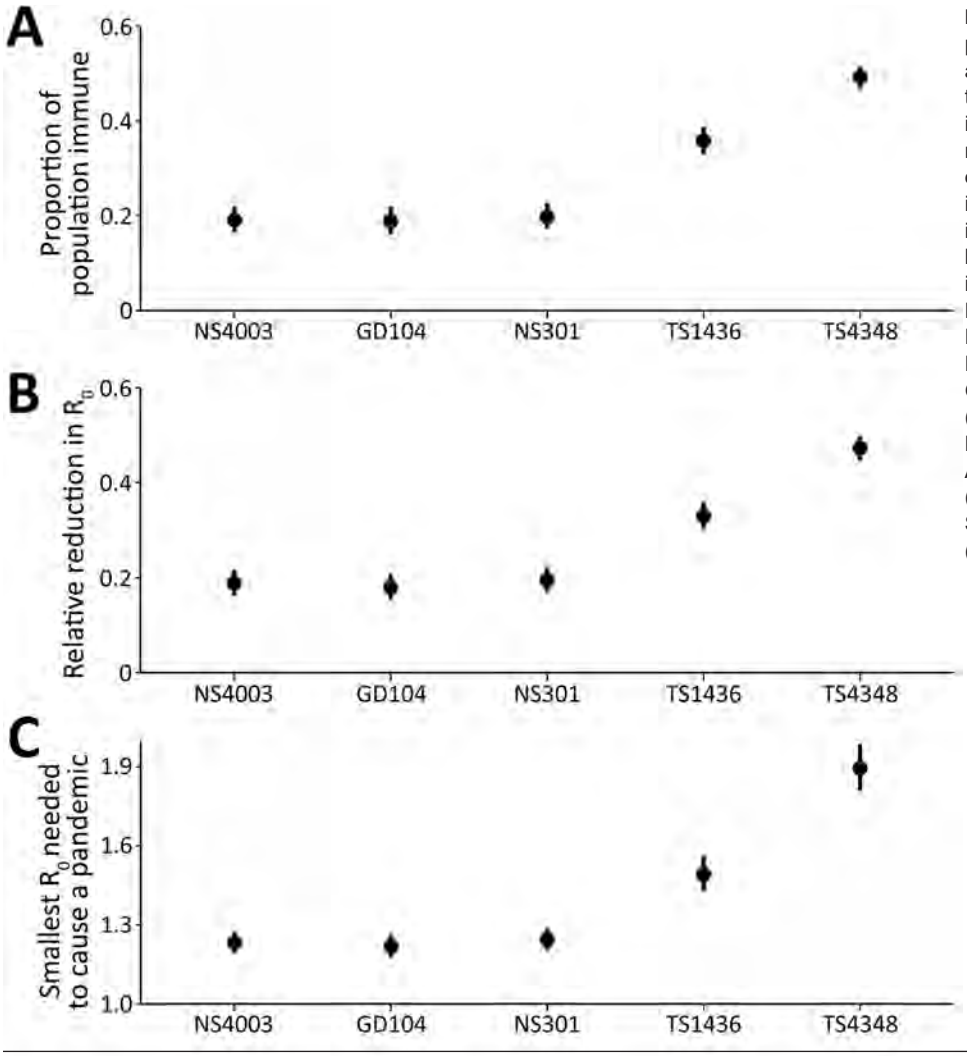

Figure 2. Estimations of overall population-level immunity against H1 and H3 viruses and the potential effect of population immunity on reproduction number in study to determine existing human population immunity as part of assessing influenza pandemic risk. Error bars represent the 95% credible intervals of the estimates. Data are shown from A/Swine/Hong Kong/NS4003/2016 (EA, H1N1) (NS4003), A/Swine/Guangdong/104/2013 (EA, H1N1) (GD104), A/Swine/Hong Kong/NS301/2013 (TR, H1N2) (NS301), A/Swine/Hong Kong/1436/2016 (pdmH1N1) (TS1436), and A/Swine/Hong Kong/4348/2016 (BD-like H3N2) (TS4348).

the smallest R_0 needed for the virus to cause a pandemic was 1.13 (95% CrI 1.11–1.16), indicating the virus would spread readily in the population, as it did in 2009. Sensitivity analysis done with the UK contact matrix showed very similar results (Appendix Table 3). A previous study showed that >40% of children were infected in that first pandemic wave, confirming the low population immunity before exposure to this virus (*33*).

From a previous study (*9*), we retrieved the HAI data for A/Singapore/1/1957 (H2N2) for 295 serum samples collected from children and adults in Hong Kong during August–December 2011 and reassessed population immunity using the methods from this study and the social contact matrices from Hong Kong (Tables 3, 4) and the United Kingdom (Appendix Table 3). Although ≈37% of the general population was immune to A/Singapore/1/1957 using either contact matrix, the resulting R_0 was 1.47 when using the Hong Kong social matrix and 1.23 when using the UK social matrix. The highly skewed age-dependent population immunity profile was markedly more sensitive to the social contact patterns in the matrices.

Discussion

We report a systematic approach for using a broad range of HAI titers in age-stratified serum samples together with data from social contact matrices to assess population immunity to viruses of pandemic concern. This approach is especially relevant in assessing risk from swine influenza viruses because levels of cross-reactive antibodies to the H1 and H3 virus subtypes vary in humans. A main reason why the H1N2 TRIG viruses, which provided the HA gene segment for the 2009 pandemic virus, were not regarded as pandemic candidates before the 2009 outbreak began, despite causing repeated previous zoonotic infections in North America, was the lack of consideration of the consequences of the low population immunity to this virus.

Table 3. Seroprevalence and geometric mean titers of hemagglutination inhibition antibodies to historical H2 and H1 pandemic viruses based on age group among persons in Hong Kong, China*

	A/California/4/2009 (H1N1pdm09)†		A/Singapore/1/1957 (H2N2pdm1957)	
Age group, y	Seroprevalence† (%), n = 600	GMT (95% CI)	Seroprevalence† (%), n = 295	GMT (95% CI)
0–10	0/72 (0)	6 (6–7)	0/24 (0)	5 (5–6)
11–20	10/107 (9.3)	8 (7–9)	0/38 (0)	5 (5–6)
21–30	3/46 (6.5)	6 (5–8)	0/39 (0)	5
31–40	5/39 (12.8)	8 (5–11)	0/37 (0)	5 (5–6)
41–50	9/125 (7.2)	6 (5–7)	13/38 (34.2)	15 (9–24)
51–60	6/131 (4.6)	6 (5–6)	40/40 (100)	243 (172–342)
61–70	1/54 (1.9)	6 (5–7)	40/40 (100)	320 (249–411)
>70	3/26 (11.5)	7 (5–10)	36/39 (92.3)	136 (89–209)

*GMT, geometric mean titer.
†Proportion of persons with hemagglutination inhibition antibody titers ≥1:40.

The estimated median R_0 was 1.8 for the 1918 pandemic, 1.65 for the 1957 pandemic, 1.8 for the 1968 pandemic, and 1.46 for the 2009 pandemic (*32*). We demonstrated that existing population immunity at the time of the emergence of the 2009 pandemic was low, which would enable the H1N1pdm09 virus to cause a pandemic if R_0 was >1.13; estimated R_0 was ≈1.46, and it did spread as a pandemic. EA H1N1 or TRIG H1N2 swine viruses now circulating in China (*11*,*13*) would face similarly low resistance from human population immunity if they were to become transmissible among humans. This finding is of particular concern because some of these viruses have 6 gene segments of H1N1pdm09 origin and are therefore potentially well adapted to human transmission (*13*). EA-lineage swine viruses have caused sporadic zoonotic infections in China, including one in which a case-patient died (*34*–*39*). One EA H1N1 virus in our study, A/Sw/HK/NS4003/2016, is of the predominant emergent EA reassortant genotype 4 (Appendix Figure 1), which was shown to have increased human infectivity (*40*). The HA1 amino acid sequences of A/Sw/HK/NS4003/2016 are similar to those of the representative genotype 4 virus A/swine/Shandong/1207/2016, with 97.9% aa identity and only 1 amino acid change (N74K, H1 numbering) in the Cb antigenic site. These 2 viruses thus pose substantial pandemic threats. In contrast, the swine Binh Duong-lineage H3N2 viruses, although they also have 6 H1N1pdm09 internal gene segments (*13*,*14*), would not cause a pandemic unless the virus had an R_0 >1.9, a much less likely situation.

We found comparable age-stratified seroprevalence in Hong Kong and Guangzhou. In an earlier study, we reported similar seroprevalence to human and avian H2N2 viruses in the United States and Hong Kong (*9*). Studies in a few large cities worldwide might provide data relevant to other large urban population centers worldwide. Whereas differences in social contact matrixes (e.g., Hong Kong vs. the United Kingdom) may have had some influence on the overall conclusions, they might not dramatically change the conclusions about the pandemic risk of a virus, unless there was a skewed age distribution of antibody prevalence, such as with the H2N2 virus.

Among our study's limitations was that we used HAI antibodies as our sole correlate of protection. Other protective mechanisms, including neuraminidase-inhibiting antibodies, HA stalk-binding antibodies, antibody-dependent cell cytotoxicity, and T-cell immune responses, would also provide measures of protection levels (*41*–*44*). However, quantitative measures of protection conferred by those immune correlates are lacking, precluding the use of similar approaches to assess their potential contributions to population immunity. Therefore, our estimates based on HAI alone provide a minimal assessment of population immunity to a given virus. Second, our estimates focused on emergence risk for a pandemic, not severity or effect. For example, because older adults were exposed to drift variants of H1N1 antigenically closer to the 1918 H1N1 pandemic virus, and because the 2009 H1N1 pandemic virus acquired the H1 from triple reassortant swine influenza viruses that had an HA closely related to the 1918 H1N1 virus, older adults had more cross-protective immunity against the H1N1pdm09 virus than did children and young adults, which reduced the overall infection rates as

Table 4. Estimations of overall population-level immunity against historical H2 and H1 pandemic viruses and the potential effect of population immunity on reproduction number among persons in Hong Kong, China*

Virus strain	Proportion of population immune (95% CI)	Relative reduction in R_0 (95% CI)	Smallest R_0 needed to cause pandemic (95% CI)
A/Singapore/1/1957 (H2N2)	0.37 (0.346–0.394)	0.321 (0.295–0.348)	1.472 (1.419–1.535)
A/California/04/2009 (H1N1)	0.117 (0.098–0.14)	0.115 (0.096–0.138)	1.13 (1.106–1.16)

*Serum samples for testing antibodies to the 1957 virus were collected in 2011 and those for testing antibodies to the 2009 virus were collected in 2008–2009.

well as severe disease and death (*45*). Third, the serum samples used in this study were collected during 2013–2015; the population immunity profile may have changed since then.

However, our main aim in this report was to provide a quantitative approach for assessing population immunity, which is a key element in determining pandemic risk from influenza viruses. This approach identified several swine viruses that need full risk assessment. Some of these viruses have 5 or 6 internal gene segments derived from H1N1pdm09 viruses, which are well adapted to humans and have efficient binding to human receptors (as do most swine influenza viruses) and to which there is low human population immunity. Changes in hemagglutinin or neuraminidase or the balance between them (*46*) may be sufficient to make them efficiently transmissible between humans and therefore pandemic threats.

Research funding came from the Research Grants Council of Hong Kong through a Theme Based Research Grant (T11-712/19-N) and US National Institute of Allergy and Infectious Diseases (NIAID) Contract 75N93021C00016.

About the Author

Dr. Cheung is a researcher at the University of Hong Kong School of Public Health. His research interests are the molecular evolutionary virology and epidemiology of zoonotic influenza viruses.

References

1. Monto AS, Webster RG. Influenza pandemics: history and lessons learned. In: Webster RG, Monto AS, Braciale TJ, Lamb RA, editors. Textbook of influenza. Hoboken (NJ): John Wiley and Sons; 2013. p. 20–34.
2. Mena I, Nelson MI, Quezada-Monroy F, Dutta J, Cortes-Fernández R, Lara-Puente JH, et al. Origins of the 2009 H1N1 influenza pandemic in swine in Mexico. eLife. 2016;5:e16777. https://doi.org/10.7554/eLife.16777
3. Wu JT, Ma ES, Lee CK, Chu DK, Ho PL, Shen AL, et al. The infection attack rate and severity of 2009 pandemic H1N1 influenza in Hong Kong. Clin Infect Dis. 2010;51:1184–91. https://doi.org/10.1086/656740
4. Jernigan DB, Cox NJ. Human influenza: one health, one world. In: Webster RG, Monto AS, Braciale TJ, Lamb RA, editors. Textbook of influenza. Hoboken (NJ): John Wiley and Sons; 2013. p. 1–19.
5. Cox NJ, Trock SC, Burke SA. Pandemic preparedness and the influenza risk assessment tool (IRAT). Curr Top Microbiol Immunol. 2014;385:119–36. https://doi.org/10.1007/82_2014_419
6. World Health Organization. Tool for influenza pandemic risk assessment (TIPRA). World Health Organization; 2016. [cited 2022 March 16] https://apps.who.int/iris/handle/10665/250130
7. Hobson D, Curry RL, Beare AS, Ward-Gardner A. The role of serum haemagglutination-inhibiting antibody in protection against challenge infection with influenza A2 and B viruses. J Hyg (Lond). 1972;70:767–77.
8. Coudeville L, Bailleux F, Riche B, Megas F, Andre P, Ecochard R. Relationship between haemagglutination-inhibiting antibody titres and clinical protection against influenza: development and application of a bayesian random-effects model. BMC Med Res Methodol. 2010;10:18. https://doi.org/10.1186/1471-2288-10-18
9. Babu TM, Perera RAPM, Wu JT, Fitzgerald T, Nolan C, Cowling BJ, et al. Population serologic immunity to human and avian H2N2 viruses in the United States and Hong Kong for pandemic risk assessment. J Infect Dis. 2018;218:1054–60. https://doi.org/10.1093/infdis/jiy291
10. Zhu H, Webby R, Lam TTY, Smith DK, Peiris JS, Guan Y. History of Swine influenza viruses in Asia. Curr Top Microbiol Immunol. 2013;370:57–68. https://doi.org/10.1007/82_2011_179
11. Vijaykrishna D, Smith GJD, Pybus OG, Zhu H, Bhatt S, Poon LLM, et al. Long-term evolution and transmission dynamics of swine influenza A virus. Nature. 2011;473:519–22. https://doi.org/10.1038/nature10004
12. Takemae N, Harada M, Nguyen PT, Nguyen T, Nguyen TN, To TL, et al. Influenza A viruses of swine (IAV-S) in Vietnam from 2010 to 2015: multiple introductions of A(H1N1)pdm09 viruses into the pig population and diversifying genetic constellations of enzootic IAV-S. J Virol. 2016;91:e01490–16.
13. Liang H, Lam TT-Y, Fan X, Chen X, Zeng Y, Zhou J, et al. Expansion of genotypic diversity and establishment of 2009 H1N1 pandemic-origin internal genes in pigs in China. J Virol. 2014;88:10864–74. https://doi.org/10.1128/JVI.01327-14
14. Baudon E, Chu DKW, Tung DD, Thi Nga P, Vu Mai Phuong H, Le Khanh Hang N, et al. Swine influenza viruses in Northern Vietnam in 2013-2014. Emerg Microbes Infect. 2018;7:123. https://doi.org/10.1038/s41426-018-0109-y
15. Cao Z, Zeng W, Hao X, Huang J, Cai M, Zhou P, et al. Continuous evolution of influenza A viruses of swine from 2013 to 2015 in Guangdong, China. PLoS One. 2019;14:e0217607. https://doi.org/10.1371/journal.pone.0217607
16. Broberg E, Nicoll A, Amato-Gauci A. Seroprevalence to influenza A(H1N1) 2009 virus—where are we? Clin Vaccine Immunol. 2011;18:1205–12. https://doi.org/10.1128/CVI.05072-11
17. Wei VWI, Wong JYT, Perera RAPM, Kwok KO, Fang VJ, Barr IG, et al. Incidence of influenza A(H3N2) virus infections in Hong Kong in a longitudinal sero-epidemiological study, 2009-2015. PLoS One. 2018;13:e0197504. https://doi.org/10.1371/journal.pone.0197504
18. Ngo LT, Hiromoto Y, Pham VP, Le HT, Nguyen HT, Le VT, et al. Isolation of novel triple-reassortant swine H3N2 influenza viruses possessing the hemagglutinin and neuraminidase genes of a seasonal influenza virus in Vietnam in 2010. Influenza Other Respir Viruses. 2012;6:6–10. https://doi.org/10.1111/j.1750-2659.2011.00267.x
19. Yang H, Chen Y, Qiao C, He X, Zhou H, Sun Y, et al. Prevalence, genetics, and transmissibility in ferrets of Eurasian avian-like H1N1 swine influenza viruses. Proc Natl Acad Sci U S A. 2016;113:392–7. https://doi.org/10.1073/pnas.1522643113
20. Hoffmann E, Neumann G, Hobom G, Webster RG, Kawaoka Y. "Ambisense" approach for the generation of influenza A virus: vRNA and mRNA synthesis from one template. Virology. 2000;267:310–7. https://doi.org/10.1006/viro.1999.0140

21. Hoffmann E, Neumann G, Kawaoka Y, Hobom G, Webster RG. A DNA transfection system for generation of influenza A virus from eight plasmids. Proc Natl Acad Sci U S A. 2000;97:6108–13. https://doi.org/10.1073/pnas.100133697
22. World Health Organization. Manual for the laboratory diagnosis and virological surveillance of influenza. Geneva: World Health Organization; 2011.
23. Nauta JJ, Beyer WE, Osterhaus AD. On the relationship between mean antibody level, seroprotection and clinical protection from influenza. Biologicals. 2009;37:216–21. https://doi.org/10.1016/j.biologicals.2009.02.002
24. Leung K, Jit M, Lau EHY, Wu JT. Social contact patterns relevant to the spread of respiratory infectious diseases in Hong Kong. Sci Rep. 2017;7:7974. https://doi.org/10.1038/s41598-017-08241-1
25. Mossong J, Hens N, Jit M, Beutels P, Auranen K, Mikolajczyk R, et al. Social contacts and mixing patterns relevant to the spread of infectious diseases. PLoS Med. 2008;5:e74. https://doi.org/10.1371/journal.pmed.0050074
26. Diekmann O, Heesterbeek JA, Metz JA. On the definition and the computation of the basic reproduction ratio R0 in models for infectious diseases in heterogeneous populations. J Math Biol. 1990;28:365–82. https://doi.org/10.1007/BF00178324
27. Diekmann O, Heesterbeek JAP, Roberts MG. The construction of next-generation matrices for compartmental epidemic models. J R Soc Interface. 2010;7:873–85. 10.1098/rsif.2009 https://doi.org/10.1098/rsif.2009.0386
28. Mak GC, Choy PW, Lee WY, Wong AH, Ng KC, Lim W. Sero-immunity and serologic response to pandemic influenza A (H1N1) 2009 virus in Hong Kong. J Med Virol. 2010;82:1809–15. https://doi.org/10.1002/jmv.21895
29. Cowling BJ, Ng S, Ma ES, Cheng CK, Wai W, Fang VJ, et al. Protective efficacy of seasonal influenza vaccination against seasonal and pandemic influenza virus infection during 2009 in Hong Kong. Clin Infect Dis. 2010;51:1370–9. https://doi.org/10.1086/657311
30. Riley S, Kwok KO, Wu KM, Ning DY, Cowling BJ, Wu JT, et al. Epidemiological characteristics of 2009 (H1N1) pandemic influenza based on paired sera from a longitudinal community cohort study. PLoS Med. 2011;8:e1000442. https://doi.org/10.1371/journal.pmed.1000442
31. Suntronwong N, Klinfueng S, Korkong S, Vichaiwattana P, Thongmee T, Vongpunsawad S, et al. Characterizing genetic and antigenic divergence from vaccine strain of influenza A and B viruses circulating in Thailand, 2017-2020. Sci Rep. 2021;11:735. https://doi.org/10.1038/s41598-020-80895-w
32. Biggerstaff M, Cauchemez S, Reed C, Gambhir M, Finelli L. Estimates of the reproduction number for seasonal, pandemic, and zoonotic influenza: a systematic review of the literature. BMC Infect Dis. 2014;14:480. https://doi.org/10.1186/1471-2334-14-480
33. Wu JT, Ma ESK, Lee CK, Chu DKW, Ho P-L, Shen AL, et al. The infection attack rate and severity of 2009 pandemic H1N1 influenza in Hong Kong. Clin Infect Dis. 2010;51:1184–91. https://doi.org/10.1086/656740
34. Xie JF, Zhang YH, Zhao L, Xiu WQ, Chen HB, Lin Q, et al. Emergence of Eurasian avian-like swine influenza A (H1N1) virus from an adult case in Fujian Province, China. Virol Sin. 2018;33:282–6. https://doi.org/10.1007/s12250-018-0034-1
35. Wang D-Y, Qi S-X, Li X-Y, Guo J-F, Tan M-J, Han G-Y, et al. Human infection with Eurasian avian-like influenza A(H1N1) virus, China. Emerg Infect Dis. 2013;19:1709–11. https://doi.org/10.3201/eid1910.130420
36. Yang H, Qiao C, Tang X, Chen Y, Xin X, Chen H. Human infection from avian-like influenza A (H1N1) viruses in pigs, China. Emerg Infect Dis. 2012;18:1144–6. https://doi.org/10.3201/eid1807.120009
37. Zhu W, Zhang H, Xiang X, Zhong L, Yang L, Guo J, et al. Reassortant Eurasian avian-like influenza A(H1N1) virus from a severely ill child, Hunan Province, China, 2015. Emerg Infect Dis. 2016;22:1930–6. https://doi.org/10.3201/eid2211.160181
38. Qi X, Cui L, Jiao Y, Pan Y, Li X, Zu R, et al. Antigenic and genetic characterization of a European avian-like H1N1 swine influenza virus from a boy in China in 2011. Arch Virol. 2013;158:39–53. https://doi.org/10.1007/s00705-012-1423-7
39. Li X, Guo L, Liu C, Cheng Y, Kong M, Yang L, et al. Human infection with a novel reassortant Eurasian-avian lineage swine H1N1 virus in northern China. Emerg Microbes Infect. 2019;8:1535–45. https://doi.org/10.1080/22221751.2019.1679611
40. Sun H, Xiao Y, Liu J, Wang D, Li F, Wang C, et al. Prevalent Eurasian avian-like H1N1 swine influenza virus with 2009 pandemic viral genes facilitating human infection. [Erratum in Proc Natl Acad Sci U S A. 2020;117:23194]. Proc Natl Acad Sci U S A. 2020;117:17204–10. https://doi.org/10.1073/pnas.1921186117
41. Ng S, Nachbagauer R, Balmaseda A, Stadlbauer D, Ojeda S, Patel M, et al. Novel correlates of protection against pandemic H1N1 influenza A virus infection. Nat Med. 2019;25:962–7. https://doi.org/10.1038/s41591-019-0463-x
42. Memoli MJ, Shaw PA, Han A, Czajkowski L, Reed S, Athota R, et al. Evaluation of antihemagglutinin and antineuraminidase antibodies as correlates of protection in an influenza A/H1N1 virus healthy human challenge model. MBio. 2016;7:e00417–16. https://doi.org/10.1128/mBio.00417-16
43. Sridhar S, Begom S, Bermingham A, Hoschler K, Adamson W, Carman W, et al. Cellular immune correlates of protection against symptomatic pandemic influenza. Nat Med. 2013;19:1305–12. https://doi.org/10.1038/nm.3350
44. Valkenburg SA, Fang VJ, Leung NH, Chu DK, Ip DK, Perera RA, et al. Cross-reactive antibody-dependent cellular cytotoxicity antibodies are increased by recent infection in a household study of influenza transmission. Clin Transl Immunology. 2019;8:e1092. https://doi.org/10.1002/cti2.1092
45. Hancock K, Veguilla V, Lu X, Zhong W, Butler EN, Sun H, et al. Cross-reactive antibody responses to the 2009 pandemic H1N1 influenza virus. N Engl J Med. 2009;361:1945–52. https://doi.org/10.1056/NEJMoa0906453
46. Yen HL, Liang CH, Wu CY, Forrest HL, Ferguson A, Choy KT, et al. Hemagglutinin-neuraminidase balance confers respiratory-droplet transmissibility of the pandemic H1N1 influenza virus in ferrets. Proc Natl Acad Sci U S A. 2011;108:14264–9. https://doi.org/10.1073/pnas.1111000108

Address for correspondence: Malik Peiris, School of Public Health, University of Hong Kong, No. 7 Sassoon Rd, Pokfulam, Hong Kong, China; email: malik@hku.hk

Disparities in First Dose COVID-19 Vaccination Coverage among Children 5–11 Years of Age, United States

Neil Chandra Murthy, Elizabeth Zell, Hannah E. Fast, Bhavini Patel Murthy, Lu Meng, Ryan Saelee, Tara Vogt, Kevin Chatham-Stephens, Christina Ottis, Lauren Shaw, Lynn Gibbs-Scharf, LaTreace Harris, Terence Chorba

We analyzed first-dose coronavirus disease vaccination coverage among US children 5–11 years of age during November–December 2021. Pediatric vaccination coverage varied widely by jurisdiction, age group, and race/ethnicity, and lagged behind vaccination coverage for adolescents aged 12–15 years during the first 2 months of vaccine rollout.

Although more common among adults, severe coronavirus disease (COVID-19) and hospitalization can occur in children. Among >8,300 hospitalized children 5–11 years of age, 1/3 required intensive care (*1*,*2*). Children can transmit severe acute respiratory syndrome coronavirus 2 to others, highlighting the need for pediatric COVID-19 vaccinations. On November 2, 2021, the US Centers for Disease Control and Prevention (CDC) recommended the use of the Pfizer-BioNTech COVID-19 vaccine (Pfizer Inc., https://www.pfizer.com) in children 5–11 years of age. We analyzed first-dose vaccination coverage among children 5–11 years of age and stratified coverage by age group, sex, race/ethnicity, and jurisdiction.

Author affiliations: Centers for Disease Control and Prevention, Atlanta, Georgia, USA (N.C. Murthy, H.E. Fast, B.P. Murthy, R. Saelee, T. Vogt, K. Chatham-Stephens, C. Ottis, L. Shaw, L. Gibbs-Scharf, L. Harris, T. Chorba); CDC COVID-19 Response Team, Atlanta (N.C. Murthy, E. Zell, H.E. Fast, B.P. Murthy, L. Meng, R. Saelee, T. Vogt, K. Chatham-Stephens, C. Ottis, L. Shaw, L. Gibbs-Scharf, L. Harris, T. Chorba); US Public Health Service Commissioned Corps, Rockville, Maryland, USA (N.C. Murthy, B.P. Murthy, K. Chatham-Stephens); Stat-Epi Associates, Inc., Ponte Vedra Beach, Florida, USA (E. Zell); General Dynamics Information Technology Inc., Falls Church, Virginia, USA (L. Meng)

DOI: https://doi.org/10.3201/eid2805.220166

The Study

We analyzed COVID-19 vaccine administration data among children 5–11 years of age in the United States during November 2–December 31, 2021. We collected data that were reported to CDC from jurisdictions, pharmacies, and federal entities through immunization information systems, the Vaccine Administration Management System, and direct data submission by January 21, 2022 (Appendix, https://wwwnc.cdc.gov/EID/article/28/5/22-0166.pdf). We calculated daily and cumulative total numbers of children receiving the first dose of Pfizer-BioNTech COVID-19 vaccine. We calculated vaccination coverage by dividing the number of children who received the first vaccine dose by the total population of children in the corresponding age group living in the defined jurisdiction. We stratified vaccine coverage by jurisdiction, age group (5–6, 7–8, and 9–11 years), and sex. We obtained the population size for children 5–11 years of age from the US Census Bureau 2020 Population Estimates (*3*). Among 82.1% of children 5–11 years of age for whom race and ethnicity data were available, we calculated the percentage of children receiving their first COVID-19 vaccine dose by race/ethnicity and compared this with the racial and ethnic makeup of the US population 5–11 years of age.

We did not conduct tests for statistical significance because these data reflect US population and not population samples. We used SAS version 9.4 (SAS Institute, Inc., https://www.sas.com) to perform analyses. This study was reviewed by CDC and conducted consistent with applicable federal law and CDC policy.

Overall, 24.0% of US children 5–11 years of age received their first COVID-19 vaccine dose during November–December 2021, and rapid initial uptake occurred during the first 2 weeks after CDC recommended the vaccine (Figure 1). Vaccination coverage varied by jurisdiction, ranging from 9.1% in Mississippi to 56.4% in Vermont. Coverage also varied by age group and was higher for children 9–11 years of age (26.8%) than children 5–6 years (20.3%) or 7–8 years (23.5%) (Figures 1, 2). Vaccination coverage did not vary by sex, 23.7% coverage for male children and 24.1% for female children (Appendix Table).

Among all US children 5–11 years of age, non-Hispanic White persons constitute 51.2% of the population, non-Hispanic Black 14.0%, and Hispanic/Latino 23.0% (*3*). However, children from these groups were underrepresented among those reporting a first COVID-19 vaccination dose; only 49.1% non-Hispanic White, 8.0% non-Hispanic Black, and 21.7% Hispanic/Latino children were vaccinated. In contrast, among vaccine recipients, 11.4% were non-Hispanic Asian children, but this group constitutes only 5.6% of the US population 5–11 years of age (Appendix Figure).

Conclusions

Vaccination coverage among children 5–11 years of age was only 24% and lagged vaccination coverage among children 12–15 years of age (33.3%) during the first 2 months of vaccine rollout (*4*). Many disparities among children 5–11 years of age emerged during the first 2 months of vaccine rollout, including racial and ethnic disparities. Children of Asian descent were overrepresented and White, Black, and Hispanic children were underrepresented. Many factors could explain these disparities. For instance, Asian Americans are less likely to live in poverty overall compared with other racial and ethnic groups (*5*). Poverty rates among Black (19.5%) and Hispanic (17.0%) communities are among the highest in the country (*6*), and lower income parents face challenges taking leave from work to get their children vaccinated or to care for children who have vaccine side effects (*7*).

Other factors that could hinder lower income parents from seeking vaccinations for their children include transportation challenges, a lack of pediatric and family medicine practices that serve as medical homes for routine pediatric care, and higher COVID-19 vaccine hesitancy among some parents (*8*,*9*). Access to a medical home could help address parental concerns about COVID-19 vaccines and improve vaccination uptake among pediatric populations. In addition, parental COVID-19 vaccination hesitancy varies by socioeconomic factors and is higher among parents whose children are publicly insured, such as through Medicaid, and parents in lower income social groups (*9*). Many factors influence parental hesitancy and additional concerted public health efforts to inform and educate parents and caregivers are needed to improve confidence in COVID-19 vaccines (*10*).

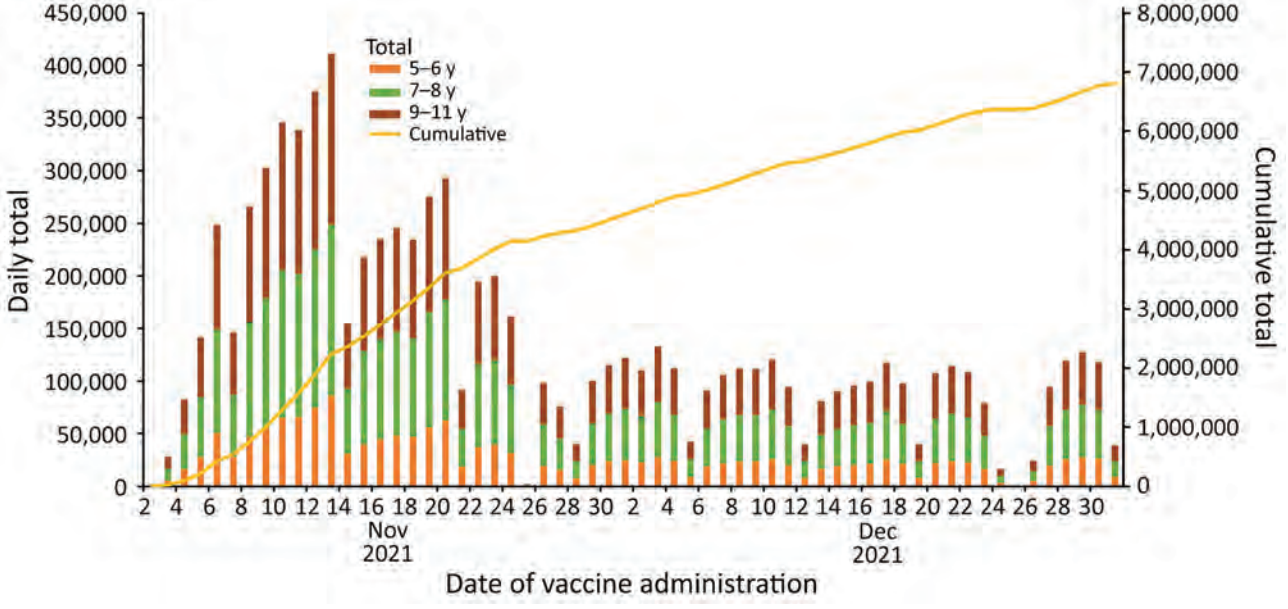

Figure 1. Daily and cumulative totals of the number of children 5–11 years of age who received the first dose of the Pfizer-BioNTech COVID-19 vaccine (Pfizer Inc., https://www.pfizer.com) by date of vaccination and age group, United States, November 2–December 31, 2021.

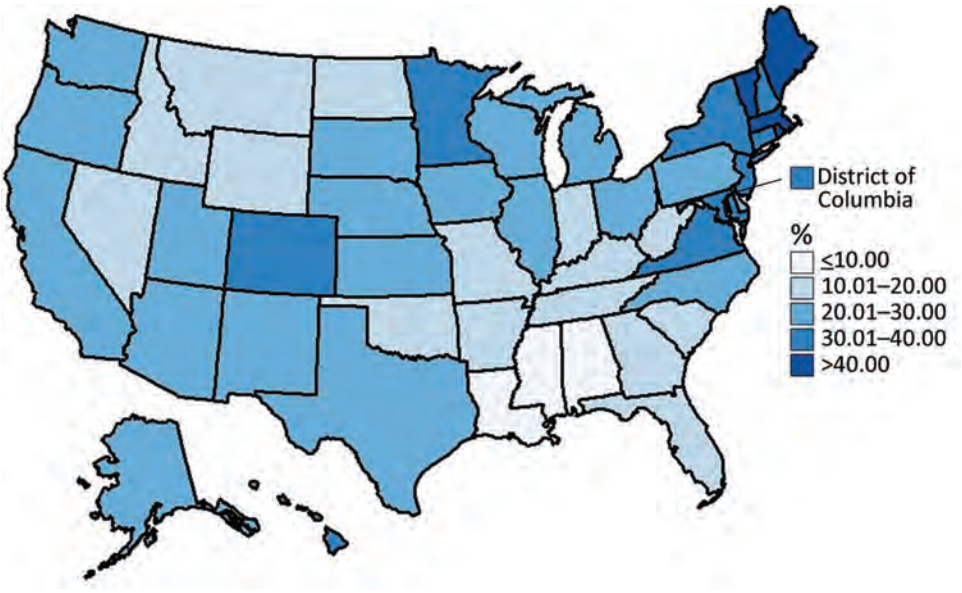

Figure 2. Percentage of vaccination coverage among children 5–11 years of age who received the first dose of the Pfizer-BioNTech COVID-19 vaccine (Pfizer Inc., https://www.pfizer.com), by jurisdiction, United States, November 2–December 31, 2021.

We found pediatric COVID-19 vaccination coverage varied widely across the United States and some jurisdictions had substantially higher vaccination coverage than others. Jurisdictions in the Northeast, including Vermont, Maine, Massachusetts, and Rhode Island, were among those with the highest vaccination coverage, and jurisdictions in the South, including Louisiana, Mississippi, and Alabama, were among those with the lowest coverage rates. This geographic variation could reflect parental vaccination status because adult vaccination coverage in the United States varied in a similar pattern (*4*). Parental COVID-19 vaccination status is one of the strongest predictors of pediatric COVID-19 vaccination (*11*), and efforts to build parental trust in COVID-19 vaccines are needed.

Furthermore, overall COVID-19 vaccination uptake among children 5–11 years of age was higher among children 9–11 years of age than children 5–6 years of age. The reasons for differences in vaccination coverage between the older and younger children are unknown but could reflect variations in parental hesitancy based on children's ages. In a recent survey of parents of children 2–17 years of age, the younger the child, the less willing the parents were to vaccinate immediately (*11*). Among surveyed parents of children 5–11 years of age, 27% said they would get their children vaccinated for COVID-19 right away, but 33% said they would wait and see, 5% said they would only vaccinate if required, and 30% said they would definitely not get their children vaccinated (*7*).

CDC recommends that everyone ≥5 years of age receive COVID-19 vaccination to reduce illness and death (*12*). Pediatric and family medicine practices that serve as medical homes, along with pharmacies and other providers, should continue to promote and offer COVID-19 vaccines to children. Vaccination clinics hosted by schools, in collaboration with a vaccinating partner like a pharmacy or public health department, also might make vaccination convenient and help increase uptake of COVID-19 vaccination among children as they have done for routine vaccinations (*13*–*15*).

Our findings have ≥2 limitations. First, missing data on race and ethnicity for 17.9% of the records could bias findings by race/ethnicity, especially if differential reporting bias based on jurisdictions or by racial or ethnic subgroups occur. In addition, the US Census does not include a race category for "Other" as noted for many jurisdictions in immunization information systems. This finding could affect the interpretation of proportions for the "Multiple/Other, non-Hispanic" category because combining "Other" with "Multiple" in the immunization records could overrepresent vaccination coverage for this category. Finally, we calculated age for 14 jurisdictions where complete date of birth was unknown, which could have misclassified some age groups.

In conclusion, we found COVID-19 vaccination coverage among children 5–11 years of age varied substantially by jurisdiction, age group, and race or ethnicity. To ensure equity, jurisdictions nationwide should devise and implement strategic efforts to strengthen vaccination programs to build vaccine confidence and reduce barriers to receiving COVID-19 vaccines.

Acknowledgments

We thank COVID-19 Vaccine Task Force; US Department of Defense; immunization program managers, immunization information system managers, and other staff members of the immunization programs in the 64 jurisdictions and 5 federal entities for providing data.

About the Author

Dr. Murthy is a Lieutenant Commander in the US Public Health Service and serves as a medical officer in the Immunization Services Division, National Center for Immunization and Respiratory Diseases, at the US Centers for Disease Control and Prevention in Atlanta, Georgia, USA, and is currently deployed on CDC's COVID-19 Response Vaccine Task Force. His research interests focus on the intersection of medicine, public health, and health communications.

References

1. Jones J. Epidemiology of COVID-19 in children aged 5–11 years. Advisory Committee on Immunization Practices (ACIP) Meeting; November 2, 2021; Atlanta, Georgia, USA [cited 2021 Nov 9]. https://www.cdc.gov/vaccines/acip/meetings/downloads/slides-2021-11-2-3/03-COVID-Jefferson-508.pdf
2. Kim L, Whitaker M, O'Halloran A, Kambhampati A, Chai SJ, Reingold A, et al.; COVID-NET Surveillance Team. Hospitalization rates and characteristics of children aged <18 years hospitalized with laboratory-confirmed COVID-19—COVID-NET, 14 states, March 1–July 25, 2020. MMWR Morb Mortal Wkly Rep. 2020;69:1081–8. https://doi.org/10.15585/mmwr.mm6932e3
3. US Census Bureau. Population and housing unit estimates [cited 2021 Nov 19]. https://www.census.gov/programs-surveys/popest.html
4. Centers for Disease Control and Prevention. COVID data tracker [cited 2022 Jan 24]. https://covid.cdc.gov/covid-data-tracker/#vaccinations_vacc-total-admin-rate-pop18
5. Budiman A, Ruiz N; Pew Research Center. Key facts about Asian Americans, a diverse and growing population 2022 [cited 2022 Feb 22]. https://www.pewresearch.org/fact-tank/2021/04/29/key-facts-about-asian-americans
6. Shrider EA, Kollar M, Chen F, Semega J; US Census Bureau. Income and poverty in the United States: 2020. Washington, DC: The Bureau; 2021.
7. Hamel L, Lopes L, Sparks G, Kirziner A, Kearney A, Stokes M, et al. Kaiser Family Foundation. KFF COVID-19 vaccine monitor: October 2021 [cited 2021 Dec 4]. https://www.kff.org/coronavirus-covid-19/poll-finding/kff-covid-19-vaccine-monitor-october-2021
8. Weller BE, Faubert SJ, Ault AK. Youth access to medical homes and medical home components by race and ethnicity. Matern Child Health J. 2020;24:241–9. https://doi.org/10.1007/s10995-019-02831-3
9. Alfieri NL, Kusma JD, Heard-Garris N, Davis MM, Golbeck E, Barrera L, et al. Parental COVID-19 vaccine hesitancy for children: vulnerability in an urban hotspot. BMC Public Health. 2021;21:1662. https://doi.org/10.1186/s12889-021-11725-5
10. Balasuriya L, Santilli A, Morone J, Ainooson J, Roy B, Njoku A, et al. COVID-19 vaccine acceptance and access among Black and Latinx communities. JAMA Netw Open. 2021;4:e2128575. https://doi.org/10.1001/jamanetworkopen.2021.28575
11. Rane MS, Robertson MM, Westmoreland DA, Teasdale CA, Grov C, Nash D. Intention to vaccinate children against COVID-19 among vaccinated and unvaccinated US parents. JAMA Pediatr. 2022;176:201–3. https://doi.org/10.1001/jamapediatrics.2021.5153
12. Centers for Disease Control and Prevention. COVID-19 vaccines for children & teens [cited 2021 Dec 5]. https://www.cdc.gov/coronavirus/2019-ncov/vaccines/recommendations/children-teens.html
13. Centers for Disease Control and Prevention. COVID-19 vaccination for children [cited 2022 Feb 22]. https://www.cdc.gov/vaccines/covid-19/planning/children.html
14. The Community Guide. Vaccination programs: schools and organized child care centers [cited 2021 Dec 5]. https://www.thecommunityguide.org/findings/vaccination-programs-schools-and-organized-child-care-centers
15. Kates J, Michaud J, Tolbert J, Artiga S, Orgera K; Kaiser Family Foundation. Vaccinating children ages 5–11: policy considerations for COVID-19 vaccine rollout [cited 2021 Dec 4]. https://www.kff.org/coronavirus-covid-19/issue-brief/vaccinating-children-ages-5-11-policy-considerations-for-covid-19-vaccine-rollout

Address for correspondence: Neil Chandra Murthy, Centers for Disease Control and Prevention, 1600 Clifton Rd NE, Mailstop H24-6, Atlanta, Georgia 30329-4027, USA; email: nmurthy@cdc.gov

Multisystem Inflammatory Syndrome in Children after SARS-CoV-2 Vaccination

Eisha Jain, Jeffrey R. Donowitz, Elizabeth Aarons, Beth C. Marshall, Michael P. Miller

Multisystem inflammatory syndrome in children (MIS-C) is a hyperinflammatory state that occurs after severe acute respiratory syndrome coronavirus 2 (SARS-CoV-2) infection. We present 2 cases of MIS-C after SARS-CoV-2 vaccination; 1 patient had evidence of recent SARS-CoV-2 infection. Our findings suggest that vaccination modulates the pathogenesis of MIS-C.

Multisystem inflammatory syndrome in children (MIS-C) was first described in 2019 during the severe acute respiratory syndrome coronavirus 2 (SARS-CoV-2) pandemic (*1*). MIS-C is a systemic hyperinflammatory state necessitating hospitalization in patients <21 years of age who experienced ≥24 hours of fever, recent SARS-CoV-2 exposure or positive testing, involvement of ≥2 organ systems, and ≥1 of the following laboratory results: elevated C-reactive protein (CRP), erythrocyte sedimentation rate, fibrinogen, procalcitonin, D-dimer, ferritin, lactate dehydrogenase, interleukin-6, neutrophils, reduced lymphocytes, or reduced albumin (*2*). It is unknown whether vaccination can precipitate or abrogate MIS-C and whether natural infection preceding or at the time of vaccination plays a role (*1*). We describe MIS-C in 2 adolescents recently vaccinated with BNT162b2 (Pfizer-BioNTech, https://www.pfizer.com) and raise the possibility of vaccination modulating MIS-C pathogenesis.

The Study

Patient 1 was a 15-year-old girl with asthma who received her first dose of BNT162b2 6 days before seeking care. She had low-grade fever and myalgia, which resolved within 2 days of vaccination. Four days later, she experienced 102°F fevers, headaches, nonbilious emesis, myalgias, chest pain, and a rash. Emergency department (ED) examination identified pharyngeal erythema, bilateral conjunctivitis, and a diffuse blanching rash. She had no respiratory or cardiovascular symptoms. At admission, laboratory test results showed leukocytosis with polymorphonuclear cell predominance and elevated CRP, fibrinogen, prothrombin time, brain natriuretic peptide (BNP), and D-dimer (Table). Urinalysis revealed trace protein, large blood, moderate leukocyte esterase, 10–20 leukocytes per high-powered field, and 1+ bacteria. Results of nasopharyngeal SARS-CoV-2 reverse transcription PCR were negative. Further tests included chest radiograph, chest computed tomography angiography, electrocardiogram, and echocardiogram; all results were unremarkable. She was admitted to the pediatric intensive care unit (ICU) and given 2 g/kg intravenous immune globulin (IVIG) for suspected of MIS-C. Symptoms rapidly improved. Leukocyte level decreased to 11.0 K/uL and D-dimer to 2.5 mg/L within 48 hours. The patient remained hemodynamically stable throughout admission and was afebrile with improved symptoms when she was discharged 3 days after admission. SARS-CoV-2 antibody test results at discharge were positive for nucleocapsid but negative for spike. Two days after discharge, the patient returned to the ED for throbbing headaches, nausea, and fatigue. CRP had downtrended since discharge to 2.71 mg/L. Magnetic resonance venography results were normal and she was discharged on antimigraine medication.

Patient 2 was a previously healthy female 17-year-old who received her first dose of BNT162b2 vaccination 7 days before seeking care. Three days after vaccination, she experienced fevers, headaches, abdominal pain, fatigue, and myalgias. Her primary care provider noted leukocytosis to 20 K/uL and referred her to the ED. She had a 103.1°F fever, diffuse abdominal tenderness, and costovertebral angle

Author affiliations: Virginia Commonwealth University School of Medicine, Richmond, Virginia, USA (E. Jain); Children's Hospital of Richmond at Virginia Commonwealth University, Richmond (J.R. Donowitz, E. Aarons, B.C. Marshall, M.P. Miller)

DOI: https://doi.org/10.3201/eid2804.212418

Table. Data for 2 adolescent patients experiencing multisystem inflammatory syndrome after initial dose of BNT162b2 vaccination against severe acute respiratory syndrome coronavirus 2, United States*

Data	Patient 1	Patient 2
Age, y/sex	15/F	17/F
Underlying conditions	Asthma, seasonal allergies	None
Time since BNT162b2 dose, d	6	7
Initial symptoms	102°F fever, headache, nonbilious emesis, myalgias, chest pain, diffuse blanching rash	103.1°F fever, headache, abdominal tenderness, fatigue, myalgias, and costovertebral angle tenderness
Initial vital signs	Blood pressure 115/56 mm Hg, pulse 105 beats/min, temperature 100.4°F, respiratory rate 20 breaths/min, oxygen saturation 100%, weight 60.8 kg	Blood pressure 104/59 mm Hg, pulse 124 beats/min, temperature 103.1°F, respiratory rate 18 breaths/min, oxygen saturation 99%, weight 58 kg
Laboratory test results (reference range)		
Leukocytes, K/μL (4.2–9.4)	17	21.1
% PMNs (39–74)	91	90
% Lymphocytes (18–50)	3	5
CRP, mg/dL (0–0.60)	15.1	36.7
ESR, mm/H (0–15)	13	83
LDH, U/, sL (130–230)	176	326
Fibrinogen, mg/dL (200–475)	516	>800
Prothrombin time, s (9–11.1)	11.4	11.3
BNP, pg/mL (<125)	169	560
Troponin, ng/mL (<0.05)	<0.05	0.18
D-dimer, mg/L (0–0.65)	2.84	2.58
Creatinine, mg/dL (0.3–1.10)	0.92	1.39
AST U/L (15–37)	16	71
ALT, U/L (12–78)	22	73
Alkaline phosphate, U/L (40–120)	73	258
Additional work-up		
Urinalysis	Trace protein, large blood, moderate leukocyte esterase, 10–20 leukocytes, 1+ bacteria	100 mg/dL of protein, moderate blood, moderate leukocyte esterase, 10–20 leukocytes, 5–10 red blood cells, no bacteria
Urine culture	Not performed	10,000 CFUs *Escherichia coli*
Blood culture	Not performed	Negative
Chest radiograph	No abnormal findings	No abnormal findings
Chest CT	No abnormal findings	Not performed
Electrocardiogram	No abnormal findings	Sinus tachycardia, nonspecific T-wave abnormalities
Echocardiogram	No abnormal findings	No abnormal findings
Abdomen/pelvis CT	Not performed	Diffuse left renal enlargement, possible polycystic ovaries
COVID-19 labs		
Nasopharyngeal RT-PCR	Negative	Negative
Spike antibody	Negative	Positive
Nucleocapsid antibody	Positive	Not performed
PICU admission	Yes	No
Treatment	2 g/kg IVIG	2 g/kg IVIG for 1 d, 30 mg IV methylprednisolone 2×/d for 3 d to continue at home orally for 2 d then 2–3 wk steroid taper, 325 mg aspirin reduced to 81 mg on day 3, cefdinir 7 d course
Length of hospital stay	1 d	3 d

*BNT162b2, Pfizer-BioNTech (https://www.pfizer.com). ALT, alanine transaminase; AST, aspartate transaminase; BNP, brain natriuretic peptide; COVID-19, coronavirus disease; CRP, C-reactive protein; CT, computed tomography; ESR, erythrocyte sedimentation rate; IVIG, intravenous immune globulin; LDH, lactate dehydrogenase; PICU, pediatric intensive care unit; PMN, polymorphonuclear cells; RT-PCR, reverse transcription PCR.

tenderness. She had no respiratory symptoms. At admission, laboratory test results showed leukocytosis with polymorphonuclear cell predominance and elevated CRP, erythrocyte sedimentation rate, lactate dehydrogenase, BNP, troponin, D-dimer, creatinine, aspartate aminotransferase, and alkaline phosphate (Table). Urinalysis revealed 100 mg/dL protein, moderate blood, moderate leukocyte esterase, 10–20 leukocytes per high-powered field, 5–10 red blood cells per high powered field, and no bacteria. Urine culture was positive for 10,000 CFU/mL of *Escherichia coli*. Blood culture results were negative. Electrocardiogram showed sinus tachycardia and nonspecific T-wave abnormalities. Abdomen and pelvis computed tomography showed diffuse left renal enlargement without hypoattenuation or hyperattenuation and possible polycystic ovaries. Results of chest radiograph and echocardiogram

were normal. Nasopharyngeal SARS-CoV-2 RT-PCR was negative. Results of SARS-CoV-2 spike antibody testing were positive; nucleocapsid antibody testing was not performed. She started 3 days of intravenous methylprednisolone (30 mg 2×/d) and 1 day IVIG (2 g/kg) for MIS-C. Troponin decreased to <0.05 within 24 hours and CRP to 16.2 within 48 hours. BNP rose to 2,024 on hospital day 2. Repeat echocardiogram showed mild right coronary artery ectasia, and she was started on 325 mg of aspirin daily. On hospital day 3, repeat echocardiogram results were normal, and she was afebrile. Aspirin was decreased to 81 mg daily. She was discharged on hospital day 4 with no fevers for 60 hours and downtrending inflammatory markers including CRP to 8.49 mg/dL. She was also treated for a possible UTI.

Conclusions

This report describes 2 cases of MIS-C within 1 week of receiving the first dose of BNT162b2. There is no specific test for MIS-C; although both patients met diagnostic criteria, alternative diagnoses were possible. Patient 2 had costovertebral angle tenderness, unilateral renal enlargement, and 10,000 CFU/mL growth of a uropathogen on culture. Given the low level of bacterial growth, lack of enhancement on her CT, and constellation of lab and imaging abnormalities not commonly seen with urinary tract infections, MIS-C remains her most likely diagnosis.

Patient 1 had a positive antinucleocapsid antibody suggesting community-acquired COVID-19 infection before MIS-C developed (P.D. Burbelo et al., unpub. data, https://doi.org/10.1101/2020.04.20.20071423). Salzman et al. describe 3 similar cases in which MIS or an MIS-like illness developed after COVID-19 vaccination, particularly in the setting of community-acquired COVID-19 (*3*). The chronology of events in these cases raises the possibility that vaccination may be involved in the pathogenesis of MIS-C when preceded by community-acquired SARS-CoV-2.

The pathogenesis of MIS-C is thought to involve immune dysregulation and hyperinflammation (*4*). Studies have identified high levels of receptor-binding protein (RBD) antibodies in children with severe MIS-C (*5*,*6*). Both natural SARS-CoV-2 infection and BNT162b2 vaccination have been shown to elicit RBD antibodies (*7*). It may be possible that the immune responses to these 2 forms of exposure to SARS-CoV-2 interact to shape the manifestations of mild MIS-C in the postinfectious period of COVID-19. Although both of these cases were mild, we have insufficient data on the pathogenesis of MIS-C to understand how vaccination may shape symptomatology.

A recent report by Zambrano et al. documented that 61/97 (62.9%) MIS-C cases in unvaccinated patients required ICU admission (*8*). That report had a small number of vaccinated cases; 1 in 5 of those vaccinated needed ICU care (*8*). An analysis of postvaccination MIS-C in 21 patients showed that 3 (14%) required invasive mechanical ventilation, 8 (38%) required vasopressors, and 12 (57%) required ICU care (A.R. Yousaf et al., unpub. data, https://doi.org/10.1101/2022.01.03.22268681). In contrast to Zambrano et al.'s vaccinated cases and our reported cases, the Yousaf et al. report suggests a similar number of ICU admissions in vaccinated and unvaccinated persons.

Studies have shown that COVID-19 vaccination is associated with reduced incidence of MIS-C, especially if 2 doses are given. A study of MIS-C cases in France during September–October 2021 found a significantly lower risk of MIS-C among vaccinated adolescents than those who were unvaccinated (*9*). Zambrano et al. found a 91% protective effect of complete (2 doses) BNT162b2 vaccination against MIS-C (*8*). Phase 2 and phase 3 clinical trials of BNT162b2 revealed 0 cases of MIS-C after vaccination (*10*). Despite the reports of postvaccination MIS-C, vaccination clearly lowers the overall MIS-C burden, probably by preventing infection. These studies also suggest low likelihood of vaccination triggering development of MIS-C.

If vaccination can play a role in MIS-C pathogenesis, it is likely an extremely rare event and may involve an underlying genetic predisposition or be contingent on extraneous factors like recent SARS-CoV-2 community exposure. Our findings in 2 cases of MIS-C within 1 week of a dose of BNT162b2 raise the possibility that vaccination may alter the symptom profile of MIS-C.

About the Author

Ms. Jain is a third-year medical student at the Virginia Commonwealth University School of Medicine in Richmond, Virginia. Her primary research interests include infectious disease and pediatric medicine.

References

1. Ahmed M, Advani S, Moreira A, Zoretic S, Martinez J, Chorath K, et al. Multisystem inflammatory syndrome in children: a systematic review. EClinicalMedicine. 2020; 26:100527. https://doi.org/10.1016/j.eclinm.2020.100527
2. Centers for Disease Control and Prevention. Information for healthcare providers about multisystem inflammatory syndrome in children (MIS-C). February 11, 2020 [cited 2021 Oct 1]. https://www.cdc.gov/mis/mis-c/hcp/index.html
3. Salzman MB, Huang C-W, O'Brien CM, Castillo RD. Multisystem inflammatory syndrome after SARS-CoV-2

infection and COVID-19 vaccination. Emerg Infect Dis. 2021;27:1944–8. https://doi.org/10.3201/eid2707.210594
4. Nakra NA, Blumberg DA, Herrera-Guerra A, Lakshminrusimha S. Multi-system inflammatory syndrome in children (MIS-C) following SARS-CoV-2 infection: review of clinical presentation, hypothetical pathogenesis, and proposed management. Children (Basel). 2020;7:69. https://doi.org/10.3390/children7070069
5. Rostad CA, Chahroudi A, Mantus G, Lapp SA, Teherani M, Macoy L, et al. Quantitative SARS-CoV-2 serology in children with multisystem inflammatory syndrome (MIS-C). Pediatrics. 2020;146:e2020018242. https://doi.org/10.1542/peds.2020-018242
6. Yonker LM, Neilan AM, Bartsch Y, Patel AB, Regan J, Arya P, et al. Pediatric severe acute respiratory syndrome coronavirus 2 (SARS-CoV-2): clinical presentation, infectivity, and immune responses. J Pediatr. 2020;227:45–52.e5. https://doi.org/10.1016/j.jpeds.2020.08.037
7. Trougakos IP, Terpos E, Zirou C, Sklirou AD, Apostolakou F, Gumeni S, et al. Comparative kinetics of SARS-CoV-2 anti-spike protein RBD IgGs and neutralizing antibodies in convalescent and naïve recipients of the BNT162b2 mRNA vaccine versus COVID-19 patients. BMC Med. 2021;19:208. https://doi.org/10.1186/s12916-021-02090-6
8. Zambrano LD, Newhams MM, Olson SM, Halasa NB, Price AM, Boom JA, et al.; Overcoming COVID-19 Investigators. Effectiveness of BNT162b2 (Pfizer-BioNTech) mRNA vaccination against multisystem inflammatory syndrome in children among persons aged 12–18 years—United States, July–December 2021. MMWR Morb Mortal Wkly Rep. 2022;71:52–8. https://doi.org/10.15585/mmwr.mm7102e1
9. Levy M, Recher M, Hubert H, Javouhey E, Fléchelles O, Leteurtre S, et al. Multisystem inflammatory syndrome in children by COVID-19 vaccination status of adolescents in France. JAMA. 2022;327:281–3. https://doi.org/10.1001/jama.2021.23262
10. Food and Drug Administration. Vaccines and Related Biological Products Advisory Committee. VRBPAC briefing document, October 26, 2021 [cited 2022 Feb 28]. https://www.fda.gov/media/153409/download

Address for correspondence: Michael P. Miller, Children's Hospital of Richmond at Virginia Commonwealth University, 5801 Bremo Rd, Richmond, VA 23226, USA; email: Michael_miller3@bshsi.org

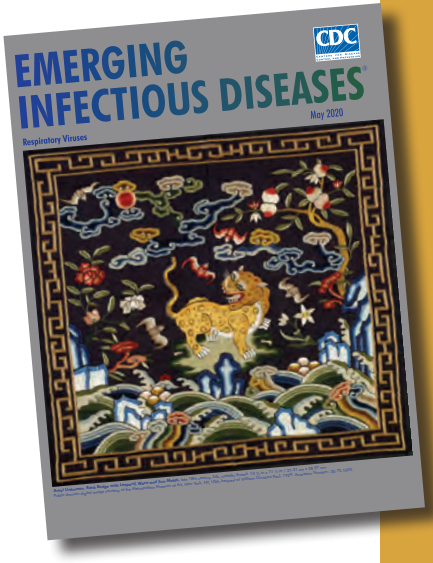

Originally published in May 2020

etymologia revisited

Coronavirus

The first coronavirus, avian infectious bronchitis virus, was discovered in 1937 by Fred Beaudette and Charles Hudson. In 1967, June Almeida and David Tyrrell performed electron microscopy on specimens from cultures of viruses known to cause colds in humans and identified particles that resembled avian infectious bronchitis virus. Almeida coined the term "coronavirus," from the Latin *corona* ("crown"), because the glycoprotein spikes of these viruses created an image similar to a solar corona. Strains that infect humans generally cause mild symptoms. However, more recently, animal coronaviruses have caused outbreaks of severe respiratory disease in humans, including severe acute respiratory syndrome (SARS), Middle East respiratory syndrome (MERS), and 2019 novel coronavirus disease (COVID-19).

Sources:

1. Almeida JD, Tyrrell DA. The morphology of three previously uncharacterized human respiratory viruses that grow in organ culture. J Gen Virol. 1967;1:175–8. https://doi.org/10.1099/0022-1317-1-2-175
2. Beaudette FR, Hudson CB. Cultivation of the virus of infectious bronchitis. J Am Vet Med Assoc. 1937;90:51–8.
3. Estola T. Coronaviruses, a new group of animal RNA viruses. Avian Dis. 1970;14:330–6. https://doi.org/10.2307/1588476
4. Groupe V. Demonstration of an interference phenomenon associated with infectious bronchitis virus of chickens. J Bacteriol. 1949;58:23–32. https://doi.org/10.1128/JB.58.1.23-32.1949

https://wwwnc.cdc.gov/eid/article/26/5/et-2605_article

Pathogens that Cause Illness Clinically Indistinguishable from Lassa Fever, Nigeria, 2018

Jonathan W. Ashcroft,[1] Adebola Olayinka, Nnaemeka Ndodo, Kuiama Lewandowski, Martin D. Curran, Chioma Dan Nwafor, Kingsley Madubuike, Helen Bagnall, Abdulmajid S. Musa, Adama Ahmad, Afolabi Akinpelu, Adesola Adeleye, Chukwuji Martin, Adejoke Akano, Michael Onoja, Akanimo Iniobong, Winifred Ukponu, Chinedu Arinze, Else Ilori, Nwando Mba, Benedict Gannon, Anthony Ahumibe, Chikwe Ihekweazu

During the 2018 Lassa fever outbreak in Nigeria, samples from patients with suspected Lassa fever but negative Lassa virus PCR results were processed through custom gene expression array cards and metagenomic sequencing. Results demonstrated no single etiology, but bacterial and viral pathogens (including mixed coinfections) were detected.

Timely and accurate laboratory differentiation of infectious agents responsible for acute febrile illness represents a major challenge for West Africa. The etiology of systemic febrile illness is particularly poorly described; numerous region-endemic diseases lead to similar initial clinical signs and symptoms (*1*).

In 2018, Nigeria experienced its largest recorded outbreak of Lassa fever; during January 11–December 31, 2018, a total of 3,498 suspected cases were reported. Of these, 633 were confirmed positive, 20 probable, 2,853 negative, and 8 undetermined (*2*). A high number of patients met the case definition for Lassa fever yet ultimately tested negative for the virus and no causative pathogen was identified. To determine the causes of the patients' illnesses, we analyzed gene expression and conducted metagenomic analysis. Ethics approval was obtained from the London School of Hygiene and Tropical Medicine Ethical Review Board (reference no. 16263) and National Health Research Ethics Committee of Nigeria (reference no. NHREC/01/01/2007–19/03/2019).

The Study

During January–December 2018, state health departments across Nigeria collected samples from persons with suspected cases according to Nigeria's National Lassa Fever Outbreak Guidance for patients who met the case definition for Lassa fever (V. Navapurkar et al., unpub. data, https://www.medrxiv.org/content/10.1101/2020.06.02.20118489v3.full.pdf) (Appendix, https://wwwnc.cdc.gov/EID/article/28/5/21-1153-App1.pdf). For sample selection, we used a convenience-based approach. Inclusion criteria were sample collection in 2018, Lassa-negative quantitative reverse transcription PCR (RT-PCR) results, malaria-negative test results (CareStart Malaria RDT; Access-Bio, https://accessbio.net), sufficient sample remaining for subsequent testing, and available basic patient demographic information.

To address the differential diagnoses, we opted to use a TaqMan Array Card (Applied Biosystems, https://www.thermofisher.com) with prespotted singleplex real time PCRs (1 sample can be simultaneously screened for 50 pathogens) (Appendix Figure 2). The assay and data analysis were conducted as previously described (*3*,*4*; S. Minot et al., unpub. data, https://www.biorxiv.org/content/biorxiv/early/2015/09/28/027607.full.pdf). We visually inspected the amplification curve of each reaction and

Author affiliations: Public Health England, London, UK (J.W. Ashcroft, H. Bagnall, B. Gannon); London School of Hygiene and Tropical Medicine, London (J.W. Ashcroft, H. Bagnall, B. Gannon); Nigeria Centre for Disease Control, Abuja, Nigeria (A. Olayinka, N. Ndodo, C. Dan Nwafor, K. Madubuike, A.S. Musa, A. Ahmad, A. Akinpelu, A. Adeleye, C. Martin, A. Akano, M. Onoja, A. Iniobong, W. Ukponu, C. Arinze, E. Ilori, N. Mba, A. Ahumibe, C. Ihekweazu); Public Health England, Porton Down, UK (K. Lewandowski); Clinical Microbiology and Public Health Laboratory, Public Health England, Cambridge, UK (M.D. Curran)

DOI: https://doi.org/10.3201/eid2805.211153

[1]Current affiliation: Army, Defence Science & Technology, Ministry of Defence, London, UK.

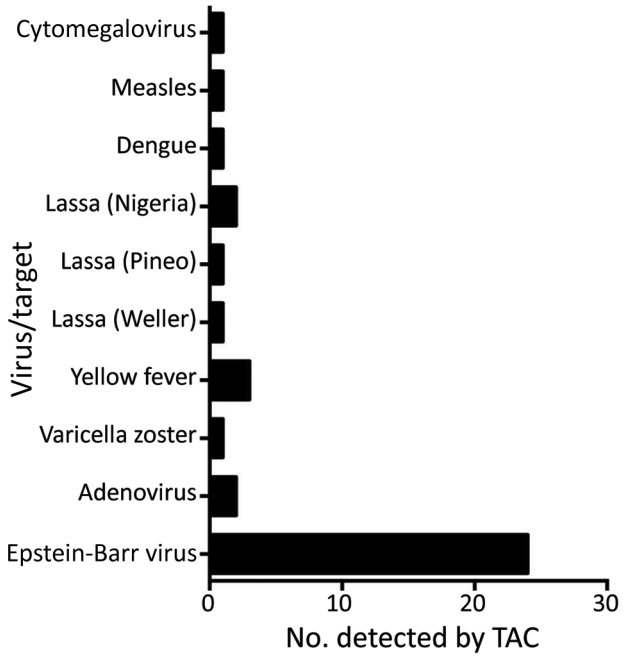

Figure 1. Number of samples from patients who met the case definition for Lassa fever that were positive for specific viral pathogens, among 160 samples tested, Nigeria, 2018. CMV, cytomegalovirus; TAC, TaqMan Array Cards (Applied Bio systems, https://www.thermofisher.com).

classified findings as positive (pathogen target detected) or negative (pathogen target not detected). We used no multicomponent or raw data plots for classification. Public Health England (Cambridge) independently reviewed the final results and found no deviations in reported interpretations. We randomly selected 12 of the samples that had been run on the TaqMan Array Cards (TACs) and subjected them to MinION sequencing by previously described methods (*5*,*6*). Of these 12, we found 0 positive TAC hits for 3 samples and 1–8 hits for the remaining 9 samples.

We examined samples collected from 21 of 37 states within Nigeria, most from Plateau (20.00%), Bauchi (15.60%), Nasarawa (11.25%), Federal Capital Territory (10.00%), Taraba (8.75%), and Kogi (6.88%). Of the 160 samples, ≈58% were from male patients; combined population ages ranged from 2 months to 70 years (median age for male and female patients was 25 years) (Appendix Table 1).

Of the 160 samples tested, TAC detected ≥1 positive bacterial or viral hit for 84 (52.5%) samples. TAC runs recorded positive hits for 8 viruses and 15 types of bacteria (Figures 1, 2; Appendix Figure 3). Virus results were positive for Lassa virus, yellow fever virus, measles virus, cytomegalovirus, adenovirus, Epstein-Barr virus, dengue virus, and varicella zoster virus. The most prevalent species of bacteria among the 15 identified were *Streptococcus* spp., *Salmonella* spp., *Enterobacteriaceae* spp., *Pseudomonas aeruginosa*, *Escherichia coli*, and *Klebsiella pneumoniae*. Cycle threshold (Ct) ranges for the positive hits ranged from a low of 16.2 (*Neisseria meningitidis*) to a high of 43.8 (*Proteus* spp.); Ct for most samples was in the 25–35 range (Appendix Figure 4).

Of the 84 samples positive by TAC, 34 registered >1 target, including mixed bacterial and viral infections (Appendix Table 2, Figure 3). Of these 84, most (95.23%) contained 1–4 detectable pathogens; the remaining samples (4.8%) contained 5–7 detectable pathogens. The pathogenic constellations of patients with higher levels of co-infection (e.g., Epstein-Barr virus, *K. pneumoniae*, and *Enterobacter cloacae*) are in line with those expected to be observed in immunocompromised persons (*7*). Although confident with the results, we cannot completely rule out the possibility of sample contamination; however, we took

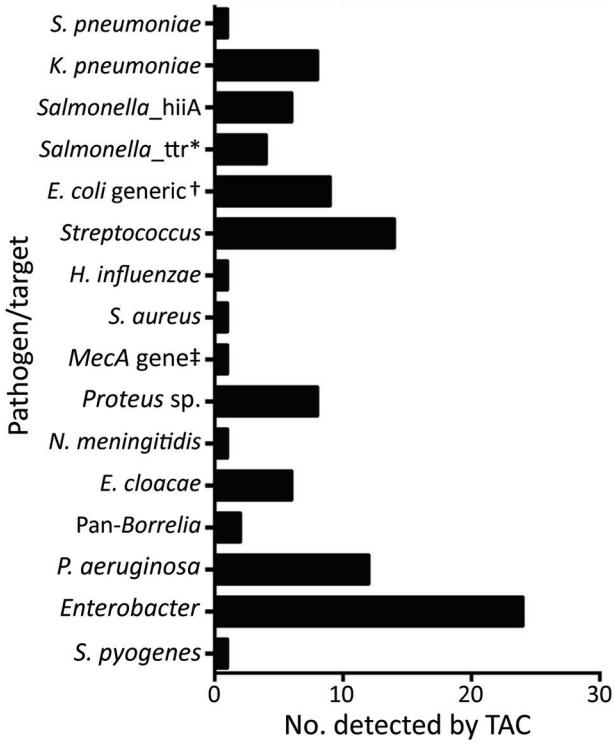

Figure 2. Number of samples from patients who met the case definition for Lassa fever that were positive for specific bacterial pathogens, among 160 samples tested, Nigeria, 2018. *All *Salmonella*_ttr–positive samples also registered as *Salmonella*_hilA–gene positive. †Includes one EAggEC. ‡Sample also positive for *Streptococcus*, *Proteus* spp., and *Pseudomonas aeruginosa*. *E. cloacae*, *Enterobacter cloacae*; EAggEC, enteroaggregative *E. coli*; *E. coli*, *Escherichia coli*; *H.*, *Haemophilus*; *K.*, *Klebsiella*; *N.*, *Neisseria*; *P.*, *Pseudomonas*; *S.*, *Streptococcus*; TAC, TaqMan Array Cards (Applied Biosystems, https://www.thermofisher.com); ttr, tetrathionate.

Table 1. Array and MinION sequencing results for a subset of samples from patients who met the case definition for Lassa fever that were positive for virus, Nigeria, 2018*

Sample	Kraken hits	TAC virus hits	Mapping hits	Mapped reads, no. (%)
307	None	None	NA	NA
165	Human mastadenovirus B	Adenovirus	Adenovirus 2	246 (0.07)
349	Yellow fever virus	Yellow fever virus	Yellow fever virus	66 (0.02)
370	None	None	NA	NA
184	None	None	NA	NA
320	None	Epstein-Barr virus	Epstein-Barr virus	22 (0.01)
344	None	None	NA	NA
279	Yellow fever	Yellow fever	Yellow fever virus	72 (0)
157	Pegivirus C (hepatitis G)	None	Pegivirus C (hepatitis G)	116 (0.01)
147	None	Dengue 2 virus	Dengue 2 virus	0
322	None	None	NA	NA
70	Lassa virus	Lassa virus	Lassa virus	16309 (5.05)-L, 8265 (2.575)-S
201	None	None	NA	NA

*MinION described in (*5*,*6*). NA, not applicable; TAC, TaqMan Array Cards (Applied Biosystems, https://www.thermofisher.com).

steps to minimize contamination (e.g., we prepared fresh RNA extractions in dedicated cabinets and used sample tracking forms).

For confirmatory sequencing using the MinION sequencing platform, we randomly selected a subset of 9 TAC-positive and 3 TAC-negative samples. Sequencing was performed in Nigeria (National Reference Laboratory, Abuja, Nigeria) and in the United Kingdom (Public Health England, Porton Down, UK). The MS2 control spike, used to demonstrate reverse transcription and sequencing efficiency, was satisfactory in all samples.

With respect to viral pathogens, the sequencing data confirmed the results registered by the TACs where available (Table 1). The only differences observed were for 2 samples: 1 weakly positive (Ct >40) for dengue but not detected via sequencing and 1 negative by TAC but proven positive for pegivirus C (a pathogen not represented on the TAC).

Of note are the yellow fever virus–positive and Lassa virus–positive results. The yellow fever virus–positive samples were from Kaduna and Kogi states; patients first displayed signs/symptoms in late July, late August, and early November 2018, the year when the Nigeria Centre for Disease Control reported a large and widespread outbreak of yellow fever in Nigeria, which affected many states. Centre data indicate that, at the time of collection of the 3 yellow fever samples that were positive by TAC with or without sequencing, those states had neither suspected nor confirmed cases of yellow fever (*8*). As such, our results confirm the presence of yellow fever virus when presence of the disease was only suspected.

For the 3 Lassa virus–positive samples, 1 had been misclassified as negative because of an initial laboratory error (e.g., undetected run fail). Of the other 2 samples, 1 was originally recorded as negative by RT-PCR, but a rerun confirmed the presence of Lassa virus (Altona, Ct = 38.51); the other registered as positive for Lassa virus (Nigeria, Pinneo strain, clade 1) but did not register a positive result on RT-PCR (Altona), possibly because of diagnostic primer sets not possessing sufficient homology.

With respect to samples that contained TAC-positive bacterial targets, because sample extracts had been prepared to favor detection of viral pathogens, we could not complete full analysis of potential bacterial pathogens. We compared potential bacterial pathogens indicated by TAC with the Kraken (https://github.com) taxonomic analysis. Read numbers were reported at the genus level (Table 2). Analysis does not rule out the presence of these pathogens; however, data are insufficient for determining presence with certainty.

Table 2. Array and MinION sequencing results for a subset of samples from patients who met the case definition for Lassa fever that were positive for bacteria, Nigeria, 2018*

Sample	TAC hits	Seq hit 1 (no. mapped reads)	Seq hit 2 (no. mapped reads)	Seq hit 3 (no. mapped reads)	Seq hit 4 (no. mapped reads)	Seq hit 5 (no. mapped reads)
307	*Klebsiella pneumoniae*	*Salmonella*_hilA (108)	*Salmonella*_ttr (55)	*Enterobacter* (55)	*Enterobacter cloacae* (55)	*Enterobacter* (56)
165	Pan-*Borrelia*	Spirochetes (27)	None	None	None	None
349	*Escherichia coli* generic	*E. coli* (58)	None	None	None	None
344	*Streptococcus*	Mec_A (591)	*Staphylococcus* (657)	*Pseudomonas aeruginosa* (3)	*Streptococcus. pyogenes* (591)	*Streptococcus* (591)
279	*Streptococcus*	*Streptococcus* (8,837)	None	None	None	None

*Only samples with hits are shown. Seq hits at the genus level (number of reads). MinION described in references *5*,*6*. TAC, TaqMan Array Cards (Applied Biosystems, https://www.thermofisher.com). Seq hit, sequencing hit.

Conclusions

When examining samples from patients who met the case definition for Lassa fever but tested negative for the Lassa virus by quantitative RT-PCR, we found that processing the samples through custom TaqMan Array Cards revealed that there was no single cause of the patients' signs/symptoms. Instead, results were far more complex, detecting a variety of bacterial and viral pathogens (including mixed co-infections). For the random TAC-positive and TAC-negative samples that underwent metagenomic sequencing, results corroborated the TAC viral results well and supported the bacterial results. It is likely that a proportion of the TAC-negative samples (47.5%) were from patients whose illness did indeed have an infectious etiology but did not register on the TAC because the pathogen for the molecular target was not represented, and a proportion might not have had an infectious origin. The pathogens identified in this study could be added to the differential diagnosis for patients with Lassa fever signs/symptoms but negative Lassa virus/malaria test results during outbreaks in West Africa.

Acknowledgments

We thank the following persons for their support: Innocent Okoli, Dan Bailey, Ruth Elderfield, Matt Catton, Anna Seale, Susan Ismaeel, Thom Banks, William Nicholas, Jimmy Whitworth, Steve Pullan, Dan Carter, Karen Osman, Sola Aruna, Colin Brown, Miles Carroll, and Tim Brooks.

The UK Public Health Rapid Support Team is a partnership between Public Health England and the London School of Hygiene & Tropical Medicine, funded by UK Aid from the Department of Health and Social Care.

About the Author

At the time of the study, Dr. Ashcroft was deputy lead microbiologist for the UK Public Health Rapid Support Team; he is now senior science advisor for the British Army. His research interests include pathogen discovery, global health security, and public health advocacy.

References

1. McCormick JB, King IJ, Webb PA, Johnson KM, O'Sullivan R, Smith ES, et al. A case-control study of the clinical diagnosis and course of Lassa fever. J Infect Dis. 1987;155:445–55. https://doi.org/10.1093/infdis/155.3.445
2. Marongiu L, Shain E, Drumright L, Lillestøl R, Somasunderam D, Curran MD. Analysis of TaqMan Array Cards data by an assumption-free improvement of the *maxRatio* algorithm is more accurate than the cycle-threshold method. PLoS One. 2016;11:e0165282. https://doi.org/10.1371/journal.pone.0165282
3. Wood DE, Lu J, Langmead B. Improved metagenomic analysis with Kraken 2. Genome Biol. 2019;20:257. https://doi.org/10.1186/s13059-019-1891-0
4. Li H, Durbin R. Fast and accurate long-read alignment with Burrows-Wheeler transform. Bioinformatics. 2010;26:589–95. https://doi.org/10.1093/bioinformatics/btp698
5. Kafetzopoulou LE, Pullan ST, Lemey P, Suchard MA, Ehichioya DU, Pahlmann M, et al. Metagenomic sequencing at the epicenter of the Nigeria 2018 Lassa fever outbreak. Science. 2019;363:74–7. https://doi.org/10.1126/science.aau9343
6. Lewandowski K, Xu Y, Pullan ST, Lumley SF, Foster D, Sanderson N, et al. Metagenomic nanopore sequencing of influenza virus direct from clinical respiratory samples. J Clin Microbiol. 2019;58:e00963–19. https://doi.org/10.1128/JCM.00963-19
7. Shields A, Patel S. Infections in the immunocompromised host: primary immunodeficiency disorders. Medicine (Baltimore). 2021;49:603–10. https://doi.org/10.1016/j.mpmed.2021.07.002
8. Nigeria Centre for Disease Control. An update of yellow fever outbreak in Nigeria [cited 2021 May 1]. https://ncdc.gov.ng/diseases/sitreps/?cat=10&name=An%20update%20of%20Yellow%20Fever%20outbreak%20in%20Nigeria

Address for correspondence: Adebola Olayinka, Nigeria Centre for Disease Control, Plot 801 Ebitu Ukiwe St, Jabi-Abuja, FCT, Nigeria; email: adebola.olayinka@ncdc.gov.ng

Duration of Infectious Virus Shedding by SARS-CoV-2 Omicron Variant–Infected Vaccinees

Kenichiro Takahashi,[1] Masahiro Ishikane,[1] Mugen Ujiie, Noriko Iwamoto, Nobumasa Okumura, Testsuro Sato, Maki Nagashima, Ataru Moriya, Michiyo Suzuki, Masayuki Hojo, Takayuki Kanno, Shinji Saito, Sho Miyamoto, Akira Ainai, Minoru Tobiume, Takeshi Arashiro, Tsuguto Fujimoto, Tomoya Saito, Masaya Yamato, Tadaki Suzuki, Norio Ohmagari

To determine virus shedding duration, we examined clinical samples collected from the upper respiratory tracts of persons infected with severe acute respiratory syndrome coronavirus 2 Omicron variant in Japan during November 29–December 18, 2021. Vaccinees with mild or asymptomatic infection shed infectious virus 6–9 days after onset or diagnosis, even after symptom resolution.

The severe acute respiratory syndrome coronavirus 2 (SARS-CoV-2) variant of concern belonging to the Pango lineage B.1.1.529, known as the Omicron variant, has spread rapidly worldwide (*1*,*2*). Several reports describe high infectivity and transmissibility of Omicron (*3*,*4*). The clinical course and the duration of virus shedding based on cycle quantification (Cq) values among 11 Omicron-infected patients has been reported (*5*). However, the relationship between duration of virus shedding and infectivity of Omicron is unknown. To help determine the criteria for patient isolation, we evaluated the duration of shedding of Omicron variant virus isolated from upper respiratory samples collected from the reported case-patients in Japan.

This study was approved by the ethics committee of the National Center for Global Health and Medicine (approval no. NCGM-G-003472–03) and the Medical Research Ethics Committee of the National Institute of Infectious Diseases (NIID) for the use of human subjects (approval no. 1178). We obtained written informed consent to publish the article.

Author affiliations: National Institute of Infectious Diseases, Tokyo, Japan (K. Takahashi, T. Kanno, S. Saito, S. Miyamoto, A. Ainai, M. Tobiume, T. Arashiro, T. Fujimoto, T. Saito, T. Suzuki); National Center for Global Health and Medicine, Tokyo (M. Ishikane, M. Ujiie, N. Iwamoto, N. Okumura, T. Sato, M. Nagashima, A. Moriya, M. Suzuki, M. Hojo, N. Ohmagari); Rinku General Medical Center, Osaka, Japan (M. Yamato)

DOI: https://doi.org/10.3201/eid2805.220197

The Study

We conducted our retrospective study on leftover clinical samples collected from Omicron-infected patients in Japan during November 29–December 18, 2021. We sequenced the Omicron variant by using whole-genome sequencing as described (*2*) and uploaded the consensus sequences to GISAID (https://www.gisaid.org) (Table).

For cases detected by SARS-CoV-2 testing at airport quarantines, samples collected for diagnosis (saliva or nasopharyngeal) were transported to the NIID to confirm Omicron. We used the residual samples for this study. The date of sample collection of the first Omicron-positive sample for each patient was defined as the diagnosis date (day 0). Nasopharyngeal samples were collected serially during hospitalization, stored at −80°C, and transported to NIID.

We quantified SARS-CoV-2 RNA by using quantitative reverse transcription PCR (qRT-PCR) and virus isolation testing. We performed qRT-PCR as described previously (*6*). We measured Cq values (i.e., viral RNA levels) by using qRT-PCR targeting the SARS-CoV-2 nucleocapsid gene (Appendix Figure 1, https://wwwnc.cdc.gov/EID/article/28/5/22-0197-App1.pdf). We analyzed samples with Cq values that were reported as negative after 40 cycles by substituting a value of 45. We performed the virus isolation assay according to described procedure (*7*). All laboratory analyses were performed at the NIID.

To examine infectious virus shedding, we classified samples according to date of diagnosis, date of symptom onset, and date of symptom resolution.

[1]These authors contributed equally to this article.

Table . Overview of 18 cases of SARS-CoV-2 infection caused by the Omicron variant, Japan, November 29–December 18, 2021*

Case no.	Patient age, y/sex	Disease severity	Vaccine, no. doses (type)	Duration of symptoms, d	Lowest Cq values (days after diagnosis, days after symptom onset)	Virus isolation, since diagnosis (days)‡
1	39/M	Mild	2 (M, M)	5	21.6 (3, 3)	Positive (3)
2	30/M	Asymptomatic	2 (M, M)	NA	25.3 (5, NA)	Positive (5)
3	25/M	Mild	2 (P, P)	6	23.2 (4, 3)	Negative
4	46/M	Mild	3 (J, P, P)	11	24.7 (9, 11)	Positive (6)
5	50/M	Asymptomatic	2 (P, P)	NA	23.1 (5, NA)	Positive (5)
6	31/M	Mild	2 (P, P)	5	25.4 (0, 0)	Negative
7	47/M	Asymptomatic	2 (P, P)	NA	34.2 (9, NA)	Negative
8	33/F	Mild	2 (M, M)	12	32.4 (0, 1)	Negative
9	64/M	Mild	2 (P, P)	4	23.9 (0, −1)	Positive (0)
10	42/M	Mild	2 (M, M)	4	27.0 (0, −1)	Negative
11	49/M	Mild	2 (M, M)	5	26.5 (0, −1)	Positive (8)
12	31/M	Mild	2 (M, M)	4	25.4 (5, 4)	Positive (7)
13	50/M	Mild	2 (M, M)	6	24.7 (5, 7)	Positive (5)
14	30/F	Mild	2 (M, M)	11	30.0 (0, 2)	Negative
15	27/M	Mild	2 (P, P)	8	25.8 (6, 10)	Negative
16	23/M	Mild	2 (P, P)	5	18.7 (3, 4)	Positive (3)
17	47/M	Mild	2 (M, M)	6	24.2 (7, 7)	Positive (0)
18	38/M	Mild	2 (P, P)	6	29.0 (7, 8)	Negative

*The consensus sequences of the viral genome have been uploaded to GISAID (https://www.gisaid.org) (identification nos. EPI_ISL_6913953, EPI_ISL_6914908, EPI_ISL_7194610, EPI_ISL_7834392, EPI_ISL_7860184, EPI_ISL_7860185, EPI_ISL_7860188, EPI_ISL_7860189, EPI_ISL_7860190, EPI_ISL_7860193, EPI_ISL_7860197, EPI_ISL_7889642, EPI_ISL_7889643, EPI_ISL_8096984, EPI_ISL_8096995, EPI_ISL_8605240, EPI_ISL_8605241, EPI_ISL_8605242). Cq, quantification cycle; J, Johnson & Johnson; M, Moderna; NA, not available; P, Pfizer/BioNTech; SARS-CoV-2, severe acute respiratory syndrome. coronavirus 2.

For cases in which multiple samples were collected in each time segment, we used the sample with the highest amount of viral RNA (i.e., lowest Cq values) in each time segment for each case for comparison. For data analysis and visualization, we used GraphPad Prism version 8.4.3 (https://www.graphpad.com). To compare the Cq values, we used Mann-Whitney *t* and Friedman tests with Dunn multiple comparisons. Statistical significance was set at p<0.05.

All 18 case-patients had been vaccinated >14 days before coronavirus disease (COVID-19) diagnosis (Table). The median (interquartile range [IQR]) duration between vaccination and diagnosis was 117 (71–131) days. Of the 18 case-patients, 15 were symptomatic and 3 were asymptomatic.

Among the 101 serially collected samples analyzed (85 nasopharyngeal and 16 saliva), we detected infectious virus in 10 (9.9%) from 10 patients (8 symptomatic and 2 asymptomatic) (Figure 1, panel A; Appendix Tables 1, 2,). The viral RNA levels analyzed by using qRT-PCR were significantly higher in samples with the infectious virus than without (p<0.0001) (Figure 1, panel A). Infectious virus was detected up to 9 days after diagnosis; the highest proportion of virus isolates (41.7%) was found in samples collected 2–5 days after diagnosis, and no isolates were detected

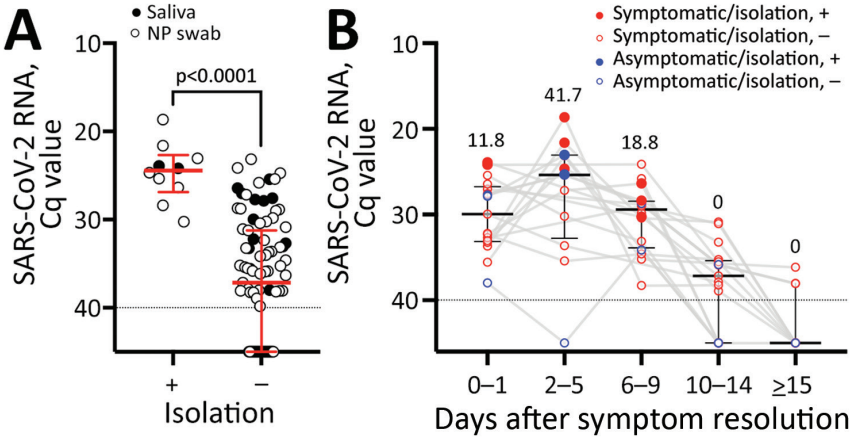

Figure 1. SARS-CoV-2 RNA level and infectious virus shedding in upper respiratory samples from symptomatic patients infected with the SARS-CoV-2 Omicron variant, Japan, November 29–December 18, 2021. A) SARS-CoV-2 RNA levels and presence of the infectious virus, by date of symptom onset. Each closed circle indicates case-patients from whom virus was isolated. Numbers above each plot indicate the proportion of case-patients from whom virus was isolated in each period. Black lines indicate median Cq values and error bars interquartile ranges; dotted lines indicate negative cutoff values. *Before symptom onset. B) SARS-CoV-2 RNA levels and presence of infectious virus, by date of symptom resolution. Closed circles indicate patients from whom virus was isolated. Numbers above each plot indicate the proportion of persons from whom virus was isolated in each period. Black lines indicate median Cq values and error bars interquartile ranges; dotted lines indicate cutoff values. †Before symptom resolution. Cq, quantification cycle; SARS-CoV-2, severe acute respiratory syndrome coronavirus 2.

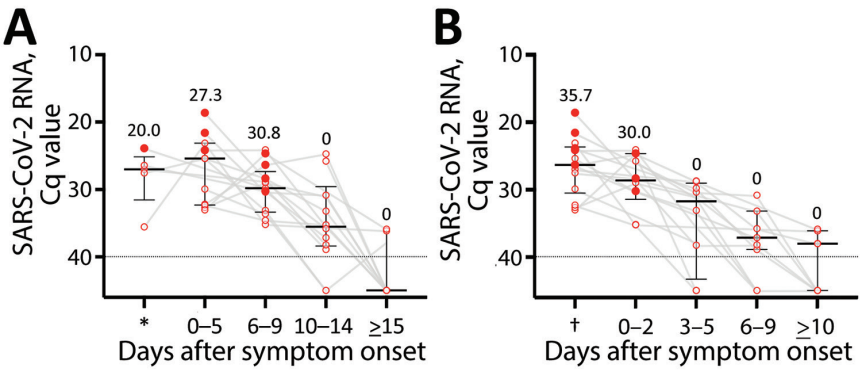

Figure 2. SARS-CoV-2 RNA level and infectious virus shedding in all upper respiratory samples from patients infected with the SARS-CoV-2 Omicron variant, Japan, November 29–December 18, 2021. A) SARS-CoV-2 RNA levels in NP swab samples (open circles) and saliva (closed circles) with or without infectious virus. Red lines indicate median Cq values and error bars interquartile ranges; dotted lines indicate negative cutoff values. The Cq values between samples from which infectious virus was isolated and samples from which infectious virus was not isolated were compared by using the Mann-Whitney test. B) SARS-CoV-2 RNA levels and presence of infectious virus organized by the days after diagnosis. Red circles indicate symptomatic case-patients; blue circles indicate asymptomatic case-patients; each closed circle indicates case-patients from whom virus was isolated. Numbers above each plot indicate the proportion of case-patients from whom virus was isolated in each period. Black lines indicate median Cq values and error bars interquartile ranges; dotted lines indicate negative cutoff values. Cq, quantification cycle; NP, nasopharyngeal; SARS-CoV-2, severe acute respiratory syndrome coronavirus 2; +, with infectious virus; –, without infectious virus.

10 days after diagnosis (Figure 1, panel B; Appendix Figure 3, panel A).

We detected infectious virus in the samples of 20%–30% symptomatic patients, ranging from before they were symptomatic to 9 days after symptom onset, but we detected no infectious virus beyond 10 days after symptom onset (Figure 2, panel A; Appendix Table 3, Figure 2, panel B, Figure 3, panel B). For ≈30% of case-patients, infectious virus shedding was detected up to 2 days after symptom resolution, but no virus was detected beyond 3 days after symptom resolution (Figure 2, panel B; Appendix Table 4, Figure 3, panel C). Many of the first samples collected were saliva samples. Of note, the results of only nasopharyngeal samples did not differ from samples including saliva after 2 days of diagnosis (Appendix Figure 4, panels A, B).

Conclusions

Omicron RNA detection was highest 2–5 days after diagnosis or after symptom onset and then decreased over time, markedly 10 days after diagnosis or symptom onset. In symptomatic case-patients with infectious virus detected on days 6–9 after symptom onset, infectious virus was also detected 0–2 days after symptom resolution. Although the sample size used in our study is small, these findings suggest the possibility of changes in the viral replication kinetics, unlike previous reports for ancestral (wild-type) strain (Wu01) strains (*8*,*9*). Cq values were frequently lower for the B.1.617.2 (Delta) variant than for the other variants (B.1.1.7 [Alpha]), and virus clearance was faster in vaccinated than in unvaccinated persons (*10*). Similar to findings for the Wu01 strain, the Alpha variant, and the Delta variant (*11*–*13*), RNA of the Omicron variant was detectable 10 days after diagnosis or symptom onset, but no virus was isolated.

In the United States, the isolation period for COVID-19 patients is 5 days after symptom onset if the symptoms are improving (*14*). In Japan, based on the outbreak situation, the results of this study, and isolation criteria in other countries, the isolation criteria for Omicron patients were changed on January 6, 2022. Two consecutive negative test results 10 days after diagnosis or symptom onset are no longer required for patients who received 2 vaccine doses.

Our first study limitation is that we identified infectious virus by infection assays among only 18 patients. We do not know about the infectivity outside of this study. In addition, there are no epidemiologic data about whether secondary infections occurred from patients with these infectious viruses. Therefore, comparing theses results with future epidemiologic studies of more samples is necessary. Our second study limitation is that the virus isolation and infectivity assay results depend on the sample collection method, storage period, and storage conditions. Therefore, negative results do not guarantee that there was no infectious virus in the sample at the time of collection. Last, for some case-patients, virus was not isolated in samples collected at the time of diagnosis. For these persons, the samples used for diagnosis were collected at the airport quarantine and were saliva, for which the quality may not be suitable for virus isolation. Although our results are insufficient to show a difference in efficiency of virus isolation between saliva and nasopharyngeal samples in Omicron-infected persons, this difference may have underestimated the presence of infectious virus at diagnosis. In conclusion, fully vaccinated COVID-19

case-patients with mild or asymptomatic infection shed infectious virus in their upper respiratory tract for 6–9 days after illness onset or diagnosis, even after symptom resolution, but not after day 10.

Acknowledgments

We thank Akiko Sataka, Asato Kojima, Izumi Kobayashi, Yuki Iwamoto, Yuko Sato, Seiya Ozono, Milagros Virhuez Mendoza, Noriko Nakajima, Kenta Takahashi, Yuichiro Hirata, Shun Iida, Harutaka Katano, Makoto Kuroda, Tsuyoshi Sekizuka, Naomi Nojiri, Hazuka, Yoshida, Nozomu Hanaoka, and Masumichi Saito for technical support. We also thank Kenji Sadamasu and Mami Nagashima for technical support with respect to SARS-CoV-2 viral RNA genome sequencing and all staff members for providing care for COVID-19 patients.

About the Author

Dr. Takahashi is a research scientist and pediatrician at the Center for Emergency Preparedness and Response, National Institute of Infectious Diseases, Tokyo, Japan. His research interests include pediatric emerging infectious diseases.

References

1. World Health Organization. Classification of omicron (B1.1.529): SARS-CoV-2 variant of concern [cited 2022 Mar 9]. https://www.who.int/news/item/26-11-2021-classification-of-omicron-(b.1.1.529)-sars-cov-2-variant-of-concern
2. Maruki T, Iwamoto N, Kanda K, Okumura N, Yamada G, Ishikane M, et al. Two cases of breakthrough SARS-CoV-2 infections caused by the Omicron variant (B.1.1.529 lineage) in international travelers to Japan. Clin Infect Dis. 2022 Jan 3; ciab1072. Online ahead of print. https://doi.org/10.1093/cid/ciab1072
3. The National Institute for Communicable Diseases. The daily COVID-19 effective reproductive number (R) in the public sector of South Africa (week 48 of 2021) [cited 2022 Mar 10]. https://www.nicd.ac.za/wp-content/uploads/2021/12/The-Daily-COVID-19-Effective-Reproductive-Number-R-in-the-public-sector-of-South-Africa-week-48-of-2021.pdf
4. UK Health Security Agency. SARS-CoV-2 variants of concern and variants under investigation in England: technical briefing 32 [cited 2022 Mar 10]. https://assets.publishing.service.gov.uk/government/uploads/system/uploads/attachment_data/file/1042688/RA_Technical_Briefing_32_DRAFT_17_December_2021_2021_12_17.pdf
5. Okumura N, Tsuzuki S, Saito S, Saito T, Takasago S, Hojo M, et al. The first eleven cases of SARS-CoV-2 Omicron variant infection in Japan: a focus on viral dynamics. Global Health & Medicine. 2021. Online ahead of print. https://doi.org/10.35772/ghm.2021.01124
6. Shirato K, Nao N, Katano H, Takayama I, Saito S, Kato F, et al. Development of genetic diagnostic methods for detection for novel coronavirus 2019(nCoV-2019) in Japan. Jpn J Infect Dis. 2020;73:304–7. https://doi.org/10.7883/yoken.JJID.2020.061
7. Yamada S, Fukushi S, Kinoshita H, Ohnishi M, Suzuki T, Fujimoto T, et al.; Virus Diagnosis Group (NIID Toyama). Assessment of SARS-CoV-2 infectivity of upper respiratory specimens from COVID-19 patients by virus isolation using VeroE6/TMPRSS2 cells. BMJ Open Respir Res. 2021;8:e000830. https://doi.org/10.1136/bmjresp-2020-000830
8. He X, Lau EHY, Wu P, Deng X, Wang J, Hao X, et al. Temporal dynamics in viral shedding and transmissibility of COVID-19. Nat Med. 2020;26:672–5. https://doi.org/10.1038/s41591-020-0869-5
9. Cheng HY, Jian SW, Liu DP, Ng TC, Huang WT, Lin HH; Taiwan COVID-19 Outbreak Investigation Team. Contact tracing assessment of COVID-19 transmission dynamics in Taiwan and risk at different exposure periods before and after symptom onset. JAMA Intern Med. 2020;180:1156–63. https://doi.org/10.1001/jamainternmed.2020.2020
10. Kissler SM, Fauver JR, Mack C, Tai CG, Breban MI, Watkins AE, et al. Viral dynamics of SARS-CoV-2 variants in vaccinated and unvaccinated persons. N Engl J Med. 2021;385:2489–91. https://doi.org/10.1056/NEJMc2102507
11. Owusu D, Pomeroy MA, Lewis NM, Wadhwa A, Yousaf AR, Whitaker B, et al.; Household Transmission Study Team. Persistent SARS-CoV-2 RNA shedding without evidence of infectiousness: a cohort study of individuals with COVID-19. J Infect Dis. 2021;224:1362–71. https://doi.org/10.1093/infdis/jiab107
12. Blanquart F, Abad C, Ambroise J, Bernard M, Cosentino G, Giannoli JM, et al. Characterisation of vaccine breakthrough infections of SARS-CoV-2 Delta and Alpha variants and within-host viral load dynamics in the community, France, June to July 2021. Euro Surveill. 2021;26:34533119. https://doi.org/10.2807/1560-7917.ES.2021.26.37.2100824
13. Siedner MJ, Boucau J, Gilbert RF, Uddin R, Luu J, Haneuse S, et al. Duration of viral shedding and culture positivity with postvaccination SARS-CoV-2 delta variant infections. JCI Insight. 2022;7:e155483. https://doi.org/10.1172/jci.insight.155483
14. Centers for Disease Control and Prevention. CDC updates and shortens recommended isolation and quarantine period for general population [cited 2022 Jan 18]. https://www.cdc.gov/media/releases/2021/s1227-isolation-quarantine-guidance.html

Address for correspondence: Masahiro Ishikane, Disease Control and Prevention Center, National Center for Global Health and Medicine 1-21-1 Toyama, Shinjuku-ku, Tokyo 162-8655, Japan; email: ishikanemasahiro@gmail.com. Tadaki Suzuki, Department of Pathology, National Institute of Infectious Diseases, 1-23-1 Toyama, Shinjuku-ku, Tokyo 162-8640, Japan; email: tksuzuki@nih.go.jp

Imported Monkeypox from International Traveler, Maryland, USA, 2021

Varea Costello, Madeleine Sowash, Aahana Gaur, Michael Cardis, Helena Pasieka, Glenn Wortmann, Sheena Ramdeen

A case of monkeypox was diagnosed in a returning traveler from Nigeria to Maryland, USA. Prompt infection control measures led to no secondary cases in 40 exposed healthcare workers. Given the global health implications, public health systems should be aware of effective strategies to mitigate the potential spread of monkeypox.

Since the eradication of smallpox, monkeypox has assumed the role of the most prominent orthopoxvirus affecting human communities (*1*). Formerly a rare disease native to Africa, monkeypox is now endemic to countries in western and central Africa, which have faced a resurgence of monkeypox outbreaks over the past decade. More confirmed cases of monkeypox have been diagnosed since 2016 than in the previous 40 years (*2*). Nigeria is in the midst of an ongoing monkeypox outbreak; as of October 2021, a total of 502 cases and 8 deaths from this disease had been reported (*3*). Because of global health implications, in 2017 the World Health Organization and the US Centers for Disease Control and Prevention (CDC) conducted an informal consultation with infectious diseases experts and researchers in countries in Africa to assess the surveillance and outbreak response to monkeypox.

Outside Africa, cases of monkeypox remain rare, but are increasing; 7 international cases have been diagnosed since 2018 (*4*–*6*). In the United States, a case was recently identified in Texas in a traveler returning from Nigeria (*7*). Before that case, the last confirmed monkeypox cases in the United States were in an outbreak involving 47 persons across 6 states; those cases were associated with contact of prairie dogs infected by imported rats from Ghana (*7*). As case rates increase, determining effective public health interventions in preventing secondary spread of monkeypox is critical and a challenge that largely has yet to be confronted in the United States. We describe a case of imported monkeypox in Maryland, USA, and the infection control measures used to prevent additional disease transmission.

The Study

A 28-year-old man sought care for a diffuse vesicular rash that had developed over the preceding 24–48 hours. He had traveled on a flight from Lagos, Nigeria, and arrived in the United States the day he sought care. While in Nigeria, he visited relatives, stayed in hotel lodging without travel to rural regions, and had no interactions with animals or animal carcasses. During his flight from Lagos, he noticed a burning sensation on his skin, followed by development of discrete vesicles on his forehead and nose, which spread to his arms, trunk, and inner thighs over several hours. He denied having associated symptoms, including fever, chills, or headache.

At examination, we observed right cervical lymphadenopathy and numerous 2–4-mm pustules on an erythematous base. Some of these pustules had central umbilication and were present diffusely with acrofacial propensity, favoring the face, neck, and hands. A few 2–3-mm round erosions were noted on the oral mucosa, and an intact pustule was observed on the lower mucosal lip (Figure 1). The patient was given intravenous acyclovir for empiric treatment of disseminated varicella zoster virus infection, admitted, and subjected to contact and airborne isolation precautions pending further evaluation. Within 24 hours of admission, no new

Author affiliations: Walter Reed National Military Medical Center, Bethesda, Maryland, USA (V. Costello); Uniformed Services University, Bethesda (V. Costello); Medstar Washington Hospital Center, Washington, DC, USA (M. Sowash, A. Gaur, M. Cardis, H. Pasieka, G. Wortmann, S. Ramdeen)

DOI: https://doi.org/10.3201/eid2805.220292eid2805.220292

Figure 1. Cutaneous manifestations of imported monkeypox from international traveler, Maryland, USA, 2021. Numerous pustules on erythematous base with some central umbilication and acrofacial propensity are shown.

lesions developed, and there was noticeable crusting of several existing vesicles.

We obtained a 4-mm punch biopsy specimen from an intact pustule on the abdomen of the patient. This specimen showed epidermal necrosis, reticular degeneration, and vesiculation by staining with hematoxylin and eosin. We found dyskeratotic keratinocytes, neutrophil exocytosis, and intracytoplasmic inclusion bodies consistent with Guarnieri bodies in the epidermis. We also detected a diffuse, mixed, superficial dermal infiltrate of lymphocytes, histiocytes, neutrophils, and occasional eosinophils (Figure 2).

Based on the travel history of the patient and histopathologic findings, we suspected monkeypox, likely acquired by human contact in the absence of any animal exposures. Additional specimens of the skin lesions were identified by the Maryland Department of Health as non–variola orthopox by real-time reverse transcription PCR (RT-PCR) and the CDC Laboratory Response Network protocol. CDC used viral culture and RT-PCR to confirm the diagnosis of monkeypox, further identifying the specimen as part of the West African clade, which has driven the outbreak in Nigeria since 2017.

Upon confirmation of the monkeypox diagnosis, we identified all healthcare workers (HCWs)

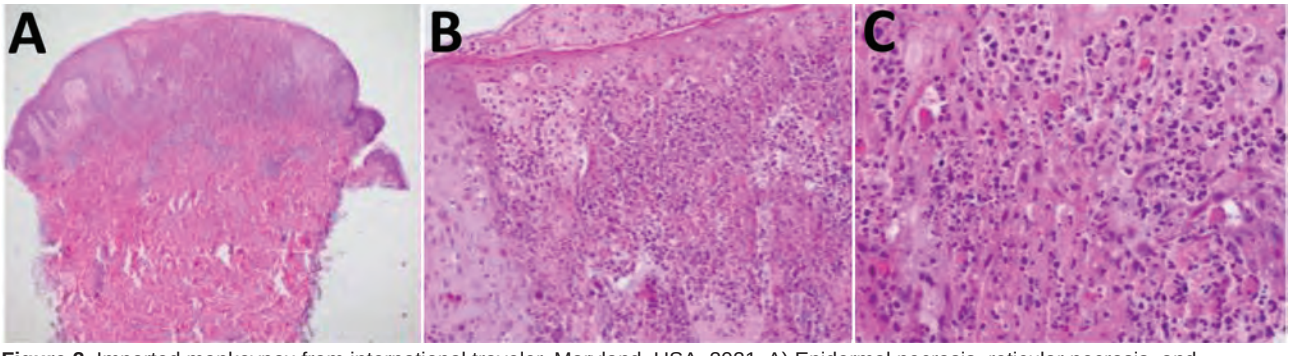

Figure 2. Imported monkeypox from international traveler, Maryland, USA, 2021. A) Epidermal necrosis, reticular necrosis, and vesiculation. In the dermis, a diffuse mixed superficial dermal infiltrate was observed. B, C) Higher magnification views showing dyskeratotic keratinocytes, neutrophil exocytosis, and intracytoplasmic inclusion bodies consistent with Guarnieri bodies in the epidermis. Hematoxylin and eosin stain; original magnification ×4 in panel A, ×20 in panel B, and ×40 in panel C.

involved in the case and classified 40 as contacts by CDC guidelines (*8*). No HCW met the criteria for high-risk exposure, and no doses of preventive smallpox vaccine were administered. Hospital-based public health officials contacted each HCW daily for 21 days (the duration of incubation period for monkeypox) and instructed them to measure their temperature twice a day and monitor any symptoms. At the conclusion of the surveillance period, we did not detect disease transmission.

Conclusions

Previously considered a rare zoonotic infection, human monkeypox has reemerged as a clinically serious disease after decades of quiescence. Monkeypox has an overall case-fatality rate of up to 11% (*1*), and increasing human populations have no immunity to poxvirus; therefore, future progress in understanding monkeypox is critical. The World Health Organization Research and Development Blueprint in 2018 classified monkeypox as an emergent disease requiring accelerated research, development, and public health action (*8*). The epidemic potential of monkeypox was demonstrated during the outbreak in the United States in 2003, and had the predominant virus strain been the more virulent and aggressive Congo Basin strain instead of a virus in the West African clade, a higher mortality rate would have been possible (*9*).

Although the public health experience addressing monkeypox in the United States has been limited, this case illustrates the effectiveness of the basic principles of infection control: rapid identification and isolation of the index patient; use of personal protective equipment by HCWs; and thorough contact tracing, including monitoring for secondary cases throughout the totality of the incubation period. Using these interventions alone, our hospital system and community were able to avoid additional disease transmission. Hospital systems should ensure that their healthcare teams, particularly frontline workers, are aware of infection control policies, especially pertaining to patients with possible infectious diseases. In particular, any patient who has a fever and disseminated vesicular or pustular rash should immediately be placed on airborne and contact precautions because these are the typical symptoms associated with orthopoxvirus infection (*10*).

Although vaccination was not required in this case, public health recommendations to prevent secondary disease transmission of monkeypox include the smallpox vaccine (*11*). The vaccine has been estimated to confer 85% protection against monkeypox (*12*), and waning population immunity since routine smallpox vaccine administration ended is postulated to have contributed to its resurgence (*2*). The 2 Food and Drug Administration–approved vaccines are ACAM2000 and JYNNEOS. Either vaccine can be administered preemptively for monkeypox exposures, which is recommended for persons involved in monkeypox outbreak investigations. JYNNEOS is a nonreplicating, live virus, licensed specifically for monkeypox prevention; ACAM2000 is the only recommended vaccine for monkeypox postexposure prophylaxis. On the basis of the effectiveness of postexposure smallpox vaccine, the CDC advises postexposure prophylaxis to high-risk contacts within 4 days and up to 14 days of initial contact with monkeypox (*11*). This intervention has been safely and effectively used by public health officials in the United States, the United Kingdom, and Singapore (*5*,*6*,*13*).

In addition to smallpox vaccine, vaccinia immune globulin is available and can be used as prophylaxis for severely immunocompromised patients (when smallpox vaccine should be avoided), although the benefit is unclear (*10*). The Food and Drug Administration–approved antiviral drugs to treat smallpox are tecovirimat and brincidofovir, which can also be used to treat monkeypox, but there are no monkeypox-specific antiviral drugs for treatment or postexposure prophylaxis. Because there are multiple orthopoxvirus vaccine guidance documents, formulation of consolidated recommendations is ongoing (*14*).

In summary, we report a case of monkeypox in a traveler returning to the United States from Nigeria and review infection control measures to prevent secondary cases. Multiple appearances beyond disease-endemic countries indicate that monkeypox has become a relevant travel-related disease, and physicians should remain vigilant in combatting transmission of this virus.

Acknowledgments

We thank the Maryland Department of Health and all medical doctors and ancillary staff involved in caring for the patient.

About the Author

Dr. Costello is an infectious diseases fellow at the Walter Reed National Military Medical Center, Bethesda, MD. His primary research interests are global medicine and emerging infectious diseases.

References

1. McCollum AM, Damon IK. Human monkeypox. Clin Infect Dis. 2014;58:260–7. https://doi.org/10.1093/cid/cit703
2. Durski KN, McCollum AM, Nakazawa Y, Petersen BW, Reynolds MG, Briand S, et al. Emergence of monkeypox—

West and Central Africa, 1970–2017. MMWR Morb Mortal Wkly Rep. 2018;67:306–10. https://doi.org/10.15585/mmwr.mm6710a5
3. Nigeria Centre for Disease Control. An update of monkeypox outbreak in Nigeria for week 43, Oct 31, 2021 [cited 2021 Dec 3]. https://ncdc.gov.ng/themes/common/files/sitreps/75e3b8532d48167c0e58fcd0eca03062.pdf
4. Erez N, Achdout H, Milrot E, Schwartz Y, Wiener-Well Y, Paran N, et al. Diagnosis of imported monkeypox, Israel, 2018. Emerg Infect Dis. 2019;25:980–3. https://doi.org/10.3201/eid2505.190076
5. Yong SE, Ng OT, Ho ZJM, Mak TM, Marimuthu K, Vasoo S, et al. Imported monkeypox, Singapore. Emerg Infect Dis. 2020;26:1826–30. https://doi.org/10.3201/eid2608.191387
6. Vaughan A, Aarons E, Astbury J, Balasegaram S, Beadsworth M, Beck CR, et al. Two cases of monkeypox imported to the United Kingdom, September 2018. Euro Surveill. 2018;23:1800509. https://doi.org/10.2807/1560-7917.ES.2018.23.38.1800509
7. Centers for Disease Control and Prevention. Monkeypox in the U.S., Nov 17, 2021 [cited 2021 Dec 3]. https://www.cdc.gov/poxvirus/monkeypox/outbreak/us-outbreaks.html
8. Centers for Disease Control and Prevention. Monitoring people who have been exposed, Nov 17, 2021 [cited 2022 Feb 18]. https://www.cdc.gov/poxvirus/monkeypox/clinicians/monitoring.html
9. World Health Organization. R&D blueprint: list of blueprint priority diseases, 2018 [cited 2022 Feb 22]. http:// www.who.int/blueprint/priority-diseases
10. Brown K, Leggat PA. Human monkeypox: current state of knowledge and implications for the future. Trop Med Infect Dis. 2016;1:8. https://doi.org/10.3390/tropicalmed1010008
11. Centers for Disease Control and Prevention. Chart 1: acute, generalized vesicular or pustular rash illness protocol. Dec 16, 2021 [cited 2022 Feb 17]. https://www.cdc.gov/smallpox/lab-personnel/laboratory-procedures/chart1.html
12. Di Giulio DB, Eckburg PB. Human monkeypox: an emerging zoonosis. Lancet Infect Dis. 2004;4:15–25. https://doi.org/10.1016/S1473-3099(03)00856-9
13. Centers for Disease Control and Prevention (CDC). Update: multistate outbreak of monkeypox—Illinois, Indiana, Kansas, Missouri, Ohio, and Wisconsin, 2003. MMWR Morb Mortal Wkly Rep. 2003;52:642–6.
14. Petersen B. Orthopoxvirus work group background and considerations, 2021. Advisory Committee on Immunization Practices (ACIP) [cited 2022 Feb 22]. https://www.cdc.gov/vaccines/acip/meetings/downloads/slides-2021-02/24-25/02-OPX-Petersen.pdf

Address for correspondence: Varea Costello, Department of Infectious Diseases, Walter Reed Military Medical Center, Bldg 7, 1st Fl, 8901 Wisconsin Ave, Bethesda, MD 20889, USA; email: varea.h.costello2.mil@mail.mil

Intercontinental Movement of Highly Pathogenic Avian Influenza A(H5N1) Clade 2.3.4.4 Virus to the United States, 2021

Sarah N. Bevins,[1] Susan A. Shriner,[1] James C. Cumbee Jr, Krista E. Dilione, Kelly E. Douglass, Jeremy W. Ellis, Mary Lea Killian, Mia K. Torchetti, Julianna B. Lenoch

We detected Eurasian-origin highly pathogenic avian influenza A(H5N1) virus belonging to the Gs/GD lineage, clade 2.3.4.4b, in wild waterfowl in 2 Atlantic coastal states in the United States. Bird banding data showed widespread movement of waterfowl within the Atlantic Flyway and between neighboring flyways and northern breeding grounds.

Influenza A viruses have a worldwide distribution, and wild birds are the primary wild reservoir. Many wild ducks in particular are often repeatedly exposed to and infected with these viruses (hereafter referred to as avian influenza viruses or AIV) with little to no sign of clinical disease (*1*), although highly pathogenic forms of the virus can sometimes cause illness and death in wild birds (*2*). Highly pathogenic lineage viruses identified in 1996 (A/goose/Guangdong/1/1996 [Gs/GD]) have repeatedly spilled over from poultry to wild birds, and eventual emergence of highly pathogenic AIV Gs/GD clade 2.3.4.4 has led to more persistent circulation of these viruses in wild birds and high numbers of illnesses and deaths in poultry on multiple continents (*3*).

One way to better understand AIV movement on the landscape or to identify routes of introduction of novel AIVs is through wild bird band-recovery data (*4*). These data have been collected as part of waterfowl management and conservation efforts in North America since the 1920s (*5*). Spatial locations of where birds are banded and later recovered are recorded and archived, providing data on wild bird movement. For waterfowl, recoveries primarily occur through banded birds being reported as part of hunter harvest activities.

The Study

Wild bird samples are routinely collected by the US Department of Agriculture, Animal Plant Health Inspection Service, Wildlife Services, National Wildlife Disease Program (National Wildlife Disease Program, US Fish and Wildlife Service permit no. MB124992 0) and screened for AIV in conjunction with the National Animal Health Laboratory Network and with the National Veterinary Services Laboratories (Ames, Iowa, USA) as part of a targeted AIV surveillance program in wild birds (*6*). Samples analyzed in this investigation came from routine wild bird surveillance activities in the US Atlantic Flyway and were primarily obtained from hunter harvest activities, live-trapping, and bird banding operations. These surveillance data, combined with bird band-recovery movement data, can shed light on AIV occurrence on the landscape, and findings in wild birds can act as an early warning system for spillover risk to poultry and humans (*6*).

For these analyses, we initially screened wild bird samples by using an influenza matrix gene real-time, reverse transcription PCR. We then tested matrix gene presumptive positive samples by using H5 and H7 subtype-specific, real-time reverse transcription PCRs. Influenza A virus RNA from wild bird samples

Author affiliations: US Department of Agriculture National Wildlife Research Center, Fort Collins, Colorado, USA (S.N. Bevins, S.A. Shriner); US Department of Agriculture National Wildlife Disease Program, Fort Collins (K.E. Dilione, J.B. Lenoch); US Department of Agriculture Wildlife Services, Columbia, South Carolina, USA (J.C. Cumbee Jr); US Department of Agriculture Wildlife Services, Raleigh, North Carolina, USA (K.E. Douglass); US Department of Agriculture Veterinary Services, Ames, Iowa, USA (M.L. Killian, M.K. Torchetti)

DOI: https://doi.org/10.3201/eid2805.220218

[1]These authors contributed equally to this article.

Figure 1. Maximum-likelihood phylogenic analysis of the hemagglutinin gene segment of the first sequenced set of wild bird isolates of highly pathogenic avian influenza A(H5N1) clade 2.3.4.4 virus, United States, 2021. Red indicates US wild bird highly pathogenic detections, and blue indicates closest virus detected in Newfoundland, Canada. MAFFT alignment and RAxML trees were generated in Geneious 11.1.5 (https://www.geneious.com) and visualized in FigTree 1.4.1 (https://tree.bio.ed.ac.uk). Scale bar indicates average nucleotide substitutions per site.

was amplified as described (*7*). After amplification was completed, we generated cDNA libraries for MiSeq by using the Nextera XT DNA Sample Preparation Kit (Illumina, https://www.illumina.com) and the 500 cycle MiSeq Reagent Kit v2 (Illumina) according to manufacturer instructions. We performed de novo and directed assembly of genome sequences by using IRMA version 0.6.7 (*8*), followed by visual verification in DNAStar SeqMan version 14 (https://www.dnastar.com). For phylogenetic analysis, we downloaded sequences from GISAID (https://www.gisaid.org) and aligned in Geneious 11.1.5 by using MAFFT (https://www.geneious.com), then generated trees by using RAxML (https://cme.h-its.org).

We queried North American Bird Banding Program data (*5*) to find all records from 1960–2021 for 11 dabbling duck species targeted for wild bird surveillance. These species were American black duck (*Anas rubripes*), American green-winged teal (*Anas crecca carolinensis*), American wigeon (*Mareca americana*), blue-winged teal (*Spatula discors*), cinnamon teal (*Spatula cyanoptera*), gadwall (*Mareca strepera*), mallard (*Anas platyrhynchos*), mottled duck (*Anas fulvigula*), northern pintail (*Anas acuta*), northern shoveler (*Spatula clypeata*), and wood duck (*Aix sponsa*). We then limited records for these species to only include birds that were either banded or encountered in North Carolina or South Carolina, USA, and ≥1 other state or province.

As part of these routine surveillance efforts, we detected Gs/GD lineage clade 2.3.4.4b H5N1 highly pathogenic AIVs in multiple wild birds sampled in North Carolina and South Carolina during December 2021 and January 2022 (Figure 1). Genetic analyses showed that all virus segments were of Eurasian origin (99.7%–99.8% similar; Appendix, https://wwwnc.cdc.gov/EID/article/28/5/22-0318-App1.pdf) and have high identity with December 2021 AIV H5N1 findings in Newfoundland, Canada (Figure 1) (*9*).

A sample was collected on December 30, 2021 from an American wigeon in Colleton County, South Carolina [A/American_wigeon/South_Carolina/AH0195145/2021(H5N1), GISAID accession no. EPI_ISL_9869760]. Immediately after this finding, there was an additional wild bird detection in South Carolina [A/blue-winged_teal/South_Carolina/AH0195150/2021(H5N1), GISAID accession no.

Table. Detections of highly pathogenic avian influenza A(H5N1) clade 2.3.4.4 virus in wild birds, United States, December 30, 2021–March 3, 2022*

State	Wild bird species	No. clade 2.3.4.4 detections
Alabama	American wigeon	1
Connecticut	Mallard	21
	American black duck	9
Delaware	American wigeon	1
	Gadwall	1
	Northern shoveler	5
	American black duck	1
Florida	Blue-winged teal	2
Georgia	American wigeon	1
	Gadwall	1
Kentucky	Gadwall	4
	Mallard	4
Maine	American black duck	6
New Hampshire	Mallard	49
New Jersey	Mallard	21
North Carolina	American green-winged teal	34
	American wigeon	53
	Gadwall	19
	Mallard	14
	Northern pintail	4
	Northern shoveler	8
	Wood duck	3
South Carolina	American wigeon	7
	Blue-winged teal	9
	Gadwall	7
	Northern shoveler	1
Tennessee	Wood duck	2
Virginia	American green-winged teal	2
	Gadwall	1
	Mallard	1
Total detections		292

*All samples collected were in conjunction with the US Department of Agriculture Wildlife Services National Wildlife Disease Program.

EPI_ISL_9876777] and detections in neighboring North Carolina (Figure 1). Another 291 detections in wild birds occurred within 2 months, indicating high susceptibility to infection with a novel virus along with continued transmission and dispersal (Table). All birds were apparently healthy live-trapped or hunter-obtained dabbling ducks (Appendix Table). North American lineage AIV was not found in any of these samples.

Analysis of North American Bird Banding Program data showed broadscale movement of waterfowl throughout North America. Across 11 species of dabbling ducks targeted in surveillance sampling that were historically banded or encountered in North Carolina or South Carolina (and subsequently or previously banded or encountered in another state or province), a total of 64.7% of bird movements were within the Atlantic Flyway, 33.6% of analyzed species were encountered in the Atlantic and the Mississippi Flyways, and 1.7% were encountered in the Atlantic and Central Flyways (Figure 2).

Conclusions

Although there has been intense focus on intercontinental movement of highly pathogenic AIV from Asia to the North American Pacific Flyway (*10*), viral movement by the trans-Atlantic pathway has been less clear (*11*). Data reported here, in combination with the recent highly pathogenic AIV findings in Newfoundland, Canada (*9*), suggest that wild bird surveillance captured the introduction of a Eurasian-origin highly pathogenic AIV into wild birds by the Atlantic Flyway of the United States. The potential introduction pathway probably includes wild bird migratory routes from northern

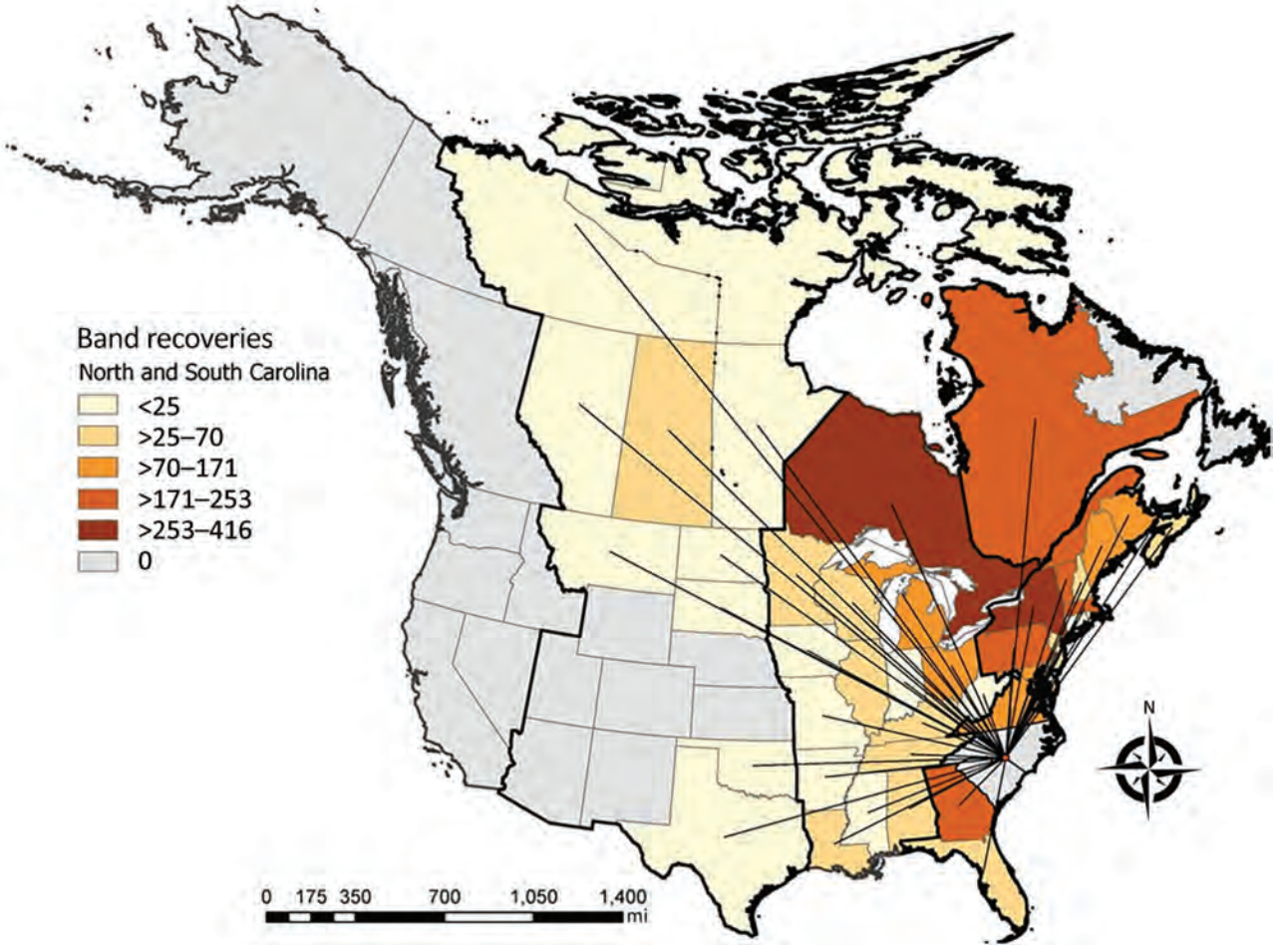

Figure 2. Dabbling duck movements to and from North Carolina and South Carolina, USA, to other states or provinces in study of highly pathogenic avian influenza A(H5N1) 2.3.4.4 virus, United States, 2021. Data are based on North American Bird Banding Program data collected during 1960–2021. Color intensities represent number of movements detected between a given state or province and North Carolina or South Carolina. Lines are positioned at the centroid of a given state or province. Bold border lines indicate administrative migratory bird flyways (from west to east: Pacific Flyway, Central Flyway, Mississippi Flyway, and Atlantic Flyway).

Europe that overlap Arctic regions of North America and then dispersal farther south into Canada and the United States (*12*).

Band recovery data showed that most dabbling ducks banded in the Atlantic Flyway are also recovered in the Atlantic Flyway, reinforcing the predominance of within flyway movement (*13*). However, data also show routine movement to other flyways, providing a potential mechanism of wider spread dispersal of the virus in North America.

In addition, sequence data indicate that these viruses cluster closely with viruses found in Western Europe during spring of 2021 (Figure 1; Appendix). If viruses were exchanged between North American and Eurasian waterfowl on northern breeding grounds during spring and summer 2021, and then carried south during fall of 2021, these viruses might already be in multiple locations in North America (Figure 2). Because wild bird surveillance has recently been limited to the Atlantic and Pacific Flyways, introductions into the Central or Mississippi Flyways might have gone undetected. Additional detections in wild birds suggest these clade 2.3.4.4b H5 viruses continue to be transmitted (Appendix Table), and further dispersal might be seen once waterfowl migrate to summer breeding areas.

Some findings of highly pathogenic AIVs in wild birds have been associated with repeated spillover of the viruses from domestic birds, which are where mutations to high pathogenicity primarily occur; however, in some cases, Gs/GD lineage viruses now appear to be maintained in wild bird populations (*14*). This potential adaptation of highly pathogenic AIV to wild birds highlights the need for continued wild bird surveillance. In addition, these findings demonstrate that targeted AIV surveillance in wild bird populations can detect newly introduced or emergent AIVs before spillover to domestic poultry. Advanced warnings from wild bird surveillance enable poultry producers to consider altering biosecurity in the face of increased AIV risk and also help inform zoonotic disease potential (*15*).

Acknowledgments

We thank Wildlife Services employees and collaborators at state wildlife agencies for contributing wildlife sampling expertise, hunters for participating in this large-scale effort, and staff at state and federal agency laboratories and at the Canadian Food Inspection Agency for providing contributions to this study.

This study was supported by the US Department of Agriculture, Animal Plant Health Inspection Service.

About the Author

Dr. Bevins is a research scientist at the US Department of Agriculture National Wildlife Research Center, Fort Collins, CO. Her primary research interest is pathogen emergence from wild animals.

References

1. Webster RG, Bean WJ, Gorman OT, Chambers TM, Kawaoka Y. Evolution and ecology of influenza A viruses. Microbiol Rev. 1992;56:152–79. https://doi.org/10.1128/mr.56.1.152-179.1992
2. Pohlmann A, Starick E, Harder T, Grund C, Höper D, Globig A, et al. Outbreaks among wild birds and domestic poultry caused by reassorted influenza A(H5N8) clade 2.3.4.4 viruses, Germany, 2016. Emerg Infect Dis. 2017;23:633–6. https://doi.org/10.3201/eid2304.161949
3. Verhagen JH, Fouchier RA, Lewis N. Highly pathogenic avian influenza viruses at the wild-domestic bird interface in Europe: future directions for research and surveillance. Viruses. 2021;13:212. https://doi.org/10.3390/v13020212
4. Franklin AB, Bevins SN, Ellis JW, Miller RS, Shriner SA, Root JJ, et al. Predicting the initial spread of novel Asian origin influenza A viruses in the continental USA by wild waterfowl. Transbound Emerg Dis. 2019;66:705–14. https://doi.org/10.1111/tbed.13070
5. Celis-Murillo A, Malorodova M, Nakash E. North American bird banding program dataset 1960–2021, retrieved 2021–07–25. US Geological Survey. 2021 [cited 2022 Mar 10]. https://www.sciencebase.gov/catalog/item/613f75d7d34e1449c5d35c77
6. United States Interagency Working Group. Surveillance plan for highly pathogenic avian influenza in wild migratory birds in the United States. USDA Avian Influenza Disease. 2017 [cited 2022 Mar 10]. https://www.aphis.usda.gov/animal_health/downloads/animal_diseases/ai/2017-hpai-surveillance-plan.pdf
7. Crossley BM, Rejmanek D, Baroch J, Stanton JB, Young KT, Killian ML, et al. Nanopore sequencing as a rapid tool for identification and pathotyping of avian influenza A viruses. J Vet Diagn Invest. 2021;33:253–60. https://doi.org/10.1177/1040638720984114
8. Shepard SS, Meno S, Bahl J, Wilson MM, Barnes J, Neuhaus E. Viral deep sequencing needs an adaptive approach: IRMA, the iterative refinement meta-assembler. BMC Genomics. 2016;17:708. https://doi.org/10.1186/s12864-016-3030-6
9. Avian influenza (04): Americas (Canada) wild bird. ProMed-mail [cited 2022 Mar 11]. https://www.promedmail.org, archive no. 20220103.8700643.
10. Lee DH, Torchetti MK, Winker K, Ip HS, Song CS, Swayne DE. Intercontinental Spread of Asian-Origin H5N8 to North America through Beringia by migratory birds. J Virol. 2015;89:6521–4. https://doi.org/10.1128/JVI.00728-15
11. Makarova NV, Kaverin NV, Krauss S, Senne D, Webster RG. Transmission of Eurasian avian H2 influenza virus to shorebirds in North America. J Gen Virol. 1999;80:3167–71. https://doi.org/10.1099/0022-1317-80-12-3167
12. Dusek RJ, Hallgrimsson GT, Ip HS, Jónsson JE, Sreevatsan S, Nashold SW, et al. North Atlantic migratory bird flyways provide routes for intercontinental movement of avian influenza viruses. PLoS One. 2014;9:e92075. https://doi.org/10.1371/journal.pone.0092075
13. Li L, Bowman AS, DeLiberto TJ, Killian ML, Krauss S, Nolting JM, et al. Genetic evidence supports sporadic and

independent introductions of subtype H5 low-pathogenic avian influenza A viruses from wild birds to domestic poultry in North America. J Virol. 2018;92:e00913-18. https://doi.org/10.1128/JVI.00913-18
14. Caliendo V, Leijten L, van de Bildt M, Germeraad E, Fouchier RA, Beerens N, et al. Tropism of highly pathogenic avian influenza H5 viruses from the 2020/2021 epizootic in wild ducks and geese. Viruses. 2022;14:280. https://doi.org/10.3390/v14020280
15. Oliver I, Roberts J, Brown CS, Byrne AM, Mellon D, Hansen R, et al. A case of avian influenza A(H5N1) in England, January 2022. Euro Surveill. 2022;27:2200061. https://doi.org/10.2807/1560-7917.ES.2022.27.5.2200061

Address for correspondence: Sarah N. Bevins, US Department of Agriculture National Wildlife Research Center, 4101 Laporte Ave, Fort Collins, CO, 80521, USA; email: sarah.n.bevins@usda.gov

Epidemiologic and Genomic Analysis of SARS-CoV-2 Delta Variant Superspreading Event in Nightclub, the Netherlands, June 2021

Jelle Koopsen,[1] Catharina E. van Ewijk,[1] Roisin Bavalia, Akke Cornelissen, Sylvia M. Bruisten, Floor de Gee, Alvin X. Han, Maarten de Jong, Menno D. de Jong, Marcel Jonges, Norin Khawaja, Fleur M.H.P.A. Koene, Mariken van der Lubben, Iris Mikulic, Sjoerd P.H. Rebers, Colin A. Russell, Janke Schinkel, Anja J.M. Schreijer, Judith A. den Uil, Matthijs R.A. Welkers, Tjalling Leenstra, on behalf of the ARGOS consortium

We report a severe acute respiratory syndrome coronavirus 2 superspreading event in the Netherlands after distancing rules were lifted in nightclubs, despite requiring a negative test or vaccination. This occurrence illustrates the potential for rapid dissemination of variants in largely unvaccinated populations under such conditions. We detected subsequent community transmission of this strain.

Because of decreasing severe acute respiratory syndrome coronavirus 2 (SARS-CoV-2) incidence rates in the Netherlands at the time, the government of the Netherlands lifted most restrictions on June 26, 2021 (week 25) (*1*). The mandate to stay at home and get tested if experiencing symptoms remained. However, wearing of facemasks was no longer mandatory if a distance of ≥1.5 meters could be maintained. Event attendees who were fully vaccinated or had tested negative for SARS-CoV-2 within the previous 40 hours (testing-for-access) did not have to wear facemasks or maintain 1.5-meter physical distancing. Persons meeting 1 of those criteria (tested or fully vaccinated) were given a QR code in the CoronaCheck application, commissioned by the government of the Netherlands (*2*), which allowed them access to events.

Author affiliations: Amsterdam University Medical Centres, University of Amsterdam, Amsterdam, the Netherlands (J. Koopsen, A.X. Han, M.D. de Jong, M. Jonges, S.P.H. Rebers, C.A. Russell, J. Schinkel, M.R.A. Welkers); Public Health Service Amsterdam, the Netherlands. (C.E. van Ewijk, R. Bavalia, A. Cornelissen, S.M. Bruisten, F. de Gee, M. de Jong, N. Khawaja, F.M.H.P.A. Koene, M. van der Lubben, I. Mikulic, A.J.M. Schreijer, J.A. den Uil, M.R.A. Welkers, T. Leenstra)

DOI: https://doi.org/10.3201/eid2805.212019

Shortly after June 26, coronavirus disease (COVID-19) cases surged in the greater Amsterdam region of the Netherlands (Appendix 1 Figure 1, https://wwwnc.cdc.gov/EID/article/28/5/21-2019-App1.pdf). Most infections were among young adults 18–30 years of age (Appendix 1 Figure 2), of whom only 14% were fully vaccinated at that time (*3*). A steep increase in reported clusters related to the hospitality sector, particularly bars and discotheques, was observed in the following weeks; 121 clusters were reported in week 27 compared with an average of 4 clusters/week in weeks 21–25 (Appendix 1 Figure 3). To gain insight into the case surge and transmission dynamics, we investigated an outbreak linked to a nightclub event in central Amsterdam on June 26. We examined whether the high number of cases linked to the nightclub were the result of a superspreading event or the attendance of multiple infectious persons.

The Study

In the Netherlands, confirmed infections are reported to the local Public Health Service (PHS), and source and contact tracing is performed with a telephone interview. Data are obtained on sociodemographics, date of symptom onset, symptoms, vaccination status (and, if applicable, vaccine type, number of doses, and dates of administration) and locations the index-patient visited during the incubation and contagious periods. Medical ethics clearance for this study was not required (Appendix 1).

We defined a case as illness in a person who visited the nightclub on June 26, tested positive for

[1]These authors contributed equally to this article.

SARS-CoV-2 within 14 days, and whose status was reported to the PHS. Cases were identified passively: persons were included only if they indicated during their PHS interview that they had visited the nightclub on June 26. The nightclub has an estimated capacity of 150 persons and was reported to be at full capacity that evening with attendees dancing and singing to loud music. A total of 60 confirmed COVID-19 cases were linked to the nightclub, raising suspicion of a superspreading event. Onset of symptoms occurred during June 27–July 3. Most case-patients were not fully vaccinated (defined as 14 days after completion of the vaccination series [Appendix 1 Figures 4, 5]): 4 (7.4%) persons were fully vaccinated and 41 (76%) were unvaccinated (Table). Most cases were in young adults (mean age 21.1 years [SD 3.3 years]) and women (60%), and most persons reported COVID-19–associated symptoms (93%). In 61% of cases, no other potential source for transmission besides the nightclub event was indicated. Of the 60 confirmed cases, 33 persons lived in the Amsterdam region and 27 resided in other regions (Table).

Samples from 23/60 cases were available for sequencing, of which 3 were not eligible because of high cycle threshold values (>32). For 19/20 samples, we successfully obtained full genome sequences; all belonged to PANGO-lineage B.1.617.2 (*4*), which was denoted as variant of concern Delta by the World Health Organization (*5*) (Appendix 1 Table). To provide for phylogenetic context, we included weekly surveillance samples from the Amsterdam region (n = 421) in the analyses, as well as all Delta variant sequences from the Netherlands available in the GISAID database (https://www.gisaid.org; n = 4,465) (Appendix 2 Table, https://wwwnc.cdc.gov/EID/article/28/5/21-2019-App2.pdf) on August 1, 2021. All nightclub-associated genomes showed characteristics of a superspreading event: a tight phylogenetic cluster closely related in time (June 27–July 3) (Appendix 1 Figure 4) and genomic diversity (Figure 1). The pairwise genetic distance between all sequences was ≤2 single-nucleotide polymorphisms (Appendix 1 Figure 6), comparable to previously observed superspreading events (*6*). In addition, all sequences formed a monophyletic cluster marked by a specific single-nucleotide polymorphism combination: a Delta variant with C4321T in the presence of (wild-type) 22792C. In our dataset, all viruses with this combination collected before July 1 were sampled from persons who were at the nightclub. This combination was not observed in our dataset or in any Netherlands Delta sequences (n = 4465) from the GISAID database before June 26 (Appendix 1 Figure 7). Furthermore, randomly collected surveillance samples in the region from the weeks preceding the nightclub event showed diverse viruses circulating in the Amsterdam region (Appendix 1 Figure 8), and samples collected from 2 other nightclubs on June 26 also showed different lineages (Appendix 1 Figure 9). This finding makes multiple introductions at the nightclub with a highly prevalent, highly similar variant unlikely. In all, these findings strongly suggest a single introduction of the C4321T + 22792C variant, which was amplified by superspreading at the nightclub.

Since the introduction of C4321T + 22792C, the variant has been increasingly detected in random genomic surveillance from the Amsterdam region: no surveillance samples were detected in week 26 compared with 33% of samples in week 28 (Figure 2). This lineage was introduced the weekend nightclubs were opened and has clearly propagated in the community, where subsequent transmission of the lineage occurred.

Conclusions

This study illustrates the amplification of a specific linage in a largely unvaccinated group under circumstances such as those observed in a nightclub where

Table. Descriptive statistics of 60 persons with confirmed SARS-CoV-2 infection after nightclub event, Amsterdam, the Netherlands, June 2021*

Characteristics	No. (%)
Sex	
F	34 (60)
M	23 (40)
Unknown	3
Mean age, y (SD)	21.1 (3.3)
Unknown	3
Symptoms	
Symptomatic	55 (93)
Asymptomatic	4 (7)
Unknown	1
Vaccination status	
Fully vaccinated†	4 (7.4)
Incomplete vaccination	9 (17)
No vaccination received	41 (76)
Unknown	6
PHS region	
PHS Amsterdam	33 (57)
Other PHS region	25 (43)
Unknown	2
Other self-reported potential sources	
None: only nightclub on June 26th	35 (61)
Other hospitality sector	17 (30)
Education	1 (1.8)
Social gathering	2 (3.5)
Supermarket	1 (1.8)
Vaccination location	1 (1.8)
Unknown	3

*PHS, Public Health Service; SARS-CoV-2, severe acute respiratory syndrome coronavirus 2.
†Fully vaccinated defined as 14 days after completion of vaccination series.

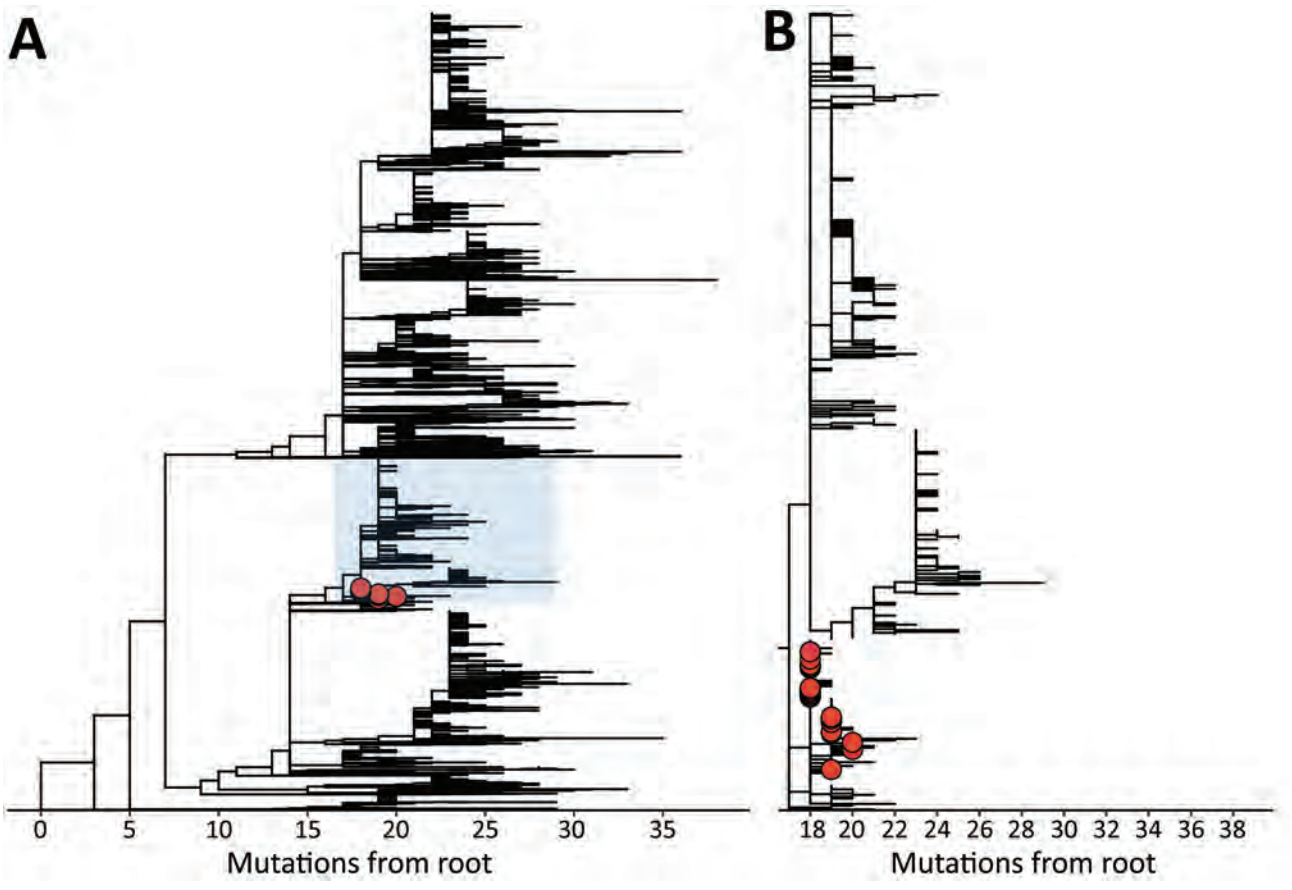

Figure 1. Clustering of severe acute respiratory syndrome coronavirus 2 cases related to nightclub event, Amsterdam, the Netherlands, June 2021. Red circles indicate sequences linked to the nightclub. A) Maximum-likelihood tree of all sequences (n = 4,905) in the dataset. B) Magnification of the clade (highlighted in blue in panel A) containing sequences linked to the nightclub (n = 1,663). Branches without tips depict other Netherlands Delta variant sequences derived from GISAID (https://www.gisaid.org).

social distancing measures and facemask requirements were lifted, despite a testing-for-access policy. In addition, our results highlight the consequence of superspreading events on subsequent transmission dynamics of SARS-CoV-2 in the community. Investigating an outbreak on June 26, 2021, the first date that social distancing measures were lifted under testing-for-access conditions, enabled us to isolate a single SARS-CoV-2 transmission event.

The role of superspreading in SARS-CoV-2 transmission has been highlighted previously (*6*,*7*), also in the context of nightclubs (*8*,*9*). Considering the potential of SARS-CoV-2 to be transmitted through aerosols (*10*,*11*), nightclubs can be a high-risk setting because of poor ventilation and sustained overcrowding. Our findings suggest that the rapid surge in cases in July 2021 was at least partially driven by superspreading events such as the event we describe.

In particular, testing-for-access, as it was put in place in the weeks following June 26, provided opportunity for infectious persons to slip through. Access was provided immediately after a single Johnson & Johnson/Janssen vaccination (https://www.janssen.com) (too soon), a negative antigen test result was valid for 40 hours (too long), and checking of QR codes was reported to be inconsistent at some venues (*12*,*13*).

This study used data collected for nonresearch purposes during scaled-down source and contact tracing and has limitations. First, cases were passively included, which could underestimate the true extent of the outbreak, because asymptomatic cases or cases tested only by self-administered antigen tests might have been missed. This factor could also explain the high percentage of symptomatic cases (*14*). Nevertheless, we believe this factor did not result in a biased selection of cases. Second, we conducted genomic analysis for only 1/121 detected hospitality sector–related clusters, limiting generalizability of our findings.

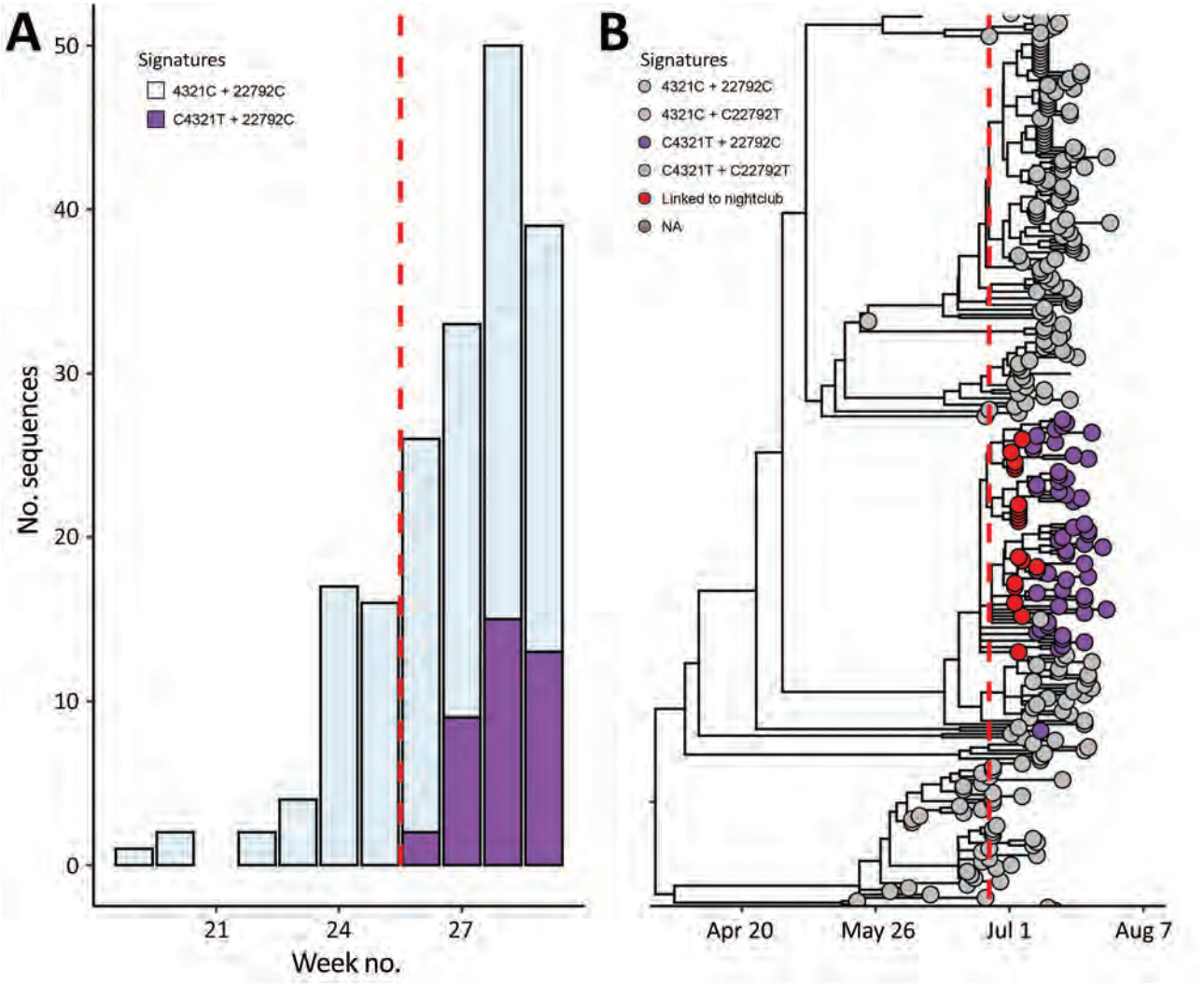

Figure 2. Detected increase of severe acute respiratory syndrome coronavirus 2 (SARS-CoV-2) sequences with signature first detected in nightclub samples, Amsterdam, the Netherlands. A) Absolute number of weekly cases in randomly selected surveillance samples in the Amsterdam region, colored by the nucleotides at position 4321 and 22792 of the SARS-CoV-2 genome. B) Time-resolved phylogenetic tree of dataset containing all Netherlands SARS-CoV-2 Delta variant sequences available in GISAID on August 1, 2021, random surveillance samples from the Amsterdam region, and samples from returning travelers to the Amsterdam region. Tips are colored by the nucleotides at position 4321 and 22792 and epidemiologic linkage to the nightclub (with signature C4321T + 22792C). Dashed red line indicates the day of lifting 1.5-meter social distancing restrictions with QR code. NA, not applicable.

In conclusion, testing-for-access did not prevent superspreading at this event, indicating the need for caution when easing social distancing measures in night life, even under more optimal testing-for-access conditions. This finding is particularly relevant in a population where vaccination coverage is low or when new variants circulate that are associated with lower vaccine effectiveness.

ARGOS (Amsterdam Regional Genomic epidemiology & Outbreak Surveillance) consortium collaborators: Roisin Bavalia (PHS Amsterdam), Akke Cornelissen (PHS Amsterdam), Sylvia M. Bruisten (PHS Amsterdam), Catharina E. van Ewijk (PHS Amsterdam), Floor de Gee (PHS Amsterdam), Alvin X. Han (Amsterdam UMC), Maarten de Jong (Amsterdam UMC), Menno D. de Jong (Amsterdam UMC), Marcel Jonges (Amsterdam UMC), Norin Khawaja (PHS Amsterdam), Fleur Koene (PHS Amsterdam, Amsterdam UMC), Jelle Koopsen (Amsterdam UMC), Tjalling Leenstra (PHS Amsterdam), Mariken van der Lubben (PHS Amsterdam), Iris Mikulic (PHS Amsterdam), Sjoerd R. Rebers (Amsterdam UMC), Colin A. Russell (Amsterdam UMC), Janke Schinkel (Amsterdam UMC), Anja J.M. Schreijer (PHS Amsterdam), Judith den Uil (PHS Amsterdam), and Matthijs Welkers (Amsterdam UMC, PHS Amsterdam)

About the Author

Mr. Koopsen is a PhD candidate at the Amsterdam University Medical Centre. His work focuses on the genomic epidemiology of SARS-CoV-2 and hepatitis C virus. Dr. van Ewijk is a public health physician in training, specializing in infectious disease control. She is also a fellow from the European Programme of Intervention Epidemiology cohort 2021 (European Centre for Disease Prevention and Control) at the National Institute for Public Health and the Environment.

References

1. Ministry of General Affairs, the Netherlands. The Netherlands takes a big step: almost everything is possible at 1.5 meters [in Dutch]. 2021 Jun 18 [cited 2021 Aug 1]. https://www.rijksoverheid.nl/actueel/nieuws/2021/06/18/nederland-zet-grote-stap-bijna-alles-kan-op-anderhalve-meter
2. Ministry of Health, Welfare and Sport, the Netherlands. CoronaCheck [cited 2021 Aug 1]. https://coronacheck.nl
3. National Institute for Public Health and the Environment, the Netherlands. COVID-19 vaccination program figures [in Dutch]. 2021 [cited 2021 Aug 1]. https://www.rivm.nl/covid-19-vaccinatie/cijfers-vaccinatieprogramma
4. O'Toole Á, Scher E, Underwood A, Jackson B, Hill V, McCrone JT, et al. Assignment of epidemiological lineages in an emerging pandemic using the pangolin tool. Virus Evol. 2021;7:b064. https://doi.org/10.1093/ve/veab064
5. World Health Organization. Tracking SARS-CoV-2 variants. 2021 [cited 2021 Aug 1]. https://www.who.int/en/activities/tracking-SARS-CoV-2-variants
6. Lemieux JE, Siddle KJ, Shaw BM, Loreth C, Schaffner SF, Gladden-Young A, et al. Phylogenetic analysis of SARS-CoV-2 in Boston highlights the impact of superspreading events. Science. 2021;371:eabe3261. https://doi.org/10.1126/science.abe3261
7. Pozderac C, Skinner B. Superspreading of SARS-CoV-2 in the USA. PLoS One. 2021;16:e0248808. https://doi.org/10.1371/journal.pone.0248808
8. Muller N, Kunze M, Steitz F, Saad NJ, Mühlemann B, Beheim-Schwarzbach JI, et al. Severe acute respiratory syndrome coronavirus 2 outbreak related to a nightclub, Germany, 2020. Emerg Infect Dis. 2020;27:645–8. https://doi.org/10.3201/eid2702.204443
9. Kang CR, Lee JY, Park Y, Huh IS, Ham HJ, Han JK, et al.; Seoul Metropolitan Government COVID-19 Rapid Response Team (SCoRR Team). Coronavirus disease exposure and spread from nightclubs, South Korea. Emerg Infect Dis. 2020;26:2499–501. https://doi.org/10.3201/eid2610.202573
10. Greenhalgh T, Jimenez JL, Prather KA, Tufekci Z, Fisman D, Schooley R. Ten scientific reasons in support of airborne transmission of SARS-CoV-2. Lancet. 2021; 397:1603–5. https://doi.org/10.1016/S0140-6736(21)00869-2
11. Centers for Disease Control and Prevention. Scientific brief: SARS-CoV-2 transmission. 2021 May 7 [cited 2022 Feb 10]. https://www.cdc.gov/coronavirus/2019-ncov/science/science-briefs/sars-cov-2-transmission.html
12. Ministry of General Affairs, the Netherlands. Verbatim text press conference Prime Minister Rutte and Minister De Jonge (18 June 2021) [in Dutch] [cited 2021 Aug 1]. https://www.rijksoverheid.nl/documenten/mediateksten/2021/06/18/letterlijke-tekst-persconferentie-minister-president-rutte-en-minister-de-jonge-18-juni-2021
13. Ministry of General Affairs, the Netherlands. Verbatim text press conference Prime Minister Rutte and Minister De Jonge (9 July 2021) [in Dutch] [cited 2021 Aug 1]. https://www.rijksoverheid.nl/documenten/mediateksten/2021/07/09/letterlijke-tekst-persconferentie-minister-president-rutte-en-minister-de-jonge-9-juli-2021
14. National Institute for Public Health and the Environment, the Netherlands. Substantive substantiation of symptomology COVID-19 and consequences for tests and measures [in Dutch] [cited 2021 Aug 1]. https://lci.rivm.nl/onderbouwing-symptomatologie

Address for correspondence: Jelle Koopsen, Amsterdam UMC, Room K3-120, Meibergdreef 9, 1105 AZ, Amsterdam, the Netherlands; email: j.koopsen@amsterdamumc.nl

Severe Multisystem Inflammatory Symptoms in 2 Adults after Short Interval between COVID-19 and Subsequent Vaccination

Elizabeth R. Jenny-Avital, Ruth A. Howe[1]

We observed multisystem inflammatory syndrome in 2 older adults in the United States who had received mRNA coronavirus disease vaccine soon after natural infection. We identified 5 similar cases from the Vaccine Adverse Events Reporting System. The timing of vaccination soon after natural infection might have an adverse effect on the occurrence of vaccine-related systemic inflammatory disorders.

The Centers for Disease Control and Prevention (CDC) recommends coronavirus disease (COVID-19) vaccination after natural severe acute respiratory syndrome coronavirus 2 (SARS-CoV-2) infection once acute symptoms resolve. We encountered 2 adults at Jacobi Medical Center (Bronx, NY, USA) who experienced severe febrile multisystem inflammatory illness, fulfilling the original CDC surveillance definition for multisystem inflammatory syndrome in adults (MIS-A) (*1*), after receiving COVID-19 mRNA vaccination 30 days after natural SARS-CoV-2 infection. We subsequently identified 5 similar cases from the Vaccine Adverse Event Reporting System (VAERS; https://www.vaers.hhs.gov) through October 2021 in hospitalized adults >30 years of age.

The Cases

Case 1 was in a 48-year-old healthcare worker with type 2 diabetes, hypertension, and obesity (body mass index 55) who experienced sinus symptoms and loss of taste and smell in January 2021 concurrent with a positive SARS-CoV-2 PCR test. Thirty days later, she received the first dose of the mRNA-1273 COVID-19 vaccine (Moderna, https://www.moderna.com). The next day, she awoke with malaise, fever, and a localized pruritic rash. Symptoms, including worsening rash, fever (103°F), headache, loose stools, and disabling joint pain, progressed over 5 days. Physical examination revealed tachycardia (130 beat/min), fever (100.2°F), relative hypotension (100/60 mm Hg), swollen hands, and a rash consisting of urticarial pink papules and confluent red plaques involving her extremities and abdomen. Laboratory tests showed leukocytosis (16.5 × 103/μL, 77% neutrophils), acute liver injury (bilirubin 2 mg/dL, aspartate aminotransferase 120 U/L, alanine transaminase 248 U/L), and elevated C-reactive protein (187 mg/L), ferritin (558 mcg/L), and D-dimer (2,698 ng/mL). Nucleoprotein (NP) antibody testing was positive, substantiating previous SARS-CoV-2 infection. Results of imaging and serologic testing (viral hepatitis, HIV, parvovirus, autoimmune arthritis) were unrevealing. Echocardiography showed a small pericardial effusion. Treatment with prednisone and topical steroids resulted in rapid clinical improvement and resolution of her liver injury. Eleven days later, the palms of the patient's hands and soles of her feet desquamated. After her second mRNA-1273 vaccine, she reported fever for 3 days. She had no symptoms after a booster with the BNT162b2 vaccine (Pfizer-BioNTech, https://www.pfizer.com).

Case 2 was in a healthy 51-year-old man who experienced self-limiting COVID-19 symptoms in mid-April 2021, concurrent with positive SARS-CoV-2 PCR tests in household contacts. He received the first dose of the mRNA BNT162b2 vaccine on May 11. Two weeks later, he experienced fever, watery diarrhea, and escalating abdominal discomfort. He sought care on May 31 for symptoms of fever (101.8°F) and

Author affiliations: Jacobi Medical Center, Bronx, New York, USA (E.R. Jenny-Avital); Albert Einstein College of Medicine, Bronx (R.A. Howe)

DOI: https://doi.org/10.3201/eid2805.212316

[1]Current affiliation: University of Washington, Seattle, Washington, USA.

diarrhea. He had tachycardia (130 beats/min), hypotension (90/60 mm Hg), leukocytosis (19.4 × 103/μL, 92% neutrophils), anemia (hemoglobin 11 g/dL), thrombocytopenia (72,000/μL), and elevated C-reactive protein (334 mg/L), Pro-Brain Natriuretic peptide (17,768 pg/mL), troponin (0.248 μg/L). NP antibody testing confirmed previous SARS-CoV-2 infection. PCR testing for SARS-CoV-2 and enteric pathogens was negative. Imaging of the chest and abdomen was initially normal. Despite fluids, he required vasopressors and overt pulmonary edema developed. Echocardiography confirmed biventricular dilatation with ejection fraction of 20%. After empiric MIS-A treatment with steroids and 1 dose of intravenous immunoglobulin (0.8 g/kg), symptoms, hemodynamics, and inflammatory markers rapidly improved; ejection fraction was normal (60%) on June 14 and June 28 while the patient was on prednisone (5 mg/d). On steroids, he experienced superficial desquamation of the palms of his hands and soles of his feet and 2 episodes of mild conjunctivitis. He remained fully recovered as of February 2022 but had no further vaccination.

We queried the VAERS database through October 2021 for hospitalized older adults (>30 years of age) using the symptom search term "Multisystem Inflammatory Syndrome/MIS" and found 19 cases (including case 2). VAERS did not substantiate MIS in 6 cases. Of the remaining cases, 3 additional cases occurred after a first vaccination given within 1 month of mild COVID-19 illness (Table). Only one other report provided information on previous COVID-19 (4 months earlier). Using search terms "myocarditis/fever" (57 cases) and "acute heart failure/fever" (12 cases), we found 1 case for each search that fulfilled criteria for MIS-A after vaccine administration soon after mild COVID-19 (Table).

Conclusions

Although case 1 fulfilled the initial 5-criteria surveillance CDC definition for MIS-A (*1*), which included acute liver injury, it does not fulfill the updated CDC definition (*2*), illustrating the dynamic and competing objectives of surveillance and precision. A broader Brighton Collaboration definition of MIS (*3*) was developed in part to be used in the evaluation of vaccine adverse events.

Table. Characteristics of 5 previously published MIS cases occurring after COVID-19 vaccine was administered within 1 month of infection, United States*

Case no. and search term	VAERS ID	Patient age, y/sex	COVID-19 date	Vaccine date, type†	Description in VAERS	Treatment and outcome
1. MIS	1396536	53/F	2021 May 7	2021 May 29, Pfizer-BioNTech	2021 May 31: febrile (101.3°F), initial GI symptoms, dyspnea; admitted June 1; hypotensive (63/48 mm Hg) requiring vasopressors; leukocytes 31.3 × 10^3 cells/μL, creatinine 4.6 mg/dL, bilirubin 5.5 mg/dL, EF 35%	Immunoglobulin infusion for prolonged hypotension despite antibiotics; weaned from vasopressors, reduced EF, and renal failure resolved
2. MIS	1282200	40/M	2020 Dec 26	2021 Jan 25, Pfizer-BioNTech	2021 Jan 29: fever, headache, neck pain, weakness, fatigue, diarrhea, abdominal pain; admitted after 2 emergency department visits with elevated cardiac inflammatory markers (BNP and troponin)	Steroids, with complete resolution
3. MIS	1154625	48/F	2021 Dec 31	2021 Jan 22, Moderna	2021 Feb 1: MIS with GI symptoms, rash, conjunctival injection, encephalopathy, elevated BNP	Immunoglobulin infusion, steroids, aspirin, with good response
4. Acute heart failure and fever	1027010	45/M	2020 Dec 30	2021 Jan 22, Pfizer-BioNTech	2021 Jan 30: fever, hypotension, morbilliform rash, cariogenic shock, EF 35%, CRP >320, BNP 3,583, SARS-CoV-2 antibody-positive	Intra-aortic balloon pump, antibiotics; resolution, with EF 67%
5. Myocarditis and fever	1088210, 1122743	46/F	2021 early Jan	2021 Feb 5‡	2021 Feb 23: 5 d fever, sore throat, swelling in hands/feet, EF 35%, hypotension requiring vasopressor, CRP >300 mg/L, ferritin 3,054 mcg/L, severe thrombocytopenia	Antibiotics, steroids, mechanical ventilation, ECMO, intra-aortic balloon pump support

*BNP, brain natriuretic peptide; COVID-19, coronavirus disease; CRP, C-reactive protein; ECMO, extracorporeal membrane oxygenation; EF, ejection fraction; FU, follow-up; GI, gastrointestinal; ID, identification; MIS, multisystem inflammatory syndrome; SARS-CoV-2, severe acute respiratory syndrome coronavirus 2; VAERS, Vaccine Adverse Event Reporting System.
†Pfizer-BioNTech, https://www.pfizer.com; Moderna, https://www.moderna.com.
‡Vaccine type not available in VAERS report.

Case 2, by contrast, unequivocally fulfills MIS-A criteria and occurred within the usual time frame for post–COVID-19 MIS-A; its occurrence after vaccine might have been coincidental. Because MIS is overwhelmingly a disease of children and young adults, these 2 rare events, both occurring soon after vaccination in older adults, raised our concern that vaccination soon after COVID-19 infection might provoke MIS-A (case 2) or some similar vaccine-related multisystem inflammatory illness (case 1) consistent with the broader Brighton definition (*3*).

Some vaccine-triggered inflammatory symptoms, such as fever and myocarditis, occur disproportionately after a second vaccination, except in persons with previous COVID-19 infection, in whom reactions occur after a first vaccination, which suggests priming by a first antigenic exposure. The mRNA vaccine trials excluded participants with previous COVID-19, but antibody tests indicated previous infection in 2.5% of participants <65 years of age in the mRNA-1273 trial (*4*). Fever after first vaccination occurred in 9.4% of participants with previous COVID-19, compared with only 0.5% in COVID-19–naive participants and increased to 15.7% in the initially COVID-19–naive after the second vaccination (*4*). Similarly, myocarditis, a well-recognized vaccine adverse reaction in adolescents and young adults, almost invariably follows a second mRNA vaccine dose (*5*,*6*). However, a well-characterized report of 23 members of the US military identified myocarditis after the first vaccination only in 3 persons who had previous COVID-19 (*6*). By analogy, vaccine-associated multisystem inflammation, including MIS-A, might occur differentially between COVID-19–naive and COVID-19–experienced persons, such as suggested by the Brighton Collaboration document (*3*).

MIS, initially described in children who were SARS-CoV-2–negative by PCR but had plausible COVID-19 exposure or NP antibodies (*7*,*8*), was interpreted as a postviral syndrome caused by a deleterious hyper-inflammatory immune response (*6*). Although subsequent MIS cases reported in adults and children had concurrently positive PCR results in more than half (*9*,*10*), this finding was attributed to prolonged SARS-CoV-2 shedding, which has been noted in up to 19% of asymptomatic convalescent outpatients (*11*), rather than to a second infection in a sensitized host. Of 6 cases of MIS-A reported by Kaiser Permanente, 3 (50%) occurred in persons who were vaccinated after natural infection, despite the fact that only 7% of the cohort was vaccinated (*12*). Of 20 MIS-A cases collected by CDC during December 2020–April 2021, 7 (35%) occurred after vaccination after natural infection (*2*). The interval from infection to MIS-A was the same regardless of intervening vaccination, suggesting that vaccination was coincidental. Miyazato et al. (*13*) reported MIS-A 5 days after vaccination in a person with severe inflammatory illness that followed unrecognized previous COVID-19 infection confirmed only by positive NP antibody. Nune et al. (*14*) coined the term MIS-V to describe a case of MIS that began as progressive local injection-site inflammation 2 days after vaccination and demonstrated evolving systemic features, without evidence of antecedent COVID-19 infection.

COVID-19 vaccination during high periods of transmission increases the likelihood of vaccination following soon after infection. Further epidemiologic observations are needed to confirm a clear causal relationship, but our results indicate that vaccination soon after natural infection may result in the occurrence of strictly defined MIS-A or of other vaccine-triggered systemic inflammatory disorders.

About the Author

Dr. Jenny-Avital is an attending physician in infectious diseases at Jacobi Medical Center and associate clinical professor of medicine at Albert Einstein College of Medicine. Dr. Howe is an intern in internal medicine at the University of Washington, Seattle, Washington. She was a fourth-year medical student at Albert Einstein College of Medicine when she cared for the first patient described in this study and initiated the case write-up.

References

1. Morris SB, Schwartz NG, Patel P, Abbo L, Beauchamps L, Balan S, et al. Case series of multisystem inflammatory syndrome in adults with SARS-CoV-2 infection—United Kingdom and United States March–August 2020. MMWR Morb Mortal Wkly Rep. 2020;69:1450–6. https://doi.org/10.15585/mmwr.mm6940e1
2. Belay ED, Godfred Cato S, Rao AK, Abrams J, Wilson WW, Lim S, et al. Multisystem inflammatory syndrome in adults after SARS-CoV-2 infection and COVID-19 vaccination. Clin Infect Dis. 2021 Nov 28 [Epub ahead of print]. https://doi.org/10.1093/cid/ciab936
3. Vogel TP, Top KA, Karatzios C, Hilmers DC, Tapia LI, Moceri P, et al. Multisystem inflammatory syndrome in children and adults (MIS-C/A): Case definition & guidelines for data collection, analysis, and presentation of immunization safety data. Vaccine. 2021;39:3037–49. https://doi.org/10.1016/j.vaccine.2021.01.054
4. Baden LR, El Sahly HM, Essink B, Kotloff K, Frey S, Novak R, et al.; COVE Study Group. Efficacy and safety of the mRNA-1273 SARS-CoV-2 vaccine. N Engl J Med. 2021;384:403–16. https://doi.org/10.1056/NEJMoa2035389
5. Dionne A, Sperotto F, Chamberlain S, Baker AL, Powell AJ, Prakash A, et al. Association of myocarditis with BNT162b2 messenger RNA COVID-19 vaccine in a case series in children. JAMA Cardiol. 2021;6:1446–50. https://doi.org/10.1001/jamacardio.2021.3471

6. Montgomery J, Ryan M, Engler R, Hoffman D, McClenathan B, Collins L, et al. Myocarditis following immunization with mRNA COVID-19 vaccines in members of the US military. JAMA Cardiol. 2021;6:1202–6. https://doi.org/10.1001/jamacardio.2021.2833
7 Riphagen S, Gomez X, Gonzalez-Martinez C, Wilkinson N, Theocharis P. Hyperinflammatory shock in children during COVID-19 pandemic. Lancet. 2020;395:1607–8. https://doi.org/10.1016/S0140-6736(20)31094-1
8. Verdoni L, Mazza A, Gervasoni A, Martelli L, Ruggeri M, Ciuffreda M, et al. An outbreak of severe Kawasaki-like disease at the Italian epicentre of the SARS-CoV-2 epidemic: an observational cohort study. Lancet. 2020;395:1771–8. https://doi.org/10.1016/S0140-6736(20)31103-X
9. Dufort EM, Koumans EH, Chow EJ, Rosenthal EM, Muse A, Rowlands J, et al.; New York State and Centers for Disease Control and Prevention Multisystem Inflammatory Syndrome in Children Investigation Team. Multisystem inflammatory syndrome in children in New York State. N Engl J Med. 2020;383:347–58. https://doi.org/10.1056/NEJMoa2021756
10. Feldstein LR, Rose EB, Horwitz SM, Collins JP, Newhams MM, Son MBF, et al. Multisystem inflammatory syndrome in US children and adolescents. N Engl J Med. 2020;383:334046. https://doi.org/10.1056/NEJMoa2021680
11. Wajnberg A, Mansour M, Leven E, Bouvier NM, Patel G, Firpo-Betancourt A, et al. Humoral response and PCR positivity in patients with COVID-19 in the New York City region, USA: an observational study. Lancet Microbe. 2020;1:e283–9. https://doi.org/10.1016/S2666-5247(20)30120-8
12. Salzman MB, Huang CW, O'Brien CM, Castillo RD. Multisystem inflammatory syndrome after SARS-CoV-2 infection and COVID-19 vaccination. Emerg Infect Dis. 2021;27:1944–8. https://doi.org/10.3201/eid2707.210594
13. Miyazato Y, Yamamoto K, Yamada G, Kubota S, Ishikane M, Sugiyama M, et al. Multisystem inflammatory syndrome in adult after first dose of mRNA vaccine. Emerg Infect Dis. 2022 Feb 11 [Epub ahead of print]. https://doi.org/10.3201/eid2804.212585
14. Nune A, Iyengar KP, Goddard C, Ahmed AE. Multisystem inflammatory syndrome in an adult following the SARS-CoV-2 vaccine (MIS-V). BMJ Case Rep. 2021;14:e243888. https://doi.org/10.1136/bcr-2021-243888

Address for correspondence: Elizabeth R. Jenny-Avital, Department of Medicine, Division of Infectious Diseases, 1400 Pelham Pkwy S, ACS Clinic Suite 146, Jacobi Medical Center, Bronx, NY 10461, USA; email: Elizabeth.jenny-avital@nychhc.org

Rapid Replacement of SARS-CoV-2 Variants by Delta and Subsequent Arrival of Omicron, Uganda, 2021

Nicholas Bbosa, Deogratius Ssemwanga, Hamidah Namagembe, Ronald Kiiza, Jocelyn Kiconco, John Kayiwa, Tom Lutalo, Julius Lutwama, Alfred Ssekagiri, Isaac Ssewanyana, Susan Nabadda, Henry Kyobe-Bbosa, Jennifer Giandhari, Sureshnee Pillay, Upasana Ramphal, Yajna Ramphal, Yeshnee Naidoo, Derek Tshiabuila, Houriiyah Tegally, Emmanuel J. San, Eduan Wilkinson, Tulio de Oliveira, Pontiano Kaleebu

Genomic surveillance in Uganda showed rapid replacement of severe acute respiratory syndrome coronavirus 2 over time by variants, dominated by Delta. However, detection of the more transmissible Omicron variant among travelers and increasing community transmission highlight the need for near–real-time genomic surveillance and adherence to infection control measures to prevent future pandemic waves.

Severe acute respiratory syndrome coronavirus 2 (SARS-CoV-2) is the etiologic agent of human coronavirus disease (COVID-19), which was declared by the World Health Organization to be a global pandemic in March 2020 (*1*). Since the beginning of the pandemic, COVID-19 has caused enormous socioeconomic destruction (*2*) and has resulted in >5 million deaths worldwide.

A study conducted by the Medical Research Council/Uganda Virus Research Institute (MRC/UVRI) and the London School of Hygiene and Tropical Medicine (LSHTM) Uganda Research Unit (Entebbe, Uganda) during the early phase of the pandemic showed that most SARS-CoV-2 infections were imported and consisted of several lineages that included A, B, B.1, B.1.1, B.1.1.1, and B.4 (*3*). A subsequent study that covered the period from December 2020 through January 2021 showed that a SARS-CoV-2 lineage A variant (A.23.1) had emerged and become the dominant variant in Uganda (*4*).

The UVRI and its partners, such as the MRC/UVRI and LSHTM, contribute to the SARS-CoV-2 response in Uganda. As part of routine national genomic surveillance, we identified circulating variants during June–December 2021 and analyzed trends of SARS-CoV-2 lineages over time.

The Study

We conducted SARS-CoV-2 whole-genome deep sequencing for 266 nasooropharyngeal samples collected during June–December 2021 from 28 travelers arriving at Entebbe International Airport and from 238 patients in Uganda from 18 districts (Kampala, Wakiso, Mpigi, Kalungu, Kalangala, Dokolo, Amudat, Moroto, Kassanda, Gulu, Arua, Koboko, Amuru, Lamwo, Kwania, Apac, Kisoro, and Mityana). All samples had tested positive for SARS-CoV-2 by reverse transcription PCR with cycle threshold values <30 and were sequenced by using Illumina MiSeq (https://www.illumina.com) (n = 236, 88.7%) and Oxford Nanopore MinION (https://nanoporetech.com) (n = 30, 11.3%) next-generation sequencing platforms. Most (77%) samples sequenced were from the central region of Uganda (mostly from Kampala, Wakiso, Mpigi, and Kalungu); fewer samples came from the northern (13.9%) and western regions (8.2%) of the country.

We assembled deep sequence reads by using the genome detective software (*5*) (for the Illumina MiSeq–generated sequence reads) and Nanopolish/Medaka

Author affiliations: Medical Research Council/Uganda Virus Research Institute, Entebbe, Uganda (N. Bbosa, D. Ssemwanga, H. Namagembe, J. Kiconco, J. Kayiwa, T. Lutalo, J. Lutwama, A. Ssekagiri, P. Kaleebu); London School of Hygiene and Tropical Medicine Uganda Virus Research Unit, Entebbe (D. Ssemwanga, R. Kiiza, J. Kiconco, J. Kayiwa, T. Lutalo, J. Lutwama, A. Ssekagirl, P. Kaleebu); Ministry of Health, Kampala, Uganda (I. Ssewanyana, S. Nabadda, H. Kyobe-Bbosa); University of KwaZulu-Natal, Durban, South Africa (J. Giandhari, S. Pillay, U. Ramphal, Y. Ramphal, Y. Naidoo, D. Tshiabuila, H. Tegally, E.J. San, E. Wilkinson, T. de Oliveira); Stellenbosch University, Stellenbosch, South Africa (E. Wilkinson, T. de Oliveira)

DOI: https://doi.org/10.3201/eid2805.220121

(https://artic.network/ncov-2019/ncov2019-bioinformatics-sop.html) (for the Nanopore–generated sequence reads) to obtain high-quality SARS-CoV-2 genomes with >80% coverage. We performed quality control of all sequences to check for adequate coverage, indels, and frameshifts. We performed mutation calling by using Nextclade (https://clades.nextstrain.org), followed by SARS-CoV-2 lineage analysis with Pangolin (https://github.com/cov-lineages/pangolin). To analyze trends of SARS-CoV-2 lineages over time, we downloaded all sequences from Uganda in GISAID (https://www.gisaid.org) (950 sequences as of January 10, 2022).

Results showed that most (195, 73.3%) of the 266 SARS-CoV-2 sequences genotyped were the Delta variant (B.1.617.2 and other AY.1, AY.4, AY.33, AY.39, AY.46, AY.46.4 sublineages), a variant of concern (https://www.who.int/en/activities/tracking-SARS-CoV-2-variants; accessed January 10, 2022). Another variant of concern we identified was the Omicron variant (B.1.1.529 and BA.1 sublineage) (28, 10.5%). We also identified the Eta variant (B.1.525) (2, 0.8%) and other variants (41, 15.4%) mostly of the A and B lineages (Figure 1).

Uganda is in the third wave of the COVID-19 pandemic (Figure 2, panel A). During the first wave (December 2020–January 2021), the A.23.1 variant dominated (*4*). During second wave (May–July 2021) and by June 2021, Delta dominated all variants reported. We report the numbers and percentage of SARS-CoV-2 genomes generated and variants reported over time based on 950 sequences from Uganda deposited in GISAID (Figure 2, panels B, C). The first Kappa variant (B.1.617.1) was identified in March 2021. However, in June 2021, the Delta variant reached its peak and comprised >90% of all circulating variants. SARS-CoV-2 variants previously reported (*3*,*4*) have since been largely replaced by Delta, and the current third wave (began in December 2021) is dominated by Delta and the highly transmissible Omicron variant.

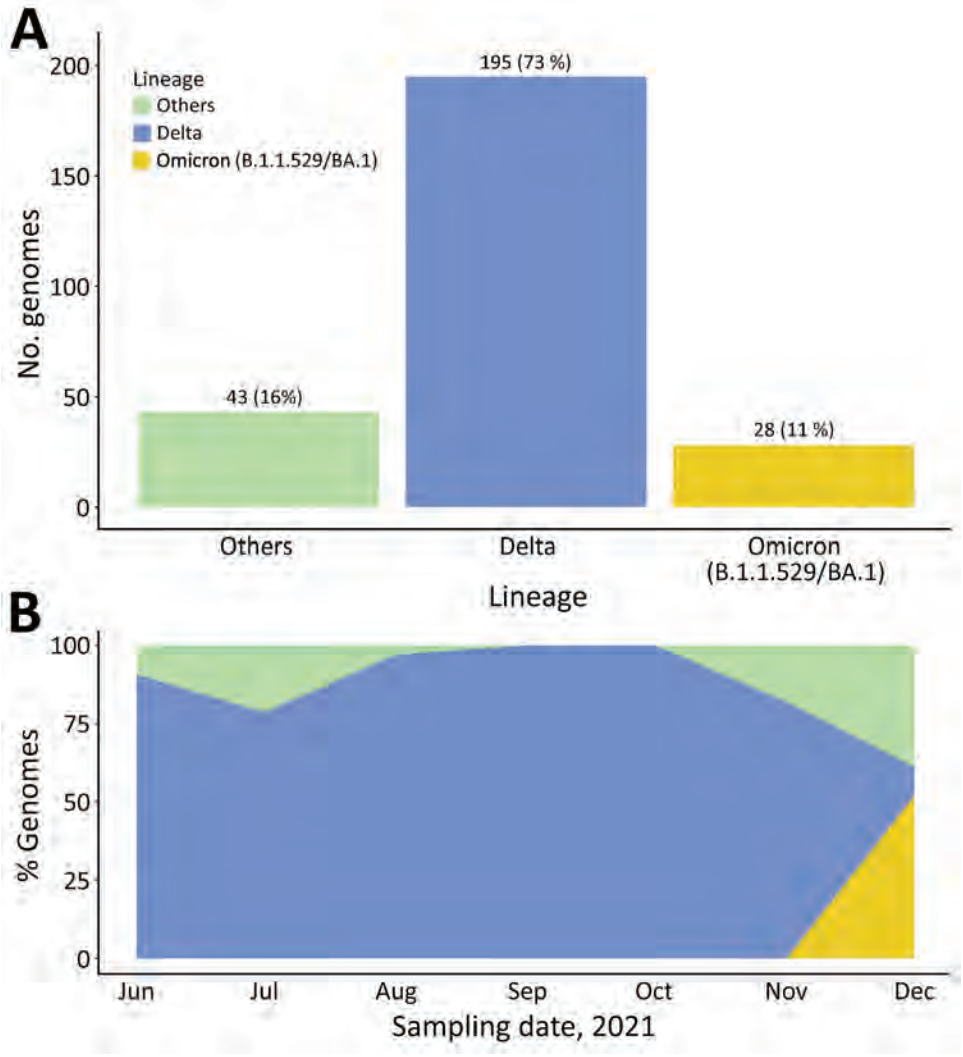

Figure 1. Distribution of severe acute respiratory syndrome coronavirus 2 (SARS-CoV-2) variants, Uganda, June–December 2021. A) Distribution of SARS-CoV-2 variants from 266 samples genotyped during June–December 2021. B) Percentage of SARS-CoV-2 variants genotyped during June–December 2021 according to sampling dates.

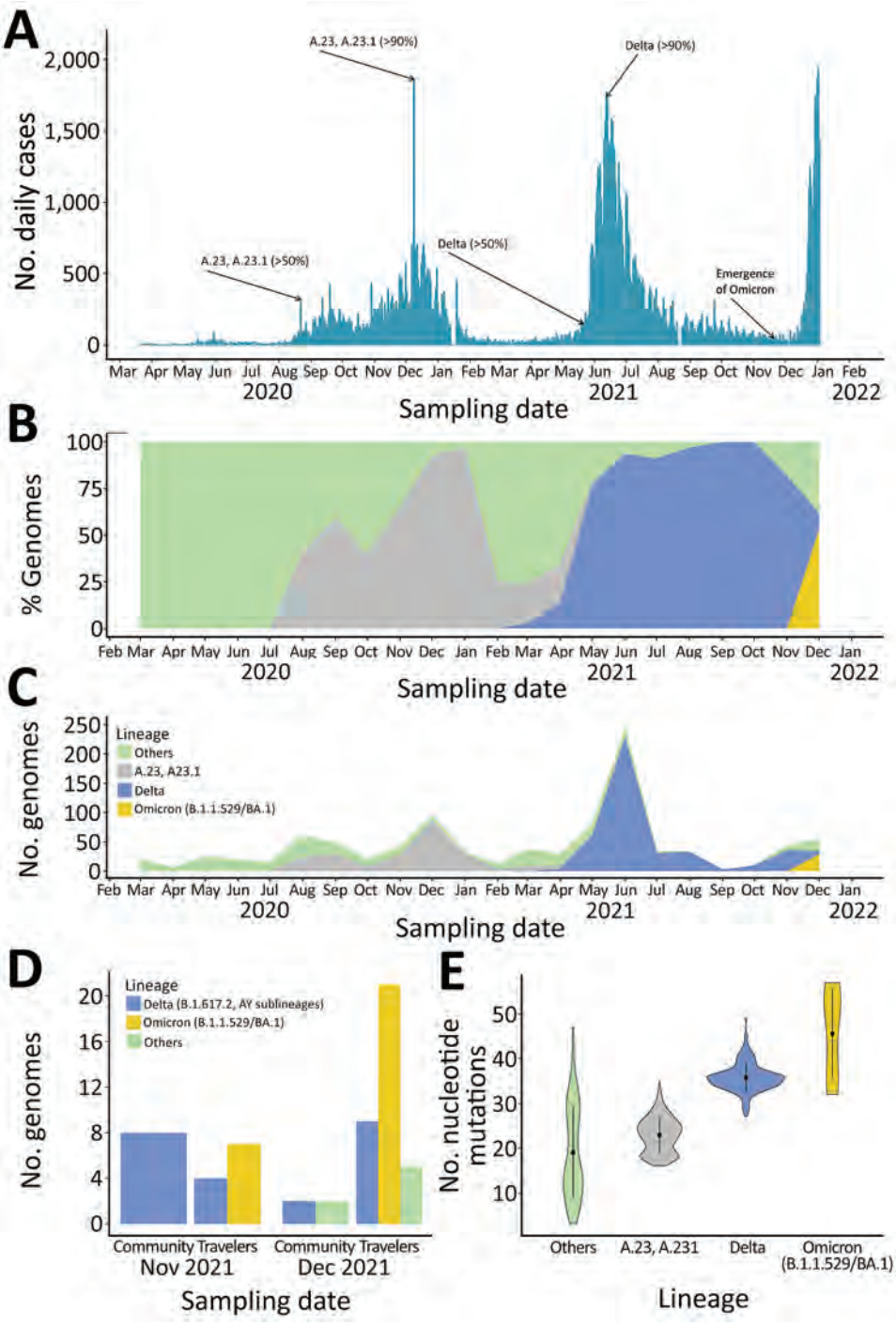

Figure 2. Rapid replacement of severe acute respiratory syndrome coronavirus 2 (SARS-CoV-2) variants by Delta and subsequent arrival of Omicron, Uganda, 2021. A) Coronavirus disease pandemic waves. Confirmed cases of daily coronavirus disease and trends of the SARS-CoV-2 pandemic over time. Three waves of the pandemic dominated by the A.23.1 in the first wave (December 2020–January 2021), Delta in the second wave (May–July 2021), and the Delta and Omicron variants in the third wave (Omicron emerged in late November 2021 and the wave began in December 2021). B, C) SARS-CoV-2 variants over time (950 genomes deposited in the GISAID database [https://www.gisaid.org] by January 10, 2022). D) SARS-CoV-2 variants during the third wave among travelers and community samples. E) Violin plots showing the distribution of whole-genome nucleotide mutations in each of the SARS-CoV-2 lineages by using the wild-type Wuhan-Hu-1/2019 isolate (GenBank accession no. MN908947) as the reference. Black dots indicate median number of nucleotide mutations. Error bars indicate interquartile ranges.

We performed a subanalysis of SARS-CoV-2 variants during the third wave (Figure 2, panel D). We also detected other Delta sublineages, such as AY.1 or B.1.617.2.1 (also known as Delta Plus and associated with a relatively higher transmissibility) (*6*), at a low prevalence. The AY.1 Delta sublineage has been associated with more antibody escaping properties because of the K417N mutation, which was identified in the Beta variant (*7*). We also provide the relative number of mutations for SARS-CoV-2 variants (Figure 2, panel E). We deposited all sequences generated during this study in the GISAID public database (accession nos. EPI ISL 4548461–543, EPI_ISL_6262724–47, EPI_ISL_8307285–411, EPI_ISL_8523904–5, EPI_ISL_6506618, EPI_ISL_6506627, EPI_ISL_6506639, EPI_ISL_6506648, EPI_ISL_6506655, EPI_ISL_6506666, EPI_ISL_6506674,

EPI_ISL_6506689, EPI_ISL_6506697, EPI_ISL_6506706, EPI_ISL_6506713, EPI_ISL_6506721, EPI_ISL_6506726, EPI_ISL_6506738, EPI_ISL_6506747, EPI_ISL_6506751, EPI_ISL_6506760, EPI_ISL_6506767, EPI_ISL_6506773, EPI_ISL_6506784, EPI_ISL_6506791, EPI_ISL_6506802, EPI_ISL_6506812, EPI_ISL_6506824, EPI_ISL_6506829, EPI_ISL_6506835, EPI_ISL_6506841, EPI_ISL_6506844, EPI_ISL_6506851, and EPI_ISL_6506857).

Conclusions

SARS-CoV-2 sequences deposited in GISAID from Uganda showed a rapid replacement of variants since the beginning of the COVID-19 pandemic. Genomic sequencing involving 266 samples collected during June–December 2021 showed that the Delta variant was the dominant virus. However, the Omicron variant emerged in late November 2021 from travelers arriving through Entebbe International Airport (39.29% from South Africa, 28.57% from Nigeria, 14.29% from Kenya, 7.14% from the Democratic Republic of the Congo, 3.57% from Ethiopia, 3.57% Rwanda, and 3.57% from the United States), and Omicron community transmissions are increasing (based on PCR genotyping). Therefore, we anticipate that Delta is gradually being replaced by Omicron, which is consistent with the observed SARS-CoV-2 variants trajectory over time.

Furthermore, results from a mutation-specific SARS-CoV-2 PCR screening (*8*,*9*) suggest that Omicron, initially becoming dominant among travelers, will likely later predominate in the community. The Omicron variant has been associated with increased transmissibility and has quickly become a global concern (*10*). Speeding up genomic sequencing from prospective samples collected at points of entry and from the community will enable faster response to outbreaks as they emerge.

A major limitation of this study was suboptimal sampling. Previously, convenience sampling that targeted points of entry and outbreak hotspots was more common. Sampling prioritized mostly moderate-to-high community transmission sites and focused less on sampling low viral transmission communities. However, plans are under way to adopt effective sampling guidelines to ensure geographically representative sampling (*11*,*12*).

In summary, the SARS-CoV-2 Delta variant rapidly replaced earlier virus variants after it was introduced into Uganda. The Omicron variant has followed the same trajectory. Our results highlight the need for surveillance and infection control measures to prevent future pandemic waves.

Acknowledgments

We thank the Uganda Ministry of Health and its COVID-19 Scientific Advisory Committee, the National COVID-19 Task Force, and the staff of the Emerging and Remerging Infections Department of the Uganda Virus Research Institute for their providing contributions; the team at the KwaZulu-Natal Research Innovation and Sequencing Platform for providing laboratory training and support; the staff at the Uganda Virus Research Institute for collecting field samples; and the persons who collected samples at borders or points of entry into Uganda.

This study was supported by the United Kingdom Medical Research Council and the United Kingdom Department for International Development under their concordat agreement. Training in genomic sequencing was supported by the African Society of Laboratory Medicine and Africa Centres for Disease Control and Prevention.

About the Author

Dr. Bbosa is a postdoctoral scientist at the Medical Research Council/Uganda Virus Research Institute and the London School of Hygiene and Tropical Medicine Uganda Research Unit, Entebbe, Uganda. His primary research interests are viral genomics, molecular epidemiology, pathogen phylodynamics and bioinformatics, and infectious disease epidemic response.

References

1. Cucinotta D, Vanelli M. WHO declares COVID-19 a pandemic. Acta Biomed. 2020;91:157–60.
2. Nicola M, Alsafi Z, Sohrabi C, Kerwan A, Al-Jabir A, Iosifidis C, et al. The socio-economic implications of the coronavirus pandemic (COVID-19): a review. Int J Surg. 2020;78:185–93. https://doi.org/10.1016/j.ijsu.2020.04.018
3. Bugembe DL, Kayiwa J, Phan MV, Tushabe P, Balinandi S, Dhaala B, et al. Main routes of entry and genomic diversity of SARS-CoV-2, Uganda. Emerg Infect Dis. 2020;26:2411–5. https://doi.org/10.3201/eid2610.202575
4. Bugembe DL, Phan MVT, Ssewanyana I, Semanda P, Nansumba H, Dhaala B, et al. Emergence and spread of a SARS-CoV-2 lineage A variant (A.23.1) with altered spike protein in Uganda. Nat Microbiol. 2021;6:1094–101. https://doi.org/10.1038/s41564-021-00933-9
5. Vilsker M, Moosa Y, Nooij S, Fonseca V, Ghysens Y, Dumon K, et al. Genome detective: an automated system for virus identification from high-throughput sequencing data. Bioinformatics. 2019;35:871–3. https://doi.org/10.1093/bioinformatics/bty695
6. Kannan SR, Spratt AN, Cohen AR, Naqvi SH, Chand HS, Quinn TP, et al. Evolutionary analysis of the Delta and Delta Plus variants of the SARS-CoV-2 viruses. J Autoimmun. 2021;124:102715. https://doi.org/10.1016/j.jaut.2021.102715
7. Rahman FI, Ether SA, Islam MR. The "Delta Plus" COVID-19 variant has evolved to become the next potential variant of concern: mutation history and measures of prevention. J Basic Clin Physiol Pharmacol. 2021;33:109–12. https://doi.org/10.1515/jbcpp-2021-0251

8. Primerdesign Ltd. SNPsig® real-time PCR SARS-CoV-2 mutation detection/allelic discrimination kit. Identification of L452R mutation [cited 2022 Jan 13]. https://genesig.com/assets/files/snpsig_sars_cov_2_l452r_version_1_01.pdf
9. Wang H, Jean S, Eltringham R, Madison J, Snyder P, Tu H, et al. Mutation-specific SARS-CoV-2 PCR screen: rapid and accurate detection of variants of concern and the identification of a newly emerging variant with spike L452R mutation. J Clin Microbiol. 2021;59:e0092621. https://doi.org/10.1128/JCM.00926-21
10. Thakur V, Ratho RK. OMICRON (B.1.1.529): a new SARS-CoV-2 variant of concern mounting worldwide fear. J Med Virol. 2021 Dec 22 [Epub ahead of print]. https://doi.org/10.1002/jmv.27541
11. Ministry of Health Uganda. A guide for genomic surveillance of COVID-19 in Uganda. The Ministry: Kampala (Uganda); 2021.
12. Africa CDC and WHO. Interim operational guidance on SARS-CoV-2 genomic surveillance in Africa: an updated guide. 2021 [cited 2022 Jan 10]. https://africacdc.org/download/interim-operational-guidance-on-sars-cov-2-genomic-surveillance-in-africa-an-updated-guide

Address for correspondence: Nicholas Bbosa, Medical Research Council/Uganda Virus Research Institute and London School of Hygiene and Tropical Medicine Uganda Research Unit, Plot 51–59 Nakiwogo Rd, Entebbe, Uganda; email: nicholas.bbosa@mrcuganda.org

SARS-CoV-2 Antibody Prevalence and Population-Based Death Rates, Greater Omdurman, Sudan

Wendelin Moser, Mohammed Ahmed Hassan Fahal,[1] Elamin Abualas,[1] Shahinaz Bedri, Mahgoub Taj Elsir, Mona Fateh El Rahman Omer Mohamed, Abdelhalim Babiker Mahmoud, Amna Ismail Ibrahim Ahmad, Mohammed A. Adam, Sami Altalib, Ola Adil DafaAllah, Salahaldin Abdallah Hmed, Andrew S. Azman, Iza Ciglenecki, Etienne Gignoux, Alan González, Christine Mwongera, Manuel Albela Miranda

In a cross-sectional survey in Omdurman, Sudan, during March–April 2021, we estimated that 54.6% of the population had detectable severe acute respiratory syndrome coronavirus 2 antibodies. Overall population death rates among those ≥50 years of age increased 74% over the first coronavirus disease pandemic year.

Many key epidemiologic and serologic characteristics of severe acute respiratory syndrome coronavirus 2 (SARS-CoV-2) remain unknown. Few seroprevalence studies have been conducted in Africa to better understand the landscape of humoral immunity. In Sudan, 32,846 confirmed cases of coronavirus disease (COVID-19) were recorded during March 13, 2020– April 10, 2021; of those, 72% were registered in the state of Khartoum alone (*1*). A study of a convenience sample of ≥1,000 participants from 22 neighborhoods of the city of Khartoum in March–July 2020 found that 35% of participants were positive by real time RT-PCR for SARS-CoV-2, and 18% had SARS-CoV-2 antibodies (*2*). Similar discrepancies between clinical confirmed cases and infection rates assessed by serology or PCR testing independent of symptoms have been described elsewhere in Africa (*3*–*5*).

The National Health Review Ethics Committee (no. 3-1-21), Médecins Sans Frontières Ethics Review Board (ID 2089c), and Khartoum State Ministry of Health approved this study. Before field data collection began, we visited the leader of the resistance committee for each block to obtain verbal consent. For the mortality survey, we obtained verbal consent from the head of the household. For the seroprevalence survey, we obtained written informed consent from adults and, for participants <18 years of age, first written informed consent from parents or legal guardians and second, oral assent from the participants themselves.

The Study

Sudan's capital, Khartoum, is a tripartite metropolis comprising Khartoum, Bahri, and Omdurman; it has >8 million inhabitants (*6*). We chose Omdurman, the largest of the 3 cities, as the study site for 2 surveys conducted in March–July 2020 (Appendix, https://wwwnc.cdc.gov/EID/article/28/5/21-1951-App1.pdf). One, a retrospective mortality survey, was conducted using a 2-stage cluster sampling methodology based on random geopoints with 2 recall periods, the prepandemic (January 1, 2019–February 29, 2020) and the pandemic period (March 1, 2020–date of survey); an adult representative of the household answered a standardized questionnaire. The second was a nested SARS-CoV-2 antibody prevalence survey; all the members of a subset of the household, regardless of age, were invited to participate in the seroprevalence study.

Capillary blood was collected on dried blood spot cards and directly tested with the STANDARD

Author affiliations: Médecins Sans Frontières, Geneva, Switzerland (W. Moser, A.S. Azman, I. Ciglenecki, A. González, C. Mwongera, M. Albela Miranda); Médecins Sans Frontières, Khartoum (M.T. Elsir, A.B. Mahmoud, A.I.I. Ahmad, M.A. Adam, S. Altalib, O.A. DafaAllah, S.A. Hmed); Khartoum State Ministry of Health, Khartoum, Sudan (M.AH. Fahal, E. Abualas, S. Bedri, M.T. Elsir, M.F.E.R.O. Mohamed, O.A. DafaAllah); National Public Health Laboratory, Khartoum (E. Abualas, S. Bedri, O.A. DafaAllah); University of Khartoum, Khartoum (A.B. Mahmoud, M.A. Adam, S. Altalib); Johns Hopkins Bloomberg School of Public Health, Baltimore, Maryland, USA (A.S. Azman); University of Geneva, Geneva (A.S. Azman); Epicentre, Paris, France (E. Gignoux)

DOI: https://doi.org/10.3201/eid2805.211951

[1]These authors contributed equally to this article.

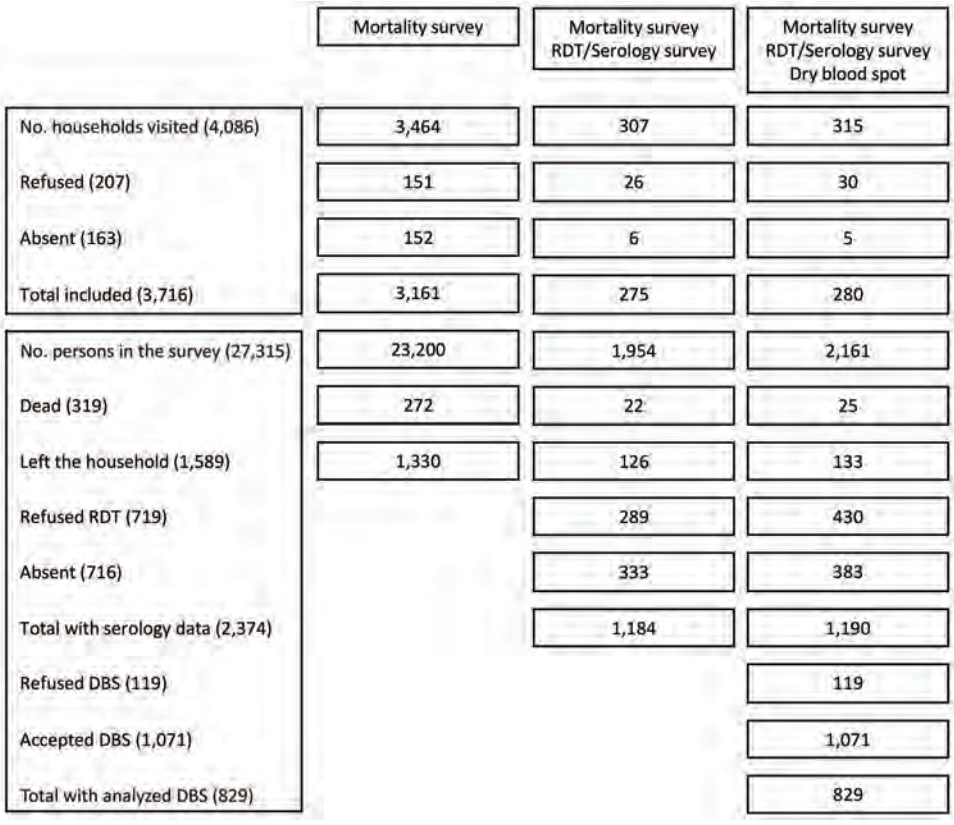

Figure 1. Survey flow for cross-sectional study of SARS-CoV-2 prevalence and population-based death rates, Omdurman, Sudan, 2021. DBS, dry blood spot; RDT, rapid diagnostic test.

Q COVID-19 IgM/IgG Combo rapid diagnostic test (RDT) (SD–Biosensor, https://www.sdbiosensor.com). All participants who tested positive for any isotype were considered seropositive. Dried blood spot cards (Euroimmun, https://www.euroimmun.com) were transferred to the National Public Health Laboratory (NPHL; Khartoum, Sudan) for further analysis by ELISA (Anti–SARS-CoV-2 ELISA [IgG, S1 domain]; Euroimmun) to compare with the rapid test results (*7*,*8*). To adjust our seroprevalence estimates using published validation data for both ELISA and RDT tests, we conducted a meta-analysis with random effects and a Bayesian latent class model (Appendix).

During March 1–April 10, 2021, a total of 2,374 (62.3%) participants from 555 households (Figure 1) agreed to provide blood; 34.3% (95% CI 32.4%–36.2%; Table 1) of them had detectable SARS-CoV-2 antibodies (IgM, IgG, or both). After adjusting for immunoassay performance for detecting previous infections, we estimated a seroprevalence of 54.6% (95% CI 51.4%–57.8%), noting a clear increase of seroprevalence risk with age (Table 1). We found the highest seroprevalence of 80.7% (95% CI 71.7%–89.7%) among participants ≥50 years of age. Assuming a population size of 3,040,604 for Omdurman on the basis of the data collected in the survey and the data provided by the Ministry of Planning, we estimate that 1,660,170 (95% CI 1,458,225–1,863,936) persons had been infected by SARS-CoV-2 at the time of the survey.

We found evidence of significant clustering of seropositivity within households; 364 households (65.6%) had ≥1 positive household member. Living

Table 1. SARS-CoV-2 antibody seroprevalence test results by age group in cross-sectional survey, Omdurman, Sudan*

	RDT results			Adjusted results		
Age group	% Positive (95% CI)	Relative risk (95% CI)	p value†	Seroprevalence (95% CI)	Relative risk (95% CI)	p value†
<5 y, = 299	18.7 (14.7–23.5)	0.4 (0.3–0.5)	<0.001	29.0 (22.4–36.9)	0.3 (0.3–0.4)	<0.001
5–19 y, = 786	30.6 (27.5–33.9)	0.6 (0.5–0.7)	<0.001	48.5 (43.3–53.9)	0.6 (0.5–0.6)	<0.001
20–34 y, = 629	35.5 (31.8–39.3)	0.7 (0.6–0.8)	<0.001	56.5 (50.5–62.8)	0.7 (0.6–0.7)	<0.001
35–49 y, = 342	39.5 (34.4–44.7)	0.8 (0.7–0.9)	0.006	63.1 (54.8–71.8)	0.8 (0.7–0.9)	<0.001
≥50 y, = 319	50.2 (44.7–55.6)	Referent		80.7 (71.7–89.7)	Referent	
Overall, = 2,375	34.3 (32.4–36.2)			54.6 (51.4–57.8)		

*RDT, rapid diagnostic test; SARS-CoV-2, severe acute respiratory syndrome coronavirus 2.
†p values indicate the difference in relative risk between the oldest age group (≥50 y) as reference and the other age groups.

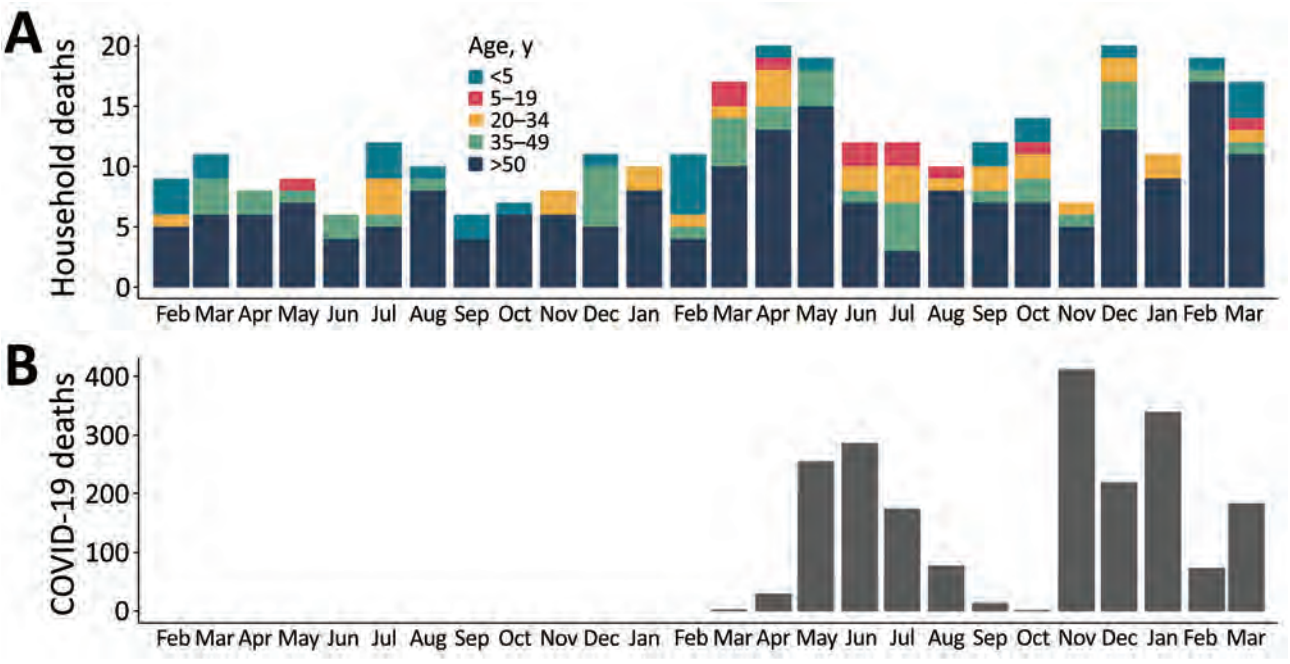

Figure 2. Comparison of estimated and reported deaths from coronavirus disease, Sudan, January 2019–April 2021. A) Distribution of all deaths as reported in a population-based cross-sectional survey in the city of Omdurman, Sudan. B) Official registered COVID-19–related deaths across Sudan.

with a person who was seropositive led to a 1.68-fold (odds ratio [OR] 95% CI 1.35–2.08; p<0.001) increase in the odds of being seropositive (Appendix). Among the 4,086 households visited (Figure 1), we enumerated 27,315 persons who had been a household member at some time after January 1, 2019. Among them, 319 deaths were reported, including 206 (64.6%) among persons ≥50 years of age and 30 (9.4%) among children <5 years of age. The deaths increased in 2020 during the pandemic period, consistent with the reported countrywide confirmed COVID-19 deaths (Figure 2).

The overall death rate for the whole recall period was 0.16 (95% CI 0.13–0.18) deaths/10,000 population/day (Table 2). The crude death rate significantly increased by 67% (95% CI 32%–110%) from 0.12 (0.10–0.14) deaths/10,000 population/day for the prepandemic period to 0.20 (0.16–0.23) deaths/10,000 population/day for the pandemic period. This difference was even more pronounced among those ≥50 years of age; deaths increased 74% (95% CI 30%–133%; p<0.001) between the 2 periods. (Table 2). On the basis of our estimates of the population size of Omdurman and the death rates, we estimated 7,113 excess deaths (95% CI 5,015–9,505) during the pandemic period and that 5,125 (95% CI 4,165–6,226) of these occurred in persons ≥50 years of age.

Conclusions

Our findings indicate that mortality rates in the overall population of Omdurman increased by 67% during the first pandemic year; the highest increase (74%) was among the population ≥50 years of age. We estimated an excess of 7,113 all-cause deaths during the pandemic period, compared with 287 COVID-19–related deaths officially reported for Omdurman; these data were obtained from the Khartoum Ministry of Health. We have considered the potential limitation of having

Table 2. Reported death rates for the prepandemic and pandemic periods from cross-sectional SARS-CoV-2 survey, Omdurman, Sudan*

	Overall		Prepandemic period		Pandemic period		Rate ratio	
Age group	No. deaths	Rate (95% CI)	No. deaths	Rate (95% CI)	No. deaths	Rate (95% CI)	Rate ratio (95% CI)	p value
<5 y	30	0.19 (0.10–0.28)	18	0.22 (0.11–0.32)	12	0.17 (0.04–0.30)	0.77 (0.34–1.70)	0.613
5–19 y	13	0.02 (0.01–0.03)	2	0.00 (0.00–0.01)	11	0.03 (0.01–0.05)	Referent	NA
20–34 y	30	0.05 (0.03–0.07)	10	0.04 (0.01–0.06)	20	0.07 (0.04–0.11)	1.75 (0.78–4.19)	0.199
35–49 y	40	0.12 (0.09–0.16)	16	0.09 (0.05–0.14)	24	0.15 (0.09–0.21)	1.67 (0.85–3.36)	0.149
≥50 y	206	0.78 (0.65–0.91)	80	0.57 (0.45–0.69)	126	0.99 (0.79–1.20)	1.74 (1.30–2.33)	<0.001
Total	319	0.16 (0.13–0.18)	126	0.12 (0.10–0.14)	193	0.20 (0.16–0.23)	1.67 (1.32–2.10)	<0.001

*No. deaths per category are reported rates. NA, not applicable; SARS-CoV-2, severe acute respiratory syndrome coronavirus 2.

a recall period >2 years for mortality estimates, which could introduce bias for deaths occurring at the beginning of the recall period. Surveyors were trained to be aware of this factor to mitigate those bias (Appendix).

The crude seroprevalence estimate shows how widespread SARS-CoV-2 infection was, affecting all age groups, especially persons ≥50 years of age. However, the estimates based on RDT results might have underestimated the seroprevalence as a result of several limitations. First, we conducted our survey 1 year after the earliest SARS-CoV-2 infection was detected in Sudan, so a varying degree of antibody decay over time could be expected (*9*,*10*). Second, when antibodies remain present in the blood, their detection is limited by the performance of the RDT (*11*). To overcome those limitations, we adjusted the crude results; we observed a 20% increase in the overall seroprevalence. With that estimation we calculated that the number of infections was 50 times higher than the number of COVID-19 cases recorded by the end of the survey, which was consistent with other case-to-infection ratios in low-income settings in Africa and Asia (*12*,*13*). Despite this high seroprevalence, another wave of infection occurred right after the survey (May–June 2021); comparing it with the previous wave, we saw that fewer cases but more deaths per case were reported. Three more waves occurred during September 2021–January 2022, the latest one reporting a record number of weekly cases (*14*). No sequencing data was available as of January 2022; therefore, it was impossible to discuss the emergence of new variants and their impact on the new waves of infections given the prior seroprevalence we estimated in this survey.

In summary, this population-based cross-sectional survey in Omdurman, Sudan, demonstrated significantly higher death rates during the COVID-19 pandemic compared with those of the prepandemic period, particularly affecting persons ≥50 years of age. We also found elevated SARS-CoV-2 seropositivity, affecting older populations the most. Our results suggest that Omdurman, one of the largest population centers in Africa, was severely affected by the COVID-19 pandemic and that excess mortality rates were much higher than reported COVID-19 deaths.

Acknowledgments

We thank all people participating in the survey, the survey surveyors for their hard work in the field, the laboratory technicians from the National Public Health Laboratory for the ELISA analysis, the team of the Innovation, Development and Research Directorate of the State Ministry of Health for their support, and Tania Kapoor for editorial support. We thank the National Public Health Laboratory, Sudan, for donating 5,000 rapid tests for the survey with kind permission from the Africa Centre for Disease Control

Medécins Sans Frontières–Switzerland (MSF–CH) funded the study, except for the tests donated by Africa CDC through the National Public Health Laboratory.

W.M., A.S.A., I.C., A.G., C.M., and M.A. had a role in the survey design, survey execution, data collection, data analysis, data interpretation, and writing of the report. W.M., M.A.H.F., M.T.E., and M.A. had full access to all data in the survey and had final responsibility for the decision to submit for publication.

The minimal data set underlying the findings of this paper are available on request, in accordance with the legal framework set forth by Médecins Sans Frontières data sharing policy (https://www.ncbi.nlm.nih.gov/pmc/articles/PMC3858219/pdf/pmed.1001562.pdf). To request the data, email data.sharing@msf.org.

About the Author

Dr. Moser is an epidemiologist with Médecins Sans Frontières, Geneva, Switzerland. His research interest includes the epidemiology of infectious and neglected tropical diseases.

References

1. Mukhtar MM, Khogali M. The accelerating COVID-19 epidemic in Sudan. Nat Immunol. 2021;22:797–8. https://doi.org/10.1038/s41590-021-00950-0
2. TEPHINET. Sudan FETP conducts targeted testing for COVID-19 in Khartoum state. 2020 [cited 2021 Feb 2]. https://www.tephinet.org/sudan-fetp-conducts-targeted-testing-for-covid-19-in-khartoum-state
3. Musa HH, Musa TH, Musa IH, Musa IH, Ranciaro A, Campbell MC. Addressing Africa's pandemic puzzle: Perspectives on COVID-19 transmission and mortality in sub-Saharan Africa. Int J Infect Dis. 2021;102:483–8. https://doi.org/10.1016/j.ijid.2020.09.1456
4. Lawal Y. Africa's low COVID-19 mortality rate: A paradox? Int J Infect Dis. 2021;102:118–22. https://doi.org/10.1016/j.ijid.2020.10.038
5. Oladipo EK, Ajayi AF, Odeyemi AN, Akindiya OE, Adebayo ET, Oguntomi AS, et al. Laboratory diagnosis of COVID-19 in Africa: availability, challenges and implications. Drug Discov Ther. 2020;14:153–60. https://doi.org/10.5582/ddt.2020.03067
6. Imperial College London. Report 39—characterizing COVID-19 epidemic dynamics and mortality under-ascertainment in Khartoum, Sudan. 2021 [cited 2021 Feb 2]. http://www.imperial.ac.uk/medicine/departments/school-public-health/infectious-disease-epidemiology/mrc-global-infectious-disease-analysis/covid-19/report-39-sudan
7. Higgins RL, Rawlings SA, Case J, Lee FY, Chan CW, Barrick B, et al. Longitudinal SARS-CoV-2 antibody study

using the Easy Check COVID-19 IgM/IgG™ lateral flow assay. PLoS One. 2021;16:e0247797. https://doi.org/10.1371/journal.pone.0247797
8. Pavlova IP, Nair SS, Kyprianou N, Tewari AK. The rapid coronavirus antibody test: can we improve accuracy? Front Med (Lausanne). 2020;7:569. https://doi.org/10.3389/fmed.2020.00569
9. Wang H, Yuan Y, Xiao M, Chen L, Zhao Y, Haiwei Zhang, et al. Dynamics of the SARS-CoV-2 antibody response up to 10 months after infection. Cell Mol Immunol. 2021;18:1832–4. https://doi.org/10.1038/s41423-021-00708-6
10. Chia WN, Zhu F, Ong SWX, Young BE, Fong S-W, Le Bert N, et al. Dynamics of SARS-CoV-2 neutralising antibody responses and duration of immunity: a longitudinal study. Lancet Microbe. 2021;2:e240–9. https://doi.org/10.1016/S2666-5247(21)00025-2
11. Uwamino Y, Wakui M, Aoki W, Kurafuji T, Yanagita E, Morita M, et al.; Keio Donner Project Team. Evaluation of the usability of various rapid antibody tests in the diagnostic application for COVID-19. Ann Clin Biochem. 2021;58:174–80. https://doi.org/10.1177/0004563220984827
12. Wiens KE, Mawien PN, Rumunu J, Slater D, Jones FK, Moheed S, et al. Seroprevalence of severe acute respiratory syndrome coronavirus 2 IgG in Juba, South Sudan, 2020. Emerg Infect Dis. 2021;27:1598–606. https://doi.org/10.3201/eid2706.210568
13. Bhuiyan TR, Hulse JD, Hegde ST, Akhtar M, Islam T, Khan ZH, et al. SARS-CoV-2 seroprevalence before Delta variant surge, Chattogram, Bangladesh, March–June 2021. Emerg Infect Dis. 2022;28:429–31. https://doi.org/10.3201/eid2802.211689
14. World Health Organization. Health emergency dashboard: Sudan.2022 [cited 2022 Jan 19]. https://covid19.who.int/region/emro/country/sd

Address for correspondence: Manuel Albela Miranda, Médecins Sans Frontières, Rue de Lausanne 78, 1202 Geneva, Switzerland; email: manuel.albela@geneva.msf.org

Evidence of Prolonged Crimean-Congo Hemorrhagic Fever Virus Endemicity by Retrospective Serosurvey, Eastern Spain

Laura Carrera-Faja, Jesús Cardells, Lola Pailler-García, Víctor Lizana, Gemma Alfaro-Deval, Johan Espunyes, Sebastian Napp,[1] Oscar Cabezón[1]

We conducted a retrospective serosurvey for antibodies against Crimean-Congo hemorrhagic fever virus in wild ungulates along the eastern Mediterranean Coast of Spain. The virus has been endemic in this region since 2010 but is mainly restricted to geographic clusters with extremely high seropositivity associated with high density of bovids.

Crimean-Congo hemorrhagic fever (CCHF) is caused by CCHF virus (CCHFV), a tickborne pathogen of the genus *Orthonairovirus*, belonging to the family *Bunyaviridae*. In humans, CCHFV can induce a severe and potentially fatal systemic hemorrhagic disease. CCHFV infections in wildlife and domestic animals are generally subclinical but, in some species, can induce enough viremia to enable virus transmission to uninfected ticks. Moreover, infected animals produce antibodies, enabling the identification of affected areas through retrospective serologic studies (*1*). CCHFV is endemic in several countries in Asia, Africa, the Middle East, and southeastern Europe and has a range similar to that of its main vectors and reservoirs, *Hyalomma* spp. ticks, which are expanding their habitat range in southern Europe (*2*).

In Spain, CCHFV was detected in *H. lusitanicum* ticks from a red deer (*Cervus elaphus*) in 2010 (*3*). Since 2013, several severe CCHF cases in humans have been reported in the country (*4*). Viral strains identified in Spain showed high genetic variability, suggesting repeated introductions from different origins, including Africa and eastern Europe (*5*,*6*). Seroprevalence studies conducted in 2017 and 2018 showed evidence that CCHFV is prevalent over large areas of central and southern Spain, which coincide with the regions where *H. marginatum* and *H. lusitanicum* ticks have been described (*4*,*6*). Along the Mediterranean Coast of eastern Spain, the existence of CCHFV vectors (*Hyalomma* ticks) and of the virus itself were uncertain until recently, when *H. lusitanicum* ticks were found in wild boars (*Sus scrofa*) from the metropolitan area of Barcelona (*7*), and CCHFV seropositivity was reported in ungulates from southern Catalonia (*8*). To evaluate the extent and duration of CCHFV circulation in eastern Spain, we conducted a retrospective serosurvey to detect CCHFV antibodies in different wildlife species in the Valencia region.

The Study

We used the CCHF Double Antigen Multi-Species ELISA kit (IDvet, https://www.id-vet.com) to test for CCHFV antibodies in serum samples collected from 332 wild boars, 126 Iberian ibexes (*Capra pyrenaica*), and 48 mouflons (*Ovis aries musimon*). Serum samples were collected during 2010–2021 within the framework of the wildlife surveillance program in the Valencia region. We chose wild boars, Iberian ibexes, and mouflons because they are the main wild ungulate species in the region. Iberian ibexes and mouflons were selected from the 2 areas where they are more abundant. We also selected serum samples taken from boars in the same 2 areas and from areas with low densities of wild ruminants. (Appendix Figure 1, https://wwnc.cdc.gov/EID/article/28/5/21-2335-App1.pdf).

Our results showed that CCHFV was already circulating in different areas of the Valencia region

Author affiliations: Universitat Autònoma de Barcelona, Bellaterra, Spain (L. Carrera-Faja, J. Espunyes, O. Cabezón); Universidad Cardenal Herrera-CEU, Valencia, Spain (J. Cardells, V. Lizana, G. Alfaro-Deval); Institut de Recerca i Tecnologia Agroalimentàries, Bellaterra (L. Pailler-García, S. Napp)

DOI: https://doi.org/10.3201/eid2805.212335

[1]These senior authors contributed equally to this article.

Table. Seropositivity of serum samples from various mammalian species tested for antibodies against Crimean-Congo hemorrhagic fever virus, Valencia region, Spain*

Year	Iberian ibex (*Capra pyrenaica*)	Mouflon (*Ovis aries musimon*)	Wild boar (*Sus scrofa*)	Total
2010	–	–	21/84 (17–36)	21/84 (17–36)
2011	–	–	12/92 (7–22)	12/92 (7–22)
2012	–	–	4/50 (3–20)	4/50 (3–20)
2013	–	–	0/12 (0–30)	0/12 (0–30)
2014	–	–	8/40 (10–36)	8/40 (10–36)
2015	–	–	6/49 (6–26)	6/49 (6–26)
2016	–	–	0/4 (0–60)	0/4 (0–60)
2017	13/13 (72–100)	–	–	13/13 (72–100)
2018	38/39 (85–100)	15/15 (75–100)	0/1 (0–95)	53/55 (86–99)
2019	51/54 (84–99)	33/33 (87–100)	–	84/87 (90–99)
2020	16/17 (69–100)	–	–	16/17 (69–100)
2021	3/3 (31–100)	–	–	3/3 (31–100)
Total	121/126 (91–99)	48/48 (91–100)	51/332 (12–20)	220/506 (39–48)

*Data are no. positive/no. tested (95% CI for percent seropositive). –, no samples tested.

by the time the virus was reported in Spain in 2010 (Table 1; Appendix Figure 2). These results are consistent with the phylogenetic analysis of the CCHFV strain obtained from a *H. lusitanicum* tick collected in western Spain in 2014 that suggested the strain had been circulating in the country for several decades (*9*). Together with the variability of CCHFV strains identified in Spain (*5*,*6*), our findings suggest an epidemiologic scenario in which CCHFV has been repeatedly introduced into different regions of Spain over many years.

Among Iberian ibex serum samples from Valencia, 96.0% (121/126) had antibodies against CCHFV, which is close to the 100% seroprevalence reported for the same species in the affected neighboring area of Catalonia (*8*). Likewise, all the mouflon (48/48) samples in this study were seropositive, indicating a high susceptibility in this species, even though CCHFV infection has not been previously described in mouflons. In contrast, only 15.5% (51/332) of the wild boar samples tested were seropositive, and wild boars in the areas of high densities of Iberian ibexes

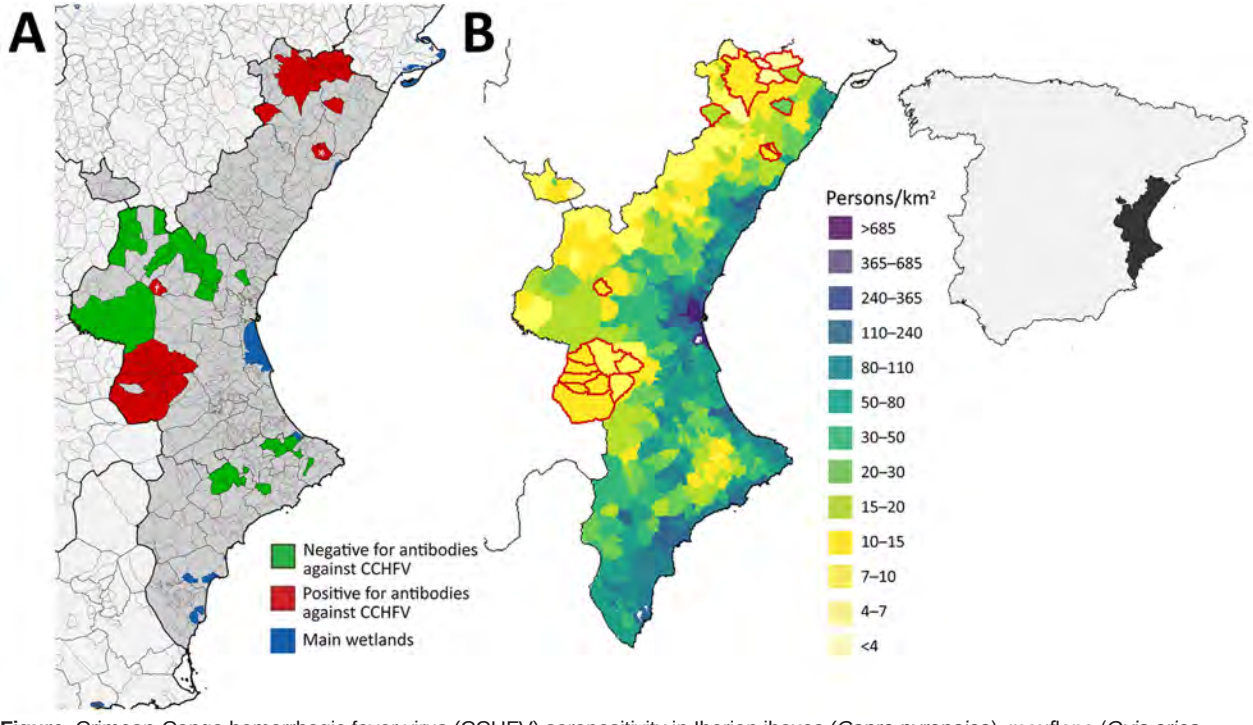

Figure. Crimean-Congo hemorrhagic fever virus (CCHFV) seropositivity in Iberian ibexes (*Capra pyrenaica*), mouflons (*Ovis aries musimon*), and wild boars (*Sus scrofa*), Valencia region, Spain, 2010–2021. A) Areas in Valencia where tested animals were seropositive and seronegative. Green indicates all samples were seronegative; red indicates ≥1 sample was seropositive; gray indicates areas not sampled. Asterisk (*) indicates Chera and dagger (†) indicates Vilanova d'Alcolea, 2 areas of CCHFV-seropositivity in wild boars outside the main areas in which Iberian ibexes and mouflons tested positive. B) Density of human population, Valencia region, Spain 2015. Areas with red outlines coincide with areas in which CCHFV-seropositive animals were sampled. Map at right shows the Valencia region in Spain.

and mouflons had seroprevalences of only 36.0% (49/136), which coincides with the results obtained in Catalonia (*8*). One possible explanation for the prevalences we found in Iberian ibexes, mouflons, and wild boars is that *Hyalomma* genus ticks feed preferably on species of the family *Bovidae* but also feed, although less prominently, in the family *Suidae* (*10*).

CCHFV seropositivity in the Valencia region clustered in 2 areas (Figure 1, panel A). One cluster was in the north in the Tinença de Benifassà Natural Park, an area of the region that is a continuation of the Ports de Tortosa-Beseit National Game Reserve, the affected area in Catalonia that is close to the Ebro Delta wetland (*8*). The other cluster was located at the Muela de Cortes y el Caroche natural area in central Valencia region, <40 km from the Albufera, the third-largest wetland in Spain. Identifying 2 main CCHFV transmission areas close to key stopover areas for migratory birds adds weight to the hypothesis of CCHFV introduction in Spain via migratory birds carrying infected ticks. In fact, the Mediterranean/Black Sea Flyway and the East Atlantic Flyway, 2 of the 3 Palaearctic-African flyways connecting Europe with Africa, converge on the Mediterranean Coast of eastern Spain.

We also detected CCHFV antibodies in a few wild boars outside the 2 main positive areas (Figure, panel A). Because wild boars are known to disperse over long distances (*11*), this species could play a key role in the spread of CCHFV outside endemic areas.

A recent study mapped the risk for CCHFV exposure among humans in mainland Spain by using red deer as an indicator of the transmission risk plus environmental variables (*12*), but that study did not predict areas of high risk that we identified in the Valencia region or those identified farther north (*8*). Those findings indicate that determinants of CCHFV circulation in central and southwestern Spain are clearly different from those in the Mediterranean area, where Iberian ibexes, and to a lesser extent wild boars and mouflons, likely play a key role.

Little information is available on the distribution of competent CCHFV vectors in the Valencia region, but a study to the north of the region reported a substantial increase during 2017–2018 in the number of persons receiving tick bites, 85% of which were caused by *H. lusitanicum* ticks (*13*). Other studies have suggested that the lack of human CCHF cases in the Mediterranean region, despite areas with widespread CCHFV, is the result of a low rate of contact between humans and infected ticks (*14*). At least in the Valencia region, this low contact seems to be the case; areas where CCHFV transmission in wildlife is concentrated coincide with the areas with the lowest human density (Figure 1, panel B). However, rising wild ungulate populations that are moving closer to densely populated areas could change the human epidemiologic situation.

Conclusions

Our results support an epidemiologic scenario in which CCHFV has been endemic in wild ungulates in different regions of Spain before it was detected in 2010. In eastern Spain, CCHFV circulation mainly occurs in geographic clusters associated with high densities of *Bovidae* species. However, as these species move into areas with higher human populations, more human CCHF cases could occur. To protect the population of the region, public health authorities should continue CCHFV surveillance among tick and ungulate species.

About the Author

Ms. Carrera-Faja is a PhD candidate at the Wildlife Conservation Medicine Research Group (WildCoM), Department of Animal Medicine and Surgery, Universitat Autònoma, Barcelona, Spain. Her current research focuses on Crimean-Congo hemorrhagic fever virus in wildlife species.

References

1. Spengler JR, Bergeron É, Rollin PE. Seroepidemiological studies of Crimean-Congo hemorrhagic fever virus in domestic and wild animals. PLoS Negl Trop Dis. 2016;10:e0004210. https://doi.org/10.1371/journal.pntd.0004210
2. Messina JP, Pigott DM, Golding N, Duda KA, Brownstein JS, Weiss DJ, et al. The global distribution of Crimean-Congo hemorrhagic fever. Trans R Soc Trop Med Hyg. 2015;109:503–13. https://doi.org/10.1093/trstmh/trv050
3. Estrada-Peña A, Palomar AM, Santibáñez P, Sánchez N, Habela MA, Portillo A, et al. Crimean-Congo hemorrhagic fever virus in ticks, Southwestern Europe, 2010. Emerg Infect Dis. 2012;18:179–80. https://doi.org/10.3201/eid1801.111040
4. Ministry of Health, Consumption and Social Welfare. Report on the situation and evaluation of the risk of transmission of the Crimean-Congo hemorrhagic fever virus in Spain, July 2019 [in Spanish] [cited 2021 Nov 9]. https://www.mscbs.gob.es/profesionales/saludPublica/ccayes/analisisituacion/doc/ER_FHCC.pdf
5. Ramírez de Arellano E, Hernández L, Goyanes MJ, Arsuaga M, Cruz AF, Negredo A, et al. Phylogenetic characterization of Crimean-Congo hemorrhagic fever virus, Spain. Emerg Infect Dis. 2017;23:2078–80. https://doi.org/10.3201/eid2312.171002
6. Moraga-Fernández A, Ruiz-Fons F, Habela MA, Royo-Hernández L, Calero-Bernal R, Gortazar C, et al. Detection of new Crimean-Congo haemorrhagic fever virus genotypes in ticks feeding on deer and wild boar, Spain. Transbound Emerg Dis. 2021;68:993–1000. https://doi.org/10.1111/tbed.13756

7. Castillo-Contreras R, Magen L, Birtles R, Varela-Castro L, Hall JL, Conejero C, et al. Ticks on wild boar in the metropolitan area of Barcelona (Spain) are infected with spotted fever group rickettsiae. Transbound Emerg Dis. 2021 Jul 31 [Epub ahead of print]. https://doi.org/10.1111/tbed.14268
8. Espunyes J, Cabezón O, Pailler-García L, Dias-Alves A, Lobato-Bailón L, Marco I, et al. Hotspot of Crimean-Congo hemorrhagic fever virus seropositivity in wildlife, Northeastern Spain. Emerg Infect Dis. 2021;27:2480–4. https://doi.org/10.3201/eid2709.211105
9. Cajimat MNB, Rodriguez SE, Schuster IUE, Swetnam DM, Ksiazek TG, Habela MA, et al. Genomic characterization of Crimean-Congo hemorrhagic fever virus in *Hyalomma* tick from Spain, 2014. Vector Borne Zoonotic Dis. 2017;17:714–9. https://doi.org/10.1089/vbz.2017.2190
10. Spengler JR, Estrada-Peña A. Host preferences support the prominent role of *Hyalomma* ticks in the ecology of Crimean-Congo hemorrhagic fever. PLoS Negl Trop Dis. 2018;12:e0006248. https://doi.org/10.1371/journal.pntd.0006248
11. Casas-Díaz E, Closa-Sebastià F, Peris A, Torrentó J, Casanovas R, Marco I, et al. Dispersal record of wild boar (*Sus scrofa*) in northeast Spain: implications for implementing disease-monitoring programs. Wildl Biol Pract. 2013;9:19–26. https://doi.org/10.2461/wbp.2013.ibeun.3
12. Cuadrado-Matías R, Cardoso B, Sas MA, García-Bocanegra I, Schuster I, González-Barrio D, et al. Red deer reveal spatial risks of Crimean-Congo haemorrhagic fever virus infection. Transbound Emerg Dis. 2021 Nov 5 [Epub ahead of print]. https://doi.org/10.1111/tbed.14385
13. Falcó Garí JV, López-Peña D, de la Torre J, Safont-Adsuara L, Bellido-Blasco J, Jiménez-Peydró R. Incidence of disease-transmitting ticks on the human population in the province of Castellón [In Spanish]. Rev Salud Ambient. 2019;19 (Espec. Congr):135. Presented at: XV Environmental Health Congress; May 22–24, 2019; Valencia, Spain.
14. Estrada-Peña A, de la Fuente J. The ecology of ticks and epidemiology of tick-borne viral diseases. Antiviral Research. 2014;108:104–28. https://doi.org/10.1016/j.antiviral.2014.05.016
15. National Air and Space Administration. Socioeconomic data and applications center (SEDAC): gridded population of the world, version 4 (GPWv4): administrative unit center points with population estimates [cited 2021 Nov 3]. https://doi.org/10.7927/H4F47M2C

Address for correspondence: Johan Espunyes; Wildlife Conservation Medicine Research Group (WildCoM), Departament de Medicina i Cirurgia Animals, Universitat Autònoma de Barcelona, 08193 Bellaterra, Spain; email: johan.espunyes@uab.cat

Lack of Evidence for Crimean–Congo Hemorrhagic Fever Virus in Ticks Collected from Animals, Corsica, France

Vincent Cicculli, Apolline Maitre, Nazli Ayhan, Stevan Mondoloni, Jean-Christophe Paoli, Laurence Vial, Xavier N. de Lamballerie, Remi Charrel, Alessandra Falchi

In Corsica, France, 9.1% of livestock serum samples collected during 2014–2016 were found to have antibodies against Crimean–Congo hemorrhagic fever virus (CCHFV), an emerging tickborne zoonotic disease. We tested 8,051 ticks for CCHFV RNA and *Nairovirus* RNA. The results indicate that Corsica is not a hotspot for CCHFV.

Crimean–Congo hemorrhagic fever (CCHF) is a tickborne zoonotic disease that is characterized by hemorrhagic fever and can progress from mild, nonspecific signs to a severe and fatal hemorrhagic disease. The CCHF virus (CCHFV) is an enveloped, segmented, negative-sense, single-stranded RNA member of the family *Nairoviridae*, genus *Orthonairovirus*. CCHFV has been detected in >35 species of ticks worldwide, among which ticks belonging to the genus *Hyalomma* are the primary vectors in humans and wild and domestic animals (*1*). Humans are infected through tick bites and direct contact with infected blood and body fluids during occupational exposure (e.g., farming, slaughtering, and medical and nursing care).

CCHF is endemic in Africa, Asia, and the Balkan region (*2*). In Western Europe, autochthonous human cases were reported only in Spain, where CCHFV was identified in *H. lusitanicum* ticks (*3*). In Corsica, a French Mediterranean island, 9.1% of livestock (i.e., cattle, goats, sheep) serum samples contained CCHFV-specific IgG during 2014–2016 (*4*). Entomologic surveys revealed that the *H. marginatum* tick, a vector of CCHFV, was present in Corsica (*5*).

Author affiliations: Laboratoire de Virologie, Université de Corse–Institut National de Santé et de la Recherche Médicale, Corte, France (V. Cicculli. A. Maitre, A. Falchi); Unité des Virus Emergents, Aix Marseille Université, Marseille, France (V. Cicculli, N. Ayhan, X.N. de Lamballerie, R. Charrel); Laboratoire de Recherches sur le Développement de l'Élevage, Institut National de la Recherche pour l'Agriculture, l'Alimentation et l'Environnement, Corte (J.-C. Paoli); Campus International de Baillarguet, Montpellier (L. Vial); Parc Naturel Régionale de Corse, Corte (S. Mondoloni)

DOI: https://doi.org/10.3201/eid2805.211996

The Study

To assess whether CCHFV circulates in Corsica, we collected 8,051 ticks from wild and domestic animals in selected sites on the island during 2016–2020 (Table, Figure). These 8,051 ticks included 7,156 ticks taken from 3,674 domestic animals and 895 ticks taken from 188 wild animals. They consisted of 4,177 *Rhipicephalus bursa* (51.8%), 2,386 *H. marginatum* (29.6%), 839 *Dermacentor marginatus* (10.4%) and 282 *H. scupense* (3.5%) ticks. We identified ticks at the species level by using a pictorial guide and confirmed morphologic identification by using sequencing of mitochondrial 16S rDNA (*5*). We then pooled up to 10 ticks per pool on the basis of developmental stage (nymphs, nonengorged females, and male adults) and host (Table). Pools, containing an average of 2.5 ticks (range 1–10 ticks) were crushed in phosphate-buffered saline with TissueLyser II (QIAGEN, https://www.qiagen.com) at 5,500 rpm for 3 min. We spiked each pool before extraction with a predefined amount of MS2 bacteriophage to monitor the subsequent steps (nucleic acid extraction, reverse transcription, and PCR amplification) and to detect the presence of inhibitors and enzymatic reactions as described (*6*). We performed DNA extraction by using QIAcube HT and a QIAamp cador Pathogen Mini Kit (QIAGEN), according to the manufacturer's instructions. We eluted DNA in 150 µL of buffer and stored at –20°C. We tested each pool for the presence of CCHFV RNA by using a real-time, reverse transcription PCR (*7*) and

the presence of *Nairovirus* RNA by using a pangeneric reverse transcription PCR (*8*).

We detected neither CCHFV RNA nor *Nairovirus* RNA in the 8,051 ticks. The absence of CCHFV or *Nairovirus* RNA was not attributable to technical problems or presence of inhibitors, which were ruled out by MS2 bacteriophage monitoring. Moreover, we detected viral RNA corresponding to new tickborne *Phleboviruses* in 40 samples (5%) and *Flavivirus* in 7 samples (0.9%); these samples remain under investigation, and results will be reported after detailed characterization.

Conclusions

We considered whether CCHFV RNA was not detected because of a low minimum infection rate (MIR) that a larger number of ticks would have been required. We calculated the theoretical power that could be achieved by using the number of ticks obtained in our study. On the basis of an expected CCHFV prevalence (P) of ≈0.2% and a pool size (k) of 2 ticks, a total of 7,676 ticks have to be tested for a prevalence estimation with a 95% CI and a precision (d) set at ±0.001 because the disease prevalence is <0.1 (10%) (*9*). Thus, with a sample of 8,051 ticks, we were able to detect a prevalence of ≥0.2%.

The rate of CCHFV-infected ticks in countries in Europe with enzootic foci ranges from 0.50% to 3.70% among *Hyalomma* spp. ticks (2.8% [44/1,579 *H. lusitanicum* ticks] in Spain, 3.7% [6/161 *H. marginatum* ticks] in Bulgaria, and 0.5% [1/199 *H. marginatum* ticks] in Kosovo) and from 1.5% to 6.2% among *Rhipicephalus* spp. (1.5% [2/123 *R. sanguineus* ticks] in Bulgaria and 6.2% (8/130 *R. bursa* ticks] in Kosovo) (*10*). Other studies conducted outside of Europe have largely reported MIR values >0.2% among ticks: 0.71% in South Africa (1.6% [15/914] *H. truncatum* and 0.2% [2/1,149] *H. rufipes*) (*11*); 2.6% in Mauritania (39/1,517 *Hyalomma* spp.) (*12*); 3.8% (20/525 *Hyalomma* spp.) in Pakistan (*13*); and 51.5% (103/200 *H. marginatum*) in Turkey (*14*). These studies were conducted during the past 5 years using methods comparable to those of our study. The number of *Hyalomma* (n = 2,682) and *Rhipicephalus* (n = 4,177) ticks that we tested are much higher than reported in these previous studies. Therefore, our study would

Table. Ticks collected, by host, number of ticks, and number of tick pools, in a study of Crimean–Congo hemorrhagic fever virus in ticks from wild and domestic animals, Corsica, France, 2016–2020

Host and tick species	No. ticks	No. tick pools
Cattle, n = 1,211		
Rhipicephalus bursa	3,413	818
Hyalomma marginatum	1,343	475
H. scupense	282	96
Boophilus annulatus	130	47
Ixodes ricinus	85	33
H. punctata	14	10
R. sanguineus	96	32
Dermacentor marginatus	2	2
Total	5,365	1,513
Horses, n = 201		
H. marginatum	1,026	247
R. bursa	637	135
R. sanguineus	27	10
Total	1,690	392
Wild boar, n = 182		
D. marginatus	837	222
H. marginatum	13	7
R. bursa	9	6
I. ricinus	13	5
R. sanguineus	1	1
Total	873	241
Sheep, n = 773		
R. bursa	101	93
Total	101	93
Deer, n = 4		
R. bursa	9	4
H. marginatum	4	1
Total	13	5
Mouflon sheep, n = 2		
R. bursa	8	5
I. ricinus	1	1
Total	9	6
Overall	8,051	2,250

have been able to recognize CCHFV presence for a prevalence ≥0.2%, which is 10 times lower than the lowest overall prevalence value reported to date in countries where CCHFV is present: 2.1% (95% CI 1.3%–2.9%) according to a recent meta-analysis (*10*). Furthermore, another study addressing the presence of CCHFV RNA in *Hyalomma* spp. ticks (362 *H. marginatum* and 135 *H. scupense*) and *Rhipicephalus* ticks (n = 518) collected in 2014 from domestic and wild animals in Corsica also provided only negative results (*15*). In all countries where CCHF cases are described, the observed MIR of ticks is ≥2.5 times higher than the detection limit in our study (0.2%). Another argument that strongly supports the contention that the lack of detection of CCHFV or *Nairovirus* RNA was not caused by technical problems is based on the consideration that the protocol used in this study enables the detection of a wide variety of different CCHFV strains, a fact that confirms the accuracy of the results (*7*,*8*).

Recent studies determine whether CCHFV is present in Corsica and to what extent it is a threat for human populations, provide contrasting data. On one hand, tick species that are able to transmit CCHFV are present and widely distributed, and a serologic study based on ELISA screening and neutralization test for confirmation supports the presence of CCHFV or an antigenically related agent. On the other hand, the absence of detection of CCHFV RNA (or an antigenically related agent) in a large number of ticks, together with the absence of a CCHF case, supports the absence of CCHFV in Corsica to date.

In any case, the absence of a documented case of CCHF together with the lack of detection of CCHFV RNA in tick species that are recognized as a competent vector enables us to declare that Corsica is not a hotspot for CCHFV and that the threat to the human population is very limited. However, this discrepant set of data pleads for a One Health approach for dealing with the CCHF question in Corsica and the potential exposure of island population. To do so, the roadmap established by the World Health Organization's R&D blueprint (https://www.who.int/teams/blueprint/about) should be followed. Because the accuracy of CCHFV serologic assays has been questioned, several tests must be combined as advocated. Then, serologic studies in animals and humans must be synchronized with virus detection in ticks and systematic screening of patients with uncharacterized febrile illness during the tick season. A need exists for a large-scale One Health prospective program for surveillance of ticks, vertebrates, and humans in Corsica.

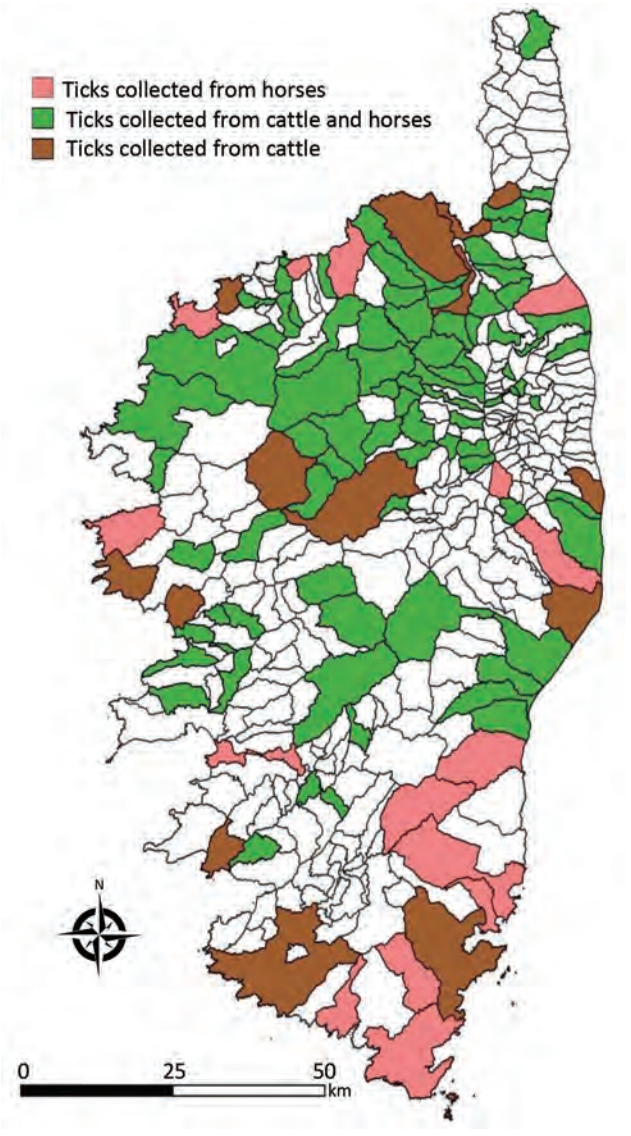

Figure. Locations of tick collection sites (for cattle and horses) for a study of Crimean–Congo Hemorrhagic fever virus in ticks from wild and domestic animals, Corsica, France, 2016–2020.

Acknowledgments

We are grateful to the staff of the slaughterhouse at Ponte-Leccia for their help in collecting ticks from cattle.

This study has been funded in part by the European Virus Archive Global Project, which has received funding from the European Union's Horizon 2020-INFRAIA-2019 research and innovation programme (grant agreement no. 871029) and by the European Union–Cepheid Innovative Medicines Initiative Joint Undertaking (as part of the Viral Haemorrhagic Fever: Modern Approaches For Developing Bedside Rapid Diagnostics [VHFMoDRAD] under grant no. 823666).

About the Author

Mr. Cicculli is a doctoral student at the University of Corsica and Aix-Marseille University. His research interests include the epidemiology of vectorborne pathogens.

References

1. Spengler JR, Bergeron É, Rollin PE. Seroepidemiological studies of Crimean-Congo hemorrhagic fever virus in domestic and wild animals. PLoS Negl Trop Dis. 2016;10:e0004210. https://doi.org/10.1371/journal.pntd.0004210
2. Portillo A, Palomar AM, Santibáñez P, Oteo JA. Epidemiological aspects of Crimean-Congo hemorrhagic fever in Western Europe: what about the future? Microorganisms. 2021;9:649. https://doi.org/10.3390/microorganisms9030649
3. Negredo A, Sánchez-Ledesma M, Llorente F, Pérez-Olmeda M, Belhassen-García M, González-Calle D, et al. Retrospective identification of early autochthonous case of Crimean-Congo hemorrhagic fever, Spain, 2013. Emerg Infect Dis. 2021;27:1754–6. https://doi.org/10.3201/eid2706.204643
4. Grech-Angelini S, Lancelot R, Ferraris O, Peyrefitte CN, Vachiery N, Pédarrieu A, et al. Crimean-Congo hemorrhagic fever virus antibodies among livestock on Corsica, France, 2014–2016. Emerg Infect Dis. 2020;26:1041–4. https://doi.org/10.3201/10.3201/eid2605.191465
5. Cicculli V, Oscar M, Casabianca F, Villechenaud N, Charrel R, de Lamballerie X, et al.; Molecular Detection of Spotted-Fever Group Rickettsiae in ticks collected from domestic and wild animals in Corsica, France. Pathogens. 2019;8:138. https://doi.org/10.3390/pathogens8030138
6. Ninove L, Nougairede A, Gazin C, Thirion L, Delogu I, Zandotti C, et al. RNA and DNA bacteriophages as molecular diagnosis controls in clinical virology: a comprehensive study of more than 45,000 routine PCR tests. PLoS One. 2011;6:e16142. https://doi.org/10.1371/journal.pone.0016142
7. Wölfel R, Paweska JT, Petersen N, Grobbelaar AA, Leman PA, Hewson R, et al. Virus detection and monitoring of viral load in Crimean–Congo hemorrhagic fever virus patients. Emerg Infect Dis. 2007;13:1097–100. https://doi.org/10.3201/eid1307.070068
8. Lambert AJ, Lanciotti RS. Consensus amplification and novel multiplex sequencing method for S segment species identification of 47 viruses of the *Orthobunyavirus*, *Phlebovirus*, and *Nairovirus* genera of the family *Bunyaviridae*. J Clin Microbiol. 2009;47:2398–404. https://doi.org/10.1128/JCM.00182-09
9. Ausvet. Epitools—epidemiological calculators. 2016 [cited 2022 Feb 19]. https://epitools.ausvet.com.au
10. Belobo JTE, Kenmoe S, Kengne-Nde C, Emoh CPD, Bowo-Ngandji A, Tchatchouang S, et al. Worldwide epidemiology of Crimean-Congo Hemorrhagic fever virus in humans, ticks and other animal species, a systematic review and meta-analysis. PLoS Negl Trop Dis. 2021;15:e0009299. https://doi.org/10.1371/journal.pntd.0009299
11. Msimang V, Weyer J, le Roux C, Kemp A, Burt FJ, Tempia S, et al. Risk factors associated with exposure to Crimean-Congo haemorrhagic fever virus in animal workers and cattle, and molecular detection in ticks, South Africa. PLoS Negl Trop Dis. 2021;15:e0009384. https://doi.org/10.1371/journal.pntd.0009384
12. Schulz A, Barry Y, Stoek F, Pickin MJ, Ba A, Chitimia-Dobler L, et al. Detection of Crimean-Congo hemorrhagic fever virus in blood-fed *Hyalomma* ticks collected from Mauritanian livestock. Parasit Vectors. 2021;14:342. https://doi.org/10.1186/s13071-021-04819-x
13. Kasi KK, von Arnim F, Schulz A, Rehman A, Chudhary A, Oneeb M, et al. Crimean-Congo haemorrhagic fever virus in ticks collected from livestock in Balochistan, Pakistan. Transbound Emerg Dis. 2020;67:1543–52. https://doi.org/10.1111/tbed.13488
14. Akyildiz G, Bente D, Keles AG, Vatansever Z, Kar S. High prevalence and different genotypes of Crimean-Congo hemorrhagic fever virus genome in questing unfed adult *Hyalomma marginatum* in Thrace, Turkey. Ticks Tick Borne Dis. 2021;12:101622. https://doi.org/10.1016/j.ttbdis.2020.101622
15. Grech-Angelini S, Stachurski F, Vayssier-Taussat M, Devillers E, Casabianca F, Lancelot R, et al. Tick-borne pathogens in ticks (Acari: Ixodidae) collected from various domestic and wild hosts in Corsica (France), a Mediterranean island environment. Transbound Emerg Dis. 2020;67:745–57. https://doi.org/10.1111/tbed.13393

Address for correspondence: Vincent Cicculli, Laboratoire de virologie, UR7310 Université de Corse, 20250, Corte, France; email: cicculli_v@univ-corse.fr

Highly Pathogenic Avian Influenza A(H5N8) Clade 2.3.4.4b Viruses in Satellite-Tracked Wild Ducks, Ningxia, China, 2020

Xinru Lv,[1] Xiang Li,[1] Heting Sun,[1] Yi Li,[1] Peng Peng, Siyuan Qin, Weidong Wang, Yuecheng Li, Qing An, Tian Fu, Fengyi Qu, Qiuzi Xu, Rongxiu Qin, Zhenliang Zhao, Meixi Wang, Yulong Wang, Yajun Wang, Xiangwei Zeng, Zhijun Hou, Chengliang Lei, Dong Chu, Yanbing Li, Hongliang Chai

During October 2020, we identified 13 highly pathogenic avian influenza A(H5N8) clade 2.3.4.4b viruses from wild ducks in Ningxia, China. These viruses were genetically related to H5N8 viruses circulating mainly in poultry in Europe during early 2020. We also determined movements of H5N8 virus–infected wild ducks and evidence for spreading of viruses.

A novel reassortant highly pathogenic avian influenza (HPAI) A(H5N8) virus belonging to clade 2.3.4.4 was detected in poultry and wild birds in South Korea during January 2014 (*1*) and spread rapidly by migration of wild birds to Asia, Europe, and North America (*2*). Clade 2.3.4.4 HPAI H5N8 viruses caused additional influenza outbreaks worldwide during 2016 and continued circulating in birds in Asia, Europe, and Africa (*3*–*5*).

In October 2020, clade 2.3.4.4b HPAI H5N8 viruses were detected in wild swans in China (*6*). A clade 2.3.4.4b H5N8 virus infection in humans was reported in Russia during December 2020, indicating a possible increased risk for these viruses crossing species barriers (*7*). In this study, we investigated the emergence of HPAI H5N8 viruses in wild ducks in Ningxia, in western China, during October 2020 and performed satellite tracking to determine the flyways of wild ducks.

Author affiliations: Northeast Forestry University College of Wildlife and Protected Area, Harbin, China (X. Lv, X. Li, Yi Li, Q. An, T. Fu, F. Qu, Q. Xu, R. Qin, Z. Zhao, M. Wang, Yulong Wang, Yajun Wang, X. Zeng, Z. Hou, H. Chai); National Forestry and Grassland Administration, Shenyang, China (H. Sun, P. Peng, S. Qin, C. Lei, D. Chu); Monitoring Center for Terrestrial Wildlife Epidemic Diseases, Yinchuan, China (W. Wang, Yuecheng Li); Harbin Veterinary Research Institute, Harbin (Yanbing Li)

DOI: https://doi.org/10.3201/eid2805.211580

The Study

Ningxia, located at the intersection of the Central Asian and East Asian-Australasian Flyways, is an ideal location for influenza surveillance. We collected 275 paired oropharyngeal and cloacal swab specimens from net-caught wild ducks at the Changshantou Reservoir in Ningxia (37°16′14″N, 105°43′5″E) during October 2020. We inoculated all samples into 10-day-old, embryonated, specific pathogen–free chicken eggs for virus isolation. Thirteen samples were positive for H5N8 subtype avian influenza virus (AIV) by reverse transcription PCR. We sequenced full-length genomes and submitted them to the GISAID EpiFlu database (https://www.gisaid.org) (Appendix Table 1, https://wwwnc.cdc.gov/EID/article/28/5/21-1580-App1.pdf).

We attached solar-powered global positioning system satellite trackers to 12 apparently healthy mallards (*Anas platyrhynchos*) at the capture site and released the birds immediately. We successfully obtained movement tracks for 9 mallards to identify their wintering and stopover sites. We isolated H5N8 viruses from 2 of the satellite-tracked mallards (birds NX-175 and NX-176), but the remaining 7 mallards were negative for AIV (Figure; Appendix Table 2, Figures 1, 2).

All H5N8 isolates were identified as HPAIVs by the amino acid sequence REKRRKR/GLF at the hemagglutinin (HA) cleavage site. H5 phylogenetic analysis classified Ningxia isolates into clade 2.3.4.4b and divided them into 2 distinct groups according to tree topology (Appendix Figure 3). Most isolates (n = 12) shared high nucleotide identities in 8 gene segments (99.6%–100%) with viruses responsible for disease outbreaks in poultry in Europe during early 2020; these segments were closely related to H5N8 viruses

[1]These authors contributed equally to this article

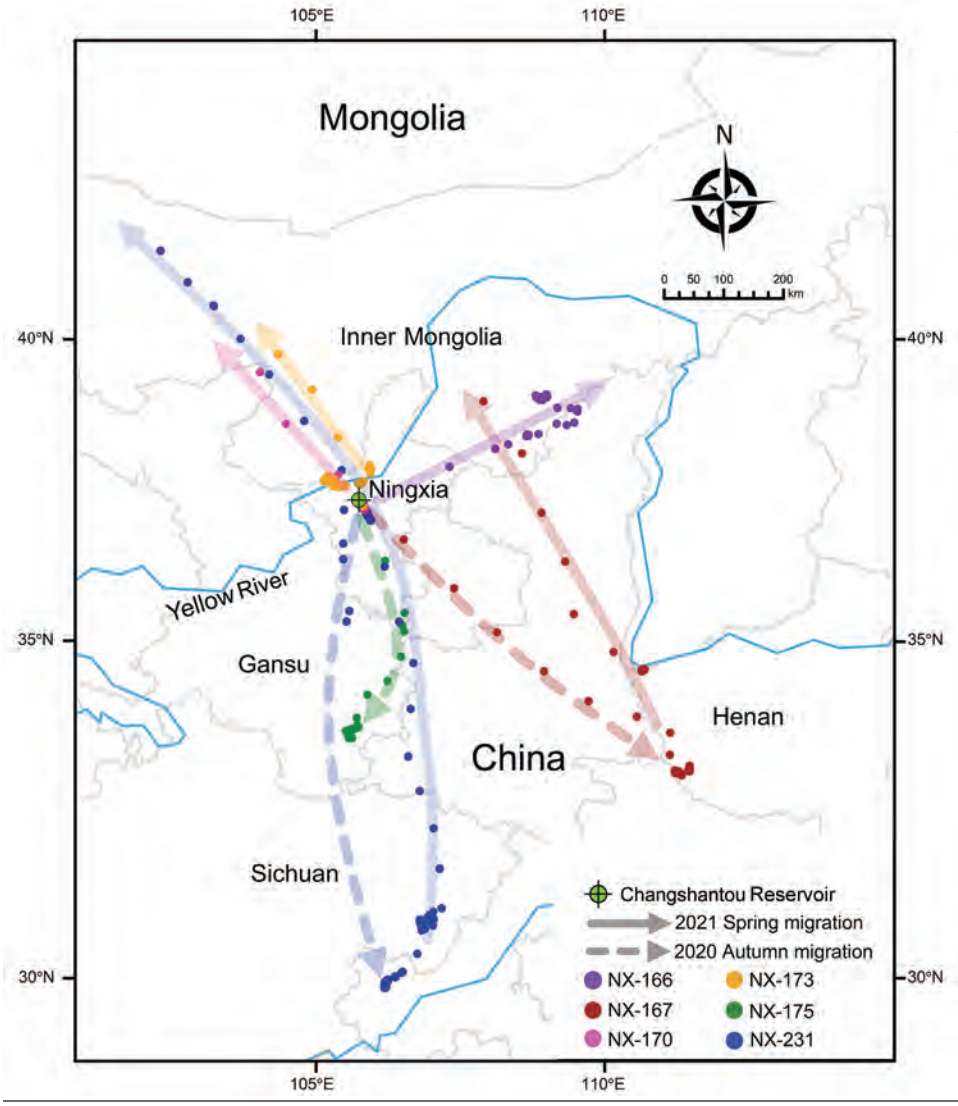

Figure. Migratory routes of 6 of 9 successfully satellite-tracked mallards infected with highly pathogenic avian influenza A(H5N8) clade 2.3.4.4b viruses, Ningxia, China, 2020. Mallards are indicated by different colors. The sampling site (Changshantou Reservoir) is indicated. Solid and dashed lines indicate spring migration in 2021 and autumn migration in 2020, respectively. Because the other 3 successfully satellite-tracked mallards (birds NX-169, NX-174, and NX-176) had been moving around the sampling point, their movements are not shown.

from South Korea and Japan, isolated in October and November 2020 and recognized as subclade 2.3.4.4b1, (Appendix Table 3). The remaining isolate, A/common teal/Ningxia/105/2020(H5N8) (from mallard NX-105), clustered with HPAI H5 viruses that were prevalent in Eurasia in autumn 2020 and recognized as subclade 2.3.4.4b2. A similar tree topology was shown in all 8 segments of Ningxia virus isolates (Appendix Figure 4). Mallard isolate NX-105 and the human isolate A/Astrakhan/3212/2020(H5N8) (human H5N8) from Russia had relatively high nucleotide identities of 99.2%–99.8% in 8 gene segments.

Bayesian phylogenetic analysis showed that the most recent common ancestor of the genome of isolate NX-105 and its neighbor strains emerged during June–October 2020. Ningxia b1 isolates emerged during August–September 2020, and East Asian lineage (b1 viruses including Ningxia subclade 2.3.4.4b1 isolates, strains from Japan and South Korea) emerged at the genome level during May–August 2020 (Appendix Table 4, Figure 5).

Several amino acid mutations in the HA protein (H5 numbering) were associated with increased binding to human–like receptor (α–2,6–sialic acid) (*8*–*11*). Both Ningxia H5N8 isolates and the human H5N8 isolate from Russia had the S133A and T156A mutations, and isolate NX-105 had extra T188I and V210I substitutions, suggesting that this isolate might be more adaptable at infecting humans than the human H5N8 virus. All isolates lacked the Q222L and G224S mutations in the HA protein, including the human H5N8 virus, and lacked the mammalian adaptation markers Q591K, E627K, and D701N mutations in the polymerase basic 2 protein (*12*). Both Ningxia H5N8 isolates and the human H5N8 virus also had other molecular markers associated with

increased virulence and transmission among mammals (Appendix Table 5).

Satellite tracking showed that 2 mallards (NX-167, negative for AIV, and NX-175, infected with H5N8 virus) migrated to the wintering ground without a long duration in Ningxia. Mallard NX-167 flew directly to Henan at a high speed (82.1–116.2 km/h). In contrast, mallard NX-175 showed a greatly decreased speed (34.1–61.8 km/h) after a short stopover at the junction of Ningxia and Gansu, and eventually reached Gansu (Appendix Figure 1). Another H5N8-infected mallard (NX-176) had been moving around the sampling site until we lost the tracking signals on December 25, 2020 (Appendix Figure 2). These results indicated that mallards could continue to migrate after being infected with HPAI H5N8 viruses, but their movements would be affected.

Conclusions

Previous studies have demonstrated a key role for wild waterfowl in the continental transmission of HPAIVs (*13*). In this study, we inferred that H5N8 viruses emerging in Ningxia were likely to be transmitted by migration of infected wild ducks. H5N8 virus outbreaks occurred in the poultry industry in Europe during spring 2020, and the responsible viruses might have been introduced into the wild-bird gene pool through contact with infected poultry (*14*). Wild ducks are short-distance migratory birds, which generally find it difficult to migrate directly from Europe to eastern Asia. Strains from eastern Asia had high nucleotide identity (99.3%–100%) at the genome level, indicating that subclade 2.3.4.4b1 H5N8 viruses might be maintained at common breeding and stopover sites of wild ducks that winter in China, Japan, and South Korea.

The long branch lengths for all segments of the East Asian lineage compared with those for strains from Europe suggested that the virus had been circulating undetected for the intervening period and seemed to have a common ancestor from older viruses during early 2020 or 2019 (Appendix Figure 4). A previous study of the origin of clade 2.3.4.4b HPAI H5N6 viruses isolated in wild ducks in Ningxia in 2017 indicated a similar transmission pattern (*15*). In addition, isolate NX-105 showed an extremely close phylogenetic relationship with the 2020 isolates from Russia (Appendix Figure 4), which also seemed to be transmitted to China by migratory wild ducks.

The movement of mallard NX-175 proved that mallards infected with HPAI H5N8 viruses could continue to migrate, resulting in potential wide spreading of HPAI H5N8 viruses (Appendix Figure 1). Satellite tracking showed that continuous and stable tracking signals for 3 mallards (NX-170, NX-173, and NX-231) migrating northward during April 2021 were suddenly lost during a high-speed flight in Inner Mongolia (Figure). Assuming no damage to the transmitters, we inferred that these 3 mallards had already flown out of China for breeding, and we will therefore not receive additional signals from overseas until the birds return to China during their autumn migration. Further satellite tracking studies are being performed to determine the breeding and stopover grounds in northern Ningxia, China, as essential means of tracing the origins of AIVs and providing future early warnings for these viruses.

Ningxia H5N8 virus isolates showed highly similar mutations to those of human H5N8 viruses, and isolate NX-105 is highly homologous at the genome level, indicating that wild duck–origin viruses could pose an increased threat to public health. Long-term surveillance of wild bird–origin AIVs and international collaboration in AIV monitoring of migratory birds will help support early warning for influenza epidemics.

Acknowledgments

We thank the authors and submitting laboratories for providing sequences to the GISAID EpiFlu Database and International Science Editing (http://www.international-scienceediting.com) for editing the manuscript.

This study was supported by the National Natural Science Foundation of China (grant 31970501) and the National Forestry and Grassland Administration.

About the Author

Ms. Lv is a graduate student at Northeast Forestry University, College of Wildlife and Protected Area, Harbin, China. Her primary research interest is the epidemiology of influenza viruses in wild birds.

References

1. Lee YJ, Kang HM, Lee EK, Song BM, Jeong J, Kwon YK, et al. Novel reassortant influenza A(H5N8) viruses, South Korea, 2014. Emerg Infect Dis. 2014;20:1087–9. https://doi.org/10.3201/eid2006.140233
2. Verhagen JH, Herfst S, Fouchier RA. Infectious disease. How a virus travels the world. Science. 2015;347:616–7. https://doi.org/10.1126/science.aaa6724
3. Li M, Liu H, Bi Y, Sun J, Wong G, Liu D, et al. Highly pathogenic avian influenza A(H5N8) virus in wild migratory birds, Qinghai Lake, China. Emerg Infect Dis. 2017;23:637–41. https://doi.org/10.3201/eid2304.161866
4. Alarcon P, Brouwer A, Venkatesh D, Duncan D, Dovas CI, Georgiades G, et al. Comparison of 2016–17 and previous

epizootics of highly pathogenic avian influenza H5 Guangdong lineage in Europe. Emerg Infect Dis. 2018;24:2270–83. https://doi.org/10.3201/eid2412.171860
5. Selim AA, Erfan AM, Hagag N, Zanaty A, Samir AH, Samy M, et al. Highly pathogenic avian influenza virus (H5N8) clade 2.3.4.4 infection in migratory birds, Egypt. Emerg Infect Dis. 2017;23:1048–51. https://doi.org/10.3201/eid2306.162056
6. Li X, Lv X, Li Y, Peng P, Zhou R, Qin S, et al. Highly pathogenic avian influenza A(H5N8) virus in swans, China, 2020. Emerg Infect Dis. 2021;27:1732–4. https://doi.org/10.3201/eid2706.204727
7. Pyankova OG, Susloparov IM, Moiseeva AA, Kolosova NP, Onkhonova GS, Danilenko AV, et al. Isolation of clade 2.3.4.4b A(H5N8), a highly pathogenic avian influenza virus, from a worker during an outbreak on a poultry farm, Russia, December 2020. Euro Surveill. 2021;26. https://doi.org/10.2807/1560-7917.ES.2021.26.24.2100439
8. Yang ZY, Wei CJ, Kong WP, Wu L, Xu L, Smith DF, et al. Immunization by avian H5 influenza hemagglutinin mutants with altered receptor binding specificity. Science. 2007;317:825–8. https://doi.org/10.1126/science.1135165
9. Wang W, Lu B, Zhou H, Suguitan AL Jr, Cheng X, Subbarao K, et al. Glycosylation at 158N of the hemagglutinin protein and receptor binding specificity synergistically affect the antigenicity and immunogenicity of a live attenuated H5N1 A/Vietnam/1203/2004 vaccine virus in ferrets. J Virol. 2010;84:6570–7. https://doi.org/10.1128/JVI.00221-10
10. Watanabe Y, Ibrahim MS, Ellakany HF, Kawashita N, Mizuike R, Hiramatsu H, et al. Acquisition of human-type receptor binding specificity by new H5N1 influenza virus sublineages during their emergence in birds in Egypt. PLoS Pathog. 2011;7:e1002068. https://doi.org/10.1371/journal.ppat.1002068
11. Chutinimitkul S, van Riel D, Munster VJ, van den Brand JM, Rimmelzwaan GF, Kuiken T, et al. In vitro assessment of attachment pattern and replication efficiency of H5N1 influenza A viruses with altered receptor specificity. J Virol. 2010;84:6825–33. https://doi.org/10.1128/JVI.02737-09
12. Yamada S, Hatta M, Staker BL, Watanabe S, Imai M, Shinya K, et al. Biological and structural characterization of a host-adapting amino acid in influenza virus. PLoS Pathog. 2010;6:e1001034. https://doi.org/10.1371/journal.ppat.1001034
13. Global Consortium for H5N8 and Related Influenza Viruses. Role for migratory wild birds in the global spread of avian influenza H5N8. Science. 2016;354:213–7. https://doi.org/10.1126/science.aaf8852
14. Lewis NS, Banyard AC, Whittard E, Karibayev T, Al Kafagi T, Chvala I, et al. Emergence and spread of novel H5N8, H5N5 and H5N1 clade 2.3.4.4 highly pathogenic avian influenza in 2020. Emerg Microbes Infect. 2021;10:148–51. https://doi.org/10.1080/22221751.2021.1872355
15. Sun J, Zhao L, Li X, Meng W, Chu D, Yang X, et al. Novel H5N6 avian influenza virus reassortants with European H5N8 isolated in migratory birds, China. Transbound Emerg Dis. 2020;67:648–60. https://doi.org/10.1111/tbed.13380

Address for correspondence: Hongliang Chai, Northeast Forestry University, College of Wildlife and Protected Area, NO.26 Hexing Rd, Xiangfang District, Harbin 150040, Heilongjiang, China; email: hongliang_chai@hotmail.com

Novel Hendra Virus Variant Circulating in Black Flying Foxes and Grey-Headed Flying Foxes, Australia

Alison J. Peel,[1] Claude Kwe Yinda,[1] Edward J. Annand, Adrienne S. Dale, Peggy Eby, John-Sebastian Eden, Devin N. Jones, Maureen K. Kessler, Tamika J. Lunn, Tim Pearson, Jonathan E. Schulz, Ina L. Smith, Vincent J. Munster,[2] Raina K. Plowright[2]; Bat One Health Group[3]

A novel Hendra virus variant, genotype 2, was recently discovered in a horse that died after acute illness and in *Pteropus* flying fox tissues in Australia. We detected the variant in flying fox urine, the pathway relevant for spillover, supporting an expanded geographic range of Hendra virus risk to horses and humans.

Hendra virus (HeV; genus *Henipavirus*, family *Paramyxoviridae*) is a well-characterised zoonotic pathogen endemic to *Pteropus* spp. bats (flying foxes) in Australia. Spillover from bats to horses has been detected 65 times; 4 of 7 persons infected from horses have died (*1*). Quantitative reverse-transcription PCR (qRT-PCR) (*2*) is a tool used for surveillance and priority disease investigation in bats and horses (*3*,*4*). The high specificity of assays limits detection to a narrow range of genotypic diversity, meaning that divergent variants might remain undetected (*3*).

In October 2021, spillover of a novel variant, HeV genotype 2 (HeV-g2), resulted in the death of a horse in New South Wales (NSW), Australia, farther south than HeV had previously been detected in horses (*5*). This spillover was detected only because diagnostic assays had been recently updated after retrospective discovery of HeV-g2 in a horse that exhibited signs of HeV disease in 2015 but tested negative through routine screening at that time (*3*). Discovery of HeV-g2 in this horse arose using broad panparamyxovirus PCRs (*6*), followed by next-generation sequencing and virus isolation. The variant showed 84% pairwise nucleotide identity genome-wide to prototype HeV (HeV-g1), and 99% similarity with partial sequences recovered from tissue samples from a grey-headed flying fox, *P. poliocephalus* (*7*). Bats submitted for lyssavirus diagnostics were opportunistically screened using an updated quantitative PCR specific for HeV-g2, which resulted in additional positive detections in tissue collected from *P. poliocephalus* in 2019–2021 and a little red flying fox (*P. scapulatus*) in 2015 (*7*).

Although HeV-g1 has been detected in tissues from all 4 flying fox species in continental Australia, excretion of the virus has been confirmed only in the black flying fox (*P. alecto*) and the spectacled flying fox (*P. conspicillatus*), suggesting these species are sources of transmission to horses (*8*,*9*). Sequence mismatches between HeV-g1 and HeV-g2 mean that PCR assays used in previous surveillance of reservoir hosts would not have detected the novel HeV-g2. To address this gap, we used a new qRT-PCR (*3*) to screen banked flying fox urine samples collected over a large extent of space and time.

Author affiliations: Griffith University Centre for Planetary Health and Food Security, Nathan, Queensland, Australia (A.J. Peel, P. Eby, T.J. Lunn); National Institutes of Health, Hamilton, Montana, USA (C.K. Yinda, J.E. Schulz, V.J. Munster); EquiEpiVet, Aireys Inlet, Victoria, Australia (E.J. Annand); Department of Agriculture, Water, and the Environment, Canberra, Australian Capital Territory, Australia (E.J. Annand); University of Sydney, Sydney, New South Wales, Australia (E.J. Annand, J.-S. Eden); Texas Tech University, Lubbock, Texas, USA (A.S. Dale); University of New South Wales, Sydney (P. Eby); Montana State University, Bozeman, Montana, USA (D.N. Jones, M.K. Kessler, R.K. Plowright); Bellingen, New South Wales, Australia (T. Pearson); CSIRO, Black Mountain, Australian Capital Territory, Australia (I.L. Smith)

DOI: https://doi.org/10.3201/eid2805.212338

[1]These authors contributed equally to this article.

[2]These senior authors contributed equally to this article.

[3]Members of Bat One Health are listed at the end of this article.

The Study

We collected pooled urine samples from plastic sheets placed underneath flying fox roosts in southeastern Queensland and mid- to north-coast NSW during December 2016–September 2020 (Figure). We placed sheets in areas of the roost where *P. alecto* flying foxes were roosting, although other species were often also present. We recorded the number and species of bats immediately above the sheets. We also captured individual bats in mist nests; recorded species, sex, and age class; then collected urine samples directly from each anaesthetised bat or from a urine collection bag attached to its holding bag. Shortly after collection, we placed samples into viral lysis buffer, virus transport media, or an empty cryovial and stored them at −80°C (Appendix, https://wwwnc.cdc.gov/EID/article/28/5/21-2338-App1.pdf).

We used the QIAamp Viral RNA Kit using a QIAcube HT automated system (QIAGEN, https://www.qiagen.com) to extract RNA, then eluted it in 150 μL of TE buffer and first screened it for HeV-g1 using a qRT-PCR assay targeting the P gene (Table 1). We stored extracted RNA at −80°C and then screened it for HeV-g2 using the new multiplexed qRT-PCR assay, targeting the M gene with primers specific for HeV-g1 and HeV-g2 (*2*,*3*) (Table 1; Appendix). We used 10-fold dilutions with a known number of genome copies to construct a standard curve, calculate copy numbers/mL, and estimate limit of detection. We amplified the partial cytochrome *b* gene from all positive samples (*10*,*11*) (Table 1) and confirmed host species identity based on sequence identity across 402-bp sequences (Appendix).

We screened 4,539 pooled urine samples collected from 129 underroost sampling sessions and 1,674 urine samples collected from individual bats over 39 catching sessions during July 2017–September 2020 (Appendix Tables 1, 2). Eight pooled urine samples and 2 samples from individual flying foxes tested positive for HeV-g2 (Table 2). Positive samples were from Sunnybank in Queensland and Clunes, Lismore, Dorroughby, Maclean, and Nambucca Heads in NSW.

We detected HeV-g2 in samples collected across all seasons. Prevalence in sessions with positive detections ranged from 2.5% to 6.5% (95% CI 0.1%–22.8%). In pooled samples, HeV-g2 was only detected in sessions when HeV-g1 was also detected (HeV-g1 prevalence range 2.5%–50.1%); however, we found no statistically significant correlation between HeV-g1 and HeV-g2 prevalence (Pearson correlation analysis ρ = 0.09; p = 0.87). Most (8/10) of the HeV-g2–positive samples had low genome copies, but 2, ARSUN015_15_1 and ARLIS002_55_1, had considerably higher copy numbers (Table 2).

Individual flying foxes that tested positive included a *P. poliocephalus* juvenile female captured in

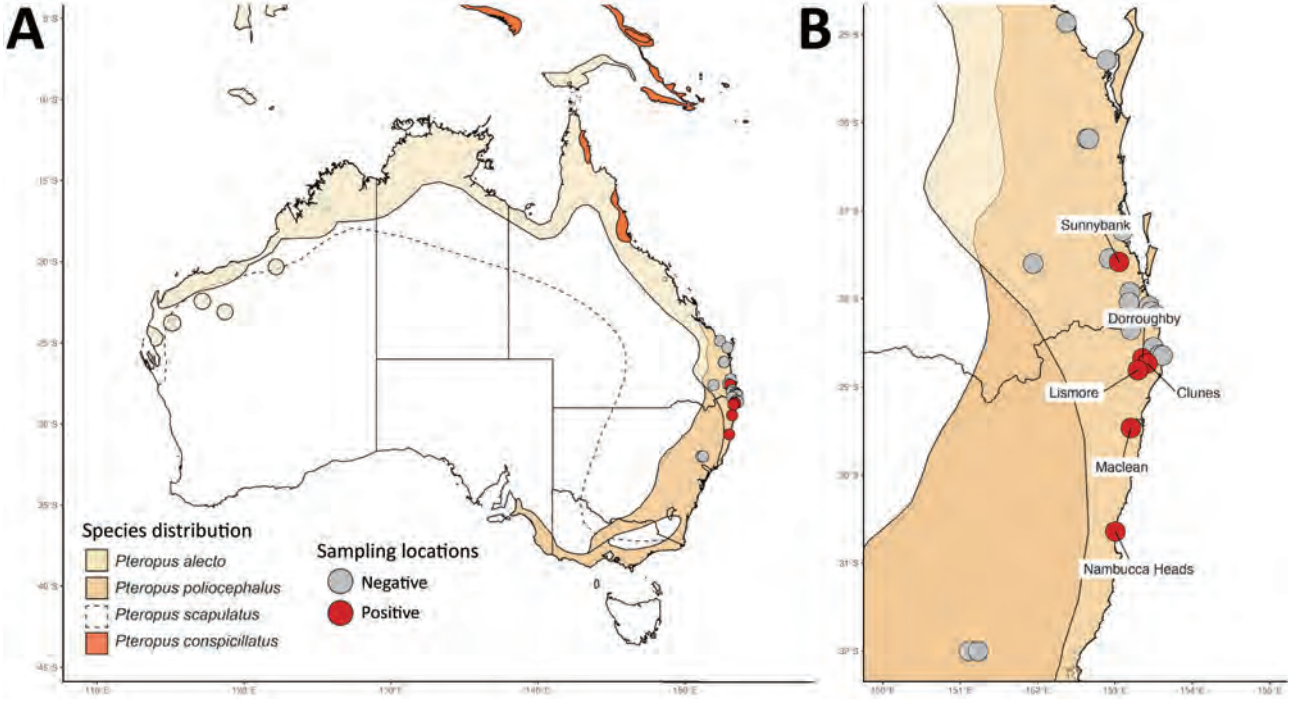

Figure. Distribution of flying fox species in Australia (*13*) and sampling locations for study of HeV variant circulating in flying foxes in southeastern Queensland and mid- to north-coast New South Wales, December 2016–September 2020. A) Locations in Australia; B) locations in study area. HeV, Hendra virus; HeV-g2, HeV genotype 2.

Table 1. Primers and probes used in PCR for study of novel Hendra virus variant circulating in black and grey-headed flying foxes, Australia*

Target	Primers and Probes	Reference
HeV-g1 P gene	F: 5′-CCCAACCAAGAAAGCAAGAG R: 5′-TTCATTCCTCGTGACAGCAC P: 5′-TTACTGCGGAGAATGTCCAACTGAGTG	This study
HeV-g1 M gene	F: 5′-CTTCGACAAAGACGGAACCAA R: 5′ TGGCATCTTTCATGCTCCATCTCGG P: 5′ CCAGCTCGTCGGACAAAATT	(*2*)
HeV-g2 M gene	F: 5′ TCTCGACAAGGACGGAGCTAA R: 5′ CCGGCTCGTCGAACAAAATT P: 5′ TGGCATCCTTCATGCTTCACCTTGG	(*3*)
Partial cytochrome b gene	F: 5′-CGAAGCTTGATATGAAAAACCATCGTTG R: 5′ AACTGCAGCCCCTCAGAATGATATTTGTCCTCA	(*10*,*11*)

*F, forward; R, reverse; P, probe.

Maclean, NSW, and a *P. alecto* adult male captured in Clunes, NSW (Appendix Table 3). We detected HeV-g2 in pooled samples from mixed-species roosts containing *P. alecto* and *P. poliocephalus* flying foxes. Cytochrome b sequencing identified DNA from *P. alecto* flying foxes in 6/8 positive underroost samples and from *P. poliocephalus* flying foxes in 2/8 (Table 2).

Conclusions

Urine is the route of HeV excretion from flying foxes and the source of virus transmission to horses. Detecting the novel Hendra variant HeV-g2 in the urine of flying foxes helped identify its distribution range, associated host species, transmission dynamics, and spillover risk. We show evidence that *P. alecto* and *P. poliocephalus* flying foxes excrete HeV-g2 in urine and both are likely competent reservoir hosts. We did not screen urine samples from *P. conspicillatus* or *P. scapulatus* flying foxes, so the potential of these species to excrete HeV-g2 in urine remains unconfirmed.

Although HeV-g1 has been detected in flying fox urine samples collected across all seasons, prevalence peaks in winter in subtropical regions (*4*,*12*), which is consistent with our preliminary HeV-g2 seasonality findings (5/8 detections in late May–late August) in the study area. The significantly lower prevalence of HeV-g2 than HeV-g1 could indicate actual lower prevalence in the sampled population. Alternatively, repeated freeze-thaw cycles in our samples or the bias toward collecting *P. alecto* urine in our sampling design might have led to lower detection. Tissue samples from flying foxes submitted for lyssavirus

Table 2. Details of urine samples collected from *Pteropus alecto* and *P. poliocephalus* flying foxes in underroost sampling sessions that tested positive for HeV-g2 and associated session-level prevalence for HeV-g1 and HeV-g2, Australia*

		HeV-g2		HeV-g1					
Site	Date	No. positive/ total	Prevalence, % (95% CI)	No. positive/ total	Prevalence, % (95% CI)	Sample ID	RNA copies/ mL†	Species recorded‡	*Cyt b* species§
Clunes, NSW	2019 Jul 27	1/36	2.8 (0.1–16.2)	0/36	0.0 (0–12.0)	ACMAC001_35_1	169	*Pa*	*Pa*
Maclean, NSW	2018 Jul 9	1/36	2.8 (0.1–16.2)	0/36	0.0 (0–12.0)	ACCLU004_22_1F	225	*Pp*	*Pp*
Clunes, NSW	2017 Aug 8	1/36	2.8 (0.1–16.2)	5/36	13.9 (5.2–30.3)	ACMAC001_35_1	174	2 *Pa*; 0 *Pp*	*Pa*
Clunes, NSW	2018 Nov 1	2/51	3.9 (0.7–14.6)	4/51	7.8 (2.5–19.7)	ARCLU002_14_1	38	0 *Pa*; 2 *Pp*	Mixed *Pp/Pa*
						ARCLU010_22_1	17	1 *Pa*; 2 *Pp*	*Pa*
Lismore, NSW	2017 Aug 27	1/48	2.1 (0.1–12.5)	21/48	43.8 (29.8–58.7)	ARCLU010_26_1	783	4 *Pa*; 0 *Pp*	NA
Nambucca Heads, NSW	2018 May 20	2/31	6.5 (1.1–22.8)	8/31	25.8 (12.5–50.1)	ARLIS002_55_1	67	0 *Pa*; 2 *Pp*	*Pa*
						ARNAM005_2_1	15	4 *Pa*; 0 *Pp*	*Pa*
Sunnybank, QLD	2018 Nov 26	1/36	2.8 (0.1–16.2)	1/36	2.8 (0.1–16.2)	ARNAM005_12_1	381,123	0 *Pa*; 4 *Pp*	*Pp*
Dorroughby, NSW	2016 Dec 16	1/18	2.5 (0.01–14.7)	1/18	2.5 (0.01–14.7)	ARSUN015_15_1	58	NR	*Pa*

**Cyt b, Cytochrome b*; HeV, Hendra virus; NSW, New South Wales; *Pa*, *P. alecto*; *Pp*, *P. poliocephalus*; QLD, Queensland; NA, not available; NR, not recorded.
†HeV-g2 viral copies/mL: the minimum copy number which would be expected to reliably give a positive PCR result in all replicates in the quantitative reverse transcription PCR assay (the limit of detection) was 5–10 copies per reaction (≈1,070–2,140 copies/mL).
‡For underroost samples, the number of flying foxes recorded by species (*P. alecto* or *P. poliocephalus*) at the time of sampling might not precisely reflect the proportion of urine collected from each species.
§Appendix Table 3 (https://wwwnc.cdc.gov/EID/article/28/5/21-2338-App1.pdf).

testing after contact with humans or pets showed higher HeV-g2 prevalence than our samples from wild populations (*7*), which might reflect higher prevalence in sick or stressed bats or geographical differences. HeV-g2 was previously detected in tissue samples from South Australia (3 positives from 4 samples), Victoria (7/64), and Western Australia (1/2) (*7*). Our findings extend the known distributional range of HeV-g2 to southeastern Queensland and mid- to north-coast NSW, areas proximate to the 2 known cases of HeV-g2 spillover to horses (*3*,*5*).

Our findings support expanding the expected geographic risk area for HeV spillover to include the distribution of *P. poliocephalus* flying foxes. Screening flying fox urine samples from a broader geographic range, including regions where *P. alecto* flying foxes are absent, should better inform epidemiologic relationships and relative prevalence of HeV variants. Given that data on the true diversity of HeV and related viruses in flying fox populations are incomplete, unbiased or *Paramyxoviridae* family–level viral surveillance in reservoir and spillover hosts might identify further variants. Developing a panel of diagnostic tools to detect a more comprehensive range of the viruses capable of spillover would substantially advance our ability to forecast spillover risk, manage biosecurity, and provide guidance to horse owners, veterinarians, and other stakeholders.

Bat One Health group members: Mandy Allonby, Remy Brooks, Liam Chirio, Caylee A. Falvo, Hamish McCallum, Ticha Padgett-Stewart, Manuel Ruiz-Aravena, Kirk A. Silas, and Rachael Smethurst.

Acknowledgments

We acknowledge the Bundjalung, Butchulla, Danggan Balun, Gomeroi, Gumbainggir, Kabi Kabi, Taribelang Bunda, Turrbal, Widjabul Wia-bal, Yugambeh, and Yuggera Ugarapul people, who are the traditional custodians of the land upon which this work was conducted. We also thank government and private landholders for granting permission for fieldwork and broader team members and volunteers for their contributions: Liam McGuire, Wyatt Madden, Justine Scaccia, Denise Karkkainen, Cara Parsons, Ariane Ananda, Emma Glennon, Emily Stanford, Jessica Mitchell, Eloise Stephenson, Kerryn Parry-Jones, Anja Divljan, Cinthia Pietromonaco, and other volunteers. We thank Allan Grolla for the design of the HeV assay and Paul Oliver for input on interpretation of cytochrome b sequencing data.

The project was supported by an NSF Coupled Dynamics of Natural and Human Systems grant DEB1716698, funding from the Defense Advanced Research Projects Agency administered through Cooperative Agreement D18AC00031-PREEMPT and support from the Intramural Research Program of the National Institute of Allergy and Infectious Diseases, National Institutes of Health. A.J.P. was supported by an ARC DECRA fellowship (DE190100710). R.K.P. was supported by the USDA National Institute of Food and Agriculture (Hatch project 1015891). E.J.A., J.S.E., and I.L.S. were supported by the Australian Government Department of Agriculture, Water and the Environment, Biosecurity Innovation Project 2020–21 Project ID 202043, Metagenomic Investigation of Horses as Sentinels.

About the Authors

Dr. Peel is a DECRA senior research fellow at Griffith University in Brisbane, Queensland, Australia. Her primary interests lie in the role of landscape change and anthropogenic influence on the dynamics and drivers of infectious disease in bats. Dr. Yinda is a postdoctoral research fellow at the Virus Ecology Section of the Rocky Mountains Laboratories, National Institute of Allergy and Infectious Diseases, National Institutes of Health. He is interested in pathogen discovery of emerging viruses, and their cross-species transmissions and disease potential.

References

1. Playford EG, McCall B, Smith G, Slinko V, Allen G, Smith I, et al. Human Hendra virus encephalitis associated with equine outbreak, Australia, 2008. Emerg Infect Dis. 2010;16:219–23. https://doi.org/10.3201/eid1602.090552
2. Smith IL, Halpin K, Warrilow D, Smith GA. Development of a fluorogenic RT-PCR assay (TaqMan) for the detection of Hendra virus. J Virol Methods. 2001;98:33–40. https://doi.org/10.1016/S0166-0934(01)00354-8
3. Annand EJ, Horsburgh BA, Xu K, Reid PA, Poole B, de Kantzow MC, et al. Novel Hendra virus variant detected by sentinel surveillance of Australian horses. Emerg Infect Dis. 2022;28:693–704. https://doi.org/10.3201/eid2803.211245
4. Field HE, Jordan D, Edson D, Morris S, Melville D, Parry-Jones K, et al. Spatiotemporal aspects of Hendra virus infection in pteropid bats (flying-foxes) in eastern Australia. Plos One. 2015;10:e0144055. https://doi.org/10.1371/journal.pone.0144055
5. ProMED. Hendra virus spillover [cited 2021 Oct 20]. https://promedmail.org, archive no. 8699079.
6. Tong S, Chern S-WW, Li Y, Pallansch MA, Anderson LJ. Sensitive and broadly reactive reverse transcription-PCR assays to detect novel paramyxoviruses. J Clin Microbiol. 2008;46:2652–8. https://doi.org/10.1128/JCM.00192-08
7. Wang J, Anderson DE, Halpin K, Hong X, Chen H, Walker S, et al. A new Hendra virus genotype found in Australian flying foxes. Virol J. 2021;18:197. https://doi.org/10.1186/s12985-021-01652-7
8. Edson D, Field H, McMichael L, Vidgen M, Goldspink L, Broos A, et al. Routes of Hendra virus excretion in naturally-infected flying-foxes: implications for viral transmission and spillover risk. PLoS One. 2015;10:e0140670.

https://doi.org/10.1371/journal.pone.0140670
9. Smith I, Broos A, de Jong C, Zeddeman A, Smith C, Smith G, et al. Identifying Hendra virus diversity in pteropid bats. PLoS One. 2011;6:e25275. https://doi.org/10.1371/journal.pone.0025275
10. Kocher T, Thomas W, Meyer A, Edwards S, Paabo S, Villablanca F, et al. Dynamics of mitochondrial DNA evolution in animals: amplification and sequencing with conserved primers. Proc National Acad Sci U S A. 1989;86:6196–200. https://doi.org/10.1073/pnas.86.16.6196
11. Hsieh H-M, Chiang H-L, Tsai L-C, Lai S-Y, Huang N-E, Linacre A, et al. Cytochrome b gene for species identification of the conservation animals. Forensic Sci Int. 2001;122:7–18. https://doi.org/10.1016/S0379-0738(01)00403-0
12. Plowright RK, Eby P, Hudson PJ, Smith IL, Westcott DA, Bryden WL, et al. Ecological dynamics of emerging bat virus spillover. Proc Biol Sci. 2015;282:20142124. https://doi.org/10.1098/rspb.2014.2124
13. Lunney D, Richards G, Dickman C Pteropus poliocephalus. The IUCN Red List of Threatened Species [cited 2021 Nov 15]. https://www.iucnredlist.org/species/18751/22085511

Address for correspondence: Alison Peel, Centre for Planetary Health and Food Security, Griffith University, Nathan Campus, Sir Samuel Griffith Centre (N78) 2.23, 170 Kessels Rd, Nathan, QLD 4111, Australia; email: a.peel@griffith.edu.au

Increased COVID-19 Severity among Pregnant Patients Infected with SARS-CoV-2 Delta Variant, France

Souheil Zayet, Vincent Gendrin, Catherine Gay, Philippe Selles, Timothée Klopfenstein

Author affiliation: Nord Franche-Comté Hospital, Trevenans, France

DOI: https://doi.org/10.3201/eid2805.212080

We conducted a retrospective study of pregnant persons hospitalized for severe acute respiratory syndrome coronavirus 2 infection in France. Delta variant infection had a relative risk of 14.33 for intensive care unit admission and 9.56 for high supplemental oxygen support. The Delta variant might cause more severe illness during pregnancy.

The obstetric practice of Nord-Franche-Comté Hospital, France, has ≈3,600 deliveries per year (*1*). A recent study warned about the possibility of more severe coronavirus disease (COVID-19) among pregnant persons infected with severe acute respiratory syndrome coronavirus 2 (SARS-CoV-2) Delta variant (*2*). In France, the Delta variant became the predominant circulating SARS-CoV-2 variant in late June 2021 (*3*). We explored whether severe COVID-19 cases among pregnant persons increased in our facility when the Delta variant was predominant.

We conducted a retrospective study on all hospitalized pregnant women diagnosed with COVID-19 by reverse transcription PCR of nasopharyngeal swab samples during March 1, 2020–November 15, 2021. We defined severe COVID-19 as a case requiring intensive care unit (ICU) admission and critical COVID-19 as a case in the ICU that required high supplemental oxygen support, either high-flow nasal cannula, noninvasive ventilation, or mechanical ventilation.

We defined the predominant SARS-CoV-2 variants during 3 periods as variants detected in >50% of all sequences analyzed nationwide. National data from epidemiologic surveillance showed that wild-type was the predominant variant until March 1, 2021 (period 1); Alpha (20I/501Y.V1) during March 2–June 28, 2021 (*4*) (period 2); and Delta (21A/478K.V1) during June 29–November 15, 2021 (period 3). Beta (20H/501Y.V2) and Gamma (20J/501Y.V3) variants also were circulating in France but were not predominant.

To compare the frequency of severe and critical COVID-19 among the 3 periods, we calculated the ratio of women of reproductive age (defined as 15–42 years) hospitalized with COVID-19 during the same period. During March 1, 2020–November 15, 2021, a total of 77 women of reproductive age were hospitalized for COVID-19 in our facility, including 30 pregnant women (Figure). Among the 30 pregnant persons, 7 were transferred to the ICU (1 confirmed Alpha variant, 6 confirmed Delta variant

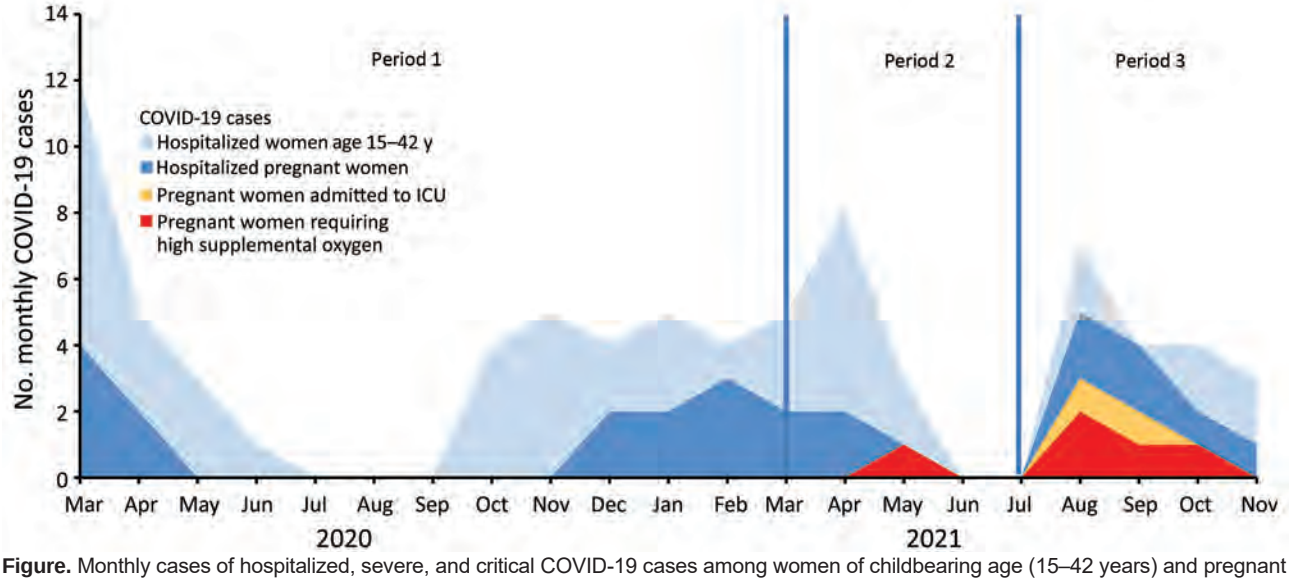

Figure. Monthly cases of hospitalized, severe, and critical COVID-19 cases among women of childbearing age (15–42 years) and pregnant women at Nord Franche-Comté Hospital, France, March 1, 2020–November 15, 2021. We assessed COVID-19 disease severity against circulating severe acute respiratory syndrome coronavirus 2 (SARS-CoV-2) variants during 3 periods of interest based on predominance of circulating variants. During period 1, wild-type virus comprised >50% of all sequenced SARS-CoV-2 variants in France; during period 2, >50% were Alpha variant; and during period 3, >50% were Delta variant. COVID-19, coronavirus disease; ICU, intensive care unit.

cases), 5 of whom required high supplemental oxygen support (1 Alpha variant, 4 Delta variant cases). None of the 7 severe or critical COVID-19 patients were vaccinated.

For each period, we calculated the ratio between severe and critical COVID-19 among pregnant women and all women of reproductive age hospitalized for COVID-19. For period 1, the ratio was <2.33% (0 severe cases; thus, <1 among 43 cases); for period 2, 6.25% (1 severe case/16 cases); and for period 3, 33.33% (6 severe cases/18 cases). The ratio between pregnant women with critical COVID-19 and all women of reproductive age hospitalized for COVID-19 was <2.33% (0 critical cases; thus, <1 among 43 cases) for period 1; 6.25% (1 critical case/16 cases) for period 2; and 22.22% (4 critical cases/18 cases) for period 3.

Based on these ratios, compared with period 1, the relative risk for ICU admission was 2.69 (95% CI 0.18–40.46) for period 2 and 14.33 (95% CI 1.86–110.70) for period 3. The relative risk for high supplemental oxygen support was 2.69 (95% CI 0.18–40.46) for period 2 and 9.56 (95% CI 1.15–79.70) for period 3.

The risk ratios for severe and critical COVID-19 during the 3 periods rebut the hypothesis that the increasing number of SARS-CoV-2 infections in younger persons, combined with low acceptance for COVID-19 vaccination during pregnancy, sufficiently explain the increased risk for severe disease noticed with the Delta variant (*5*). SARS-CoV-2 lineage B.1.617 (Delta) probably is associated with increased COVID-19 severity among pregnant persons compared with previous variants (*2*,*6*). This consistent difference suggests a change in pathogenicity in pregnant persons and requires further investigation. A large retrospective cohort study comparing similar groups of pregnant women with COVID-19 during the pre-Delta period (n = 224) and the Delta period (n = 69) suggested an increase in critical illness and adverse perinatal outcomes associated with the Delta variant during pregnancy (*7*). Another study showed that pregnant patients infected with the Delta variant were more symptomatic and were diagnosed earlier than patients diagnosed before Delta was prevalent (*8*). Our results support the possibility of increased COVID-19 severity with Delta compared with previous SARS-CoV-2 variants.

Our study's first limitation is that standard care and hospitalization criteria changed between the 3 periods, which could have affected our results. We suspect thresholds for ICU admission were lower for pregnant persons during periods 2 and 3 than during period 1 because of a partial ICU bed saturation during the first COVID-19 wave (*9*). COVID-19 treatment progressively improved and standard care was more optimal during periods 2 and 3 than period 1(Appendix, https://wwwnc.cdc.gov/EID/article/28/5/21-2080-App1.pdf); thus, we should have expected fewer severe and critical COVID-19 patients in periods 2 and 3, but we observed the opposite. The main limitation of our study is the small sample size in a monocentric study, which prevents us from issuing any conclusions.

Despite the small number of cases, our findings on COVID-19 severity among pregnant persons infected with the Delta variant are consistent with those of other studies (*2*,*6*–*8*). A larger national cohort study, such as the one conducted by the UK Obstetric Surveillance System (N. Vousden et al., unpub. data, https://www.medrxiv.org/content/10.1101/2021.07.22.21261000v1), could confirm our findings. Nonetheless, our results show that SARS-CoV-2 prevention measures, especially COVID-19 vaccination, are needed during pregnancy.

Acknowledgments

We thank Azzedine Rahmani, Julien Huot, Elodie Bouvier, and Emmanuel Siess for their input into this work.

About the Author

Dr. Zayet is a specialist in the Infectious Diseases Department of Nord Franche-Comte Hospital, Trevenans, France. His primary research interests focus on hepatitis and tuberculosis, especially in HIV-infected patients.

References

1. North Franche-Comté Hospital [in French] [cited 2022 Feb 1]. https://www.hnfc.fr/l-hopital,198,343.html
2. Adhikari EH, SoRelle JA, McIntire DD, Spong CY. Increasing severity of COVID-19 in pregnancy with Delta (B.1.617.2) variant surge. Am J Obstet Gynecol. 2022;226;149–51. https://doi.org/10.1016/j.ajog.2021.09.008
3. Public Health France. Coronavirus: circulation of SARS-CoV-2 variants [in French] [cited 2021 Sep 23]. https://www.santepubliquefrance.fr/dossiers/coronavirus-covid-19/coronavirus-circulation-des-variants-du-sars-cov-2
4. Gaymard A, Bosetti P, Feri A, Destras G, Enouf V, Andronico A, et al.; ANRS MIE AC43 COVID-19; French viro COVID group. Early assessment of diffusion and possible expansion of SARS-CoV-2 lineage 20I/501Y.V1 (B.1.1.7, variant of concern 202012/01) in France, January to March 2021. Euro Surveill. 2021;26:2100133. https://doi.org/10.2807/1560-7917.ES.2021.26.9.2100133
5. Lapinsky SE, Adhikari NK. COVID-19, variants of concern and pregnancy outcome. Obstet Med. 2021;14:65–6. https://doi.org/10.1177/1753495X211028499
6. Stirrup O, Boshier F, Venturini C, Guerra-Assunção JA, Alcolea-Medina A, Beckett A, et al.; COG-UK-HOCI Variant substudy consortium; COVID-19 Genomics UK (COG-UK) consortium. SARS-CoV-2 lineage B.1.1.7 is associated with

greater disease severity among hospitalised women but not men: multicentre cohort study. BMJ Open Respir Res. 2021;8:e001029. https://doi.org/10.1136/bmjresp-2021-001029
7. Seasely AR, Blanchard CT, Arora N, Battarbee AN, Casey BM, Dionne-Odom J, et al.; CWRH COVID-19 Working Group. Maternal and perinatal outcomes associated with the severe acute respiratory syndrome coronavirus 2 (SARS-CoV-2) Delta (B.1.617.2) variant. Obstet Gynecol. 2021;138:842–4. https://doi.org/10.1097/AOG.0000000000004607
8. Wang AM, Berry M, Moutos CP, Omere C, Clark SM, Harirah HM, et al. Association of the Delta (B.1.617.2) variant of severe acute respiratory syndrome coronavirus 2 (SARS-CoV-2) with pregnancy outcomes. Obstet Gynecol. 2021; 138:838–41. https://doi.org/10.1097/AOG.0000000000004595
9. Klopfenstein T, Zayet S, Lohse A, Selles P, Zahra H, Kadiane-Oussou NJ, et al.; HNF Hospital Tocilizumab multidisciplinary team. Impact of tocilizumab on mortality and/or invasive mechanical ventilation requirement in a cohort of 206 COVID-19 patients. Int J Infect Dis. 2020; 99:491–5. https://doi.org/10.1016/j.ijid.2020.08.024

Address for correspondence: Timothee Klopfenstein, Department of Infectious Disease, Nord Franche-Comte Hospital, 90400 Trevenans, France; email: timothee.klopfenstein@hnfc.fr

Cross-Variant Neutralizing Serum Activity after SARS-CoV-2 Breakthrough Infections

Pinkus Tober-Lau,[1] Henning Gruell,[1] Kanika Vanshylla,[1] Willi M. Koch, David Hillus, Philipp Schommers, Isabelle Suárez, Norbert Suttorp, Leif Erik Sander,[2] Florian Klein,[2] Florian Kurth[2]

Author affiliations: Charité–Universitätsmedizin Berlin, Berlin, Germany (P. Tober-Lau, W.M. Koch, D. Hillus, N. Suttorp, L.E. Sander, F. Kurth); University of Cologne, Cologne, Germany (H. Gruell, K. Vanshylla, P. Schommers, I. Suárez, F. Klein); German Center for Infection Research, Bonn-Cologne, Germany (F. Klein); Bernhard Nocht Institute for Tropical Medicine, Hamburg, Germany (F. Kurth); University Medical Centre Hamburg-Eppendorf, 20359, Hamburg (F. Kurth)

DOI: https://doi.org/10.3201/eid2805.220271

[1]These authors contributed equally to this article.

[2]These authors co-led this study.

To determine neutralizing activity against the severe acute respiratory syndrome coronavirus 2 ancestral strain and 4 variants of concern, we tested serum from 30 persons with breakthrough infection after 2-dose vaccination. Cross-variant neutralizing activity was comparable to that after 3-dose vaccination. Shorter intervals between vaccination and breakthrough infection correlated with lower neutralizing titers.

The B.1.1.529 (Omicron) variant of concern of severe acute respiratory syndrome coronavirus 2 (SARS-CoV-2) carries a high number of nonsynonymous mutations in the spike glycoprotein, relative to that of the ancestral (wild-type) strain (Wu01). Those mutations result in a strong immune evasion phenotype, as demonstrated by severely reduced serum neutralization after vaccination or previous infection with ancestral variants in most persons (*1*–*3*), lower vaccine effectiveness, and increased rates of reinfection (N. Andrews et al., unpub. data, https://www.medrxiv.org/content/10.1101/2021.12.14.21267615v1). However, booster vaccinations with 1 dose of mRNA vaccine after priming with an initial 2 doses induce high levels of serum neutralizing activity against Omicron (*1*,*4*). Substantial efforts have therefore been made to speed up booster vaccination campaigns in light of the rapid spread of Omicron and the recent surge of infections worldwide. Breakthrough infections after 2-dose mRNA vaccination can result in a natural boost to humoral immunity against SARS-CoV-2 (*5*; L.J. Abu-Raddad et al., unpub. data, https://www.medrxiv.org/content/10.1101/2022.01.18.222694502v2), and emerging evidence suggests that breakthrough infections with non-Omicron SARS-CoV-2 variants also elicit cross-neutralizing serum activity against Omicron (*6*).

We determined serum neutralizing activity against the spike pseudotypes of SARS-CoV-2 Wu01 strain and 4 variants of concern (Alpha, Beta, Delta, Omicron [BA.1]) in 20 persons with non-Omicron (Alpha, Delta) SARS-CoV-2 infection after 2-dose mRNA vaccination with BNT162b2 (Comirnaty; Pfizer-BioNTech, https://www.comirnaty.com) or heterologous vaccination with ChAdOx1 (Vaxzevria; AstraZeneca, https://www.astrazeneca.com) and BNT162b2 (Appendix, https://wwwnc.cdc.gov/EID/article/28/5/22-0271-App1.pdf). We compared serum neutralization activity for this cohort with that of 2 age-matched cohorts, 1 consisting of 20 persons who received 2 or 3 doses of mRNA vaccine (*1*) and did not experience breakthrough infection and another cohort of 10 persons who experienced

Omicron breakthrough infection after 2-dose vaccination (Figure, panel A; Appendix Table).

We detected significantly higher serum neutralizing activity against all investigated variants in serum from vaccinated persons with subsequent non-Omicron SARS-CoV-2 infection (Figure, panel B) than in serum from persons who received the regular 2 doses of vaccine and experienced no subsequent infection. The geometric mean 50% inhibitory serum dilution (ID_{50}) against Wu01 was 6.3-fold higher after breakthrough infection (640 [95% CI 409–1,003] vs. 4,056 [95% CI 2,174–7,568]). This difference in serum neutralizing activity was particularly pronounced against the Beta (23.5-fold higher ID_{50}, 49 [95% CI 28–85] vs. 1,148 [95% CI 524–2,514]) and Omicron (23.8-fold higher ID_{50}, 9 [95% CI 5–13] vs. 202 [95% CI 79–515]) variants, each of which exhibits substantial immune escape. The boosting effect of non-Omicron breakthrough infections was highly variable (Figure, panel B) because serum

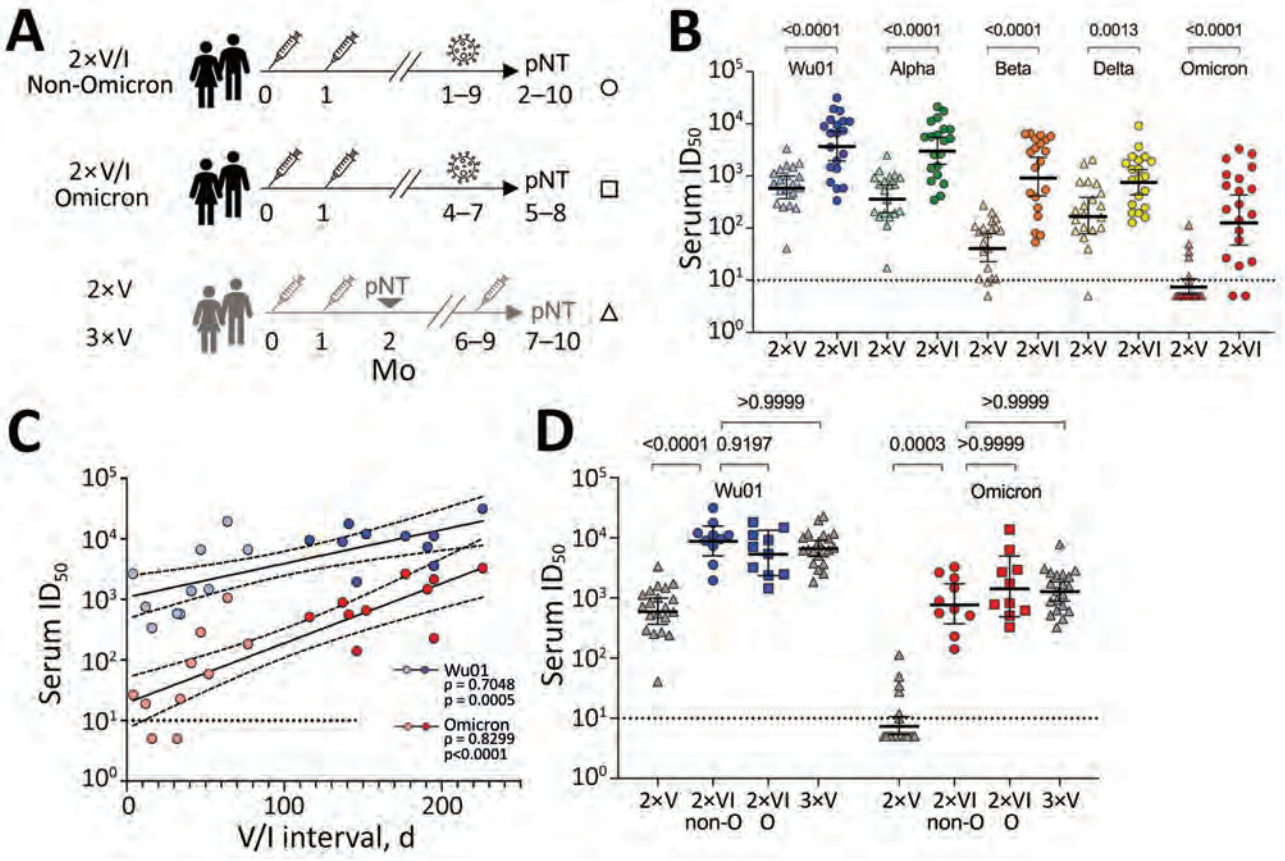

Figure. SARS-CoV-2 serum neutralizing titers across variants after postvaccination breakthrough infection. A) Schematic of the study cohort of 2×VI patients and age-matched reference cohorts (1). B) Serum neutralizing activity against Wu01 and SARS-CoV-2 variants in 2×V persons (triangles) and 2×V/I persons (circles). Horizontal lines indicate geometric mean ID50s; error bars, 95% CIs. Groups were compared by using the Mann-Whitney test. p values are shown at top. C) Correlation of serum neutralizing activity against SARS-CoV-2 Wu01 (blue) or Omicron (red) and interval between second vaccination and non-Omicron breakthrough infection (Spearman ρ and p values). Breakthrough infections within 3 months (90 days) from vaccination are indicated by light shaded symbols. Solid lines indicate linear regression, and dashed lines indicate 95% CIs. Correlation was determined by Spearman ρ. D) Serum neutralizing activity against SARS-CoV-2 Wu01 (blue) and Omicron (red) in 2×V or 3×V persons (triangles) compared with 2×V/I non-Omicron (circles) or Omicron (triangles) persons after 2 and 3 doses of mRNA vaccine. Only persons with vaccine-to-infection intervals >3 months are shown. Groups were compared by using the Kruskal-Wallis test with the Dunn multiple testing correction. Horizontal lines indicate geometric mean ID50s; error bars, 95% CIs. p values are shown at top. Black dotted lines in panels B, C, and D indicate the lower limit of quantification (ID50 = 10); ID50s <10 were imputed to half the lower limit of quantification (ID50 = 5). ID50, 50% inhibitory serum dilution; O, Omicron; pNT, pseudovirus neutralization test; SARS-CoV-2, severe acute respiratory syndrome coronavirus 2; V/I, vaccination with subsequent breakthrough infection; Wu01, ancestral (wild-type) SARS-CoV-2 strain; 2xV/I non-Omicron, vaccinated persons with non-Omicron breakthrough infection that occurred 1–8 months after vaccination (circles); 2xV/I Omicron, vaccinated persons with Omicron breakthrough infection that occurred 4–7 months after vaccination (squares); 2xV, vaccinated persons after 2 doses of mRNA vaccine; 3xV, vaccinated persons after 3 doses of mRNA vaccine (triangles).

neutralizing titers (ID_{50}) showed a strong correlation with the interval between second vaccination and diagnosis of breakthrough infection (Omicron, Spearman ρ = 0.8299, p<0.0001; Wu01, ρ = 0.7048, p = 0.0005) (Figure, panel C; Appendix Figure, panels A–C). Breakthrough infections acquired >3 months after the second vaccination resulted in serum neutralizing capacity against both Wu01 and Omicron, which was comparable to that after 3-dose vaccination. This effect was observed after both non-Omicron and Omicron breakthrough infections (Figure, panel D). Similarly, neutralizing capacity against the Delta variant was increased after Omicron breakthrough infections (Appendix Figure, panel D). Limitations of this study include limited sample size and application of a pseudovirus-based neutralization assay.

In summary, we found that Omicron and non-Omicron SARS-CoV-2 breakthrough infections elicit cross-variant neutralizing antibodies. Our results suggest that short vaccination-to-infection intervals correlate with lower neutralizing titers, which may be relevant for recommendations concerning additional booster vaccination of persons who experience early breakthrough infections after initial immunization.

Acknowledgments

We are grateful to all study participants. We also thank Florian Behr, Julia Blum, Annelene Kossow, Göksu Oral, Elham Rezaei, Maike Schlotz, and the members of the EICOV/COVIM Study Group for sample acquisition and processing as well as logistical support: Yvonne Ahlgrimm, Ben Al-Rim, Kerstin Behn, Norma Bethke, Harald Bias, Tobias Bleicker, Dana Briesemeister, Claudia Conrad, Victor Max Corman, Chantip Dang-Heine, Doris Frey, Julie-Anne Gabelich, Janine Gerdes, Ute Gläser, Andreas Hetey, Lisbeth Hasler, Anja Heiduk, Elisa-Theresa Helbig, Alexandra Horn, Claudia Hülso, Stefanie Jentzsch, Luisa Kegel, Paolo Kroneberg, Sebastian Kühn, Irmgard Landgraf, Ngoc Han Le, Michelle Lisy, Lena Johanna Lippert, Constanze Dorothea Lüttke, Pedro de Macedo Gomes, Birgit Maeß, Janine Michel, Friederike Münn, Andreas Nitsche, Anne-Maria Ollech, Christina Pley, Anita Pioch, Annelie Richter, Mira Risham, Carolin Rubisch, Angela Sanchez Rezza, Lisa Ruby, Isabelle Schellenberger, Jenny Schlesinger, Angelika Schliephake, Georg Schwanitz, Tatjana Schwarz, Sevda Senaydin, Alexandra Stege, Sarah Steinbrecher, Paula Stubbemann, Charlotte Thibeault, Denise Treue, and Saskia Zvorc.

This work was supported by grants from COVIM: "NaFoUniMedCovid19" (FKZ: 01KX2021 to L.E.S. and F.K.L.), the Federal Institute for Drugs and Medical Devices (V-2021.3 / 1503_68403 / 2021-2022 to L.E.S. and F.K.U.), the German Center for Infection Research (DZIF) (to F.K.L.), and the Deutsche Forschungsgemeinschaft (DFG) (CRC1310 to F.K.L. and SFB-TR84 to N.S. and L.E.S.). The funders of the study had no role in study design, data collection, data analysis, data interpretation, or writing of the report.

H.G., K.V., and F.K.L. are listed as inventors on pending patent application(s) on SARS-CoV-2-neutralizing antibodies filed by the University of Cologne.

About the Author

Dr. Tober-Lau is a physician and researcher at the Department of Infectious Diseases and Respiratory Medicine at Charité–Universitätsmedizin Berlin, Germany. His research interests focus on infectious diseases and global health.

References

1. Gruell H, Vanshylla K, Tober-Lau P, Hillus D, Schommers P, Lehmann C, et al. mRNA booster immunization elicits potent neutralizing serum activity against the SARS-CoV-2 Omicron variant. Nat Med. 2022 Jan 19 [Epub ahead of print]. https://doi.org/10.1038/s41591-021-01676-0
2. Schmidt F, Muecksch F, Weisblum Y, Da Silva J, Bednarski E, Cho A, et al. Plasma neutralization of the SARS-CoV-2 Omicron variant. N Engl J Med. 2021;386:599–601. https://doi.org/10.1056/NEJMc2119641
3. Carreño JM, Alshammary H, Tcheou J, Singh G, Raskin AJ, Kawabata H, et al.; PSP-PARIS Study Group. Activity of convalescent and vaccine serum against SARS-CoV-2 Omicron. Nature. 2021;602:682–8.
4. Nemet I, Kliker L, Lustig Y, Zuckerman N, Erster O, Cohen C, et al. Third BNT162b2 vaccination neutralization of SARS-CoV-2 Omicron infection. N Engl J Med. 2021;386:492–4. https://doi.org/10.1056/NEJMc2119358 386(5):492-49.
5. Bates TA, McBride SK, Winders B, Schoen D, Trautmann L, Curlin ME, et al. Antibody response and variant cross-neutralization after SARS-CoV-2 breakthrough infection. JAMA. 2022;327:179–81. https://doi.org/10.1001/jama.2021.22898
6. Rössler A, Riepler L, Bante D, von Laer D, Kimpel J. SARS-CoV-2 Omicron variant neutralization in serum from vaccinated and convalescent persons. N Engl J Med. 2022;386:698–700. https://doi.org/10.1056/NEJMc2119236

Address for correspondence: Florian Kurth, Charité–Universitätsmedizin Berlin, corporate member of Freie Universität Berlin and Humboldt-Universität zu Berlin, Department of Infectious Diseases and Respiratory Medicine, Augustenburger Platz 1, D-13353 Berlin, Germany; email: florian.kurth@charite.de

Mathematical Modeling for Removing Border Entry and Quarantine Requirements for COVID-19, Vanuatu

Caroline van Gemert,[1] Len Tarivonda, Posikai Samuel Tapo, Sereana Natuman, Geoff Clark, Joanne Mariasua, Nick Scott, Adam Craig, Myriam Abel, Matthew J. Cornish, Margaret Hellard, Rachel Sacks-Davis

Author affiliations: The University of Melbourne, Carlton, Victoria, Australia (C. van Gemert); Vanuatu Health Program, Port Vila, Vanuatu (C. van Gemert, G. Clark); The Burnet Institute, Melbourne, Victoria, Australia (C. van Gemert, N. Scott, M. Hellard, R. Sacks-Davis); Ministry of Health, Iatika Complex, Port Vila (L. Tarivonda, P.S. Tapo, S. Natuman, J. Mariasua); Oxford University, Oxford, UK (N. Scott); University of New South Wales, Sydney, New South Wales, Australia (A. Craig); World Health Organization, Port Vila (M. Abel); Dokta Blong Mi, Port Vila (M.J. Cornish)

DOI: https://doi.org/10.3201/eid2805.211757

The Pacific Island country of Vanuatu is considering strategies to remove border restrictions implemented during 2020 to prevent imported coronavirus disease. We performed mathematical modeling to estimate the number of infectious travelers who had different entry scenarios and testing strategies. Travel bubbles and testing on entry have the greatest importation risk reduction.

Many Pacific Island Countries and Territories (PICTs) implemented border entry restrictions and mandatory quarantine in 2020 to prevent imported coronavirus disease (COVID-19). Although some PICTs have experienced large-scale community transmission of COVID-19 (such as Fiji, Papua New Guinea, French Polynesia, and Guam), many PICTs have not (as of January 2022) experienced community transmission, including Vanuatu. Since March 2020, Vanuatu (population 301,695) has restricted entry to citizens and residents and required all incoming travelers to a complete 14-day quarantine period (*1*). As of January 10, 2022, a total of 7 border cases have been reported among travelers in quarantine in Vanuatu, and no community transmission (*2*).

The government of Vanuatu is considering various strategies to remove border restrictions and quarantine, including opening borders, creating travel bubbles with neighboring point-prevalence countries, and restricting entry to vaccinated travelers. We performed mathematical modeling to estimate the expected number of infected arrivals expected for each of these scenarios and through different testing strategies. This modeling complements other modeling that assessed importation risks of COVID-19 with higher point prevalence in the origin countries (*3*) and different outcomes, such as the expected time delay associated with different scenarios (*4*).

We developed an individual stochastic model to estimate the potential number of infectious travelers who would arrive in Vanuatu. We modeled 3 border scenarios and 4 testing strategies (Table). The probability of a traveler being infected on entry into Vanuatu was assumed to be a function of the point prevalence in the country of origin and the distributions of latent, presymptomatic and infectious, and symptomatic (or asymptomatic) infectious periods and test sensitivity. We used point prevalence estimates based on the epidemiologic situation on July 19, 2021, for neighboring countries, including New Caledonia (<0.001%) and New Zealand (0.001%) (*5*).

We assumed that passengers returning with a positive pretravel test result did not travel, those tested on arrival isolated until results were provided, and those tested on day 5 were in the community for 6 days (including time for testing and provision of results). We simulated 10,000 infected travelers stochastically and used 1,000 bootstrap samples to estimate uncertainty intervals. We applied the model to 40,000 passengers (15% of the number of arrivals in 2019) (*6*) (Appendix, https://wwwnc.cdc.gov/EID/article/28/5/21-1757-App1.pdf). We did not include additional variables, such as group size, masking, and hygiene measures.

The number of infectious persons in the community decreased by 98%–99% when travel was restricted entry to persons from low point-prevalence countries, compared with no restrictions on the country of departure for travelers (Figure). The number decreased further, by 61%–63% for each testing strategy, when travel was further restricted to vaccinated travelers only. For all scenarios, the number of infectious persons in the community was inversely proportional to the number of tests conducted. The greatest decrease was observed for testing on arrival (compared with no testing), for which the number of infectious cases in the community decreased by 42%–44%. The proportional decrease was 10%–14% when predeparture plus arrival testing was included. Although adding day 5 testing (in addition to predeparture and on arrival testing) did not result in further

[1]Current affiliation: The Burnet Institute, Melbourne, Victoria, Australia.

decrease in the number infectious persons in the community, it did identify 56%–67% of cases after entry, which would enable contact tracing to reduce risk for onward transmission.

Our analysis highlights that the scenario with the greatest importation risk reduction for Vanuatu is travel bubbles with low point-prevalence countries. The risk for case importation through quarantine-free travel with low COVID-19 incidence countries is <3.2 cases/40,000 travelers, an importation risk reduction of ≈100-fold compared with open borders. Several countries in the Pacific region have a low or zero COVID-19 point prevalence (*5*). Furthermore, country-level incidence might decrease as vaccination coverage increases because there is evidence that several COVID-19 vaccines might reduce transmission (*7*). On the basis of our results, many PICTs could be considered for quarantine-free travel with low risk for importation to Vanuatu.

Our results also demonstrate that COVID-19 testing on arrival is useful in all scenarios, but especially for open borders. Testing becomes increasingly useful as the point prevalence of COVID-19 increases in countries of travel origin. Testing 5 days after arrival enables detection of an additional 10%–14% of infections for all scenarios, and these cases can be contact traced and those infected quarantined for part of their infectious period. Since late 2020, Vanuatu has conducted arrival testing for all international arrivals (in addition to routine testing during quarantine). Our results confirm the usefulness of this strategy.

A limitation of our study is that the model does not estimate the number of secondary cases. Assumptions for parameters were based on published evidence for the original variant; these parameters might differ with new and emerging variants. In summary, as Vanuatu and other PICTs move toward removing border restrictions and importation prevention measures, on-arrival testing and restricting entry to travelers from low point-prevalence settings are essential strategies to limit COVID-19 cases.

Table. Characteristics considered in the model for removing border entry and quarantine requirements for coronavirus disease, Vanuatu

Characteristic	Description
Border opening scenarios	
Scenario 1	Open border with no restrictions
Scenario 2	Travel bubble with low point-prevalence neighboring countries
Scenario 3	Travel bubble with low point-prevalence neighboring countries plus vaccination for all incoming travelers
Testing strategies	
Test strategy 1	No testing
Test strategy 2	Testing on arrival only
Test strategy 3	Predeparture plus on arrival
Test strategy 4	Predeparture plus on arrival plus day 5 after arrival

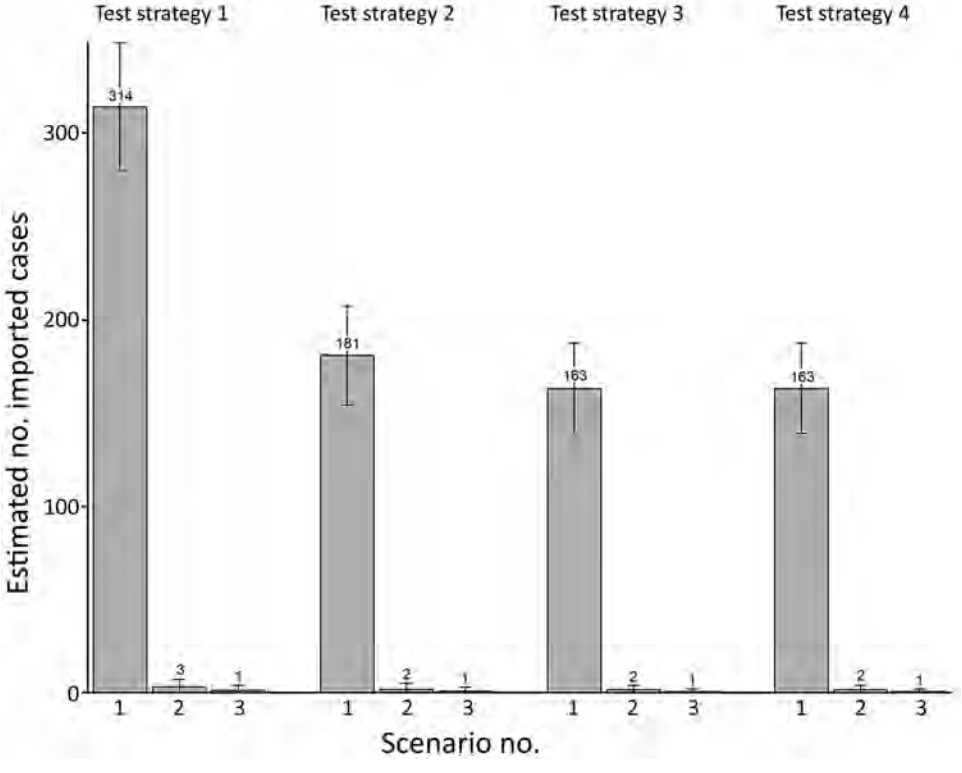

Figure. Number of imported cases of coronavirus disease in the community per 40,000 arrivals, by test strategy and epidemiologic scenario, Vanuatu. Error bars indicate 95% CIs.

The Vanuatu Health Program is supported by the Australian Department of Foreign Affairs and Trade Australian Aid Program. C.v.G. is a recipient of an Early Career Research Fellowship, supported by the Australian National Health and Medical Research Council.

About the Author

Dr. van Gemert is an epidemiologist and postdoctoral research fellow in the Vanuatu Health Program, Port Vila, Vanuatu, and with the Burnet Institute, Melbourne, Victoria, Australia. Her primary research interest is surveillance of infectious disease in resource-poor settings.

References

1. Vanuatu Government Office of the President. Extraordinary Gazette Numbero Special No. 3. Extension of Declaration of State of Emergency Order No. 93 of 2020 [cited 2020 Jul 13]. https://www.gov.vu/index.php/events/news/86-extension-of-the-declaration-of-the-soe-order-no-93-of-2020
2. Vanuatu Ministry of Health. Vanuatu situation report 59—23 December 2021 [cited 2022 Jan 10]. https://covid19.gov.vu/images/Situation-reports/19122021_Vanuatu_COVID19_NHEOC_SitRep_59_2.pdf
3. Yang B, Tsang TK, Wong JY, He Y, Gao H, Ho F, et al. The differential importation risks of COVID-19 from inbound travellers and the feasibility of targeted travel controls: a case study in Hong Kong. Lancet Reg Health West Pac. 2021;13:100184. https://doi.org/10.1016/j.lanwpc.2021.100184
4. Clifford S, Pearson CA, Klepac P, Van Zandvoort K, Quilty BJ, Eggo RM, et al.; CMMID COVID-19 working group. Effectiveness of interventions targeting air travellers for delaying local outbreaks of SARS-CoV-2. J Travel Med. 2020;27:taaa068. https://doi.org/10.1093/jtm/taaa068
5. World Health Organization. WHO coronavirus (COVID-19) dashboard 2022 [cited 2022 Jan 10]. https://covid19.who.int/
6. Vanuatu National Statistics Office. Statistics update: international visitor arrivals. December 2020 provisional highlights [cited 2021 Feb 10]. https://www.stats.govt.nz/information-releases/international-travel-december-2021
7. Pritchard E, Matthews PC, Stoesser N, Eyre DW, Gethings O, Vihta KD, et al. Impact of vaccination on new SARS-CoV-2 infections in the United Kingdom. Nat Med. 2021;27:1370–8. https://doi.org/10.1038/s41591-021-01410-w

Address for correspondence: Caroline van Gemert, The Burnet Institute, 85 Commercial Rd, Melbourne, VIC 3004, Australia; email: caroline.vangemert@burnet.edu.au

SARS-CoV-2 Seroprevalence after Third Wave of Infections, South Africa

Jackie Kleynhans, Stefano Tempia, Nicole Wolter, Anne von Gottberg, Jinal N. Bhiman, Amelia Buys, Jocelyn Moyes, Meredith L. McMorrow, Kathleen Kahn, F. Xavier Gómez-Olivé, Stephen Tollman, Neil A. Martinson, Floidy Wafawanaka, Limakatso Lebina, Jacques D. du Toit, Waasila Jassat, Mzimasi Neti, Marieke Brauer, Cheryl Cohen, for the PHIRST-C Group[1]

Author affiliations: National Institute for Communicable Diseases of the National Health Laboratory Service, Johannesburg, South Africa (J. Kleynhans, S. Tempia, N. Wolter, A. von Gottberg, J.N. Bhiman, A. Buys, J. Moyes, W. Jassat, M. Neti, C. Cohen); University of the Witwatersrand, Johannesburg (J. Kleynhans, S. Tempia, N. Wolter, A. von Gottberg, J.N. Bhiman, J. Moyes, C. Cohen); US Centers for Disease Control and Prevention, Atlanta, Georgia, USA (S. Tempia, M.L. McMorrow); US Centers for Disease Control and Prevention, Pretoria, South Africa (M.L. McMorrow); MRC/Wits Rural Public Health and Health Transitions Research Unit (Agincourt), University of the Witwatersrand, Johannesburg (K. Kahn, F.X. Gómez-Olivé, S. Tollman, F. Wafawanaka, J. du Toit); Johns Hopkins University Center for Tuberculosis Research, Baltimore, Maryland, USA (N.A. Martinson); Perinatal HIV Research Unit, University of the Witwatersrand, Johannesburg (N.A. Martinson, L. Lebina); Africa Health Research Institute, Durban, South Africa (L. Lebina); Ampath Pathology, Pretoria (M. Brauer)

DOI: https://doi.org/10.3201/eid2805.220278

By November 2021, after the third wave of severe acute respiratory syndrome coronavirus 2 infections in South Africa, seroprevalence was 60% in a rural community and 70% in an urban community. High seroprevalence before the Omicron variant emerged may have contributed to reduced illness severity observed in the fourth wave.

South Africa has experienced 4 waves of severe acute respiratory syndrome coronavirus 2 (SARS-CoV-2) infections, the fourth dominated by the Omicron variant of concern (*1*). Data on the proportion of the population with serologic evidence of previous infection at the time of Omicron emergence are important to contextualize the observed rapid increases and subsequent quick decline in case numbers (*1*), as well as the lower severity compared with previous variants (*2*).

[1]Additional members of the PHIRST-C group who contributed to this article are listed at the end of this article.

We previously described the seroprevalence of SARS-CoV-2 in the PHIRST-C (Prospective Household Study of SARSCoV-2, Influenza, and Respiratory Syncytial Virus Community Burden, Transmission Dynamics, and Viral Interaction) cohort in a rural and an urban community at 5 timepoints during July 2020–March 2021 (*3*). By using the same methods (Appendix, https://wwwnc.cdc.gov/EID/article/28/5/22-0278-App1.pdf), we report seroprevalence at 4 additional timepoints through November 27, 2021, spanning the third, Delta-dominated wave (Appendix Figure 1), ending the week Omicron was identified (*4*). We tested serum samples by using the Roche Elecsys Anti-SARS-CoV-2 assay (Roche Diagnostics, https://www.roche.com); we considered a cutoff index ≥1.0 an indication of prior infection. The immunoassay detects nucleocapsid (N) antibodies; thus, it does not detect postvaccination antibody responses. We obtained seroprevalence 95% credible intervals (CrIs) by using Bayesian inference with 10,000 posterior draws (*5*). We estimated the age- and sex-adjusted number of infections and age-adjusted diagnosed cases, hospitalizations, deaths, case-to-infection ratio (CIR), hospitalization-to-infection ratio (HIR), and in-hospital and excess death fatality-to-infection ratio (FIR), as described previously (*3*) (Appendix). Third-wave infections were defined as participants who had a paired blood draw (BD) from the fifth timepoint of the previous study (BD5) (collected March 22–April 11, 2021) and from the ninth timepoint of this study (BD9) (collected November 15–27, 2021) and who were seronegative at BD5 and seropositive at BD9 or seropositive at BD5 but had a ≥2-fold higher cutoff index in BD9 (because 38 possible reinfections occurred after BD5 [Appendix]). We obtained vaccination status through reviewing vaccine cards that participants kept at home. The study was approved by the University of the Witwatersrand Human Research Ethics Committee (reference no. 150808); the US Centers for Disease Control and Prevention relied on local clearance (IRB approval no. 6840).

Overall, pre–third wave (BD5) SARS-CoV-2 seroprevalence adjusted for assay sensitivity and specificity was 26% (95% CrI 22%–29%) in the rural and 41% (95% CrI 37%–45%) in the urban community. After the third wave (BD9), overall seroprevalence increased to 60% (95% CrI 56%–64%) in the rural community and 70% (95% CrI 66%–74%) in the urban community (Figure; Appendix Table 1). In both communities, the largest increase in seroprevalence was seen in children 13–18 years of age, who also had the highest seroprevalence of all ages after the third wave: 80% (95% CrI 70%–88%) in the rural community (a 49% increase) and 83% (95% CrI 73%–90%) in the urban community (a 19% increase).

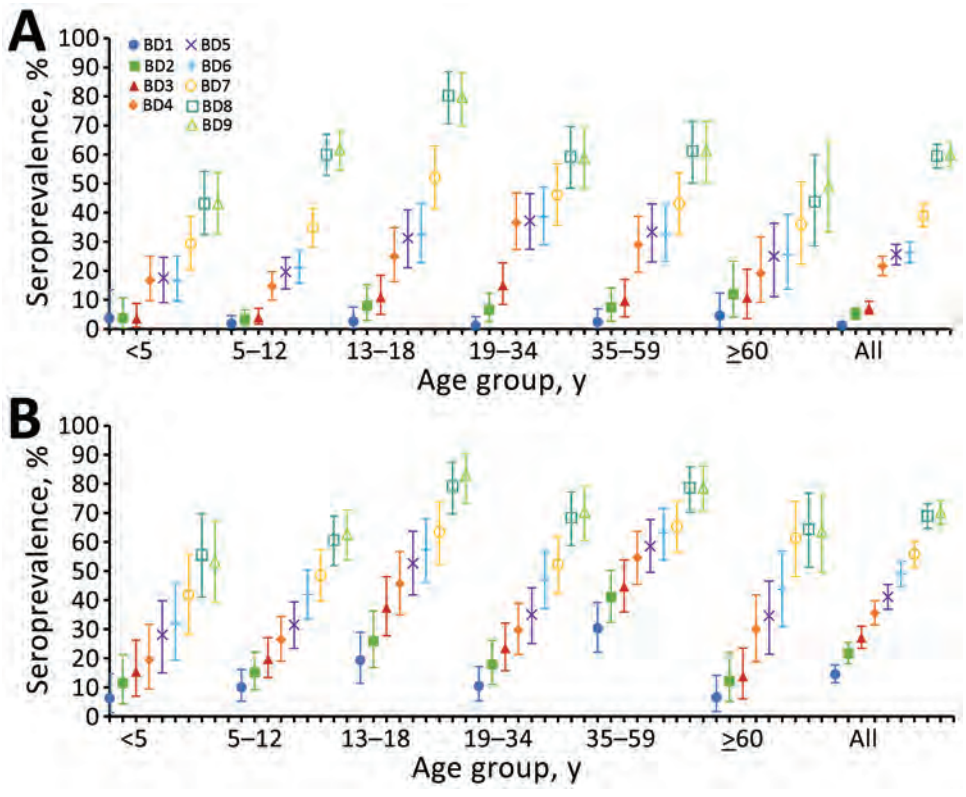

Figure. Severe acute respiratory syndrome coronavirus 2 seroprevalence at each blood collection, by age group, in a rural community (A) and urban community (B), South Africa, March 2020–November 2021. Baseline blood draw (BD1) collected July 20–September 17, 2020; second draw (BD2), September 21 – October 10, 2020; third draw (BD3), November 23–December 12, 2020; fourth draw (BD4), January 25–February 20, 2021; fifth draw (BD5), March 22–April 11, 2021; sixth draw (BD6), May 20–June 9, 2021; seventh draw (BD7), July 19–August 5, 2021; eighth draw (BD8), September 13–25, 2021; ninth draw (BD9), November 15–27, 2021. Error bars represent 95% credible intervals. Seroprevalence estimates adjusted for sensitivity and specificity of assay.

During the third wave of infections, the incidence at the rural site was 39% (95% CrI 24%–55%), resulting in a CIR of 3% (95% CI 2%–5%). HIR was 0.5% (95% CI 0.3%–0.7%) and in-hospital FIR was 0.1% (95% CI 0.1%–0.2%); excess deaths FIR was 0.5% (95% CI 0.4%–0.8%) (Figure; Appendix Figure 2).

In the urban community, the incidence during the third wave was 40% (95% CrI 26%–54%). CIR was a 5% (95% CI 4%–8%), and HIR was 2% (95% CI 2%–4%). In-hospital FIR was 0.4% (95% CI 0.3%–0.6%) and excess deaths FIR was 0.6% (95% CI 0.4%–0.9%) (Figure; Appendix Figure 2).

HIR and FIR were similar between wave 2 and 3 (Appendix Figure 3). SARS-CoV-2 vaccines became available in South Africa in February 2021, after the second wave. By the end of wave 3, only 8% (49/609) of participants were fully vaccinated (1 dose of Johnson & Johnson/Janssen or 2 doses of Pfizer-BioNTech) in the rural community and 19% (97/512) in the urban community (Appendix Table 2). Considering the overall low vaccination coverage in these communities during the study period, the similar HIR and FIR in wave 2 and 3 were likely driven by a combination of natural immunity and potentially a moderate effect attributable to vaccination.

Taken together, by the end of November 2021, just before the emergence of Omicron, the combined proportion of persons who had serologic evidence of previous infection (at any timepoint), were fully vaccinated, or both was 62% (389/631) at the rural community and 72% (411/568) at the urban community (Appendix Table 3).

After the third wave of infections in South Africa, we observed a ≥60% overall seroprevalence attributable to SARS-CoV-2 infection, ranging from 43% in rural community children <5 years of age to 83% in urban community children 13–18 years of age (Figure). CIR, HIR, and FIRs were similar between the second and third waves. Similar to our data, results from a study in Gauteng Province found seroprevalence of 56%–80% attributable to natural infection before the emergence of Omicron (*6*). The high seroprevalence before Omicron emergence may have contributed to reduced illness severity observed in the fourth wave (*2*).

Additional members of the PHIRST-C Group who contributed: Kgaugelo Patricia Kgasago, Linda de Gouveia, Maimuna Carrim, Mignon du Plessis, Retshidisitswe Kotane, and Tumelo Moloantoa.

Acknowledgments

We thank all persons participating in the study and the field teams for their hard work and dedication to the study, the laboratory teams, the PHIRST-C scientific and safety committee, the national SARS-CoV-2 National Institute for Communicable Diseases (NICD) surveillance team, and NICD Information Technology.

This work was supported by the NICD of the National Health Laboratory Service and the US Centers for Disease Control and Prevention (cooperative agreement no. 6U01IP001048-04-02 awarded to C.C.). The funders had no role in study design, data collection and analysis, decision to publish, or preparation of the manuscript. C.C. received grant funds from US Centers for Disease Control and Prevention, Wellcome Trust, and South African Medical Research Council. N.W. and A.v.G. received grant funds from Sanofi and the Gates Foundation.

The investigators welcome enquiries about possible collaborations and requests for access to the dataset. Data will be shared after approval of a proposal and with a signed data access agreement. Investigators interested in more details about this study, or in accessing these resources, should contact the corresponding author.

About the Author

Ms. Kleynhans is an epidemiologist in the Centre for Respiratory Diseases and Meningitis, National Institute for Communicable Diseases. Her primary research interests include the epidemiology of respiratory diseases like influenza and COVID-19, vaccine impact studies, and modelling of infectious disease transmission dynamics.

References

1. National Institute for Communicable Diseases. COVID-19 weekly epidemiology brief week 3. 2022 Jan 26 [cited 2022 Jan 31]. https://www.nicd.ac.za/wp-content/uploads/2022/01/COVID-19-Weekly-Epidemiology-Brief-week-3-2022.pdf
2. Wolter N, Jassat W, Walaza S, Welch R, Moultrie H, Groome M, et al. Early assessment of the clinical severity of the SARS-CoV-2 omicron variant in South Africa: a data linkage study. Lancet. 2022;399:437–46. https://doi.org/10.1016/S0140-6736(22)00017-4
3. Kleynhans J, Tempia S, Wolter N, von Gottberg A, Bhiman JN, Buys A, et al.; PHIRST-C Group. PHIRST-C Group. SARS-CoV-2 seroprevalence in a rural and urban household cohort during first and second waves of infections, South Africa, July 2020–March 2021. Emerg Infect Dis. 2021;27:3020–9. https://doi.org/10.3201/eid2712.211465
4. World Health Organization. Classification of Omicron (B.1.1.529): SARS-CoV-2 variant of concern. 2021 Nov 26 [cited 2022 Jan 5]. https://www.who.int/news/item/26-11-2021-classification-of-omicron-(b.1.1.529)-sars-cov-2-variant-of-concern
5. Larremore DB, Fosdick BK, Bubar KM, Zhang S, Kissler SM, Metcalf CJE, et al. Estimating SARS-CoV-2 seroprevalence and epidemiological parameters with uncertainty from serological surveys. eLife. 2021;10:e64206. https://doi.org/10.7554/eLife.64206

6. Madhi SA, Kwatra G, Myers JE, Jassat W, Dhar N, Mukendi CK, et al. Population immunity and Covid-19 severity with Omicron variant in South Africa. N Engl J Med. 2022;NEJMoa2119658. https://doi.org/10.1056/NEJMoa2119658

Address for correspondence: Jackie Kleynhans, Centre for Respiratory Diseases and Meningitis, National Institute for Communicable Diseases of the National Health Laboratory Service, 1 Modderfontein Rd, Sandringham, 2192, Johannesburg, South Africa; email: jackiel@nicd.ac.za

Angiostrongylus cantonensis in a Red Ruffed Lemur at a Zoo, Louisiana, USA

Jessica Rizor, Ryan A. Yanez, Tuddow Thaiwong, Matti Kiupel

Authors affiliation: Michigan State University Veterinary Diagnostic Laboratory, Lansing, Michigan, USA

DOI: https://doi.org/10.3201/eid2805.212287

A red ruffed lemur (*Varecia rubra*) from a zoo in Louisiana, USA, was euthanized for worsening paresis. Brain and spinal cord histology identified eosinophilic meningoencephalomyelitis with intralesional adult *Angiostrongylus* sp. nematodes. PCR and sequencing confirmed *A. cantonensis* infection, indicating this parasite constitutes an emerging zoonosis in the southeastern United States.

Angiostrongylus cantonensis is a parasitic metastrongyloid nematode that has a neurotropic larval stage and is endemic throughout Southeast Asia and the Pacific Islands. The rat (*Rattus* spp.) is the main definitive host and a variety of gastropods serve as intermediate hosts. In rats, infections cause no brain damage and only some pulmonary disease in severe infections. However, in aberrant hosts, including humans and nonhuman primates, larvae cause severe eosinophilic meningoencephalitis. Clinical signs are associated with migration of the larvae and the immune response to dead or dying nematodes (*1*).

In 1987, *A. cantonensis* nematodes were detected in rats in New Orleans, Louisiana, USA (*2*); in 1995, a human case of eosinophilic meningitis was reported in North America in a child from New Orleans (*3*). *A. cantonensis* nematodes have now become endemic in the southeastern United States, as evidenced by reports of infection in a child in Texas (*4*); a horse from Mississippi (*5*); captive Geoffroy's tamarins (*Saguinus geoffroyi*) in Alabama (*6*); and several animals in Florida, including a white-handed gibbon (*Hylobates lar*), an orangutan (*Pongo pygmaeus*), a white-throated capuchin monkey (*Cebus capucinus*), a red ruffed lemur (*Varecia rubra*), and a nine-banded armadillo (*Dasypus novemcinctus*) (*7*,*8*). Ingestion of infected gastropods and paratenic hosts or unwashed contaminated vegetables are proposed routes of infection for aberrant hosts.

The International Union for Conservation of Nature lists red ruffed lemurs (*Varecia rubra*) as critically endangered (*9*). In June 2021, a 9-year-old male red ruffed lemur from a zoo in Louisiana was humanely euthanized because of hind limb paresis and a right head tilt that worsened over an 8-day period. The lemur was housed in a troop of 5 adult lemurs in an outdoor exhibit. Various snail species are common in the enclosure, but no other lemurs were clinically affected.

A necropsy performed at the Michigan State University Veterinary Diagnostic Laboratory (Lansing, Michigan, USA) identified no gross lesions. The laboratory formalin-fixed and processed the brain, the entire spinal cord, and all major organs for histopathology. Histopathologic examination revealed multiple transverse and longitudinal sections of adult nematodes within the subarachnoid space and neuropil of the cerebellum and brainstem. Nematodes were ≈50–70 μm in diameter and had a 3–4-μm thick smooth, eosinophilic cuticle and prominent lateral cords. Adult nematodes had coelomyarian musculature, and the pseudocoelom contained a reproductive tract and an intestinal tract lined by multinucleated cells with flocculent eosinophilic to brown material in the lumen (Figure). Nematodes were surrounded by hemorrhage and small numbers of eosinophils, neutrophils, macrophages, and glial cells. Several cerebellar folia were effaced by invading nematodes, hemorrhage, and inflammation. The cerebellar meninges were expanded by numerous eosinophils, fewer neutrophils, foamy macrophages, multinucleated giant cells, and lymphocytes. A representative section of thoracic spinal cord contained an identical single adult nematode in the subdural space. Another adult nematode had regionally effaced the dorsal horn in a section of lumbar spinal cord. The affected spinal cord had regional rarefaction of both gray and white

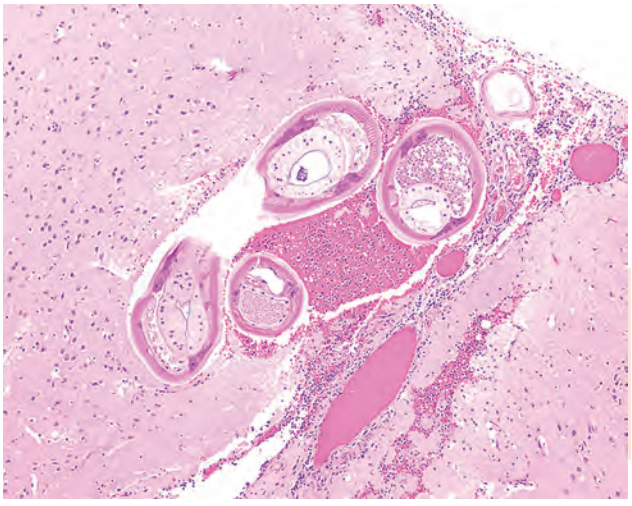

Figure. Formalin-fixed brainstem specimen from red ruffed lemur (*Varecia rubra*) infected with *Angiostrongylus cantonensis* nematodes at a zoo in Louisiana, USA. Hematoxylin and eosin stain shows adult nematodes measuring ≈50–70 μm in diameter with 3–4 μm thick, smooth, eosinophilic cuticle and prominent lateral cords. Nematodes have a coelomyarain musculature and a pseudocoelom that contains a reproductive tract and an intestinal tract, lined by multinucleated cells. Original magnification ×10.

matter and marked variation in myelin sheath size. The spinal cord meninges were similarly expanded by moderate numbers of eosinophils, lymphocytes, plasma cells, and fewer eosinophils.

We suspected *Angiostrongylus* sp. nematode infection on the basis of histomorphologic findings and anatomic features of migrating nematodes. We extracted nematode DNA by using a QIAamp DNA FFPE Tissue Kit (QIAGEN, https://www.qiagen.com) following the manufacturer's instructions. We performed species identification by PCR on paraffin-embedded brain tissue using primers (forward 5′-TGA AAT CGT TGA AGT GGA ACC-3′ and reverse 5′-GTC GCA ACC TGT ACG CTC TAC-3′) that we designed specifically to amplify an ≈500-bp product of the 28S ribosomal RNA gene. Sanger sequencing of the amplicon revealed >99% similarity to *A. cantonensis* (GenBank accession no. AY292792.1), 92% to *A. vasorum* (GenBank accession no. AM039758.1), and 91% to *A. chabaudi* (GenBank accession no. KM216825.1).

In the southeastern United States, *A. cantonensis* nematodes have emerged as clinically significant parasites in mammals, including humans, causing severe neurologic disease and death. Our findings illustrate another example of a nonhuman primate succumbing to infection and should raise awareness of the potential risk for infection in endemic areas. Diagnosing *A. cantonensis* infection in a live patient is challenging because of nonspecific clinical signs, ineffective serologic testing, and inability to detect adult nematodes in cerebrospinal fluid. Real time PCR performed on cerebrospinal fluid has detected DNA remnants of larvae in 22 of 33 human patients with eosinophilic meningitis (*10*). Because diagnosing and treating *A. cantonensis* infection is difficult, awareness and prevention are key. Humans and animals should only consume thoroughly cleaned vegetables and fully cooked gastropods and paratenic hosts. Persons living in affected areas can reduce risks for invasive gastropod species to become established by protecting food storage areas and local gardens from rats and gastropods.

In conclusion, the *A. cantonensis* nematode is emerging in the southeastern United States, and its range seems to be expanding. Because this parasite can infect a wide variety of mammals, including humans, both human and veterinary caretakers should remain vigilant for this zoonotic pathogen.

Acknowledgments

We thank Zoosiana in Broussard, Louisiana, and All Creatures Veterinary Hospital in New Iberia, Louisiana, for their dedication in caring for these animals.

About the Author

Ms. Rizor is a third-year doctor of veterinary medicine candidate at Michigan State University College of Veterinary Medicine in Lansing, Michigan, USA. Her main research interests are immunology and infectious diseases.

References

1. da Silva AJ, Morassutti AL. *Angiostrongylus* spp. (Nematoda; Metastrongyloidea) of global public health importance. Res Vet Sci. 2021;135:397–403. https://doi.org/10.1016/j.rvsc.2020.10.023
2. Kim DY, Stewart TB, Bauer RW, Mitchell M. *Parastrongylus* (=*Angiostrongylus*) *cantonensis* now endemic in Louisiana wildlife. J Parasitol. 2002;88:1024–6. https://doi.org/10.1645/0022-3395(2002)088[1024:PACNEI]2.0.CO;2
3. New D, Little MD, Cross J. *Angiostrongylus cantonensis* infection from eating raw snails. N Engl J Med. 1995;332:1105–6. https://doi.org/10.1056/NEJM199504203321619
4. Al Hammoud R, Nayes SL, Murphy JR, Heresi GP, Butler IJ, Pérez N. *Angiostrongylus cantonensis* meningitis and myelitis, Texas, USA. Emerg Infect Dis. 2017;23:1037–8. https://doi.org/10.3201/eid2306.161683
5. Costa LRR, McClure JJ, Snider III TG, Stewart TB. Verminous meningoencephalomyelitis by *Angiostrongylus* (=*Parastrongylus*) *cantonensis* in an American miniature horse. Equine Vet Educ. 2000;12:2–6. https://doi.org/10.1111/j.2042-3292.2000.tb01754.x
6. Kottwitz JJ, Perry KK, Rose HH, Hendrix CM. *Angiostrongylus cantonensis* infection in captive Geoffroy's tamarins (Saguinus geoffroyi). J Am Vet Med

Assoc. 2014;245:821–7. https://doi.org/10.2460/javma.245.7.821
7. Duffy MS, Miller CL, Kinsella JM, de Lahunta A. *Parastrongylus cantonensis* in a nonhuman primate, Florida. Emerg Infect Dis. 2004;10:2207–10. https://doi.org/10.3201/eid1012.040319
8. Walden HDS, Slapcinsky J, Rosenberg J, Wellehan JFX. *Angiostrongylus cantonensis* (rat lungworm) in Florida, USA: current status. Parasitology. 2021;148:149–52. https://doi.org/10.1017/S0031182020001286
9. Borgerson C, Eppley TM, Patel E, Johnson S, Louis EE, Razafindramanana J. *Varecia rubra*. IUCN red list of threatened species 2018 [cited 2018 July 5]. https://www.iucnredlist.org/species/22920/115574598
10. Qvarnstrom Y, Xayavong M, da Silva AC, Park SY, Whelen AC, Calimlim PS, et al. Real-time polymerase chain reaction detection of *Angiostrongylus cantonensis* DNA in cerebrospinal fluid from patients with eosinophilic meningitis. Am J Trop Med Hyg. 2016;94:176–81. https://doi.org/10.4269/ajtmh.15-0146

Address for correspondence: Matti Kiupel, Michigan State University Veterinary Diagnostic Laboratory, 4125 Beaumont Rd, Lansing, MI 48910, USA; email: kiupel@msu.edu

Breast Milk as Route of Tick-Borne Encephalitis Virus Transmission from Mother to Infant

Jana Kerlik, Mária Avdičová, Monika Musilová, Jana Bérešová, Roman Mezencev

Author affiliations: Regional Public Health Authority, Banská Bystrica, Slovakia (J. Kerlik, M. Avdičová, M. Musilová, J. Bérešová); Slovak Medical University Faculty of Medicine, Bratislava, Slovakia (M. Avdičová); Georgia Institute of Technology, Atlanta, Georgia, USA (R. Mezencev)

DOI: https://doi.org/10.3201/eid2805.212457

Tick-borne encephalitis virus (TBEV) is transmitted mainly by tick bites, but humans can acquire infection through consuming unpasteurized milk from infected animals. Interhuman transmission of TBEV by breast milk has not been confirmed or ruled out. We report a case of probable transmission of TBEV from an unvaccinated mother to an infant through breast-feeding.

Alimentary outbreaks of tickborne encephalitis (TBE) have been caused by consuming unpasteurized milk from infected goats, sheep, and rarely also from cows (*1*). Although tick-borne encephalitis virus (TBEV) has been isolated from milk of infected animals (*2*–*4*), interhuman transmission through breast milk has not yet been established (*5*).

At the end of May 2020, a 29-year-old woman had temporal lobe headache, neck stiffness, muscle weakness, and her temperature increased to 38.5°C. Her condition did not improve for 3–4 days, and on May 29, she was admitted to an emergency care facility. At admission, the patient reported having a transient fever 1 week before her admission that lasted several days. Her clinical evaluation led to an initial diagnosis of a neuroinfection.

Subsequently, the patient had peripheral paresis develop in the right upper limb and paresthesia in the left hand. On the second day of hospitalization, she had a generalized seizure, low peripheral O_2 saturation of 80%, and stupor. Test results for TBEV IgM were positive for serum and cerebrospinal fluid.

Before hospitalization, the patient was breastfeeding her 8-month-old infant, including the entire period when she had clinical symptoms. On May 31, when the patient was transferred to an intensive care unit, the infant was admitted to an inpatient care unit because of fever (temperature ≤40°C) since the previous day. The infant did not show signs of meningeal irritation, and cerebrospinal fluid was negative for TBEV IgM. Therefore, the infant was discharged and started home care on June 4. Tests for detection of the TBEV RNA by reverse transcription PCR were not performed.

In the days after discharge, the temperature of the infant increased to 38°C. On June 11, the infant was evaluated in an emergency medical facility because of a low-grade fever and more prominent apathy. However, the infant was not admitted to an in-patient care unit and was discharged because the condition was not considered clinically serious and was thought to represent teething effects. However, on June 25, a serum specimen from the infant was collected at the office of a district pediatrician and tested for TBEV antibody. The test result was positive for TBEV IgM.

Cases of TBE in infants have been infrequently reported. However, the increasing number of cases reported more recently from several countries in Europe implies that TBE might be underreported and not exceedingly rare in infants (*6*). Some of these cases that lack a history of tick bites might have resulted from another route of transmission.

Breast-feeding is a probable route of mother-to-child transmission of TBEV because alimentary infections by unpasteurized raw milk and dairy products from infected animals have been confirmed in humans (*1*–*4*), and mother-to-child transmission during breastfeeding has been demonstrated for Zika virus, another flavivirus that can also cross the intestinal barrier in experimental models (*7*). Depending on the animal species, TBEV is typically present in blood of infected ungulates for 1–5 days and in their milk for 2–8 days (*3*,*4*).

Conversely, this mode of transmission has not yet been conclusively demonstrated in humans. Thus far, transmission by breast milk has been suggested in a single report of serologically confirmed TBE in a mother and her breast-fed 10-day old newborn from Lithuania (*5*). We report another probable case of mother-to-infant transmission of TBEV by breast milk that is supported by clinical, epidemiologic, and serologic findings.

The incubation period for TBE is usually 7–14 days for tickborne disease but only 3–4 days for alimentary infection (*8*). These findings are consistent with the observed incubation period in the infant. The mother was hospitalized on May 29, a week after she had a transient fever. The infant had initial clinical signs of TBE on May 30.

The family lived in a disease-endemic area of Banská Bystrica, Slovakia, that had the highest rate of TBE illness in this country. According to her husband, the mother consumed dairy products from an animal farm and had a tick bite 1 month before her hospitalization. He also reported lack of tick bites and denied the infant had consumed unpasteurized dairy products. The mother had not been vaccinated against TBE.

Vaccination against TBE has showed 99% efficacy (*9*) and provides short-term protection to newborns and infants through transplacental transfer of antibodies from vaccinated mothers (*10*). Because vaccination of children is recommended at 1 year of age, only nonpharmaceutical measures are available to prevent TBE in younger children.

Although alimentary transmission of TBEV from infected animals to humans by drinking raw milk has been confirmed (*1*,*4*–*8*), mother-to-child transmission through breast milk has not (*2*). The case in this study indicates probable transmission of TBEV from an unvaccinated mother to her offspring through breast milk. This mode of transmission, if further confirmed, can have considerable implications for management of breast-feeding in unvaccinated mothers after tick bites in TBEV-endemic areas.

About the Author

Dr. Kerlik is an epidemiologist at the Regional Health Authority, Banská Bystrica, Slovakia. Her primary research interests are vector-borne diseases with a focus on tick-borne encephalitis.

References

1. Kerlik J, Avdičová M, Štefkovičová M, Tarkovská V, Pántiková Valachová M, Molčányi T, et al. Slovakia reports highest occurrence of alimentary tick-borne encephalitis in Europe: analysis of tick-borne encephalitis outbreaks in Slovakia during 2007–2016. Travel Med Infect Dis. 2018;26:37–42. https://doi.org/10.1016/j.tmaid.2018.07.001
2. Grešíková M. Excretion of tick-borne encephalitis virus by goat's milk [in Slovak]. Veterinársky Casopis Slovenskej Akadémie Vied. 1957;6:177–83.
3. Grešíková M. Excretion of the tickborne encephalitis virus in the milk of subcutaneously infected cows [in Slovak]. Acta Virol. 1958;2:188–92.
4. Grešíková M. Recovery of the tick-borne encephalitis virus from the blood and milk of subcutaneously infected sheep [in Slovak]. Acta Virol. 1958;2:113–9.
5. Vaisvieliene D. TBE in Lithuania. In: Süss, J, Kahl O, editors. Proceedings of the Fourth International Potsdam Symposium on Tick-Borne Diseases; Potsdam, Germany; February 21–22, 1997. Lengerich (Germany): Pabst Science Publishers; 1997. p. 100–13.
6. Steffen R. Tick-borne encephalitis (TBE) in children in Europe: epidemiology, clinical outcome and comparison of vaccination recommendations. Ticks Tick Borne Dis. 2019;10:100–10. https://doi.org/10.1016/j.ttbdis.2018.08.003
7. Desgraupes S, Hubert M, Gessain A, Ceccaldi PE, Vidy A. Mother-to-child transmission of arboviruses during breastfeeding: from epidemiology to cellular mechanisms. Viruses. 2021;13:1312. https://doi.org/10.3390/v13071312
8. Dumpis U, Crook D, Oksi J. Tick-borne encephalitis. Clin Infect Dis. 1999;28:882–90. https://doi.org/10.1086/515195
9. Heinz FX, Holzmann H, Essl A, Kundi M. Field effectiveness of vaccination against tick-borne encephalitis. Vaccine. 2007;25:7559–67. https://doi.org/10.1016/j.vaccine.2007.08.024
10. Eder G, Kollaritsch H. Antigen dependent adverse reactions and seroconversion of a tick-borne encephalitis vaccine in children. Vaccine. 2003;21:3575–83. https://doi.org/10.1016/S0264-410X(03)00422-5

Address for correspondence: Jana Kerlik, Regional Health Authority, Cesta k Nemocnici 1, Banská Bystrica 97556, Slovakia; email: jana.kerlik@vzbb.sk

atpE Mutation in *Mycobacterium tuberculosis* Not Always Predictive of Bedaquiline Treatment Failure

Laure Fournier Le Ray, Alexandra Aubry, Wladimir Sougakoff, Matthieu Revest, Jérôme Robert, Isabelle Bonnet, Nicolas Veziris, Florence Morel

Author affiliations: Sorbonne Université, Institut National de la Santé et de la Recherche Médicale, Paris, France (L. Fournier Le Ray, A. Aubry, W. Sougakoff, J. Robert, I. Bonnet, N. Veziris, F. Morel); Hôpital Pitié-Salpêtrière, Assistance Publique–Hôpitaux de Paris, Sorbonne Université, Paris, France (A. Aubry, W. Sougakoff, J. Robert, I. Bonnet, F. Morel); Pontchaillou University Hospital, Rennes, France (M. Revest); Université de Rennes, Institut National de la Santé et de la Recherche Médicale, Rennes (M. Revest); Hôpital Saint-Antoine, Assistance Publique–Hôpitaux de Paris, Sorbonne Université, Paris (N. Veziris)

DOI: https://doi.org/10.3201/eid2805.212517

We report the emergence of an *atpE* mutation in a clinical *Mycobacterium tuberculosis* strain. Genotypic and phenotypic bedaquiline susceptibility testing displayed variable results over time and ultimately were not predictive of treatment outcome. This observation highlights the limits of current genotypic and phenotypic methods for detection of bedaquiline resistance.

Bedaquiline is one of the core drugs used to treat multidrug-resistant (MDR) tuberculosis (TB) and extensively drug-resistant TB (XDR TB) (*1*). Bedaquiline resistance is now part of the revised definition of XDR TB, and its incidence is rising alarmingly (*2*,*3*). Resistance to bedaquiline is mainly caused by mutations in *Rv0678* (*mmpR*), which encodes the repressor of the efflux pump MmpL5−MmpS5, usually leading to low-level resistance (*4*). Conversely, mutations in *atpE*, which encodes the target of bedaquiline, the c subunit of the ATP synthase, are rarely described in clinical strains (*5*) and are associated with high increase of MICs (*4*). Mutations in *pepQ* and *Rv1979c* are also reported, but their effect on bedaquiline susceptibility is unclear. We report a case of an *atpE* mutation in a bedaquiline-resistant clinical strain of *Mybobacterium tuberculosis* and discuss the performances of current methods for susceptibility testing (Appendix, https://wwwnc.cdc.gov/EID/article/28/5/21-2517-App1.pdf) and their clinical implications (*6*).

A 32-year-old man from Georgia received a diagnosis of bilateral cavitary lung MDR TB upon his arrival in France in January 2020. Three consecutive treatment regimens of bedaquiline and clofazimine had failed. A fourth regimen combining bedaquiline, linezolid, cycloserine, clofazimine, delamanid, and amoxicillin/clavulanate + meropenem was initiated on arrival.

The first isolate from January 2020 (S1) was bedaquiline-resistant with a MIC one dilution above the breakpoint (MIC = 2 mg/L) and clofazimine-susceptible with a MIC close to the breakpoint (MIC = 1 mg/L). We detected 2 deletions (P129fs [15%] and G66fs [54%]) in Rv0678 (Figure).

At the end of March 2020, cycloserine was withdrawn because of phenotypic resistance, and bedaquiline, which had been stopped 1 month earlier, was resumed; the patient underwent a lobectomy. One month after, sputum microscopic examination and culture were still positive. The second isolate (S2) from April 2020 had an increased bedaquiline MIC (4 mg/L) but clofazimine MIC remained unchanged (1 mg/L). No mutation in Rv0678 was detected, but we observed an AtpE I66M (63%) substitution (Figure).

Two months later in June, the patient was sputum smear-negative but remained culture positive. Isolate S3 was susceptible to bedaquiline (MIC = 0.5 mg/L) and clofazimine resistant (MIC = 2 mg/L). A deletion was found in Rv0678 different from those identified in S1: deletion at position 293 (N98fs) (97%), whereas no mutation was identified in atpE (Figure). Verapamil and ethionamide were added and amoxicillin-clavulanate + meropenem was stopped. Finally, samples from September 2020 were culture negative, with regression of pulmonary lesions. The outcome was classified as treatment success in February 2021 after 13 months of treatment and was still favorable as of December 2021.

All 3 isolates shared the same spoligotype (SIT1) (Beijing lineage) and displayed only 3 single-nucleotide variants (SNVs) of difference by pairwise comparison. The SNVs were all nonsynonymous. Two SNVs were only recovered in strain S2, 1 corresponding to the AtpE: I66M substitution and 1 located in *Rv0243* (L136P substitution) encoding the acetyl−CoA acyltransferase FadA2 and probably implicated in lipid degradation. One SNV was only found in S1 in *Rv3909* (M683L substitution), encoding a protein of unknown function. No mutations were observed in *pepQ*, its promoter, or in *Rv1979c* (*7*).

As this case illustrates, identifying bedaquiline resistance in the laboratory and its effects on patient management appear complex. Over a 6-month period, we tested 3 *M. tuberculosis* isolates with different genotypic and phenotypic patterns regarding

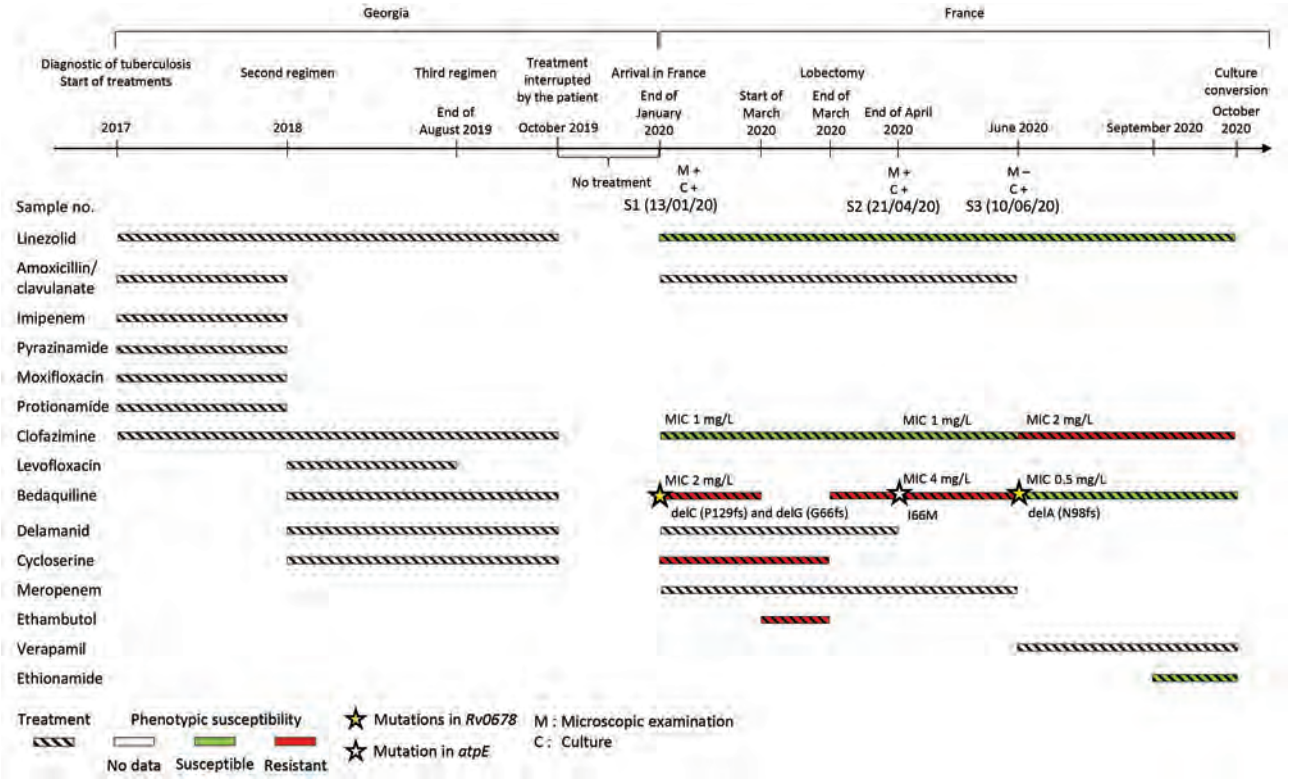

Figure. Timeline of treatment regimen and microbiologic data for patient with multidrug-resistant tuberculosis before and after his arrival in France from Georgia. Timeline for each antibiotic indicates treatment (striped), phenotypic resistance (red), and susceptibility (green), as indicated in patient records. M, microscopic examination; C, culture.

bedaquiline, exhibiting various MIC levels and mutations in genes involved in bedaquiline resistance. These isolates displayed only 3 SNVs by pairwise comparison of their genomes, excluding a reinfection by a new strain or a mixed infection.

Of note, mutations in *atpE* or *Rv0678* were found only once and were not found at subsequent timepoints. Despite continuous bedaquiline treatment, resistant strain S2 with the *atpE* mutation was not selected, and the patient was cured. A previous in vitro study suggested that, whereas *Rv0678* mutations were dynamic over time, *atpE* mutations were fixed once they appeared (*8*). This observation was not confirmed by our clinical case. One possible explanation for nonfixation of these mutations could be the associated fitness cost. However, an in vitro study did not show any fitness cost because of the I66M substitution (*9*). Because fitness also depends on the genetic background, the results of this in vitro study might not be transposable here. Regarding *Rv0678*, 2 mutations have been studied and did not have fitness impact (E138G and R94Q) (*4*). Additional in vivo and epidemiologic studies would help evaluate the fitness cost of such mutations. Another explanation for the variability of genotypic and phenotypic bedaquiline susceptibility over time could be a spatial heterogeneity in the lesions as already described (*10*).

This case raises concerns about the ability of current phenotypic and genotypic methods to detect bedaquiline resistance. Further studies are needed before relying on these methods for therapeutic decisions. In the meantime, these data can help improve the World Health Organization database of drug resistance–related mutations (*11*). Overall, this case underlines the complexity of bedaquiline-resistance mechanisms and of the dynamics of mutation emergence and selection.

Acknowledgments

We thank the technicians of NRC MyRMA for their technical assistance.

We wish to honor the memory of our colleague, Wladimir Sougakoff, who passed away in January 2022.

NRC MyRMA is supported by annual grant of Santé Publique France. L.F.L.R. was supported by a grant for Fondation du Souffle. The laboratory has received a research grant from Janssen for study on bedaquiline antimycobacterial activity.

About the Author

Dr. Fournier Le Ray recently successfully defended a PhD thesis in microbiology. Her research was focused on the in vivo emergence of bedaquiline resistance.

References

1. Van Deun A, Decroo T, Piubello A, de Jong BC, Lynen L, Rieder HL. Principles for constructing a tuberculosis treatment regimen: the role and definition of core and companion drugs. Int J Tuberc Lung Dis. 2018;22:239–45. https://doi.org/10.5588/ijtld.17.0660
2. World Health Organization. Meeting report of the WHO expert consultation on the definition of extensively drug-resistant tuberculosis, 27–29 October 2020 [cited 2021 Feb 5]. https://www.who.int/publications/i/item/meeting-report-of-the-who-expert-consultation-on-the-definition-of-extensively-drug-resistant-tuberculosis
3. Andres S, Merker M, Heyckendorf J, Kalsdorf B, Rumetshofer R, Indra A, et al. Bedaquiline-resistant tuberculosis: dark clouds on the horizon. Am J Respir Crit Care Med. 2020;201:1564–8. https://doi.org/10.1164/rccm.201909-1819LE
4. Andries K, Villellas C, Coeck N, Thys K, Gevers T, Vranckx L, et al. Acquired resistance of *Mycobacterium tuberculosis* to bedaquiline. PLoS One. 2014;9:e102135. https://doi.org/10.1371/journal.pone.0102135
5. Peretokina IV, Krylova LY, Antonova OV, Kholina MS, Kulagina EV, Nosova EY, et al. Reduced susceptibility and resistance to bedaquiline in clinical *M. tuberculosis* isolates. J Infect. 2020;80:527–35. https://doi.org/10.1016/j.jinf.2020.01.007
6. World Health Organization. Technical manual for drug susceptibility testing of medicines used in the treatment of tuberculosis. 2018 [cited 2018 Oct 18]. https://apps.who.int/iris/handle/10665/275469
7. Battaglia S, Spitaleri A, Cabibbe AM, Meehan CJ, Utpatel C, Ismail N, et al. Characterization of genomic variants associated with resistance to bedaquiline and delamanid in naive mycobacterium tuberculosis clinical strains. J Clin Microbiol. 2020;58:1304–24. https://doi.org/10.1128/JCM.01304-20
8. Ismail N, Ismail NA, Omar SV, Peters RPH. In vitro study of stepwise acquisition of rv0678 and atpE mutations conferring bedaquiline resistance. Antimicrob Agents Chemother. 2019;63:e00292–19. https://doi.org/10.1128/AAC.00292-19
9. Huitric E, Verhasselt P, Koul A, Andries K, Hoffner S, Andersson DI. Rates and mechanisms of resistance development in *Mycobacterium tuberculosis* to a novel diarylquinoline ATP synthase inhibitor. Antimicrob Agents Chemother. 2010;54:1022–8. https://doi.org/10.1128/AAC.01611-09
10. Kaplan G, Post FA, Moreira AL, Wainwright H, Kreiswirth BN, Tanverdi M, et al. *Mycobacterium tuberculosis* growth at the cavity surface: a microenvironment with failed immunity. Infect Immun. 2003;71:7099–108. https://doi.org/10.1128/IAI.71.12.7099-7108.2003
11. World Health Organization. Catalogue of mutations in *Mycobacterium tuberculosis* complex and their association with drug resistance [cited 2022 Jan 18]. https://www.who.int/publications-detail-redirect/9789240028173

Address for correspondence: Nicolas Veziris, Faculté de Médecine Sorbonne Université, 91, boulevard de l'hôpital, 75013 Paris, France; email: nicolas.veziris@sorbonne-universite.fr

Emerging Novel Reassortant Influenza A(H5N6) Viruses in Poultry and Humans, China, 2021

Wenming Jiang, Chunxia Dong, Shuo Liu, Cheng Peng, Xin Yin, Shaobo Liang, Lin Zhang, Jinping Li, Xiaohui Yu, Yang Li, Jingjing Wang, Guangyu Hou, Zheng Zeng, Hualei Liu

Author affiliations: China Animal Health and Epidemiology Center, Qingdao, China (W. Jiang, S. Liu, C. Peng, X. Yin, S. Liang, L. Zhang, J. Li, X. Yu, Y. Li, J. Wang, G. Hou, H. Liu); Chongqing Animal Disease Prevention and Control Center, Chongqing, China (C. Dong, Z. Zeng)

DOI: https://doi.org/10.3201/eid2805.212163

A novel highly pathogenic avian influenza A(H5N6) clade 2.3.4.4b virus was isolated from a poultry market in China that a person with a confirmed case had visited. Most genes of the avian and human H5N6 isolates were closely related. The virus also exhibited distinct antigenicity to the Re-11 vaccine strain.

Highly pathogenic avian influenza A(H5N1) virus emerged in China in 1996. H5 viruses have spread to Eurasia since 2003, Africa since 2005, and North America since 2014–2015. These viruses cause huge economic losses to the poultry industry and pose substantial threats to human health. By March 2022, a total of 75 confirmed cases of human infection with influenza A(H5N6) virus had been reported, including 48 cases in China since 2021 (https://www.who.int/teams/global-influenza-programme/avian-influenza/monthly-risk-assessment-summary).

On July 9, 2021, a human case of H5N6 infection was reported in Chongqing, China. One day later, we conducted an epidemiologic survey in the poultry market the patient had visited and collected swab samples from poultry. We identified the samples as H5N6 subtype by using H5- and N6-specific primers and probes. We propagated the virus in 10-day-old specific pathogen–free chicken embryos and designated the isolate as A/chicken/Chonqqing/H1/2021(H5N6) (CK/CQ/H1). We sequenced the viral genome by using the Sanger method and deposited the sequences in GISAID (https://www.gisaid.org; accession nos. EPI1937512–9).

Phylogenetic analysis of the hemagglutinin (HA) genes showed that CK/CQ/H1 and A/Chongqing/

02/2021 were closely related genetically and belonged to subclade 2.3.4.4b, along with H5N6 human isolates from Sichuan (2021) and Hunan (2021) Provinces, indicating that their HA genes likely derived from wild bird strains that arrived in China in 2020 (Figure). Phylogenetic analysis of the neuraminidase (NA) genes showed that the isolate were most closely related to H5N6 isolates (subclade 2.3.4.4h) from China (Figure). The H5N8 viruses that arrived in China in late 2020 appear to have reassorted with clade 2.3.4.4h H5N6 viruses already circulating.

Sequence analysis suggested that the polymerase basic protein 1, polymerase acidic protein, and nucleoprotein genes of CK/CQ/H1 were closely related to those of H5N6 viruses in China, such as A/Environment/Guangdong/C18277136/2018(H5N6) and A/Muscovy duck/China/FJFZ21/2020(H5N6). The matrix protein gene was most closely related to those of H5N8 viruses in Korea and China such as A/wild bird/Korea/H496–3/2020(H5N8) and A/Cygnus columbianus/Hubei/49/2020(H5N8), the polymerase basic protein 2 gene to those of A/Environment/Guangxi/28753/2014(H3N2), and the nonstructural protein gene to those of A/Environment/Jiangxi/47054/2016(H4N2) (Appendix Table 1, https://wwwnc.cdc.gov/EID/article/28/5/21-2163-App1.pdf). These findings indicate that CK/CQ/H1 is a new reassortant virus with genes derived from different avian influenza virus subtypes in eastern Asia.

Analysis based on the HA amino acid sequence revealed the presence of a cleavage site (PLREKRRKR/GLF), suggesting that the isolate was highly pathogenic in chickens. The presence of receptor binding sites Q226 and G228 (H3 numbering) indicate that the isolate would preferentially bind to avian-like receptors (*1*). However, the receptor binding site mutations A137, N158, A160, N186, I192, Q222, and R227 (H3 numbering) could increase binding to human-like receptors (*2*–*5*).

Bioinformatics analysis identified many mutations that would increase virulence in mice, such as R114 and I115 (H3 numbering) of the HA gene; D30, M43, and A215 of the matrix protein 1 gene; S42, E55E, E66, M106, and F138 of the nonstructural protein 1 gene; the nonstructural protein 1 C-terminal ESEV motif of the PDZ domain at position aa 227–230; V89, D309, K339, G477, V495, E627, and T676 of

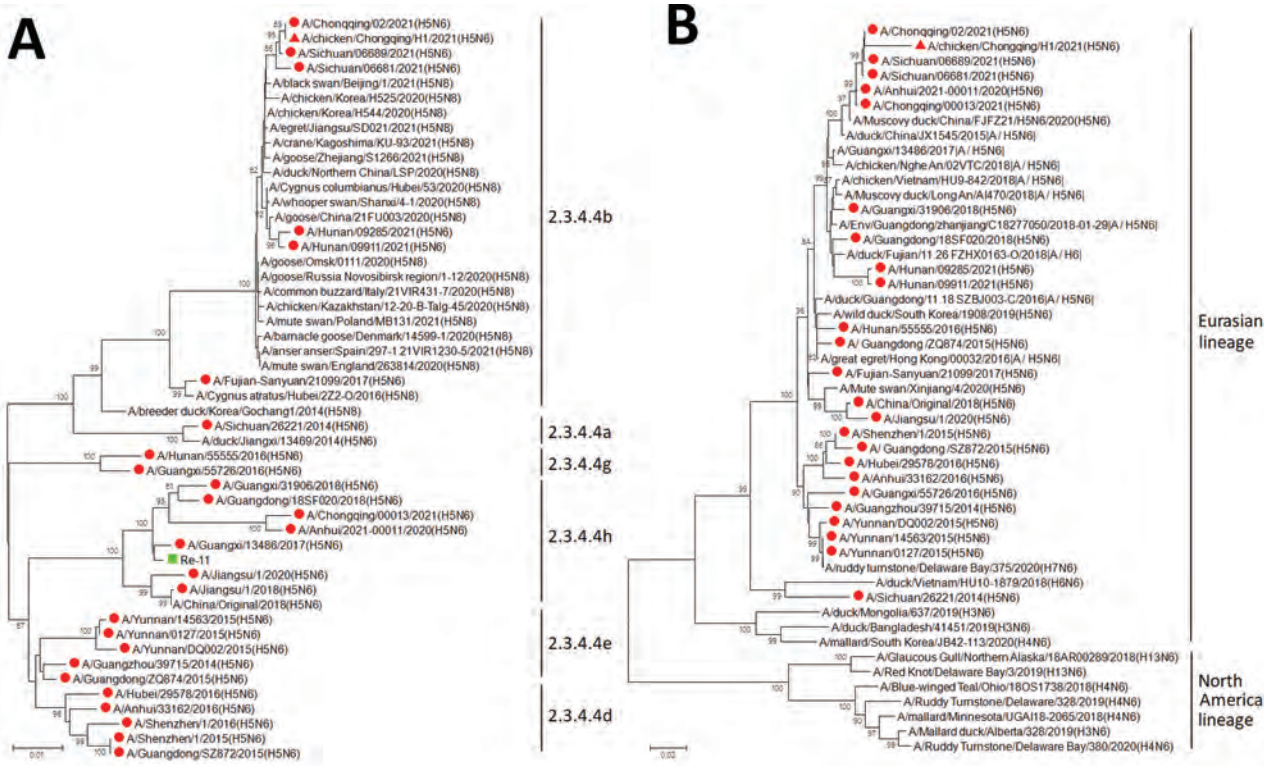

Figure. Phylogenetic trees of hemagglutinin (A) and neuraminidase (B) genes of H5 and N6 subtype influenza viruses collected from poultry and humans in China, 2021, and reference viruses. Red triangles indicate virus obtained in this study; red circles indicate human-infected avian influenza viruses; green squares indicate H5 Re-11 vaccine strain. Clade numbers and lineages are indicated on the right in panel. Trees were constructed with MEGA 5.10 software (https://www.megasoftware.net) using the neighbor-joining method. Bootstrap analysis was performed with 1,000 replications. Scale bars indicate nucleotide substitutions per site.

the polymerase basic protein 2 gene; V3 and G622 of the polymerase basic protein 1 gene; and D383 of the polymerase acidic protein gene (*6*). Mice inoculated with CK/CQ/H1 experienced a rapid and dramatic weight loss of >30%, had signs of illness, and died within 8 days (Appendix Figure).

Since 2019, the inactivated reassortant vaccine H5 Re-11 (clade 2.3.4.4h) has been used in China to control clade 2.3.4.4 viruses. We analyzed differences in antigenicity between CK/CQ/H1 and Re-11. The hemagglutination inhibition titer of Re-11 antiserum against CK/CQ/H1 was 5 $\log_2$ lower than that against the homologous Re-11 antigen, indicating that CK/CQ/H1 exhibited greater antigenic drift relative to the Re-11 vaccine strain. The variations of antigenicity-associated amino acid sites on HA might indicate the potential antigenic drift of CK/CQ/H1 (*7*) (Appendix Table 2).

We also evaluated the protective efficiency of Re-11 vaccine against the isolate. We vaccinated 3-week-old specific pathogen–free chickens with the Re-11 vaccine. At 21 days after vaccination, the vaccine induced very high levels of antibody against the vaccine antigen. Then, the birds were intranasally challenged with 10^6 50% egg infectious dose of CK/CQ/H1. All vaccinated birds displayed no clinical signs and survived, but 2 of them shed virus (Appendix Table 3). The results were inconsistent with those of Cui et al. (*8*), which may be related to bird species and immune background.

Novel H5N8 viruses of clade 2.3.4.4b virus have spread to China through migratory birds in late 2020 (*9*,*10*). These viruses are similar to those that were dominant in Europe from the autumn of 2020 through 2021 but have undergone reassortment since arriving in China, producing novel viruses like CK/CQ/H1. The novel virus we identified is highly pathogenic to both chickens and mice and exhibited distinct antigenicity to the Re-11 vaccine strain, which could not provide complete protection. Under field conditions, birds are unlikely to get sustained high levels of antibody and would more likely be susceptible to infection and virus shedding. New antigen-matched vaccines and more productive measures are needed to prevent and control novel H5N6 infection in poultry and humans.

This work was supported by the National Key Research and Development Program (grant no. 2021YFD1800201).

About the Author

Dr. Jiang is a veterinary researcher at the China Animal Health and Epidemiology Center. His research interests are the epidemiology and control of avian influenza virus.

References

1. Tharakaraman K, Raman R, Viswanathan K, Stebbins NW, Jayaraman A, Krishnan A, et al. Structural determinants for naturally evolving H5N1 hemagglutinin to switch its receptor specificity. Cell. 2013;153:1475–85. https://doi.org/10.1016/j.cell.2013.05.035
2. Yang ZY, Wei CJ, Kong WP, Wu L, Xu L, Smith DF, et al. Immunization by avian H5 influenza hemagglutinin mutants with altered receptor binding specificity. Science. 2007;317:825–8. https://doi.org/10.1126/science.1135165
3. Wang W, Lu B, Zhou H, Suguitan AL Jr, Cheng X, Subbarao K, et al. Glycosylation at 158N of the hemagglutinin protein and receptor binding specificity synergistically affect the antigenicity and immunogenicity of a live attenuated H5N1 A/Vietnam/1203/2004 vaccine virus in ferrets. J Virol. 2010;84:6570–7. https://doi.org/10.1128/JVI.00221-10
4. Gao Y, Zhang Y, Shinya K, Deng G, Jiang Y, Li Z, et al. Identification of amino acids in HA and PB2 critical for the transmission of H5N1 avian influenza viruses in a mammalian host. PLoS Pathog. 2009;5:e1000709. https://doi.org/10.1371/journal.ppat.1000709
5. Guo H, de Vries E, McBride R, Dekkers J, Peng W, Bouwman KM, et al. Highly pathogenic influenza A(H5Nx) viruses with altered H5 receptor-binding specificity. Emerg Infect Dis. 2017;23:220–31. https://doi.org/10.3201/eid2302.161072
6. Suttie A, Deng YM, Greenhill AR, Dussart P, Horwood PF, Karlsson EA. Inventory of molecular markers affecting biological characteristics of avian influenza A viruses. Virus Genes. 2019;55:739–68. https://doi.org/10.1007/s11262-019-01700-z
7. Li J, Zhang C, Cao J, Yang Y, Dong H, Cui Y, et al. Re-emergence of H5N8 highly pathogenic avian influenza virus in wild birds, China. Emerg Microbes Infect. 2021;10:1819–23. https://doi.org/10.1080/22221751.2021.1968317
8. Cui P, Zeng X, Li X, Li Y, Shi J, Zhao C, et al. Genetic and biological characteristics of the globally circulating H5N8 avian influenza viruses and the protective efficacy offered by the poultry vaccine currently used in China. Sci China Life Sci. 2021. https://doi.org/10.1007/s11427-021-2025-y
9. Li X, Lv X, Li Y, Peng P, Zhou R, Qin S, et al. Highly pathogenic avian influenza A(H5N8) virus in swans, China, 2020. Emerg Infect Dis. 2021;27:1732–4. https://doi.org/10.3201/eid2706.204727
10. He G, Ming L, Li X, Song Y, Tang L, Ma M, et al. Genetically divergent highly pathogenic avian influenza A(H5N8) viruses in wild birds, eastern China. Emerg Infect Dis. 2021;27:2940–3. https://doi.org/10.3201/eid2711.204893

Address for correspondence: Hualei Liu, Avian Diseases Surveillance Laboratory, China Animal Health and Epidemiology Center, No. 369 Nanjing Rd, Qingdao, 266032, China; email: liuhualei@cahec.cn

Mycobacterium lepromatosis as Cause of Leprosy, Colombia

Nora Cardona-Castro, María Victoria Escobar-Builes, Héctor Serrano-Coll, Linda B. Adams, Ramanuj Lahiri

Author affiliations: Colombian Institute of Tropical Medicine–CES University, Antioquia, Colombia (N. Cardona-Castro, M.V. Escobar-Builes, H. Serrano-Coll); US Department of Health and Human Services, Health Resources and Services Administration, Health Systems Bureau, National Hansen's Disease Program, Baton Rouge, Louisiana, USA (L.B. Adams, R. Lahiri)

DOI: https://doi.org/10.3201/eid2805.212015

Leprosy is a granulomatous infection caused by infection with *Mycobacterium leprae* or *M. lepromatosis*. We evaluated skin biopsy and slit skin smear samples from 92 leprosy patients in Colombia by quantitative PCR. Five (5.4%) patients tested positive for *M. lepromatosis*, providing evidence of the presence of this pathogen in Colombia.

The primary causal agent of leprosy is *Mycobacterium leprae*; however, as of February 2012, *M. lepromatosis* has been established as another etiologic agent that is still underexplored in many leprosy-endemic countries (*1*). Dual infections caused by both species have also been reported (*2*). The similarities between these bacteria initially led researchers to think *M. lepromatosis* was a new strain of *M. leprae*; however, it is now considered a new species because of ≈9% difference in whole-genome sequences (*3*).

The global prevalence and extent of *M. lepromatosis* infection are still unknown. Also unknown is whether *M. lepromatosis* can cause substantially different disease severity from *M. leprae* manifested as nerve damage, leprosy reactions (type I/II), relapse rate, and overall prognosis; these factors are essential to understanding the clinical implications and case management of patients with *M. lepromatosis* infection or co-infection. We report the presence of *M. lepromatosis* in patients in Colombia.

We performed *M. lepromatosis*– and *M. leprae*–specific real-time quantitative PCR (qPCR) on 67 skin lesion biopsies and 25 earlobe slit skin smears (SSS) from 92 multibacillary leprosy patients identified during 2006–2016. The participants were from 11 provinces: Atlántico, Antioquia, Bolívar, Chocó, Cesar, Cundinamarca, Magdalena, Santander, Norte de Santander, Sucre, and Tolima. All samples belonged to the Colombian Institute of Tropical Medicine (Antioquia, Colombia) and were stored in 70% ethanol. Before sample collection, all participants gave written informed consent for future research, and the institutional ethics committee for human research at CES University endorsed such use. We processed samples at the National Hansen's Disease Program (NHDP) Laboratory (Baton Rouge, LA, USA). We conducted *M. lepromatosis*– and *M. leprae*–specific qPCR on these samples following DNA extraction with DNeasy Kit (QIAGEN, https://www.qiagen.com) and using previously described primers and probes (*4*,*5*). Both these qPCR tests are Clinical Laboratory Improvement Amendments validated and are now used as routine diagnostic tests at the NHDP (*6*).

Of the study participants, 87% were male. Median age was 51.5 years (range 12–84 years). Thirty-seven percent of the participants lived in Santander and 34.8% in Atlantic Coast (Appendix Table 1, https://wwwnc.cdc.gov/EID/article/28/5/21-2015-App1.pdf). qPCRs amplified the repetitive element region specific to *M. lepromatosis* in 5 patients and the repetitive element region specific to *M. leprae* in all samples evaluated. Thus, 5.4% of the patient samples were positive for both *M. leprae* and *M. lepromatosis* and 94.6% (87 patients) were positive for *M. leprae* only (Table). The 5 patients coinfected with *M. lepromatosis* and *M. leprae* resided in geographic areas with a high burden of leprosy: Santander, Atlántico, and Chocó. Four had lepromatous leprosy (LL) and one had dimorphic LL; 1 of the patients had a history of type I leprosy reaction (Appendix Table 2).

Most leprosy-endemic countries do not conduct routine surveillance for *M. lepromatosis*, and so its true distribution and clinical effect are unknown as of 2022. However, this knowledge is crucial for clinical management and to understand the transmission network of leprosy-causing organisms. The earliest known population-based study to analyze the presence of both mycobacteria indicates that *M. lepromatosis* arrived in America with human populations that migrated from Asia through the Bering Strait, in contrast to *M. leprae*, which arrived

Table. *Mycobacterium lepromatosis* real-time quantitative PCR results for samples from 92 multibacillary leprosy patients identified during 2006–2016 in Columbia*

Characteristic	No. (%) positive
Biological samples	
Skin biopsies	67 (72.8)
SSS	25 (27.2)
Quantitative PCR	
RLEP positive (*M. leprae*)	87 (94.6)
M. lepromatosis and *M. leprae* positive	5 (5.4)

*RLEP, repetitive element in *M. leprae*, SSS, slit skin smears.

in America with the settlers and as a result of the slave trade (*7*). To clarify the clinical outcomes of *M. lepromatosis* infection, a study in Mexico associated both mycobacteria with the forms already classified by Ridley and Jopling (*8*). That study found that, of the 55 cases with *M. lepromatosis* as the sole etiologic agent, 34 manifested LL, 13 developed diffuse LL, and the remaining 8 had other forms of leprosy. Fourteen patients carried both mycobacteria and showed all clinical forms (*2*). In contrast, 15% of leprosy patients in Brazil who had *M. lepromatosis* as the sole agent had polar tuberculoid leprosy, none had LL, and patients with infection by both mycobacteria had LL (*7*). The same study evaluated 8 patients in Myanmar and found *M. lepromatosis* in 2 patients, both of whom had LL (*7*).

This study demonstrates presence of *M. lepromatosis* in samples taken by our research group before 2008 when this mycobacterium was first reported (*1*). Therefore, we infer that *M. lepromatosis* has coexisted with *M. leprae* in Colombia for some time. Finally, this report confirms *M. lepromatosis* in Colombia. Genomic surveillance is needed to monitor the infection dynamics of both mycobacteria among leprosy patients and contacts to stop transmission and limit the dire physical, social, economic, and emotional consequences that these organisms cause among susceptible persons.

Acknowledgments

We thank the patients and personnel of the leprosy control programs of Colombia for their collaboration.

The financial support for this work was assumed by the Colombian Institute of Tropical Medicine–CES University, Sabaneta, Antioquia, Colombia, and by United States Department of Health and Human Services, Health Resources and Services Administration, Health Systems Bureau, National Hansen's Disease Program, Baton Rouge, Louisiana, USA.

About the Author

Dr. Cardona-Castro is a full professor and senior researcher at the Colombian Institute of Tropical Medicine affiliated with CES University in Medellin, Colombia. Her research and teaching interests are focused on neglected and tropical infectious diseases.

References

1. Han XY, Seo Y-H, Sizer KC, Schoberle T, May GS, Spencer JS, et al. A new Mycobacterium species causing diffuse lepromatous leprosy. Am J Clin Pathol. 2008;130:856–64. https://doi.org/10.1309/AJCPP72FJZZRRVMM
2. Han XY, Sizer KC, Velarde-Félix JS, Frias-Castro LO, Vargas-Ocampo F. The leprosy agents Mycobacterium lepromatosis and Mycobacterium leprae in Mexico. Int J Dermatol. 2012;51:952–9. https://doi.org/10.1111/j.1365-4632.2011.05414.x
3. Levis WR, Zhang S, Martiniuk F. Mycobacterium lepromatosis: emerging strain or species? J Drugs Dermatol. 2012;11:158.
4. Sharma R, Singh P, McCoy RC, Lenz SM, Donovan K, Ochoa MT, et al. Isolation of Mycobacterium lepromatosis and development of molecular diagnostic assays to distinguish Mycobacterium leprae and M. lepromatosis. Clin Infect Dis. 2020;71:e262–9. https://doi.org/10.1093/cid/ciz1121
5. Truman RW, Andrews PK, Robbins NY, Adams LB, Krahenbuhl JL, Gillis TP. Enumeration of Mycobacterium leprae using real-time PCR. PLoS Negl Trop Dis. 2008;2:e328. https://doi.org/10.1371/journal.pntd.0000328
6. Kowalska M, Kowalik A. Mycobacterium leprae: pathogenic agent in leprosy. Discovery of new species Mycobacterium lepromatosis. Perspectives in research and diagnosis of leprosy. Int Marit Health. 2012;63:213–8.
7. Han XY, Aung FM, Choon SE, Werner B. Analysis of the leprosy agents Mycobacterium leprae and Mycobacterium lepromatosis in four countries. Am J Clin Pathol. 2014;142:524–32.
8. Ridley DS, Jopling WH. Classification of leprosy according to immunity. A five-group system. Int J Lepr Other Mycobact Dis. 1966;34:255-73.

Address for correspondence: Nora Cardona-Castro, Colombian Institute of Tropical Medicine–CES University. Cra 43 A # 52 Sur 99. Sabaneta, Antioquia, 055450, Colombia; email: ncardona@ces.edu.co

Rare Case of Rickettsiosis Caused by *Rickettsia monacensis*, Portugal, 2021

Rita de Sousa, Marta Leal dos Santos, Claudina Cruz, Vasco Almeida, Ana Raquel Garrote, Freddy Ramirez, Diana Seixas, Maria J. Manata, Fernando Maltez

Author affiliations: National Institute of Health Dr. Ricardo Jorge, Águas de Moura, Portugal (R. de Sousa); Hospital de Curry Cabral, Lisbon, Portugal (M. Leal dos Santos, C. Cruz, V. Almeida, A.R. Garrote, F. Ramirez, D. Seixas, M.J. Manata, F. Maltez)

DOI: https://doi.org/10.3201/eid2805.211836

We report a case of rickettsiosis caused by *Rickettsia monacensis* in an immunocompetent 67-year-old man in Portugal who had eschar, erythematous rash, and an attached *Ixodes ricinus* tick. Seroconversion and eschar biopsy led to confirmed diagnosis by PCR. Physicians should be aware of this rare rickettsiosis, especially in geographic regions with the vector.

Rickettsia monacensis, spotted fever group rickettsiae (SFGR), are bacteria transmitted by *Ixodes* spp. ticks and are rarely reported as causing disease in humans. Few cases have been documented and laboratory confirmed (*1*–*4*). *R. monacensis* infection causing Mediterranean spotted fever (MSF)–like rickettsiosis was described in 2007 for 2 patients from La Rioja and the Basque Country, Spain, followed by 1 case in Italy (2012) and 2 cases in South Korea (2017 and 2019) (*1*–*4*). Despite the few human infections described, *R. monacensis* is frequently found (0.5%– 42.5%) in *Ixodes ricinus* ticks in Europe, including Portugal and North Africa, and in another *Ixodes* species tick in Asia (*3*–*5*).

Three previously reported rickettsioses in Portugal were MSF caused by *R. conorii*, tick-borne lymphadenopathy caused by *R. slovaca*, and lymphangitis-associated rickettsiosis caused by *R. sibirica mongolitimonae* (*6*–*8*). We report *R. monacensis* infection in a human and *Rickettsia* in the attached tick.

In February 2021, a 67-year-old man with alcoholism–associated dilated cardiomyopathy and diabetes mellitus type 2 was hospitalized in Lisbon, Portugal. The patient reported a 5-day history of fever and appearance of rash on day 3 of fever onset. He lived in Lisbon and had traveled to a rural area 5 days before symptom onset. At admission, he had fever, fatigue, myalgia, and anorexia. Physical examination showed disperse upper-body erythematous exanthema, palmo-plantar erythema, and an eschar surrounded by erythema on his upper left back (Figure). An engorged female *I. ricinus* tick was removed from the patient. Laboratory evaluation showed hematologic, hepatic, and renal abnormalities; anemia (hemoglobin 9.7 g/dL); lymphopenia (420 cells/μL); thrombocytopenia (38,000 platelets/mm^3); and increased serum levels of creatinine (2.23 mg/dL), alanine aminotransferase (73 IU/L), aspartate aminotransferase (89 IU/L), creatine phosphokinase (116 IU/dL), lactate dehydrogenase (148 IU/L), and C-reactive protein (159.5 mg/L). Electrocardiography findings were unremarkable. Oral doxycycline (200 mg/d) was empirically started on hospitalization day 1.

After the patient had been hospitalized for 12 hours and received 1 dose of doxycycline, we biopsied the eschar and collected a blood sample. PCR and DNA sequence analysis of partial fragments of *omp*A and *glt*A genes from the tick and biopsy samples showed 100% identity with nucleotide sequences of *R. monacensis* (GenBank accession no. LN794217). Screening for *Borrelia* DNA in the tick was negative.

For antibody testing we used an immunofluorescence assay from FOCUS Diagnostics (https://www.focusdx.com), which used commercial *R. conorii* IFA substrate slides for IgG and IgM; results demonstrated seroconversion within 2 weeks in consecutively collected samples. We detected no antibodies in the acute-phase serum sample collected on day 6 after symptom onset, and we detected reactive antibodies against SFGR (IgM titer 32, IgG titer 128) in the second sample only, collected 3 weeks after illness onset (*9*). Supplemental methods and results are in the Appendix (https://wwwnc.cdc.gov/EID/article/28/5/21-1836-App1.pdf).

Figure. Patient with rickettsiosis caused by *Rickettsia monacensis*, Portugal, 2021. A) Rash and eschar; B) rash on soles; C) rash on palms.

Table. Clinical features and laboratory diagnosis of patients with *Rickettsia monacensis* infection, 2003–2021

Feature	Patient 1, La Rioja, Spain (*1*)	Patient 2, Basque, Spain (*1*)	Patient 3, Sardinia, Italy (*2*)	Patient 4, South Korea (*3*)	Patient 5, South Korea (*4*)	Patient 6, Portugal (this study)
Epidemiologic						
Age, y/ sex	84/M	59/F	28/M	73/M	75/F	67/M
Date of onset	Jun 2003	Sep 2003	Apr 2011	2006	Oct 2019	Feb 2021
Tick bite history	NK	Yes	NK	NK	NK	Yes
Clinical						
Fever, ºC (ºF)	Yes, 39.5º (103.1º)	Yes, 38º (100.4º)	Yes, 38.2º (100.8º)	Yes, 40º (104.0º)	Yes, 38.4º (101.1º)	Yes, 39.9º (103.8º)
Eschar (location)	No	No	Yes (calf)	Yes (back)	Yes (scalp)	Yes (back)
Rash	Yes	Yes	No	Yes	Yes	Yes
Type	Maculopapular	Erythematous		Maculopapular	Maculopapular	Erythematous
Including palm and soles	Yes					Yes
Headache	Yes	Yes	Yes	Yes	NK	Yes
Lymphadenopathy	NK	NK	NK	Yes	Yes	NK
Laboratory test results						
SFGR IFA titer						
Sample 1	<40 IgG	2,560 IgG	128 IgG	320 (IgM + IgG)	<16 IgM/32 IgG, negative	Negative
Sample 2	1,280 IgG (26 wk later)	1,280 IgG	NA	NA	16 IgM/128 IgG (2 mo)	32 IgM /128 IgG (2 wk)
Culture, blood/biopsy	Positive	Negative	NA	Positive	NA	NA
PCR detection, blood and/or skin biopsy	Positive	Positive	Positive	NK	Positive	Positive
Co-infections with other pathogens	NK	NK	NK	NK	*Orientia tsutsugamushi*	NK
Treatment						
Hospitalization	NA	NA	Yes	Yes	Yes	Yes
Antimicrobial drug	Doxycycline 100 mg every 12 h for 10 d	Doxycycline 100 mg every 12 h for 10 d	Doxycycline 100 mg every 12 h for 7 d	Azithromycin 500 mg, 1 dose	Doxycycline 200 mg/d	Doxycycline 200 mg/d

After 48 hours of antimicrobial therapy, the patient was afebrile; after 4 days, exanthema was completely resolved; and after 7 days, all symptoms had resolved. The patient was discharged and scheduled for outpatient follow-up.

We confirm that *R. monacensis* caused disease in this patient. Very few cases of human infection with *R. monacensis* have been reported, possibly because this species is not considered to be very pathogenic and for most patients might cause self-limited infection (*1*–*5*). Another hypothesis is that cases have been misdiagnosed or confirmed by serology only, which cannot distinguish among SFGR species (*8*,*9*). Moreover, if cases occur in the autumn/winter, when adult *I. ricinus* ticks are more active and outside the peak season (June–September) for MSF, some physicians might not think of rickettsiosis as the cause, particularly if there is no epidemiologic context and clinical findings are not highly suggestive.

For the patient reported here, we identified an eschar, as was done for the 3 other patients from Italy and South Korea (Table). However, the first 2 patients identified in Spain did not have any sign of an eschar. We are unaware whether any specific patient host factors could be associated with *R. monacensis* infection, but alcoholism in the patient reported here could have been a risk factor for severity (*8*). With exception of the patient from Italy, all patients were >59 years of age, including the patient from Portugal, and at least 3 were hospitalized. In general, it would seem that older persons are more susceptible to disease, even when infected with low-pathogenicity *Rickettsia*. For instance, in the case report of an 8-year-old child from Croatia with Lyme borreliosis, in whom *R. monacensis* DNA was also detected in a skin biopsy of the erythema migrans tissue, antibodies against *Borrelia* were detected but not antibodies against SFGR (*10*).

This case of infection with *R. monacensis*, formerly considered to be of low pathogenicity and found in *Ixodes* spp. ticks, was associated with disease in an immunocompetent patient. Other cases may be underdiagnosed, particularly outside the usual summer months when MSF cases peak in Portugal. Moreover, because *R. monacensis* shares the same vector as *Borrelia* spp. and these co-infections have been detected, physicians should be aware of this rickettsiosis, especially in areas where the vector is present.

About the Author

Dr. de Sousa is a public health microbiologist responsible for the Rickettsial and the Gastrointestinal Viral Infections Units at the National Institute of Health Dr. Ricardo Jorge. She works on research and diagnosis of rickettsial diseases.

References

1. Jado I, Oteo JA, Aldámiz M, Gil H, Escudero R, Ibarra V, et al. *Rickettsia monacensis* and human disease, Spain. Emerg Infect Dis. 2007;13:1405–7. https://doi.org/10.3201/eid1309.060186
2. Madeddu G, Mancini F, Caddeo A, Ciervo A, Babudieri S, Maida I, et al. *Rickettsia monacensis* as cause of Mediterranean spotted fever-like illness, Italy. Emerg Infect Dis. 2012;18:702–4. https://doi.org/10.3201/eid1804.111583
3. Kim YS, Choi YJ, Lee KM, Ahn KJ, Kim HC, Klein T, et al. First isolation of *Rickettsia monacensis* from a patient in South Korea. Microbiol Immunol. 2017;61:258–63. https://doi.org/10.1111/1348-0421.12496
4. Kim SW, Kim CM, Kim DM, Yun NR. Case report: coinfection with *Rickettsia monacensis* and *Oraientia tsutsugamushi.* Am J Trop Med Hyg. 2019;101:332–5. https://doi.org/10.4269/ajtmh.18-0631
5. Parola P, Paddock CD, Socolovschi C, Labruna MB, Mediannikov O, Kernif T, et al. Update on tick-borne rickettsioses around the world: a geographic approach. Clin Microbiol Rev. 2013;26:657–702. https://doi.org/10.1128/CMR.00032-13
6. de Sousa R, Pereira BI, Nazareth C, Cabral S, Ventura C, Crespo P, et al. *Rickettsia slovaca* infection in humans, Portugal. Emerg Infect Dis. 2013;19:1627–9. https://doi.org/10.3201/eid1910.130376
7. de Sousa R, Barata C, Vitorino L, Santos-Silva M, Carrapato C, Torgal J, et al. *Rickettsia sibirica* isolation from a patient and detection in ticks, Portugal. Emerg Infect Dis. 2006;12:1103–8. https://doi.org/10.3201/eid1207.051494
8. Sousa R, França A, Dória Nòbrega S, Belo A, Amaro M, Abreu T, et al. Host- and microbe-related risk factors for and pathophysiology of fatal *Rickettsia conorii* infection in Portuguese patients. J Infect Dis. 2008;198:576–85. https://doi.org/10.1086/590211
9. Portillo A, de Sousa R, Santibáñez S, Duarte A, Edouard S, Fonseca IP, et al. Guidelines for the detection of *Rickettsia* spp. Vector Borne Zoonotic Dis. 2017;17:23–32. https://doi.org/10.1089/vbz.2016.1966
10. Tijsse-Klasen E, Sprong H, Pandak N. Co-infection of *Borrelia burgdorferi* sensu lato and *Rickettsia* species in ticks and in an erythema migrans patient. Parasit Vectors. 2013;6:347.

Address for correspondence: Rita de Sousa, Av. Da Liberdade n°5, 2965, Águas de Moura, Portugal; email: rsr.desousa@gmail.com

Domestic Dogs as Sentinels for West Nile Virus but not *Aedes*-borne Flaviviruses, Mexico

Edward Davila,[1] Nadia A. Fernández-Santos,[1] José Guillermo Estrada-Franco, Lihua Wei, Jesús A. Aguilar-Durán, María de J. López-López, Roberto Solís-Hernández, Rosario García-Miranda, Doireyner Daniel Velázquez-Ramírez, Jasiel Torres-Romero, Susana Arellano Chávez, Raúl Cruz-Cadena, Roberto Navarro-López, Adalberto A. Pérez de León,[2] Carlos Guichard-Romero, Estelle Martin,[3] Wendy Tang, Matthias Frank, Monica Borucki, Michael J. Turell, Alex Pauvolid-Corrêa, Mario A. Rodríguez-Pérez, Héctor Ochoa-Díaz-López, Sarah A. Hamer, Gabriel L. Hamer

Author affiliations: Texas A&M University, College Station, Texas, USA (E. Davila, E. Martin, W. Tang, A. Pauvolid-Corrêa, S.A. Hamer, G.L. Hamer); Instituto Politécnico Nacional, Reynosa, México (N.A. Fernández-Santos, J.G. Estrada-Franco, L. Wei, J.A. Aguilar-Durán, M. de J. López-López, M.A. Rodríguez-Pérez); El Colegio de la Frontera Sur, San Cristóbal de Las Casas, México (R. Solís-Hernández, R. García-Miranda, D.D. Velázquez-Ramírez, J. Torres-Romero, H. Ochoa-Díaz-López); Universidad Autónoma de Chiapas, Tuxtla Gutiérrez, México (S. Arellano Chávez); Universidad Autónoma de Chiapas, Ocozocoautla de Espinosa, México (R. Cruz-Cadena); Comisión México-Estados Unidos para la Prevención de la Fiebre Aftosa y Otras Enfermedades Exóticas de los Animales, México City (R. Navarro-López); US Department of Agriculture Agricultural Research Service Knipling-Bushland Livestock Insects Research Laboratory, Kerrville, Texas, USA (A.A. Pérez de León); Zoológico Miguel Álvarez del Toro, Tuxtla Gutiérrez (C. Guichard-Romero); Lawrence Livermore National Laboratory, Livermore, California, USA (M. Frank, M. Borucki); VectorID LLC, Frederick, Maryland, USA (M.J. Turell)

DOI: https://doi.org/10.3201/eid2805.211879

We tested 294 domestic pet dogs in Mexico for neutralizing antibodies for mosquito-borne flaviviruses. We found high (42.6%) exposure to West Nile virus in Reynosa (northern Mexico) and low (1.2%) exposure in Tuxtla Gutierrez (southern Mexico) but very limited exposure to *Aedes*-borne flaviviruses. Domestic dogs may be useful sentinels for West Nile virus.

[1]These authors contributed equally to this article.

[2]Current affiliation: US Department of Agriculture Agricultural Research Service San Joaquin Valley Agricultural Sciences Center, Parlier, California, USA.

[3]Current affiliation: University of Florida, Gainesville, Florida, USA.

Mosquito-transmitted viruses represent substantial health burdens across the Americas. Despite the broad geographic ranges of *Aedes* spp. and *Culex* spp. mosquitoes, the endemicity of human arboviral diseases is incongruent with these vector distributions (*1*,*2*). Animal sentinels may therefore be useful for signaling areas of virus transmission and human risk, especially in resource-poor settings where human diseases may be underreported. Although *Ae. aegypti* mosquitoes have been considered to feed predominantly on humans and *Cx. quinquefasciatus* mosquitoes on birds, our recent work studying host feeding patterns in southern Texas, USA (*3*), and northern Mexico (*4*) has documented substantial feeding on dogs for both species, presenting a novel opportunity to evaluate dogs for possible sentinel surveillance. Because dogs are ubiquitous and share the domestic environment with humans, tracking their exposures might provide evidence for understanding human risk and a sensitive indicator of geographic variation for mosquito-borne disease risk. We aimed to estimate domestic dog exposure to Zika virus (ZIKV), dengue virus 1 (DENV-1) and DENV-2, and West Nile virus (WNV) in northern and southern Mexico based on the presence and quantity of specific neutralizing antibodies as a proxy for human risk.

During 2018–2019, we sampled pet dogs from 3 residential areas in the city of Tuxtla Gutierrez, Chiapas, in southern Mexico and 8 neighborhoods in the city of Reynosa, Tamaulipas, in northern Mexico (Figure). We initially screened serum or plasma samples at a 1:10 dilution, then further tested those that neutralized PFUs by ≥90% in duplicates at serial 2-fold dilutions that ranged from 1:10 to 1:320 to determine 90% endpoint titers (Appendix, https://wwwnc.cdc.gov/EID/article/28/5/21-1879-App1.pdf).

We tested blood samples from 294 pet dogs (predominantly mixed breeds, chihuahuas, and pit bulls). Canine exposure to WNV was widespread, and we found a higher prevalence of neutralizing antibodies to WNV in dogs from Reynosa (72/169, 42.6%) than in those from Tuxtla Gutierrez (1/87, 1.2%; Appendix). In contrast, only 2 (0.7%) dogs from Tuxtla Gutierrez had neutralizing antibodies for ZIKV exposure, showing endpoint titers of 40 and 10. However, the dog with a ZIKV titer of 40 also had a 90% plaque-reduction neutralization test titer of 20 for WNV; we could not screen the dog with a ZIKV titer of 10 for other viruses because of low sample volume. A single dog from Tuxtla Gutierrez had a low titer monotypic reaction for DENV-2, the only evidence of exposure to an *Aedes*-borne flavivirus (Appendix). A sample size analysis indicated that the level of sampling we conducted supports 95% confidence that true prevalence of neutralizing antibodies in these canine populations did not exceed 1% for each of these *Aedes*-borne flaviviruses.

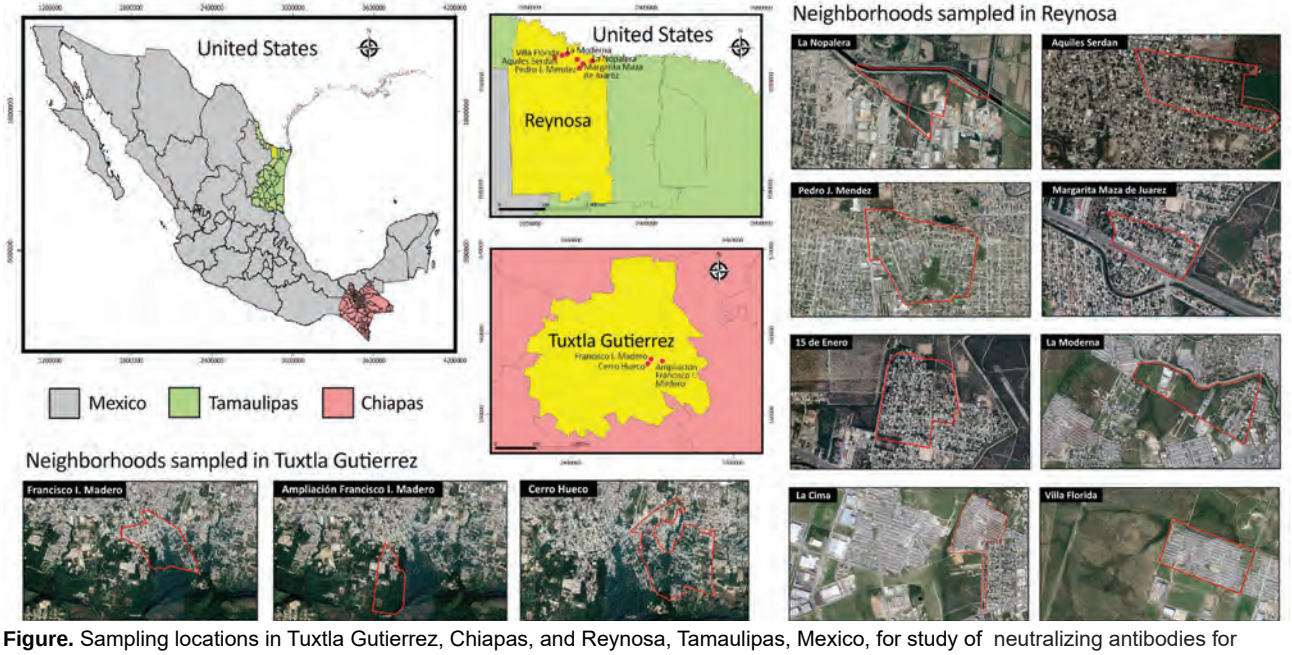

Figure. Sampling locations in Tuxtla Gutierrez, Chiapas, and Reynosa, Tamaulipas, Mexico, for study of neutralizing antibodies for mosquito-borne flaviviruses in domestic dogs. Map was created using QGIS 3.18.2 (https://qgis.org/en/site) with public domain map data from Instituto Nacional de Estadística, Geografía e Informatica (National Institute of Statistics, Geography, and Computer Science [INEGI]; https://www.inegi.org.mx/app/mapas) and satellite images from Google Maps (https://www.google.com.mx/maps).

Our data suggested substantial WNV enzootic activity in Reynosa and corroborated prior observations of high use of dogs as blood meal hosts by *Cx. quinquefasciatus* mosquitoes. Despite detecting neutralizing antibodies for WNV in 42.6% of dogs from Reynosa, the number of reported human WNV cases in Mexico has remained low (*5*), suggesting that transmission occurs among domestic animals but either humans have not been infected or cases have not been reported. Texas has a high number of reported human WNV cases (Texas Department of State Health Services, https://dshs.texas.gov/idcu/disease/arboviral/westNile/#stats). The lower reported numbers of WNV cases in Mexico might be in part because of the high seroprevalence of antibodies for other flaviviruses, which have been shown to protect against severe clinical infection from WNV, thus leading to reduced testing (*6*). Low WNV seroprevalence among dogs in Tuxtla Gutierrez might reflect a larger diversity of vertebrates with lower WNV competence, fed upon by *Culex* mosquitoes in the study area.

The relative lack of canine exposure to *Aedes*-borne flaviviruses suggests not an absence of these viruses circulating in these communities but that dogs are likely insensitive sentinels of the viruses' transmission in Mexico. In Chiapas, 7,972 human cases of dengue and 763 cases of Zika had been reported during 2016–2020 (*7*,*8*). Considering the timing of our sampling and the ages of the dogs, we expect that ≈75% of sampled dogs were living in these communities during DENV and ZIKV transmission activity. In the state of Tamaulipas, there were 3,988 human cases of dengue (*7*) and 733 cases of Zika during 2016–2020 (*8*). Given recent quantification that >50% of *Ae. aegypti* in southern Texas and northern Mexico feed on dogs (*3*,*4*), our serologic data suggest that either the probability of virus spillover into dogs is low or that, although dogs are susceptible to infection, neutralizing antibodies developed weakly or waned rapidly (*9*).

Our study suggests substantial WNV enzootic activity in Reynosa, Mexico and corroborates observations that *Cx. quinquefasciatus* mosquitoes, a primary vector of WNV, use high numbers of dogs for blood meals. Therefore, domestic pet dogs may be useful sentinels of WNV transmission, as previously suggested in other regions (*10*).

Acknowledgments

We thank the World Reference Center for Emerging Viruses and Arboviruses at the University of Texas Medical Branch and the Centers for Disease Control and Prevention for providing the viruses used in this study. We appreciate field sampling assistance in Tamaulipas from Sofia Rodríguez, Irma Cobos, Cristian Delgado, Mónica Duarte, Diana Navarrate, Elisa Rodarte, Luis Sánchez, Ricardo Palacios, Adebiyi Adeniran, and Ester Carbajal. We appreciate field sampling assistance in Chiapas from Paola Ruiz, Daniela Mendoza, Ali Fajardo, Azucena, Katia Hernandez, Ma. Fernanda Escobar, Emiliano Escobar, Nathan Penagos, and Cristel Nandayapa.

Our work was performed, in part, under the auspices of the US Department of Energy by Lawrence Livermore National Laboratory under contract DE-AC52-07NA27344 to G.L.H., M.F., M.K.B. Additional support came from the Texas A&M University-Consejo Nacional de Ciencia y Tecnologia Collaborative Research Program grant (no. 2018-041-1) and a Texas A&M AgriLife Insect Vector seed grant. J.G.E.F. was supported by grants from Secretaría de Investigación y Posgrado of Instituto Politécnico Nacional (Nos. 20196759, 20200843, and 20202442).

About the Author

Mr. Davila is a PhD student at the Texas A&M University College of Veterinary Medicine and Biomedical Sciences. His primary research interests include animals as sentinels for human disease and the epidemiology of emerging infectious diseases.

References

1. Kraemer MU, Sinka ME, Duda KA, Mylne AQ, Shearer FM, Barker CM, et al. The global distribution of the arbovirus vectors Aedes aegypti and Ae. albopictus. eLife. 2015;4:e08347. https://doi.org/10.7554/eLife.08347
2. Rochlin I, Faraji A, Healy K, Andreadis TG. West Nile virus mosquito vectors in North America. J Med Entomol. 2019;56:1475–90. https://doi.org/10.1093/jme/tjz146
3. Olson MF, Ndeffo-Mbah ML, Juarez JG, Garcia-Luna S, Martin E, Borucki MK, et al. High rate of non-human feeding by Aedes aegypti reduces Zika virus transmission in South Texas. Viruses. 2020;12:E453. https://doi.org/10.3390/v12040453
4. Estrada-Franco JG, Fernández-Santos NA, Adebiyi AA, López-López MJ, Aguilar-Durán JA, Hernández-Triana LM, et al. Vertebrate-Aedes aegypti and Culex quinquefasciatus (Diptera) arbovirus transmission networks: non-human feeding revealed by meta-barcoding and next-generation sequencing. PLoS Negl Trop Dis. 2020;14:e0008867. https://doi.org/10.1371/journal.pntd.0008867
5. Elizondo-Quiroga D, Elizondo-Quiroga A. West Nile virus and its theories, a big puzzle in Mexico and Latin America. J Glob Infect Dis. 2013;5:168–75. https://doi.org/10.4103/0974-777X.122014
6. Tesh RB, Travassos da Rosa AP, Guzman H, Araujo TP, Xiao SY. Immunization with heterologous flaviviruses protective against fatal West Nile encephalitis. Emerg Infect Dis. 2002;8:245–51. https://doi.org/10.3201/eid0803.010238
7. Dirección General de Epidemiología, Secretaría de Salud México. Historical epidemiological bulletin [in Spanish]

[cited 2022 Jan 26]. https://www.gob.mx/salud/acciones-y-programas/historico-boletin-epidemiologico
8. Pan American Health Organization. Zika: confirmed cases in Mexico, 2017 [cited 2020 Jun 19]. https://www3.paho.org/data/index.php/en/?option=com_content&view=article&id=526:zika-mex-en&Itemid=352
9. Thongyuan S, Kittayapong P. First evidence of dengue infection in domestic dogs living in different ecological settings in Thailand. PLoS One. 2017;12:e0180013. https://doi.org/10.1371/journal.pone.0180013
10. Resnick MP, Grunenwald P, Blackmar D, Hailey C, Bueno R, Murray KO. Juvenile dogs as potential sentinels for West Nile virus surveillance. Zoonoses Public Health. 2008;55:443–7. https://doi.org/10.1111/j.1863-2378.2008.01116.x

Address for correspondence: Gabriel Hamer, Texas A&M University, TAMU 2475, College Station, TX, 77843, USA; email: ghamer@tamu.edu; Héctor Ochoa-Díaz-López, El Colegio de la Frontera Sur, Departamento de Salud, San Cristóbal de Las Casas, Chiapas, México, CP. 29290; email: hochoa@ecosur.mx; Mario A. Rodríguez-Pérez, Instituto Politécnico Nacional, Centro de Biotecnología Genómica, Blvd. del Maestro esquina Elías Piña s/n, Colonia Narciso Mendoza, 88170, Cd. Reynosa, Tamaulipas, México; email: mrodriguez@ipn.mx

Viral Hepatitis E Outbreaks in Refugees and Internally Displaced Populations, sub-Saharan Africa, 2010–2020

Angel N. Desai, Amir M. Mohareb, Mubarak Mustafa Elkarsany, Hailemichael Desalegn, Lawrence C. Madoff, Britta Lassmann

Author affiliations: University of California–Davis, Sacramento, California, USA (A.N. Desai); International Society for Infectious Diseases, Brookline, Massachusetts, USA (A.N. Desai, M.M. Elkarsany, L.C. Madoff, B. Lassmann); Massachusetts General Hospital, Boston, Massachusetts, USA (A.M. Mohareb); Karary University, Khartoum, Sudan (M.M. Elkarsany); St. Paul's Hospital MMC, Addis Ababa, Ethiopia (H.D. Desalegn); University of Massachusetts Medical School, Worcester, Massachusetts, USA (L.C. Madoff)

DOI: https://doi.org/10.3201/eid2805.212546

Hepatitis E virus is a common cause of acute viral hepatitis. We analyzed reports of hepatitis E outbreaks among forcibly displaced populations in sub-Saharan Africa during 2010–2020. Twelve independent outbreaks occurred, and >30,000 cases were reported. Transmission was attributed to poor sanitation and overcrowding.

Hepatitis E virus (HEV) is a common etiology of acute viral hepatitis worldwide (*1*). Large-scale, often protracted outbreaks caused by HEV infection in refugee and internally displaced person (IDP) settlements and camps have occurred (*1*), particularly in sub-Saharan Africa, a region with nearly one third of the global forcibly displaced population (*2*). Previous epidemiologic studies of HEV infections in forcibly displaced persons have focused on singular events (*3*,*4*). The objective of this study was to identify trends in HEV outbreaks among forcibly displaced populations in sub-Saharan Africa.

We conducted a focused review of all English-language curated reports posted on ProMED-mail (ProMED) during 2010–2020 concerning HEV in forcibly displaced populations in sub-Saharan Africa. ProMED uses formal and informal disease surveillance mechanisms to rapidly report emerging disease events in animals, humans, and plants globally (*5*). It has been validated as a rapid and accurate tool for determining and describing global outbreaks. We verified all reports via PubMed, ReliefWeb, the UN High Commission for Refugees, World Health Organization (WHO), and references secondarily collected from ProMED. We used the keyword "hepatitis E" in applicable search engines for reports published during 2010–2020. We included records documenting "refugee(s) and/or asylum seeker(s) and/or internally displaced person(s)" in sub-Saharan Africa as defined by the World Bank (*6*). We considered outbreaks unique on the basis of date and location of cases. When screening ProMED reports, we used the most recent report pertaining to an outbreak. In cases where discrepancies existed between data sources reporting on the same outbreak, we retained the higher number of case counts. Three independent investigators (A.D., B.L., and A.M.) manually reviewed the databases.

Twelve hepatitis E outbreaks among forcibly displaced persons resulting in a total of >30,000 suspected or confirmed cases of acute HEV and ≥610 deaths were reported during 2010–2020 (Appendix Table, https://wwwnc.cdc.gov/EID/article/28/5/21-2546-App1.pdf). Outbreaks occurred in Sudan, South Sudan, Ethiopia, Chad, Niger, Namibia, Burkina Faso, Kenya, and Nigeria (Figure). One outbreak in displaced persons in South Sudan's Bentiu camp for

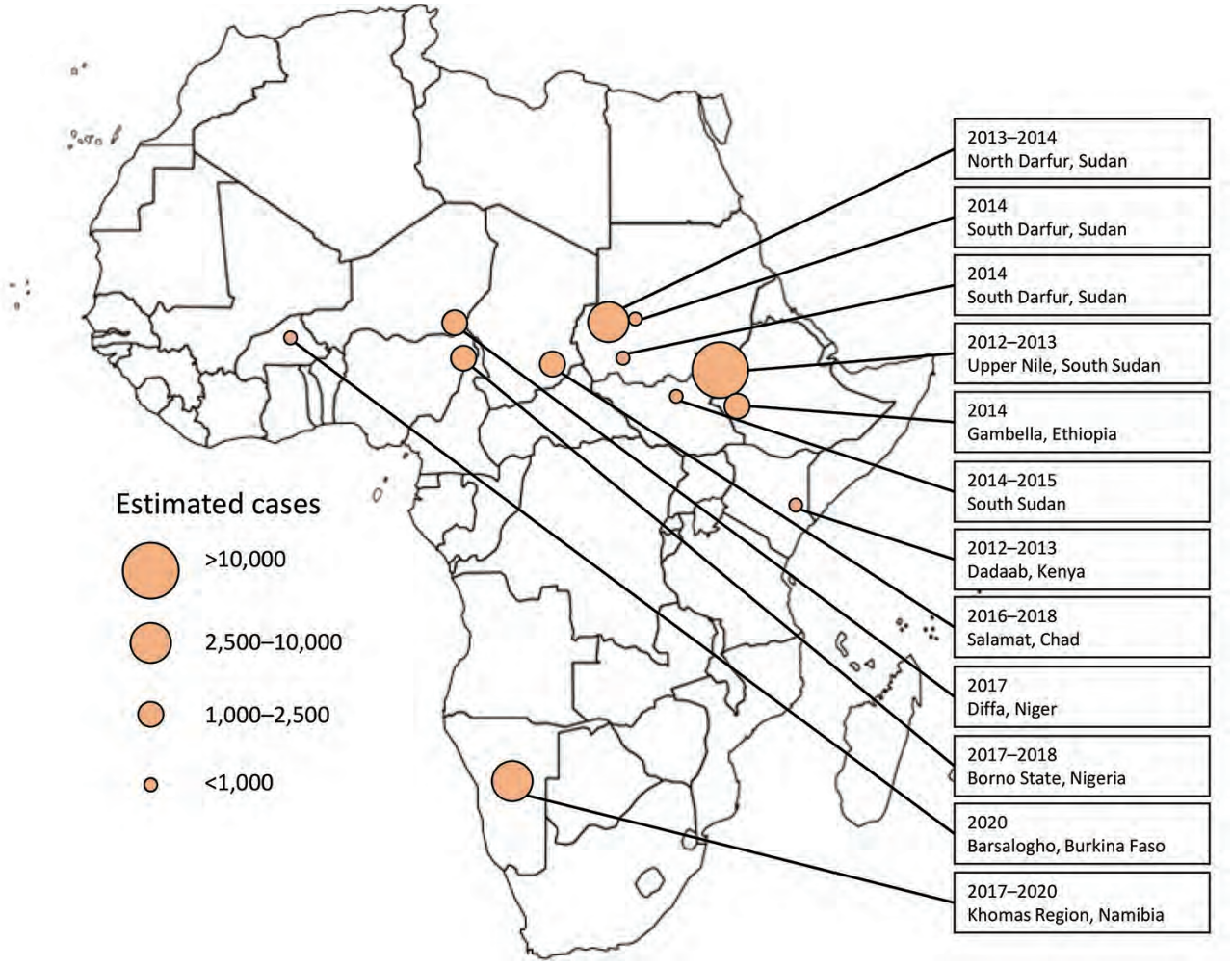

Figure. Geographic distribution of acute hepatitis E virus outbreaks reported among displaced persons in sub-Saharan Africa, 2010–2020.

internally displaced persons that included >1,000 cases since 2019 was not included in this analysis because it continued beyond 2020. The largest outbreak of acute HEV infections (>11,000 cases) was reported in a protracted outbreak in the Upper Nile, South Sudan, during July 2012–October 2013, among persons fleeing violence in Sudan in 2011. The most common contributors to hepatitis E outbreaks reported were overcrowding, poor sanitation, and flooding.

Prior studies have demonstrated the proclivity of HEV transmission in settings such as refugee and IDP camps; close quarters, inadequate sanitation and hygiene, and the constant introduction of new, susceptible persons into camps provided the conditions necessary for forward transmission (*3*,*4*). We could not calculate accurate case-fatality rates given the uncertainty surrounding the total number of true cases and deaths reported. Population-based studies during disease outbreaks of hepatitis E have placed mortality rates at 0.07%–0.6%; we noted substantial variability particularly for high-risk populations such as pregnant women (*1*). Cases and fatalities in pregnant women were reported for 3 hepatitis E outbreaks in this series: 2 reported deaths among 18 cases in pregnant women in Ethiopia (2014); 17 reported deaths in pregnant women in Niger (2017), comprising 45% of the recorded deaths in that outbreak; and 12 reported deaths in pregnant women in Namibia (2019).

The first limitation of this study is that case definitions may vary between settings, and confirmatory testing was not always reported. Second, mild and asymptomatic cases are often unreported, and the relatively long incubation period for HEV infection may hinder diagnosis and reporting. Third, misclassification bias is possible, especially because many of the settings are endemic for other causes of acute jaundice syndrome, such as malaria and yellow fever, and diagnostic testing was infrequent. Those factors also limited our ability to conduct a pooled analysis on the data.

Despite these limitations, this study demonstrates the high potential for HEV to cause outbreaks in communities with recently displaced persons. Of note, all of the reported outbreaks in this study occurred in the context of highly crowded camps or settlements, supporting the association between hepatitis E outbreaks and those environments. Given that some of the outbreaks noted in this analysis appeared to cross national borders, genetic sequencing to validate related strains may be useful for disease surveillance and prevention efforts. Additional data are needed to evaluate the potential utility of HEV vaccination in outbreaks and the barriers to vaccinating residents of refugee and IDP settlements. Water, sanitation, and hygiene measures are critical to reducing disease outbreaks, as is improved cross-border communication to prevent and manage future outbreaks. Clinicians and relief staff working with displaced populations should be vigilant for signs of hepatitis E disease, particularly among high-risk hosts such as pregnant women. Resources must be devoted to improving HEV surveillance, diagnostic capabilities, and response efforts for refugee and displaced populations.

Acknowledgments

We thank ProMED editors, moderators, and staff for their work in generating and providing context for the reports.

About the Author

Dr. Desai is an infectious disease physician and researcher whose primary focus is the application of informal surveillance methods for displaced populations, as well as for emerging and reemerging infectious disease threats.

References

1. Bagulo H, Majekodunmi AO, Welburn SC. Hepatitis E in sub-Saharan Africa—a significant emerging disease. One Health. 2020;11:100186. https://doi.org/10.1016/j.onehlt.2020.100186
2. UN High Commission for Refugees. Global trends: forced displacement in 2017. 2017 [cited 2019 May 30]. http://www.unhcr.org/en-us/statistics
3. Browne LB, Menkir Z, Kahi V, Maina G, Asnakew S, Tubman M, et al.; Centers for Disease Control and Prevention (CDC). Notes from the field: hepatitis E outbreak among refugees from South Sudan—Gambella, Ethiopia, April 2014-January 2015. MMWR Morb Mortal Wkly Rep. 2015;64:537.
4. Lagare A, Ibrahim A, Ousmane S, Issaka B, Zaneidou M, Kadadé G, et al. Outbreak of hepatitis E virus infection in displaced persons camps in Diffa Region, Niger, 2017. Am J Trop Med Hyg. 2018;99:1055–7. https://doi.org/10.4269/ajtmh.17-0950
5. Bijkerk P, Monnier AA, Fanoy EB, Kardamanidis K, Friesema IH, Knol MJ. ECDC round table report and ProMed-mail most useful international information sources for the Netherlands Early Warning Committee. Euro Surveill. 2017;22:pii=30502. https://doi.org/10.2807/1560-7917.ES.2017.22.14.30502
6. World Bank Group. Sub-Saharan Africa [cited 2019 May 28]. http://data.worldbank.org/region/sub-saharan-africa

Address for correspondence: Angel N. Desai, University of California Davis Health System—Internal Medicine, Division of Infectious Diseases, 4150 V St, Sacramento, CA 95817-2201, USA; email: angel.n.desai@gmail.com

Usutu Virus Africa 3 Lineage, Luxembourg, 2020

Chantal J. Snoeck, Aurélie Sausy, Serge Losch, Félix Wildschutz, Manon Bourg, Judith M. Hübschen

Author affiliations: Luxembourg Institute of Health, Esch-sur-Alzette, Luxembourg (C.J. Snoeck, A. Sausy, J.M. Hübschen); Administration des Services Vétérinaires de l'Etat, Ministère de l'Agriculture, de la Viticulture et du Développement rural, Luxembourg (S. Losch, F. Wildschutz, M. Bourg)

DOI: https://doi.org/10.3201/eid2805.212012

We detected Usutu virus in a dead Eurasian blackbird (*Turdus merula*) in Luxembourg in September 2020. The strain clustered within the Africa 3.1 lineage identified in Western Europe since 2016. Our results suggest maintenance of the virus in Europe despite little reporting during 2019–2020, rather than a new introduction.

West Nile virus (WNV) and Usutu virus (USUV), members of the family *Flaviviridae*, share several epidemiologic traits and cocirculate in Europe. Both viruses are maintained through a transmission cycle involving bird and mosquito vectors. Migratory birds likely play a role in long-distance spread of USUV, similarly to WNV, and in the recent introduction of the virus to Europe from Africa (*1*).

In Europe, USUV has been associated with bird dieoff events since 2001 (*2*) and seems notably pathogenic for passerines and owls (*3*). Massive dieoff

events of Eurasian blackbirds (*Turdus merula*) have become a hallmark of USUV circulation in Western Europe, enabling its detection through passive surveillance (*2*,*4*,*5*).

WNV and USUV are also occasionally transmitted through a mosquito bite to mammals (such as humans or horses), which are considered dead-end hosts (*3*) and experience a wide range of clinical signs up to neuroinvasive syndromes. Although most persons infected with USUV experience no or limited symptoms, USUV can cause more severe disease in certain persons or be detected in blood donations with yet-unknown consequences for the blood product recipients (*6*). The apparent intense virus circulation in countries neighboring Luxembourg that began in 2016, coupled with accumulating reports of USUV infections in humans (*7*), prompted us to initiate passive surveillance in Luxembourg as an early warning system for mosquitoborne *Flaviviridae* circulation.

During October 2018–September 2020, a total of 61 samples from 33 birds (Table) were submitted for investigation of WNV or USUV infection. The animals were found dead or died shortly after arrival at a wildlife rehabilitation center. All samples were screened for the presence of WNV and USUV by real-time reverse transcription PCR (Appendix, https://wwwnc.cdc.gov/EID/article/28/5/21-2012-App1.pdf). All tested negative for WNV. In September 2020, one brain sample from a Eurasian blackbird found dead in a home garden near the capital city tested positive for USUV (cycle threshold 22.09) (Table). Before death, the animal exhibited neurologic symptoms (disorientation, loss of coordination). The presence of USUV RNA was confirmed by a second real-time reverse transcription PCR test, and the whole genome was sequenced for further strain characterization.

Phylogenetic analyses assigned the USUV strain from Luxembourg to the Africa 3 lineage. This lineage was first identified in Germany in 2014 (*4*); since then, it has been regularly described in Belgium, France, Germany, and the Netherlands (*4*,*5*) and has occasionally been reported in the Czech Republic (2018) (*8*) and the United Kingdom (2020) (*9*) (Figure). More precisely, the USUV strain from Luxembourg grouped within the Africa 3.1 sublineage, which is the least represented lineage (*5*). It clustered together with strains from blackbirds and a common scoter (*Melanitta nigra*) detected in Belgium, Germany, France, and the Netherlands in 2016 and 2018 (Appendix Figure). The intermingling of the only 2 strains reported in 2020 from Luxembourg and the United Kingdom within Africa 3.1 and 3.2 together with earlier Western Europe strains suggests local virus spread rather than a new virus introduction in Europe. However, little reporting in 2019 and 2020 and the lack of sequences from Africa hamper definite conclusion. The time gaps between the estimated ancestors of the Africa 3 lineage (2009) and Europe 3 lineage (2002) (*5*) and the earliest sequences available (2014 for Africa 3 and 2010 for Europe 3) further suggest that silent USUV circulation is not uncommon. In addition, passive surveillance in Luxembourg might have missed earlier cases, as was reposted in Austria, where only an estimated 0.2% of blackbirds killed by USUV were identified during 2003–2005 (*10*).

The transmission of both WNV and USUV is governed by a combination of factors, such as temperature, which influences both the developmental cycles of mosquitoes and virus transmissibility (*10*). Unusually high temperatures likely promoted the unprecedented USUV circulation in Western Europe (*4*,*10*). Expanding USUV geographic distribution is considered by some to be an indicator of WNV dispersion potential (*11*,*12*).

Table. Samples collected in the framework of WNV and USUV passive surveillance, Luxembourg, 2018–2020*

Year	Bird species	Location	No. samples tested	Sample types	No. birds positive/no. total	
					WNV	USUV
2018	*Turdus merula*	Rehabilitation center	4	Liver, brain, kidney, heart	0/1	0/1
	Tyto alba	Rehabilitation center	6	Liver, brain, kidney, heart, tracheal swab, cloacal swab	0/1	0/1
	Pica pica	Esch-sur-Alzette	4	Liver, brain, kidney, heart	0/1	0/1
2019	*T. merula*	Rehabilitation center	10	Brain	0/10	0/10
	Corvus corone	Rehabilitation center	2	Brain	0/2	0/2
	Corvus frugilegus	Rehabilitation center	3	Brain	0/3	0/3
	Corvus sp.	Rehabilitation center	1	Brain	0/1	0/1
2020	*Sturnus vulgaris*	Lamadelaine, Pétange	20	Brain, tracheal swab, cloacal swab	0/9	0/9
	Corvus sp.	Pétange	10	Brain, tracheal swab, cloacal swab	0/4	0/4
	T. merula	Strassen	1	Brain	0/1	1/1
Total			61		0/33	1/33

*USUV, Usutu virus; WNV, West Nile virus.

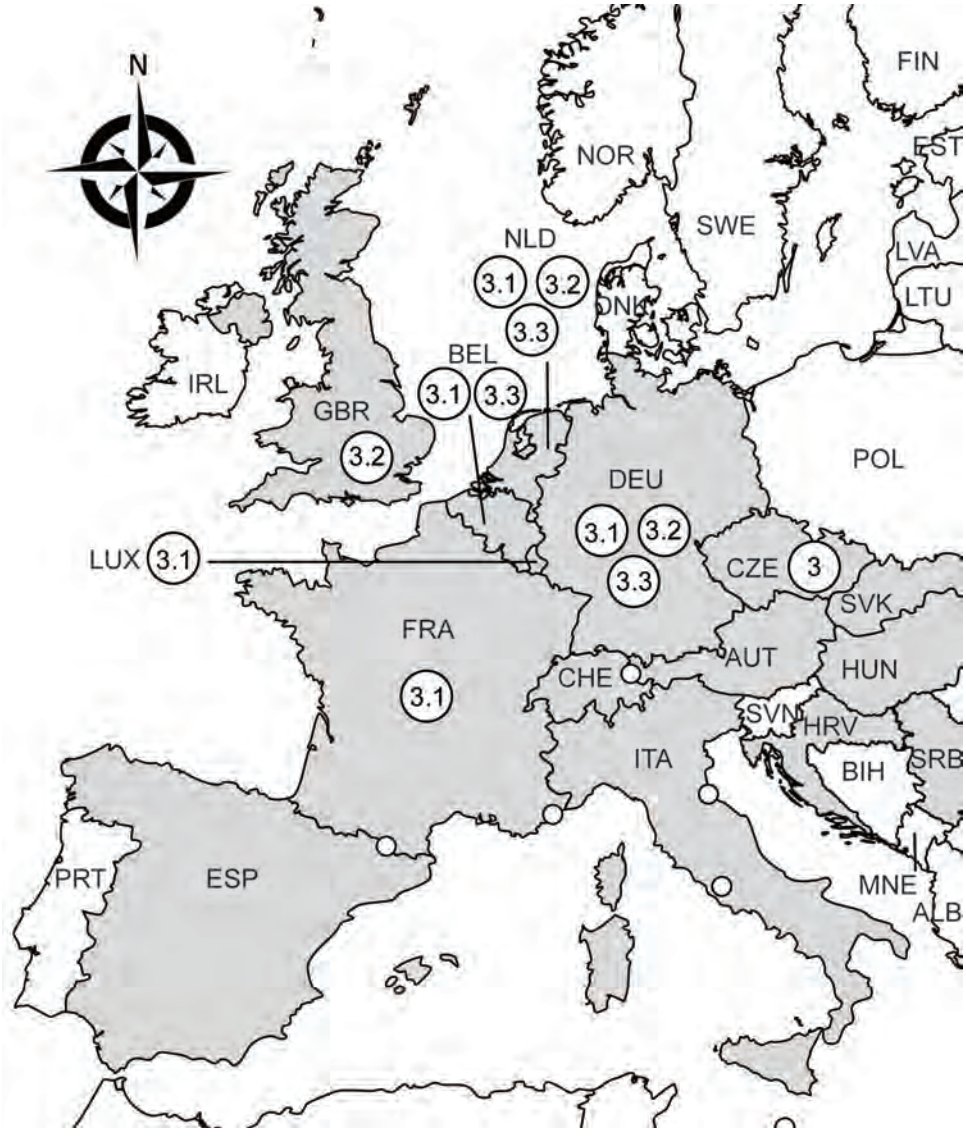

Figure. Geographic distribution of Usutu virus Africa 3 lineage in Europe. Countries are identified by 3-letter International Organization for Standardization codes (https://www.iso.org); gray indicates those where Usutu sequences were reported (partial E gene, partial NS5 gene, or complete polyprotein coding viral sequences available on GenBank). Large white circles indicate locations where Africa 3 lineage has been identified; sublineages are indicated within circles. Only partial NS5 sequence was available for Africa 3 strain from Czech Republic, preventing sub-lineage attribution. Small white circles delineate European microstates (AND, MCO, LIE, SMR and Vatican city); no Usutu virus circulation was reported. Map created with https://www.mapchart.net.

The spread of WNV to Germany in 2018 and the Netherlands in 2020 corroborates this hypothesis. Because of the increasing frequencies of climatic anomalies, Luxembourg is also at risk for WNV to be introduced. Surveillance of mosquitoborne viruses such as USUV and WNV in animal hosts should be maintained and strengthened in the country as an early warning system to inform public health authorities.

Acknowledgments

We thank the staff from the rehabilitation center Centre de Soins pour la Faune sauvage, Natur&Ëmwelt, for their collaboration.

This study was funded by the Ministère de l'Agriculture, de la Viticulture et du Développement rural, Luxembourg.

About the Author

Dr. Snoeck is a researcher at the Luxembourg Institute of Health. Her primary research interests include the epidemiology of zoonotic viruses.

References

1. Engel D, Jöst H, Wink M, Börstler J, Bosch S, Garigliany MM, et al. Reconstruction of the evolutionary history and dispersal of Usutu virus, a neglected emerging arbovirus in Europe and Africa. MBio. 2016;7:e01938–15. https://doi.org/10.1128/mBio.01938-15
2. Weissenböck H, Kolodziejek J, Url A, Lussy H, Rebel-Bauder B, Nowotny N. Emergence of Usutu virus, an African mosquito-borne flavivirus of the Japanese encephalitis virus group, central Europe. Emerg Infect Dis. 2002;8:652–6. https://doi.org/10.3201/eid0807.020094

3. Benzarti E, Linden A, Desmecht D, Garigliany M. Mosquito-borne epornitic flaviviruses: an update and review. J Gen Virol. 2019;100:119–32. https://doi.org/10.1099/jgv.0.001203
4. Cadar D, Lühken R, van der Jeugd H, Garigliany M, Ziegler U, Keller M, et al. Widespread activity of multiple lineages of Usutu virus, western Europe, 2016. Euro Surveill. 2017;22:30452. https://doi.org/10.2807/1560-7917.ES.2017.22.4.30452
5. Oude Munnink BB, Münger E, Nieuwenhuijse DF, Kohl R, van der Linden A, Schapendonk CME, et al. Genomic monitoring to understand the emergence and spread of Usutu virus in the Netherlands, 2016–2018. Sci Rep. 2020;10:2798. https://doi.org/10.1038/s41598-020-59692-y
6. Aberle SW, Kolodziejek J, Jungbauer C, Stiasny K, Aberle JH, Zoufaly A, et al. Increase in human West Nile and Usutu virus infections, Austria, 2018. Euro Surveill. 2018;23:23. https://doi.org/10.2807/1560-7917.ES.2018.23.43.1800545
7. Vilibic-Cavlek T, Petrovic T, Savic V, Barbic L, Tabain I, Stevanovic V, et al. Epidemiology of Usutu virus: the European scenario. Pathogens. 2020;9:E699. https://doi.org/10.3390/pathogens9090699
8. Hönig V, Palus M, Kaspar T, Zemanova M, Majerova K, Hofmannova L, et al. Multiple lineages of Usutu virus (Flaviviridae, Flavivirus) in blackbirds (Turdus merula) and mosquitoes (Culex pipiens, Cx. modestus) in the Czech Republic (2016–2019). Microorganisms. 2019;7:568. https://doi.org/10.3390/microorganisms7110568
9. Folly AJ, Lawson B, Lean FZ, McCracken F, Spiro S, John SK, et al. Detection of Usutu virus infection in wild birds in the United Kingdom, 2020. Euro Surveill. 2020;25:2001732. https://doi.org/10.2807/1560-7917.ES.2020.25.41.2001732
10. Rubel F, Brugger K, Hantel M, Chvala-Mannsberger S, Bakonyi T, Weissenböck H, et al. Explaining Usutu virus dynamics in Austria: model development and calibration. Prev Vet Med. 2008;85:166–86. https://doi.org/10.1016/j.prevetmed.2008.01.006
11. Zannoli S, Sambri V. West Nile virus and Usutu virus co-circulation in Europe: epidemiology and implications. Microorganisms. 2019;7:E184. https://doi.org/10.3390/microorganisms7070184
12. Fros JJ, Miesen P, Vogels CB, Gaibani P, Sambri V, Martina BE, et al. Comparative Usutu and West Nile virus transmission potential by local Culex pipiens mosquitoes in northwestern Europe. One Health. 2015;1:31–6. https://doi.org/10.1016/j.onehlt.2015.08.002

Address for correspondence: Chantal J. Snoeck, Department of Infection and Immunity, Luxembourg Institute of Health, 29 rue Henri Koch, L-4354 Esch-sur-Alzette, Luxembourg; email: chantal.snoeck@lih.lu

COMMENT LETTERS

Guillain-Barré Syndrome Associated with COVID-19 Vaccination

Josef Finsterer, Fulvio A. Scorza, Carla A. Scorza

Author affiliations: Neurology and Neurophysiology Center, Vienna, Austria (J. Finsterer); Disciplina de Neurociência. Universidade Federal de São Paulo/Escola Paulista de Medicina, São Paulo, Brazil (J. Finsterer, F.A. Scorza, C.A. Scorza)

DOI: https://doi.org/10.3201/eid2805.212145

To the Editor: With interest we read the article by Shao et al. (*1*) about the frequency of severe acute respiratory syndrome coronavirus 2 (SARS-CoV-2) vaccination–associated Guillain-Barré syndrome (SCoVaG) among 18,269 healthcare workers in Taiwan who had received the AstraZeneca vaccine (AZV; https://www.astrazeneca.com). Only 1 vaccinee experienced SCoVaG during the study period (*1*). The study is appealing but raises concerns.

Recently, our review of 19 SCoVaG patients, for whom data were collected through June 2021, was published (*2*). The 9 men and 10 women in the study were 20–86 years of age. All patients experienced SCoVaG after the first vaccine dose. AZV was given to 14 patients, the Pfizer-BioNTech (https://www.pfizer.com) vaccine to 4 patients, and the Johnson & Johnson (https://www.jnj.com) vaccine to 1 patient. Latency between vaccination and SCoVaG onset ranged from 3 hours to 39 days. Patients received intravenous immune globulin (n = 13), steroids (n = 3), or no therapy (n = 3). Six patients required mechanical ventilation. One patient recovered completely; 9 achieved partial recovery (*2*). Only 1 of the studies included in our review mentioned the total number of vaccinated persons (*3*); in that study, 7 persons among 1.2 million vaccinated persons were found to have SCoVaG (*3*).

In addition, data on 389 patients with SCoVaG were collected in a recent review about the neurologic adverse events of SARS-CoV-2 vaccination (*4*). However, no individual data were provided for 337

of these patients (*4*). Among the 53 patients for whom individual data were available, AZV was given to 39 patients, Pfizer-BioNTech vaccine to 9 patients, and Johnson & Johnson vaccine to 2 patients.

For the Shao et al. report (*1*), we wondered why the oldest healthcare worker was 86 years of age. Also missing were the specific treatment and outcome of the patient with SCoVaG.

Available data suggest that SCoVaG is a rare complication of SARS-CoV-2 vaccination, irrespective of the vaccine brand used. SCoVaG should be diagnosed early so treatment can be initiated promptly. Whether the beneficial effect of SARS-CoV-2 vaccination outweighs the risk for adverse events (e.g., Guillain-Barré syndrome) remains a matter of discussion (*5*).

References

1. Shao SC, Wang CH, Chang KC, Hung MJ, Chen HY, Liao SC. Guillain-Barré syndrome associated with COVID-19 vaccination. Emerg Infect Dis. 2021;27:3175–8. https://doi.org/10.3201/eid2712.211634
2. Finsterer J, Scorza FA, Scorza CA. Post SARS-CoV-2 vaccination Guillain-Barre syndrome in 19 patients. Clinics (São Paulo). 2021;76:e3286. https://doi.org/10.6061/clinics/2021/e3286
3. Maramattom BV, Krishnan P, Paul R, Padmanabhan S, Cherukudal Vishnu Nampoothiri S, Syed AA, et al. Guillain-Barré syndrome following ChAdOx1-S/nCoV-19 vaccine. Ann Neurol. 2021;90:312–4. https://doi.org/10.1002/ana.26143
4. Finsterer J. Neurological side effects of SARS-CoV-2 vaccinations. Acta Neurol Scand. 2021. https://doi.org/10.1111/ane.13451
5. Koike H, Chiba A, Katsuno M. Emerging infection, vaccination, and Guillain-Barré syndrome: a review. Neurol Ther. 2021;10:523–37. https://doi.org/10.1007/s40120-021-00261-4

Address for correspondence: Josef Finsterer, Neurology and Neurophysiology Center Vienna, Postfach 20, 1180 Vienna, Austria; email: fifigs1@yahoo.de

SARS-CoV-2 Cross-Reactivity in Prepandemic Serum from Rural Malaria-Infected Persons, Cambodia

Jillian T. Grassia, Christine F. Markwalter, Wendy P. O'Meara, Steve M. Taylor, Andrew A. Obala

DOI: https://doi.org/10.3201/eid2805.220404

To the Editor: We read with interest the observations by Manning et al. (*1*) that serum collected from malaria-infected persons in Cambodia before the coronavirus disease (COVID-19) pandemic harbored seroreactivity against severe acute respiratory syndrome coronavirus 2 (SARS-CoV-2) antigens but lacked neutralizing activity. These results suggest that malaria exposure may increase background reactivity in SARS-CoV-2 serosurveys and more specific measures of exposure, such as surrogate virus neutralization tests (sVNTs), may be necessary to capture functional SARS-CoV-2 seroreactivity in malaria-endemic areas. Additional studies in settings with distinct malaria transmission intensities would generalize and strengthen these findings.

One hypothesis for the unexpectedly moderate burden of SARS-CoV-2 in malaria-endemic countries in Africa is that exposure to *Plasmodium falciparum* confers functional protection against COVID-19 through cross-reactivity or general immune activation. To test this hypothesis, we analyzed 237 dried blood spot samples taken in January 2020 (prepandemic) from *P. falciparum*–exposed persons in a high-transmission setting in western Kenya for the presence of SARS-CoV-2 neutralizing antibodies (nAbs) using the GenScript SARS-CoV2 sVNT assay (https://www.genscript.com). Monthly *P. falciparum* real-time PCR results were collected in a previous study (*2*) for 138/237 persons in the 12 months prior to January 2020. Of these, 131 (95%) were infected with *P. falciparum* at least 1 time in 2019, suggesting that most persons included in this screening had been recently exposed to malaria parasites.

Consistent with findings in Manning et al. (*1*), none of the 237 people harbored SARS-CoV-2 nAbs, despite high prior levels of exposure to *P. falciparum*. Although nAbs are subject to decay after infection (*3*), this lack of nAb activity suggests that sVNTs offer a more specific measure of SARS-CoV-2 exposure than standard ELISAs (*4*). We further suggest that, given that protection from SARS-CoV-2 infection may be associated with the presence of nAbs (*5*), their absence in samples from both the Manning et al. study

(*1*) and our study does not support the notion that *P. falciparum* infections elicit functional humoral responses against COVID-19.

This work was supported by the National Institute of Allergy and Infectious Diseases (R21AI167242 to W.P.O. and S.M.T. and F32AI149950 to C.F.M.)

References

1. Manning J, Zaidi I, Lon C, Rosas LA, Park J-K, Ponce A, et al. SARS-CoV-2 cross-reactivity in prepandemic serum from rural malaria-infected persons, Cambodia. Emerg Infect Dis. 2022;28:440–4. https://doi.org/10.3201/eid2802.211725
2. Sumner KM, Mangeni JN, Obala AA, Freedman E, Abel L, Meshnick SR, et al. Impact of asymptomatic *Plasmodium falciparum* infection on the risk of subsequent symptomatic malaria in a longitudinal cohort in Kenya. eLife. 2021;10:e68812. https://doi.org/10.7554/eLife.68812
3. Chia WN, Zhu F, Ong SWX, Young BE, Fong S-W, Le Bert N, et al. Dynamics of SARS-CoV-2 neutralising antibody responses and duration of immunity: a longitudinal study. Lancet Microbe. 2021;2:e240–9. https://doi.org/10.1016/S2666-5247(21)00025-2
4. Tan CW, Chia WN, Qin X, Liu P, Chen MIC, Tiu C, et al. A SARS-CoV-2 surrogate virus neutralization test based on antibody-mediated blockage of ACE2-spike protein-protein interaction. Nat Biotechnol. 2020;38:1073–8. https://doi.org/10.1038/s41587-020-0631-z
5. Addetia A, Crawford KHD, Dingens A, Zhu H, Roychoudhury P, Huang M-L, et al. Neutralizing antibodies correlate with protection from SARS-CoV-2 in humans during a fishery vessel outbreak with a high attack rate. J Clin Microbiol. 2020;58:e02107–20. https://doi.org/10.1128/JCM.02107-20

Address for correspondence: Christine Markwalter, Duke Global Health Institute, 310 Trent Dr, Durham, NC, 27707, USA; email: christine.markwalter@duke.edu

Melioidosis in Children, Brazil, 1989–2019

Bijayini Behera, Anjuna Radhakrishnan, Sonali Mohapatra, Baijayantimala Mishra

Author affiliation: All India Institute of Medical Sciences, Bhubaneswar, India

DOI: https://doi.org/10.3201/eid2805.211473

To the Editor: We read with great interest the article by Lima et al. (*1*), in which the authors have discussed 20 confirmed or suspected melioidosis cases in children over a period of 30 years, concluding that childhood melioidosis is more severe in Brazil. This conclusion seems far-fetched based on findings described in the article, although the authors state that the high death rate and clinical severity might have been attributed to underreporting of mild cases,

Melioidosis is not a notifiable disease in India. Even so, from a single tertiary-care teaching hospital at Odisha, we have reported >100 cases of culture-confirmed cases during 2016–2021 (*2*–*4*), of which 10 cases were in the pediatric population (8 cases of superficial pyogenic infections in otherwise healthy children and 2 cases of septicemic melioidosis). All case-patients survived except 1 of the 2 with septicemic melioidosis, an 11-year-old boy who had systemic lupus erythematosus and died despite adequate intensive therapy. The second septicemic case was a 3-year-old girl with underlying acute lymphoblastic leukemia; she was treated with intravenous meropenem for 10 days and was discharged with a regimen of oral cotrimoxazole for 12 weeks.

Clinical severity of melioidosis is predominantly a function of host immunity (*5*). At a more pragmatic level, we would like to emphasize that, in melioidosis-endemic regions, most immunocompetent children with melioidosis experience localized infections and have better clinical outcomes, whereas in children with risk factors such as immunosuppression and childhood malignancies, the clinical course may be sudden and severe. In our view, frequent environmental exposures may not entirely explain the severity of childhood melioidosis. Lima et al. should have provided additional evidence to support their conclusion that childhood melioidosis is more severe in the population in Brazil.

About the Author

Dr. Behera is an additional professor in the department of microbiology at All India Institute of Medical Sciences, Bhubaneswar, India. Her primary research interests are melioidosis, rickettsial diseases, and antimicrobial resistance.

References

1. Lima RXR, Rolim DB. Melioidosis in children, Brazil, 1989–2019. Emerg Infect Dis. 2021;27:1705–8. https://doi.org/10.3201/eid2706.200154
2. Behera B, Mohanty S, Mahapatra A, Hallur VK, Mishra B, Dey A, et al. Melioidosis in Odisha: a clinico-microbiological and epidemiological description of culture-confirmed cases

over a 2-year period. Indian J Med Microbiol. 2019;37:430–2. https://doi.org/10.4103/ijmm.IJMM_19_367
3. Radhakrishnan A, Behera B, Mishra B, Mohapatra PR, Kumar R, Singh AK. Clinico-microbiological description and evaluation of rapid lateral flow immunoassay and PCR for detection of *Burkholderia pseudomallei* from patients hospitalized with sepsis and pneumonia: a twenty-one months study from Odisha, India. Acta Trop. 2021;221:105994. https://doi.org/10.1016/j.actatropica.2021.105994
4. Purushotham P, Mohanty S, Chappity P, Mishra TS, Mahapatra A. Identification and characterization of *Burkholderia pseudomallei* from localized pyogenic infections in eastern India: a clinico-microbiological study. Am J Trop Med Hyg. 2021;104:1252–9. https://doi.org/10.4269/ajtmh.20-1386
5. Webb JR, Sarovich DS, Price EP, Ward LM, Mayo M, Currie BJ. *Burkholderia pseudomallei* lipopolysaccharide genotype does not correlate with severity or outcome in melioidosis: host risk factors remain the critical determinant. Open Forum Infect Dis. 2019;6:ofz091. https://doi.org/10.1093/ofid/ofz091

Address for correspondence: Bijayini Behera, AIIMS Bhubaneswar, Microbiology, 2nd Fl, Academic block, All India institute of Medical Sciences, Bhubaneswar, Bhubaneswar, Odisha 751019 India; email: drbinny2004@gmail.com

In Response: We would like to respectfully clarify a few points in the comments by Behera et al. (*1*). We did not conclude that the severity of melioidosis in children in Brazil is greater than in other countries; we discussed it as a possibility (*2*). We also discussed that mild to moderate cases are the most prevalent forms in children and that they are underdiagnosed. However, it is possible that the severity of childhood melioidosis in Brazil may be like that in other melioidosis-endemic countries. By emphasizing disease severity, we aimed to draw attention to the detection of melioidosis in children, which can result in high death rates (*3*). Because the severe cases in our study occurred in healthy children, we did not discuss host immunity; this fact does not invalidate the role of immunity in melioidosis pathophysiology. Our objective was the same as that of Wiersinga et al. (*4*).

We described the intense environmental exposure of this age group in our region and recognized the importance of the environment to melioidosis epidemiology. We do not claim that exposure is the only explanation for disease severity, nor that it is a direct cause of severity. Furthermore, we acknowledge that human behavior and habits vary in different regions of the world; for example, tropical areas in which children play outdoors have a higher risk for melioidosis. Currie et al. have recommended additional studies (*5*).

We observed diverse genetic, cultural, and economic factors in the countries where melioidosis is found, whether it is well recognized or not. All of these factors could influence the distribution and severity of the disease (*6*). At this time, we believe a descriptive study can draw attention to melioidosis in tropical regions, such as Brazil and Latin American countries. The goal is to improve detection and reduce deaths from melioidosis in all parts of the world.

Rachel Ximenes Ribeiro Lima, Dionne Bezerra Rolim

Author affiliations: Municipal Department of Health, Fortaleza, Brazil (R.X.R. Lima); University of Fortaleza Medical School (R.X.R. Lima, D.B. Rolim); Ceará State University, Fortaleza (D.B. Rolim)

DOI: https://doi.org/10.3201/eid2805.220479

References

1. Behera B, Radhakrishnan A, Mohapatra S, Mishra B. Melioidosis in children, Brazil, 1989–2019. Emerg Infect Dis. 2022 Mar 28 [Epub ahead of print]. https://doi.org/10.3201/eid2805.211473
2. Lima RXR, Rolim DB. Melioidosis in children, Brazil, 1989–2019. Emerg Infect Dis. 2021;27:1705–8. https://doi.org/10.3201/eid2706.200154
3. Wiersinga WJ, Currie BJ, Peacock SJ. Melioidosis.. N Engl J Med. 2012;367:1035–44. https://doi.org/10.1056/NEJMra1204699
4. Wiersinga WJ, Virk HS, Torres AG, Currie BJ, Peacock SJ, Dance DAB, et al. Melioidosis. Nat Rev Dis Primers. 2018;4:17107. https://doi.org/10.1038/nrdp.2017.107
5. Currie BJ, Jacups SP. Intensity of rainfall and severity of melioidosis, Australia. Emerg Infect Dis. 2003;9:1538–42. https://doi.org/10.3201/eid0912.020750
6. Limmathurotsakul D, Golding N, Dance DAB, Messina JP, Pigott DM, Moyes CL, et al. Predicted global distribution of Burkholderia pseudomallei and burden of melioidosis. Nat Microbiol. 2016;1:15008 https://doi.org/10.1038/nmicrobiol.2015.8

Address for correspondence: Rachel Lima, Universidade de Fortaleza, Washington Soares Av, 1321, Fortaleza 60811-905 Brazil; email: quel0505@gmail.com

High-Dose Convalescent Plasma for Treatment of Severe COVID-19

Daniele Focosi, Arturo Casadevall

Author affiliations: Pisa University Hospital, Pisa, Italy (D. Focosi); Johns Hopkins School of Public Health and School of Medicine, Baltimore, Maryland, USA (A. Casadevall)

DOI: https://doi.org/10.3201/eid2805.220191

To the Editor: We commend our colleagues in Brazil for completing a multicenter, open-label, randomized controlled trial (RCT) of coronavirus disease (COVID-19) convalescent plasma (CCP) against wild-type severe acute respiratory syndrome coronavirus 2 (SARS-CoV-2) (*1*). This RCT had some strengths, including use of high-dose CCP (600 mL CCP for 3 days at a median neutralizing antibody titer of 1:128). The overall results were negative, but the authors caution that this finding probably reflects inclusion of patients late in disease, as evident by enrollment criteria (oxygen saturation <93%, partial pressure of oxygen/fraction of inspired oxygen <300, or need for mechanical ventilation), median transfusion at day 9 after symptom onset, 100% seropositivity, and 35% requiring hemodialysis at enrollment. The severity of disease in those patients means that disease was driven by inflammation as opposed to ongoing virus replication. To date, 2 CCP RCTs have shown benefit, 1 that provided outpatient treatment (D. Sullivan, et al., unpub. data, https://www.medrxiv.org/content/10.1101/2021.12.10.2126748v1) and 1 that provided inpatient treatment within 3 days of symptom onset (*2*). Hence, we caution against negative conclusions about the efficacy of CCP based on these data.

We find it remarkable that despite late CCP use, the authors observed a lower mortality rate among CCP-treated patients (31%) than controls (35%), given that the prevailing view is that this therapy functions as an antiviral and should not be effective in late disease. A similar finding is apparent in most other RCTs of hospitalized patients (*3*). This reduced mortality rate did not reach statistical significance because of the low sample size, which was estimated by assuming a 50% reduction in mortality rate from the intervention, much higher than that assumed in the RCTs of anti-spike monoclonal antibodies (typically in the range of 20%); further, recruitment was halted at 110 out of 120 patients. A recent article suggests that there is a population with high World Health Organization severity scores that benefits from CCP (*4*). We wonder if the authors can reanalyze their data by using the treatment benefit calculator (https://covid-convalescentplasma-tbi-calc.org) (*4*) to gain more insight into whether a small subset of patients benefited from CCP.

A.C. was a co-investigator in the CSSC-004 RCT. D.F. was a co-investigator in the TSUNAMI RCT.

D.F. conceived the manuscript and wrote the first draft. A.C. revised the manuscript.

References

1. De Santis GC, Oliveira LC, Garibaldi PMM, Almado CEL, Croda J, Arcanjo GGA, et al. High-dose convalescent plasma for treatment of severe COVID-19. Emerg Infect Dis. 2022;28:548–55. PubMed https://doi.org/10.3201/eid2803.212299
2. Arnold Egloff SA, Junglen A, Restivo JSA, Wongskhauluang M, Martin C, Doshi P, et al. Association of convalescent plasma treatment with reduced mortality and improved clinical trajectory in patients hospitalized with COVID-19 in the community setting. JAMA. 2021;325:1185–95. https://doi.org/10.1001/jama.2021.2747
3. Focosi D, Franchini M, Pirofski L, Burnouf T, Paneth N, Joyner MJ, et al. COVID-19 convalescent plasma and clinical trials: understanding conflicting outcomes. Clin Microbiol Rev. 2022;e00200-21. https://doi.org/10.1128/cmr.00200-21
4. Park H, Tarpey T, Liu M, Goldfeld K, Wu Y, Wu D, et al. Development and validation of a treatment benefit index to identify hospitalized patients with COVID-19 who may benefit from convalescent plasma. JAMA Netw Open. 2022;5:e2147375. https://doi.org/10.1001/jamanetworkopen.2021.47375

Address for correspondence: Daniele Focosi, Pisa University Hospital, Building 2K, via Paradisa 2, 56124 Pisa, Italy; email: daniele.focosi@gmail.com

In Response: We thank Focosi and Casadevall for their comments (*1*). One strong contribution of our study was the high dose (i.e., 1,800 mL in 3 days) of coronavirus disease (COVID-19) convalescent plasma (CCP), which, in our opinion, would be more likely to benefit patients than a lower dose (e.g., 200–600 mL in 1 or 2 doses), as is the protocol in most CCP studies (including but not limited to COVID-19 treatment) (*2*).

The weak point of our study was the relatively large therapeutic window (up to 10 days of signs/symptoms) for CCP transfusion, which may have included the later inflammatory process of illness. One early trial suggested benefit for COVID-19 patients who received CCP within the first 14 days (*3*). Nevertheless, subsequent trials showed that CCP (or serum) administration could be most beneficial for COVID-19 patients when administered as prophylaxis or within the first days of infection (*4*,*5*), ideally, within the first 3 days (*6*) but perhaps not later (*7*,*8*).

We emphasize that CCP transfusion was considered experimental at the beginning of the pandemic, and inclusion criteria comprised only patients with severe illness, for whom ≥7 days of infection are needed for illness to become evident.

We think that applying the suggested formula to identify which COVID-19 patients are likely to benefit from CCP (higher risk for progression to severe disease) would not be applicable to our study because it was envisaged for patients not receiving mechanical ventilation (*9*), whereas the patients in our study had severe disease (90% receiving mechanical ventilation).

In summary, our study emphasizes that CCP should not be transfused late in the course of disease, when the clinical course is driven by inflammation. This conclusion does not exclude the possibility of transfusing CCP as soon as patients are identified for potential benefit, as suggested by other studies (*6*,*7*).

Gil C. De Santis, Rodrigo T. Calado

Author affiliation: University of São Paulo, São Paulo, Brazil

DOI: https://doi.org/10.3201/eid2805.220363

References

1. Focosi D, Casadevall A. High-dose convalescent plasma for treatment of severe COVID-19. Emerg Infect Dis. 2022 Apr XX [Epub ahead of print]. https://doi.org/10.3201/eid2805.220191
2. Bloch EM, Shoham S, Casadevall A, Sachais BS, Shaz B, Winters JL, et al. Deployment of convalescent plasma for the prevention and treatment of COVID-19. J Clin Invest. 2020;130:2757–65. https://doi.org/10.1172/JCI138745
3. Cheng Y, Wong R, Soo YO, Wong WS, Lee CK, Ng MH, et al. Use of convalescent plasma therapy in SARS patients in Hong Kong. Eur J Clin Microbiol Infect Dis. 2005;24:44–6. https://doi.org/10.1007/s10096-004-1271-9
4. Focosi D, Franchini M, Pirofski LA, Burnouf T, Fairweather D, Joyner MJ, et al. COVID-19 convalescent plasma is more than neutralizing antibodies: a narrative review of potential beneficial and detrimental co-factors. Viruses. 2021;13:1594. https://doi.org/10.3390/v13081594
5. Casadevall A, Scharff MD. Serum therapy revisited: animal models of infection and development of passive antibody therapy. Antimicrob Agents Chemother. 1994;38:1695–702. https://doi.org/10.1128/AAC.38.8.1695
6. Libster R, Pérez Marc G, Wappner D, Coviello S, Bianchi A, Braem V, et al.; Fundación INFANT–COVID-19 Group. Early high-titer plasma therapy to prevent severe Covid-19 in older adults. N Engl J Med. 2021;384:610–8. https://doi.org/10.1056/NEJMoa2033700
7. Korley FK, Durkalski-Mauldin V, Yeatts SD, Schulman K, Davenport RD, Dumont LJ, et al.; SIREN-C3PO Investigators. Early convalescent plasma for high-risk outpatients with Covid-19. N Engl J Med. 2021;385:1951–60. https://doi.org/10.1056/NEJMoa2103784
8. Simonovich VA, Burgos Pratx LD, Scibona P, Beruto MV, Vallone MG, Vázquez C, et al.; PlasmAr Study Group. A randomized trial of convalescent plasma in Covid-19 severe pneumonia. N Engl J Med. 2021;384:619–29. https://doi.org/10.1056/NEJMoa2031304
9. Park H, Tarpey T, Liu M, Goldfeld K, Wu Y, Wu D, et al. Development and validation of a treatment benefit index to identify hospitalized patients with COVID-19 who may benefit from convalescent plasma. JAMA Netw Open. 2022;5:e2147375. https://doi.org/10.1001/jamanetworkopen.2021.47375

Address for correspondence: Gil C. De Santis, Rua Tenente Catão Roxo, 2501 Ribeirão Preto, 14051-140 SP, Brazil; email: gil@hemocentro.fmrp.usp.br

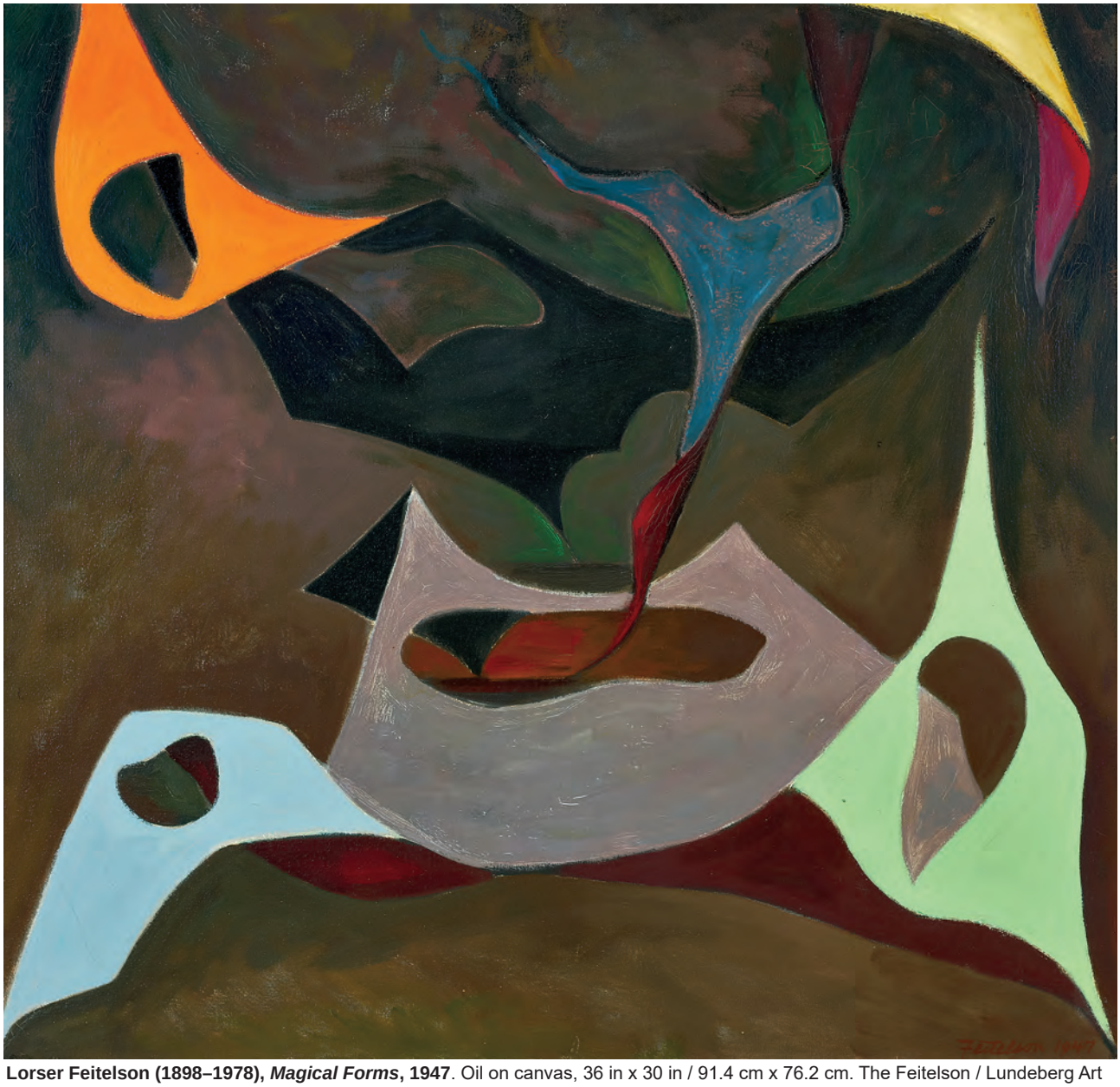

Lorser Feitelson (1898–1978), *Magical Forms*, 1947. Oil on canvas, 36 in x 30 in / 91.4 cm x 76.2 cm. The Feitelson / Lundeberg Art Foundation Collection, courtesy Louis Stern Fine Arts © The Feitelson / Lundeberg Art Foundation, Portland, Oregon, USA.

Durable Vitality and Magical Forms

Byron Breedlove

Lorser Feitelson grew up in New York City, and his interest in art was apparent when he was quite young. When young Feitelson was only six years old, his father started teaching him an analytical approach to drawing. His father's extensive collection of books and periodicals provided the young artist the means to self-study classic and modern artwork. After attending the Armory Show of 1913—an event that included works by Cezanne, Van Gogh, Gauguin, Matisse, and Picasso, and is considered

Author affiliation: Centers for Disease Control and Prevention, Atlanta, Georgia, USA

DOI: https://doi.org/10.3201/eid2805.AC02805

the beginning of Modernism in America—Feitelson decided to pursue painting as a career. At the age of 18, he rented a studio in Greenwich Village and from 1919–1927, made several trips abroad, living and studying in Paris.

In 1927, Feitelson moved to Los Angeles, where he lived and worked for most of his life. In addition to painting, he started what would be a 50-year career as an art instructor. Among his students was Helen Lundeberg, with whom he forged a working and a romantic relationship and married in 1956. The Smithsonian American Art Museum states, "Together, they adapted European surrealism into a new art movement known as subjective classicism. They rejected dreamlike free associations and instead placed objects together deliberately to evoke a particular idea." The Feitelson/Lundeberg Art Foundation explains that their approach, also called Post-Surrealism, "did not rely on random, dream, personally symbolic, or arbitrary imagery. Instead, carefully planned objects or props were used to guide the viewer through the painting, gradually revealing a deeper and inter-connected meaning."

For a time, Feitelson may have been better known as the host of "Feitelson on Art," his popular, unscripted, live television show that aired from 1956 through 1963, than for his artwork now found in many private collections, museums, and galleries. The Feitelson/Lundeberg Art Foundation notes that on his weekly TV show, "Over the years, Feitelson presented all eras, cultures and methods of making art from prehistoric through contemporary mid 1950s through early 1960s."

During 1940–1960, Feitelson experimented with abstract forms and his compositions shifted from organic imagery to geometric forms, culminating with his minimalistic "ribbon" paintings. This month's cover image, *Magical Forms*, is one of several such paintings that share this title or variation of it. A series of tapered, twisting shapes, all with hollow centers, glide and drift across the canvas, emerging from and returning to the dark background. The brightly colored shapes along the edges appear to rise from the darkness, while the darker shapes seem to be receding. Their movements quietly evoke stingrays gliding under the ocean's surface or bats pirouetting in twilight. The viewer is unsure what these magical forms represent, but the rhythm and balance of shapes and background are transfixing.

Feitelson's notes on these paintings are telling: "There is nothing fortuitous or 'automatic' in the creation of these Magical Space Forms, fantastic though they are. Because I am concerned with durable vitality, rather than momentary frenzy, I find my work demands full participation of both my sensibilities and critical faculties."

During the 1890s, the same decade in which Feitelson was born, major breakthroughs occurred in virology. Dmitri Ivanovsky discovered that sap from diseased tobacco plants after being strained through filters that trapped bacteria could infect healthy plants, and Martinus Beijerinck, whose filtration experiments yielded the same results, named this pathogen a "virus." In 1939, eight years after Ernst Ruska and Max Knoll built the first electron microscope, Ruska, Gustav Kausche, and Edgar Pfankuch used an electron microscope to record the first images of the tobacco mosaic virus with its rodlike shape.

Before viruses were clearly understood and actually seen, they may have also seemed like magical forms. Viruses were determined to be submicroscopic parasites that cannot reproduce outside of a host and that have few components, essentially a single- or double-stranded nucleic acid and a protein coat in the form of a capsid. The structure and shape of viruses enable them to infect different types of cells and hosts, sometimes killing their hosts and sometimes coexisting without harming them. This high degree of specialization among viruses in a sense echoes Feitelson and Lundeberg's notion of placing objects together deliberately to evoke a particular response.

Given the abundance and diversity of viruses, it might have been expected that viruses would be found in a staggering array of shapes. After all, researcher Curtis Suttle notes, "If we compare the number of viruses in the oceans to the number of stars in the universe, there are about 10^{23} stars in the universe. In contrast, there are about 10 million-fold more viruses in the ocean than there are stars in the universe." Infectious disease specialist David Pride wrote, "Biologists estimate that 380 trillion viruses are living on and inside your body right now—10 times the number of bacteria. Some can cause illness, but many simply coexist with you."

Despite those nearly unfathomable numbers, most viruses are categorized as having one of three shapes: helical, icosahedral, or complex viruses. Helical viruses, or filamentous viruses, have rodlike, elongated shapes. Icosahedral viruses, or isometric viruses, possess 20 triangular sides or faces and 12 vertices, and 60 asymmetrical units. Complex viruses have multiple structural components that do not fit neatly into the other classifications.

Since the 1980s, millions of people have been killed or sickened by a number of viruses, including

human immunodeficiency viruses, coronaviruses, hantaviruses, hepatitis viruses, Ebola and Marburg viruses, dengue viruses, influenza viruses, and the measles virus. Because their evolution has yielded a wide diversity, viruses have maintained a durable vitality. Ensuring that public health infrastructure has a similar durable vitality for responding to emerging viral diseases and cyclic pandemics remains a high priority.

Bibliography

1. Curtis C. Feitelson's serene and anxious forms. Los Angeles Times, October 5, 1990, p. 24. [cited 2022 Mar 23] https://www.latimes.com/archives/la-xpm-1990-10-05-ca-1796-story.html
2. Feitelson L. Lorser Feitelson and Helen Lundeberg papers, circa 1890s–2002. Box 8, Folder 47: magical space forms, 1950s−1960s [cited 2022 Mar 28]. https://www.aaa.si.edu/collections/lorser-feitelson-and-helen-lundeberg-papers-7341/series-7/box-8-folder-47
3. The Feitelson/Lundeberg Art Foundation. Lorser Feitelson [cited 2022 Mar 8]. https://www.thefeitelsonlundebergartfoundation.org/biography
4. Goldsmith CS, Miller SE. Modern uses of electron microscopy for detection of viruses. Clin Microbiol Rev. 2009;22:552–63. https://doi.org/10.1128/CMR.00027-09
5. Laguna Art Museum. Lorser Feitelson [cited 2022 Mar 12]. https://lagunaartmuseum.org/artist/lorser-feitelson
6. Louten J. Virus structure and classification. In: Louten J, editor. Essential human virology; 2016. p. 19–29. https://doi.org/10.1016/B978-0-12-800947-5.00002-8
7. National Institutes of Health, National Institute of Allergy and Infectious Diseases. NIAID emerging infectious diseases/pathogens [cited 2022 Mar 12]. https://www.niaid.nih.gov/research/emerging-infectious-diseases-pathogens
8. Pride D. Viruses can help us as well as harm us [cited 2022 Mar 20]. Scientific American. https://www.scientificamerican.com/article/viruses-can-help-us-as-well-as-harm-us
9. Smithsonian American Art Museum. Lorser Feitelson [cited 2022 Mar 12]. https://americanart.si.edu/artist/lorser-feitelson-1509
10. Suttle CA. Viruses: unlocking the greatest biodiversity on earth. Genome. 2013;56:542–4. https://doi.org/10.1139/gen-2013-0152
11. The University of Queensland Institute for Molecular Bioscience. What's the difference between bacteria and viruses? [cited 2022 Mar 20] https://imb.uq.edu.au/article/2020/04/difference-between-bacteria-and-viruses

Address for correspondence: Byron Breedlove, EID Journal, Centers for Disease Control and Prevention, 1600 Clifton Rd NE, Mailstop H16-2, Atlanta, GA 30329-4027, USA; email: wbb1@cdc.gov

etymologia revisited

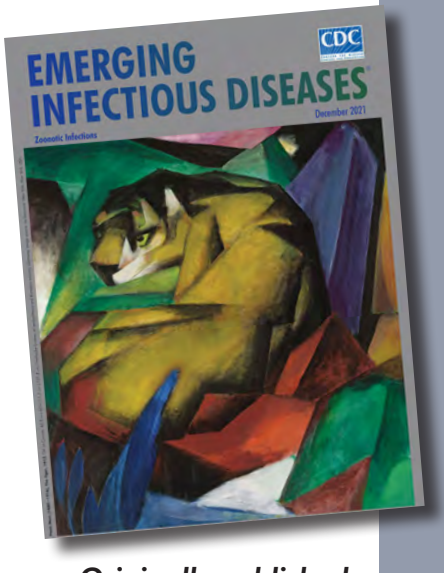

Originally published in December 2021

Trichinella spiralis

[tri·kuh·neh′·luh spr·a′·luhs]

Trichinella is derived from the Greek words *trichos* (hair) and *ella* (diminutive); *spiralis* means spiral. In 1835, Richard Owen (1804–1892) and James Paget (1814–1899) described a spiral worm (*Trichina spiralis*)–lined sandy diaphragm of a cadaver. In 1895, Alcide Raillet (1852–1930) renamed it as *Trichinella spiralis* because *Trichina* was attributed to an insect in 1830. In 1859, Rudolf Virchow (1821–1902) described the life cycle. The genus includes many distinct species, several genotypes, and encapsulated and nonencapsulated clades based on the presence/absence of a collagen capsule.

Sources

1. Campbell WC. History of trichinosis: Paget, Owens and the discovery of *Trichinella spiralis*. Bull Hist Med. 1979;53:520–52.
2. Centers for Disease Control and Prevention. Trichinellosis: general information [cited 2021 May 11]. https://www.cdc.gov/parasites/trichinellosis/ gen_info/faqs.html
3. Gottstein B, Pozio E, Nöckler K. Epidemiology, diagnosis, treatment, and control of trichinellosis. Clin Microbiol Rev. 2009;22:127–45. https://doi.org/10.1128/CMR.00026-08
4. Observations on *Trichina spiralis*. Boston Med Surg J. 1860; 63:294–8. https://doi.org/10.1056/NEJM186011080631504
5. Zarlenga D, Thompson P, Pozio E. *Trichinella* species and genotypes. Res Vet Sci. 2020;133:289–96. https://doi.org/10.1016/j.rvsc.2020.08.012

https//wwwnc.cdc.gov/eid/article/27/12/et-2712_article

EMERGING INFECTIOUS DISEASES®

Upcoming Issue • June 2022

- Cross-Sectional Study of Clinical Predictors of Coccidioidomycosis, Arizona, USA
- Detection of SARS-CoV-2 B.1.351 (Beta) Variant through Wastewater Surveillance Before Case Detection in a Community, Oregon
- Divergent Rabies Virus Variant of Probable Bat Origin in 2 Gray Foxes, New Mexico, USA
- Effects of Acute Dengue Infection in Men on Sperm and Virus Clearance in Body Fluids
- Retrospective Genomic Characterization of a 2017 Dengue Virus Outbreak, Burkina Faso
- Impact of Recombinant Vesicular Stomatitis Virus, Zaire
- Ebola Virus Vaccination on Ebola Virus Disease Illness and Death, Democratic Republic of the Congo
- Characterization of Healthcare-Associated and Community-Associated *Clostridioides difficile* Infections among Adults, Canada, 2015–2019
- Economic Burden of Reported Lyme Disease in High-Incidence Areas, United States, 2014–2016
- *Angiostrongylus cantonensis* Nematode Invasion Pathway, Mallorca, Spain
- SARS-CoV-2 Antibody Response to CoronaVac followed by a Booster Dose of BNT162b2 Vaccine
- *Burkholderia pseudomallei* in Environment of Adolescent Siblings with Melioidosis, Kerala, India, 2019
- Outbreak of Imported Seventh Pandemic *Vibrio cholerae* O1 El Tor, Algeria, 2018
- Lizards as Silent Hosts of *Trypanosoma cruzi*
- Introduction and Rapid Spread of SARS-CoV-2 Omicron Variant and Dynamics of BA.1 and BA.1.1 Sublineages, Finland, December 2021
- Rapid Increase of Community SARS-CoV-2 Seroprevalence during Second Wave of COVID-19 Epidemic, Yaoundé, Cameroon
- Secondary Attack Rate, Transmission and Incubation Periods, and Serial Interval of SARS-CoV-2 Omicron Variant, Spain
- Molecular Diagnosis of *Pseudoterranova decipiens* Sensu Stricto Infections, South Korea, 2002–2020
- Identifying Japanese Encephalitis Virus by Metatranscriptomic Sequencing, Xinjiang, China
- Multistate Outbreak of Infection with SARS-CoV-2 Omicron Variant after Event in Chicago, Illinois, USA, November–December 2021
- Detecting SARS-CoV-2 Omicron B.1.1.529 Variant in Wastewater Samples by Using Nanopore Sequencing
- Viral Zoonoses in Small Wild Mammals and Detection Of Hantavirus, Spain
- Serum Neutralization of SARS-CoV-2 Omicron BA.1 and BA.2 after BNT162b2 Booster Vaccination
- Detection of Recombinant BA.1/BA.2 SARS-CoV-2 Virus in Arriving Travelers, Hong Kong, February 2022
- Experimental Infection of Mink with SARS-COV-2 Omicron Variant and Subsequent Clinical Disease with Lung Pathology and Transmission
- Expansion of L452R-positive SARS-CoV-2 Omicron Variant, Northern Lombardy, Italy

Complete list of articles in the June issue at https://wwwnc.cdc.gov/eid/#issue-289

Earning CME Credit

To obtain credit, you should first read the journal article. After reading the article, you should be able to answer the following, related, multiple-choice questions. To complete the questions (with a minimum 75% passing score) and earn continuing medical education (CME) credit, please go to http://www.medscape.org/journal/eid. Credit cannot be obtained for tests completed on paper, although you may use the worksheet below to keep a record of your answers.

You must be a registered user on http://www.medscape.org. If you are not registered on http://www.medscape.org, please click on the "Register" link on the right hand side of the website.

Only one answer is correct for each question. Once you successfully answer all post-test questions, you will be able to view and/or print your certificate. For questions regarding this activity, contact the accredited provider, CME@medscape.net. For technical assistance, contact CME@medscape.net. American Medical Association's Physician's Recognition Award (AMA PRA) credits are accepted in the US as evidence of participation in CME activities. For further information on this award, please go to https://www.ama-assn.org. The AMA has determined that physicians not licensed in the US who participate in this CME activity are eligible for AMA PRA Category 1 Credits™. Through agreements that the AMA has made with agencies in some countries, AMA PRA credit may be acceptable as evidence of participation in CME activities. If you are not licensed in the US, please complete the questions online, print the AMA PRA CME credit certificate, and present it to your national medical association for review.

Article Title

Invasive Group A *Streptococcus* Outbreaks Associated with Home Healthcare, England, 2018–2019

CME Questions

1. Which one of the following statements regarding invasive group A *Streptococcus* (iGAS) infections is most accurate?

A. The mortality rate of iGAS is between 1% and 2%
B. Asymptomatic passage of GAS is not known to occur
C. GAS can persist on fomites for up to 1 week
D. Throat, nose, skin, and anogenital carriage of GAS have been implicated in healthcare-associated outbreaks

2. Which one of the following characteristics was noted in the current case series of outbreaks of iGAS?

A. Most outbreaks involved at least 200 cases of iGAS
B. The case-fatality rate was 4%
C. The median age of cases was 51 years
D. Nearly all cases featured care administered by home healthcare (HHC) nurses

3. Which one of the following statements regarding the mode of transmission of GAS in the current study is most accurate?

A. Throat swabs from nearly half of HHC workers were positive for GAS
B. PCCs were more likely to recommend screening after age 75 years
C. Fomites were involved in most cases of iGAS
D. The source of GAS was not definitively identified in any outbreak

4. All of the following infection control methods were employed during outbreaks of iGAS in the current study except:

A. HHC worker antibiotic treatment
B. Replacement of equipment
C. Wide antibiotic prophylaxis among patients
D. Antibiotic treatment of patients with wounds positive for GAS

Earning CME Credit

To obtain credit, you should first read the journal article. After reading the article, you should be able to answer the following, related, multiple-choice questions. To complete the questions (with a minimum 75% passing score) and earn continuing medical education (CME) credit, please go to http://www.medscape.org/journal/eid. Credit cannot be obtained for tests completed on paper, although you may use the worksheet below to keep a record of your answers.

You must be a registered user on http://www.medscape.org. If you are not registered on http://www.medscape.org, please click on the "Register" link on the right hand side of the website.

Only one answer is correct for each question. Once you successfully answer all post-test questions, you will be able to view and/or print your certificate. For questions regarding this activity, contact the accredited provider, CME@medscape.net. For technical assistance, contact CME@medscape.net. American Medical Association's Physician's Recognition Award (AMA PRA) credits are accepted in the US as evidence of participation in CME activities. For further information on this award, please go to https://www.ama-assn.org. The AMA has determined that physicians not licensed in the US who participate in this CME activity are eligible for AMA PRA Category 1 Credits™. Through agreements that the AMA has made with agencies in some countries, AMA PRA credit may be acceptable as evidence of participation in CME activities. If you are not licensed in the US, please complete the questions online, print the AMA PRA CME credit certificate, and present it to your national medical association for review.

Article Title

Genomic Epidemiology of Global Carbapenemase-Producing *Escherichia coli,* 2015–2017

CME Questions

1. You are advising a large hospital system about emerging antibiotic resistance of *Escherichia coli*. On the basis of the genome sequencing study of 229 carbapenemase-producing *E. coli* (2015–17) from 36 countries by Peirano and colleagues, which one of the following statements about global distribution of different carbapenemase genes is correct?

A. KPC-2 and NDM-1 were the 2 most common carbapenemases
B. Of 5 dominant sequence types (STs), ST410 and ST131 were limited to Turkey
C. OXA-181 was frequent in Jordan (because of ST410-B4/H24RxC subclade) and Turkey (because of ST1284)
D. OXA-48 was frequent in Egypt, Thailand, and Vietnam

2. According to the genome sequencing study of 229 carbapenemase-producing *E. coli* (2015–17) from 36 countries by Peirano and colleagues, which one of the following statements about antimicrobial resistance determinants and plasmid replicon types, virulence-associated factors, and carbapenemase gene flanking regions and plasmid analysis is correct?

A. Among antimicrobial resistance determinants, this study examined only carbapenemase genes
B. The investigators found nearly identical IncX3-blaOXA-181 plasmids among 11 STs from 12 countries
C. Most isolates had papA and iha virulence factors
D. All NDM genes were situated within Tn2013 harbored on near-identical IncX3 plasmids

3. On the basis of the genome sequencing study of 229 carbapenemase-producing *E. coli* (2015–17) from 36 countries by Peirano and colleagues, which one of the following statements about public health implications of global distribution of different carbapenemase genes and associated factors is correct?

A. A World Health Organization (WHO) report showed adequate surveillance for carbapenem-resistant *E. coli* in most lower- and middle-income countries
B. Global multidrug-resistant surveillance does not require characterization of individual carbapenemases
C. The most frequent individual carbapenemases in this survey were similar to those in carbapenemase-producing *Klebsiella pneumoniae* and *Enterobacter cloacae* complex
D. A public health priority should be control of IncX3 plasmids, which were mainly responsible for global distribution of OXA-181 genes, the most common carbapenemase in this study